Journal of Mathematics

Soft Computing Algorithms Based on Fuzzy Extensions 2022

Lead Guest Editor: Naeem Jan
Guest Editors: Lazim Abdullah and Ewa Rak

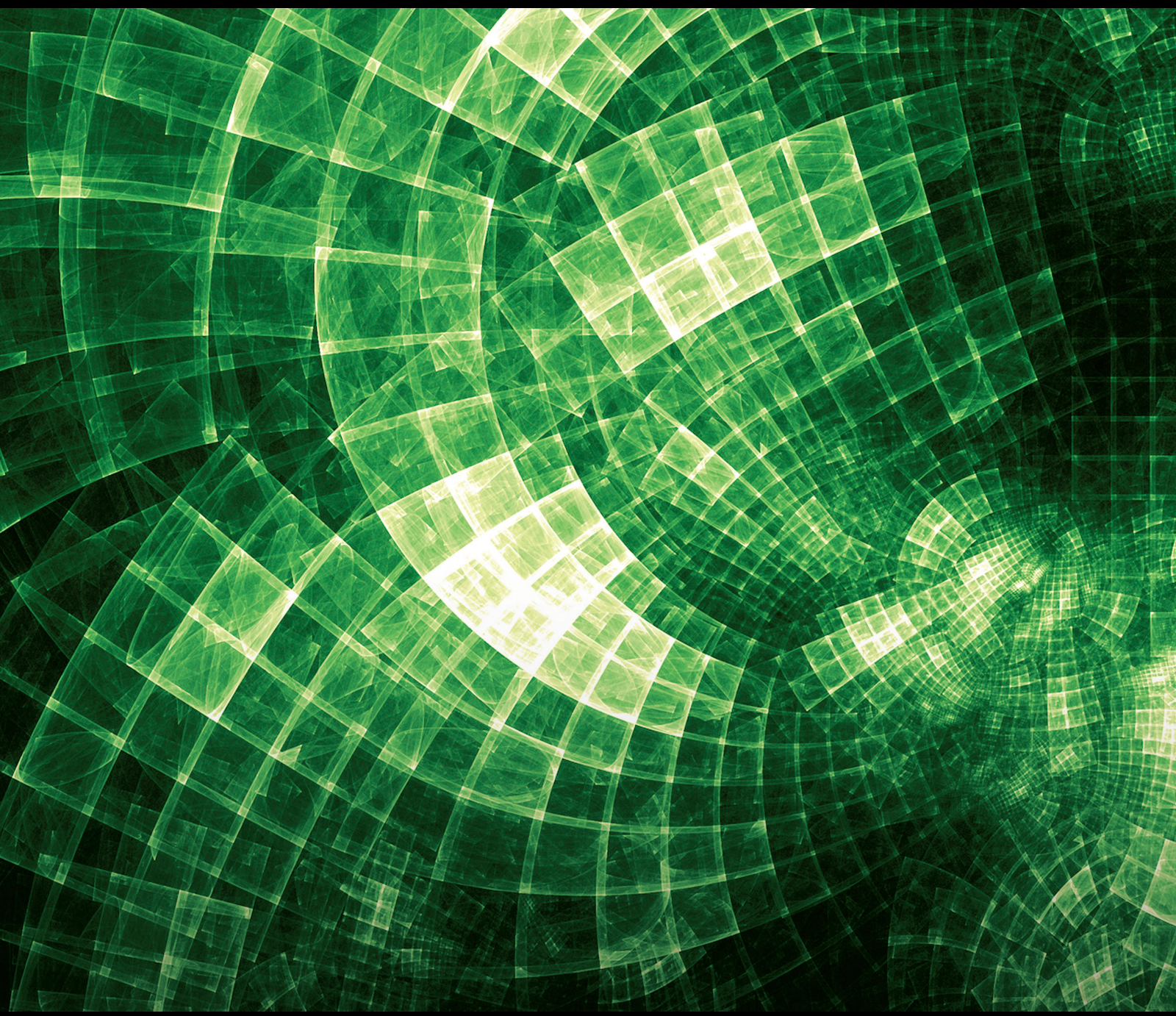

Soft Computing Algorithms Based on Fuzzy Extensions 2022

Journal of Mathematics

Soft Computing Algorithms Based on Fuzzy Extensions 2022

Lead Guest Editor: Naeem Jan
Guest Editors: Lazim Abdullah and Ewa Rak

Probability and Statistics

Contents

Contents

Contents

Hindawi
Journal of Mathematics
Volume 2024, Article ID 9857507, 1 page
https://doi.org/10.1155/2024/9857507

Retraction

Retracted: Dynamic Wavelength Scheduling by Multiobjectives in OBS Networks

Journal of Mathematics

Received 23 January 2024; Accepted 23 January 2024; Published 24 January 2024

This article has been retracted by Hindawi following an investigation undertaken by the publisher [1]. This investigation has uncovered evidence of one or more of the following indicators of systematic manipulation of the publication process:

(1) Discrepancies in scope

(2) Discrepancies in the description of the research reported

(3) Discrepancies between the availability of data and the research described

(4) Inappropriate citations

(5) Incoherent, meaningless and/or irrelevant content included in the article

(6) Manipulated or compromised peer review

The presence of these indicators undermines our confidence in the integrity of the article's content and we cannot, therefore, vouch for its reliability. Please note that this notice is intended solely to alert readers that the content of this article is unreliable. We have not investigated whether authors were aware of or involved in the systematic manipulation of the publication process.

Wiley and Hindawi regrets that the usual quality checks did not identify these issues before publication and have since put additional measures in place to safeguard research integrity.

We wish to credit our own Research Integrity and Research Publishing teams and anonymous and named external researchers and research integrity experts for contributing to this investigation.

The corresponding author, as the representative of all authors, has been given the opportunity to register their agreement or disagreement to this retraction. We have kept a record of any response received.

References

[1] V. K. A. Kumar, M. R. Kumar, N. Shribala et al., "Dynamic Wavelength Scheduling by Multiobjectives in OBS Networks," *Journal of Mathematics*, vol. 2022, Article ID 3806018, 10 pages, 2022.

Hindawi
Journal of Mathematics
Volume 2024, Article ID 9806508, 1 page
https://doi.org/10.1155/2024/9806508

Retraction

Retracted: Novel Concepts in Rough Cayley Fuzzy Graphs with Applications

Journal of Mathematics

Received 23 January 2024; Accepted 23 January 2024; Published 24 January 2024

This article has been retracted by Hindawi following an investigation undertaken by the publisher [1]. This investigation has uncovered evidence of one or more of the following indicators of systematic manipulation of the publication process:

(1) Discrepancies in scope

(2) Discrepancies in the description of the research reported

(3) Discrepancies between the availability of data and the research described

(4) Inappropriate citations

(5) Incoherent, meaningless and/or irrelevant content included in the article

(6) Manipulated or compromised peer review

The presence of these indicators undermines our confidence in the integrity of the article's content and we cannot, therefore, vouch for its reliability. Please note that this notice is intended solely to alert readers that the content of this article is unreliable. We have not investigated whether authors were aware of or involved in the systematic manipulation of the publication process.

Wiley and Hindawi regrets that the usual quality checks did not identify these issues before publication and have since put additional measures in place to safeguard research integrity.

We wish to credit our own Research Integrity and Research Publishing teams and anonymous and named external researchers and research integrity experts for contributing to this investigation.

The corresponding author, as the representative of all authors, has been given the opportunity to register their agreement or disagreement to this retraction. We have kept a record of any response received.

References

[1] Y. Rao, Q. Zhou, M. Akhoundi, A. A. Talebi, S. Omidbakhsh Amiri, and G. Muhiuddin, "Novel Concepts in Rough Cayley Fuzzy Graphs with Applications," *Journal of Mathematics*, vol. 2023, Article ID 2244801, 11 pages, 2023.

Hindawi
Journal of Mathematics
Volume 2024, Article ID 9793057, 1 page
https://doi.org/10.1155/2024/9793057

Retraction

Retracted: Extended DPL-VIKOR Method for Risk Assessment of Technological Innovation Using Dual Probabilistic Linguistic Information

Journal of Mathematics

Received 23 January 2024; Accepted 23 January 2024; Published 24 January 2024

This article has been retracted by Hindawi following an investigation undertaken by the publisher [1]. This investigation has uncovered evidence of one or more of the following indicators of systematic manipulation of the publication process:

(1) Discrepancies in scope

(2) Discrepancies in the description of the research reported

(3) Discrepancies between the availability of data and the research described

(4) Inappropriate citations

(5) Incoherent, meaningless and/or irrelevant content included in the article

(6) Manipulated or compromised peer review

The presence of these indicators undermines our confidence in the integrity of the article's content and we cannot, therefore, vouch for its reliability. Please note that this notice is intended solely to alert readers that the content of this article is unreliable. We have not investigated whether authors were aware of or involved in the systematic manipulation of the publication process.

Wiley and Hindawi regrets that the usual quality checks did not identify these issues before publication and have since put additional measures in place to safeguard research integrity.

We wish to credit our own Research Integrity and Research Publishing teams and anonymous and named external researchers and research integrity experts for contributing to this investigation.

The corresponding author, as the representative of all authors, has been given the opportunity to register their agreement or disagreement to this retraction. We have kept a record of any response received.

References

[1] S. Ashraf, M. Ijaz, M. Naeem, S. Abdullah, and L. B. Alphonse-Roger, "Extended DPL-VIKOR Method for Risk Assessment of Technological Innovation Using Dual Probabilistic Linguistic Information," *Journal of Mathematics*, vol. 2023, Article ID 7570984, 15 pages, 2023.

Hindawi
Journal of Mathematics
Volume 2023, Article ID 9838794, 1 page
https://doi.org/10.1155/2023/9838794

Retraction

Retracted: On Some Classes of Estimators Derived from the Positive Part of James–Stein Estimator

Journal of Mathematics

Received 19 December 2023; Accepted 19 December 2023; Published 20 December 2023

This article has been retracted by Hindawi following an investigation undertaken by the publisher [1]. This investigation has uncovered evidence of one or more of the following indicators of systematic manipulation of the publication process:

(1) Discrepancies in scope

(2) Discrepancies in the description of the research reported

(3) Discrepancies between the availability of data and the research described

(4) Inappropriate citations

(5) Incoherent, meaningless and/or irrelevant content included in the article

(6) Manipulated or compromised peer review

The presence of these indicators undermines our confidence in the integrity of the article's content and we cannot, therefore, vouch for its reliability. Please note that this notice is intended solely to alert readers that the content of this article is unreliable. We have not investigated whether authors were aware of or involved in the systematic manipulation of the publication process.

Wiley and Hindawi regrets that the usual quality checks did not identify these issues before publication and have since put additional measures in place to safeguard research integrity.

We wish to credit our own Research Integrity and Research Publishing teams and anonymous and named external researchers and research integrity experts for contributing to this investigation.

The corresponding author, as the representative of all authors, has been given the opportunity to register their agreement or disagreement to this retraction. We have kept a record of any response received.

References

[1] A. Hamdaoui, A. Benkhaled, M. Alshahrani, M. Terbeche, W. Almutiry, and A. Alahmadi, "On Some Classes of Estimators Derived from the Positive Part of James–Stein Estimator," *Journal of Mathematics*, vol. 2023, Article ID 5221061, 12 pages, 2023.

Hindawi
Journal of Mathematics
Volume 2023, Article ID 9760174, 1 page
https://doi.org/10.1155/2023/9760174

Retraction

Retracted: Optimized CNN-Based Recognition of District Names of Punjab State in Gurmukhi Script

Journal of Mathematics

Received 19 December 2023; Accepted 19 December 2023; Published 20 December 2023

This article has been retracted by Hindawi following an investigation undertaken by the publisher [1]. This investigation has uncovered evidence of one or more of the following indicators of systematic manipulation of the publication process:

(1) Discrepancies in scope

(2) Discrepancies in the description of the research reported

(3) Discrepancies between the availability of data and the research described

(4) Inappropriate citations

(5) Incoherent, meaningless and/or irrelevant content included in the article

(6) Manipulated or compromised peer review

The presence of these indicators undermines our confidence in the integrity of the article's content and we cannot, therefore, vouch for its reliability. Please note that this notice is intended solely to alert readers that the content of this article is unreliable. We have not investigated whether authors were aware of or involved in the systematic manipulation of the publication process.

Wiley and Hindawi regrets that the usual quality checks did not identify these issues before publication and have since put additional measures in place to safeguard research integrity.

We wish to credit our own Research Integrity and Research Publishing teams and anonymous and named external researchers and research integrity experts for contributing to this investigation.

The corresponding author, as the representative of all authors, has been given the opportunity to register their agreement or disagreement to this retraction. We have kept a record of any response received.

References

[1] S. Sharma, S. Gupta, D. Gupta et al., "Optimized CNN-Based Recognition of District Names of Punjab State in Gurmukhi Script," *Journal of Mathematics*, vol. 2022, Article ID 6580839, 10 pages, 2022.

Hindawi
Journal of Mathematics
Volume 2023, Article ID 9893017, 1 page
https://doi.org/10.1155/2023/9893017

Retraction

Retracted: Research on the Flow Space Planning Model of a Classical Garden Based on an Ant Colony Optimization Algorithm

Journal of Mathematics

Received 10 October 2023; Accepted 10 October 2023; Published 11 October 2023

This article has been retracted by Hindawi following an investigation undertaken by the publisher [1]. This investigation has uncovered evidence of one or more of the following indicators of systematic manipulation of the publication process:

(1) Discrepancies in scope
(2) Discrepancies in the description of the research reported
(3) Discrepancies between the availability of data and the research described
(4) Inappropriate citations
(5) Incoherent, meaningless and/or irrelevant content included in the article
(6) Peer-review manipulation

The presence of these indicators undermines our confidence in the integrity of the article's content and we cannot, therefore, vouch for its reliability. Please note that this notice is intended solely to alert readers that the content of this article is unreliable. We have not investigated whether authors were aware of or involved in the systematic manipulation of the publication process.

Wiley and Hindawi regrets that the usual quality checks did not identify these issues before publication and have since put additional measures in place to safeguard research integrity.

We wish to credit our own Research Integrity and Research Publishing teams and anonymous and named external researchers and research integrity experts for contributing to this investigation.

The corresponding author, as the representative of all authors, has been given the opportunity to register their agreement or disagreement to this retraction. We have kept a record of any response received.

References

[1] Y. Tang and Z. Madina, "Research on the Flow Space Planning Model of a Classical Garden Based on an Ant Colony Optimization Algorithm," *Journal of Mathematics*, vol. 2022, Article ID 2001084, 8 pages, 2022.

Hindawi
Journal of Mathematics
Volume 2023, Article ID 9878505, 1 page
https://doi.org/10.1155/2023/9878505

Retraction

Retracted: Classical and Bayesian Inference of Marshall-Olkin Extended Gompertz Makeham Model with Modeling of Physics Data

Journal of Mathematics

Received 10 October 2023; Accepted 10 October 2023; Published 11 October 2023

This article has been retracted by Hindawi following an investigation undertaken by the publisher [1]. This investigation has uncovered evidence of one or more of the following indicators of systematic manipulation of the publication process:

(1) Discrepancies in scope

(2) Discrepancies in the description of the research reported

(3) Discrepancies between the availability of data and the research described

(4) Inappropriate citations

(5) Incoherent, meaningless and/or irrelevant content included in the article

(6) Peer-review manipulation

The presence of these indicators undermines our confidence in the integrity of the article's content and we cannot, therefore, vouch for its reliability. Please note that this notice is intended solely to alert readers that the content of this article is unreliable. We have not investigated whether authors were aware of or involved in the systematic manipulation of the publication process.

Wiley and Hindawi regrets that the usual quality checks did not identify these issues before publication and have since put additional measures in place to safeguard research integrity.

We wish to credit our own Research Integrity and Research Publishing teams and anonymous and named external researchers and research integrity experts for contributing to this investigation.

The corresponding author, as the representative of all authors, has been given the opportunity to register their agreement or disagreement to this retraction. We have kept a record of any response received.

References

[1] R. A. H. Mohamed, A. A. Al-Babtain, I. Elbatal, E. M. Almetwally, and H. M. Almongy, "Classical and Bayesian Inference of Marshall-Olkin Extended Gompertz Makeham Model with Modeling of Physics Data," *Journal of Mathematics*, vol. 2022, Article ID 2528583, 14 pages, 2022.

Hindawi
Journal of Mathematics
Volume 2023, Article ID 9874714, 1 page
https://doi.org/10.1155/2023/9874714

Retraction

Retracted: International Chinese Education Expert System Based on Artificial Intelligence and Machine Learning Algorithms

Journal of Mathematics

Received 10 October 2023; Accepted 10 October 2023; Published 11 October 2023

This article has been retracted by Hindawi following an investigation undertaken by the publisher [1]. This investigation has uncovered evidence of one or more of the following indicators of systematic manipulation of the publication process:

(1) Discrepancies in scope

(2) Discrepancies in the description of the research reported

(3) Discrepancies between the availability of data and the research described

(4) Inappropriate citations

(5) Incoherent, meaningless and/or irrelevant content included in the article

(6) Peer-review manipulation

The presence of these indicators undermines our confidence in the integrity of the article's content and we cannot, therefore, vouch for its reliability. Please note that this notice is intended solely to alert readers that the content of this article is unreliable. We have not investigated whether authors were aware of or involved in the systematic manipulation of the publication process.

Wiley and Hindawi regrets that the usual quality checks did not identify these issues before publication and have since put additional measures in place to safeguard research integrity.

We wish to credit our own Research Integrity and Research Publishing teams and anonymous and named external researchers and research integrity experts for contributing to this investigation.

The corresponding author, as the representative of all authors, has been given the opportunity to register their agreement or disagreement to this retraction. We have kept a record of any response received.

References

[1] L. Shen and F. Latif, "International Chinese Education Expert System Based on Artificial Intelligence and Machine Learning Algorithms," *Journal of Mathematics*, vol. 2022, Article ID 2160289, 12 pages, 2022.

Hindawi
Journal of Mathematics
Volume 2023, Article ID 9829645, 1 page
https://doi.org/10.1155/2023/9829645

Retraction

Retracted: A Novel Multicriteria Decision-Making Approach for Einstein Weighted Average Operator under Pythagorean Fuzzy Hypersoft Environment

Journal of Mathematics

Received 10 October 2023; Accepted 10 October 2023; Published 11 October 2023

This article has been retracted by Hindawi following an investigation undertaken by the publisher [1]. This investigation has uncovered evidence of one or more of the following indicators of systematic manipulation of the publication process:

(1) Discrepancies in scope

(2) Discrepancies in the description of the research reported

(3) Discrepancies between the availability of data and the research described

(4) Inappropriate citations

(5) Incoherent, meaningless and/or irrelevant content included in the article

(6) Peer-review manipulation

The presence of these indicators undermines our confidence in the integrity of the article's content and we cannot, therefore, vouch for its reliability. Please note that this notice is intended solely to alert readers that the content of this article is unreliable. We have not investigated whether authors were aware of or involved in the systematic manipulation of the publication process.

Wiley and Hindawi regrets that the usual quality checks did not identify these issues before publication and have since put additional measures in place to safeguard research integrity.

We wish to credit our own Research Integrity and Research Publishing teams and anonymous and named external researchers and research integrity experts for contributing to this investigation.

The corresponding author, as the representative of all authors, has been given the opportunity to register their agreement or disagreement to this retraction. We have kept a record of any response received.

References

[1] P. Sunthrayuth, F. Jarad, J. Majdoubi, R. M. Zulqarnain, A. Iampan, and I. Siddique, "A Novel Multicriteria Decision-Making Approach for Einstein Weighted Average Operator under Pythagorean Fuzzy Hypersoft Environment," *Journal of Mathematics*, vol. 2022, Article ID 1951389, 24 pages, 2022.

Hindawi
Journal of Mathematics
Volume 2023, Article ID 9806481, 1 page
https://doi.org/10.1155/2023/9806481

Retraction

Retracted: A New Four-Parameter Inverse Weibull Model: Statistical Properties and Applications

Journal of Mathematics

Received 10 October 2023; Accepted 10 October 2023; Published 11 October 2023

This article has been retracted by Hindawi following an investigation undertaken by the publisher [1]. This investigation has uncovered evidence of one or more of the following indicators of systematic manipulation of the publication process:

(1) Discrepancies in scope

(2) Discrepancies in the description of the research reported

(3) Discrepancies between the availability of data and the research described

(4) Inappropriate citations

(5) Incoherent, meaningless and/or irrelevant content included in the article

(6) Peer-review manipulation

The presence of these indicators undermines our confidence in the integrity of the article's content and we cannot, therefore, vouch for its reliability. Please note that this notice is intended solely to alert readers that the content of this article is unreliable. We have not investigated whether authors were aware of or involved in the systematic manipulation of the publication process.

Wiley and Hindawi regrets that the usual quality checks did not identify these issues before publication and have since put additional measures in place to safeguard research integrity.

We wish to credit our own Research Integrity and Research Publishing teams and anonymous and named external researchers and research integrity experts for contributing to this investigation.

The corresponding author, as the representative of all authors, has been given the opportunity to register their agreement or disagreement to this retraction. We have kept a record of any response received.

References

[1] N. Yahia and N. Alsadat, "A New Four-Parameter Inverse Weibull Model: Statistical Properties and Applications," *Journal of Mathematics*, vol. 2022, Article ID 5936783, 6 pages, 2022.

Hindawi
Journal of Mathematics
Volume 2023, Article ID 9793012, 1 page
https://doi.org/10.1155/2023/9793012

Retraction

Retracted: Fuzzy Intelligence in Physical Immersion Teaching System Based on Digital Simulation Technology

Journal of Mathematics

Received 10 October 2023; Accepted 10 October 2023; Published 11 October 2023

This article has been retracted by Hindawi following an investigation undertaken by the publisher [1]. This investigation has uncovered evidence of one or more of the following indicators of systematic manipulation of the publication process:

(1) Discrepancies in scope

(2) Discrepancies in the description of the research reported

(3) Discrepancies between the availability of data and the research described

(4) Inappropriate citations

(5) Incoherent, meaningless and/or irrelevant content included in the article

(6) Peer-review manipulation

The presence of these indicators undermines our confidence in the integrity of the article's content and we cannot, therefore, vouch for its reliability. Please note that this notice is intended solely to alert readers that the content of this article is unreliable. We have not investigated whether authors were aware of or involved in the systematic manipulation of the publication process.

Wiley and Hindawi regrets that the usual quality checks did not identify these issues before publication and have since put additional measures in place to safeguard research integrity.

We wish to credit our own Research Integrity and Research Publishing teams and anonymous and named external researchers and research integrity experts for contributing to this investigation.

The corresponding author, as the representative of all authors, has been given the opportunity to register their agreement or disagreement to this retraction. We have kept a record of any response received.

References

[1] A. Du, "Fuzzy Intelligence in Physical Immersion Teaching System Based on Digital Simulation Technology," *Journal of Mathematics*, vol. 2022, Article ID 3741475, 10 pages, 2022.

Hindawi
Journal of Mathematics
Volume 2023, Article ID 9785391, 1 page
https://doi.org/10.1155/2023/9785391

Retraction

Retracted: Linguistic Analysis of Hindi-English Mixed Tweets for Depression Detection

Journal of Mathematics

Received 10 October 2023; Accepted 10 October 2023; Published 11 October 2023

This article has been retracted by Hindawi following an investigation undertaken by the publisher [1]. This investigation has uncovered evidence of one or more of the following indicators of systematic manipulation of the publication process:

(1) Discrepancies in scope

(2) Discrepancies in the description of the research reported

(3) Discrepancies between the availability of data and the research described

(4) Inappropriate citations

(5) Incoherent, meaningless and/or irrelevant content included in the article

(6) Peer-review manipulation

The presence of these indicators undermines our confidence in the integrity of the article's content and we cannot, therefore, vouch for its reliability. Please note that this notice is intended solely to alert readers that the content of this article is unreliable. We have not investigated whether authors were aware of or involved in the systematic manipulation of the publication process.

Wiley and Hindawi regrets that the usual quality checks did not identify these issues before publication and have since put additional measures in place to safeguard research integrity.

We wish to credit our own Research Integrity and Research Publishing teams and anonymous and named external researchers and research integrity experts for contributing to this investigation.

The corresponding author, as the representative of all authors, has been given the opportunity to register their agreement or disagreement to this retraction. We have kept a record of any response received.

References

[1] C. M. B. M. J, R. S, M. Arif, D. K. V, A. K. K, and A. G, "Linguistic Analysis of Hindi-English Mixed Tweets for Depression Detection," *Journal of Mathematics*, vol. 2022, Article ID 3225920, 7 pages, 2022.

Hindawi
Journal of Mathematics
Volume 2023, Article ID 9784719, 1 page
https://doi.org/10.1155/2023/9784719

Retraction

Retracted: Statistical Inference and Mathematical Properties of Burr X Logistic-Exponential Distribution with Applications to Engineering Data

Journal of Mathematics

Received 10 October 2023; Accepted 10 October 2023; Published 11 October 2023

This article has been retracted by Hindawi following an investigation undertaken by the publisher [1]. This investigation has uncovered evidence of one or more of the following indicators of systematic manipulation of the publication process:

(1) Discrepancies in scope

(2) Discrepancies in the description of the research reported

(3) Discrepancies between the availability of data and the research described

(4) Inappropriate citations

(5) Incoherent, meaningless and/or irrelevant content included in the article

(6) Peer-review manipulation

The presence of these indicators undermines our confidence in the integrity of the article's content and we cannot, therefore, vouch for its reliability. Please note that this notice is intended solely to alert readers that the content of this article is unreliable. We have not investigated whether authors were aware of or involved in the systematic manipulation of the publication process.

Wiley and Hindawi regrets that the usual quality checks did not identify these issues before publication and have since put additional measures in place to safeguard research integrity.

We wish to credit our own Research Integrity and Research Publishing teams and anonymous and named external researchers and research integrity experts for contributing to this investigation.

The corresponding author, as the representative of all authors, has been given the opportunity to register their agreement or disagreement to this retraction. We have kept a record of any response received.

References

[1] M. M. Al Sobhi, "Statistical Inference and Mathematical Properties of Burr X Logistic-Exponential Distribution with Applications to Engineering Data," *Journal of Mathematics*, vol. 2022, Article ID 4688871, 21 pages, 2022.

Hindawi
Journal of Mathematics
Volume 2023, Article ID 9768364, 1 page
https://doi.org/10.1155/2023/9768364

Retraction

Retracted: Leveraging Digital Library to Enhance Research and Learning Experience of College Students: An In-Depth Study

Journal of Mathematics

Received 10 October 2023; Accepted 10 October 2023; Published 11 October 2023

This article has been retracted by Hindawi following an investigation undertaken by the publisher [1]. This investigation has uncovered evidence of one or more of the following indicators of systematic manipulation of the publication process:

(1) Discrepancies in scope

(2) Discrepancies in the description of the research reported

(3) Discrepancies between the availability of data and the research described

(4) Inappropriate citations

(5) Incoherent, meaningless and/or irrelevant content included in the article

(6) Peer-review manipulation

The presence of these indicators undermines our confidence in the integrity of the article's content and we cannot, therefore, vouch for its reliability. Please note that this notice is intended solely to alert readers that the content of this article is unreliable. We have not investigated whether authors were aware of or involved in the systematic manipulation of the publication process.

Wiley and Hindawi regrets that the usual quality checks did not identify these issues before publication and have since put additional measures in place to safeguard research integrity.

We wish to credit our own Research Integrity and Research Publishing teams and anonymous and named external researchers and research integrity experts for contributing to this investigation.

The corresponding author, as the representative of all authors, has been given the opportunity to register their agreement or disagreement to this retraction. We have kept a record of any response received.

References

[1] C. Yang, "Leveraging Digital Library to Enhance Research and Learning Experience of College Students: An In-Depth Study," *Journal of Mathematics*, vol. 2022, Article ID 8046962, 8 pages, 2022.

Hindawi
Journal of Mathematics
Volume 2023, Article ID 9783969, 1 page
https://doi.org/10.1155/2023/9783969

Retraction

Retracted: The Application of the Internet of Things Framework in the Ideological and Political Teaching System

Journal of Mathematics

Received 13 September 2023; Accepted 13 September 2023; Published 14 September 2023

This article has been retracted by Hindawi following an investigation undertaken by the publisher [1]. This investigation has uncovered evidence of one or more of the following indicators of systematic manipulation of the publication process:

(1) Discrepancies in scope

(2) Discrepancies in the description of the research reported

(3) Discrepancies between the availability of data and the research described

(4) Inappropriate citations

(5) Incoherent, meaningless and/or irrelevant content included in the article

(6) Peer-review manipulation

The presence of these indicators undermines our confidence in the integrity of the article's content and we cannot, therefore, vouch for its reliability. Please note that this notice is intended solely to alert readers that the content of this article is unreliable. We have not investigated whether authors were aware of or involved in the systematic manipulation of the publication process.

Wiley and Hindawi regrets that the usual quality checks did not identify these issues before publication and have since put additional measures in place to safeguard research integrity.

We wish to credit our own Research Integrity and Research Publishing teams and anonymous and named external researchers and research integrity experts for contributing to this investigation.

The corresponding author, as the representative of all authors, has been given the opportunity to register their agreement or disagreement to this retraction. We have kept a record of any response received.

References

[1] B. Qiu and P. Ikram, "The Application of the Internet of Things Framework in the Ideological and Political Teaching System," *Journal of Mathematics*, vol. 2022, Article ID 2846103, 9 pages, 2022.

Hindawi
Journal of Mathematics
Volume 2023, Article ID 9865757, 1 page
https://doi.org/10.1155/2023/9865757

Retraction

Retracted: Dynamic Alterations and the Affecting Attributes of the Unbalanced Economic Development in the Basin of the Yellow River: Analysis Utilizing Population-Weighted Coefficient of Variation

Journal of Mathematics

Received 13 September 2023; Accepted 13 September 2023; Published 14 September 2023

This article has been retracted by Hindawi following an investigation undertaken by the publisher [1]. This investigation has uncovered evidence of one or more of the following indicators of systematic manipulation of the publication process:

(1) Discrepancies in scope
(2) Discrepancies in the description of the research reported
(3) Discrepancies between the availability of data and the research described
(4) Inappropriate citations
(5) Incoherent, meaningless and/or irrelevant content included in the article
(6) Peer-review manipulation

The presence of these indicators undermines our confidence in the integrity of the article's content and we cannot, therefore, vouch for its reliability. Please note that this notice is intended solely to alert readers that the content of this article is unreliable. We have not investigated whether authors were aware of or involved in the systematic manipulation of the publication process.

Wiley and Hindawi regrets that the usual quality checks did not identify these issues before publication and have since put additional measures in place to safeguard research integrity.

We wish to credit our own Research Integrity and Research Publishing teams and anonymous and named external researchers and research integrity experts for contributing to this investigation.

The corresponding author, as the representative of all authors, has been given the opportunity to register their agreement or disagreement to this retraction. We have kept a record of any response received.

References

[1] Z. Zhao, "Dynamic Alterations and the Affecting Attributes of the Unbalanced Economic Development in the Basin of the Yellow River: Analysis Utilizing Population-Weighted Coefficient of Variation," *Journal of Mathematics*, vol. 2022, Article ID 3549510, 8 pages, 2022.

Hindawi
Journal of Mathematics
Volume 2024, Article ID 9793057, 1 page
https://doi.org/10.1155/2024/9793057

Retraction

Retracted: Extended DPL-VIKOR Method for Risk Assessment of Technological Innovation Using Dual Probabilistic Linguistic Information

Journal of Mathematics

Received 23 January 2024; Accepted 23 January 2024; Published 24 January 2024

This article has been retracted by Hindawi following an investigation undertaken by the publisher [1]. This investigation has uncovered evidence of one or more of the following indicators of systematic manipulation of the publication process:

(1) Discrepancies in scope

(2) Discrepancies in the description of the research reported

(3) Discrepancies between the availability of data and the research described

(4) Inappropriate citations

(5) Incoherent, meaningless and/or irrelevant content included in the article

(6) Manipulated or compromised peer review

The presence of these indicators undermines our confidence in the integrity of the article's content and we cannot, therefore, vouch for its reliability. Please note that this notice is intended solely to alert readers that the content of this article is unreliable. We have not investigated whether authors were aware of or involved in the systematic manipulation of the publication process.

Wiley and Hindawi regrets that the usual quality checks did not identify these issues before publication and have since put additional measures in place to safeguard research integrity.

We wish to credit our own Research Integrity and Research Publishing teams and anonymous and named external researchers and research integrity experts for contributing to this investigation.

The corresponding author, as the representative of all authors, has been given the opportunity to register their agreement or disagreement to this retraction. We have kept a record of any response received.

References

[1] S. Ashraf, M. Ijaz, M. Naeem, S. Abdullah, and L. B. Alphonse-Roger, "Extended DPL-VIKOR Method for Risk Assessment of Technological Innovation Using Dual Probabilistic Linguistic Information," *Journal of Mathematics*, vol. 2023, Article ID 7570984, 15 pages, 2023.

Hindawi
Journal of Mathematics
Volume 2023, Article ID 7570984, 15 pages
https://doi.org/10.1155/2023/7570984

Research Article

Extended DPL-VIKOR Method for Risk Assessment of Technological Innovation Using Dual Probabilistic Linguistic Information

Shahzaib Ashraf,[1] Muhammad Ijaz,[2] Muhammad Naeem ,[3] Saleem Abdullah,[4] and Lula Babole Alphonse-Roger [5]

[1]*Institute of Mathematics, Khwaja Fareed University of Engineering & Information Technology, Rahim Yar Khan 64200, Pakistan*
[2]*Department of Mathematics, Central South University, Changsha, China*
[3]*Department of Mathematics, Deanship of Applied Sciences, Umm Al-Qura University, Makkah, Saudi Arabia*
[4]*Department of Mathematics, Abdul Wali Khan University, Mardan 23200, Pakistan*
[5]*Department of Mathematics and Computer Science, University of Kinshasa, Kinshasa, Congo*

Correspondence should be addressed to Lula Babole Alphonse-Roger; lulababole@gmail.com

Received 9 May 2022; Revised 28 July 2022; Accepted 7 April 2023; Published 20 May 2023

Academic Editor: Naeem Jan

The main objective of the present study is to evaluate the multicriteria group decision-making problem in risk management for technological innovation projects (TIPs) under dual-probabilistic linguistic information. The suggested approach is based on an enhanced dual probabilistic linguistic-vise kriterijumska optimizacija kompromisno resenje (DPL-VIKOR) technique to assess risk management in TIP employing probabilistic linguistic information. The conventional VIKOR approach is incapable of dealing with the complexity and difficulty of risk assessment in TIP. Therefore, we incorporated the information included in the dual probabilistic linguistic term set. In DPL-VIKOR, we investigated the relationship between the positive ideal solution (PIS) of the alternative and the negative ideal solution (NIS). To deal with the multicriteria group decision-making problem of risk assessment in TIP, we proposed the extended DPL-VIKOR approach rather than the traditional VIKOR method. We compared the findings to those of several decision-making problem techniques and examined the effectiveness and reliability, as well as advantages of the proposed approach. From the comparison and sensitivity analysis, we conclude that the proposed method is more reliable and effective for evaluating the best alternative in risk management problems for TIP.

1. Introduction

Innovation is crucial for economic development and employment potential, benefiting both society and the economy. Purchasing goods or services from low-wage nations such as China and western economies can only compete and thrive via innovation, characterized as the development of new and improved technologies and operational processes [1]. According to Afuah [2], innovation entails the application of prior knowledge in order to develop a new product or service that customers desire. The term "innovation" refers to the commercialization of a novel concept. Process innovation refers to the introduction of a new or modified method of manufacturing a product. The term "product innovation" refers to the production or modification of an existing product. Innovations available in a variety of manifestations and degrees of uniqueness. This shows that organizations take risks in order to create and launch new products successfully and promptly. Thus, risk identification and management are viewed as critical capabilities in innovative organizations [3]. Organizations that want to survive must innovate at a rapid speed despite

simultaneously contending with market uncertainty. This leads into an improvement in the risk level of organizations. The risk is the potential of an unpredictable event occurring and its outcomes. Any aspect that has an effect on a project's performance might be a source of risk. The risk occurs whenever this influence has an unexpected and material effect on the project's performance [4]. Companies get into collaborative partnerships in order to limit the risks involved with innovation, because they possess the requisite resources, including expertise [5]. The risk assessment of technological innovation initiatives is a problem for both researchers and practitioners. Fierce competition in technology and marketing urges technological innovation projects (TIP) focused companies to occupy an advantageous position in the process of accelerating industrial integration [6].

However, some internal and external risks of the business, such as technical risks, market risks, policy risks, and management risks are always affected by TIP [7]. As a consequence, these risks may cause companies to underperform to attain their objectives and incur large losses, and their effect is sometimes difficult to precisely evaluate. Thus, objective risk identification, quantifiable risk assessment, and comprehensive risk management are very important for TIP [6, 8]. This will not only enable business managers to make the correct decision, such as slowing or continuing the introduction of TIP but can also attract the attention of venture finance firms to ensure the project's successful completion.

The risk assessment project is a multi-criteria group decision-making (MCGDM) [9, 10] process with probability and fuzzy uncertainty that plays a crucial role in choosing suitable scientific research initiatives. In the MCGDM process, several individuals are typically want to participate in decision making [11, 12], and decision-makers (DMs) also want to provide their decision matrix, rank and choose the good method [13, 14]. Many DM require to evaluate the risk factor indices (criteria) for risk assessment of TIP, provide the weight data of each metric, and provide their assessment [15, 16]. Due to the external environment's uncertainty and imperfection, evaluating weight data and assessing each substitute or criterion for internal business growth is complex for decision-makers at this step and achieving a comprehensive and reliable judgment is challenging. In addition, linguistic knowledge has special significance for decision makers, because verbal judgments about occurrences may result in imprecise ambiguity [13]. In this context, DPLTS is an improved the precision expressions model relevant to risk assessment of the TIP in the MCGDM phase. Since this not only consisting of other potential linguistic words but also includes their possibilities or levels of confidence, that can help DM more reliably assess and compare each alternatives or criteria [17–19]. For illustration, an effective team of ten analysts is selected to evaluate innovative threat under a few competing parameters using the linguistic variable set to evaluate risk assessment for a TIP [20].

$$\mathbb{k} = \{k_{-2} = \text{low}, k_{-1} = \text{slightly low}, k_0 = \text{medium}, k_1 = \text{slightly high}, k_2 = \text{high}\}. \quad (1)$$

For one situation, the expert may claim that he/she is 40% confident that the risk is average, and 60% confident that the risk is relatively high. From the other scenario, four specialists are allowed to assume that the threat is mild, while six experts are allowed to insure also that risk is relatively higher. Then, these two linguistic terms can describe the value of the linguistic terms of these two instances $\text{DPLTS} = \{\text{medium}(0.4), \text{slightly high}(0.6)\}$.

Even so, we discovered on the basis of literary works that the DPLTS system coupled both with DM methods is unusual for risk assessment of TIP. As we know, when solving MCGDM problems, there are two solutions that are Pareto's best option [21]. Since a set of preinferior options is often created by MCGDM, it often contrasts with our primary idea. As a result, it is difficult to choose only one or more of the best choices to be the best fit for Pareto. Although evaluating the degree of proximity of a specific approach to the optimal solution is the basic principle of reasonable compromise, consensus technology offers an efficient way to deal with contradictory parameters [17, 22]. But a collaboration solution concept is much more fitting. While the measurement falsity in risk assessment for technical innovation plans caused by probability uncertainties and fuzzy uncertainty can be compensated [13, 14]. And, a paper considers that the MCGDM is much more suitable based on the method of agreement programming with DPLTSs. After all, most researchers use traditional approaches, such as the analytical hierarchy process (AHP), on the study basis the outlook relating to the risk management model of TIP [23], approach to Bayesian network [24], BP neural network [21], etc. To find the best optimum solutions, which can also lead to the risk assessment outcomes being biassed. For the path, graph-based AHP for risk objectivity in TIP can be used by Huang et al. [22]. For risk assessments, applicable to allow the use of AHP and fault tree analysis (FTA), shield tunneling machine (TBM). In addition, many papers use consensus methods to assess risk. In addition to lack of probabilistic linguistic knowledge, they have also reached certain types of results. For example, VIKOR is one of the most common concession approaches for solving MCGDM problems. Many techniques of compromise solutions,used often such as the LINMAP process [21], ORESTE method [25], and Vahdani et al. [26]. In order to enhance the risk assessment process, a new FMEA approach was introduced by incorporating a fuzzy belief system and TOPSIS. Li et al. [27] presented the inhanced VIKOR modle to takcle the risk

evaluation in projects of technological innovation under probabilistic linguistic information.

In this paper, we proposed VIKOR method with DPLTSs to carry out risk evaluations of TIP in order to improve the precision and impartiality of risk evaluation of TIP. Since VIKOR is among the most common solution methods, choosing a sensible compromise that's also nearest to the perfect suitable response is the key concept of the VIKOR technique. A PL-VIKOR procedure was introduced by Zhang and Xing integrating the PTLSs, [28]. However, the traditional PL-VIKOR method only considers the connection between each alternative and the optimistic ideal, while ignoring the connection between each alternative and the NIS. The goal of our work is to first improve the current PL-VIKOR approach, and then, based on these research gaps, to propose improved DPL-VIKOR method under probabilistic linguistic uncertainty. In this new process we introduce the connection between each alternative and the detrimental ideal way to improve the DPL-VIKOR method, they add the relationship between each alternate and NIS. In addition, this article utilizes the improved DPL-VIKOR approach to make probabilistic linguistic knowledge accessible for risk assessment of TIP. The paper contributions can be summed up in the three folds as follows:

(1) To solve the MCGDM problem more accurately and comprehensively in the probabilistic linguistic setting, we are developing a new approach called the improved DPL-VIKOR method. The improved method of DPL-VIKOR also considers the relationship between each alternative and PIS and the relationship between each alternative and NIS. Therefore, this new method makes up for the shortcomings of the traditional PL-VIKOR method. The conventional PL-VIKOR technique only reflects the relationship between each alternative and the PIS, but overlooks the relationship between each alternative and the NIS. We use a more appropriate method to normalize DPLTS and ensure that when scheming the distance measure between two PLTS to get the three measures, they take the same number of linguistic terms with the similar normal distribution.

(2) Its the first time that DPLTSs have adopted the improved DPL-VIKOR approach to counter the danger of TIP. In contrast with traditional approaches, the improved DPL-VIKOR approach is more suitable for risk assessment. In addition, combined with the value of DPLTSs, this compromise approach framework will make the risk assessment more detailed and analytical, filling the current research gap.

(3) For the company's managers and the venture capital firms, having a detailed and objective risk assessment of the TIP has clear practical guiding importance. Using the improved PL-VIKOR method and DPLTS to determine and deal with TIP risks is more conducive for officials to allow TIP goals and risk reduction goals throughout the process, which not only reduces DM mistakes and losses but also reduces them to a certain extent Company cost. In addition, the scientific method and template for determining the risks of TIP would be used for risk evaluations.

This article is structured as follows. In Section 2, the fundamental principles related to DPLTSs are reviewed. The enhanced DPL-VIKOR technique for MCGDM is developed in Section 3. Section 4 introduces the improved DPL-VIKOR approach to resolve the practical issue of danger to venture capital from TIP. Section 5 presented the comparison analysis of the established methodology with existing methods in the literature. In Section 6, some findings and possible studies are summarized.

2. Preliminaries

Usually experts tend to issue linguistic terms to express their preferences, rather than objective assessments, such as quantitative assessments. When dealing with MCGDM challenges, such as "good," "medium," or "bad," there are several linguistic expression methods, such as a set of unwilling fuzzy linguistic terms [29], types 2 fuzzy set, double hierarchy hesitant fuzzy linguistic term set [30], linguistic terms with weakened hedges [31], and 2-tuple linguistic model [32].

Even so, not available the current linguistic interpretation methods to reflect the confidence of the linguistic terms assessed by individuals or the meaning of the probability distribution of the overall language terms of all community DM experts. To overcome the shortcoming, the concept of PLTS was defined by Pang et al. [17] in which the probabilities are involved to the assessment provided by the experts to calculate them extra correctly.

Let $\mathbb{k} = \{k_r \mid r = -t, \ldots, -1, 0, 1, \ldots, t\}$ be a LTS, the DPLTSs can be defined as

$$D^L(p) = \left\{ \left\langle \begin{array}{c} L_{(k)}p_{(k)}, M_{(k)}q_{(k)} \mid L_{(k)}, M_{(k)} \in \mathbb{k}, P_{(k)}q_{(k)} \geq 0, k = 1, 2, \ldots, *D^L(p), *D^L(q), \\ \sum_{k=1}^{*L(p),L(q)} p_{(k)}, q_{(k)} \leq 1 \end{array} \right\rangle \right\}, \quad (2)$$

where $L_{(k)}(p_{(k)})$ the linguistic word correlated with likehood is $(p_{(k)})$ and $M_{(k)}(q_{(k)})$ is the linguistic term associated with the probability $(q_{(k)})$, $*L_{(k)}, M_{(k)}$. In all the various linguistic words, the number is the $D^L(p)$ with the DPLTSs. In addition to presenting several possible linguistic values on an object (alternative or attribute), the experts may also represent the probabilistic data of the value set [33]. Relative to other approaches to the modelling of linguistic knowledge for representation, in the DPLTSs DM may assist in defining the object simultaneously of the perspective linguistic expressions and probability. For example, we all see the number of linguistic words with DPLTS is less than 1. For the sake of calculating innocence, Pang et al. [17] defiend a strategy for normalising in DPLTSs. Given a DPLTS as $\sum_{k=1}^{*L(p),L(q)} p_{(k)}, q_{(k)} < 1$, then the normalized DPLTSs

$$D^{\dot{L}}(p) = \left\{ \left\langle \left\langle \dot{L}_{(k)}\dot{p}_{(k)}, \dot{M}_{(k)}\dot{q}_{(k)} \right\rangle \middle| \dot{L}_{(k)}, \dot{M}_{(k)} \in \mathbb{k}, \left(\dot{p}_{(k)}\right)\left(\dot{q}_{(k)}\right) \geq 0, \right\rangle \right\}, \quad k = 1, 2, \ldots, *D^L(p), *D^L(q) \tag{3}$$

where

$$\left(\dot{p}_{(k)}\right)\left(\dot{q}_{(k)}\right) = \sum_{k=1}^{*D^L(p),*D^L(q)} p_{(k)}, q_{(k)} \leq 1 \quad \forall k = 1, 2, \ldots, *D^L(p), *D^L(q). \tag{4}$$

Some transfermation function for *DPLTS* is introduced by Gou et al. [34] to defiend some operational laws on the basis of these function.

Definition 1. Let $\mathbb{k} = \{k_r \mid r = -t, \ldots, -1, 0, 1, \ldots, t\}$ be a LTS the expression for equivlanet information for membership and nonmembership grade can be define as

$$\begin{aligned} f\colon [-\varphi, \varphi] &\longrightarrow [0,1], f(k_r) = \frac{t}{\varphi} + \frac{1}{2} = \tau, \\ f\colon [-\varphi, \varphi] &\longrightarrow [0,1], f(k_r) = \frac{t}{\varphi} + \frac{1}{2} = v. \end{aligned} \tag{5}$$

Definition 2. The inverse function that can show the equivalent information for limguistic term k_t can be describe as

$$\begin{aligned} f^{-1}\colon [0,1] &\longrightarrow [-\varphi, \varphi], f^{-1}(\tau) = k_{(2\tau-1)t} = k_t, \\ f^{-1}\colon [0,1] &\longrightarrow [-\varphi, \varphi], f^{-1}(v) = k_{(2v-1)t} = k_t, \end{aligned} \tag{6}$$

on the basis of above definition, some opreational laws are define as follows.

Definition 3. Let $\mathbb{k} = \{k_r \mid r = -t, \ldots, -1, 0, 1, \ldots, t\}$ be an LTS, $D^L(p), D^L(p_1), D^L(p_2)$ be three DPLTSs, and for a possitive real number λ can be define as follows:

(1) $D^L(p_1) \oplus D^L(p_2) = f^{-1}$
$\left(\bigcup_{v_1^i \in f(L_1), v_1^j \in f(L_2)} \left\{ \begin{array}{c} (v_1^i + v_2^j - v_1^i v_2^j)(p_1^i p_2^j), \\ \{(v_1^i v_2^j)(q_1^i q_2^j)\} \end{array} \right\} \right)$,
$i = 1, 2, \ldots, *D^L(p_1),\ j = 1, 2, \ldots *D^L(p_2)$

(2) $D^L(p_1) \otimes D^L(p_2) = f^{-1}$
$\left(\bigcup_{v_1^i \in f(M_1), v_1^j \in f(M_2)} \begin{array}{c} \{(v_1^i v_2^j)(q_1^i q_2^j)\}, \\ \{(v_1^i + v_2^j - v_1^i v_2^j)(p_1^i p_2^j)\} \end{array} \right)$,
$i = 1, 2, \ldots, *D^L(p_1),\ j = 1, 2, \ldots *D^L(p_2)$

(3) $\lambda D^L(p) = f^{-1}$
$\left(\bigcup_{v^i \in f(M)} \{(1 - (1 - v^i)^\lambda (p^i)), (v^i)^\lambda (q^i)\} \right)$,
$i = 1, 2, \ldots *D^L(p)$

(4) $(D^L(p))^\lambda = f^{-1}$
$\left(\bigcup_{v^i \in f(M)} \{(v^i)^\lambda (q^i)\}, (1 - (1 - v^i)^\lambda (p^i)) \right)$,
$i = 1, 2, \ldots, *D^L(p)$

(5) $\overline{(D^L(p))} = f^{-1} \left(\bigcup_{v^i \in f(M)} \{(1 - v^i)(p^i), (v^i)^\lambda (q^i)\} \right)$,
$i = 1, 2, \ldots, *D^L(p)$

On the basis of equations (5) and (6), the score and deviation function for a DPLTS can be define as follows.

Definition 4. Let

$$D^L(p) = \left\{ \left\langle L_{(k)}p_{(k)}, M_{(k)}q_{(k)} \mid L_{(k)}, M_{(k)} \in \mathbb{k}, P_{(k)}q_{(k)} \geq 0, k = 1, 2, \ldots, *\overset{L}{\underset{P}{D}}, *\overset{L}{\underset{q}{D}} \right\rangle \right\}, \tag{7}$$

be a DPLTS. Then there is the score and deviation function of $D^L(p)$ Can be found as, respectively,

$$E\left(D^L(p)\right) = \frac{\sum_{k=1}^{*D^L(p)} f\left(L_{(k)}\right) p_{(k)} / \sum_{k=1}^{*D^L(p)} p_{(k)} + \sum_{k=1}^{*D^L(p)} f\left(M_k\right) q_{(k)} / \sum_{k=1}^{*D^L(p)} q_{(k)}}{2}$$

$$\cdot \left(\sum_{k=1}^{*D^L(p)} f\left(L_{(k)}\right) - E\left(D^L(p)\right)^2 p_{(k)} \right)^{1/2} / \sum_{k=1}^{*D^L(p)} p_{(k)} + \tag{8}$$

$$\tau\left(D^L(p)\right) = \frac{\left(\sum_{k=1}^{*D^L(p)} f\left(M_{(k)}\right) - E\left(D^L(p)\right)^2 q_{(k)} \right)^{1/2} / \sum_{k=1}^{*D^L(p)} q_{(k)}}{2},$$

for two DPLTS $D^L(p_1)$ and $D^L(p_2)$, it is possible to do a comparison between DPLTS:

(1) If $E(D^L(p_1)) > E(D^L(p_2))$,then $D^L(p_1)$ is superior $D^L(p_2)$denoted by $(D^L(p_1)) > (D^L(p_2))$

(2) If $E(D^L(p_1)) = E(D^L(p_2))$, then

(a) If $\tau(D^L(p_1)) > \tau(D^L(p_2))$, then $D^L(p_1)$ is superior $D^L(p_2)$, denoted by $(D^L(p_1)) > (D^L(p_2))$

(b) If $\tau(D^L(p_1)) = \tau(D^L(p_2))$, then $D^L(p_1)$ is indifferent to $D^L(p_2)$, denoted by $(D^L(p_1)) \sim (D^L(p_2))$

The PL-VIKOR technique is built on this foundation of Wu et al. [35] will establish the distance measurement between two DPLTS developed an adaptation method to ensure that two DPLTS use a similar number of linguistic words and probability distributions. The DPLTSs $(D^L(p_1))$ and $(D^L(p_2))$. The normalise corresponding DPLTSs are

$$\begin{aligned} D^L(p_1) &= \left\{ \left\langle \left\langle \bullet L_{1(k)} \bullet p_{1(k)}, \bullet \overset{\bullet}{M}_{1(k)} \bullet q_{1(k)} \right\rangle \mid k = 1, 2, \ldots, K \right\rangle \right\}, \\ D^L(p_2) &= \left\{ \left\langle \left\langle \bullet L_{2(k)} \bullet p_{2(k)}, \bullet \overset{\bullet}{M}_{2(k)} \bullet q_{2(k)} \right\rangle \mid k = 1, 2, \ldots, K \right\rangle \right\}, \end{aligned} \tag{9}$$

then

$$d\left(\left(D^L(p_1)\right), \left(D^L(p_2)\right)\right) = \frac{1}{2} \left(\begin{array}{c} \sum_{k=1}^{*D^L(p)} p_{(k)} \left(\left(f\left(D^L(p_1)\right) - f\left(D^L(p_2)\right) \right)^2 \right) + \\ \sum_{k=1}^{*D^L(p)} q_{(k)} \left(f\left(D^L(p_1)\right) - f\left(D^L(p_2)\right) \right)^2 \end{array} \right)^{(1/2)}. \tag{10}$$

Example 1. Let $\mathbb{k} = \{k_r \mid r = -t, \ldots, -1, 0, 1, \ldots, t\}$ be LTS,

$$\begin{aligned} D^L(p_1) &= \left\langle \begin{array}{c} \{s_0(0.3)s_1(0.7), \mu_0(0.5)\mu_1(0.5)\}, \{s_1(0.5)s_2(0.5), \mu_0(1)\}, \\ \{s_{-1}(0.4)s_{-2}(0.6), \mu_1(0.5)\mu_2(0.5)\} \end{array} \right\rangle \\ D^L(p_2) &= \left\langle \begin{array}{c} \{s_{-1}(0.3)s_0(0.7), \mu_1(0.5)\mu_2(0.5)\}, \{s_1(0.5)s_2(0.5), \mu_0(1)\}, \\ \{s_{-1}(0.4)s_{-2}(0.6), \mu_0(0.5)\mu_1(0.5)\} \end{array} \right\rangle. \end{aligned} \tag{11}$$

Then the distance of $D^L(p_1)$ and $D^L(p_2)$ can be calculated as

$$d\left(\left(D^L(p_1)\right),\left(D^L(p_2)\right)\right) = \sqrt{\begin{pmatrix} 0.3\times\left(f(s_0)-f(s_{-1})+0.7\times\left(f(s_1)-f(s_0)+0.5\times\right.\right. \\ \left(f(s_1)-f(s_1)+0.5\times\left(f(s_2)-f(s_2)\right.\right. \\ +0.4\times\left(f(s_{-1})-f(s_{-1})+0.6\times\left(f(s_{-2})-f(s_{-2})\right.\right. \\ +0.5\times\left(f(\mu_0)-f(\mu_1)+0.5\times\left(f(\mu_1)-f(\mu_2)\right)^2\right. \\ +1\times\left(f(\mu_2)-f(\mu_2)\right)^2+0.5\times\left(f(\mu_1)-f(\mu_0)\right)^2 \\ +0.5\times\left(f(\mu_2)-f(\mu_1)\right)^2 \end{pmatrix}^2} \quad (12)$$

$$= 0.2545.$$

3. Improved DPL-VIKOR Method of MCGDM System

The VIKOR (VIse Kriterijumska Optimizacija kompromisno Resenje in Serbian; a solution that implies multistandard optimization compromise) is a useful but DM method for voting on compromise options. In dealing with MCGDM issues, the VIKOR approach is very rational, particularly when they have criteria that are incompatible and incompatible. All of the VIKOR techniques were created with the basic measure of "Intimacy" in mind, as well as the "ideal" solution known as the Lp-metric, which is used as an aggregation tool in compromise programming. The primary characteristics of VIKOR's measures are as follows:

(1) Linear standardization

(2) The optimum solution must be documented

(3) Distances from optimal solutions are approximated

(4) Calculation of substitute compromise assessments

(5) Collect franchise alternatives by franchise value

The VIKOR approach is now widely employed in a variety of sectors, including mountain destination selection, forest protection and afforestation, and earthquake reconstruction.

However, in the current research, almost all VIKOR methods in the context of DM only include the connection between each alternative and PIS, while ignoring the connection between each alternative and NIS. As a result, in a probabilistic linguistic context, this study improves the existing PL-VIKOR approach and introduces a new DPL-VIKOR method.

First and foremost, the DPLTS MCGDM problem can be summarized as follows.

Let $A = \{A_1, A_2, \ldots A_n\}$, be a set of alternatives, $C = \{c_1, c_2, \ldots, c_m\}$ is a set of m criteria, and $W = \{\omega_1, \omega_2, \ldots, \omega_n\}^T$ its weight vector with $W_j \geq 0$ and $\sum_{j=1}^{n} W_j = 1$. Numerous experts $U = \{e_1, e_2, \ldots, e_k\}$ are invited to provide their assessments on each alternative for each standard of a given LTS. $T = \{T_t/t = -\varphi, \ldots. -1, 0, 1, \ldots, \varphi\}$, and the weight vector of experts is $W = \{\omega_1, \omega_2, \ldots, \omega_r\}^T$ with $\omega_n \geq 0$, $n = 1, 2, \ldots, m$ and $\sum_{n=1}^{R} W_n = 1$. The assessment of each expert can be a dual probabilistic linguistic decision matrix,is denoted by DPLTSs and then all these evaluations. $D^{DL}(p) = (L^{c(k)}(p_i), M^{c(k)}(q_i))_{m\times n}$ By gathering all elements into a set in the same area, where

$$D^{cL}(p_1) = \{\langle (L^{c(k)}(p_i), M^{c(k)}(q_i)) \mid k = 1, 2, \ldots, K\rangle\}. \quad (13)$$

And, then we can choose the optimum value of the $D^{+L}(p_1)$. And, the worst value of the $D^{-L}(p_1)$ and associated with each criterion c_j based on the following rules:

$$D^{+L}(p_1) = \left\{ \begin{array}{c} \max\limits_{i=1,2,\ldots m} L^c_{(i)}(p_j), M^c_{(i)}(q_j) \text{for the benefit criterion } c_j \\ \min\limits_{i=1,2,\ldots,m} L^c_{(i)}(p_j), M^c_{(i)}(q_j) \text{for the cost criterrion } c_j \\ \text{for all } j = 1, 2, \ldots, n \end{array} \right\}, \quad (14)$$

$$D^{-L}(p_1) = \left\{ \begin{array}{c} \min\limits_{i=1,2,\ldots,m} L^c_{(i)}(p_j), M^c_{(i)}(q_j) \text{ for the benefit criterion } c_j \\ \max\limits_{i=1,2,\ldots m} L^c_{(i)}(p_j), M^c_{(i)}(q_j) \text{for the cost criterrion } c_j \\ \text{for all } j = 1, 2, \ldots, n \end{array} \right\}, \quad (15)$$

Then, the PIS $D^{+L}(p) = \{D^{+L}(p_1), D^{+L}(p_2), \ldots, D^{+L}(p_n)\}$ and the NIS $D^{-L}(p) = \{D^{-L}(p_1), D^{-L}(p_2), \ldots, D^{-L}(p_n)\}$ can be obtained. An example of the aggregating technique and rules can be put up as follows.

Example 2. Let $\mathbb{k} = \{k_r \mid r = -t, \ldots, -1, 0, 1, \ldots, t\}$ be an LTS ,and $A = \{A_1, A_2, A_3\}$, is a set of three possibilities, $c = \{c_1, c_2, c_3\}$ is a set of three criterian, two experts decision metrices are

$$D^L(p_1) = \begin{pmatrix} \{s_0(0.6)s_1(0.4), \mu_0(0.6)\mu_1(0.4)\}, \{s_1(0.3)s_2(0.7), \mu_{-1}(0.7)\mu_0(0.3)\}, \\ \{s_{-1}(1), \mu_0(1)\}\{s_0(1), \mu_{-2}(1)\}, \{s_0(0.6)s_1(0.4), \mu_{-2}(0.4)\mu_{-1}(0.6)\}, \\ \{s_{-2}(0.5)s_{-1}(0.5), \mu_0(0.5)\mu_1(0.5)\}\{s_0(0.6)s_1(0.4), \mu_1(0.4)\mu_2(0.6)\}, \\ \{s_1(01), \mu_0(1)\}, \{s_{-1}(0.2)s_{-2}(0.8), \mu_0(0.4)\mu_1(0.6)\} \end{pmatrix},$$
$$D^L(p_2) = \begin{pmatrix} \{s_0(0.2)s_1(0.8), \mu_0(0.4)\mu_1(0.6)\}, \{s_1(0.3)s_2(0.7), \mu_{-1}(0.7)\mu_0(0.3)\}, \\ \{s_{-2}(0.5)s_{-1}(0.5), \mu_0(1)\}\{s_0(1), \mu_{-1}(0.5)\mu_{-2}(0.5)\}, \\ \{s_0(0.5)s_1(0.5), \mu_{-2}(0.5)\mu_{-1}(0.5)\}, \{s_{-1}(0.3)s_{-2}(0.5), \mu_0(0.5)\mu_1(0.5)\} \\ \{s_1(1), \mu_1(0.5)\mu_2(0.5)\}, \{s_1(0.5)s_2(0.5), \mu_0(1)\}, \{s_{-1}(0.5)s_{-2}(0.5), \mu_1(1)\} \end{pmatrix}. \tag{16}$$

Represents the weight vector of the expert is $w = \{0.3, 0.3\}^{\mathrm{T}}$. Therefore, the collective selection matrix can be calculated as follows:

$$D^{cL}(p) = \begin{pmatrix} \{s_0(0.32)s_1(0.12)s_2(0.56), \mu_0(0.46)\mu_1(0.54)\}, \\ \{s_1(0.30)s_2(0.7), \mu_{-1}(0.7)\mu_0(0.3)\}, \\ \{s_{-1}(0.65)s_{-2}(0.35), \mu_0(1)\}\{s_{-1}(1), \mu_{-1}(0.35)\mu_{-2}(0.65)\}, \\ \{s_0(0.53)s_1(0.47), \mu_{-1}(0.47)\mu_{-2}(0.53)\}, \\ \{s_{-1}(0.5)s_{-2}(0.5), \mu_0(0.85)\mu_1(0.15)\} \\ \{s_0(0.18)s_1(0.82), \mu_1(0.47)\mu_2(0.53)\}, \\ \{s_1(0.55)s_2(0.35), \mu_0(1)\}, \\ \{s_{-1}(0.41)s_{-2}(0.59), \mu_0(1)\mu_1(0.82)\} \end{pmatrix}. \tag{17}$$

Furthermore, if c_1 and c_2 are the income criteria and c_2 is the cost criterion, PIS and NIS can be calculated using equations (14) and (15).

$$D^{+L}(p) = \begin{Bmatrix} \{s_0(0.18)s_1(0.82), \mu_1(0.47)\mu_2(0.53)\}, \\ \{s_0(0.53)s_1(0.47), \mu_{-1}(0.47)\mu_{-2}(0.53)\}, \\ \{s_{-1}(0.5)s_{-2}(0.5), \mu_0(0.85)\mu_1(0.15)\} \end{Bmatrix},$$
$$D^{-L}(p) = \begin{Bmatrix} \{s_{-1}(1), \mu_{-1}(0.35)\mu_{-2}(0.65)\}, \\ \{s_1(0.55)s_2(0.35), \mu_0(1)\}, \\ \{s_{-1}(0.65)s_{-2}(0.35), \mu_0(1)\} \end{Bmatrix}. \tag{18}$$

The three development metrics mentioned above are obtained for MCGDM, according to the collective decision matrix, to express how close a solution is to the ideal solution. In the first location, the discrete form, respectively $D_\lambda^L(p)$ – metric, based on equation (10). The relation between each alternative and the NIS is introduced as a new definition of Dual probabilistic Linguistic Euclidean $D_\lambda^L(p)$ – metric is established. The calculation shown is as follows.

$$D^{\lambda L}(p) = \left(\sum_{j=1}^{n} \left(w_n \frac{d\left(\left(D^{+L}(p_j), D^{cL}(p_{ij})\right)\right) - d\left(D^{-L}(p_j), \left(D^{cL}(p_{ij})\right)\right)}{d\left(D^{+L}(p_j), D^{-L}(p_j)\right)} \right)^{\lambda} \right)^{1/\lambda}, \tag{19}$$

$$1 \le \lambda \le \infty, \quad i = 1, 2, \ldots, m, \tag{20}$$

in equation (10), there is

$$\frac{d\left(\left(D^{+L}(p_j), D^{cL}(p_{ij})\right)\right) - d\left(D^{-L}(p_j), \left(D^{cL}(p_{ij})\right)\right)}{d\left(D^{+L}(p_j), D^{-L}(p_j)\right)} \in [-1, 1]. \tag{21}$$

Definition 5. The Dual linguistic probabilistic Euclidean $D_\lambda^L(p)$ – metric. For an optional choice, A_i is defined as follows.

However, if a parameter λ is even number and when

$$\frac{d\left(\left(D^{+L}(p_j), D^{cL}(p_{ij})\right)\right) - d\left(D^{-L}(p_j), \left(D^{cL}(p_{ij})\right)\right)}{d\left(D^{+L}(p_j), D^{-L}(p_j)\right)} \in [-1, 0]. \tag{22}$$

The negative outcome will be changed to a possible outcome. To resolve this shortcoming, therefore, to make the Dual linguistic probabilistic Euclidean $D_\lambda^L(p)$ – metric Simper measure, we will let you measure, $\lambda = 1$ equation (19) can be reduced from Dual linguistic Probabilisticto Measure of Group Utility (DPLGU).

$$D^{\mathrm{LGU}_i}(p) = \left(\sum_{j=1}^{n} w_n \frac{d\left(\left(D^{+L}(p_i)\right), \left(D^{cL}(p_{ij})\right)\right) - d\left(\left(D^{-L}(p_i)\right), \left(D^{cL}(p_{ij})\right)\right)}{d\left(\left(D^{+L}(p_j)\right), \left(D^{-L}(p_{ji})\right)\right)} \right), \quad i = 1, 2, \ldots, m. \tag{23}$$

In fact, the Dual Linguistic Probabilistic individual regrets

$$D^{LIR_i}(p) = \max_{j=1,2,\ldots n} \left\{ w_n \frac{d\left(\left(D^{+L}(p_i)\right), \left(D^{cL}(p_{ij})\right)\right) - d\left(\left(D^{-L}(p_i)\right), \left(D^{c}(p_{ij})\right)\right)}{d\left(\left(D^{+L}(p_j)\right), \left(D^{-L}(p_{ji})\right)\right)} \right\}, \quad i = 1, 2, \ldots, m. \tag{24}$$

Completely, $D^{LUG_i}(p_i) \in [-1, 1]$ and $D^{LIR_i}(p_i) \in [-1, 1]$. Centered on these two steps, the Dual Linguistic Probabilistic Compromise $D^{Lc_i}(p)$ measure for the alternative A_i is determined as follows:

$$D^{Lc_i}(p_i) = \theta \frac{D^{\mathrm{LGU}_i}(p) - D^{+LGU}(p)}{D^{-LGU}(p) - D^{+LGU}(p)} + (1 - \theta) \frac{D^{LIR_i}(p) - D^{+LIR}(p)}{D^{-LIR}(p) - D^{+LIR}(p)}, \tag{25}$$

where $D^{+LGU}(p) = \min_i D^{\mathrm{LGU}_i}(p)$, $D^{-LGU}(p) = \max_i D^{\mathrm{LGU}_i}(p)$, $D^{+LIR}(p) = \min_i D^{LIR_i}(p)$, and $\theta (0 \le \theta \le 1)$ a parameter is a variable that can be changed.so without the loss of equality, we can put $\theta = 0.5$ on the basis of these three measures $D^{\mathrm{LGU}_i}(p)$, $D^{LIR_i}(p)$, and $D^{Lc_i}(p)$, we can find that the compromise solution should also be the best solution

with the smallest value among the options of $D^{\mathrm{LGU}_i}(p), D^{LIR_i}(p)$, and $D^{Lc_i}(p)$. Therefore, we need to rank $D^{\mathrm{LGU}_i}(p), D^{LIR_i}(p)$, and $D^{Lc_i}(p)$ Increment in order to get the final compromise solution.

Still, it is very difficult to get a compromise solution that fulfils the metric $D^{\mathrm{LGU}_i}(p), D^{LIR_i}(p)$, and $D^{Lc_i}(p)$ simultaneously in most cases. Therefore, in order to obtain the best compromise, the following rules are given.

With the measure $D^{Lc_i}(p)$, assume that the right selection of alternatives are $A = \{A^{\tau(1)}, A^{\tau(2)}, \ldots, A^{\tau(n)}\}$. The alternative is the better compromise option, then $A^{\tau(1)}$ complies concurrently with the following two conditions:

(1) $D^{Lc_{A^{\tau(2)}}}(p) - D^{Lc_{A^{\tau(1)}}}(p) \geq 1/(m-1)$, where $A^{\tau(2)}$ is the alternative which ranks second in $D^{Lc_i}(p)$.

(2) In both $D^{\mathrm{LGU}_i}(p)$ and $D^{LIR_i}(p)$ the alternative $A^{\tau(1)}$ should also rank first. Furthermore, if one of the aforementioned factors is not met, the best method to reach a compromise is to consider other options.

(a) If only condition 2 is not met, then both conditions are satisfied. $A^{\tau(1)}$ and $A^{\tau(2)}$. The best compromise options are known to be.

(b) If condition 1 is satisfied, then $A^{\tau(1)}, A^{\tau(2)}, \ldots, A^{\tau(k)}, 1 \leq k \leq m$ the best options for compromise are $A^{\tau(k)}$ can be obtained on the basis of $D^{Lc_{A^{\tau(k)}}} - D^{Lc_{A^{\tau(1)}}} < /(m-1)$ with maximum k. Based on the description above, an algorithm is developed to demonstrate the MCGDMM process for improving the PL-VIKOR approach.

3.1. The Improved DLP-VIKOR Algorithm for MCGDM Problems

Input: the set of alternatives $A = \{A_1, A_2, \ldots, A_m\}$, the set of criteria $c = \{c_1, c_2, \ldots, c_n\}$ and the decision matrices $D^{DL}(p) = (L^{r(k)}(p_i), M^{r(k)}(q_i))_{m\times n}\ (r = 1, 2, \ldots, R)$ assembled by experts.

Output: the right solution for compromise.

Step 1: computing all matrices for decisions $D^{DL}(p) = (L_{ij}^{r(k)}(p_{ij}), M_{ij}^{r(k)}(q_{ij}))_{m\times n}$, $(r = 1, 2, \ldots, R)$. Through the matrix of mutual decisions $D^{cL}(p) = (L_{ij}^{c_{(k)}}(p_{ij}), M_{ij}^{c_{(k)}}(q_{ij}))_{m\times n}$.

Step 2: calculate the measures $D^{\mathrm{LGU}_i}(p)$, $D^{LIR_i}(p)$, and $D^{Lc_i}(p)$ for each alternative A_i depend on equations (23) and (26)

Step 3: in increasing orderd $D^{\mathrm{LGU}_i}(p)$, $D^{LIR_i}(p)$, and $D^{Lc_i}(p)$ rank three measures.

Step 4: based on these two circumstances and the two rules described above, come up with a compromise.

Step 5: end.

4. Implementing the Improved DPL-VIKOR Method to Carry Out a Case Study of Risk Assesment of Technological Innovation Projects

A TIP still requires a lot of funds from venture capital companies. Its drive is to achieve corresponding investment income by industrializing TIP [36]. Before conducting a risk assessment, first define the risk category, then create a risk index method and evaluate the weight of the risk scale. When completing these measures, the enhanced PL-VIKOR approach can be carried out a TIP risk assessment.

4.1. Risk Identification of Projects for Technical Advancement. The risk classification of TIP is primarily focused on internal risk for organizations and external risk for businesses [37]. Technological risks, management risks, production risks, and financial risks are internal risks. Environmental risk and business risk are also internal risks.

The technical risk of TIP is related to the potential failure of the wrong research field in the R&D process [38]. In TIP, some R&D ventures require enormous investment and long-term periods. The harm will be extreme once the incorrect research path or reproductive cells technology was selected.

The possibility of TIP being handled due to poor management of the TIP [39] refers to the lack of innovation. Inadequate organization and teamwork, insufficient attention from senior executives, or stubbornly making the incorrect judgments can all contribute to a lack of technological advancement.

The market risk of TIP means that, owing to the uncertain and rapidly evolving market, the new outcomes does not satisfy market demand [40]. The market risk mainly includes adaptive capabilities with regard to business changes, sensitivity to the business environment, and changing customer needs. The market outlook can be very strong before theTIP is launched,while the innovation is finished, a lot of changes have occurred in the market prospect. Customers could not accept the new product anymore.

The likelihood of failure induced by elements such as social policies, national or municipal legislation, rules, and policies is linked to the environmental risks of technological innovation initiatives. TIP may not be compliant with environmental, energy, technology, or science policies, or it may be unable to secure a license to import raw tools and equipment. Consequently, it is not possible to effectively execute technical break through programmers.

4.1.1. Evaluate the System's Indicator Scores and Measure the Number of Risk Indicators. Any risk factors may be involved in the TIP, and the connection between these elements are

difficult. The structure of the risk index system must therefore be consistent with the systemic principle, the science concept, and the global morality [41]. The systematic concept means that the layout of risk index schemes should systematically reflect the main risks of various aspects and the precise way of industrial technological innovation. According to scientific theory, the quantity of danger indicators must be appropriate and adequate. If there are many risk indicators, the risk indicator system does not fully represent the enterprise's technological progress risk. Therefore, the successful setting of the risk index ensures that the main index is included, minimizes overlapping indexes and makes them clear and relevant. The universal principle means that the common choice for most companies should be the risk index. The danger of technological progress is centered on subjective viewpoints.

According to the three principles and the literature given above, [37–40]. The risk index framework is constructed according to risk identification and the above-given concepts on the basis of technology risks, environmental risk, management risks, and market risk [42]. And, through expert surveys, statistical analysis and other methods, the developed framework is refined, updated, supplemented and finalised. Table 1 displays the final risk index system. This risk evaluation methodology has four levels of risk indices.

In the TIP, the relative value of each risk index varies from one another [43]. The weights should be correctly and allocated into order to represent the significance of each risk index. In this article, we invite three risk management experts to send out scores according to the significance of risk indices, and we use the AHP [44, 45] Methodology for assessing the weight of individual risk indexes, as shown in Table 2.

We are interviewing a venture capital company to learn about their three alternative technology innovation venture capital plans. The alternative is expressed as $A = \{A_1, A_2, A_3\}$. There are four criteria to be determined easily according in Table 2, and we put fourth-level criteria into our calculations. All parameters are denoted as $C = \{c_1, c_2, c_3, c_4\}$ on the basis of the given LTS.

$$R = \{r_{-2} = \text{low}, r_{-1} = \text{slightlylow}, r_0 = \text{medium}, r_1 = \text{slightlyhigh}, r_2 = \text{high}\}. \tag{26}$$

Three of the experts we invited were $u^r = \{e_1, e_2, e_3\}$. They are invited to analyse the alternatives on the basis of four parameters and to carry out their evaluations with equal significance. The tests are seen in $D^L(p) = (L_{ij}^{r_{(k)}}(p_{ij}), M_{ij}^{r_{(k)}}(q_{ij}))_{3\times 4}$, $(r = 1, 2, \ldots, R)$.

$$D^{L1}(p) = \left\{ \begin{array}{c} \left(\begin{array}{c} \{s_0(0.4)s_1(0.6), \mu_0(0.6)\mu_1(0.4)\}, \{s_{-1}(0.5)s_{-2}(0.5), \mu_1(0.4)\mu_2(0.6)\}, \\ \{s_1(0.6)s_2(0.4), \mu_{-2}(0.6)\mu_{-1}(0.4)\}, \{s_{-2}(0.4)s_{-1}(0.6), \mu_1(0.6)\mu_2(0.4)\} \end{array} \right) \\ \left(\begin{array}{c} \{s_1(0.6)s_2(0.4), \mu_0(0.6)\mu_1(0.4)\}, \{s_{-2}(0.4)s_{-1}(0.6), \mu_0(0.5)\mu_1(0.5)\}, \\ \{s_0(0.3)s_1(0.7), \mu_{-2}(0.6)\mu_{-1}(0.4)\}, \{s_1(0.2)s_2(0.8), \mu_0(0.4)\} \end{array} \right) \\ \left(\begin{array}{c} \{s_{-2}(0.7)s_{-1}(0.3), \mu_1(0.5)\mu_2(0.5)\}, \{s_1(1), \mu_1(0.3)\mu_2(0.7)\}, \\ \{s_{-2}(0.4)s_{-1}(0.6), \mu_0(1)\}, \{s_1(0.5)s_2(0.5), \mu_0(0.4)\mu_1(0.4)\} \end{array} \right) \end{array} \right\},$$

$$D^{L2}(p) = \left\{ \begin{array}{c} \left(\begin{array}{c} \{s_0(0.6)s_1(0.4), \mu_0(0.6)\mu_1(0.4)\}, \{s_{-1}(0.5)s_{-2}(0.5), \mu_1(0.5)\mu_2(0.5)\}, \\ \{s_1(0.6)s_2(0.4), \mu_{-2}(0.3)\mu_{-1}(0.7)\}, \{s_{-2}(0.4)s_{-1}(0.6), \mu_1(0.6)\mu_2(0.4)\} \end{array} \right) \\ \left(\begin{array}{c} \{s_1(0.8)s_2(0.2), \mu_0(0.6)\mu_1(0.4)\}, \{s_{-2}(0.6)s_{-1}(0.4), \mu_0(0.8)\mu_1(0.2)\}, \\ \{s_0(0.2)s_1(0.8), \mu_{-2}(0.6)\mu_{-1}(0.4)\}, \{s_1(0.6)s_2(0.4), \mu_0(1)\} \end{array} \right) \\ \left(\begin{array}{c} \{s_{-2}(0.8)s_{-1}(0.2), \mu_1(0.8)\mu_2(0.2)\}, \{s_1(1), \mu_1(0.4)\mu_2(0.6)\}, \\ \{s_{-2}(0.8)s_{-1}(0.2), \mu_0(1)\}, \{s_1(0.8)s_2(0.2), \mu_0(0.6)\mu_1(0.4)\} \end{array} \right) \end{array} \right\}, \tag{27}$$

$$D^{L3}(p) = \left\{ \begin{array}{c} \left(\begin{array}{c} \{s_1(1), \mu_0(0.4)\mu_1(0.6)\}, \{s_{-1}(0.4)s_{-2}(0.6), \mu_1(0.3)\mu_2(0.7)\}, \\ \{s_1(0.3)s_2(0.7), \mu_{-2}(0.3)\mu_{-1}(0.7)\}, \{s_{-2}(1), \mu_1(1)\mu_2\} \end{array} \right) \\ \left(\begin{array}{c} \{s_1(0.6)s_2(0.4), \mu_0(0.5)\mu_1(0.5)\}, \{s_{-2}(1), \mu_0(0.2)\mu_1(0.8)\}, \\ \{s_0(0.3)s_1(0.7), \mu_{-2}(0.5)\mu_{-1}(0.5)\}, \{s_1(0.2)s_2(0.8), \mu_0(1)\} \end{array} \right) \\ \left(\begin{array}{c} \{s_{-2}(0.8)s_{-1}(0.2), \mu_1(0.8)\mu_2(0.2)\}, \{s_1(0.5)s_2(0.5), \mu_1(1)\}, \\ \{s_{-2}(0.3)s_{-1}(0.7), \mu_0(0.8)\mu_1(0.2)\}, \{s_1(0.8)s_2(0.2), \mu_1(1)\} \end{array} \right) \end{array} \right\}.$$

Table 1: The measures DPLGU_i, DPLIR_i, and DPLC_i for alternatives.

	A_1	A_2	A_3
DPLGU_i	0.076	−0.3246	−0.0281
DPLIR_i	0.3164	0.2201	0.2876
DPLC_i	0.8013	0.2761	0.7453

Then, to deal with this MCGDM issue, we can use the improved DLP-VIKOR method and carry out the risk assessment of these projects. The comparative study between the improved method of DPL-VIKOR and some current methods of decision-making is also completed.

4.1.2. The Improving DLP-VIKOR Method Solves This MCGDM Problem Based on Algorithm 1

Table 2: Risk index and weight indexes.

Risk categories	Weight of the index
Technology c_1	0.26
Environment c_2	0.27
Management c_3	0.22
Market c_4	0.25

Step 1. Aggregate all DMs $D^{DL}(p) = (L_{ij}^{r(k)}(p_{ij}), M_{ij}^{r(k)}(q_{ij}))_{3\times4}$, $(r = 1, 2, \ldots, R)$

Through the common matrix of decisions

$$D^{cL}(p) = \left(L_{ij}^{c(k)}\left(p_{ij}\right), M_{ij}^{c(k)}\left(q_{ij}\right)\right)_{3\times4}, \tag{28}$$

based on expert's weight vectors $\omega = \{0.3, 0.4, 0.3\}$:

$$D^{cL}(p) = \left\{ \begin{pmatrix} \left\{s_0\left(\frac{9}{25}\right)s_1\left(\frac{16}{25}\right), \mu_0\left(\frac{27}{50}\right)\mu_1\left(\frac{23}{50}\right)\right\}, \left\{s_{-1}\left(\frac{47}{100}\right)s_{-2}\left(\frac{53}{100}\right), \mu_1\left(\frac{41}{25}\right)\mu_2\left(\frac{59}{100}\right)\right\}, \\ \left\{s_1\left(\frac{51}{100}\right)s_2\left(\frac{49}{100}\right), \mu_{-2}\left(\frac{33}{100}\right)\mu_{-1}\left(\frac{67}{100}\right)\right\}, \left\{s_{-2}\left(\frac{29}{50}\right)s_{-1}\left(\frac{21}{50}\right), \mu_1\left(\frac{18}{25}\right)\mu_2\left(\frac{7}{25}\right)\right\} \end{pmatrix} \right. \\ \begin{pmatrix} \left\{s_1\left(\frac{17}{25}\right)s_2\left(\frac{8}{25}\right), \mu_0\left(\frac{57}{100}\right)\mu_1\left(\frac{43}{100}\right)\right\}, \left\{s_{-2}\left(\frac{33}{50}\right)s_{-1}\left(\frac{17}{50}\right), \mu_0\left(s_{-2}\left(\frac{53}{50}\right)\right)\mu_1\left(s_{-2}\left(\frac{47}{100}\right)\right)\right\}, \\ \left\{s_0\left(\frac{13}{50}\right)s_1\left(\frac{37}{50}\right), \mu_{-2}\left(\frac{57}{100}\right)\mu_{-1}\left(\frac{43}{100}\right)\right\}, \left\{s_1\left(\frac{9}{25}\right)s_2\left(\frac{16}{25}\right), \mu_0(1)\right\} \end{pmatrix} \\ \left. \begin{pmatrix} \left\{s_{-2}\left(\frac{77}{100}\right)s_{-1}\left(\frac{23}{100}\right), \mu_1\left(\frac{71}{100}\right)\mu_2\left(\frac{29}{100}\right)\right\}, \left\{s_1\left(\frac{17}{20}\right)s_2\left(\frac{3}{20}\right), \mu_1\left(\frac{11}{50}\right)\mu_2\left(\frac{9}{20}\right)\right\}, \\ \left\{s_{-2}\left(\frac{53}{100}\right)s_{-1}\left(\frac{47}{100}\right), \mu_0\left(\frac{47}{50}\right)\mu_1\left(\frac{3}{50}\right)\right\}, \left\{s_1\left(\frac{71}{100}\right)s_2\left(\frac{29}{100}\right), \mu_0\left(\frac{9}{25}\right)\mu_1\left(\frac{16}{25}\right)\right\} \end{pmatrix} \right\}. \tag{29}$$

Step 2. To measure $D^{\mathrm{LGU}_i}(p)$, $D^{LIR_i}(p)$, and $D^{Lc_i}(p)$. Based on equations (11)–(13) for any alternate A_i. Table 1, shows that the lower the risk index value, the better the performance of technological innovation venture capital projects, especially because the risk index value is a cost criterion.

Step 3. According to the obtained measurement values, as shown in Table 1, the ranking order of the alternatives can be obtained according to each indicator.

(1) In DPLGU_i steps, we take $A_2 > A_3 > A_1$

(2) In DPLIR_i steps, we take $A_2 > A_3 > A_1$

(3) In the DPLC_i steps, we take $A_2 > A_3 > A_1$

Step 4. Determine the compromise solution DPLGU_i, DPLIR_i, and DPLC_i, based on the above-given three measures. Hence, the optimal alternative is A_2.

Step 5. End.

5. Comparative Analysis

In this section, we presented the comparison analysis of the developed concept DLPTS based methodology with some existions methods in the literature. We divided this section into two parts.

One is based on DPLTS scores and differences and the other one is focus on the comparison of one linguistic

probability variable with another linguistic probability variable. To begin, the score and deviation functions of the DPLTSs projected in this work are more accurate than the other two ways because the value received via the transfer function is more expressive than the value gained through the subscript. Furthermore, the utilisation of multiple dimensions, namely, probabilistic information and linguistic term subscriptions, will result in some data loss.

5.1. A Comparison of the Improved DLP-VIKOR and PL-VIKOR. These three phases can be calculated and shown on the basis of the PL-VIKOR method, respectively [28] inclosed in Table 3.

In the measures of $PLGU'_i$, $PLIR'_i$, PLC'_i listed in Table 3 cannot meet the recommended conditions:

(1) $PLC'_{A^{\sigma(2)}} - PLC'_{A^{\sigma(1)}} = 0.3280 - 0.2261 = 1019 < 0.5$

(2) The alternative A_2 ranks first in the PLC'_i, and $PLIR'_i$, tests but second in the $PLGU'_i$

Therefore, we are unable to get the perfect alternative.

However, we can get the optimal alternative through the improved DPL-VIKOR method.

5.2. Comparisons between the Enhanced System of PL-VIKOR and Current Methods. Over view of some current methods under the probabilistic linguistic environment to deal with the MCGDM process [17, 46, 47]. It is possible to obtain the DM results and view them in Table 4.

Based on the above-given two comparisons, the summary is as follows:

(1) This is shown in Table 4, which is based on the standard PL-VIKOR approach [28]. It is impossible to find the best compromise solution. This technique only considers the link between some of the alternatives and the PIS, but it ignores the relationship between the alternatives and the NIS. Furthermore, the distance metric employed in the classic PL-VIKOR approach is based on a normalisation procedure that necessitates the inclusion of certain components to the shorter PLTS. As a result, the enhanced DPL-VIKOR approach is more accurate and reasonable than the standard PL-VIKOR method.

(2) Some DM outcomes can be obtained in Table 4, based on some existing methods [17, 46, 47, 49, 55]. For the aggregation operators [17], the PL-TOPSIS method [17], the PL-MULTIMOORA method [46], the PL-DNMA method [48], and the PL-LINMAP [49] method the DM outcome is the same as that of the improved PL-VIKOR process. The PL-TOPSIS Method [17]; however, it only takes into account the degrees of deviation (or distance) between the alternative and the PIS and the degrees of deviation (or distance) between the alternative and the NIS, but it neglects the degrees of deviation (or distance) between the ideal positive solution and the ideal negative solution. In addition, the process of PL-MULTIMOORA [46]: three measures are required, but the third measure, called the Probabilistic Linguistic Full-Multiplicative Type Model, is unable to function if only the profit criteria or cost criteria are present in the decision-making problem.

Table 3: Final Ranking Results.

	A_1	A_2	A_3	Ranking order
$PLGU'_i$	0.7378	0.5980	0.4826	$A_3 > A_2 > A_1$
$PLIR'_i$	0.2600	0.1728	0.2300	$A_2 > A_3 > A_1$
PLC'_i	1.0000	0.2261	0.3280	$A_2 > A_3 > A_1$

Table 4: Results of decision-making based on certain current processes.

Authors	Methods	Ranking order
Pang et al. [17]	Aggregation operators	$A_2 \succ A_3 \succ A_1$
Pang et al. [17]	PL TOPSIS method	$A_2 \succ A_3 \succ A_1$
Wu et al. [46]	PL MULTIMOORA method	$A_2 \succ A_3 \succ A_1$
Liao and Wu [48]	PL DNMA	$A_2 \succ A_3 \succ A_1$
Liao et al. [49]	PL LINMAP method	$A_2 \succ A_3 \succ A_1$
Teng and Liu [50]	PL TODIM method	$A_3 \succ A_2 \succ A_1$
Wu et al. [46]	PL GLDS method	$A_2 \succ A_1 \succ A_3$
Wu and Liao [51]	PL ORESTE method	$A_2 \succ A_1 \succ A_3$
Liao et al. [52]	PL ELECTRE	$A_2 \succ A_1 \succ A_3$
Wu et al. [53]	PL PROMETHEE	$A_2 \succ A_1 \succ A_3$
Feng et al. [54]	PL QUALIFLEX	$A_2 \succ A_1 \succ A_3$
Liang et al. [47]	PL GRA	$A_2 \succ A_1 \succ A_3$
The proposed method	Improvedd DLP VIKOR	$A_2 \succ A_3 \succ A_1$

The following is an overview of the major benefits: the modified DPL-VIKOR technique considers the alternative's link with the PIS as well as the alternative's interaction with the NIS. Second, the PLTS normalization process is more reasonable than the classic PL-VIKOR distance calculation method. Finally, when it comes to assessing the risk of TIP MCGDM with PLTSs, the enhanced DPL-VIKOR approach is a good tool to improve risk assessment outcomes and incentive's managers to do scientific risk analysis.

6. Conclusions and Future Directions for Study

Every organization aspires to be successful. Profit growth, market share leadership supported by customer satisfaction, and the ability to innovate define success today. The role of technological innovation projects in the presence of dual-probability linguistic information was investigated in this article. The TIP is always vulnerable to external and internal risks. The impact of these risks may result in failures, and these failures may result in significant losses for the company. It is necessary to develop a risk assessment target for these uncertain risks. As a result, in order to conduct a reasonable risk assessment of TIP, some DM methods, such as the VIKOR method in conjunction with the probabilistic linguistic term set, should be recommended. The PL-VIKOR method, on the other hand, failed to explain

the relationship between each alternative and NIS and PIS. To avoid this gap, the risk evolution system in the TIP must be accurate and comprehensive. Our research looks at a new method called the improved DPL-VIKOR method, which clarifies the relationship between each alternative and PIS as well as between each alternative and NIS and is used to solve the dual probabilistic linguistic system MCGDM under risk assessment. In order to show the superiority of our proposed method, we compared our proposed model with existing methods [33] (such as aggregation-based methods), PL-TOPSIS method [32] for risk evaluation of TIP under Probabilistic Linguistic system.

In the future, we will eventually provide more logical decision-making procedures in a probabilistic linguistic framework. We will also extend our work to the Dombi norms, Yager norms, and Frank norms. Furthermore, we will use our proposed work for various methods like TOPSIS method and TODIM method.

Data Availability

The data used in the manuscript are hypothetical and can be used by anyone by just citing this article.

Ethical Approval

This article does not contain any studies with human participants or animals performed by any of the authors.

Conflicts of Interest

The authors declare that they have no conflicts of interest.

Authors' Contributions

All authors have contributed equally to this article.

Acknowledgments

The authors would like to thank the Deanship of Scientific Research at Umm Al-Qura University for supporting this work under Grant no. 22UQU4310396DSR34.

References

[1] J. Storey and S. Salaman, *Managers of Innovation*, Blackwell Publishing, Hoboken, NJ, USA, 2005.

[2] A. Afuah, *Innovation Management: Strategies, Implementation, and Profits*, Oxford University Press, Oxford, UK, 2003.

[3] J. G. Vargas-Hernández, M. R. Noruzi, and N. Sariolghalam, "Risk or innovation, which one is far more preferable in innovation projects?" *International Journal ofMarketing Studies*, vol. 2, no. 1, pp. 233–244, 2010.

[4] R. Taplin, *Risk Management and Innovation in Japan, Britain and the United States*, Routledge, England, UK, 2005.

[5] P. J. Edwards and P. A. Bowen, *Risk Management in Project Organization*, University of New South Wales Press Ltd, Randwick, Australia, 2005.

[6] P. Bromiley, D. Rau, and M. K. McShane, "Can strategic risk management contribute to enterprise risk management? A strategic management perspective," *The Routledge Companion to Strategic Risk Management*, pp. 140–156, Routledge, England, UK, 2016.

[7] M. F. Malik, M. Zaman, and S. Buckby, "Enterprise risk management and firm performance: role of the risk committee," *Journal of Contemporary Accounting and Economics*, vol. 16, no. 1, Article ID 100178, 2020.

[8] N. M. Cavaco and V. C. Machado, "Sustainable competitiveness based on resilience and innovation – an alternative approach," *International Journal of Management Science and Engineering Management*, vol. 10, no. 2, pp. 155–164, 2015.

[9] S. Ashraf, S. Abdullah, T. Mahmood, F. Ghani, and T. Mahmood, "Spherical fuzzy sets and their applications in multi-attribute decision making problems," *Journal of Intelligent and Fuzzy Systems*, vol. 36, no. 3, pp. 2829–2844, 2019.

[10] S. Ashraf and S. Abdullah, "Spherical aggregation operators and their application in multiattribute group decision-making," *International Journal of Intelligent Systems*, vol. 34-, no. 3, pp. 493–523, 2019.

[11] S. Ashraf, S. N. Abbasi, M. Naeem, and S. M. Eldin, "Novel decision aid model for green supplier selection based on extended EDAS approach under pythagorean fuzzy Z-numbers," *Frontiers in Environmental Science*, vol. 11, p. 342, 2023.

[12] S. Ashraf, H. Razzaque, M. Naeem, and T. Botmart, "Spherical q-linear Diophantine fuzzy aggregation information: application in decision support systems," *AIMS Mathematics*, vol. 8, no. 3, pp. 6651–6681, 2023.

[13] S. Ebrahimnejad, S. Mousavi, R. Tavakkoli-Moghaddam, and M. Heydar, "Evaluating high risks in large-scale projects using an extended VIKOR method under a fuzzy environment," *International Journal of Industrial Engineering Computations*, vol. 3, no. 3, pp. 463–476, 2012.

[14] T. K. Biswas and K. Zaman, "A fuzzy-based risk assessment methodology for construction projects under epistemic uncertainty," *International Journal of Fuzzy Systems*, vol. 21, no. 4, pp. 1221–1240, 2019.

[15] S. Ashraf, S. Abdullah, and R. Chinram, "Emergency decision support modeling under generalized spherical fuzzy Einstein aggregation information," *Journal of Ambient Intelligence and Humanized Computing*, vol. 13, no. 4, pp. 2091–2117, 2022.

[16] S. Ashraf, S. Abdullah, and T. Mahmood, "Aggregation operators of cubic picture fuzzy quantities and their application in decision support systems," *Korean Journal of Mathematics*, vol. 28, no. 2, pp. 343–359, 2020.

[17] Q. Pang, H. Wang, and Z. Xu, "Probabilistic linguistic term sets in multi-attribute group decision making," *Information Sciences*, vol. 369, pp. 128–143, 2016.

[18] Y. Choi, X. Ye, L. Zhao, and A. C. Luo, "Optimizing enterprise risk management: a literature review and critical analysis of the work of? Wu and Olson," *Annals of Operations Research*, vol. 237, no. 1-2, pp. 281–300, 2015.

[19] S. Ashraf, T. Mahmood, S. Abdullah, and Q. Khan, "Different approaches to multi-criteria group decision making problems for picture fuzzy environment," *Bulletin of the Brazilian Mathematical Society, New Series*, vol. 50, no. 2, pp. 373–397, 2019.

[20] S. Xian, J. Chai, and Y. Yin, "A visual comparison method and similarity measure for probabilistic linguistic term sets and their applications in multi-criteria decision making," *International Journal of Fuzzy Systems*, vol. 21, no. 4, pp. 1154–1169, 2019.

[21] Y. Changwei, L. Zonghao, G. Xueyan, Y. Wenying, J. Jing, and Z. Liang, "Application of BP neural network model in risk

evaluation of railway construction," *Complexity*, vol. 2019, Article ID 2946158, 12 pages, 2019.

[22] Y. S. Huang, J. X. Qi, and J. H. Zhou, "Method of risk discernment in technological innovation based on path graph and variable weight fuzzy synthetic evaluation," in *Proceedings of the Fuzzy Systems and Knowledge Discovery: Second International Conference*, pp. 635–644, Berlin ,Germany, August 2005.

[23] F. Tüysüz and C. Kahraman, "Project risk evaluation using a fuzzy analytic hierarchy process: an application to information technology projects," *International Journal of Intelligent Systems*, vol. 21, no. 6, pp. 559–584, 2006.

[24] M. Yazdi and S. Kabir, "A fuzzy Bayesian network approach for risk analysis in process industries," *Process Safety and Environmental Protection*, vol. 111, pp. 507–519, 2017.

[25] H. Jafari, "Identification and prioritization of grain discharging operations risks by using ORESTE method," *American Journal of Public Health Research*, vol. 1, no. 8, pp. 214–220, 2013.

[26] B. Vahdani, M. Salimi, and M. Charkhchian, "A new FMEA method by integrating fuzzy belief structure and TOPSIS to improve risk evaluation process," *The International Journal of Advanced Manufacturing Technology*, vol. 77, no. 1-4, pp. 357–368, 2015.

[27] L. Li, Q. Chen, X. Li, and X. Gou, "An improved PL-VIKOR model for risk evaluation of technological innovation projects with probabilistic linguistic term sets," *International Journal of Fuzzy Systems*, vol. 23, no. 2, pp. 419–433, 2021.

[28] X. Zhang and X. Xing, "Probabilistic linguistic VIKOR method to evaluate green supply chain initiatives," *Sustainability*, vol. 9, no. 7, pp. 1231–1249, 2017.

[29] M. Kong, Z. Pei, F. Ren, and F. Hao, "New operations on generalized hesitant fuzzy linguistic term sets for linguistic decision making," *International Journal of Fuzzy Systems*, vol. 21, no. 1, pp. 243–262, 2019.

[30] X. Gou, H. Liao, Z. Xu, and F. Herrera, "Double hierarchy hesitant fuzzy linguistic term set and MULTIMOORA method. A case of study to evaluate the implementation status of haze controlling measures," *Information Fusion*, vol. 38, pp. 22–34, 2017.

[31] H. Wang, X. Pan, and S. He, "A new interval type-2 fuzzy VIKOR method for multi-attribute decision making," *International Journal of Fuzzy Systems*, vol. 21, no. 1, pp. 145–156, 2019.

[32] G. Wei, J. Wang, J. Lu et al., "VIKOR method for multiple criteria group decision making under 2-tuple linguistic neutrosophic environment," *Economic Research-Ekonomska Istraživanja*, vol. 33, no. 1, pp. 3185–3208, 2019.

[33] C. Bai, R. Zhang, S. Shen, C. Huang, and X. Fan, "Interval-valued probabilistic linguistic term sets in multi-criteria group decision making," *International Journal of Intelligent Systems*, vol. 33, no. 6, pp. 1301–1321, 2018.

[34] X. Gou and Z. Xu, "Novel basic operational laws for linguistic terms, hesitant fuzzy linguistic term sets and probabilistic linguistic term sets," *Information Sciences*, vol. 372, pp. 407–427, 2016.

[35] C. Bai, R. Zhang, L. Qian, and Y. Wu, "Comparisons of probabilistic linguistic term sets for multi-criteria decision making," *Knowledge-Based Systems*, vol. 119, pp. 284–291, 2017.

[36] S. Kortum and J. Lerner, "Assessing the contribution of venture capital to innovation," *The RAND Journal of Economics*, vol. 31, no. 4, pp. 674–692, 2000.

[37] M. Abdel-Basset, M. Gunasekaran, M. Mohamed, and N. Chilamkurti, "RETRACTED: a framework for risk assessment, management and evaluation: economic tool for quantifying risks in supply chain," *Future Generation Computer Systems*, vol. 90, pp. 489–502, 2019.

[38] B. W. Nocco and R. M. Stulz, "Enterprise risk management: theory and practice," *The Journal of Applied Corporate Finance*, vol. 18, no. 4, pp. 8–20, 2006.

[39] L. Tchankova, "Risk identification – basic stage in risk management," *Environmental Management and Health*, vol. 13, no. 3, pp. 290–297, 2002.

[40] S. Ward and C. Chapman, "Transforming project risk management into project uncertainty management," *International Journal of Project Management*, vol. 21, no. 2, pp. 97–105, 2003.

[41] S. N. Luko, "Risk management principles and guidelines," *Quality Engineering*, vol. 25, no. 4, pp. 451–454, 2013.

[42] J. Wang, W. Lin, and Y.-H. Huang, "A performance-oriented risk management framework for innovative R&D projects," *Technovation*, vol. 30, no. 11-12, pp. 601–611, 2010.

[43] O. Golichenko and S. Samovoleva, "Mapping risk factors of innovation activity enterprises," *International Journal of Innovation and Regional Development*, vol. 5, no. 2, pp. 149–164, 2013.

[44] W. Ho and X. Ma, "The state-of-the-art integrations and applications of the analytic hierarchy process," *European Journal of Operational Research*, vol. 267, no. 2, pp. 399–414, 2018.

[45] Y. Li and X. Wang, "Risk assessment for public–private partnership projects: using a fuzzy analytic hierarchical process method and expert opinion in China," *Journal of Risk Research*, vol. 21, no. 8, pp. 952–973, 2018.

[46] X. L. Wu, H. C. Liao, Z. S. Xu, A. Hafezalkotob, and F. Herrera, "Probabilistic linguistic multimoora: a multicriteria decision making method based on the probabilistic linguistic expectation function and the improved borda rule," *IEEE Transactions on Fuzzy Systems*, vol. 26, no. 6, pp. 3688–3702, 2018.

[47] D. C. Liang, A. Kobina, and W. Quan, "Grey relational analysis method for probabilistic linguistic multi-criteria group decision-making based on geometric Bonferroni mean," *International Journal of Fuzzy Systems*, vol. 20, no. 7, pp. 2234–2244, 2018.

[48] H. C. Liao, X. M. Mi, and Z. S. Xu, "A survey of decision-making methods with probabilistic linguistic information: bibliometrics, preliminaries, methodologies, applications and future directions," *Fuzzy Optimization and Decision Making*, vol. 19, no. 1, pp. 81–134, 2019.

[49] H. C. Liao, L. S. Jiang, Z. S. Xu, J. P. Xu, and F. Herrera, "A linear programming method for multiple criteria decision making with probabilistic linguistic information," *Information Sciences*, vol. 415-416, pp. 341–355, 2017.

[50] P. Liu and F. Teng, "Probabilistic linguistic TODIM method for selecting products through online product reviews," *Information Sciences*, vol. 485, pp. 441–455, 2019.

[51] X. L. Wu and H. C. Liao, "An approach to quality function deployment based on probabilistic linguistic term sets and

Hindawi
Journal of Mathematics
Volume 2023, Article ID 5671089, 8 pages
https://doi.org/10.1155/2023/5671089

Research Article

A Mathematical Modeling and an Optimization Algorithm for Marine Ship Route Planning

Lili Huang

Zhengzhou Tourism College, Zhengzhou, Henan 451464, China

Correspondence should be addressed to Lili Huang; huanglili@zztrc.edu.cn

Received 25 April 2022; Revised 2 July 2022; Accepted 6 July 2022; Published 24 April 2023

Academic Editor: Naeem Jan

In order to solve the problem of ship route planning at sea, we reduce the economic cost of ship navigation planning and improve the efficiency of ship navigation. As a result, the goal of this work is to delve into the mathematical modeling and the best algorithm for marine ship route planning. To begin, a mathematical model of ship route planning is created, taking into account the impact of nonuniformity in the offshore wind field on ship route planning, with the shortest ship sailing time as the goal. Based on the mathematical model, the ant colony algorithm is used to optimize the initial route of the ship. Finally, through the optimization of the ant colony algorithm, the optimal route with the shortest total length and the smaller steering angle is obtained, and the optimal ship navigation planning scheme is obtained. The simulation results show that, when compared to artificial intelligence and genetic algorithms, the optimization algorithm suggested in this research produces the best ship route planning outcomes and has the lowest economic cost, which may effectively increase the efficiency of ship route work.

1. Introduction

Ship route planning is a research hotspot in the field of maritime transportation. If there is a collision accident in the process of transportation, the ship and its cargo are also prone to losses. At the same time, the pollution caused by the collision accident to the marine environment is also very serious. The main purpose of the research on route planning of ship collision avoidance is to reduce the probability of traffic accidents. Therefore, it becomes very important to plan the route of ship collision avoidance. Science and technology such as artificial intelligence and deep learning are frequently appearing in various domains of social public life as a result of the rapid growth of computer technology. New technologies such as artificial intelligence also have an important impact on marine transportation, effectively promoting the rapid development of ship unmanned technology and intelligent navigation technology. In the process of the gradual development of ship unmanned technology, the more important core technology is ship route planning technology, especially in complex sea areas.

In the transportation activities of real maritime traffic, the traffic environment faced by ships is very complex, and the probability of ship accidents increases greatly in complex and changeable sea areas. In recent years, frequent maritime traffic accidents have prompted people to pay attention to solve different problems faced in maritime transportation. How to reduce the probability of maritime traffic accidents and ensure the safety of staff and property to the greatest extent is an important problem that needs to be solved urgently. Ship navigation and autopilot are efficient ways to effectively solve the current problems. In the process of ship intelligent navigation, automatic route planning is an important link. To some extent, it is related to the labor intensity of ship drivers and the ship safety performance and will have a direct impact on the safety of social public life and property. Therefore, the research on ship route planning, especially the route planning of ships in complex waters, is of great significance.

The innovations of this paper are as follows:

(1) Considering the impact of the heterogeneity of the offshore wind field on ship route planning, taking the shortest ship sailing time as the goal, this paper constructs the mathematical model of ship route planning. The ship's initial route is optimized using the ant colony algorithm, and the optimum route with the shortest total length and the smallest steering angle is found.

(2) The simulation results show that compared with other algorithms, the ship route planning result of the optimization algorithm proposed in this paper is the best, and the planning economic cost is the lowest, which can effectively improve the ship route work efficiency.

2. Related Work

Maritime waters are areas where maritime traffic accidents occur frequently. Because of the complex and changeable characteristics of maritime waters, it is difficult for ships to plan their routes at sea. The planning and development of ship routes in special waters is the focus of current research in the field of ship routes, and there have been many literature research results. In order to improve the scientificity of ship route automatic driving, Pan et al. comprehensively considered the influencing factors of the ship route environment and put forward the route planning of the intelligent ship route. Based on the Delaunay triangulation algorithm, the environment model is constructed, and the area prohibited from ship navigation in the environment model is searched by using the ship navigation safety theory. The tangent diagram approach is used to construct the ship route network, the interference force of the ship route is modeled using ship mechanics principles, and a ship route correction algorithm based on the environmental interference force is provided. The intelligent ship route planning algorithm is applied to a sea area for simulation and analysis. The analysis results show that the algorithm can plan the ship route in different environments and make the ship adapt to ship route planning in various environments. Although the feasibility of this method is relatively high, work efficiency is poor due to the complex process [1]. Wang et al. designed an optimization planning method integrating ship navigation characteristics, comprehensively considered the constraints existing in ship maneuverability, obtained accurate ship route planning, and constructed a ship turning model. In order to complete the detection of the ship planned route and position at the sea, a detection algorithm based on quadtree and the irregular boundary was adopted to solve the planning problem of avoiding collision between static obstacles and dynamic obstacles. The path planning based on the quadratic genetic algorithm is designed to realize the efficient solution of marine ship route planning. The validation analysis is carried out on the simulated ship route platform. This method optimizes five route planning, which proves the effectiveness of the algorithm, but the feasibility of this method is poor due to the complex process [2]. Yao et al. designed a ship route planning method that integrates massive data through the ship navigation trajectory. Firstly, the ship navigation trajectory data is processed by the Doug Las Peucker algorithm, and then the ship trajectory data processed by the DBSCAN algorithm is clustered to extract the turning points of the ship route, it clarified the connection relationship between the turning points with the geographic data and corrected the navigation near the obstacles. The maritime network diagram was constructed, the ship route density was calculated, the density value was taken as the pheromone concentration, the optimal route of ship navigation was solved, and the navigation trajectory data of a bulk carrier was taken as the sample. Simulation experiments show that although the convergence speed of this method is fast, the process is complex, resulting in poor work efficiency [3]. Han et al. designed a ship route planning algorithm based on the depth network, it is proposed to provide simulated routes in the electronic sea area map, in order to form suitable ship route planning, in order to effectively solve the problems of traditional ship route planning for inexperienced reference routes and not meeting the actual navigation needs. This algorithm needs to use the two-layer neural network structure of the neural network and the target neural network, so as to achieve the purpose of disrupting the data, store the experience, and use the randomly sampled data to avoid local convergence, so as to complete the route planning of the untrained electronic sea area map. Computer simulation and actual planning are used to verify that this method has good practicability, but there is still a problem of poor efficiency [4].

3. Mathematical Model of Ship Route Planning at the Sea

3.1. Coordinate System. Ship navigation often uses satellite navigation's geodetic coordinates for placement, as well as an electronic chart. A plane rectangular coordinate system is built based on the chart, and geodetic coordinates are translated into plane rectangular coordinates to make the calculation easier [5, 6]. The slow increasing rate of latitude is ignored while translating coordinates due to the high quantity of the navigation chart. Therefore, rectangular coordinates converted from geodetic coordinates to the plane are expressed as

$$(a, b) = f(\alpha, \beta). \tag{1}$$

In formula (1), (α, β) represents the geodetic coordinates of a point where the ship navigates in the chart, (a, b) represents the rectangular coordinates of the corresponding plane, and f represents the mapping relationship between (a, b) and (α, β). Formula (1) can also be expressed as

$$\frac{\alpha - \alpha_0}{\beta - \beta_0} = \frac{b - b_0}{a - a_0}. \tag{2}$$

That is, the ratio between the longitude difference and the latitude difference of any two points within the scope of

Table 1: Initial data of key position points related to route planning.

Critical position point	Geodetic coordinates	Plane Cartesian coordinates	The direction of the wind	The wind speed
Weather station 1	(α_1, β_1)	(a_1, b_1)	d_1	s_1
Weather station 2	(α_2, β_2)	(a_2, b_2)	d_2	s_2
...	...	...	...	...
Weather station k	(α_k, β_k)	(a_k, b_k)	d_k	s_k
The starting point	(α_s, β_s)	(a_s, b_s)		
At the end of	(α_d, β_d)	(a_d, b_d)		

the chart. In the plane rectangular coordinate system, the ratio of the ordinate difference and the abscissa difference is equal [7, 8]. In formula (2), (α_0, β_0) represents the geodetic coordinates of any point in the chart, and (a_0, b_0) represents the rectangular coordinates of the corresponding plane.

3.2. Digitization of Wind Farm. Generally, the wind vector data at different locations cannot be accurately measured at the sea. Only the wind vector data of meteorological ships or meteorological buoy stations can be obtained [9, 10]. Table 1 shows the position coordinates of key points related to ship route planning and corresponding plane rectangular coordinates, as well as the data of the wind vector of the meteorological station.

Most of the objects on the sea surface have no shelter, and the wind field changes evenly. Therefore, the overall wind vector data is obtained by the interpolation method. Querying the wind vector data of the wind field can obtain the wind vector data of any point within the scope of the chart.

There are many interpolation methods. This paper mainly adopts the inverse distance weighted interpolation method. We find the meteorological station close to the interpolation point, and interpolate the data of the meteorological station according to the size of the area, which is expressed by the following formula:

$$f(x, y) = \sum_{j=1}^{k} \frac{z_j}{d_j^p}, \tag{3}$$

$$d_j = \sqrt{\left(x - x_j\right)^2 + \left(y - y_j\right)^2}. \tag{4}$$

In formulas (3) and (4), z_j represents the wind speed value at the rectangular coordinates (x_j, y_j) of the sea area plane, d_j represents the horizontal distance between the ship's navigation point (x, y) and the ship's navigation point (x_j, y_j), $j = 1, 2, \ldots, k$, p represents a constant greater than 0, which can be called the weighted index. In this paper, p is taken as 1.

After interpolation, the wind speed value of the offshore wind field can form matrix M. The local wind speed value and the navigation of the ship in the wind field are shown in Figure 1. In Figure 1, the curve represents the wind speed contour, * represents the position of the turning point of the ship in the wind field, and the arrow between the turning points represents the navigation route.

3.3. Objective Function. Taking the overall ship navigation time T_i as the objective function, the optimization model

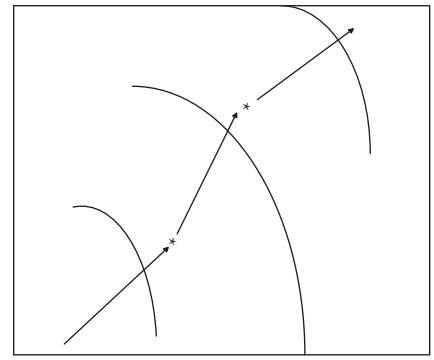

Figure 1: Local wind speed and sailing course in the wind field.

with the shortest time of the ship on the planned route as the objective is constructed, which is expressed as

$$T_i = \sum_{j=1}^{C} t_j, \quad j = 1, 2, \ldots, C. \tag{5}$$

In formula (5), t_j represents the time taken for the ship to sail from the previous turning point A to the next turning point B. Because the wind field between points A and B changes unevenly, it is difficult to directly calculate the time used by the ship during this navigation [11, 12]. In this paper, the integral idea is used for calculation. Assuming that the wind field in l0 of the ship navigation section is uniform, the starting point of point l_0 is the ship navigation speed instead of the average ship speed of the ship in this navigation section, the wind direction and wind speed at this position are obtained by using the wind speed value matrix M, and the ship navigation direction from point A to point $B\theta_1$ is substituted into formulas (7) and (8) to calculate the ship speed, and the navigation time of leg l_0 is accumulated, which is approximately t_j. In this paper, the value of l_0 is 0.5, and the sailing time from point A to point B is expressed as

$$t_j = \int_A^B dt \approx \sum_{i=1}^{n} \frac{l_0}{v_i}. \tag{6}$$

In formula (6), n represents the distance and the l0 ratio between two turning points of ship navigation, $v_i = f_{v\theta}(M(a_{ij}, b_{ij}))$, (a_{ij}, b_{ij}) represents the rectangular coordinates of any point plane in the wind field of ship navigation, $M(a_{ij}, b_{ij})$ represents the data of wind vector at this point, and $f_{v\theta}$ represents the calculation of apparent wind speed.

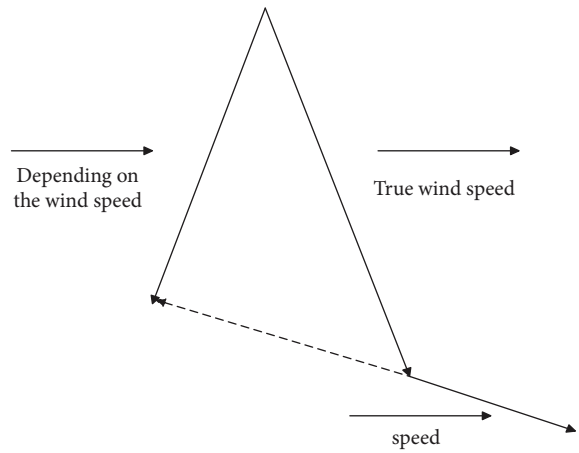

Figure 2: Vector relationship between true wind speed and apparent wind speed.

As shown in Figure 2, the vector relationship between true wind speed and ship speed and apparent wind speed is expressed as apparent wind speed = true wind speed - ship speed. The apparent wind speed can be calculated as

$$v = \sqrt{\left(-v_1 \sin\theta_1 + v_2 \sin\theta_2\right)^2 + \left(-v_1 \cos\theta_1 + v_2 \cos\theta_2\right)^2} \tag{7}$$

$$\theta = \theta_2 - \left(\frac{v_1 \sin\left(\theta_1 + \theta_2\right)}{\sqrt{\left(-v_1 \sin\theta_1 + v_2 \sin\theta_2\right)^2 + \left(-v_1 \cos\theta_1 + v_2 \cos\theta_2\right)^2}}\right)\arcsin\theta. \tag{8}$$

In formulas (7) and (8), v represents the apparent wind speed of ship navigation, θ represents the direction of the apparent wind speed of the ship, v_1 represents the speed of the ship, θ_1 represents the sailing direction of the ship, v_2 represents the true wind speed of the ship, and θ_2 represents the true wind speed direction of the ship.

4. Mathematical Modeling and Optimization of the Initial Ship Route Based on the Ant Colony Algorithm

Combined with the ship navigation mathematical model constructed above, the ant colony algorithm is used to optimize the ship navigation mathematical model.

4.1. Discretization of Workspace. If L_i represents the link line of free space and $p_i^{(0)}$ and $p_i^{(1)}$ represent the two endpoints of L_i, other points on the link line are represented as

$$p_i\left(h_i\right) = \left(p_i^{(1)} - p_i^{(0)}\right) \times h_i, h_i \in [0,1], \quad i = 1,2,3\ldots,N \tag{9}$$

In formula (9), $p_i(h_i)$ represents any point on the navigation link line of the ship, h_i represents a random number from 0 to 1, which is mainly used to represent the parameter of the proportion between the two endpoints, and N represents the number of nodes through which the link passes.

Before using the ant colony optimization algorithm to optimize the ship route planning model, we must make the working space discrete, we can divide the link line and adopt the fixed length division method. In order to meet the requirements of the constraint distance of ship route planning and the minimum distance $D_{\min}$ of the dangerous area, each link line L is divided into scores:

$$N_i = \begin{cases} \mathrm{Int}\left(\dfrac{L_i}{D_{\min}}\right), \mathrm{Int}\left(\dfrac{L_i}{D_{\min}}\right) \text{Even numbers} \\ \\ \mathrm{Int}\left(\dfrac{L_i}{D_{\min}}\right) + 1, \mathrm{Int}\left(\dfrac{L_i}{D_{\min}}\right) + 1 \text{ Odd number} \end{cases} \tag{10}$$

In formula (10), Int function represents the rounding function. When $\mathrm{Int}(L_i/D_{\min})$ is an odd number, in order to ensure that the midpoint of the link line is an equidistant point, after discretization, there will be $N_i + 1$ navigation routes that can be selected from the ship route link line L_i–1 $\mathrm{Int}(L_i/D_{\min})$ to the adjacent ship navigation link line L_i.

4.2. Ant Path Search and Pheromone Update. After searching the planned route from the beginning to the end of each ship's navigation, the corresponding parameter set of the ship navigation route $(h_i, h_2, \ldots, h_k)$ will be generated. In the process of the ship movement, when the ant is on the navigation link line L_i, the method of selecting the heading

node j on the next navigation link line L_{i+1} is to calculate the probability P_{ij} selected from the node i to the next ship route node j in turn. According to the selected probability P_{ij}, the roulette method is used to find the next ship route node j, and the calculation of P_{ij} is expressed as

$$P_{ij} = \frac{\tau_{i,j} \times \eta_{ij}^{\beta}}{\sum_{\omega \in I} \tau_{i,\omega} \times \eta_{i,\omega}^{\beta}}. \tag{11}$$

In formula (11), $\eta_{i,j}$ represents the heuristic value and $\tau_{i,j}$ represents the pheromone. The higher the concentration of the pheromone, the greater the probability $P_{ij}$of selection. When a node is selected during the movement of the ship route, the node will release the pheromone and update the pheromone of the node, which is expressed as

$$\tau_{i,j} = (1 - \rho_1) \times \tau_{i,j} + \tau_0. \tag{12}$$

In formula (12), τ_0 represents the initial value of the pheromone and ρ_1 represents the parameter of the interval. When all ants complete the search, the shortest path length is saved and the pheromone of each point is updated [13, 14]. Update can be called pheromone volatilization update, and the pheromone volatilization formula of the ship route is expressed as

$$\tau_{i,j} = \tau_{i,j}(1 - \rho_2). \tag{13}$$

In formula (13), ρ_2 represents the volatilization parameter of the ship route pheromone, and the value of ρ_2 is 0.003.

4.3. Ant Colony Algorithm for Optimizing Ship Route Turning Angle. When ants search for the next node p_i on node p_{i-1}, if the selected route node $p_i^{(0)}$ and $p_i^{(1)}$ is in the straight line, and the angle α between the starting point S and the ending point T of the ship's route is small, the p_i^1 point is the priority point, as shown in Figure 3.

In Figure 3, $p_i^{(0)}$ and $p_i^{(1)}$ represent the two endpoints of the link, point S is the starting point of the ship's route, point T is the ending point of the ship's route planning, point p_{i-1} is the ant's current position, p_i^1 and p_i^2 are the alternative node locations for the next search location of the ship's route, and α_1 1 and α_2 represent the current position of the ship's route, the connection between the alternative node locations, and the angle between the starting point S and the ending point T. When using the ant colony algorithm to optimize the ship route, in order to ensure that ants will select p_i^1 node with a greater probability, α is introduced into the pheromone update formula when the ship route pheromone is updated to complete the ants' selection of the next node which constitutes α smaller route node with a greater probability, and the modified ship route pheromone update is expressed as

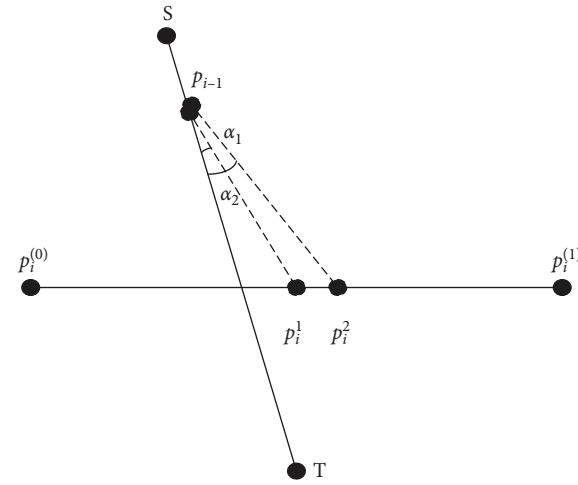

Figure 3: Optimization of the steering angle.

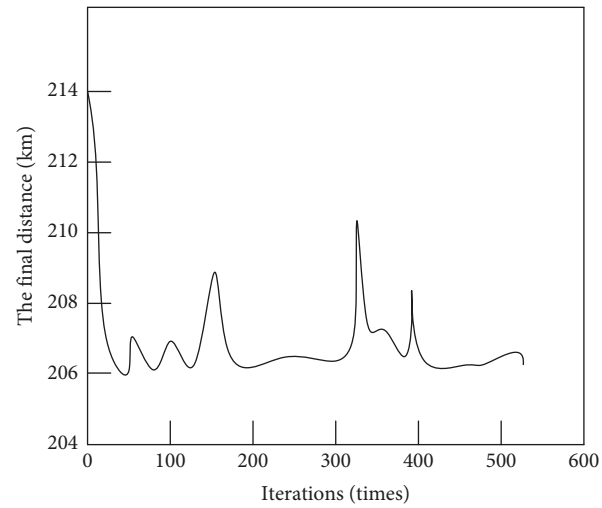

Figure 4: Convergence process of the ant colony algorithm.

Table 2: Test results.

Methods	Iterations/times
Artificial intelligence algorithm	249
Genetic algorithm (ga)	234
In this paper, algorithm	222

$$\tau_{i,j} = \lambda_{ij} \times \left[(1 - \rho_1) \times \tau_{i,j} + \tau_0\right], \tag{14}$$

$$\lambda_{ij} = \left\{1 + \frac{\pi/2 - \left|\alpha_{ij}\right|}{\pi/2}\right\}. \tag{15}$$

Formula (14) is the updated formula of the ship pheromone after correction. λ_{ij} represents the correction factor of the newly introduced ship's route pheromone update. Formula (15) is the calculation formula of the ship's route pheromone correction factor. Among them, α_{ij} is the angle between the current position of the ship's route and the

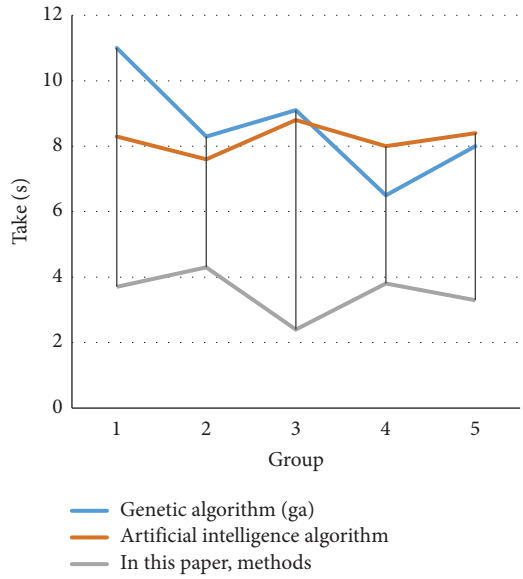

Figure 5: Comparison of average time-consuming results of different algorithms.

alternative position and the starting and ending position, which eliminates the positive and negative influence of the angle.

When using the ant colony algorithm to optimize ship route planning, 10 ants will search the optimal path in each iteration. In order to effectively observe the convergence process of the ant colony algorithm in searching the optimal ship route, as shown in Figure 4. The following Figure 4 shows the convergence process of the initial solution of the optimization of the ship route planning model by the ant colony algorithm [15,16].

5. Analysis of Experimental Results

In order to verify the effectiveness of the ship route planning optimization algorithm based on the ant colony algorithm [17] proposed in this paper, the simulation experiment is carried out, and the simulation experiment environment is established according to the needs of the experimental test. Combined with the application characteristics of visual control in MATLAB software, GUI control is selected as the visual program design of the simulation experiment. In order to test the planning effect based on ant colony algorithm, artificial intelligence algorithm, genetic algorithm, and ant colony algorithm proposed in this paper are selected to solve the mathematical model of the marine ship route, and the number of iterations of the three methods is counted. The test results are shown in Table 2.

From the test results in Table 1, it can be seen that the number of iterations of the methods mentioned in this paper is significantly lower than that of the artificial intelligence algorithm and the genetic algorithm, which can effectively reduce optimization time and improve the efficiency of optimization. Therefore, the optimization performance based on the ant colony algorithm in this paper is better. To further verify the optimization performance of the algorithms presented in this paper, three algorithms are optimized, repeated five times, and the time-consuming results are compared. The average time-consuming results of different algorithms are compared as shown in Figure 5.

Through the analysis of Figure 5, it can be seen that the average ship route based on the ant colony algorithm proposed in this paper takes less time, indicating that the route planning effect is good, while the initial time based on the artificial intelligence algorithm is relatively long. With the increase of times, although fluctuates slightly, the overall time-consuming is more. The genetic algorithm is roughly the same as the artificial intelligence algorithm, and the time-consuming is relatively long. This shows that the algorithm proposed in this paper can effectively reduce the redundancy of ship route planning and calculation, so as to reduce the time-consuming of the ship route mathematical model. The success rate of ship route planning and the planned path length of the optimal ship route are selected as the rating indicators of the ship route planning performance, as shown in Table 3.

As can be seen from Table 3, the success rate of the ship route planning algorithm proposed in this paper is 96.3%, which is significantly higher than the ship route planning algorithm based on the artificial intelligence algorithm and the genetic algorithm. Compared with the other two algorithms, the path length of the optimal ship route planning algorithm proposed in this paper is shorter, which can effectively reduce the economic cost of ship navigation planning. Figures 6 and 7 show the fuel consumption of three mathematical models of ship navigation planning under the conditions of sailing distance of 1200 nm and 2400 nm. The smaller the value, the better the performance of the mathematical model.

It can be seen from the data in Figures 6 and 7 that if the planned route of the ship is to avoid obstacles, it can be regarded as a failed route. Under the condition of different sailing distance, the mathematical model of ship route planning in the figure can avoid obstacles at the sea and plan

Table 3: Performance comparison of ship route planning with different methods.

Methods	The success rate of (%)	Optimal path length
Artificial intelligence algorithm	91.20	1862
Genetic algorithm (ga)	93.40	1796
In this paper, algorithm	96.30	1699

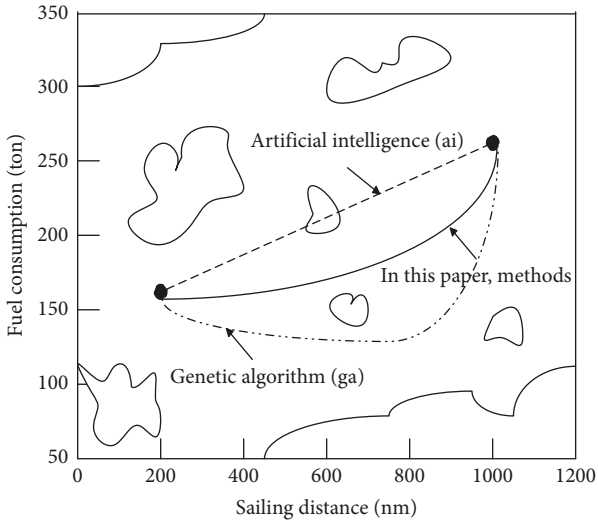

Figure 6: Fuel consumption for distance 1200 nm.

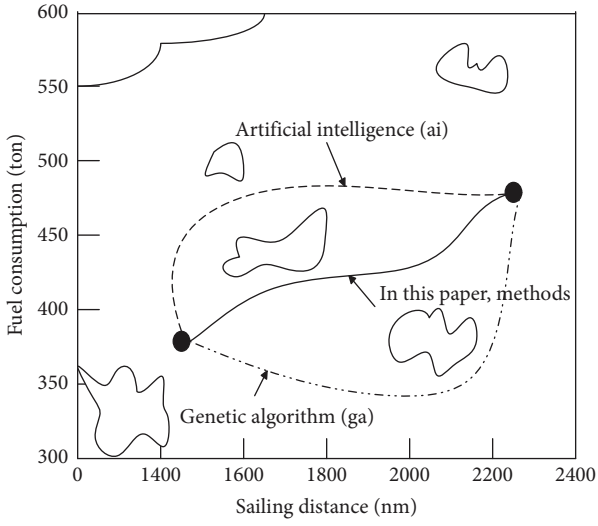

Figure 7: Fuel consumption for distance 2400 nm.

the optimal route. With the increase of sailing distance, the fuel consumption of the method proposed in this paper is always the least of the three methods, which shows that the method proposed in this paper can effectively reduce the economic cost of ship route operation and improve the efficiency of ship navigation.

6. Conclusion

Planning the ideal ship route, when combined with the above contents, may effectively increase ship navigation safety and reduce ship risk, which is critical, as well as improve the degree of ship route planning. Therefore, this paper designs a ship route planning model based on the ant colony algorithm, and the simulation results show that the iteration times of the method proposed in this paper are relatively small, which can effectively shorten the optimization time of the mathematical model, so as to increase work efficiency and has a high reference value.

Data Availability

Data are available from the corresponding author upon request.

Conflicts of Interest

The authors declare that there are no conflicts of interest for the publication of this work.

References

[1] W. Pan, Q. L. Dong, and X. W. Xu, "Route planning of intelligent ships considering navigation environment factors," *Journal of Shanghai Maritime University*, vol. 42, no. 3, pp. 76–84, 2021.

[2] L. P. Wang, Z. Zhang, and S. Ma, "Improved genetic algorithm-based ship route planning considering ship maneuverability constraints," *Journal of Harbin Engineering University*, vol. 42, no. 7, pp. 1056–1062, 2021.

[3] X. X. Yao, Q. Y. Hu, and C. Yang, "Route planning of vessels with ant colony algorithm and massive AIS data," *Journal of Transport Information and Safety*, vol. 37, no. 3, pp. 79–85, 2019.

[4] Z. H. Han, Y. B. Zhang, and Y. Zhang, "Automatic ship route planning based on deep reinforcement learning," *Navigation of China*, vol. 44, no. 1, pp. 100–105, 2021.

[5] G. X. Wang, L. C. Wang, and J. Zheng, "Dynamic route planning method for intelligent ships considering complex meteorological changes," *Journal of Shanghai Maritime University*, vol. 42, no. 1, pp. 1–6, 2021.

[6] Y. Liu, X. L. Xie, and A. He, "Planning ship route through area of multi-construction sites in series," *Navigation of China*, vol. 42, no. 3, pp. 51–54, 2019.

[7] J. L. Duan and Y. Han, "Route planning algorithm based on historical track statistics," *Journal of Shanghai Scientific Research Institute of Shipping*, vol. 43, no. 2, pp. 10–14, 2020.

[8] M. Y. Pan, Y. S. Liu, and Q. Li, "Improved A algorithm based route planning and its application for inland waterway network," *Journal of Shanghai Maritime University*, vol. 41, no. 1, pp. 40–45, 2020.

[9] J. H. Jin, J. Sun, and T. ZhangA, "USV path planning based on quantum-behaved particle swarm optimization," *Journal of Ship Mechanics*, vol. 24, no. 3, pp. 352–361, 2020.

[10] M. ZhangL and F. WuX, "Optimization planning method of freight ship distribution route under low carbon condition," *Ship Science and Technology*, vol. 43, no. 18, pp. 181–183, 2021.

[11] M. N. Rahmatdin, N. S. F. A. Rahman, and M. K. Othman, "An empirical study on the current feeder shipping network patterns among Malaysian feeder service providers," *The*

Asian Journal of Shipping and Logistics, vol. 33, no. 4, pp. 177–188, 2017.

[12] A. BalakrishnanBalakrishnan and C. V. Karsten, "Container shipping service selection and cargo routing with transshipment limits," *European Journal of Operational Research*, vol. 263, no. 2, pp. 652–663, 2017.

[13] M. A. Dulebenets, "The vessel scheduling problem in a liner shipping route with heterogeneous fleet," *International Journal of Civil Engineering*, vol. 16, no. 1, pp. 19–32, 2018.

[14] J. Bhagwat, "Maritime shipping on the northern sea route: need for greater emphasis on mutual cooperation and a non-negotiable safety culture. Part I," *Arctic and North*, vol. 39, no. 39, pp. 5–25, 2020.

[15] H. Idris and M. F. Ramli, "Southeast asian region maritime connectivity and the potential development of the northern sea route for commercial shipping," *Journal of Southeast Asian Studies*, vol. 23, no. 2, pp. 25–46, 2018.

[16] D. Dalaklis, M. L. Drewniak, and J. U. Schröder-Hinrichs, "Shipping operations support in the "high north": examining availability of icebreakers along the Northern Sea Route," *Wmu Journal of Maritime Affairs*, vol. 17, no. 2, pp. 129–147, 2018.

[17] L. Pan, J. Liang, and B. Qu, *Bio-inspired Computing: Theories and Applications: 14th International Conference, BIC-TA 2019, Zhengzhou, China, November 22–25, 2019, Revised Selected Papers, Part I*, Vol. 1159, Springer Nature, Berlin, Germany, 2020.

Hindawi
Journal of Mathematics
Volume 2023, Article ID 2260153, 16 pages
https://doi.org/10.1155/2023/2260153

Research Article

Common Fixed Point Results for Intuitionistic Fuzzy Hybrid Contractions with Related Applications

Mohammed Shehu Shagari,[1] **Shazia Kanwal**,[2] **Akbar Azam**,[3] **Hassen Aydi**,[4,5,6] **and Yaé Ulrich Gaba**[6,7,8]

[1]*Department of Mathematics, Faculty of Physical Sciences, Ahmadu Bello University, Zaria, Nigeria*
[2]*Department of Mathematics, Government College University, Faisalabad, Pakistan*
[3]*Department of Mathematics, Grand Asian University, Sialkot, 7KM, Pasrur Road, Sialkot 51310, Pakistan*
[4]*Institut Supérieur D'Informatique et des Techniques de Communication, Université de Sousse, Sousse 4000, Tunisia*
[5]*China Medical University Hospital, China Medical University, Taichung 40402, Taiwan*
[6]*Department of Mathematics and Applied Mathematics, Sefako Makgatho Health Sciences University, Ga-Rankuwa, South Africa*
[7]*Quantum Leap Africa (QLA), AIMS Rwanda Centre, Remera Sector KN 3, Kigali, Rwanda*
[8]*African Center for Advanced Studies (ACAS), P.O. Box 4477, Yaoundé, Cameroon*

Correspondence should be addressed to Hassen Aydi; hassen.aydi@isima.rnu.tn and Yaé Ulrich Gaba; yaeulrich.gaba@gmail.com

Received 4 June 2022; Accepted 15 July 2022; Published 22 April 2023

Academic Editor: Ching-Feng Wen

Over time, hybrid fixed point results have been examined merely in the framework of classical mathematics. This one way research has clearly dropped-off a great amount of important results, considering the fact that a fuzzy set is a natural enhancement of a crisp set. In order to entrench hybrid fixed notions in fuzzy mathematics, this paper focuses on introducing a new idea under the name intuitionistic fuzzy p-hybrid contractions in the realm of -metric spaces. Sufficient conditions for the existence of common intuitionistic fuzzy fixed points for such maps are established. In the instance where our presented results are slimmed down to their equivalent nonfuzzy counterparts, the concept investigated herein unifies and generalizes a significant number of well-known fixed point theorems in the setting of both single-valued and multivalued mappings in the corresponding literature. A handful of these special cases are highlighted and analysed as corollaries. A nontrivial example is put together to indicate that the hypotheses of our results are valid.

1. Introduction

In practical, if a model asserts that conclusions drawn from it have some bearings on reality, then two major complications are immediate, namely, real situations are often not crisp and deterministic; a complete description of real systems often requires more detailed data than human beings could recognize simultaneously, process, and understand. Whence, by using classical mathematical tools, as the difficulty of a practical system increases, our ability to come up with precise and significant statements reduces until a threshold is reached after which accuracy become an almost mutually exclusive characteristics, see [1]. These restrictions in everyday systems paved the way to the launching of the fuzzy set by Zadeh [2], which is a flexible mathematical device to design mathematical approaches in line with practical issues. At present, the primitive ideas of the fuzzy set have been upgraded in a multifarious framework. Following this development, Heilpern [3] employed the idea of the fuzzy set to initiate a class of fuzzy set-valued mappings and presented a fixed point(Fp) theorem which is a fuzzy version of the Fp result of Nadler [4]. Thereafter, a substantial number of authors have studied the existence of Fp of fuzzy set-valued maps, for example, see [5–10]. Following Zadeh [2], an intuitionistic fuzzy set (IFS) was brought up by Atanassov [11] as an additional refinement of the notions of

fuzzy set. IFS gives relevant frames to take care of inaccuracy and hesitancy due to inadequate information. IFS is more useful than a fuzzy set as it evaluates the degrees of both membership and nonmembership. Whence, it has attracted enormous applications in several fields. At present, work on IFS have been rising at a faster speed and varying views have been discovered in different arms. Along this direction, Azam et al. [12] came up with a modern way for examining the existence of Fp of intuitionistic fuzzy set-valued maps defined on a complete metric space. Later after, [13] presented criteria for investigating coincidence points for intuitionistic fuzzy set-valued maps and employed their results to examine conditions for the existence of solutions to a system of integral equations. Of recent, [14, 15] coined the idea of Fp results for two intuitionistic fuzzy set-valued maps using $(\mathscr{T}, \mathscr{N}, \breve{\alpha})$-cut set.

The well-celebrated Banach contraction has laid a solid foundation for the development of the metric fixed point theory. The prototypical concept of the contraction mapping principle has been refined in several domains (e.g., see [16–20]). Along the lane, hybrid Fp theory emerged and has so far been studied only in the context of classical mathematics. This one way investigation has obviously neglected a great amount of useful results, considering the fact that a fuzzy set is a natural generalization of a crisp set. Whence, in order to entrench hybrid fixed point notions in fuzzy mathematics, the aim of this paper is to introduce new concepts under the name intuitionistic fuzzy p-hybrid contractions in the framework of b-metric space. Sufficient criteria for the existence of common intuitionistic fuzzy Fp for such mappings are established. It is observed that at the instance where our results are reduced to their corresponding crisp ideas, the concepts examined herein harmonize and generalize a significant number of Fp results in the setting of both point-valued and set-valued mappings in the related literature. A few of these particular cases are pinned down and discussed. A comparative example is designed to validate the hypotheses of our obtained results.

2. Preliminaries

We collect herewith specific fundamentals that will be needed later on. These basis are some extracts from [2, 4, 21, 22].

Definition 1 [21]. Let $\mho$ be a nonempty set and $\widehat{\eta} \geq 1$ be a constant. Suppose that the mapping $\widehat{\mu}: \mho \times \mho \longrightarrow \mathbb{R}_+$ satisfies the following criteria for all $\varsigma, \omega, \xi \in \mho$:

(i) $\widehat{\mu}(\varsigma, \omega) = 0 \Leftrightarrow \varsigma = \omega$;

(ii) $\widehat{\mu}(\varsigma, \omega) = \widehat{\mu}(\omega, \varsigma)$;

(iii) $\widehat{\mu}(\varsigma, \omega) \leq \widehat{\eta}[\widehat{\mu}(\varsigma, \xi) + \widehat{\mu}(\xi, \omega)]$.

Then, $(\mho, \widehat{\mu}, \widehat{\eta})$ is called as a b-metric space.

Definition 2 [23]. Consider a b-metric space $(\mho, \widehat{\mu}, \widehat{\eta})$. A sequence $\{\varsigma_\wp\}_{\wp \in \mathbb{N}}$ is called:

(i) convergent $\Leftrightarrow \varsigma \in \mho$ is such that $\widehat{\mu}(\varsigma_\wp, \varsigma) \longrightarrow 0$ as $\wp \longrightarrow \infty$.

(ii) Cauchy if $\widehat{\mu}(\varsigma_\wp, \varsigma_\varpi) \longrightarrow 0$ as $\wp, \varpi \longrightarrow \infty$.

(iii) complete if every Cauchy sequence in $\mho$ is convergent.

In a b-metric space, the limit of a sequence is not always unique. However, if a b-metric is continuous, then every convergent sequence has a unique limit.

Definition 3 [23]. Consider a b-metric space $(\mho, \widehat{\mu}, \widehat{\eta})$. A subset $\widetilde{\nabla}$ of $\mho$ is called:

(i) compact $\Leftrightarrow$ for every sequence of elements of $\widetilde{\nabla}$, we can find a subsequence that converges to an element of $\widetilde{\nabla}$.

(ii) closed $\Leftrightarrow$ for every sequence $\{\varsigma_\wp\}_{\wp \in \mathbb{N}}$ of elements of $\widetilde{\nabla}$ that converges to an element ς, we have $\varsigma \in \widetilde{\nabla}$.

Definition 4 [24]. A nonempty subset $\widetilde{\nabla}$ of $\mho$ is called proximal if, for each $\varsigma \in \mho$, we can find $a \in \widetilde{\nabla}$ such that $\widehat{\mu}(\varsigma, a) = \widehat{\mu}(\varsigma, \widetilde{\nabla})$.

We denote by $\mathscr{N}(\mho)$, $CB(\mho)$, $P^r(\mho)$, $P_b^r(\mho)$ and $\mathscr{K}(\mho)$, the family of all nonempty subsets of $\mho$, the class of all nonempty closed and bounded subsets of $\mho$, the collection of all nonempty proximal subsets of $\mho$, the totality of all bounded proximal subsets of $\mho$ and the class of nonempty compact subsets of $\mho$, respectively.

Consider a b-metric space $(\mho, \widehat{\mu}, \widehat{\eta})$. For $\widetilde{\nabla}, \widetilde{\nabla} \in \mathscr{P}^r(\mho)$, the function $\aleph: \mathscr{P}^r(\mho) \times \mathscr{P}^r(\mho) \longrightarrow \mathbb{R}_+$, defined by

$$\aleph(\widetilde{\nabla}, \widetilde{\Delta}) = \max\left\{\sup_{\varsigma \in \widetilde{\nabla}} \widehat{\mu}(\varsigma, \widetilde{\Delta}), \sup_{\varsigma \in \widetilde{\Delta}} \widehat{\mu}(\varsigma, \widetilde{\nabla})\right\}, \tag{1}$$

is called a Hausdorff-Pompeiu b-metric on $\mathscr{P}^r(\mho)$ generated by $\widehat{\mu}$, where

$$\widehat{\mu}(\varsigma, \widetilde{\nabla}) = \inf_{\omega \in \nabla} \widehat{\mu}(\varsigma, \omega). \tag{2}$$

Remark 1. Since every compact set is proximal and every proximal set is closed (see [24]), whence:

$$\mathscr{K}(\mho) \subseteq \mathscr{P}^r(\mho) \subseteq CB(\mho) \subseteq \mathscr{N}(\mho). \tag{3}$$

Let $\mho$ be a universal set. A fuzzy set in $\mho$ is a function with domain $\mho$ and values in $[0, 1] = I$. If $\widetilde{\nabla}_f$ is a fuzzy set in $\mho$, then the function value $\widetilde{\nabla}_f(\varsigma)$ is called the grade of membership of ς in $\widetilde{\nabla}_f$. The $\breve{\alpha}$-level set of a fuzzy set $\widetilde{\nabla}_f$ is denoted by $[\widetilde{\nabla}_f]_{\breve{\alpha}}$ and is given as follows:

$$\left[\widetilde{\nabla}_f\right]_{\breve{\alpha}} = \begin{cases} \overline{\{\varsigma \in \mathcal{O}: \widetilde{\nabla}(\varsigma) > 0\}}, & \text{if } \breve{\alpha} = 0 \\ \{\varsigma \in \mathcal{O}: \widetilde{\nabla}(\varsigma) \geq \breve{\alpha}\}, & \text{if } \breve{\alpha} \in (0,1], \end{cases} \tag{4}$$

where by $\overline{M}$, we mean the closure of the crisp set M. We denote the family of all fuzzy sets in $\mathcal{O}$ by $I^{\mathcal{O}}$.

A fuzzy set $\widetilde{\nabla}_f$ in a metric space V is called an approximate quantity if and only if $[\widetilde{\nabla}_f]_{\breve{\alpha}}$ is compact and convex in V and $\sup_{\varsigma \in V} \widetilde{\nabla}(\varsigma) = 1$. Denote the collection of all approximate quantities in V by $W(V)$. If we can find an $\breve{\alpha} \in [0,1]$ such that $[\widetilde{\nabla}_f]_{\breve{\alpha}}, [\widetilde{\triangle}_f]_{\breve{\alpha}} \in \mathscr{P}_b^r(\mathcal{O})$, then define

$$\begin{aligned} D_{\breve{\alpha}}\left(\widetilde{\nabla}_f, \widetilde{\triangle}_f\right) &= \aleph\left(\left[\widetilde{\nabla}_f\right]_{\breve{\alpha}}, \left[\widetilde{\triangle}_f\right]_{\breve{\alpha}}\right), \\ \widehat{\mu}_{\infty}\left(\widetilde{\nabla}_f, \widetilde{\triangle}_f\right) &= \sup_{\breve{\alpha}} D_{\breve{\alpha}}(\widetilde{\nabla}, \widetilde{\triangle}). \end{aligned} \tag{5}$$

Definition 5 [3]. Let $\mathcal{O}$ be a nonempty set. The mapping $\Xi: \mathcal{O} \longrightarrow I^{\mathcal{O}}$ is called a fuzzy set-valued map. A point $u \in \mathcal{O}$ is called a fuzzy Fp of Ξ if we can find an $\breve{\alpha} \in (0,1]$ such that $u \in [\Xi u]_{\breve{\alpha}}$.

Definition 6 [11]. Let $\mathcal{O}$ be a nonempty set. An IFS $\widetilde{\nabla}$ in $\mathcal{O}$ is a set:

$$\widetilde{\nabla} = \left\{\langle J, \widehat{\mu}_{\widetilde{\nabla}}(J), \nu_{\widetilde{\nabla}}(J)\rangle: J \in \mathcal{O}\right\}, \tag{6}$$

where $\widehat{\mu}_{\widetilde{\nabla}}: \mathcal{O} \longrightarrow [0,1]$ and $\nu_{\widetilde{\nabla}}: \mathcal{O} \longrightarrow [0,1]$ define the degrees of membership and non-membership, accordingly of J in $\mathcal{O}$ and fulfil $0 \leq \widehat{\mu}_{\widetilde{\nabla}} + \nu_{\widetilde{\nabla}} \leq 1$, for each $J \in \mathcal{O}$.

We depict the set of all IFS in $\mathcal{O}$ as $(IFS)^{\mathcal{O}}$.

Definition 7 [11]. Let $\widetilde{\nabla}$ be an IFS in $\mathcal{O}$. Then the $\breve{\alpha}$-level set of $\widetilde{\nabla}$ is a crisp subset of $\mathcal{O}$ denoted by $[\widetilde{\nabla}]_{\breve{\alpha}}$ and is given as follows:

$$[\widetilde{\nabla}]_{\breve{\alpha}} = \left\{J \in \mathcal{O}: \widehat{\mu}_{\widetilde{\nabla}}(J) \geq \breve{\alpha} \text{ and } \nu_{\widetilde{\nabla}}(J) \leq 1 - \breve{\alpha}\right\}, \text{if } \breve{\alpha} \in [0,1]. \tag{7}$$

Definition 8 [12]. Let $L = \left\{(\breve{\alpha}, \breve{\beta}): \breve{\alpha} + \breve{\beta} \leq 1, (\breve{\alpha}, \breve{\beta}) \in (0,1] \times t[0,1)\right\}$ and $\widetilde{\nabla}$ is an IFS in $\mathcal{O}$. Then the $(\breve{\alpha}, \breve{\beta})$-level set of $\widetilde{\nabla}$ is given as follows:

$$[\widetilde{\nabla}]_{(\breve{\alpha},\breve{\beta})} = \left\{J \in \mathcal{O}: \widehat{\mu}_{\widetilde{\nabla}}(J) \geq \breve{\alpha} \text{ and } \nu_{\widetilde{\nabla}}(J) \leq \breve{\beta}\right\}. \tag{8}$$

A modification of Definition 2.9 in [13] is the following.

Definition 9 [13]. The $(\widetilde{M}, \widetilde{\omega})$-level set of an intuitionistic fuzzy set $\widetilde{\nabla}$ in $\mathcal{O}$ is given as follows:

$$[\widetilde{\nabla}]_{(\widetilde{M},\widetilde{\omega})} = \left\{\varsigma \in \mathcal{O}: \widehat{\mu}_{\widetilde{\nabla}}(\varsigma) = \widetilde{M} \text{ and } \nu_{\widetilde{\nabla}}(\varsigma) = \widetilde{\omega}\right\}, \tag{9}$$

with

$$\widetilde{M} = \max_{\varsigma \in \mathcal{O}} \widehat{\mu}_{\widetilde{\nabla}}(\varsigma) \text{ and } \widetilde{\omega} = \min_{\varsigma \in \mathcal{O}} \nu_{\widetilde{\nabla}}(\varsigma). \tag{10}$$

Example 1. Let $\mathcal{O} = \{J_1, J_2, J_3, J_4, J_5\}$ and $\widetilde{\nabla}$ be an IFS in $\mathcal{O}$ given by

$$\widetilde{\nabla} = \{(J_1, 0.6, 0.2), (J_2, 0.5, 0.4), (J_3, 0.1, 0.7), (J_4, 0.3, 0.5), (J_5, 0.4, 0.3)\}. \tag{11}$$

Then the $(\breve{\alpha}, \breve{\beta})$-level sets of $\widetilde{\nabla}$ are given by.
$[\widetilde{\nabla}]_{(0.4,0.3)} = \{J_1, J_5\}$.
$[\widetilde{\nabla}]_{(0.1,0.7)} = \{J_1, J_2, J_3, J_4, J_5\}$.
$[\widetilde{\nabla}]_{(0.3,0.5)} = \{J_1, J_2, J_4, J_5\}$.

Definition 10 [12]. Let $\mathcal{O}$ be a nonempty set. The map $\Upsilon = \langle \widehat{\mu}_{\Upsilon}, \nu_{\Upsilon}\rangle: \mathcal{O} \longrightarrow (IFS)^{\mathcal{O}}$ is called an intuitionistic fuzzy set-valued map. An element $u \in \mathcal{O}$ is named an intuitionistic fuzzy Fp of Υ if we can find $(\breve{\alpha}, \beta) \in (0,1] \times t[0,1)$ such that $u \in [\Upsilon u]_{(\breve{\alpha},\breve{\beta})}$.

Definition 11 [22, 25]. An increasing function $\widehat{\varphi}: \mathbb{R}_+ \longrightarrow \mathbb{R}_+$ is called:

(i) a c-comparison function if $\widehat{\varphi}^{\wp}(t) \longrightarrow 0$ as $\wp \longrightarrow \infty$ for every $t \in \mathbb{R}_+$;

(ii) a b-comparison function if we can find $k_0 \in \mathbb{N}$, $\lambda \in (0,1)$ and a convergent non-negative series $\sum_{\wp=1}^{\infty} \varsigma_{\wp}$: $\widehat{\eta}^{k+1}\widehat{\varphi}^{k+1}(t) \leq \lambda \widehat{\eta}^{k}\widehat{\varphi}^{k}(t) + \varsigma_k$, for $\widehat{\eta} \geq 1, k \geq k_0$ and any $t \geq 0$, where $\widehat{\varphi}^{\wp}$ denotes the $\wp^{th}$ iterate of $\widehat{\varphi}$

Denote by Ω, the class of functions $\widehat{\varphi}: \mathbb{R}_+ \longrightarrow \mathbb{R}_+$ obeying:

(i) $\widehat{\varphi}$ is a b-comparison function;

(ii) $\widehat{\varphi}(t) = 0 \Leftrightarrow t = 0$;

(iii) $\widehat{\varphi}$ is continuous.

Lemma 1 [25]. *For every comparison function $\widehat{\varphi}: \mathbb{R}_+ \longrightarrow \mathbb{R}_+$, we have the following points:*

(i) each iterate $\widehat{\varphi}^{\wp}, \wp \in \mathbb{N}$ is also a comparison function;

(iii) $\widehat{\varphi}(t) < t$ for all $t > 0$.

Lemma 2 [25]. *Let $\widehat{\varphi}: \mathbb{R}_+ \longrightarrow \mathbb{R}_+$ be a b-comparison function. Then, the series $\sum_{k=0}^{\infty} \widehat{\eta}^{k}\widehat{\varphi}^{k}(t)$ converges for every $t \in \mathbb{R}_+$.*

Remark 2 [22]. In Lemma 2, every b-comparison function is a comparison function and thus, in Lemma 1, every b-comparison function satisfies $\widehat{\varphi}(t) < t$.

Lemma 3 ([26]). *Consider a b-metric space $(\mho, \widehat{\mu}, \widehat{\eta})$. For $\widetilde{\nabla}, \widetilde{\triangle} \in \mathscr{K}(\mho)$ and $\varsigma, \omega \in \mho$, the following criteria hold:*

(i) $\widehat{\mu}(\varsigma, \widetilde{\triangle}) \leq \aleph(\widetilde{\nabla}, \widetilde{\triangle})$, *for any* $\varsigma \in \widetilde{\nabla}$.
(ii) $\widehat{\mu}(\varsigma, \widetilde{\nabla}) \leq \widehat{\eta}[\widehat{\mu}(\varsigma, \omega) + \widehat{\mu}(\omega, \widetilde{\nabla})]$.
(iii) $\widehat{\mu}(\varsigma, \widetilde{\nabla}) = 0 \Leftrightarrow \varsigma \in \widetilde{\nabla}$.
(iv) $\aleph(\widetilde{\nabla}, \widetilde{\triangle}) = 0 \Leftrightarrow \widetilde{\nabla} = \widetilde{\triangle}$.
(v) $\aleph(\widetilde{\nabla}, \widetilde{\triangle}) = \aleph(\widetilde{\triangle}, \widetilde{\nabla})$.
(vi) $\aleph(\widetilde{\nabla}, \widetilde{\triangle}) \leq \widehat{\eta}[\aleph_b(\widetilde{\nabla}, C) + \aleph_b(C, \widetilde{\triangle})]$.

3. Main Results

We commence this section with the notion of intuitionistic fuzzy p-hybrid contractions on a b-metric space in the following manner.

Definition 12. Consider a b-metric space $(\mho, \widehat{\mu}, \widehat{\eta})$ and $\Upsilon, \Psi: \mho \longrightarrow (IFS)^{\mho}$ be intuitionistic fuzzy set-valued maps. Then, the pair (Υ, Ψ) is said to form an intuitionistic fuzzy p-hybrid contraction, if for all $\varsigma, \omega \in \mho$, we can find $(\breve{\alpha}, \breve{\beta})_{\Upsilon(\varsigma)}, (\breve{\alpha}, \breve{\beta})_{\Psi(\omega)} \in (0,1] \times t[0,1)$ such that

$$\aleph\left([\Upsilon\varsigma]_{(\breve{\alpha},\breve{\beta})_{\Upsilon(\varsigma)}}, [\Psi\omega]_{(\breve{\alpha},\breve{\beta})_{\Psi(\omega)}}\right) \leq \widehat{\varphi}\mathscr{C}^{p}_{(\Upsilon,\Psi)}\left(\varsigma, \omega, (\breve{\alpha}, \breve{\beta})_{\Upsilon(\varsigma)}, (\breve{\alpha}, \breve{\beta})_{\Psi(\omega)}\right), \tag{12}$$

where $\widehat{\varphi} \in \Omega$, $p \geq 0$, $a_i \geq 0$, $i = 1, 2, 3, 4$ with $\sum_{i=1}^{4} a_i = 1$ and

$$\mathscr{C}^{p}_{(\Upsilon,\Psi)}\left(\varsigma, \omega, (\breve{\alpha}, \breve{\beta})_{\Upsilon(\varsigma)}, (\breve{\alpha}, \breve{\beta})_{\Psi(\omega)}\right) = \tag{13}$$

$$\begin{cases} \left[a_1(\widehat{\mu}(\varsigma,\omega))^p + a_2\left(\widehat{\mu}(\varsigma), [\Upsilon\varsigma]_{(\breve{\alpha},\breve{\beta})_{\Upsilon(\varsigma)}}\right)^p \right. \\ \left. + a_3\left(\widehat{\mu}\left(\omega, [\Psi\omega]_{(\breve{\alpha},\breve{\beta})_{\Psi(\omega)}}\right)\right)^p + a_4\left(\dfrac{\widehat{\mu}\left(\omega, [\Upsilon\varsigma]_{(\breve{\alpha},\breve{\beta})_{\Upsilon(\varsigma)}}\right) + \widehat{\mu}\left(\varsigma, [\Psi\omega]_{(\breve{\alpha},\breve{\beta})_{\Psi(\omega)}}\right)}{2\widehat{\eta}}\right)^p\right]^{1/p}, \\ \left(\widehat{\mu}(\varsigma,\omega)^{a_1}\left(\widehat{\mu}\left(\varsigma, [\Upsilon\varsigma]_{(\breve{\alpha},\breve{\beta})_{\Upsilon(\varsigma)}}\right)\right)^{a_2}\left(\widehat{\mu}\left(\omega, [\Psi\omega]_{(\breve{\alpha},\breve{\beta})_{\Psi(\omega)}}\right)\right)\right)^{a_3} \\ \times\left(\dfrac{\widehat{\mu}\left(\varsigma, [\Psi\omega]_{(\breve{\alpha},\breve{\beta})_{\Psi(\omega)}}\right) + \widehat{\mu}\left(\omega, [\Upsilon\varsigma]_{(\breve{\alpha},\breve{\beta})_{\Upsilon(\varsigma)}}\right)}{2\widehat{\eta}}\right)^{a_4}, \\ \text{for } p = 0, \varsigma, \omega \in \mho \setminus \mathscr{F}_{ix}(\Upsilon, \Psi), \end{cases} \tag{14}$$

where

$$\mathscr{F}_{ix}(\Upsilon, \Psi) = \left\{\varsigma, \omega \in \mho: \varsigma \in [\Upsilon\varsigma]_{(\breve{\alpha},\breve{\beta})_{\Upsilon(\varsigma)}}, \omega \in [\Psi\omega]_{(\breve{\alpha},\breve{\beta})_{\Psi(\omega)}}\right\}. \tag{15}$$

In particular, if (12) holds for $p = 0$, then we say that the pair (Υ, Ψ) forms an intuitionistic fuzzy 0-hybrid contraction. Our first main result is presented hereunder.

Theorem 1. *Let $(\mho, \widehat{\mu}, \widehat{\eta})$ be a complete b-metric space and $\Upsilon, \Psi: \mho \longrightarrow (IFS)^{\mho}$ be intuitionistic fuzzy set-valued maps. Suppose that for each $\varsigma \in \mho$, we can find $(\breve{\alpha}, \beta)_{\Upsilon(\varsigma)}$, $(\breve{\alpha}, \beta)_{\Psi(\varsigma)} \in (0,1] \times t[0,1)$ such that $[\Upsilon\varsigma]_{(\breve{\alpha},\breve{\beta})_{\Upsilon(\varsigma)}}$ and $[\Psi\varsigma]_{(\breve{\alpha},\breve{\beta})_{\Psi(\varsigma)}}$ are nonempty bounded proximal subsets of $\mho$. If the pair (Υ, Ψ) forms an intuitionistic fuzzy p-hybrid contraction, then Υ and Ψ have a common intuitionistic fuzzy Fp in $\mho$.*

Proof. Let $\varsigma_0 \in \mho$, then, by hypotheses, we can find $(\breve{\alpha}, \breve{\beta})_{\Upsilon(\varsigma_0)} \in (0,1] \times t[0,1)$ such that $[\Upsilon\varsigma_0]_{(\breve{\alpha},\breve{\beta})_{\Upsilon(\varsigma_0)}} \in \mathscr{P}^{r}_{b}(\mho)$. Take $\varsigma_1 \in [\Upsilon\ \varsigma_0]_{(\breve{\alpha},\breve{\beta})_{\Upsilon(\varsigma_0)}}$ such that $\widehat{\mu}(\varsigma_0, \varsigma_1) = \widehat{\mu}(\varsigma_0, [\Upsilon\varsigma_0]_{(\breve{\alpha},\breve{\beta})_{\Upsilon(\varsigma_0)}})$. Similarly, $[\Psi\varsigma_1]_{(\breve{\alpha},\breve{\beta})_{\Upsilon(\varsigma_1)}} \in \mathscr{P}^{r}_{b}(\mho)$, by hypothesis. So, we can find $\varsigma_2 \in [\Psi\varsigma_1]_{(\breve{\alpha},\breve{\beta})_{\Upsilon(\varsigma_1)}}$ so that by proximality of Ψ, $\widehat{\mu}(\varsigma_1, \varsigma_2) = \widehat{\mu}(\varsigma_1, [\Psi\varsigma_1]_{(\breve{\alpha},\breve{\beta})_{\Upsilon(\varsigma_1)}})$. Continuing in this direction, we can construct a sequence $\{\varsigma_\wp\}_{\wp\in\mathbb{N}}$ of elements of $\mho$ such that

$$\varsigma_{2k+1} \in [\Upsilon\varsigma_{2k}]_{(\breve{\alpha},\breve{\beta})_{\Upsilon(\varsigma_{2k})}}, \varsigma_{2k+2} \in [\Psi\varsigma_{2k+1}]_{(\breve{\alpha},\breve{\beta})_{\Upsilon(\varsigma_{2k+1})}} \tag{16}$$

and

$$\begin{aligned}\widehat{\mu}(\varsigma_{2k},\varsigma_{2k+1}) &= \widehat{\mu}\left(\varsigma_{2k},\left[\Upsilon\varsigma_{2k}\right]_{(\breve{\alpha},\breve{\beta})_{\Upsilon(\varsigma_{2k})}}\right),\\ \widehat{\mu}(\varsigma_{2k+1},\varsigma_{2k+2}) &= \widehat{\mu}\left(\varsigma_{2k+1},\left[\Psi\varsigma_{2k+1}\right]_{(\breve{\alpha},\breve{\beta})_{\Upsilon(\varsigma_{2k+1})}}\right), k\in\mathbb{N}.\end{aligned} \tag{17}$$

By Lemma 3 and the above relations, we have

$$\widehat{\mu}(\varsigma_{2k},\varsigma_{2k+1}) \le \aleph\left(\left[\Upsilon\varsigma_{2k}\right]_{(\breve{\alpha},\breve{\beta})_{\Upsilon(\varsigma_{2k})}},\left[\Psi\varsigma_{2k-1}\right]_{(\breve{\alpha},\breve{\beta})_{\Upsilon(\varsigma_{2k-1})}}\right), \tag{18}$$

and

$$\widehat{\mu}(\varsigma_{2k+1},\varsigma_{2k+2}) \le \aleph\left(\left[\Upsilon\varsigma_{2k}\right]_{(\breve{\alpha},\breve{\beta})_{\Upsilon(\varsigma_{2k})}},\left[\Psi\varsigma_{2k+1}\right]_{(\breve{\alpha},\breve{\beta})_{\Upsilon(\varsigma_{2k+1})}}\right). \tag{19}$$

Suppose that $\varsigma_{2k}=\varsigma_{2k+1}$, for some $k\in\mathbb{N}$ and $p>0$. Then, from (13), we have

$$\begin{aligned}&\mathscr{C}^{p}_{(\Upsilon,\Psi)}\left(\varsigma_{2k},\varsigma_{2k+1},(\breve{\alpha},\breve{\beta})_{\Upsilon(2k)},(\breve{\alpha},\breve{\beta})_{\Psi(2k+1)}\right)\\ &=\left[a_1\left(\widehat{\mu}(\varsigma_{2k},\varsigma_{2k+1})\right)^p + a_2\left(\widehat{\mu}\left(\varsigma_{2k},\left[\Upsilon\varsigma_{2k}\right]_{(\breve{\alpha},\breve{\beta})_{\Upsilon(\varsigma_{2k})}}\right)\right)^p + a_3\left(\widehat{\mu}\left(\varsigma_{2k+1},\left[\Psi\varsigma_{2k+1}\right]_{(\breve{\alpha},\breve{\beta})_{\Upsilon(\varsigma_{2k+1})}}\right)\right)^p + a_4\left(\frac{\widehat{\mu}\left(\varsigma_{2k+1},\left[\Upsilon\varsigma_{2k}\right]_{(\breve{\alpha},\breve{\beta})_{\Upsilon(\varsigma_{2k})}}\right)+\widehat{\mu}\left(\varsigma_{2k},\left[\Psi\varsigma_{2k+1}\right]_{(\breve{\alpha},\breve{\beta})_{\Upsilon(\varsigma_{2k+1})}}\right)}{2\widehat{\eta}}\right)^p\right]^{1/p}\\ &=\left[a_1\left(\widehat{\mu}(\varsigma_{2k},\varsigma_{2k+1})\right)^p + a_2\left(\widehat{\mu}(\varsigma_{2k+1},\varsigma_{2k+1})\right)^p + a_3\left(\widehat{\mu}(\varsigma_{2k+1},\varsigma_{2k+2})\right)^p + a_4\left(\frac{\left(\widehat{\mu}(\varsigma_{2k+1},\varsigma_{2k+1})\right)^p+\left(\widehat{\mu}(\varsigma_{2k+1},\varsigma_{2k+2})\right)}{2\widehat{\eta}}\right)^p\right]^{1/p}\\ &\le\left[a_3\left(\widehat{\mu}(\varsigma_{2k+1},\varsigma_{2k+2})\right)^p + a_4\left(\widehat{\eta}\left(\frac{\widehat{\mu}(\varsigma_{2k},\varsigma_{2k+1})+\widehat{\mu}(\varsigma_{2k+1},\varsigma_{2k+2})}{2\widehat{\eta}}\right)\right)^p\right]^{1/p}\\ &\le\left[a_3\left(\widehat{\mu}(\varsigma_{2k+1},\varsigma_{2k+2})\right)^p + a_4\left(\widehat{\mu}(\varsigma_{2k+1},\varsigma_{2k+2})\right)^p\right]^{1/p}\\ &=\left(a_3+a_4\right)^{1/p}\widehat{\mu}(\varsigma_{2k+1},\varsigma_{2k+2})=\widehat{\mu}(\varsigma_{2k+1},\varsigma_{2k+2})\, as\ p\longrightarrow\infty.\end{aligned} \tag{20}$$

Whence, using Lemma 1, we have

$$\begin{aligned}\widehat{\mu}(\varsigma_{2k+1},\varsigma_{2k+2}) &\le \aleph\left(\left[\Upsilon\varsigma_{2k}\right]_{(\breve{\alpha},\breve{\beta})_{\Upsilon(\varsigma_{2k})}},\left[\Psi\varsigma_{2k+1}\right]_{(\breve{\alpha},\breve{\beta})_{\Upsilon(\varsigma_{2k+1})}}\right)\\ &\le \widehat{\varphi}\left(\widehat{\mu}(\varsigma_{2k+1},\varsigma_{2k+2})\right) < \widehat{\mu}(\varsigma_{2k+1},\varsigma_{2k+2}),\end{aligned} \tag{21}$$

a contradiction. It follows that for all $k\in\mathbb{N}$,

$$\varsigma_{2k}=\varsigma_{2k+1}\in\left[\Upsilon\varsigma_{2k}\right]_{(\breve{\alpha},\breve{\beta})_{\Upsilon(\varsigma_{2k})}}, \tag{22}$$

$$\begin{aligned}\varsigma_{2k}=\varsigma_{2k+1}=\varsigma_{2k+2}&\in\left[\Psi\varsigma_{2k+1}\right]_{(\breve{\alpha},\breve{\beta})_{\Upsilon(\varsigma_{2k+1})}}\\ &=\left[\Psi\varsigma_{2k}\right]_{(\breve{\alpha},\breve{\beta})_{\Upsilon(\varsigma_{2k})}}.\end{aligned} \tag{23}$$

It follows that ς_{2k} is the common intuitionistic fuzzy Fp of Υ and Ψ.

Again, for $p = 0$ and $\varsigma_{2k} = \varsigma_{2k+1}$, for some $k \in \mathbb{N}$, we get $\mathscr{C}^{p}_{(\Upsilon,\Psi)}(\varsigma_{2k}, \varsigma_{2k+1}, (\breve{\alpha}, \breve{\beta})_{\Upsilon(2k)}, (\breve{\alpha}, \breve{\beta})_{\Psi(2k+1)}) = 0$, for all $k \in \mathbb{N}$. Whence, by property (ii) of Ω, one obtains $\widehat{\mu}(\varsigma_{2k+1}, \varsigma_{2k+2}) = 0$, for all $k \in \mathbb{N}$; from which, on similar arguments as above, the same conclusion follows that $\varsigma_{2k} \in [\Upsilon\varsigma_{2k}]_{(\breve{\alpha},\breve{\beta})_{\Upsilon(\varsigma_{2k})}} \cap [\Upsilon\varsigma_{2k}]_{(\breve{\alpha},\breve{\beta})_{\Upsilon(\varsigma_{2k})}}$. Hereafter, we assume that for all $k \in \mathbb{N}$, $\varsigma_{k+1} \neq \varsigma_k$ if and only if $\widehat{\mu}(\varsigma_{k+1}, \varsigma_k) > 0$.

Now, in view of (13), setting $\varsigma = \varsigma_{2k}$ and $\omega = \varsigma_{2k-1}$, we have

$$\mathscr{C}^{p}_{(\Upsilon,\Psi)}\left(\varsigma_{2k}, \varsigma_{2k-1}, (\breve{\alpha}, \breve{\beta})_{\Upsilon(2k-1)}, (\breve{\alpha}, \breve{\beta})_{\Psi(2k+1)}\right)$$

$$= \begin{cases} \left[a_1\left(\widehat{\mu}(\varsigma_{2k}, \varsigma_{2k-1})\right)^p + a_2\left(\widehat{\mu}\left(\varsigma_{2k}, [\Upsilon\varsigma_{2k}]_{(\breve{\alpha},\breve{\beta})_{\Upsilon(\varsigma_{2k})}}\right)\right)^p \right. \\ \left. + a_3\widehat{\mu}\left(\varsigma_{2k-1}, [\Psi\varsigma_{2k-1}]_{(\breve{\alpha},\breve{\beta})_{\Upsilon(\varsigma_{2k})}}\right)^p + a_4\left(\dfrac{\widehat{\mu}\left(\varsigma_{2k-1}, [\Upsilon\varsigma_{2k}]_{(\breve{\alpha},\breve{\beta})_{\Upsilon(\varsigma_{2k})}}\right) + \widehat{\mu}\left(\varsigma_{2k}, [\Psi\varsigma_{2k-1}]_{(\breve{\alpha},\breve{\beta})_{\Upsilon(\varsigma_{2k})}}\right)}{2\widehat{\eta}}\right)^p\right]^{1/p}, \\ for\ p > 0, \\ \left(\widehat{\mu}(\varsigma_{2k}, \varsigma_{2k-1})\right)^{a_1}\left(\widehat{\mu}\left(\varsigma_{2k}, [\Upsilon\varsigma_{2k}]_{(\breve{\alpha},\breve{\beta})_{\Upsilon(\varsigma_{2k})}}\right)\right)^{a_2}\left(\widehat{\mu}\left(\varsigma_{2k-1}, [\Psi\varsigma_{2k-1}]_{(\breve{\alpha},\breve{\beta})_{\Upsilon(\varsigma_{2k})}}\right)\right)^{a_3} \\ \times\left(\dfrac{\widehat{\mu}\left(\varsigma_{2k}, [\Psi\varsigma_{2k-1}]_{(\breve{\alpha},\breve{\beta})_{\Upsilon(\varsigma_{2k})}}\right) + \widehat{\mu}\left(\varsigma_{2k-1}, [\Upsilon\varsigma_{2k}]_{(\breve{\alpha},\breve{\beta})_{\Upsilon(\varsigma_{2k})}}\right)}{2\widehat{\eta}}\right)^{a_4}, \text{for } p = 0. \end{cases} \tag{24}$$

That is,

$$\mathscr{C}^{p}_{(\Upsilon,\Psi)}\left(\varsigma_{2k}, \varsigma_{2k-1}, (\breve{\alpha}, \breve{\beta})_{\Upsilon(2k)}, (\breve{\alpha}, \breve{\beta})_{\Psi(2k-1)}\right) = \tag{25}$$

$$\begin{cases} \left[a_1\left(\widehat{\mu}(\varsigma_{2k}, \varsigma_{2k-1})\right)^p + a_2\left(\widehat{\mu}(\varsigma_{2k}, \varsigma_{2k+1})\right)^p \right. \\ \left. + a_3\left(\widehat{\mu}(\varsigma_{2k-1}, \varsigma_{2k})\right)^p + a_4\left(\dfrac{\widehat{\mu}(\varsigma_{2k-1}, \varsigma_{2k+1}) + \widehat{\mu}(\varsigma_{2k}, \varsigma_{2k})}{2\widehat{\eta}}\right)^p\right]^{1/p} \\ \text{for } p > 0, \\ \left(\widehat{\mu}(\varsigma_{2k}, \varsigma_{2k-1})\right)^{a_1}\left(\widehat{\mu}(\varsigma_{2k}, \varsigma_{2k+1})\right)^{a_2}\left(\widehat{\mu}(\varsigma_{2k-1}, \varsigma_{2k})\right)^{a_3} \\ \times\left(\dfrac{\widehat{\mu}(\varsigma_{2k}, \varsigma_{2k}) + \widehat{\mu}(\varsigma_{2k-1}, \varsigma_{2k+1})}{2\widehat{\eta}}\right)^{a_4}, \\ \text{for } p = 0. \end{cases} \tag{26}$$

Now, we consider the following two cases: □

Case 1. $p>0$. Suppose that $\widehat{\mu}(\varsigma_{2k},\varsigma_{2k+1})\geq\widehat{\mu}(\varsigma_{2k-1},\varsigma_{2k})$, then from (25), we have

$$\begin{aligned}
&\mathscr{C}^{p}_{(\Upsilon,\Psi)}\Big(\varsigma_{2k},\varsigma_{2k-1},(\breve{\alpha},\breve{\beta})_{\Upsilon(2k)},(\breve{\alpha},\breve{\beta})_{\Psi(2k-1)}\Big)\\
&\leq\Big[a_1\left(\widehat{\mu}(\varsigma_{2k+1},\varsigma_{2k})\right)^{p}+a_2\left(\widehat{\mu}(\varsigma_{2k+1},\varsigma_{2k})\right)^{p}\\
&\quad+a_3\left(\widehat{\mu}(\varsigma_{2k+1},\varsigma_{2k})\right)^{p}+a_4\left(\widehat{\eta}\left(\frac{\widehat{\mu}(\varsigma_{2k+1},\varsigma_{2k})+\widehat{\mu}(\varsigma_{2k},\varsigma_{2k-1})}{2\widehat{\eta}}\right)\right)^{p}\Big]^{1/p}\\
&\leq\Big[a_1\left(\widehat{\mu}(\varsigma_{2k+1},\varsigma_{2k})\right)^{p}+a_2\left(\widehat{\mu}(\varsigma_{2k+1},\varsigma_{2k})\right)^{p}+a_3\left(\widehat{\mu}(\varsigma_{2k+1},\varsigma_{2k})\right)^{p}\\
&\quad+a_4\left(\widehat{\eta}\left(\frac{\widehat{\mu}(\varsigma_{2k+1},\varsigma_{2k})+\widehat{\mu}(\varsigma_{2k+1},\varsigma_{2k})}{2\widehat{\eta}}\right)^{p}\right)\Big]^{1/p}\\
&\leq\Big[a_1\left(\widehat{\mu}(\varsigma_{2k+1},\varsigma_{2k})\right)^{p}+a_2\left(\widehat{\mu}(\varsigma_{2k+1},\varsigma_{2k})\right)^{p}\\
&\quad+a_3\left(\widehat{\mu}(\varsigma_{2k+1},\varsigma_{2k})\right)^{p}+a_4\left(\widehat{\mu}(\varsigma_{2k+1},\varsigma_{2k})\right)^{p}\Big]^{1/p}\\
&=\Big[(a_1+a_2+a_3+a_4)\widehat{\mu}(\varsigma_{2k+1},\varsigma_{2k})^{p}\Big]^{1/p}\\
&=\widehat{\mu}(\varsigma_{2k+1},\varsigma_{2k})\left(\sum_{i=1}^{4}a_i\right)^{1/p}=\widehat{\mu}(\varsigma_{2k+1},\varsigma_{2k}).
\end{aligned}\tag{27}$$

Hence, from (12) and (27), we have

$$\widehat{\mu}(\varsigma_{2k+1},\varsigma_{2k})\leq\widehat{\varphi}\left(\widehat{\mu}(\varsigma_{2k+1},\varsigma_{2k})\right).\tag{28}$$

Given that $\widehat{\varphi}$ is a b-comparison function, (28) implies

$$\widehat{\mu}(\varsigma_{2k+1},\varsigma_{2k})<\widehat{\mu}(\varsigma_{2k+1},\varsigma_{2k}),\tag{29}$$

which is a contradiction. Whence, it follows that $\widehat{\mu}(\varsigma_{2k+1},\varsigma_{2k})\leq\widehat{\mu}(\varsigma_{2k},\varsigma_{2k-1})$. Thus, from (28), we obtain

$$\widehat{\mu}(\varsigma_{2k+1},\varsigma_{2k})\leq\widehat{\varphi}\left(\widehat{\mu}(\varsigma_{2k},\varsigma_{2k-1})\right).\tag{30}$$

Setting $\wp=2k\in\mathbb{N}$ in (30), yields

$$\begin{aligned}
\widehat{\mu}(\varsigma_{\wp+1},\varsigma_{\wp})&\leq\widehat{\varphi}\left(\widehat{\mu}(\varsigma_{\wp},\varsigma_{\wp-1})\right)\\
&\leq\widehat{\varphi}^{2}\left(\widehat{\mu}(\varsigma_{\wp-1},\varsigma_{\wp-2})\right)\\
&\leq\widehat{\varphi}^{3}\left(\widehat{\mu}(\varsigma_{\wp-2},\varsigma_{\wp-3})\right)\\
&\vdots\quad\vdots\\
&\leq\widehat{\varphi}^{\wp}\left(\widehat{\mu}(\varsigma_1,\varsigma_0)\right).
\end{aligned}\tag{31}$$

From (31), by triangle inequality on $(\mho,\widehat{\mu},\widehat{\eta})$, for all $k\geq1$, we have

$$\begin{aligned}
\widehat{\mu}(\varsigma_{\wp+k},\varsigma_{\wp})&\leq\widehat{\eta}\left(\widehat{\mu}(\varsigma_{\wp+k},\varsigma_{\wp+1})+\widehat{\mu}(\varsigma_{\wp+1},\varsigma_{\wp})\right)\\
&\leq\frac{1}{\widehat{\eta}^{\wp-1}}\sum_{i=\wp}^{\wp+k-1}\widehat{\eta}^{k}\widehat{\mu}(\varsigma_i,\varsigma_{i+1})\\
&\leq\frac{1}{\widehat{\eta}^{\wp-1}}\sum_{i=\wp}^{\wp+k-1}\widehat{\eta}^{k}\widehat{\varphi}^{k}\left(\widehat{\mu}(\varsigma_1,\varsigma_0)\right)\\
&\leq\frac{1}{\widehat{\eta}^{\wp-1}}\sum_{i=\wp}^{\infty}\widehat{\eta}^{i}\widehat{\varphi}^{i}\left(\widehat{\mu}(\varsigma_1,\varsigma_0)\right).
\end{aligned}\tag{32}$$

Letting $\wp \longrightarrow \infty$ in (32) and applying Lemma 2, we find that $\lim_{\wp\longrightarrow\infty}\widehat{\mu}(\varsigma_{\wp+k}, \varsigma_{\wp}) = 0$. Whence, $\{\varsigma_{\wp}\}_{\wp\in\mathbb{N}}$ is a Cauchy sequence of points of $(\overline{\mathcal{O}}, \widehat{\mu}, \widehat{\eta})$. The completeness of this space implies that we can find $u \in \overline{\mathcal{O}}$ such that

$$\lim_{\wp\longrightarrow\infty}\widehat{\mu}\left(\varsigma_{\wp}, u\right) = 0. \tag{33}$$

Now, we show that u is the anticipated common intuitionistic fuzzy Fp of Υ and Ψ. First, assume that $u \notin [\Upsilon u]_{(\breve{\alpha},\breve{\beta})_{\Upsilon(u)}}$ so that $\widehat{\mu}(u, [\Upsilon u]_{(\breve{\alpha},\breve{\beta})_{\Upsilon(u)}}) > 0$. Then, by Lemma 3 and for $p > 0$ in the contractive inequality (3.1), we have

$$\begin{aligned}
\widehat{\mu}\left(u, [\Upsilon u]_{(\breve{\alpha},\breve{\beta})_{\Upsilon(u)}}\right) &\leq \widehat{\eta}\widehat{\mu}\left(u, \varsigma_{\wp}\right) + \widehat{\eta}\widehat{\mu}\left(\varsigma_{\wp}, [\Upsilon u]_{(\breve{\alpha},\breve{\beta})_{\Upsilon(u)}}\right) \leq \widehat{\eta}\widehat{\mu}\left(u, \varsigma_{\wp}\right) + \widehat{\eta}\aleph\left([\Upsilon u]_{(\breve{\alpha},\breve{\beta})_{\Upsilon(u)}}, \left[\Psi\varsigma_{\wp-1}\right]_{(\breve{\alpha},\breve{\beta})_{\Psi}\left(\varsigma_{\wp-1}\right)}\right) \\
&\leq \widehat{\eta}\widehat{\mu}\left(u, \varsigma_{\wp}\right) + \widehat{\eta}\widehat{\varphi}\left(\mathscr{C}^{p}_{(\Upsilon,\Psi)}\left(u, \varsigma_{\wp-1}\right)\right) = \widehat{\eta}\widehat{\mu}\left(u, \varsigma_{\wp}\right) + \widehat{\eta}\widehat{\varphi}\left(\left[a_1\left(\widehat{\mu}\left(u, \varsigma_{\wp-1}\right)\right)^{p} + a_2\left(\widehat{\mu}\left(u, [\Upsilon u]_{(\breve{\alpha},\breve{\beta})_{\Upsilon(u)}}\right)\right)\right]\right)^{p} \\
&\quad + a_3\left(\widehat{\mu}\left(\varsigma_{\wp-1}, \left[\Psi\varsigma_{\wp-1}\right]_{(\breve{\alpha},\breve{\beta})_{\Psi}\left(\varsigma_{\wp-1}\right)}\right)\right)^{p} + a_4\left(\frac{\widehat{\mu}\left(\varsigma_{\wp-1}, [\Upsilon u]_{(\breve{\alpha},\breve{\beta})_{\Upsilon(u)}}\right) + \widehat{\mu}\left(u, \left[\Psi\varsigma_{\wp-1}\right]_{(\breve{\alpha},\breve{\beta})_{\Psi}\left(\varsigma_{\wp-1}\right)}\right)}{2\widehat{\eta}}\right)^{p}\Bigg]^{1/p}\Bigg) \\
&= \widehat{\eta}\widehat{\mu}\left(u, \varsigma_{\wp}\right) + \widehat{\eta}\widehat{\varphi}\left(a_1\left(\widehat{\mu}\left(u, \varsigma_{\wp-1}\right)\right)^{p} + a_2\left(\widehat{\mu}\left(u, [\Upsilon u]_{(\breve{\alpha},\breve{\beta})_{\Upsilon(u)}}\right)\right)\right)^{p} + a_3\left(\widehat{\mu}\left(\varsigma_{\wp-1}, \varsigma_{\wp}\right)\right)^{p} \\
&\quad + a_4\left(\frac{\widehat{\mu}\left(\varsigma_{\wp-1}, [\Upsilon u]_{(\breve{\alpha},\breve{\beta})_{\Upsilon(u)}}\right) + \widehat{\mu}\left(u, \varsigma_{\wp}\right)}{2\widehat{\eta}}\right)^{p}\Bigg]^{1/p}\Bigg).
\end{aligned} \tag{34}$$

Letting $\wp \longrightarrow \infty$ in (34), and using the properties of $\widehat{\varphi} \in \Omega$, gives

$$\widehat{\mu}\left(u, [\Upsilon u]_{(\breve{\alpha},\breve{\beta})_{\Upsilon(u)}}\right) < \widehat{\eta}\widehat{\mu}\left(u, [\Upsilon u]_{(\breve{\alpha},\breve{\beta})_{\Upsilon(u)}}\right)\left(a_2 + a_4\right)^{1/p}, \tag{35}$$

and as $p \longrightarrow \infty$,

$$\widehat{\mu}\left(u, [\Upsilon u]_{(\breve{\alpha},\breve{\beta})_{\Upsilon(u)}}\right) < \widehat{\eta}\widehat{\mu}\left(u, [\Upsilon u]_{(\breve{\alpha},\breve{\beta})_{\Upsilon(u)}}\right), \tag{36}$$

which is a contradiction for $\widehat{\eta} = 1$. Thus, $\widehat{\mu}(u, [\Upsilon u]_{(\breve{\alpha},\breve{\beta})_{\Upsilon(u)}}) = 0$, which further implies that $u \in [\Upsilon u]_{(\breve{\alpha},\breve{\beta})_{\Upsilon(u)}}$. On similar steps, by assuming that u is not an intuitionistic fuzzy Fp of Ψ, and considering

$$\begin{aligned}
\widehat{\mu}\left(u, [\Psi u]_{(\breve{\alpha},\breve{\beta})_{\Upsilon(u)}}\right) &\leq \widehat{\eta}\widehat{\mu}\left(u, \varsigma_{\wp}\right) + \widehat{\eta}\widehat{\mu}\left(\varsigma_{\wp}, [\Psi u]_{(\breve{\alpha},\breve{\beta})_{\Upsilon(u)}}\right) \\
&\leq \widehat{\eta}\widehat{\mu}\left(u, \varsigma_{\wp}\right) + \widehat{\eta}\aleph\left(\left[\Upsilon\varsigma_{\wp-1}\right]_{(\breve{\alpha},\breve{\beta})_{\Upsilon(u)}}, [\Psi u]_{(\breve{\alpha},\breve{\beta})_{\Upsilon(u)}}\right) \\
&\leq \widehat{\eta}\widehat{\mu}\left(u, \varsigma_{\wp}\right) + \widehat{\eta}\widehat{\varphi}\left(\mathscr{C}^{p}_{(\Psi,\Upsilon)}\left(\varsigma_{\wp-1}, u, (\breve{\alpha}, \breve{\beta})_{\Psi}\left(\varsigma_{\wp-1}\right), (\breve{\alpha}, \breve{\beta})_{\Upsilon(u)}\right)\right),
\end{aligned} \tag{37}$$

we can show that $u \in [\Psi u]_{(\breve{\alpha},\breve{\beta})_{\Psi(u)}}$. Whence, for $p > 0$, we can find $u \in \breve{\mathcal{O}}$ such that $u \in [\Upsilon u]_{(\breve{\alpha},\breve{\beta})_{\Upsilon(u)}} \cap [\Psi u]_{(\breve{\alpha},\breve{\beta})_{\Psi(u)}}$.

Case 2. $p = 0$. Applying the inequality (25) on account of b-comparison of $\widehat{\varphi}$, we have

$$\begin{aligned}
\widehat{\mu}(\varsigma_{2k}, \varsigma_{2k-1}) &\leq \aleph\left([\Upsilon\varsigma_{2k-1}]_{(\breve{\alpha},\breve{\beta})_{\Upsilon(2k-1)}}, [\Psi\varsigma_{2k-2}]_{(\breve{\alpha},\breve{\beta})_{\Psi(2k-2)}} \right) \\
&\leq \widehat{\varphi}\left(\mathscr{C}^{p}_{(\Upsilon,\Psi)}(\varsigma_{2k-1}, \varsigma_{2k-2}), (\breve{\alpha},\breve{\beta})_{\Upsilon(2k-1)}, (\breve{\alpha},\breve{\beta})_{\Psi(2k-2)} \right) \\
&< \left(\widehat{\mu}(\varsigma_{2k-1}, \varsigma_{2k-2})\right)^{a_1} \left(\varsigma_{2k-1}, [\Upsilon\varsigma_{2k-1}]_{(\breve{\alpha},\breve{\beta})_{\Upsilon(2k-1)}} \right)^{a_2} \left(\widehat{\mu}\left(\varsigma_{2k-2}, [\Psi\varsigma_{2k-2}]_{(\breve{\alpha},\breve{\beta})_{\Psi(2k-2)}} \right) \right)^{a_3} \\
&\quad \times \left(\frac{\widehat{\mu}\left(\varsigma_{2k-2}, [\Psi\varsigma_{2k-2}]_{(\breve{\alpha},\breve{\beta})_{\Psi(2k-2)}} \right) + \widehat{\mu}\left(\varsigma_{2k-2}, [\Upsilon\varsigma_{2k-1}]_{(\breve{\alpha},\breve{\beta})_{\Upsilon(2k-1)}} \right)}{2\widehat{\eta}} \right)^{a_4} \\
&= \left(\widehat{\mu}(\varsigma_{2k-1}, \varsigma_{2k-2})\right)^{a_1} \left(\widehat{\mu}(\varsigma_{2k-1}, \varsigma_{2k})\right)^{a_2} \left(\widehat{\mu}(\varsigma_{2k-2}, \varsigma_{2k-1})\right)^{a_3} \\
&\quad \times \left(\frac{\widehat{\mu}(\varsigma_{2k-1}, \varsigma_{2k-1}) + \widehat{\mu}(\varsigma_{2k-2}, \varsigma_{2k})}{2\widehat{\eta}} \right)^{a_4} \\
&\leq \left(\widehat{\mu}(\varsigma_{2k-1}, \varsigma_{2k-2})\right)^{a_1} \left(\widehat{\mu}(\varsigma_{2k-1}, \varsigma_{2k})\right)^{a_2} \left(\widehat{\mu}(\varsigma_{2k-2}, \varsigma_{2k-1})\right)^{a_3} \\
&\quad \times \left(\frac{\widehat{\mu}(\varsigma_{2k}, \varsigma_{2k-1}) + \widehat{\mu}(\varsigma_{2k-1}, \varsigma_{2k-2})}{2} \right)^{a_4} \\
&= \left(\widehat{\mu}(\varsigma_{2k-1}, \varsigma_{2k-2})\right)^{a_1+a_3} \left(\widehat{\mu}(\varsigma_{2k-1}, \varsigma_{2k})\right)^{a_2} \\
&\quad \times \left(\frac{\widehat{\mu}(\varsigma_{2k}, \varsigma_{2k-1}) + \widehat{\mu}(\varsigma_{2k-1}, \varsigma_{2k-2})}{2} \right)^{1-a_1-a_2-a_3}.
\end{aligned} \tag{38}$$

Assume that $\widehat{\mu}(\varsigma_{2k-1}, \varsigma_{2k-2}) \leq \widehat{\mu}(\varsigma_{2k}, \varsigma_{2k-1})$, then (3.14) gives

$$\begin{aligned}
\widehat{\mu}(\varsigma_{2k}, \varsigma_{2k-1}) &\leq \widehat{\varphi}\left(\mathscr{C}^{p}_{(\Upsilon,\Psi)}\left(\varsigma_{2k-1}, \varsigma_{2k-2}, (\breve{\alpha},\breve{\beta})_{\Upsilon(\varsigma_{2k-1})}, (\breve{\alpha},\breve{\beta})_{\Psi(\varsigma_{2k-2})} \right) \right) \\
&< \left(\widehat{\mu}(\varsigma_{2k}, \varsigma_{2k-1})\right)^{a_1+a_2+a_3} \left(\widehat{\mu}(\varsigma_{2k}, \varsigma_{2k-1})\right)^{1-a_1-a_2-a_3} \\
&= \widehat{\mu}(\varsigma_{2k}, \varsigma_{2k-1}),
\end{aligned} \tag{39}$$

a contradiction. Whence,

$$\widehat{\mu}(\varsigma_{2k}, \varsigma_{2k-1}) \leq \widehat{\mu}(\varsigma_{2k-1}, \varsigma_{2k-2}). \tag{40}$$

Using (38) and (40), we obtain

$$\widehat{\mu}(\varsigma_{2k}, \varsigma_{2k-1}) \leq \widehat{\varphi}\left(\widehat{\mu}(\varsigma_{2k-1}, \varsigma_{2k-2})\right). \tag{41}$$

Note that, (41) is equivalent to (3.9). So, on similar steps, we infer that the sequence $\{\varsigma_{\wp}\}_{\wp\in\mathbb{N}}$ is Cauchy in $(\breve{\mathcal{O}}, \widehat{\mu}, \widehat{\eta})$. Thus, the completeness of this space guarantees that $\widehat{\mu}(\varsigma_{\wp}, u) \longrightarrow 0$ as $\wp \longrightarrow \infty$, for some $u \in \breve{\mathcal{O}}$.

To see that u is a common intuitionistic fuzzy Fp of Ψ and Υ, we employ Lemma 3 and inequality (3.5) as follows:

$$\begin{aligned}\widehat{\mu}\left(u, [\Psi u]_{(\breve{\alpha},\breve{\beta})_{\Psi(u)}}\right) &\leq \widehat{\eta}\widehat{\mu}\left(u, \varsigma_{\wp}\right) + \widehat{\eta}\widehat{\mu}\left(\varsigma_{\wp}, [\Psi u]_{(\breve{\alpha},\breve{\beta})_{\Psi(u)}}\right)\\ &\leq \widehat{\eta}\widehat{\mu}\left(u, \varsigma_{\wp}\right) + \widehat{\eta}\aleph\left(\left[\Upsilon\varsigma_{\wp-1}\right]_{(\breve{\alpha},\breve{\beta})_{\Upsilon\left(\varsigma_{\wp-1}\right)}}, [\Psi u]_{(\breve{\alpha},\breve{\beta})_{\Psi(u)}}\right)\\ &\leq \widehat{\eta}\widehat{\mu}\left(u, \varsigma_{\wp}\right) + \widehat{\eta}\widehat{\varphi}\left(\mathscr{C}^{p}_{(\Upsilon,\Psi)}\left(\varsigma_{\wp-1}, u, (\breve{\alpha},\breve{\beta})_{\Upsilon(u)}, (\breve{\alpha},\breve{\beta})\right)\right),\end{aligned} \tag{42}$$

where

$$\begin{aligned}&\mathscr{C}^{p}_{(\Upsilon,\Psi)}\left(\varsigma_{\wp-1}, u, (\breve{\alpha},\breve{\beta})_{\Upsilon\left(\varsigma_{\wp-1}\right)}, (\breve{\alpha},\breve{\beta})_{\Psi(u)}\right)\\ &= \left(\widehat{\mu}\left(\varsigma_{\wp-1}, u\right)\right)^{a_1}\left(\widehat{\mu}\left(\varsigma_{\wp-1}, \left[\Upsilon\varsigma_{\wp-1}\right]_{(\breve{\alpha},\breve{\beta})_{\Upsilon_{\varsigma_{\wp-1}}}}\right)\right)^{a_2}\left(\widehat{\mu}\left(u, [\Psi u]_{(\breve{\alpha},\breve{\beta})_{\Psi(u)}}\right)\right)^{a_3}\\ &\quad\times\left(\frac{\widehat{\mu}\left(\varsigma_{\wp-1}, [\Psi u]_{(\breve{\alpha},\breve{\beta})_{\Psi(u)}}\right) + \widehat{\mu}\left(u, \left[\Upsilon\varsigma_{\wp-1}\right]_{(\breve{\alpha},\breve{\beta})_{\Upsilon_{\varsigma_{\wp-1}}}}\right)}{2\widehat{\eta}}\right)^{a_4}\\ &= \left(\widehat{\mu}\left(\varsigma_{\wp-1}, u\right)\right)^{a_1}\left(\widehat{\mu}\left(\varsigma_{\wp-1}, \varsigma_{\wp}\right)\right)^{a_2}\left(\widehat{\mu}\left(u, [\Psi u]_{(\breve{\alpha},\breve{\beta})_{\Psi(u)}}\right)\right)^{a_3}\\ &\quad\times\left(\frac{\widehat{\mu}\left(\varsigma_{\wp-1}, [\Psi u]_{(\breve{\alpha},\breve{\beta})_{\Psi(u)}}\right) + \widehat{\mu}\left(u, \varsigma_{\wp}\right)}{2\widehat{\eta}}\right)^{a_4}.\end{aligned} \tag{43}$$

We see that $\lim_{\wp\longrightarrow\infty}\mathscr{C}^{p}_{(\Upsilon,\Psi)}(\varsigma_{\wp-1}, u, (\breve{\alpha},\breve{\beta})_{\Upsilon(\varsigma_{\wp-1})}, (\breve{\alpha},\beta)_{\Psi(u)}) = 0$. Hence, under this limiting case, (3.17) becomes

$$\widehat{\mu}(u, \Psi u) \leq \widehat{\eta}\widehat{\varphi}(0). \tag{44}$$

By criterion (*ii*) of $\widehat{\varphi}$, (3.18) implies that $\widehat{\mu}(u, [\Psi u]_{(\breve{\alpha},\breve{\beta})_{\Psi(u)}}) = 0$. Whence, $u \in [\Psi u]_{(\breve{\alpha},\breve{\beta})_{\Psi(u)}}$. On similar steps, we can show that $u \in [\Upsilon u]_{(\breve{\alpha},\breve{\beta})_{\Upsilon(u)}}$. Whence, we can find $(\breve{\alpha},\breve{\beta})_{\Upsilon(u)}, (\breve{\alpha},\breve{\beta})_{\Psi(u)} \in (0,1]\times t[0,1)$ such that $u \in [\Upsilon u]_{(\breve{\alpha},\breve{\beta})_{\Upsilon(u)}} \cap [\Psi u]_{(\breve{\alpha},\breve{\beta})_{\Upsilon(u)}}$.

From Case 2 in the Proof of Theorem 1, we have also proved the next result.

Theorem 2. *Let $(\overline{\sigma}, \widehat{\mu}, \widehat{\eta})$ be a complete b-metric space and Υ, Ψ: $\overline{\sigma} \longrightarrow (IFS)^{\overline{\sigma}}$ be intuitionistic fuzzy set-valued maps. Suppose that for each $\varsigma \in \overline{\sigma}$, we can find $(\breve{\alpha},\breve{\beta})_{\Upsilon(\varsigma)}$, $(\breve{\alpha},\breve{\beta})_{\Psi(\varsigma)} \in (0,1]\times t[0,1)$ such that $[\Upsilon\varsigma]_{(\breve{\alpha},\breve{\beta})_{\Upsilon(\varsigma)}}$ and $[\Psi\varsigma]_{(\breve{\alpha},\breve{\beta})_{\Psi(\varsigma)}}$ are nonempty bounded proximal subsets of $\overline{\sigma}$. If the pair (Υ, Ψ) forms a 0-hybrid intuitionistic fuzzy contraction, then Υ and Ψ have a common intuitionistic fuzzy Fp in $\overline{\sigma}$.*

Next, we examine the idea of intuitionistic fuzzy p-hybrid contractions in view of $(\widetilde{M}, \widetilde{\omega})$-level set (see [13]) and $\widehat{\mu}_{(\infty,\infty)}$-distance as some consequences of Theorem 1. It is important to point out that the investigation of Fp of intuitionistic fuzzy set-valued maps in the frame of $\widehat{\mu}_{(\infty,\infty)}$-metric is of great significant in computing Hausdorff dimensions. These dimensions aid us to grasp the basis of ε^{∞}-space which is of enormous significant in higher energy physics. Consistent with Azam and Tabassum [12], we give some needed auxiliary concepts in the framework of a b-metric space as follows. Consider a b-metric space $(\overline{\sigma}, \widehat{\mu}, \widehat{\eta})$ and take $(\breve{\alpha},\beta) \in (0,1]\times t[0,1)$ such that $[\widetilde{\nabla}]_{(\breve{\alpha},\breve{\beta})}, [\widetilde{\Delta}]_{(\breve{\alpha},\breve{\beta})} \in \mathscr{P}^{r}_{b}(\overline{\sigma})$. Then, define

$$\begin{aligned}p_{(\breve{\alpha},\breve{\beta})}(\widetilde{\nabla}, \widetilde{\Delta}) &= \inf_{\varsigma\in\widetilde{[\nabla]}_{(\breve{\alpha},t\breve{\beta})}, \omega\in\widetilde{[\Delta]}_{(\breve{\alpha},\breve{\beta})}} \widehat{\mu}(\varsigma, \omega),\\ D_{(\breve{\alpha},\breve{\beta})}(\widetilde{\nabla}, \widetilde{\Delta}) &= \aleph\left([\widetilde{\nabla}]_{(\breve{\alpha},\breve{\beta})}, [\widetilde{\Delta}]_{(\breve{\alpha},\breve{\beta})}\right),\\ p(\widetilde{\nabla}, \widetilde{\Delta}) &= \sup_{(\breve{\alpha},\breve{\beta})} p_{(\breve{\alpha},\breve{\beta})}(\widetilde{\nabla}, \widetilde{\Delta}),\\ \widehat{\mu}_{(\infty,\infty)}(\widetilde{\nabla}, \widetilde{\Delta}) &= \sup_{(\breve{\alpha},\breve{\beta})} D_{(\breve{\alpha},\breve{\beta})}(\widetilde{\nabla}, \widetilde{\Delta}).\end{aligned} \tag{45}$$

Note that, $\widehat{\mu}_{(\infty,\infty)}$ is a metric on $\mathscr{P}^{r}_{b}(\overline{\sigma})$ (induced by the Hausdorff metric $\aleph$) and the completeness of $(\overline{\sigma}, \widehat{\mu}, \widehat{\eta})$

implies the completeness of the corresponding metric space $(\mathscr{K}_{\mathscr{JFS}}(\mathscr{O}), \widehat{\mu}_{(\infty,\infty)})$. Moreover, $(\mathscr{O}, \widehat{\mu}, \widehat{\eta}) \mapsto (\mathscr{P}_b^r(\mathscr{O}), \aleph) \mapsto (\mathscr{K}_{\mathscr{JFS}}(\mathscr{O}), \widehat{\mu}_{(\infty,\infty)}, \widehat{\eta})$, are isometric embeddings via the relations $\varsigma \longrightarrow \{\varsigma\}$ and $M \longrightarrow \chi_M$, respectively; where

$$\mathscr{K}_{\mathscr{JFS}}(\mathscr{O}) = \left\{\widetilde{\nabla} \in (IFS)^{\mathscr{O}}: [\widetilde{\nabla}]_{(\breve{\alpha},t\breve{\beta})} \in \mathscr{P}_b^r(\mathscr{O}), \text{for each } \breve{\alpha}, \breve{\beta} \in (0,1] \times t[0,1)\right\}, \tag{46}$$

and χ_M is the characteristic function of M.

Theorem 3. *Let $(\mathscr{O}, \widehat{\mu}, \widehat{\eta})$ be a complete b-metric space and $\Upsilon, \Psi: \mathscr{O} \longrightarrow (IFS)^{\mathscr{O}}$ be intuitionistic fuzzy set-valued maps. Assume that the following criteria are obeyed:*

(i) $[\Upsilon\varsigma]_{(\widetilde{M},\widetilde{\omega})_{\Upsilon(\varsigma)}}$ and $[\Psi\varsigma]_{(\widetilde{M},\widetilde{\omega})_{\Psi(\varsigma)}}$ are nonempty bounded proximal subsets of $\mathscr{O}$, for each $\varsigma \in \mathscr{O}$;

(ii) for each $\varsigma, \omega \in \mathscr{O}$,

$$\widehat{\mu}_{(\infty,\infty)}(\Upsilon(\varsigma), \Psi(\omega)) \leq \widehat{\varphi}\left(\mathscr{C}^p_{(\Upsilon,\Psi)}\varsigma, \omega, (\widetilde{M}, \widetilde{\omega})_{\Upsilon(\varsigma)}, (\widetilde{M}, \widetilde{\omega})_{\Psi(\varsigma)}\right), \tag{47}$$

where $\widehat{\varphi} \in \Omega$, $p \geq 0$, $a_i \geq 0$, $i = 1, 2, 3, 4$ with $\sum_{i=1}^4 a_i = 1$ and

$$\mathscr{C}^p_{(\Upsilon,\Psi)}\left(\varsigma, \omega, (\widetilde{M}, \widetilde{\omega})_{\Upsilon(\varsigma)}, (\widetilde{M}, \widetilde{\omega})_{\Psi(\omega)}\right) = \begin{cases} \left[a_1(\widehat{\mu}(\varsigma,\omega))^p + a_2\left(\widehat{\mu}(\varsigma), [\Upsilon\varsigma]_{(\widetilde{M},\widetilde{\omega})_{\Upsilon(\varsigma)}}\right)^p \right. \\ \left. + a_3\left(\widehat{\mu}\left(\omega, [\Psi\omega]_{(\widetilde{M},\widetilde{\omega})_{\Psi(\omega)}}\right)^p\right) + a_4\left(\dfrac{\widehat{\mu}\left(\omega, [\Upsilon\varsigma]_{(\widetilde{M},\widetilde{\omega})_{\Upsilon\varsigma}}\right)^p + \widehat{\mu}\left(\varsigma, [\Psi\omega]_{(\widetilde{M},\widetilde{\omega})_{\Psi(\omega)}}\right)^p}{2\widehat{\eta}}\right)\right]^{1/p} \\ \text{for } p > 0,\ \varsigma, \omega \in \mathscr{O}, \\ \left((\widehat{\mu}(\varsigma,\omega))^{a_1}\left(\widehat{\mu}\left(\varsigma, [\Upsilon\varsigma]_{(\widetilde{M},\widetilde{\omega})_{\Upsilon(\varsigma)}}\right)\right)\right)^{a_2}\left(\widehat{\mu}\left(\omega, [\Psi\omega]_{(\widetilde{M},\widetilde{\omega})_{\Psi(\omega)}}\right)\right)^{a_3} \\ \times\left(\dfrac{\widehat{\mu}\left(\varsigma, [\Psi\omega]_{(\widetilde{M},\widetilde{\omega})_{\Psi(\omega)}}\right) + \widehat{\mu}\left(\omega, [\Upsilon\varsigma]_{(\widetilde{M},\widetilde{\omega})_{\Upsilon(\varsigma)}}\right)}{2\widehat{\eta}}\right)^{a_4} \\ \text{for } p = 0, \varsigma, \omega \in \mathscr{O} \setminus \mathscr{F}_{ix}(\Upsilon, \Psi). \end{cases} \tag{48}$$

Then, Υ and Ψ have a common intuitionistic fuzzy Fp in $\mathscr{O}$.

Proof. Let $\varsigma \in \mathscr{O}$. Then, by assumption, $[\Upsilon(\varsigma)]_{(M,\wp)_{\Upsilon(\varsigma)}}$ and $[\Psi(\varsigma)]_{(M,\wp)_{\Psi(\varsigma)}}$ are nonempty bounded proximal subsets of $\mathscr{O}$. Hence, for each $\varsigma, \omega \in \mathscr{O}$,

$$\begin{aligned} &\aleph\left([\Upsilon(\varsigma)]_{(\widetilde{M},\widetilde{\omega})_{\Upsilon(\varsigma)}}, [\Psi(\omega)]_{(M,\widetilde{\omega})_{\Psi(\omega)}}\right) \\ &= D_{(\widetilde{M},\widetilde{\omega})}(\Upsilon(\varsigma), \Psi(\omega)) \leq \widehat{\mu}_{(\infty,\infty)}(\Upsilon(\varsigma), \Psi(\omega)) \\ &\leq \widehat{\varphi}\left(\mathscr{C}^p_{(\Upsilon,\Psi)}\left(\varsigma, \omega, (\widetilde{M}, \widetilde{\omega})_{\Upsilon(\varsigma)}, (\widetilde{M}, \widetilde{\omega})_{\Psi(\omega)}\right)\right). \end{aligned} \tag{49}$$

Whence, it follows from Theorem 1 that Υ and Ψ have a common intuitionistic fuzzy Fp in $\mathscr{O}$. □

Theorem 4. *Let $(\mathscr{O}, \widehat{\mu}, \widehat{\eta})$ be a complete b-metric space and $\Upsilon, \Psi: \mathscr{O} \longrightarrow \mathscr{K}_{\mathscr{JFS}}(\mathscr{O})$ be intuitionistic fuzzy set-valued maps such that*

$$\widehat{\mu}_{(\infty,\infty)}(\Upsilon(\varsigma), \Psi(\omega)) \leq \widehat{\varphi}\left(\mathscr{G}^p_{(\Upsilon,\Psi)}(\varsigma, \omega)\right), \tag{50}$$

where $\widehat{\varphi} \in \Omega$, $p \geq 0$, $a_i \geq 0$, $i = 1, 2, 3, 4$ with $\sum_{i=1}^4 a_i = 1$ and

$$\mathscr{G}^{p}_{(\Upsilon,\Psi)}(\varsigma,\omega)=\begin{cases}\left[a_1(\widehat{\mu}(\varsigma,\omega))^p+a_2(p(\varsigma,\Upsilon(\varsigma)))^p+a_3(p(\omega,\Psi(\omega)))^p+a_4\left(\dfrac{p(\omega,\Upsilon(\varsigma))+p(\varsigma,\Psi(\omega))}{2\widehat{\eta}}\right)^p\right]^{1/p}, & \text{for } p>0,\ \varsigma,\omega\in\overline{\sigma},\\ (p(\varsigma,\omega))^{a_1}(p(\varsigma,\Upsilon(\varsigma)))^{a_2}(p(\omega,\Psi(\omega)))^{a_3}\left(\dfrac{p(\varsigma,\Psi(\omega))+p(\omega,\Upsilon(\varsigma))}{2\widehat{\eta}}\right)^{a_4}, & \text{for } p=0,\varsigma,\omega\in\overline{\sigma}\setminus\mathscr{F}^{*}_{i.x}(\Upsilon,\Psi),\end{cases}\tag{51}$$

where

$$\mathscr{F}^{*}_{i.x}(\Upsilon,\Psi)=\{\varsigma,\omega\in\overline{\sigma}:\{\varsigma\}\subset\Upsilon(\varsigma),\{\omega\}\subset\Psi(\omega)\}.\tag{52}$$

Then, we can find $u\in\overline{\sigma}$ *such that* $\{u\}\subset\Upsilon(u)\cap\Psi(u)$.

Proof. Choose $\varsigma\in\overline{\sigma}$. For each $\varsigma\in\overline{\sigma}$, define two functions $\breve{\alpha}_{\Upsilon},\beta_{\Psi}:\overline{\sigma}\longrightarrow[0,1]$ by $\breve{\alpha}_{\Upsilon}(\varsigma):=\breve{\alpha}(\varsigma)=1$ and $\beta_{\Psi}(\varsigma):=\beta(\varsigma)=0$. Then, by hypothesis, $[\Upsilon\varsigma]_{(1,0)}$ and $[\Psi\varsigma]_{(1,0)}$ are nonempty bounded proximal subsets of $\overline{\sigma}$. Now, for all $\varsigma,\omega\in\overline{\sigma}$,

$$\begin{aligned}D_{(1,0)}(\Upsilon(\varsigma),\Psi(\omega))&\le\widehat{\mu}_{(\infty,\infty)}(\Upsilon(\varsigma),\Psi(\omega))\\&\le\widehat{\varphi}\left(\mathscr{G}^{p}_{(\Upsilon,\Psi)}(\varsigma,\omega)\right).\end{aligned}\tag{53}$$

Since $[\Upsilon\varsigma]_{(1,0)_{\Upsilon(\varsigma)}}\subseteq[\Upsilon\varsigma]_{(\breve{\alpha},\breve{\beta})_{\Upsilon(\varsigma)}}\in\mathscr{P}^{r}_{b}(\overline{\sigma})$ for each $(\breve{\alpha},\breve{\beta})_{\Upsilon(\varsigma)}\in(0,1]\times t[0,1)$, then $\widehat{\mu}(\varsigma,[\Upsilon\varsigma]_{(\breve{\alpha},\breve{\beta})_{\Upsilon(\varsigma)}})\le\widehat{\mu}(\varsigma,[\Upsilon\varsigma]_{(1,0)_{\Upsilon(\varsigma)}})$ for each $(\breve{\alpha},\breve{\beta})_{\Upsilon(\varsigma)}\in(0,1]\times t[0,1)$. So, $p(\varsigma,\Upsilon(\varsigma))\le\widehat{\mu}(\varsigma,[\Upsilon\varsigma]_{(1,0)_{\Upsilon(\varsigma)}})$. This further implies that we can find $(\breve{\alpha},\breve{\beta})_{\Upsilon(\varsigma)},(\breve{\alpha},\breve{\beta})_{\Psi(\omega)}\in(0,1]\times t[0,1)$ for each $\varsigma,\omega\in\overline{\sigma}$:

$$\begin{aligned}&\aleph\left([\Upsilon\varsigma]_{(1,0)_{\Upsilon(\varsigma)}},[\Psi\omega]_{(1,0)_{\Psi(\omega)}}\right)\\&\le\widehat{\varphi}\left(\mathscr{C}^{p}_{(\Upsilon,\Psi)}\left(\varsigma,\omega,(1,0)_{\Upsilon(\varsigma)},(1,0)_{\Psi(\omega)}\right)\right).\end{aligned}\tag{54}$$

Hence, Theorem 1 can be applied to find $u\in\overline{\sigma}$ such that $u\in[\Upsilon u]_{(1,0)_{\Upsilon(u)}}\cap[\Psi u]_{(1,0)_{\Psi(u)}}$. □

Remark 3. By putting $\widehat{\eta}=1$, $p=1$ and $h=1-\widehat{\mu}_{\Upsilon}-\nu_{\Psi}=0$, Theorem 2 can be applied to deduce the main results of [27], Theorems 10 and 11] as special cases. Also, Theorem 2 is a proper extension of the results of [28, 29] and some references therein.

The following example is constructed to verify the hypotheses of Theorem 1.

Example 2. Let $\overline{\sigma}=[0,\infty)$ and $\widehat{\mu}(\varsigma,\omega)=|\varsigma-\omega|^2$ for all $\varsigma,\omega\in\overline{\sigma}$. Then, $(\overline{\sigma},\widehat{\mu},\widehat{\eta}=2)$ is a complete b-metric space. Note that $(\overline{\sigma},\widehat{\mu},\widehat{\eta}=2)$ is not a metric space, since for $\varsigma=1$, $\omega=4$ and $\xi=2$,

$$\widehat{\mu}(\varsigma,\omega)=9>5=\widehat{\mu}(\varsigma,\xi)+\widehat{\mu}(\xi,\omega).\tag{55}$$

Take $\gamma,\lambda\in(0,1]$. Then, for each $\varsigma\in\overline{\sigma}$, consider two intuitionistic fuzzy set-valued maps $\Upsilon,\Psi:\overline{\sigma}\longrightarrow(IFS)^{\overline{\sigma}}$ defined as follows:

If $\varsigma=0$,

$$\widehat{\mu}_{\Upsilon(\varsigma)}(t)=\widehat{\mu}_{\Psi(\varsigma)}(t)=\begin{cases}\dfrac{\gamma}{6}, & \text{if } t=0,\\ 0, & \text{if } t\neq0.\end{cases}\qquad \nu_{\Upsilon(\varsigma)}(t)=\nu_{\Psi(\varsigma)}(t)=\begin{cases}0, & \text{if } t=0,\\ \dfrac{\lambda}{2}, & \text{if } t\neq0.\end{cases}\tag{56}$$

If $\varsigma\in(0,1]$,

$$\widehat{\mu}_{\Upsilon(\varsigma)}(t)=\begin{cases}\dfrac{\gamma}{4}, & \text{if } 0\le t\le\varsigma-\dfrac{\varsigma^2}{40},\\ \dfrac{\gamma}{6}, & \text{if } \varsigma-\dfrac{\varsigma^2}{40}<t\le\varsigma-\dfrac{\varsigma^2}{12},\\ 0, & \text{if } \varsigma-\dfrac{\varsigma^2}{12}<t<\infty,\end{cases}\qquad \nu_{\Upsilon(\varsigma)}(t)=\begin{cases}0, & \text{if } 0\le t\le\varsigma-\dfrac{\varsigma^2}{100},\\ \dfrac{\lambda}{4}, & \text{if } \varsigma-\dfrac{\varsigma^2}{100}<t\le\varsigma-\dfrac{\varsigma^2}{12}\\ \lambda, & \text{if } \varsigma-\dfrac{\varsigma^2}{12}<t<\infty,\end{cases}\tag{57}$$

$$\widehat{\mu}_{\Psi(\varsigma)}(t)=\begin{cases}\dfrac{\gamma}{3}, & \text{if } 0\le t\le\varsigma-\dfrac{\varsigma^2}{50},\\ \dfrac{\gamma}{6}, & \text{if } \varsigma-\dfrac{\varsigma^2}{50}<t\le\varsigma-\dfrac{\varsigma^2}{12},\\ 0, & \text{if } \varsigma-\dfrac{\varsigma^2}{12}<t<\infty,\end{cases}\qquad \nu_{\Psi(\varsigma)}(t)=\begin{cases}0, & \text{if } 0\le t\le\varsigma-\dfrac{\varsigma^2}{70},\\ \dfrac{\lambda}{4}, & \text{if } \varsigma-\dfrac{\varsigma^2}{70}<t\le\varsigma-\dfrac{\varsigma^2}{12},\\ \dfrac{\lambda}{2}, & \text{if } \varsigma-\dfrac{\varsigma^2}{12}<t<\infty.\end{cases}\tag{58}$$

If $\varsigma>1$,

$$\widehat{\mu}_{\Upsilon(\varsigma)}(t) = \widehat{\mu}_{\Psi(\varsigma)}(t) = \begin{cases} \frac{\gamma}{6}, & \text{if } 0 \le t \le 9, \\ 0, & \text{if } t > 9, \end{cases} \tag{59}$$

$$\nu_{\Upsilon(\varsigma)}(t) = \nu_{\Psi(\varsigma)}(t) = \begin{cases} 0, & \text{if } 0 \le t \le 9, \\ \lambda, & \text{if } t > 9. \end{cases} \tag{60}$$

Define the function $\widehat{\varphi}$: $\mathbb{R}_+ \longrightarrow \mathbb{R}_+$ by

$$\widehat{\varphi}(t) = \begin{cases} t - \frac{t^2}{12}, & \text{if } 0 \le t \le 1, \\ \frac{1}{12}, & \text{if } t > 1. \end{cases} \tag{61}$$

Obviously, $\widehat{\varphi}(t) < t$ for all $t > 0$. Suppose that $(\breve{\alpha}, \breve{\beta}) = (\gamma/6, \lambda/4)$. Then, clearly, we can find $(\breve{\alpha}, \breve{\beta})_{\Upsilon(\varsigma)}$, $(\breve{\alpha}, \breve{\beta})_{\Psi(\varsigma)} \in (0,1] \times t[0,1)$ such that $[\Upsilon\varsigma]_{(\breve{\alpha},\breve{\beta})_{\Upsilon(\varsigma)}}$ and $[\Psi\varsigma]_{(\breve{\alpha},\breve{\beta})_{\Psi(\varsigma)}}$ are nonempty bounded proximal subsets of $\overline{\sigma}$ for each $\varsigma \in \overline{\sigma}$. Now, to check the inequality 3.1, consider the following possibilities:

Case 1. If $\varsigma = \omega = 0$, $p = 0$, then for all $a_i \ge 0$ $(i = 1,2,3,4)$, we have $[\Upsilon\varsigma]_{(\gamma/6,\lambda/4)_{\Upsilon(\varsigma)}} = [\Psi\omega]_{(\gamma/6,\lambda/4)_{\Psi(\varsigma)}}$ and hence,

$$\begin{aligned} &\aleph\left([\Upsilon\varsigma]_{(\gamma/6,\lambda/4)_{\Upsilon(\varsigma)}}, [\Psi\omega]_{(\gamma/6,\lambda/4)_{\Psi(\varsigma)}}\right) \\ &\quad = 0 \le \widehat{\varphi}\left(\mathscr{C}^p_{(\Upsilon,\Psi)}\left(\varsigma, \omega, (\breve{\alpha}, \breve{\beta})_{\Upsilon(\varsigma)}, (\breve{\alpha}, \breve{\beta})_{\Psi(\varsigma)}\right)\right). \end{aligned} \tag{62}$$

Case 2. If $\varsigma = 0, \omega \in (0,1]$, $p = 1$, $a_1 = 1$ and $a_2 = a_3 = a_4 = 0$, we have

$$[\Upsilon 0]_{(\gamma/6,\lambda/4)_{\Upsilon(0)}} = \{0\}, [\Psi\omega]_{(\gamma/6,\lambda/4)_{\Psi(\varsigma)}} = \left[0, \omega - \frac{\omega^2}{12}\right]. \tag{63}$$

Thus,

$$\begin{aligned} &\aleph\left([\Upsilon 0]_{(\gamma/6,\lambda/4)_{\Upsilon(0)}}, [\Psi\omega]_{(\gamma/6,\lambda/4)_{\Psi(\varsigma)}}\right) \\ &\quad = \left|\omega - \frac{\omega^2}{12}\right|^2 \\ &\quad = \widehat{\varphi}\left(|\omega - 0|^2\right) \\ &\quad \le \widehat{\varphi}\left(\mathscr{C}^p_{(\Upsilon,\Psi)}\left(\varsigma, \omega, \left(\frac{\gamma}{6}, \frac{\lambda}{4}\right)_{\Upsilon(\varsigma)}, \left(\frac{\gamma}{6}, \frac{\lambda}{4}\right)_{\Psi(\omega)}\right)\right). \end{aligned} \tag{64}$$

Note that, if $\omega = 0, \varsigma \in (0,1]$, $p = 1$, $a_1 = 1$ and $a_2 = a_3 = a_4 = 0$, we obtain same conclusion as in Case 2.

Case 3. If $\varsigma, \omega \in (0,1]$, $p = 1$, $a_1 = 1$ and $a_2 = a_3 = a_4 = 0$, we have

$$\begin{aligned} &\aleph\left([\Upsilon\varsigma]_{(\gamma/6,\lambda/4)_{\Upsilon(\varsigma)}}, [\Psi\omega]_{(\gamma/6,\lambda/4)_{\Psi(\varsigma)}}\right) \\ &\quad = \aleph\left(\left[0, \varsigma - \frac{\varsigma^2}{12}\right], \left[0, \omega - \frac{\omega^2}{12}\right]\right) \\ &\quad = \left|\varsigma - \frac{\varsigma^2}{12} - \omega + \frac{\omega^2}{12}\right|^2 \\ &\quad = \left|(\varsigma - \omega) - \frac{1}{12}\left(\varsigma^2 - \omega^2\right)\right|^2 \\ &\quad = \left|(\varsigma - \omega)\left(1 - \frac{|\varsigma + \omega|}{12}\right)\right|^2 \\ &\quad \le \varsigma - \omega\left|\left(1 - \frac{|\varsigma + \omega|}{12}\right)\right|^2 \\ &\quad = \varsigma - \omega\left|-\frac{|\varsigma + \omega|}{12}\right|^2 \\ &\quad = \widehat{\varphi}\left(|\varsigma - \omega|^2\right) \\ &\quad \le \widehat{\varphi}\left(\mathscr{C}^p_{(\Upsilon,\Psi)}\left(\varsigma, \omega, \left(\frac{\gamma}{6}, \frac{\lambda}{4}\right)_{\Upsilon(\varsigma)}, \left(\frac{\gamma}{6}, \frac{\lambda}{4}\right)_{\Psi(\omega)}\right)\right). \end{aligned} \tag{65}$$

Case 4. If $\varsigma, \omega \in (1, \infty)$, then for all $a_i \ge 0$ $(i = 1,2,3,4)$, $p > 0$, we get $[\Upsilon\varsigma]_{(\gamma/6,\lambda/4)_{\Upsilon(\varsigma)}} = [\Psi\omega]_{(\gamma/6,\lambda/4)_{\Psi(\varsigma)}}$ and

$$\begin{aligned} &\aleph\left([\Upsilon\varsigma]_{(\gamma/6,\lambda/4)_{\Upsilon(\varsigma)}}, [\Psi\omega]_{(\gamma/6,\lambda/4)_{\Psi(\varsigma)}}\right) \\ &\quad = 0 \le \widehat{\varphi}\left(\mathscr{C}^p_{(\Upsilon,\Psi)}\left(\varsigma, \omega, \left(\frac{\gamma}{6}, \frac{\lambda}{4}\right)_{\Upsilon(\varsigma)}, \left(\frac{\gamma}{6}, \frac{\lambda}{4}\right)_{\Psi(\omega)}\right)\right). \end{aligned} \tag{66}$$

Thus, all the assumptions of Theorem 1 are obeyed. It follows that Υ and Ψ have a common intuitionistic fuzzy Fp in $\overline{\sigma}$.

In what follows, we discuss further consequences of our main results.

Corollary 1. *Let $(\overline{\sigma}, \widehat{\mu}, \widehat{\eta})$ be a complete b-metric space and Υ: $\overline{\sigma} \longrightarrow (IFS)^{\overline{\sigma}}$ be an intuitionistic fuzzy set-valued map. Suppose that for each $\varsigma \in \overline{\sigma}$, we can find an $(\breve{\alpha}, \breve{\beta})_{\Upsilon(\varsigma)} \in (0,1] \times t[0,1)$ such that $[\Upsilon\varsigma]_{(\breve{\alpha},\breve{\beta})_{\Upsilon(\varsigma)}}$ is a nonempty bounded proximal subsets of $\overline{\sigma}$. If*

$$\aleph\left([\Upsilon\varsigma]_{(\breve{\alpha},\breve{\beta})_{\Upsilon(\varsigma)}}, [\Upsilon\omega]_{(\breve{\alpha},\breve{\beta})_{\Upsilon(\omega)}}\right) \le \widehat{\varphi}\left(\frac{1}{4}\mathscr{C}^p_{(\Upsilon)}(\varsigma, \omega)\right), \tag{67}$$

for all $\varsigma, \omega \in \overline{\sigma}$, where $\widehat{\varphi} \in \Omega$ and

$$\begin{aligned} \mathscr{C}^p_{(\Upsilon)} = {} & \widehat{\mu}(\varsigma, \omega) + \widehat{\mu}\left(\varsigma, [\Upsilon\varsigma]_{(\breve{\alpha},\breve{\beta})_{\Upsilon(\varsigma)}}\right) + \widehat{\mu}\left(\omega, [\Upsilon\omega]_{(\breve{\alpha},\breve{\beta})_{\Upsilon(\omega)}}\right) \\ & + \frac{\widehat{\mu}\left(\omega, [\Upsilon\varsigma]_{(\breve{\alpha},\breve{\beta})_{\Upsilon(\varsigma)}}\right) + \widehat{\mu}\left(\varsigma, [\Upsilon\omega]_{(\breve{\alpha},\breve{\beta})_{\Upsilon(\omega)}}\right)}{2\widehat{\eta}}. \end{aligned} \tag{68}$$

then, we can find $u \in \overline{\sigma}$ such that $u \in [\Upsilon u]_{(\breve{\alpha},\breve{\beta})_{\Upsilon(u)}}$.

Proof. Put $\Upsilon = \Psi$, $p = 1$ and $a_1 = a_2 = a_3 = a_4 = 1/4$ in Theorem 1. □

Corollary 2. *Let $(\overline{\sigma}, \widehat{\mu}, \widehat{\eta})$ be a complete b-metric space and $\Upsilon, \Psi: \overline{\sigma} \longrightarrow (IFS)^{\overline{\sigma}}$ be intuitionistic fuzzy set-valued maps. Suppose that for each $\varsigma, \omega \in \overline{\sigma}$, we can find $(\breve{\alpha}, \breve{\beta})_{\Upsilon(\varsigma)}$, $(\breve{\alpha}, \breve{\beta})_{\Psi(\omega)} \in (0,1] \times t[0,1)$ such that $[\Upsilon\varsigma]_{(\breve{\alpha},\breve{\beta})_{\Upsilon(\varsigma)}}$ and $[\Psi\omega]_{(\breve{\alpha},\breve{\beta})_{\Psi(\omega)}}$ are nonempty bounded proximal subsets of $\overline{\sigma}$. If we can find $\lambda \in [0,1)$:*

$$\aleph\left([\Upsilon\varsigma]_{(\breve{\alpha},\breve{\beta})_{\Upsilon(\varsigma)}}, [\Psi\omega]_{(\breve{\alpha},\breve{\beta})_{\Psi(\omega)}}\right) \leq \lambda \cdot \left(\sqrt[4]{\left(\widehat{\mu}(\varsigma,\omega)\widehat{\mu}\left(\varsigma, [\Upsilon\varsigma]_{(\breve{\alpha},t\breve{\beta})_{\Upsilon(\varsigma)}}\right)\widehat{\mu}\left(\omega, [\Psi\omega]_{(\breve{\alpha},t\breve{\beta})_{\Psi(\omega)}}\right)\right)\left(\frac{\widehat{\mu}\left(\varsigma, [\Psi\omega]_{(\breve{\alpha},t\breve{\beta})_{\Psi(\omega)}}\right) + \widehat{\mu}\left(\omega, [\Psi\omega]_{(\breve{\alpha},t\breve{\beta})_{\Psi(\omega)}}\right)}{2\widehat{\eta}}\right)}\right), \tag{69}$$

then Υ and Ψ have a common intuitionistic fuzzy Fp in $\overline{\sigma}$.

Proof. Take $a_1 = a_2 = a_3 = a_4 = 1/4$, $\widehat{\varphi}(t) = \lambda t$ for all $t \geq 0$ and $p = 0$ in Theorem 1. □

Corollary 3. *Let $(\overline{\sigma}, \widehat{\mu}, \widehat{\eta})$ be a complete b-metric space and $\Upsilon, \Psi: \overline{\sigma} \longrightarrow (IFS)^{\overline{\sigma}}$ be intuitionistic fuzzy set-valued maps. Suppose that for each $\varsigma, \omega \in \overline{\sigma}$, we can find $(\breve{\alpha}, \breve{\beta})_{\Upsilon(\varsigma)}$, $(\breve{\alpha}, \breve{\beta})_{\Psi(\omega)} \in (0,1] \times t[0,1)$ such that $[\Upsilon\varsigma]_{(\breve{\alpha},\breve{\beta})_{\Upsilon(\varsigma)}}$ and $[\Psi\omega]_{(\breve{\alpha},\breve{\beta})_{\Psi(\omega)}}$ are nonempty bounded proximal subsets of $\overline{\sigma}$. If*

$$\aleph\left([\Upsilon\varsigma]_{(\breve{\alpha},\breve{\beta})_{\Upsilon(\varsigma)}}, [\Psi\omega]_{(\breve{\alpha},\breve{\beta})_{\Psi(\omega)}}\right) \leq \widehat{\varphi}\left(\max\left\{\begin{array}{l}\widehat{\mu}(\varsigma,\omega), \widehat{\mu}\left(\varsigma, [\Upsilon\varsigma]_{(\breve{\alpha},\breve{\beta})_{\Upsilon(\varsigma)}}\right), \widehat{\mu}\left(\omega, [\Psi\omega]_{(\breve{\alpha},\breve{\beta})_{\Psi(\omega)}}\right) \\ \\ \frac{1}{2}\left[\widehat{\mu}\left(\varsigma, [\Psi\omega]_{(\breve{\alpha},\breve{\beta})_{\Psi(\omega)}}\right) + \widehat{\mu}\left(\omega, [\Upsilon\varsigma]_{(\breve{\alpha},\breve{\beta})_{\Upsilon(\varsigma)}}\right)\right]\end{array}\right\}\right), \tag{70}$$

then, we can find $u \in \overline{\sigma}$ such that $u \in [\Upsilon\varsigma]_{(\breve{\alpha},\breve{\beta})_{\Upsilon(\varsigma)}} \cap [\Psi\omega]_{(\breve{\alpha},\breve{\beta})_{\Psi(\omega)}}$.

Corollary 4. *(Nadler-type (see [4])) Let $(\overline{\sigma}, \widehat{\mu}, \widehat{\eta})$ be a complete b-metric space and $\Upsilon: \overline{\sigma} \longrightarrow (IFS)^{\overline{\sigma}}$ be an intuitionistic fuzzy set-valued map. Suppose that for each $\varsigma \in \overline{\sigma}$, we can find $(\breve{\alpha}, \breve{\beta})_{\Upsilon(\varsigma)}$ such that $[\Upsilon\varsigma]_{(\breve{\alpha},\breve{\beta})_{\Upsilon(\varsigma)}}$ is a nonempty bounded proximal subsets of $\overline{\sigma}$. If there exists $\lambda \in [0,1)$:*

$$\aleph\left([\Upsilon\varsigma]_{(\breve{\alpha},\breve{\beta})_{\Upsilon(\varsigma)}}, [\Upsilon\omega]_{(\breve{\alpha},\breve{\beta})_{\Upsilon(\varsigma)}}\right) \leq \lambda\widehat{\mu}(\varsigma,\omega), \tag{71}$$

then, we can find $u \in \overline{\sigma}$ such that $u \in [\Upsilon\varsigma]_{(\breve{\alpha},\breve{\beta})_{\Upsilon(\varsigma)}}$.

Proof. Put $\Upsilon = \Psi$, $a_1 = p = 1$, $a_2 = a_3 = a_4 = 0$ and $\widehat{\varphi}(t) = \lambda t$, $t \geq 0$ in Theorem 1. □

Consistent with the proof of Theorem 2, the next result can easily be obtained by applying Corollary 4.

Corollary 5. *(Heilpern-type* (see [3])) *Let $(\overline{\sigma}, \widehat{\mu}, \widehat{\eta})$ be a complete b-metric space and $\Upsilon: \overline{\sigma} \longrightarrow \mathscr{K}_{\mathcal{IFS}}(\overline{\sigma})$ be an intuitinoistic fuzzy set-valued map. Suppose that for each $\varsigma, \omega \in \overline{\sigma}$, we can find $\lambda \in [0,1)$:*

$$\widehat{\mu}_{(\infty,\infty)}(\Upsilon(\varsigma), \Upsilon(\omega)) \leq \lambda\widehat{\mu}(\varsigma,\omega). \tag{72}$$

Then, we can find $u \in \overline{\sigma}$ such that $\{u\} \subset \Upsilon(u)$.

4. Applications to Multivalued and Single-Valued Mappings

In this section, we apply some results from previous the section to deduce their corresponding crisp Fp results of multivalued and single-valued mappings.

Corollary 6. *Let $(\overline{\sigma}, \widehat{\mu}, \widehat{\eta})$ be a complete b-metric space and $\Theta, \Lambda: \overline{\sigma} \longrightarrow \mathscr{K}(\overline{\sigma})$ be multivalued mappings. If for all $\varsigma, \omega \in \overline{\sigma}$,*

$$\aleph(\Theta\varsigma, \Lambda\omega) \leq \widehat{\varphi}\left(\max\left\{\begin{array}{l}\widehat{\mu}(\varsigma,\omega), \widehat{\mu}(\varsigma,\Theta\varsigma), \widehat{\mu}(\omega,\Lambda\omega), \\ \\ \frac{1}{2}[\widehat{\mu}(\varsigma,\Lambda\omega) + \widehat{\mu}(\omega,\Theta\varsigma)]\end{array}\right\}\right), \tag{73}$$

then, we can find $u \in \overline{\sigma}$ such that $u \in \Theta u \cap \Lambda u$.

Proof. Consider the intuitionistic fuzzy set-valued maps $\Upsilon, \Psi: \overline{\sigma} \longrightarrow (IFS)^{\overline{\sigma}}$ defined by

$$\widehat{\mu}_{\Upsilon(\varsigma)}(t)=\begin{cases}1, & \text{if } t\in\Theta\varsigma,\\ 0, & \text{if } t\notin\Theta\varsigma,\end{cases}\quad \nu_{\Upsilon(\varsigma)}(t)=\begin{cases}0, & \text{if } t\in\Theta\varsigma,\\ 1, & \text{if } t\notin\Theta\varsigma.\end{cases}\tag{74}$$

and

$$\widehat{\mu}_{\Psi(\varsigma)}(t)=\begin{cases}1, & \text{if } t\in\Lambda\varsigma,\\ 0, & \text{if } t\notin\Lambda\varsigma,\end{cases}\quad \nu_{\Psi(\varsigma)}(t)=\begin{cases}0, & \text{if } t\in\Lambda\varsigma,\\ 1, & \text{if } t\notin\Lambda\varsigma.\end{cases}\tag{75}$$

Take $(\breve{\alpha},\breve{\beta})=(1,0)$. Then $[\Upsilon\varsigma]_{(1,0)_{\Upsilon(u)}}=\Theta\varsigma$ and $[\Psi\varsigma]_{(1,0)_{\Psi(u)}}=\Lambda\varsigma$ for each $\varsigma\in\overline{\sigma}$. Whence, Corollary 3.10 can be applied to find a point $u\in\overline{\sigma}$ such that $u\in[\Upsilon u]_{(1,0)_{\Upsilon(u)}}\cap[\Psi u]_{(1,0)_{\Psi(u)}}=\Theta u\cap\Lambda u$. □

Following the Proof of Corollary 6, we can easily derive the next result by applying Corollary 1.

Corollary 7. *[30] Let $(\overline{\sigma},\widehat{\mu},\widehat{\eta})$ be a complete b-metric space and $\Theta\colon\overline{\sigma}\longrightarrow\mathscr{P}_b^r(\overline{\sigma})$ be a multivalued mapping:*

$$\aleph(\Theta\varsigma,\Theta\omega)\le\widehat{\varphi}\left(\frac{1}{4}\mathscr{C}_{(\Theta)}^p(\varsigma,\omega)\right),\tag{76}$$

for all $\varsigma,\omega\in\overline{\sigma}$, where $\widehat{\varphi}\in\Omega$ and

$$\mathscr{C}_{(\Theta)}^p=\widehat{\mu}(\varsigma,\omega)+\widehat{\mu}(\varsigma,\Theta\varsigma)+\widehat{\mu}(\omega,\Theta\omega)+\frac{\widehat{\mu}(\omega,\Theta\varsigma)+\widehat{\mu}(\varsigma,\Theta\omega)}{2\widehat{\eta}}.\tag{77}$$

Then, we can find $u\in\overline{\sigma}$ such that $u\in\Upsilon u$.

Corollary 8. *[22], Theorem 1] Let $(\overline{\sigma},\widehat{\mu},\widehat{\eta})$ be a complete b-metric space and $g\colon\overline{\sigma}\longrightarrow\overline{\sigma}$ be a single-valued mapping. If*

$$\widehat{\mu}(g\varsigma,g\omega)\le\widehat{\varphi}\left(\mathscr{C}_g^p(\varsigma,\omega)\right)\tag{78}$$

for all $\varsigma,\omega\in\overline{\sigma}$, where $\widehat{\varphi}\in\Omega$, $p\ge0$, $a_i\ge0$, $i=1,2,3,4$ with $\sum_{i=1}^4 a_i=1$ and

$$\mathscr{C}_g^p(\varsigma,\omega)=\begin{cases}\left[a_1(\widehat{\mu}(\varsigma,\omega))^p+a_2(\widehat{\mu}(\varsigma,g\varsigma))^p+a_3(\widehat{\mu}(\omega,g\omega))^p+a_4\left(\dfrac{\widehat{\mu}(\omega,g\varsigma)+\widehat{\mu}(\varsigma,g\omega)}{2\widehat{\eta}}\right)^p\right]^{1/p}, & \text{for } p>0,\ \varsigma,\omega\in\overline{\sigma}\\ (\widehat{\mu}(\varsigma,\omega))^{a_1}(\widehat{\mu}(\varsigma,g\varsigma))^{a_2}(\widehat{\mu}(\omega,g\omega))^{a_3}\left(\dfrac{\widehat{\mu}(\varsigma,g\omega)+\widehat{\mu}(\omega,g\varsigma)}{2\widehat{\eta}}\right)^{a_4}, & \text{for } p=0,\varsigma,\omega\in\overline{\sigma}\setminus\mathscr{F}_{ix}(g).\end{cases}\tag{79}$$

where

$$\mathscr{F}_{ix}(g)=\{\varsigma\in\overline{\sigma}\colon\varsigma=g\varsigma\}.\tag{80}$$

Then, we can find $u\in\overline{\sigma}$ such that $u=gu$.

Proof. Consider an intuitionistic fuzzy set-valued map $\Upsilon\colon\overline{\sigma}\longrightarrow(IFS)^{\overline{\sigma}}$ defined by

$$\widehat{\mu}_{\Upsilon(\varsigma)}(t)=\begin{cases}1, & \text{if } t\in\Theta\varsigma,\\ 0, & \text{if } t\notin\Theta\varsigma,\end{cases}\quad \nu_{\Upsilon(\varsigma)}(t)=\begin{cases}0, & \text{if } t=g\varsigma,\\ 1, & \text{if } t\ne g\varsigma.\end{cases}\tag{81}$$

Put $(\breve{\alpha},\breve{\beta})=(1,0)$. Then $[\Upsilon\varsigma]_{(1,0)_{\Upsilon(u)}}=\{g\varsigma\}$. Obviously, $\{g\varsigma\}\in\mathscr{P}_b^r(\overline{\sigma})$, for each $\varsigma\in\overline{\sigma}$. Notice that in this case, for all $\varsigma,\omega\in\overline{\sigma}$,

$$\aleph\left([\Upsilon\varsigma]_{(1,0)_{\Upsilon(\varsigma)}},[\Upsilon\omega]_{(1,0)_{\Upsilon(\omega)}}\right)=\widehat{\mu}(g(\varsigma),g(\omega)).\tag{82}$$

Hence, by Theorem 1, we can find $u\in\overline{\sigma}$ such that $u\in[\Upsilon u]_{(1,0)_{\Upsilon(u)}}=\{g(u)\}$; which further implies that $g(u)=u$. □

By using the method of proving Corollary 7, we can deduce the next Fp result due to Czerwik [21] by applying Corollary 5.

(i) For $\widehat{\eta}=1$ and $h=1-\widehat{\mu}_\Upsilon-\nu_\Upsilon=0$ in Corollary 6, we deduce the result of [27], Theorem 7].

(ii) It is clear that if we let $\widehat{\eta}=1$ in all the above-given results, we can deduce their analogues in the setting of metric space. Also, by setting $h=1-\widehat{\mu}_\Upsilon-\nu_\Upsilon=0$ all our main results reduce to their crisp analogues.

Corollary 9 [21]. *Let $(\overline{\sigma},\widehat{\mu},\widehat{\eta})$ be a complete b-metric space and $g\colon\overline{\sigma}\longrightarrow\overline{\sigma}$ be a point-valued mapping. If we can find $\lambda\in(0,1)$ such that for all $\varsigma,\omega\in\overline{\sigma}$,*

$$\widehat{\mu}(g(\varsigma),g(\omega))\le\lambda\widehat{\mu}(\varsigma,\omega)\tag{83}$$

then, there exists $u\in\overline{\sigma}$ such that $g(u)=u$.

Remark 4.

Data Availability

No data were used to support this study.

Conflicts of Interest

The authors declare that they have no conflicts of interest.

Authors' Contributions

Conceptualization was done by M. S. Shagari; Methodology was done by S. Kanwal; Formal analysis was done by A. Azam, H. Aydi; Review and editing was done by A. Azam;

Writing, review, and editing were done by M. S. Shagari. H. Aydi, Y.U. Gaba; Funding was done by Y.U. Gaba.

Acknowledgments

The fifth author (Y. U. G.) would like to acknowledge that this publication was made possible by a grant from Carnegie Corporation of New York (provided through the AIMS - Quantum Leap Africa). The statements made and views expressed are solely the responsibility of the author.

References

[1] K. K. Ali, A. Mukheimer, J. Y. Younis, M. A. Abd El Salam, and H. Aydi, "Spectral collocation approach with shifted Chebyshev sixth-kind series approximation for generalized space fractional partial differential equations," *AIMS Mathematics*, vol. 7, no. 5, pp. 8622–8644, 2022.

[2] L. A. Zadeh, "Fuzzy sets," *Information and Control*, vol. 8, no. 3, pp. 338–353, 1965.

[3] S. Heilpern, "Fuzzy mappings and fixed point theorem," *Journal of Mathematical Analysis and Applications*, vol. 83, no. 2, pp. 566–569, 1981.

[4] S. B. Nadler, "Multi-valued contraction mappings," *Pacific Journal of Mathematics*, vol. 30, no. 2, pp. 475–488, 1969.

[5] A. Georgieva, "Solving two-dimensional nonlinear fuzzy Volterra integral equations by homotopy analysis method," *Demonstratio Mathematica*, vol. 54, no. 1, pp. 11–24, 2021.

[6] B. D. Pant, S. Chauhan, Y. J. Cho, and M. E. Gordji, "Fixed points of weakly compatible mappings in fuzzy metric spaces," *Kuwait Journal of Science*, vol. 42, no. 2, pp. 107–127, 2015.

[7] A. F. Roldan-Lopez-de-Hierro, A. Fulga, E. Karapinar, and N. Shahzad, "Proinov-type fixed-point results in non-Archimedean fuzzy metric spaces," *Mathematics*, vol. 9, no. 14, p. 1594, 2021.

[8] M. Samreen and T. Kamran, "Fixed point theorems for weakly contractive mappings on a metric space endowed with a graph," *Filomat*, vol. 28, no. 3, pp. 441–450, 2014.

[9] J. Wu and H. Yang, "On metrization of the topologies induced by fuzzy metrics," *Journal of Mathematics*, vol. 2020, Article ID 4731357, 5 pages, 2020.

[10] M. Zhou, N. Saleem, X. Liu, A. Fulga, and A. F. Roldan-Lopez-de-Hierro, "A new approach to proinov-type fixed-point results in non-archimedean fuzzy metric spaces," *Mathematics*, vol. 9, no. 23, p. 3001, 2021.

[11] K. T. Atanassov, "Intuitionistic fuzzy sets," *Fuzzy Sets and Systems*, vol. 20, no. 1, pp. 87–96, 1986.

[12] A. Azam, R. Tabassum, and M. Rashid, "Coincidence and fixed point theorems of intuitionistic fuzzy mappings with applications," *Journal of Mathematical Analysis*, vol. 8, no. 4, pp. 56–77, 2017.

[13] A. Azam and R. Tabassum, "Existence of common coincidence point of intuitionistic fuzzy maps," *Journal of Intelligent and Fuzzy Systems*, vol. 35, no. 4, pp. 4795–4805, 2018.

[14] R. Tabassum, M. S. Shagari, A. Azam, O. K. S. K. Mohamed, and A. A. Bakery, "Intuitionistic fuzzy fixed point theorems in complex-valued metric spaces with applications to fractional differential equations," *Journal of Function Spaces*, vol. 2022, p. 17, Article ID 2261199, 2022.

[15] R. Tabassum, A. Azam, and S. S. Mohammed, "Existence results of delay and fractional differential equations via fuzzy weakly contraction mapping principle," *Applied General Topology*, vol. 20, no. 2, pp. 449–469, 2019.

[16] G. J. de Cabral-García, K. Baquero-Mariaca, and J. Villa-Morales, "A fixed point theorem in the space of integrable functions and applications," *Rendiconti del Circolo Matematico di Palermo Series*, vol. 2, pp. 1–18, 2022.

[17] A. J. Gnanaprakasam, S. M. Boulaaras, G. Mani, B. Cherif, and S. A. Idris, "Solving system of linear equations via bicomplex valued metric space," *Demonstratio Mathematica*, vol. 54, no. 1, pp. 474–487, 2021.

[18] K. S. Kim, "Coupled fixed point theorems under new coupled implicit relation in Hilbert spaces," *Demonstratio Mathematica*, vol. 55, no. 1, pp. 81–89, 2022.

[19] A. Kondo, "Ishikawa type mean convergence theorems for finding common fixed points of nonlinear mappings in Hilbert spaces," *Rendiconti del Circolo Matematico di Palermo Series*, vol. 2, pp. 1–19, 2022.

[20] R. Shukla and R. Panicker, "Some fixed point theorems for generalized enriched nonexpansive mappings in Banach spaces," *Rendiconti del Circolo Matematico di Palermo Series*, vol. 2, pp. 1–15, 2022.

[21] S. Czerwik, "Contraction mappings in b-metric spaces," *Acta Mathematica Informatica Universitatis Ostraviensis*, vol. 1, no. 1, pp. 5–11, 1993.

[22] E. Karapinar and A. Fulga, "New hybrid contractions on b-metric spaces," *Mathematics*, vol. 7, no. 7, p. 578, 2019.

[23] M. Boriceanu, "Fixed point theory for multivalued generalized contraction on a set with two b-metrics," *Studia Universitatis Babes-Bolyai, Mathematica*, vol. 4, no. 3, pp. 126–132, 2009.

[24] H. Kaneko and S. Sessa, "Fixed point theorems for compatible multi-valued and single-valued mappings," *International Journal of Mathematics and Mathematical Sciences*, vol. 12, no. 2, pp. 257–262, 1989.

[25] I. A. Rus, "Generalized contractions and applications," *Cluj University Press*, vol. 2, no. 6, pp. 60–71, 2001.

[26] S. L. Singh and B. Prasad, "Some coincidence theorems and stability of iterative procedures," *Computers & Mathematics with Applications*, vol. 55, no. 11, pp. 2512–2520, 2008.

[27] A. Azam, M. Arshad, and P. Vetro, "On a pair of fuzzy $\widehat{\varphi}$-contractive mappings," *Mathematical and Computer Modelling*, vol. 52, no. 1-2, pp. 207–214, 2010.

[28] B. Soo Lee, G. Myung Lee, S. Jin Cho, and D. Sang Kim, "A common fixed point theorem for a pair of fuzzy mappings," *Fuzzy Sets and Systems*, vol. 98, no. 1, pp. 133–136, 1998.

[29] J. Y. Park and J. Ug Jeong, "Fixed point theorems for fuzzy mappings," *Fuzzy Sets and Systems*, vol. 87, no. 1, pp. 111–116, 1997.

[30] M. Alansari, S. S. Mohammed, A. Azam, and N. Hussain, "On multivalued hybrid contractions with applications," *Journal of Function Spaces*, vol. 2020, Article ID 8401403, 13 pages, 2020.

Hindawi
Journal of Mathematics
Volume 2023, Article ID 3359858, 10 pages
https://doi.org/10.1155/2023/3359858

Research Article

Multi-Criteria Decision-Making with Novel Pythagorean Fuzzy Aggregation Operators

Mohammed M. Al-Shamiri,[1,2] **Rashad Ismail**,[1,2] **Saqib Mazher Qurashi**,[3] **Fareeha Dilawar**,[4] **and Faria Ahmed Shami**[5]

[1]*Department of Mathematics, Faculty of Science and Arts Mahayl Assir, King Khalid University, Abha, Saudi Arabia*
[2]*Department of Mathematics and Computer, Faculty of Science, Ibb University, Ibb, Yemen*
[3]*Government College University Faisalabad, Faisalabad, Pakistan*
[4]*Government College Women University Faisalabad, Faisalabad, Pakistan*
[5]*Department of Mathematics, Bangabandhu Sheikh Mujibur Rahman Science and Technology University, Gopalganj, Bangladesh*

Correspondence should be addressed to Saqib Mazher Qurashi; saqibmazhar@gcuf.edu.pk and Faria Ahmed Shami; fariashami@bsmrstu.edu.bd

Received 8 April 2022; Revised 24 May 2022; Accepted 2 June 2022; Published 18 April 2023

Academic Editor: Naeem Jan

Unpredictability and fuzziness coexist in decision-making analysis due to the complexity of the decision-making environment. "Pythagorean fuzzy numbers" (PFNs) outperform "intuitionistic fuzzy numbers" (IFNs) when dealing with unclear data. The "Pythagorean fuzzy set" (PFS) is a useful tool because it removes the restriction that the sum of membership degrees be less than or equal to one by substituting the square sum for the sum of membership degrees. This study proposes two aggregating operators (AOs). The recommended operators outperform the already specified PFN operators. The proposed operator is utilised in the multicriteria decision-making process to identify the best candidate for instruction (MCDM).

1. Introduction

Today's decision-making mechanism is becoming increasingly complicated, rendering it even more challenging for decision-makers to make sound judgments. This is mostly due to the fact that the intelligence acquired has a huge number of discrepancies. The data are given as discrete or interval numbers acquired from the reflecting journals or corresponding centers. Nonetheless, with the rising complexity of everyday activities, it is difficult to pinpoint actual information. In other sense, the major disadvantage of crisp sets is their failure to handle uncertainty. To conclude, if we analyse the recorded data as they are, the computed findings may lead to the conflicting selection. To deal with ambiguities in data, Zadeh [1] proposed a fuzzy set (FS) theory, in which every element is defined by its membership degree (MSD), which ranges from 0 to 1. Later, Atanassov [2] extended the FSs to intuitionistic FSs (IFSs) by combining nonmembership degrees (NMSDs) and MDs in such a way that their sum does not exceed one. The PFS was created by Yager [3–5], in which the squared sum of the MSDs and NMSDs is less than one. The main advantages of such prolonged FSs are that they use MSD and NMSD to express ambiguous information.

Data analysis is critical for making decision in the sectors of organizational, societal, clinical, scientific, cognitive, and machine intelligence. Generally, understanding of the alternate has been viewed as a crisp number or linguist number. Unfortunately, due to its unpredictability, the data cannot simply be pooled. In reality, AOs are crucial in the context of MCDM difficulties, as their primary goal is to agglomerate a bunch of inputs into a single value. The famous "Maclaurin symmetric mean" (MSM) AOs linked to IFSs were introduced by Liu and Qin [6]. Gul [7] pioneered the concept of Fermatean fuzzy SAW, VIKOR, and ARAS, which he applied to the COVID-19 testing laboratory prediction phase. MCDM technique based on fuzzy rough sets was introduced by Ye et al. [8]. Mu et al. [9] constructed power MSM AOs using PFS extension as interval-valued.

Pythagorean probabilistic hesitant fuzzy AOs were proposed by Batool et al. [10]. Peng and Yuan [11] introduced Pythagorean fuzzy averaging AOs, while Rehman et al. [12] proposed geometric AOs. Deli and Çagman [13] proposed intuitionistic fuzzy parameterized soft set.

Wang and Garg [14] proposed the idea of "Archimedean based Pythagorean fuzzy interactive" based operations and AOs with application to MCDM. Wang et al. [15] gave the "PF-interactive Hamacher power" AOs with applications to the assessment of express service quality. Huang et al. [16] initiated the idea of PF-MULTIMOORA approach with applications. Lin et al. [17] and Lin et al. [18] proposed some measures for PFSs. Meng et al. [19] proposed the idea of knowledge diffusion trajectories PFSs. Lin et al. [20] gave the "bibliometric analysis" for the PFSs. Chen et al. [21] proposed the framework of MCDM for the "sustainable building material selection." Using comparable linguistic ELECTRE III, he [22] also established expert knowledge bid assessment for building project selection. Chen et al. [23] presented the novel idea of using online-review analysis to determine passenger requirements and assess the level of customer satisfaction. Wei and Lu [24] gave the idea of "PF-power AOs," Wu and Wei [25] presented the idea of "PF-Hamacher AOs" and Garg [26] proposed "confidence levels based PF AOs" with application.

The remainder of this article will be organised in the following manner. Section 2 discusses several important PFS concepts. Section 3 considers a number of hybrid AOs for PFSs. Section 4 describes a technique for solving MCDM issues with new AOs. Section 5 is a call for details on proposed AOs. Section 6 concludes with some final remarks and future recommendations.

2. Preliminaries

In this part, we will go through the fundamentals of FSs, IFs, and PFS-sets.

Definition 1. [1] Let $\mathfrak{X}^{\Theta}$ be the reference set. A fuzzy set (FS) $\mathfrak{H}$ is

$$\mathfrak{H} = \left\{ < \wp^{\Lambda}, \mu_{\mathfrak{H}}^{\beth}\left(\wp^{\Lambda}\right) > : \wp^{\Lambda} \in \mathfrak{X}^{\Theta} \right\}, \tag{1}$$

where $\mu_{\mathfrak{H}}^{\beth}$: $\mathfrak{X}^{\Theta} \longrightarrow [0,1]$ is the MSD of $\mathfrak{H}$, which assigns a single real value to each alternative in the unit closed interval $[0,1]$.

Definition 2. [2] An intuitionistic fuzzy sets (IFSs) is

$$T = \left\{ < \wp^{\Lambda}, \mu_{T}^{\beth}\left(\wp^{\Lambda}\right), \nu_{T}^{\beth}\left(\wp^{\Lambda}\right) > : \wp^{\Lambda} \in \mathfrak{X}^{\Theta} \right\}, \tag{2}$$

which is represented by MSD $\mu_{T}^{\beth}(\wp^{\Lambda})$: $\mathfrak{X}^{\Theta} \longrightarrow [0,1]$ and N-MSD $\nu_{T}^{\beth}(\wp^{\Lambda})$: $\mathfrak{X}^{\Theta} \longrightarrow [0,1]$ with the constraint $0 \le \mu_{T}^{\beth}(\wp^{\Lambda}) + \nu_{T}^{\beth}(\wp^{\Lambda}) \le 1$, $\forall \wp^{\Lambda} \in \mathfrak{X}^{\Theta}$.

Definition 3. [4] A Pythagorean fuzzy set (PFS) in a universe $\mathfrak{X}^{\Theta}$ is

$$\vartheta^{\aleph} = \left\{ < \wp^{\Lambda}, \mu_{\vartheta^{\aleph}}^{\beth}\left(\wp^{\Lambda}\right), \nu_{\vartheta^{\aleph}}^{\beth}\left(\wp^{\Lambda}\right) > : \wp^{\Lambda} \in \mathfrak{X}^{\Theta} \right\}, \tag{3}$$

where $\mu_{\vartheta^{\aleph}}^{\beth}(\wp^{\Lambda})$: $\mathfrak{X}^{\Theta} \longrightarrow [0,1]$ shows the MSD and $\nu_{\vartheta^{\aleph}}^{\beth}(\wp^{\Lambda})$: $\mathfrak{X}^{\Theta} \longrightarrow [0,1]$ shows the N-MSD of the element $\wp^{\Lambda} \in \mathfrak{X}^{\Theta}$ to the set $\vartheta^{\aleph}$, respectively, with the condition that $0 \le \mu_{\vartheta^{\aleph}}^{\beth}(\wp^{\Lambda})^2 + \nu_{\vartheta^{\aleph}}^{\beth}(\wp^{\Lambda})^2 \le 1$.

A basic element of the form $\left\langle \mu_{\vartheta^{\aleph}}^{\beth}(\wp^{\Lambda}), \nu_{\vartheta^{\aleph}}^{\beth}(\wp^{\Lambda}) \right\rangle$ in a PFS $\vartheta^{\aleph}$ is called "Pythagorean fuzzy number" (PFN). It is denoted by $\vartheta^{\aleph} = \left\langle \mu_{\vartheta^{\aleph}}^{\beth}, \nu_{\vartheta^{\aleph}}^{\beth} \right\rangle$.

2.1. Operational Laws for PFSs

Definition 4. [4] Let $\vartheta_1^{\aleph} = \left\langle \mu_{\vartheta_1^{\aleph}}^{\beth}(\wp^{\Lambda}), \nu_{\vartheta_1^{\aleph}}^{\beth}(\wp^{\Lambda}) \right\rangle$ and $\vartheta_2^{\aleph} = \left\langle \mu_{\vartheta_2^{\aleph}}^{\beth}(\wp^{\Lambda}), \nu_{\vartheta_2^{\aleph}}^{\beth}(\wp^{\Lambda}) \right\rangle$ be PFSs on a $\mathfrak{X}^{\Theta}$. Then,

(1) $\overline{\vartheta_1^{\aleph}} = \left\langle \nu_{\vartheta_1^{\aleph}}^{\beth}(\wp^{\Lambda}), \mu_{\vartheta_1^{\aleph}}^{\beth}(\wp^{\Lambda}) \right\rangle$.

(2) $\vartheta_1^{\aleph} \subseteq \vartheta_2^{\aleph}$ iff $\mu_{\vartheta_1^{\aleph}}^{\beth}(\wp^{\Lambda}) \le \mu_{\vartheta_2^{\aleph}}^{\beth}(\wp^{\Lambda})$ and $\nu_{\vartheta_2^{\aleph}}^{\beth}(\wp^{\Lambda}) \le \nu_{\vartheta_1^{\aleph}}^{\beth}(\wp^{\Lambda})$.

(3) $\vartheta_1^{\aleph} = \vartheta_2^{\aleph}$ iff $\vartheta_1^{\aleph} \subseteq \vartheta_2^{\aleph}$ and $\vartheta_2^{\aleph} \subseteq \vartheta_1^{\aleph}$.

(4) $\vartheta_1^{\aleph} \cup \vartheta_2^{\aleph} = \{\langle \wp^{\Lambda}, ma\wp^{\Lambda} \left\{ \mu_{\vartheta_1^{\aleph}}^{\beth}(\wp^{\Lambda}), \mu_{\vartheta_2^{\aleph}}^{\beth}(\wp^{\Lambda}) \right\}, \min\left\{ \nu_{\vartheta_1^{\aleph}}^{\beth}(\wp^{\Lambda}), \nu_{\vartheta_2^{\aleph}}^{\beth}(\wp^{\Lambda}) \right\} \rangle | \wp^{\Lambda} \in \mathfrak{X}^{\Theta}\}$.

(5) $\vartheta_1^{\aleph} \cap \vartheta_2^{\aleph} = \left\{ \left\langle \wp^{\Lambda}, \min\left\{ \mu_{\vartheta_1^{\aleph}}^{\beth}(\wp^{\Lambda}), \mu_{\vartheta_2^{\aleph}}^{\beth}(\wp^{\Lambda}) \right\}, ma\wp^{\Lambda} \left\{ \nu_{\vartheta_1^{\aleph}}^{\beth}(\wp^{\Lambda}), \nu_{\vartheta_2^{\aleph}}^{\beth}(\wp^{\Lambda}) \right\} \right\rangle | \wp^{\Lambda} \in \mathfrak{X}^{\Theta} \right\}$.

(6) $\vartheta_1^{\aleph} + \vartheta_2^{\aleph} = \left\{ \left\langle \wp^{\Lambda}, \sqrt{(\mu_{\vartheta_1^{\aleph}}^{\beth}(\wp^{\Lambda})^2 + \mu_{\vartheta_2^{\aleph}}^{\beth}} (\wp^{\Lambda})^2 - \mu_{\vartheta_1^{\aleph}}^{\beth}(\wp^{\Lambda})^2 \mu_{\vartheta_2^{\aleph}}^{\beth}(\wp^{\Lambda})^2), \nu_{\vartheta_1^{\aleph}}^{\beth}(\wp^{\Lambda}) \nu_{\vartheta_2^{\aleph}}^{\beth}(\wp^{\Lambda}) \right\rangle | \wp^{\Lambda} \in \mathfrak{X}^{\Theta} \right\}$.

(7) $\vartheta_1^{\aleph} \cdot \vartheta_2^{\aleph} = \left\{ \left\langle \wp^{\Lambda}, (\mu_{\vartheta_1^{\aleph}}(\wp^{\Lambda}) \mu_{\vartheta_2^{\aleph}}^{\beth}(\wp^{\Lambda}), \sqrt{\nu_{\vartheta_1^{\aleph}}^{\beth}(\wp^{\Lambda})^2} + \nu_{\vartheta_2^{\aleph}}^{\beth}(\wp^{\Lambda})^2 - \nu_{\vartheta_1^{\aleph}}^{\beth}(\wp^{\Lambda})^2 \nu_{\vartheta_2^{\aleph}}^{\beth}(\wp^{\Lambda})^2 \right\rangle | \wp^{\Lambda} \in \mathfrak{X}^{\Theta} \right\}$.

(8) $\beth \vartheta_1^{\aleph} = \left\{ \left\langle \wp^{\Lambda}, \sqrt{(1 - (1 - \mu_{\vartheta_1^{\aleph}}^{\beth}(\wp^{\Lambda})^2)^{\beth})}, \nu_{\vartheta_1^{\aleph}}^{\beth}(\wp^{\Lambda})^{\beth} \right\rangle \right\}$.

(9) $\vartheta_1^{\aleph\beth} = \left\{ \left\langle \wp^{\Lambda}, \mu_{\vartheta_1^{\aleph}}^{\beth}(\wp^{\Lambda})^{\beth}, \sqrt{(1 - (1 - \nu_{\vartheta_1^{\aleph}}^{\beth}(\wp^{\Lambda})^2)^{\beth})}, \right\rangle \right\}$.

Theorem 1. *[4] Let* $\mathrm{P}^{\beth}$, $\mathrm{B}^{\beth}$, *and* $\mathrm{C}^{\beth}$ *be any PFSs over the reference set* $\mathfrak{X}^{\Theta}$. *Let* $\widetilde{U}$ *be absolute PFS and* $\widetilde{\varnothing}$ *be the null PFS. Then,*

(i) $\mathrm{P}^{\beth} \cup \mathrm{P}^{\beth} = \mathrm{P}^{\beth}$.

(ii) $\mathrm{P}^{\beth} \cap \mathrm{P}^{\beth} = \mathrm{P}^{\beth}$.

(iii) $(\mathrm{P}^{\beth} \cup \mathrm{B}^{\beth}) \cup \mathrm{C}^{\beth} = \mathrm{P}^{\beth} \cup (\mathrm{B}^{\beth} \cup \mathrm{C}^{\beth})$.

(iv) $(\mathrm{P}^{\beth} \cap \mathrm{B}^{\beth}) \cap \mathrm{C}^{\beth} = \mathrm{P}^{\beth} \cap (\mathrm{B}^{\beth} \cap \mathrm{C}^{\beth})$.

(v) $\mathrm{P}^{\beth} \cup (\mathrm{B}^{\beth} \cap \mathrm{C}^{\beth}) = (\mathrm{P}^{\beth} \cup \mathrm{B}^{\beth}) \cap (\mathrm{P}^{\beth} \cup \mathrm{C}^{\beth})$.

(vi) $\mathrm{P}^{\beth} \cap (\mathrm{B}^{\beth} \cup \mathrm{C}^{\beth}) = (\mathrm{P}^{\beth} \cap \mathrm{B}^{\beth}) \cup (\mathrm{P}^{\beth} \cap \mathrm{C}^{\beth})$.

(vii) $\mathrm{P}^{\beth} \cup \widetilde{\varnothing} = \mathrm{P}^{\beth}$ *and* $\mathrm{P}^{\beth} \cap \widetilde{\varnothing} = \widetilde{\varnothing}$

(viii) $\mathrm{P}^{\beth} \cup \widetilde{U} = \widetilde{U}$ *and* $\mathrm{P}^{\beth} \cap \widetilde{U} = \mathrm{P}^{\beth}$

(ix) $(\mathrm{P}^{\beth c})^{c} = \mathrm{P}^{\beth}$.

(x) $\widetilde{U}^{c} = \widetilde{\varnothing}$ **<i>and** $\widetilde{\varnothing}^{c} = \widetilde{U}$.

Theorem 2. *Let* $\mathrm{P}^{\beth}$ *and* $\mathrm{B}^{\beth}$ *be two PFSs over the reference set* $\mathfrak{X}^{\Theta}$. *Then,*

(a) $(\mathrm{P}^{\beth} \cup \mathrm{B}^{\beth})^{c} = \mathrm{P}^{\beth c} \cap \mathrm{B}^{\beth c}$ *and*

(b) $(\mathrm{P}^{\beth} \cap \mathrm{B}^{\beth})^{c} = \mathrm{P}^{\beth c} \cup \mathrm{B}^{\beth c}$.

2.2. Operational Laws for PFNs

Definition 5. [4] Suppose $\Upsilon_1^\zeta = \langle \mu_1^\lrcorner, \nu_1^\lrcorner \rangle$ and $\Upsilon_2^\zeta = \langle \mu_2^\lrcorner, \nu_2^\lrcorner \rangle$ are the two PFNs. Then,

(1) $\overline{\Upsilon_1^\zeta} = \langle \nu_1^\lrcorner, \mu_1^\lrcorner \rangle$
(2) $\Upsilon_1^\zeta \vee \Upsilon_2^\zeta = \langle \max\{\mu_1^\lrcorner, \nu_1^\lrcorner\}, \min\{\mu_2^\lrcorner, \nu_2^\lrcorner\} \rangle$
(3) $\Upsilon_1^\zeta \wedge \Upsilon_2^\zeta = \langle \min\{\mu_1^\lrcorner, \nu_1^\lrcorner\}, \max\{\mu_2^\lrcorner, \nu_2^\lrcorner\} \rangle$
(4) $\Upsilon_1^\zeta \oplus \Upsilon_2^\zeta = \left\langle \sqrt{\mu_1^{\lrcorner 2} + \mu_2^{\lrcorner 2} - \mu_1^{\lrcorner 2}\mu_2^{\lrcorner 2}}, \nu_1^\lrcorner \nu_2^\lrcorner \right\rangle$
(5) $\Upsilon_1^\zeta \otimes \Upsilon_2^\zeta = \left\langle \mu_1^\lrcorner \mu_2^\lrcorner, \sqrt{\nu_1^{\lrcorner 2} + \nu_2^{\lrcorner 2} - \nu_1^{\lrcorner 2}\nu_2^{\lrcorner 2}} \right\rangle$
(6) $\sqsupset \Upsilon_1^\zeta = \left\langle \sqrt{(1 - (1 - \mu_1^{\lrcorner 2})^{\sqsupset})}, \nu_1^{\lrcorner \sqsupset} \right\rangle$
(7) $\Upsilon_1^{\zeta \Upsilon_1^\zeta} = \left\langle \mu_1^{\lrcorner \sqsupset}, \sqrt{(1 - (1 - \nu_1^{\lrcorner 2})^{\sqsupset})} \right\rangle$

Theorem 3. *[4] Suppose $\Upsilon_1^\zeta = \langle \mu_1^\lrcorner, \nu_1^\lrcorner \rangle$ and $\Upsilon_2^\zeta = \langle \mu_2^\lrcorner, \nu_2^\lrcorner \rangle$ are any PFNs on $a\mathfrak{X}^\Theta$, and $n_1, n_2 > 0$, then*

(1) $\Upsilon_1^\zeta \oplus \Upsilon_2^\zeta = \Upsilon_2^\zeta \oplus \Upsilon_1^\zeta$
(2) $\Upsilon_1^\zeta \otimes \Upsilon_2^\zeta = \Upsilon_2^\zeta \otimes \Upsilon_1^\zeta$
(3) $n(\Upsilon_1^\zeta \oplus \Upsilon_2^\zeta) = n\Upsilon_1^\zeta \oplus n\Upsilon_2^\zeta$
(4) $n_1\Upsilon_1^\zeta \oplus n_2\Upsilon_2^\zeta = (n_1 + n_2)\Upsilon_1^\zeta$
(5) $\Upsilon_1^{\zeta n_1} \otimes \Upsilon_1^{\zeta n_2} = \Upsilon_1^{\zeta n_1 + n_2}$
(6) $\Upsilon_1^{\zeta n} \otimes \Upsilon_1^{\zeta n} = (\Upsilon_1^\zeta \otimes \Upsilon_2^\zeta)^n$

Definition 6. [4] Let $\vartheta^\aleph = \langle \mu^\lrcorner, \nu^\lrcorner \rangle$ be the PFN, then a "score function" (SF) $\widetilde{\neg}$ of $\vartheta^\aleph$ is given as

$$\widetilde{\neg}\left(\vartheta^\aleph\right) = \mu^{\lrcorner 2} - \nu^{\lrcorner 2}. \tag{4}$$

$\widetilde{\neg}(\vartheta^\aleph) \in [-1, 1]$. If the SF is high, the PFN is also significant. Unfortunately, in the many situations of PFN, the SF is ineffective. For example: let $\Upsilon_1^\zeta = \langle 0.6138, 0.2534 \rangle$ and $\Upsilon_2^\zeta = \langle 0.7147, 0.4453 \rangle$ be two PFNs. Then, SF of Υ_1^ζ is $\widetilde{\neg}(\Upsilon_1^\zeta) = 0.3125$ and the SF of Υ_2^ζ is $\widetilde{\neg}(\Upsilon_2^\zeta) = 0.3125$. This demonstrates that the SF is insufficient for comparing the PFNs. We employ another function called the "accuracy function" (AF) to tackle this difficulty.

Definition 7. [4] Let $\vartheta^\aleph = \langle \mu^\lrcorner, \nu^\lrcorner \rangle$ be the PFN. Then, the AF $\coprod$ of $\vartheta^\aleph$ is defined as

$$\coprod\left(\vartheta^\aleph\right) = \mu^{\lrcorner 2} + \nu^{\lrcorner 2}, \tag{5}$$

where $\coprod(\vartheta^\aleph) \in [0, 1]$. If the AF is high, the PFN is also significant.

For example, $\Upsilon_1^\zeta = \langle 0.6138, 0.2534 \rangle$ and $\Upsilon_2^\zeta = \langle 0.7147, 0.4453 \rangle$. The AFs are $\coprod(\Upsilon_1^\zeta) = 0.4410$ and $\coprod(\Upsilon_2^\zeta) = 0.7091$. Thus we can write $\Upsilon_1^\zeta < \Upsilon_2^\zeta$.

Definition 8. [4] Let $s = \langle \mu_s^\lrcorner, \nu_s^\lrcorner \rangle$ and $t = \langle \mu_t^\lrcorner, \nu_t^\lrcorner \rangle$ be any two PFNs. Let $\widetilde{\neg}(s)$, $\widetilde{\neg}(t)$ be the SFs of s and t and $\coprod(s)$, $\coprod(t)$ be the AFs of s and t, respectively. Then,

(1) If $\widetilde{\neg}(s)$, $\widetilde{\neg}(t)$, then $s > t$
(2) If $\widetilde{\neg}(s)$, $\widetilde{\neg}(t)$, then

If $\coprod(s) > \coprod(t)$, then $s > t$,
If $\coprod(s) > \coprod(t)$, then $s = t$.

2.3. Some Basic AOs Related to PFNs

Definition 9. [11] Let $\breve{\Upsilon}_k^\zeta = \left\langle \mu_k^\lrcorner, \nu_k^\lrcorner \right\rangle$ be the conglomeration of PFNs. Define (PFWA): $\mathfrak{X}^{\Theta n} \longrightarrow \mathfrak{X}^\Theta$ given by

$$\begin{aligned}(\text{PFWG})\left(\breve{\Upsilon}_1^\zeta, \breve{\Upsilon}_2^\zeta, \ldots, \breve{\Upsilon}_n^\zeta\right) &= \sum_{k=1}^n \mathfrak{G}_k^\lrcorner \breve{\Upsilon}_k^\zeta \\ &= \mathfrak{G}_1^\lrcorner \breve{\Upsilon}_1^\zeta \otimes \mathfrak{G}_2^\lrcorner \breve{\Upsilon}_2^\zeta \otimes, \ldots, \mathfrak{G}_n^\lrcorner \breve{\Upsilon}_n^\zeta,\end{aligned} \tag{6}$$

where T^n is the set of all PFNs and $\mathfrak{G}^\lrcorner = (\mathfrak{G}_1^\lrcorner, \mathfrak{G}_2^\lrcorner, \ldots, \mathfrak{G}_n^\lrcorner)^T$ is the "weight vector" (WV) of $(\breve{\Upsilon}_1^\zeta, \breve{\Upsilon}_2^\zeta, \ldots, \breve{\Upsilon}_n^\zeta)$, s.t. $0 \le \mathfrak{G}_k^\lrcorner \le 1$, and $\sum_{k=1}^n \mathfrak{G}_k^\lrcorner = 1$. Then, the PFWA is the "Pythagorean fuzzy weighted averaging (PFWA) operator."

We can evaluate PFWA using the operating laws of PFNs, as shown by the preceding theorem.

Theorem 4. *[11] Let $\breve{\Upsilon}_k^\zeta = \left\langle \mu_k^\lrcorner, \nu_k^\lrcorner \right\rangle (k = 1, 2, \ldots, n)$ be the conglomeration of PFNs, we also evaluate the PFWA by*

$$(\text{PFWA})\left(\breve{\Upsilon}_1^\zeta, \breve{\Upsilon}_2^\zeta, \ldots, \breve{\Upsilon}_n^\zeta\right) = \left\langle \sqrt{\left(1 - \prod_{k=1}^n \left(1 - \mu_k^\lrcorner\right)^{\mathfrak{G}_k^\lrcorner}\right)}, \prod_{k=1}^n \nu_k^{\lrcorner \mathfrak{G}_k^\lrcorner} \right\rangle. \tag{7}$$

Example 1. Let $\breve{\Upsilon}_1^\zeta = (0.70, 0.50)$, $\breve{\Upsilon}_2^\zeta = (0.30, 0.50)$, and $\breve{\Upsilon}_3^\zeta = (0.60, 0.70)$ be the three PFNs and $w = (0.30, 0.30, 0.40)$ be the WV of $(\breve{\Upsilon}_1^\zeta, \breve{\Upsilon}_2^\zeta, \breve{\Upsilon}_3^\zeta)$. We use PFWA operator to aggregate the three PFNs by using equation (1):

$$\begin{aligned}(\text{PFWA})\left(\breve{\Upsilon}_1^\zeta, \breve{\Upsilon}_2^\zeta, \breve{\Upsilon}_3^\zeta\right) &= \left\langle \sqrt{\left(1 - \prod_{k=1}^3 \left(1 - \mu_k^\lrcorner\right)^{\mathfrak{G}_k^\lrcorner}\right)}, \prod_{k=1}^3 \nu_k^{\lrcorner \mathfrak{G}_k^\lrcorner} \right\rangle \\ &= (0.591, 0.572).\end{aligned} \tag{8}$$

Definition 10. [12] Let $\breve{\Upsilon}_k^{\zeta} = \langle \mu_k^{\beth}, \nu_k^{\beth} \rangle$ be the conglomeration of PFN, and (PFWG): $\mathfrak{X}^{\Theta n} \longrightarrow \mathfrak{X}^{\Theta}$, if

$$(\text{PFWG})\left(\breve{\Upsilon}\zeta_1 t, n\breve{\Upsilon} q\zeta_2 h, \ldots x, 7\breve{\Upsilon} C\zeta_n\right) = \sum_{k=1}^{n} \breve{\Upsilon}\zeta_k^{\mathfrak{G}_k^{\beth}} = \breve{\Upsilon}\zeta_1^{\mathfrak{G}_1^{\beth}} \otimes \breve{\Upsilon}\zeta_2^{\mathfrak{G}_2^{\beth}} \otimes, \ldots, \breve{\Upsilon}\zeta_n^{\mathfrak{G}_n^{\beth}}, \tag{9}$$

where $\mathfrak{G}^{\beth} = (\mathfrak{G}_1^{\beth}, \mathfrak{G}_2^{\beth}, \ldots, \mathfrak{G}_n^{\beth})^T$ is WV of $(\breve{\Upsilon}_1^{\zeta}, \breve{\Upsilon}_2^{\zeta}, \ldots, \breve{\Upsilon}_n^{\zeta})$, s.t. $0 \le \mathfrak{G}_k^{\beth} \le 1$, and $\sum_{k=1}^{n} \mathfrak{G}_k^{\beth} = 1$. Then, the PFWG is the "Pythagorean fuzzy weighted geometric (PFWG) operator."

We can evaluate PFWG using the operating laws of PFNs, as shown by the preceding theorem.

Theorem 5. *[12] Let $\breve{\Upsilon}_k^{\zeta} = \langle \mu_k^{\beth}, \nu_k^{\beth} \rangle$ be the conglomeration of PFNs, we can find PFWG by*

$$(\text{PFWG})\left(\breve{\Upsilon}_1^{\zeta}, \breve{\Upsilon}_2^{\zeta}, \ldots, \breve{\Upsilon}_n^{\zeta}\right) = \left\langle \prod_{k=1}^{n} \mu_k^{\beth \mathfrak{G}_k^{\beth}}, \left(1 - \prod_{k=1}^{n} \left(1 - \nu_k^{\beth}\right)^{\mathfrak{G}_k^{\beth}}\right)^{1/2} \right\rangle. \tag{10}$$

Example 2. Let $\breve{\Upsilon}_1^{\zeta} = (0.70, 0.50)$, $\breve{\Upsilon}_2^{\zeta} = (0.30, 0.50)$, and $\breve{\Upsilon}_3^{\zeta} = (0.60, 0.70)$ be the three PFNs and $\mathfrak{G}^{\beth} = (0.30, 0.30, 0.40)$ be the WV of $(\breve{\Upsilon}_1^{\zeta}, \breve{\Upsilon}_2^{\zeta}, \breve{\Upsilon}_3^{\zeta})$. We use PFWG operator to aggregate the three PFNs by using equation (2):

$$\begin{aligned}(\text{PFWG})\left(\breve{\Upsilon}_1^{\zeta}, \breve{\Upsilon}_2^{\zeta}, \breve{\Upsilon}_3^{\zeta}\right) &= \left\langle \prod_{k=1}^{3} \mu_k^{\beth \mathfrak{G}_k^{\beth}}, \left(1 - \prod_{k=1}^{3} \left(1 - \nu_k^{\beth q}\right)^{\mathfrak{G}_k^{\beth}}\right)^{1/2} \right\rangle \\ &= (0.510, 0.603).\end{aligned} \tag{11}$$

2.4. Some Deficiencies of PFWA and PFWG Operators. As we all know, PFWA and PFWG operators are utilised to accumulate knowledge in different MCDM issues. Therefore, whenever some values go toward the upper justifications or highest weights, their summed values may imply some absurd results. In this section, we will look at two scenarios.

Case 1. Take two PFNs s.t. $\breve{\Upsilon}_1^{\zeta} = (0.001, 0)$, $\breve{\Upsilon}_2^{\zeta} = (1, 0)$ with weights $\mathfrak{G}_1^{\beth} = 0.9$ and $\mathfrak{G}_2^{\beth} = 0.1$. By equations (7) and (10) we get

$$\begin{aligned}\text{PFWA}\left(\breve{\Upsilon}_1^{\zeta}, \breve{\Upsilon}_2^{\zeta}\right) &= (1, 0), \\ \text{PFWG}\left(\breve{\Upsilon}_1^{\zeta}, \breve{\Upsilon}_2^{\zeta}\right) &= (0.002, 0).\end{aligned} \tag{12}$$

Case 2. Take two PFNs s.t. $\breve{\Upsilon}_1^{\zeta} = (0.001, 0)$, $\breve{\Upsilon}_2^{\zeta} = (1, 0)$ with weights $\mathfrak{G}_1^{\beth} = 0.1$ and $\mathfrak{G}_2^{\beth} = 0.9$. By equations (7) and (10) we get

$$\begin{aligned}\text{PFWA}\left(\breve{\Upsilon}_1^{\zeta}, \breve{\Upsilon}_2^{\zeta}\right) &= (1, 0), \\ \text{PFWG}\left(\breve{\Upsilon}_1^{\zeta}, \breve{\Upsilon}_2^{\zeta}\right) &= (0.501, 0).\end{aligned} \tag{13}$$

We can see from these data that the PFWA and PFWG operators managed to provide reasonable outcomes in these two circumstances. As a result, in order to address these inadequacies or limitations, we must strengthen the AOs.

3. Some Hybrid Aggregation Operators of PFNs

In this part, we suggest a novel hybrid AOs to fill the gaps left by the PFWA and PFGA operators.

3.1. PFHWAGA Operator. Assume that $\breve{\Upsilon}_k^{\zeta} = \langle \mu_k^{\beth}, \nu_k^{\beth} \rangle$ $(k = 1, 2, \ldots, n)$ is a conglomeration of PFN and (PFHWAGA): $\mathfrak{X}^{\Theta n} \longrightarrow \mathfrak{X}^{\Theta}$, if

$$(\text{PFHWAGA})\left(\breve{\Upsilon}_1^{\zeta}, \breve{\Upsilon}_2^{\zeta}, \ldots, \breve{\Upsilon}_n^{\zeta}\right) = \left(\sum_{k=1}^{n} \mathfrak{G}_k^{\beth} \breve{\Upsilon}_2^{\zeta}\right)^{\beth} \left(\sum_{k=1}^{n} \breve{\Upsilon}_2^{\zeta \mathfrak{G}_k^{\beth}}\right)^{1-\beth}, \tag{14}$$

where, $\beth$ is any real number in $[0, 1]$ and $\mathfrak{G}^{\beth} = (\mathfrak{G}_1^{\beth}, \mathfrak{G}_2^{\beth}, \ldots, \mathfrak{G}_n^{\beth})^T$ is WV of $(\breve{\Upsilon}_1^{\zeta}, \breve{\Upsilon}_2^{\zeta}, \ldots, \breve{\Upsilon}_n^{\zeta})$, s.t. $0 \le \mathfrak{G}_k^{\beth} \le 1$ and $\sum_{k=1}^{n} \mathfrak{G}_k^{\beth} = 1$. Then, the PFHWAGA is called the PFHWAGA operator. The preceding theorem can be used to find PFHWAGA based on the operating principles of PFNs.

Theorem 6. *Let* $\breve{\Upsilon}_k^{\zeta} = \langle \mu_k^{\beth}, \nu_k^{\beth} \rangle$ *be the conglomeration of PFN, we can find PFHWAGA by*

$$\begin{aligned}
&(\mathrm{PFHWAGA})\left(\breve{\Upsilon}_1^{\zeta}, \breve{\Upsilon}_2^{\zeta}, \ldots, \breve{\Upsilon}_n^{\zeta}\right) \\
&= \left(\sum_{k=1}^{n} \mathfrak{G}_k^{\beth} \breve{\Upsilon}_k^{\zeta}\right)^{\beth} \left(\sum_{k=1}^{n} \breve{\Upsilon}_k^{\zeta \mathfrak{G}_k^{\beth}}\right)^{1-\beth} \\
&= \left\langle \left(1 - \prod_{k=1}^{n} \left(1 - \left(\mu_k^{\beth}\right)^2\right)^{w_k}\right)^{\beth/2} \left(\prod_{k=1}^{n} \mu_k^{\beth w_k}\right)^{1-\beth}, \sqrt{1 - \left(1 - \left(\prod_{k=1}^{n} \left(\nu_k^{\beth}\right)^{w_k}\right)^2\right)^{\beth} \left(\prod_{k=1}^{n} \left(1 - \left(\nu_k^{\beth}\right)^2\right)^{w_k}\right)^{1-\beth}} \right\rangle,
\end{aligned} \tag{15}$$

where $\beth$ *is any number from* $[0, 1]$. $\mathfrak{G}^{\beth} = (\mathfrak{G}_1^{\beth}, \mathfrak{G}_2^{\beth}, \ldots, \mathfrak{G}_n^{\beth})^T$ *is the WV of* $(\breve{\Upsilon}_1^{\zeta}, \breve{\Upsilon}_2^{\zeta}, \ldots, \breve{\Upsilon}_n^{\zeta})$, *s.t.* $0 \le \mathfrak{G}_k^{\beth} \le 1$, *and* $\sum_{k=1}^{n} \mathfrak{G}_k^{\beth} = 1$.

Proof. Based on PFWA and PFGA operators and the operational laws of PFSs.

$$\begin{aligned}
&(\mathrm{PFHWAGA})\left(\breve{\Upsilon}_1^{\zeta}, \breve{\Upsilon}_2^{\zeta}, \ldots, \breve{\Upsilon}_n^{\zeta}\right) \\
&= \left(\sum_{k=1}^{n} \mathfrak{G}_k^{\beth} \breve{\Upsilon}_k^{\zeta}\right)^{\beth} \left(\sum_{k=1}^{n} \breve{\Upsilon}_k^{\zeta \mathfrak{G}_k^{\beth}}\right)^{1-\beth} \\
&= \left\langle \left(1 - \prod_{k=1}^{n} \left(1 - \mu_k^{\beth 2}\right)^{\mathfrak{G}_k^{\beth}}\right)^{1/2}, \prod_{k=1}^{n} \nu_k^{\beth \mathfrak{G}_k^{\beth}} \right\rangle^{\beth} \left\langle \left(\prod_{k=1}^{n} \mu_k^{\beth \mathfrak{G}_k^{\beth}}, \left(1 - \prod_{k=1}^{n} \left(1 - \nu_k^{\beth 2}\right)^{\mathfrak{G}_k^{\beth}}\right)^{1/2}\right) \right\rangle^{1-\beth} \\
&= \left\langle \left(\left(1 - \prod_{k=1}^{n} \left(1 - \mu_k^{\beth 2}\right)^{\mathfrak{G}_k^{\beth}}\right)^{\beth/2}, \left(1 - \left(1 - \left(\prod_{k=1}^{n} \nu_k^{\beth \mathfrak{G}_k^{\beth}}\right)^2\right)^{\beth}\right)^{1/2}\right) \left(\left(\prod_{k=1}^{n} \mu_k^{\beth \mathfrak{G}_k^{\beth}}\right)^{1-\beth}, \left(1 - \left(\prod_{k=1}^{n} \left(1 - \nu_k^{\beth 2}\right)^{\mathfrak{G}_k^{\beth}}\right)^{1-\beth}\right)^{1/2}\right) \right\rangle \\
&= \left\langle \left(1 - \prod_{k=1}^{n} \left(1 - \mu_k^{\beth 2}\right)^{\mathfrak{G}_k^{\beth}}\right)^{\beth/2} \cdot \left(\prod_{k=1}^{n} \mu_k^{\beth \mathfrak{G}_k^{\beth}}\right)^{1-\beth}, \right. \\
&\left. \sqrt{\left(1 - \left(1 - \left(\prod_{k=1}^{n} \nu_k^{\beth \mathfrak{G}_k^{\beth}}\right)^2\right)^{\beth}\right)^{2/2} + \left(1 - \left(\prod_{k=1}^{n} \left(1 - \nu_k^{\beth 2}\right)^{\mathfrak{G}_k^{\beth}}\right)^{1-\beth}\right)^{2/2} - \left(1 - \left(1 - \left(\prod_{k=1}^{n} \nu_k^{\beth \mathfrak{G}_k^{\beth}}\right)^2\right)^{\beth}\right) \left(1 - \left(\prod_{k=1}^{n} \left(1 - \nu_k^{\beth 2}\right)^{\mathfrak{G}_k^{\beth}}\right)^{1-\beth}\right)} \right\rangle \\
&= \left\langle \left(1 - \prod_{k=1}^{n} \left(1 - \left(\mu_k^{\beth}\right)^2\right)^{\mathfrak{G}_k^{\beth}}\right)^{\beth/2} \left(\prod_{k=1}^{n} \mu_k^{\beth \mathfrak{G}_k^{\beth}}\right)^{1-\beth}, \right. \\
&\left. \sqrt{\left(1 - \left(1 - \left(\prod_{k=1}^{n} \nu_k^{\beth \mathfrak{G}_k^{\beth}}\right)^2\right)^{\beth}\right) + \left(1 - \left(\prod_{k=1}^{n} \left(1 - \nu_k^{\beth 2}\right)^{\mathfrak{G}_k^{\beth}}\right)^{1-\beth}\right)^{2/2} - 1 + \left(\prod_{k=1}^{n} \left(1 - \nu_k^{\beth 2}\right)^{\mathfrak{G}_k^{\beth}}\right)^{1-\beth} + \left(1 - \left(\prod_{k=1}^{n} \nu_k^{\beth \mathfrak{G}_k^{\beth}}\right)^2\right)^{\beth} - \left(1 - \left(\prod_{k=1}^{n} \left(1 - \nu_k^{\beth 2}\right)^{\mathfrak{G}_k^{\beth}}\right)^{1-\beth}\right) \left(1 - \left(\prod_{k=1}^{n} \nu_k^{\beth \mathfrak{G}_k^{\beth}}\right)^2\right)^{\beth}} \right\rangle \\
&= \left\langle \left(1 - \prod_{k=1}^{n} \left(1 - \left(\mu_k^{\beth}\right)^2\right)^{\mathfrak{G}_k^{\beth}}\right)^{\beth/2} \left(\prod_{k=1}^{n} \mu_k^{\beth \mathfrak{G}_k^{\beth}}\right), \sqrt{1 - \left(1 - \left(\prod_{k=1}^{n} \left(\nu_k^{\beth}\right)^{\mathfrak{G}_k^{\beth}}\right)^2\right)^{\beth} \left(\prod_{k=1}^{n} \left(1 - \left(\nu_k^{\beth}\right)^2\right)^{\mathfrak{G}_k^{\beth}}\right)^{1-\beth}} \right\rangle.
\end{aligned} \tag{16}$$

Therefore, this complete the proof of equation (15).
ב-1 □

Remark 1. It is feasible to explore the many families of the PFHWAGA operator independently for different values of $\beth \in [0, 1]$. When we consider a particular situation, such as $\beth = 1$, the PFHWAGA operator is converted to the PFWA operator. The PFHWAGA operator is simplified to the PFWG operator if $\beth = 0$. The PFHWAGA operator is the mean of the PFWA and PFWG operators if $\beth = 0.5$.

Example 3. Let $\breve{\Upsilon}_1^{\zeta} = (0.71, 0.52)$, $\breve{\Upsilon}_2^{\zeta} = (0.34, 0.56)$, and $\breve{\Upsilon}_3^{\zeta} = (0.57, 0.68)$ be the three PFNs, $\mathfrak{G}^{\beth} = (0.5, 0.3, 0.2)$ be the WV of $(\breve{\Upsilon}_1^{\zeta}, \breve{\Upsilon}_2^{\zeta}, \breve{\Upsilon}_3^{\zeta})$, and $\beth = 0.5$. We use PFHWAGA operator to aggregate the three PFNs by using equation (15).

$$\begin{aligned}(\text{PFHWAGA})\left(\breve{\Upsilon}_1^{\zeta},\breve{\Upsilon}_2^{\zeta},\breve{\Upsilon}_3^{\zeta}\right)&=\left(1-\prod_{k=1}^{3}\left(1-\left(\mu_k^{\beth}\right)^2\right)^{w_k}\right)^{0.5/2}\left(\prod_{k=1}^{3}\mu_k^{\beth w_k}\right)^{1-0.5},\\&\cdot\sqrt{1-\left(1-\left(\prod_{k=1}^{3}\left(\nu_k^{\beth}\right)^{w_k}\right)^2\right)^{0.5}\left(\prod_{k=1}^{3}\left(1-\left(\nu_k^{\beth}\right)^2\right)^{w_k}\right)^{1-0.5}}\\&=(0.582,0.567).\end{aligned}\tag{17}$$

It is clear from the characteristics of the PFWA and PFWG operators that the PFHWAGA operator has idempotency, boundedness, and monotonicity as well.

Theorem 7. *Let* $\breve{\Upsilon}_k^{\zeta}=\left\langle\mu_k^{\beth},\nu_k^{\beth}\right\rangle(k=1,2,\ldots,n)$*is a conglomeration of PFNs. Then,*

(1) (Idempotency) if$\breve{\Upsilon}_k^{\zeta}=\breve{\Upsilon}^{\zeta}=\langle\mu^{\beth},\nu^{\beth}\rangle$*for allk, then*

$$\text{PFHWAGA}\left(\breve{\Upsilon}_1^{\zeta},\breve{\Upsilon}_2^{\zeta},\ldots,\breve{\Upsilon}_n^{\zeta}\right)=\breve{\Upsilon}^{\zeta}\tag{18}$$

(2) (Boundedness) if$\breve{\Upsilon}^{\zeta^-}=(\min(\mu_k^{\beth}),\max(\nu_k^{\beth}))$*and*$\breve{\Upsilon}^{\zeta^+}=(\max(\mu_k^{\beth}),\min(\nu_k^{\beth}))$*, then we obtain*

$$\breve{\Upsilon}^{\zeta^-}\le\text{PFHWAGA}\left(\breve{\Upsilon}_1^{\zeta},\breve{\Upsilon}_2^{\zeta},\ldots,\breve{\Upsilon}_n^{\zeta}\right)\le\breve{\Upsilon}^{\zeta^+}.\tag{19}$$

(3) (Monotonicity) if $\breve{\Upsilon}_k^{\zeta}=\left\langle\mu_k^{\beth},\nu_k^{\beth}\right\rangle$ *and* $\breve{\Upsilon}_k^{\zeta^*}=\left\langle\mu_k^{\beth^*},\nu_k^{\beth^*}\right\rangle$ *are two sets of PFNs.If*$\mu_k^{\beth}\ge\mu_k^{\beth^*},\nu_k^{\beth}\le\nu_k^{\beth^*}$ *for allkthen,*

$$\text{PFHWAGA}\left(\breve{\Upsilon}_1^{\zeta},\breve{\Upsilon}_2^{\zeta},\ldots,\breve{\Upsilon}_n^{\zeta}\right)\ge\text{PFHWAGA}\left(\breve{\Upsilon}_1^{\zeta^*},\breve{\Upsilon}_2^{\zeta^*},\ldots,\breve{\Upsilon}_n^{\zeta^*}\right).\tag{20}$$

3.2. PFHOWAGA Operator. Assume that $\breve{\Upsilon}_k^{\zeta}=\left\langle\mu_k^{\beth},\nu_k^{\beth}\right\rangle$ is a conglomeration of PFNs, and (PFHOWAGA): $\mathfrak{X}^{\Theta n}\longrightarrow\mathfrak{X}^{\Theta}$, if

$$(\text{PFHWAGA})\left(\breve{\Upsilon}_1^{\zeta},\breve{\Upsilon}_2^{\zeta},\ldots,\breve{\Upsilon}_n^{\zeta}\right)=\left(\sum_{k=1}^{n}\mathfrak{G}_k^{\beth}\breve{\Upsilon}_{\beth(k)}^{\zeta}\right)^{\beth}\left(\sum_{k=1}^{n}\breve{\Upsilon}_{\beth(k)}^{\zeta^{\mathfrak{G}_k^{\beth}}}\right)^{1-\beth},\tag{21}$$

where T^n is the set of all PFNs, $(\breve{\beth}(1),\breve{\beth}(2),\ldots,\breve{\beth}(k))$ is a permutation of $(1,2,\ldots,n)$ s.t. $\breve{\Upsilon}_{\beth(j-1)}\ge\breve{\Upsilon}_{\beth(j)}$ for any k, $\beth$ is any real number in the interval $[0,1]$, and $\mathfrak{G}^{\beth}=(\mathfrak{G}_1^{\beth},\mathfrak{G}_2^{\beth},\ldots,\mathfrak{G}_n^{\beth})^T$ is WV of $(\breve{\Upsilon}_1,\breve{\Upsilon}_2,\ldots,\breve{\Upsilon}_n)$, s.t. $0\le\mathfrak{G}_k^{\beth}\le1$ and $\sum_{k=1}^{n}\mathfrak{G}_k^{\beth}=1$. Then, the PFHOWAGA is called the PFHOWAGA operator.

We can also find PFHOWAGA operator by the following theorem.

Theorem 8. *Let* $\breve{\Upsilon}_k^{\zeta}=\left\langle\mu_k^{\beth},\nu_k^{\beth}\right\rangle$ *be a conglomeration of PFNs. We can find PFHOWAGA by*

$$\begin{aligned}(\text{PFHWAGA})\left(\breve{\Upsilon}_1^{\zeta},\breve{\Upsilon}_2^{\zeta},\ldots,\breve{\Upsilon}_n^{\zeta}\right)&=\left(\sum_{k=1}^{n}\mathfrak{G}_k^{\beth}\breve{\Upsilon}_{\beth(k)}^{\zeta}\right)^{\beth}\left(\sum_{k=1}^{n}\breve{\Upsilon}_{\beth(k)}^{\zeta^{\mathfrak{G}_k^{\beth}}}\right)^{1-\beth}\\&=\left(1-\prod_{k=1}^{n}\left(1-\left(\mu_{\beth(k)}^{\beth}\right)^2\right)^{\mathfrak{G}_k^{\beth}}\right)^{\beth/2}\left(\prod_{k=1}^{n}\mu_{\beth(k)}^{\beth^{\mathfrak{G}_k^{\beth}}}\right)^{1-\beth}\\&\cdot\sqrt{1-\left(1-\left(\prod_{k=1}^{n}\left(\nu_{\beth(k)}^{\beth}\right)^{\mathfrak{G}_k^{\beth}}\right)^2\right)^{\beth}\left(\prod_{k=1}^{n}\left(1-\left(\nu_{\beth(k)}^{\beth}\right)^2\right)^{\mathfrak{G}_k^{\beth}}\right)^{1-\beth}},\end{aligned}\tag{22}$$

where $\beth$ *is any real number in the interval* $[0, 1]$.

Proof. The proof can be made by similar way to proof of Theorem 6, so we omit the proof. ∎

Example 4. Let $\ddot{a}_1 = (0.71, 0.52), \ddot{a}_2 = (0.34, 0.56)$, and $\ddot{a}_3 = (0.57, 0.68)$ be the three PFNs, $\mathfrak{G}^{\beth} = (0.5, 0.3, 0.2)$ be the WV of $(\ddot{a}_1, \ddot{a}_2, \ddot{a}_3)$, and $\beth = 0.5$.By SF, we rank these PFNs:

$$\begin{aligned} \widetilde{\gimel}(\ddot{a}_1) &= 0.181, \\ \widetilde{\gimel}(\ddot{a}_2) &= -0.085, \\ \widetilde{\gimel}(\ddot{a}_3) &= -0.108. \end{aligned} \tag{23}$$

Now, $\breve{\Upsilon}_1^{\zeta} = \ddot{a}_1, \breve{\Upsilon}_2^{\zeta} = \ddot{a}_2, \breve{\Upsilon}_3^{\zeta} = \ddot{a}_3$. We use PFHOWAGA operator to aggregate by using equation (24).

$$\begin{aligned} (\mathrm{PFHOWAGA})\left(\breve{\Upsilon}_1^{\zeta}, \breve{\Upsilon}_2^{\zeta}, \breve{\Upsilon}_3^{\zeta}\right) &= \left(1 - \prod_{k=1}^{3}\left(1 - \left(\mu_{\beth(k)}^{\beth}\right)^2\right)^{w_k}\right)^{0.5/2} \left(\prod_{k=1}^{3} \mu_{\beth(k)}^{\beth w_k}\right)^{1-0.5} \\ &\cdot \sqrt{1 - \left(1 - \left(\prod_{k=1}^{3}\left(\nu_{\beth(k)}^{\beth}\right)^{w_k}\right)^2\right)^{0.5} \left(\prod_{k=1}^{3}\left(1 - \left(\nu_{\beth(k)}^{\beth}\right)^2\right)^{w_k}\right)^{1-0.5}} \\ &= (0.582, 0.567). \end{aligned} \tag{24}$$

Theorem 9. *Let* $\breve{\Upsilon}_k^{\zeta} = \langle \mu_k^{\beth}, \nu_k^{\beth} \rangle$ *is a conglomeration of PFNs. Then,*

(1) (Idempotency) If $\breve{\Upsilon}_k^{\zeta} = \breve{\Upsilon}^{\zeta} = \langle \mu^{\beth}, \nu^{\beth} \rangle$ *for allk, then*

$$\mathrm{PFHOWAGA}\left(\breve{\Upsilon}_1^{\zeta}, \breve{\Upsilon}_2^{\zeta}, \ldots, \breve{\Upsilon}_n^{\zeta}\right) = \breve{\Upsilon}^{\zeta} \tag{25}$$

(2) (Boundedness) if $\breve{\Upsilon}^{\zeta^-} = (\min(\mu_k^{\beth}), \max(v_k))$ *and* $\breve{\Upsilon}^{\zeta^+} = (\max(\mu_k^{\beth}), \min(\nu_k^{\beth}))$*, then we have*

$$\breve{\Upsilon}^{\zeta^-} \le \mathrm{PFHOWAGA}\left(\breve{\Upsilon}_1^{\zeta}, \breve{\Upsilon}_2^{\zeta}, \ldots, \breve{\Upsilon}_n^{\zeta}\right) \le \breve{\Upsilon}^{\zeta^+}. \tag{26}$$

(3) (Monotonicity) if $\breve{\Upsilon}_k^{\zeta} = \langle \mu_k^{\beth}, \nu_k^{\beth} \rangle$ *and* $\breve{\Upsilon}_k^{\zeta^*} = \langle \mu_k^{\beth *}, \nu_k^{\beth *} \rangle$ *are two sets of PFNs. If* $\mu_k^{\beth} \ge \mu_k^{\beth *}, \nu_k^{\beth} \le \nu_k^{\beth *}$ *for allk, then*

$$\mathrm{PFHOWAGA}\left(\breve{\Upsilon}_1^{\zeta}, \breve{\Upsilon}_2^{\zeta}, \ldots, \breve{\Upsilon}_n^{\zeta}\right) \ge \mathrm{PFHOWAGA}\left(\breve{\Upsilon}_1^{\zeta^*}, \breve{\Upsilon}_2^{\zeta^*}, \ldots, \breve{\Upsilon}_n^{\zeta^*}\right). \tag{27}$$

3.3. Numerical Example. To demonstrate the correctness of the aggregated values of the PFHWAGA and PFHOWAGA operations, we consider the first scenario in Section 2.4. If $\beth = 0.5$, we will utilize the PFHWAGA and PFHOWAGA operations.

For Case 1, by equation (15), there is $\mathrm{PFHWAGA}(\breve{\Upsilon}_1^{\zeta}, \breve{\Upsilon}_2^{\zeta}) = (0.045, 0)$, which is between $\mathrm{PFWA}(\breve{\Upsilon}_1^{\zeta}, \breve{\Upsilon}_2^{\zeta}) = (1, 0)$ and $\mathrm{PFWG}(\breve{\Upsilon}_1^{\zeta}, \breve{\Upsilon}_2^{\zeta}) = (0.002, 0)$.

The moderate values are indicated in the above case by new advanced operators. These operators are clearly capable of overcoming the shortcomings of PFWA and PFWG operators. As a result, the PFHWAGA and PFHOWAGA operators are more efficient and acceptable in aggregating data.

4. Multi-Criteria Decision-Making Method

Suppose that $\breve{\Upsilon}^{\zeta} = \left\{(\breve{\Upsilon}_1^{\zeta}, \breve{\Upsilon}_2^{\zeta}, \ldots, \breve{\Upsilon}_p^{\zeta})\right\}$ and $\mathscr{V}^{\sigma} = \left\{\mathscr{V}_1^{\sigma}, \mathscr{V}_2^{\sigma}, \ldots, \mathscr{V}_q^{\sigma}\right\}$ are the assemblage of alternatives and attributes. Consider $\mathfrak{G}^{\beth}$ be the WV of all criterion, s.t. $\mathfrak{G}_j^{\beth} \in [0, 1]$, $\sum_{j=1}^{n} \mathfrak{G}_j^{\beth} = 1$, and $\mathfrak{G}_j^{\beth}$ represent the weight of $\mathscr{V}_j^{\sigma}$. The DM assesses alternatives based on parameters and the evaluation parameters are in PFNs. Consider $(\breve{\coprod}_{ij})_{p\times q} = \left\langle \mu_{ij}^{\beth}, \nu_{ij}^{\beth} \right\rangle$ is the decision matrix given by the DM, $(\breve{\coprod}_{ij})$ represents a PFNs for alternative $\breve{\Upsilon}_i^{\zeta}$ associated with the criterions $\mathscr{V}_j^{\sigma}$. With this Algorithm 1, some constraints are included s.t

(1) $\mu_{ij}^{\beth} and \nu_{ij}^{\beth} \in [0, 1]$

(2) $0 \le \mu_A^{\beth}(\mathfrak{G}^{\beth})^2 + \nu_A^{\beth}(\mathfrak{G}^{\beth})^2 \le 1, (q \ge 1)$.

We now design Algorithm 1 to tackle the specified issue. The flow chart of Algorithm 1 is given by Figure 1.

5. MCDM Problem Related to Selection of Appropriate Candidate

Example 5. Consider the choosing of a university professor as a fairly straightforward decision-making dilemma. For the choosing, there are four teachers accessible,

Phase i. Obtain the decision matrix from DMs. $(\breve{\coprod}_{ij})_{p\times q} = \langle \mu_{ij}^{\beth}, \nu_{ij}^{\beth} \rangle$.
Phase ii. The decision matrix should be normalised. When we have various kinds of criteria or attributes, such as cost and benefit, we normalise the decision matrix by taking the complement of the cost criteria.
Phase iii. Find β_i^{γ} = PFHWAGA$(\beta_{i1}^{\gamma}, \beta_{i2}^{\gamma}, \ldots, \beta_{in}^{\gamma})$ or β_i^{γ} = PFHOWAGA$(\beta_{i1}^{\gamma}, \beta_{i2}^{\gamma}, \ldots, \beta_{in}^{\gamma})$ for each $i = 1, 2, \ldots, q$.
Phase iv. Evaluate the SFs for all β_i^{γ} for the collective overall PFNs.
Phase v. Rank all the β_i^{γ} $(i = 1, 2, \ldots, p)$ according to the score values.

Algorithm 1: Decision-making algorithm.

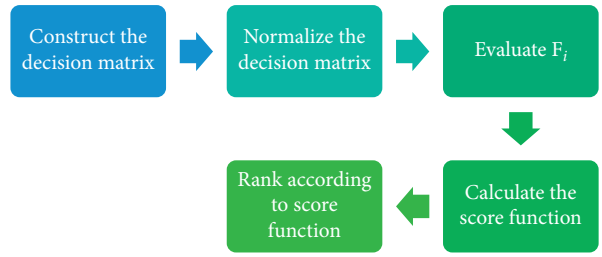

Figure 1: Flow chart of Algorithm 1.

	$\mathscr{V}_1^{\eth}$	$\mathscr{V}_2^{\eth}$	$\mathscr{V}_3^{\eth}$	$\mathscr{V}_4^{\eth}$
$\breve{\coprod}_1$	(0.320, 0.610)	(0.410, 0.450)	(0.330, 0.560)	(0.660, 0.530)
$\breve{\coprod}_2$	(0.610, 0.520)	(0.340, 0.560)	(0.570, 0.680)	(0.610, 0.490)
$\breve{\coprod}_3$	(0.720, 0.320)	(0.360, 0.490)	(0.600, 0.420)	(0.700, 0.210)
$\breve{\coprod}_4$	(0.760, 0.120)	(0.820, 0.320)	(0.910, 0.120)	(0.600, 0.130)

$D = \left\{ \breve{\coprod}_i, i = 1, 2, 3, 4 \right\}$. To evaluate the professor, we consider given criterion $P = \left\{ \mathscr{V}_i^{\eth}, i = 1, 2, 3, 4 \right\}$ given as

$$\begin{aligned} \mathscr{V}_1^{\eth} &= \text{experience}, \\ \mathscr{V}_2^{\eth} &= \text{research background}, \\ \mathscr{V}_3^{\eth} &= \text{teaching methodology}, \\ \mathscr{V}_4^{\eth} &= \text{personality}. \end{aligned} \tag{28}$$

PFNs are used in this challenge to evaluate the four feasible alternatives $\breve{\coprod}_i (i = 1, 2, 3, 4)$ based on the four criteria listed above. Let $q = 3$, a WV $\mathfrak{G}^{\beth}$ is $(0.20, 0.30, 0.10, 0.40)^T$, and the controlling index is $\beth = 0.5$.

Now, we will solve the MCDM issue using Algorithm 1. The following sections detail the procedure phases:

Phase i. Evaluating the choice matrix provided by the individual based on PF information.

Phase ii. The decision matrix is already in normalised form.

Phase iii. Compute β_i^{γ} = PFHWAGA$(\beta_{i1}^{\gamma}, \beta_{i2}^{\gamma}, \ldots, \beta_{in}^{\gamma})$ for each i. Thus we find aggregated PFNs by using equation (15).

$$\begin{aligned} \beta_1^{\gamma} &= (0.4980, 0.5270), \\ \beta_2^{\gamma} &= (0.5310, 0.5390), \\ \beta_3^{\gamma} &= (0.6020, 0.3510), \\ \beta_4^{\gamma} &= (0.7420, 0.1990). \end{aligned} \tag{29}$$

Phase iv. Evaluate the SFs for all β_i^{γ} for the collective overall PFNs.

$$\begin{aligned} \tilde{\gimel}(\beta_1^{\gamma}) &= -0.0230, \\ \tilde{\gimel}(\beta_2^{\gamma}) &= -0.0070, \\ \tilde{\gimel}(\beta_3^{\gamma}) &= 0.1750, \\ \tilde{\gimel}(\beta_4^{\gamma}) &= 0.4010. \end{aligned} \tag{30}$$

Phase v. Rank all the β_i^{γ} $(i = 1, 2, 3, 4)$ according to the score values.

$$\beta_4^{\gamma} \succ \beta_3^{\gamma} \succ \beta_2^{\gamma} \succ \beta_1^{\gamma}, \tag{31}$$

and thus β_4^{γ} is the most desirable alternative.

6. Conclusion

AOs, such as the PFWA and PFWG operators, are significant mathematical tools for integrating PF data. We designed two operators, namely the "Pythagorean fuzzy hybrid weighted arithmetic geometric aggregation (PFHWAGA) operator" and the "Pythagorean fuzzy hybrid ordered weighted arithmetic geometric aggregation (PFHOWAGA) operator" to address some of the shortcomings of the PFWA and PFWG operators in various real-world problems. Several characteristics of the PFHWAGA and PFHOWAGA operators were discovered. The recommended operators outperform the existing PFN-defined operators. With the use of examples, we enlarged on the proposed operators. Underneath the PF environment, designed operators are more robust and efficient than existing operators. Based on the PFHWAGA and PFHOWAGA operators, we devised an MCDM technique for selecting the best candidate for the position of teacher. We will use this concept in future to develope better other AOs, namely Einstein AOs, Hamacher AOs, and Dombi AOs in future.

Data Availability

The paper includes the information used to verify the study's findings.

Conflicts of Interest

The authors declare that they have no conflicts of interest.

Acknowledgments

The authors extend their appreciation to the "Deanship of Scientific Research at King Khalid University" for funding this work through general research project under R.G.P.2/48/43.

References

[1] L. A. Zadeh, "Fuzzy sets," *Information and Control*, vol. 8, no. 3, pp. 338–353, 1965.

[2] K. T. Atanassov, "Intuitionistic fuzzy sets," *Fuzzy Sets and Systems*, vol. 20, no. 1, pp. 87–96, 1986.

[3] R. R. Yager and A. M. Abbasov, "Pythagorean membership grades, complex numbers, and decision making," *International Journal of Intelligent Systems*, vol. 28, no. 5, pp. 436–452, 2013.

[4] R. R. Yager, "Pythagorean membership grades in multi criteria decision-making," *IEEE Transactions on Fuzzy Systems*, vol. 22, no. 4, pp. 958–965, 2014.

[5] R. R. Yager, "Pythagorean fuzzy subsets," in *Proceedings of the IFSA World Congress and NAFIPS Annual Meeting (IFSA/NAFIPS), 2013 Joint*, pp. 57–61, IEEE, Edmonton, Canada, 2013.

[6] P. Liu and X. Qin, "Maclaurin symmetric mean operators of linguistic intuitionistic fuzzy numbers and their application to multiple-attribute decision-making," *Journal of Experimental & Theoretical Artificial Intelligence*, vol. 29, no. 6, pp. 1173–1202, 2017.

[7] S. Gul, "Fermatean fuzzy set extensions of SAW, ARAS, andVIKOR with application s in COVID-19 testing laboratoryselection problem," *Expert Systems*, vol. 38, no. 8, Article ID e12769, 2021.

[8] J. Ye, J. Zhan, and Z. S. Xu, "A novel multi-attribute decision-making method based on fuzzy rough sets," *Computers & Industrial Engineering*, vol. 155, Article ID 107136, 2021.

[9] Z. Mu, S. Zeng, and P. Wang, "Novel approach to multi-attribute group decision-making based on interval-valued pythagorean fuzzy power maclaurin symmetric mean operator," *Computers & Industrial Engineering*, vol. 155, Article ID 107049, 2021.

[10] B. Batool, S. Abdullah, S. Ashraf, and M. Ahmad, "Pythagorean probabilistic hesitant fuzzy aggregation operators and their application in decision-making," *Kybernetes*, vol. 51, 2021.

[11] X. D. Peng and H. Yuan, "Fundamental properties of pythagorean fuzzy aggregation operators," *Fundamenta Informaticae*, vol. 147, no. 4, pp. 415–446, 2016.

[12] K. Rahman, S. Abdullah, F. Husain, and M. S. A. Khan, "Approaches to pythagorean fuzzy geometric aggregation operators," *International Journal of Computer Science and Information Security*, vol. 14, no. 9, pp. 174–200, 2016.

[13] I. Deli and N. Çağman, "Intuitionistic fuzzy parameterized soft set theory and its decision making," *Applied Soft Computing*, vol. 28, pp. 109–113, 2015.

[14] L. Wang and H. Garg, "Algorithm for multiple attribute decision-making with interactive archimedean norm operations under pythagorean fuzzy uncertainty," *International Journal of Computational Intelligence Systems*, vol. 14, no. 1, p. 503, 2020.

[15] L. Wang, H. Garg, and N. Li, "Pythagorean fuzzy interactive hamacher power aggregation operators for assessment of express service quality with entropy weight," *Soft Computing*, vol. 25, no. 2, pp. 973–993, 2021.

[16] C. Huang, M. Lin, and Z. Xu, "Pythagorean fuzzy MULTIMOORA method based on distance measure and score function: its application in multicriteria decision making process," *Knowledge and Information Systems*, vol. 62, no. 11, pp. 4373–4406, 2020.

[17] M. Lin, C. Huang, R. Chen, H. Fujita, and X. Wang, "Directional correlation coefficient measures for pythagorean fuzzy sets: their applications to medical diagnosis and cluster analysis," *Complex & Intelligent Systems*, vol. 7, no. 2, pp. 1025–1043, 2021.

[18] M. Lin, C. Huang, and Z. Xu, "TOPSIS method based on correlation coefficient and entropy measure for linguistic pythagorean fuzzy sets and its application to multiple attribute decision making," *Complexity*, vol. 2019, Article ID 6967390, 16 pages, 2019.

[19] L. Meng, Z. Chonghui, Y. Chenhong, and Y. Yujing, "Knowledge diffusion trajectories in the pythagorean fuzzy field based on main path analysis," *International Journal of Intelligent Computing and Cybernetics*, vol. 15, no. 1, pp. 124–143, 2021.

[20] M. Lin, Y. Chen, and R. Chen, "Bibliometric analysis on pythagorean fuzzy sets during 20132020," *International Journal of Intelligent Computing and Cybernetics*, vol. 14, no. 2, pp. 104–121, 2021.

[21] Z. S. Chen, L. L. Yang, K. S. Chin et al., "Sustainable building material selection: an integrated multi-criteria large group

decision making framework," *Applied Soft Computing*, vol. 113, Article ID 107903, 2021.

[22] Z. S. Chen, X. Zhang, R. M. Rodríguez, W. Pedrycz, and L. Martínez, "Expertise-based bid evaluation for construction-contractor selection with generalized comparative linguistic ELECTRE III," *Automation in Construction*, vol. 125, Article ID 103578, 2021.

[23] Z. S. Chen, X. L. Liu, K. S. Chin, W. Pedrycz, K. L. Tsui, and M. J. Skibniewski, "Online-review analysis based large-scale group decision-making for determining passenger demands and evaluating passenger satisfaction: case study of high-speed rail system in China," *Information Fusion*, vol. 69, pp. 22–39, 2021.

[24] G. Wei and M. Lu, "Pythagorean fuzzy power aggregation operators in multiple attribute decision making," *International Journal of Intelligent Systems*, vol. 33, no. 1, pp. 169–186, 2018.

[25] S. J. Wu and G. W. Wei, "Pythagorean fuzzy Hamacher aggregation operators and their application to multiple attribute decision making," *International Journal of Knowledge-Based and Intelligent Engineering Systems*, vol. 21, no. 3, pp. 189–201, 2017.

[26] H. Garg, "Confidence levels based Pythagorean fuzzy aggregation operators and its application to decision-making process," *Computational & Mathematical Organization Theory*, vol. 23, no. 4, pp. 546–571, 2017.

Hindawi
Journal of Mathematics
Volume 2024, Article ID 9806508, 1 page
https://doi.org/10.1155/2024/9806508

Retraction

Retracted: Novel Concepts in Rough Cayley Fuzzy Graphs with Applications

Journal of Mathematics

Received 23 January 2024; Accepted 23 January 2024; Published 24 January 2024

This article has been retracted by Hindawi following an investigation undertaken by the publisher [1]. This investigation has uncovered evidence of one or more of the following indicators of systematic manipulation of the publication process:

(1) Discrepancies in scope

(2) Discrepancies in the description of the research reported

(3) Discrepancies between the availability of data and the research described

(4) Inappropriate citations

(5) Incoherent, meaningless and/or irrelevant content included in the article

(6) Manipulated or compromised peer review

The presence of these indicators undermines our confidence in the integrity of the article's content and we cannot, therefore, vouch for its reliability. Please note that this notice is intended solely to alert readers that the content of this article is unreliable. We have not investigated whether authors were aware of or involved in the systematic manipulation of the publication process.

Wiley and Hindawi regrets that the usual quality checks did not identify these issues before publication and have since put additional measures in place to safeguard research integrity.

We wish to credit our own Research Integrity and Research Publishing teams and anonymous and named external researchers and research integrity experts for contributing to this investigation.

The corresponding author, as the representative of all authors, has been given the opportunity to register their agreement or disagreement to this retraction. We have kept a record of any response received.

References

[1] Y. Rao, Q. Zhou, M. Akhoundi, A. A. Talebi, S. Omidbakhsh Amiri, and G. Muhiuddin, "Novel Concepts in Rough Cayley Fuzzy Graphs with Applications," *Journal of Mathematics*, vol. 2023, Article ID 2244801, 11 pages, 2023.

Hindawi
Journal of Mathematics
Volume 2023, Article ID 2244801, 11 pages
https://doi.org/10.1155/2023/2244801

Research Article

Novel Concepts in Rough Cayley Fuzzy Graphs with Applications

Yongsheng Rao,[1] **Qixin Zhou**,[1] **Maryam Akhoundi**,[2] **A. A. Talebi**,[3] **S. Omidbakhsh Amiri**,[3] **and G. Muhiuddin**[4]

[1]*Institute of Computing Science and Technology, Guangzhou University, Guangzhou 510006, China*
[2]*Clinical Research Development Unit of Rouhani Hospital, Babol Univetsity of Medical Sciences, Babol, Iran*
[3]*Department of Mathematics, University of Mazandaran, Babolsar, Iran*
[4]*Department of Mathematics, University of Tabuk, Tabuk 71491, Saudi Arabia*

Correspondence should be addressed to Maryam Akhoundi; maryam.akhoundi@mubabol.ac.ir

Received 4 May 2022; Revised 23 June 2022; Accepted 9 July 2022; Published 8 April 2023

Academic Editor: Naeem Jan

Today, fuzzy graphs (FGs) have a variety of applications in other fields of study, including medicine, engineering, and psychology, and for this reason, many researchers around the world are trying to identify their properties and use them in computer sciences as well as finding the smallest problem in a network. The concept of a Cayley fuzzy graph has become a standard part of the toolkit used to investigate and describe groups. Also, Cayley fuzzy graphs are good models for interconnection networks, and they are useful in semigroup theory for establishing which elements are ℓ and R related. The previous definition limitations in the FGs have directed us to offer a new classification in terms of Cayley fuzzy graphs. So, in this paper, two new definitions of Cayley fuzzy graphs (CFGs) and pseudo-Cayley fuzzy graphs (PCFGs) are discussed and their rough approximations are studied. Also, some properties of fuzzy rough sets (FRSs) in CFGs and PCFGs have been investigated. Finally, we presented the determination of the most effective person in the Water and Sewerage Organization and the importance of using refereeing facilities in football matches between club teams, by using CFG in the presented applications.

1. Introduction

FG is one of the most widely used topics in fuzzy theory, which has been studied by many researchers today. One of the advantages of FG is its flexibility in reducing time and costs in economic issues, which has been welcomed by all managers of institutions and companies. FGs were introduced by Rosenfeld [1], ten years after Zadeh's innovative paper (Fuzzy Sets) [2]. In 1878, the Cayley graph (CGs) was considered for finite groups by Cayley. Dehn introduced CGs under the name Gruppenbid (group diagram) from 1909 to 1910. Alshehri and Akram defined Cayley bipolar fuzzy graphs in a group [3]. Naboothiri et al. [4] discussed CFGs. Akram et al. [5] introduced the notation of Cayley's intuitionistic fuzzy graphs on groups and investigated some of their properties. Borzooei and Rashmanlou [6] defined Cayley interval-valued fuzzy graphs. The concept of RS was originally proposed by Pawlak [7] as a mathematical approach to handle uncertainty in data analysis. Skowron and Ziarko [8, 9] introduced RS, FS, and knowledge discovery. The fundamental factors in RS theory are approximations. Biswas and Nanda [10] presented the notion of rough subgroups. Kuroki and Mordeson [11] defined RSs as the structure and rough groups. He and Shi [12] introduced the RG definition and studied some operations on it. Shahzamanian et al. [13] defined the concepts of rough approximations of CGs and rough edge CGs. Chakrabarty et al. [14] introduced the LAs and UAs in FS theory to obtain FRS. Wu et al. [15] studied the concept of generalized FRSs. Mahapatra et al. [16–20] investigated several concepts in radio fuzzy graphs and planar graphs. Shi and Kosari [21] proposed some properties of domination in product vague graphs. Shao et al. [22] defined new concepts in intuitionistic fuzzy graphs. CFG is used to illustrate real-world phenomena using Cayley fuzzy models in a variety of fields, including technology, social networking, and biological

sciences. It is evident that CFGs are very useful tools in theoretical computer science. CFGs are used for interconnection networks as great models. They are utilized in many applied problems in graph and group theory. In physics, CFGs seem to appear in the study of quantum walks. Therefore, in this paper, two new algebraic definitions called CFGs and PCFGs have been proposed and their rough approximations have been studied. Finally, two basic applications are presented, which we will be explained using this graph. In the first application, due to the vital importance of water in human life and better management in its consumption, we introduced the most efficient and literate person in the water organization and we expressed his mastery of technology using the CFG. Using refereeing facilities (video check camera, the use of yellow and red cards, experienced referee and assistant referee, etc.) is very important and we use CFG to express the use of these facilities in various competitions.

2. Preliminaries

All the basic notations are shown in Table 1. A fuzzy subset (FSS) of M is a function from M into $I = [0,1]$. The class of all subsets of M (fuzzy subsets) will be denoted by $\mathscr{P}(M)(\mathscr{F}(M))$. Let $\psi \in \mathscr{F}(M)$. For $\beta \in I$, ψ_β and $\psi_{\beta+}$ are defined as follows:

$$\begin{aligned} \psi_\beta &= \{r \mid r \in M, \psi(r) \geq \beta\}, \\ \psi_{\beta+} &= \{r \mid r \in M, \psi(r) > \beta\}, \end{aligned} \tag{1}$$

and are called the β-cut and the strong β-cut (or β-level and strong β-level) of ψ, respectively.

Let V be a nonempty set. A FG is a triple (V, ψ, φ) so that ψ is a FSS of V and φ is a symmetric FR on ψ. That is, $\psi: V \longrightarrow [0,1]$ and $\varphi: V \times V \longrightarrow [0,1]$ so that $\varphi(r,p) \leq \psi(r) \wedge \psi(p)$, $\forall r, p \in V$.

Let P and Q be two finite and nonempty universes. A FSS $T \in \mathscr{F}(P \times Q)$ is defined as a FBR from P to Q. A relation $T \in \mathscr{F}(P \times Q)$ is called reflexive if $T(r,r) = 1$, symmetric if $T(r,p) = T(p,r)$, and transitive if $T(r,k) \geq \vee_{p \in P}(T(r,p) \wedge T(p,k))$, for all $r, k \in P$.

Let G be a group. A FSS ψ of a group G is called a FSG of the group G if

(i) $\psi(rp) \geq \min\{\psi(r), \psi(p)\}$, for each $r, p \in G$

(ii) $\psi(r^{-1}) = \psi(r)$, for every $r \in G$

A FSS ψ of a group G is a FSG of the group G iff $\psi(rp^{-1}) \geq \min\{\psi(r), \psi(p)\}$, for each $r, p \in G$.

Definition 1 (see [23]). A fuzzy graph (G, ψ, φ) is complete if

$$\varphi(r,p) = \psi(r) \wedge \psi(p), \quad \forall r, p \in G. \tag{2}$$

Accordingly, some definitions are summarized which can be found in [15]. Let P and Q be two finite universes. Suppose that T be an optional relation from P to Q. We can define a set-valued function $F: P \longrightarrow \mathscr{P}(Q)$ by

Table 1: Some basic notations.

Notation	Meaning
RS	Rough set
FS	Fuzzy set
RG	Rough graph
FG	Fuzzy graph
CG	Cayley graph
CFG	Cayley fuzzy graph
CCFG	Complete Cayley fuzzy graph
PCFG	Pseudo-Cayley fuzzy graph
FSG	Fuzzy subgroup
CSS	Cayley subset
AS	Approximation space
ACFG	Approximation Cayley fuzzy graph
FR	Fuzzy relation
FSS	Fuzzy subset
CFSS	Cayley fuzzy subset
FBR	Fuzzy binary relation
FAS	Fuzzy approximation space
LA	Lower approximation
LG	Lower generalized
UA	Upper approximation
UG	Upper generalized
FAO	Fuzzy approximation operator
FRS	Fuzzy rough set
PFSG	Partial fuzzy subgraph

$$F(r) = \{p \in Q: (r,p) \in T\}, \quad r \in P. \tag{3}$$

Obviously, any set-valued function of F from P to Q defines a binary relation from P to Q by setting $T = \{(r,p) \in P \times Q: p \in F(r)\}$. The triple (P,Q,T) is referred to as a generalized AS. For any set $B \subseteq Q$, a pair of LAs and UAs, $\underline{T}(B)$ and $\overline{T}(B)$, are defined by

$$\begin{aligned} \underline{T}(B) &= \{r \in P: F(r) \subseteq C\}, \\ \overline{T}(B) &= \{r \in P: F(r) \cap C \neq \varnothing\}. \end{aligned} \tag{4}$$

The pair $\underline{T}(B)$, $\overline{R}(B)$ is referred to as a generalized RS.

Let T be an optional FR from P to Q. We define the mapping of $F: P \longrightarrow \mathscr{F}(Q)$ by

$$F(r)(p) = T(r,p), (r,p) \in P \times Q. \tag{5}$$

For any $\beta \in I$, we further define $F_\beta: P \longrightarrow \mathscr{P}(Q)$ by

$$F_\beta(r) = \{p \in Q: F(r)(p) \geq \beta\}, \quad r \in U. \tag{6}$$

Also for any $M \in \mathscr{P}(Q)$, the LAs and UAs of M with respect to the AS (P,Q,H_β) are defined as follows:

$$\begin{aligned} \underline{F}_\beta(M) &= \{r \in P: F_\beta(r) \subseteq M\}, \\ \overline{F}_\beta(M) &= \{r \in P: F_\beta(r) \cap M \neq \varnothing\}. \end{aligned} \tag{7}$$

Definition 2. Let T be an optional FR from P to Q and $B \in \mathscr{F}(Q)$. The triple (P,Q,T) is defined as the generalized FAS. We define the LG and UG FAOs $\underline{F}$ and $\overline{F}$ with respect to (P,Q,T) by

$$\underline{F}(B) = \vee_{\beta\in I}\left(\beta\wedge\underline{F}_{1-\beta}\left(B_{\beta+}\right)\right),$$
$$\overline{F}(B) = \vee_{\beta\in I}\left(\beta\wedge\overline{H}_{\beta}\left(B_{\beta}\right)\right). \tag{8}$$

The pair $(\underline{F}(B), \overline{F}(B))$ is described as generalized FRS.

Theorem 1. *If T is an optional FR from P to Q, then the pair of FAOs is satisfied in the following cases.*

For all $B, D \in \mathcal{F}(Q)$ and $\beta \in I$,

(a) $\underline{F}(B) = \sim(\overline{F}(\sim B))$
(b) $\overline{F}(B) = \sim(\underline{F}(\sim B))$
(c) $\underline{F}(B\vee\widehat{\beta}) = \underline{F}(B)\vee\widehat{\beta}$
(d) $\overline{F}(B\wedge\widehat{\beta}) = \overline{F}(B)\vee\widehat{\beta}$
(e) $\underline{F}(B\wedge D) = \underline{F}(B)\wedge\underline{F}(D)$
(f) $\underline{F}(B\vee D) = \overline{F}(B)\vee\overline{F}(D)$
(g) $B\subseteq D\Rightarrow\underline{F}(B)\subseteq\underline{F}(D)$
(h) $B\subseteq D\Rightarrow\overline{F}(B)\subseteq\overline{F}(D)$
(i) $\underline{F}(B\vee D)\supseteq\underline{F}(B)\vee\underline{F}(D)$
(j) $\overline{F}(B\wedge D)\subseteq\overline{F}(B)\wedge\overline{F}(D)$

$\widehat{\beta}$ is the constant FS: $\widehat{\alpha}(r) = \alpha$, $\forall r \in P$ and $r \in Q$.

3. Cayley Fuzzy Graph and Pseudo-Cayley Fuzzy Graphs

Definition 3. Let G be a group and ψ be a FSG of G and suppose φ is a subset of ψ so that $\varphi(rp^{-1}) \le \psi(r)\wedge\psi(p)$, for all $r, p \in G$ and $\varphi(r) \neq 0$ and $\varphi(r) = \varphi(r^{-1})$, $\forall r \in G$. The FG (G, ψ, ν) so that mapping ν is defined by $\nu(r,p) = \varphi(rp^{-1})\wedge\psi(r)\wedge\psi(p)$ for all $(r,p) \in G\times G$, $r \neq p$ is called the CFG of ψ in G relative to φ and is denoted by $\mathrm{Cay}F(G,\psi,\varphi)$. The FSS φ with the above properties is referred to as a CFSS of ψ in G.

Example 1. Consider $G = Z_4$ is the additive group of integers modulo 4 and ψ: $Z_4 \longrightarrow [0,1]$ is defined by $\psi(0) = 1$, $\psi(2) = 0.9$, and $\psi(1) = \psi(3) = 0.6$. Let $\varphi(0) = \varphi(2) = 0.5$ and $\varphi(1) = \varphi(3) = 0.6$. Then, the CFG $K = \mathrm{Cay}(Z_4, \psi, \varphi)$ is given in Figure 1.

Theorem 2. *A CFG, $K = Cay\,F(G,\psi,\varphi)$ is a complete fuzzy graph if and only if $\psi(rp^{-1}) = \psi(r)\wedge\psi(p)$, $\forall r, p \in G$, and $\psi(r) = \varphi(r)$, $\forall r \in G$.*

Proof. Assume that $K = \mathrm{Cay}F(G,\psi,\varphi)$ is CCFG. Then,

$$\varphi\left(rp^{-1}\right) = \psi(r)\wedge\psi(p), \quad \forall r, p \in G, \tag{9}$$

Hence,

$$\varphi(r) = \varphi\left(re^{-1}\right) = \psi(r)\wedge\psi\left(e^{-1}\right) = \psi(r), \forall, r \in G\}, \tag{10}$$

and also

$$\psi\left(rp^{-1}\right) = \varphi\left(rp^{-1}\right) = \psi(r)\wedge\psi(p), \quad \forall r, p \in G. \tag{11}$$

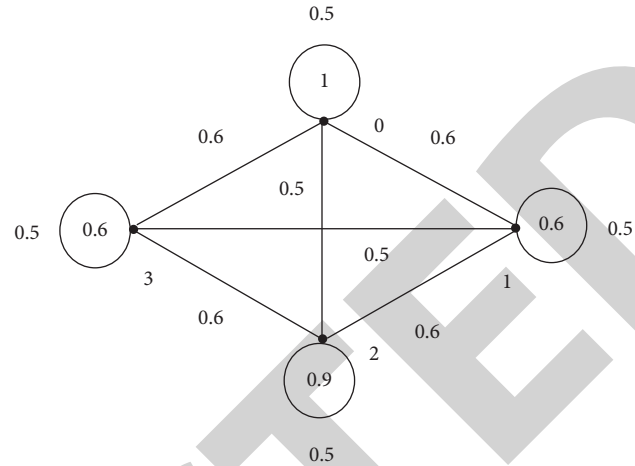

Figure 1: Cay $F(Z_4, \psi, \varphi)$.

Conversely, let $\psi(r) = \varphi(r)$, $\forall r \in G$ and $\psi(rp^{-1}) = \psi(r)\wedge\psi(p)$, $\forall r, p \in G$. Then, we have $\psi(rp^{-1}) = \varphi(rp^{-1}) = \psi(r)\wedge\psi(p), \forall r, p \in G$; hence, k is complete. □

Definition 4. Suppose that G is a group and ψ is a FSG of G. Let τ be a subset of ψ so that $\tau(r) = \tau(r^{-1})$, $\forall r \in G$. For a CSS φ of ψ, the FG (G, τ, ν) so that mapping ν is defined by $\nu(r,p) = \varphi(rp^{-1})\wedge\tau(r)\wedge\tau(p)$, $\forall (r,p) \in G\times G$, and $r \neq p$ is named the PCFG of τ in G relative to φ and is shown by $P\mathrm{Cay}F(G,\tau,\sigma)$.

Example 2. Consider $G = Z_4$ is the additive group of integers modulo 4. ψ is defined by the condition of Example 1 and let $\varphi(x) = 0.5$, $\forall r \in Z_4$. Let τ be a FSS of ψ so that $\tau(0) = 0.5$, $\tau(1) = \tau(3) = 0.6$, and $\tau(2) = 0.8$. Then, $K = P\mathrm{Cay}\,F(Z_4, \tau, \sigma)$ is PCFG.

Theorem 3. *If $K_1 = Cay\,F(G,\psi_1,\varphi_1)$ and $K_2 = Cay\,F(G,\psi_2,\varphi_2)$ are CFGs, then*

(1) $K_1\cup K_2 = Cay\,F(G,\psi_1\cup\psi_2,\varphi_1\cup\varphi_2)$, if $\psi_1\subseteq\psi_2$ or $\psi_2\subseteq\psi_1$
(2) $K_1\cap K_2 = Cay\,F(G,\psi_1\cap\psi_2,\varphi_1\cap\varphi_2)$

Proof

(1) Let $\psi_1\subseteq\psi_2$, so $\psi_1\cup\psi_2 = \psi_2$. For $r, p \in G$, we have

$$\begin{aligned}(\varphi_1\cup\varphi_2)\left(rp^{-1}\right) &= \varphi_1\left(rp^{-1}\right)\vee\varphi_2\left(rp^{-1}\right)\\ &\le (\psi_1(r)\wedge\psi_1(p))\vee(\psi_2(r)\wedge\psi_2(p))\\ &= (\psi_2(r)\wedge\psi_2(p)),\\ (\varphi_1\cup\varphi_2)\left(r^{-1}\right) &= \varphi_1\left(r^{-1}\right)\vee\varphi_2\left(r^{-1}\right)\\ &= \varphi_1(r)\vee\varphi_2(r)\\ &= (\varphi_1\cup\varphi_2)(r).\end{aligned} \tag{12}$$

(2) For $x, y \in G$, we have

$$\begin{aligned}(\varphi_1 \cap \varphi_2)\left(rp^{-1}\right) &= \varphi_1\left(rp^{-1}\right) \wedge \varphi_2\left(rp^{-1}\right) \\ &\leq (\psi_1(r) \wedge \psi_1(p)) \wedge (\psi_2(r) \wedge \psi_2(p)) \\ &= (\psi_1(r) \wedge \psi_2(r)) \wedge (\psi_1(p) \wedge \psi_2(p) \\ &= (\psi_1 \cap \psi_2)(r) \wedge (\psi_1 \cap \psi_2)(p),\end{aligned} \tag{13}$$

also

$$\begin{aligned}(\varphi_1 \cap \varphi_2)\left(r^{-1}\right) &= \varphi_1\left(r^{-1}\right) \wedge \varphi_2\left(r^{-1}\right) \\ &= \varphi_1(r) \wedge \varphi_2(r) \\ &= (\varphi_1 \cap \varphi_2)(r).\end{aligned} \tag{14}$$

□

Theorem 4. *If $K_1 = Cay\,F(G, \psi_1, \varphi_1)$ and $K_2 = Cay\,F(G, \psi_2, \varphi_2)$ are CFGs, then*

$$\begin{aligned}&K_1 \subseteq K_2 \Leftrightarrow \psi_1 \subseteq \psi_2, \\ &\varphi_1 \subseteq \varphi_1.\end{aligned} \tag{15}$$

Proof. According to the definition of the fuzzy subgraph, the proof is obvious. □

Theorem 5. *Let G be a group, ψ be an FSG of G. If $K_1 = PCayF(G, \tau_1, \varphi_1)$ and $K_2 = PCayF(G, \tau_2, \varphi_2)$ are PCFG, then*

(1) $K_1 \cup K_2 = PCayF(G, \tau_1 \cup \tau_2, \varphi_1 \cup \varphi_2)$

(2) $K_1 \cap K_2 = PCayF(G, \tau_1 \cap \tau_2, \varphi_1 \cap \varphi_2)$

Proof

(1) Since τ_1 and $\tau_2 \subseteq \psi$, then $\tau_1 \cup \tau_2 \subseteq \psi$. According to the PCFGs definition,

$$\begin{aligned}(\tau_1 \cup \tau_2)(r) &= \tau_1(r) \vee \tau_2(r) = \tau_1\left(r^{-1}\right) \vee \tau_2\left(r^{-1}\right) \\ &= (\tau_1 \cup \tau_2)\left(r^{-1}\right), \\ (\varphi_1 \cup \varphi_2)(r) &= \varphi_1(r) \vee \varphi_2(r) = \varphi_1\left(r^{-1}\right) \vee \varphi_2\left(r^{-1}\right) \\ &= (\varphi_1 \cup \varphi_2)\left(r^{-1}\right).\end{aligned} \tag{16}$$

(2) It is similar to the proof of (1). □

4. Rough Cayley Fuzzy Graphs

Definition 5. Let ψ be a FSG of the group G so that $\psi(rp^{-1}) = \psi(r^{-1}p^{-1})$, $\forall r, p \in G$. Let R be the FR from G to G, defined by $R(r, p) = \psi(rp^{-1})$, $\forall r, p \in G$. Then, by Definition 2, we have

$$\begin{aligned}\underline{F}(\varphi)(r) &= \vee\left\{\beta \in I; r \in \underline{F}_{1-\beta}\left(\varphi_{\beta^+}\right)\right\}, \\ \overline{F}(\varphi)(r) &= \vee\left\{\beta \in I; r \in \overline{F}_{\beta}\left(\varphi_{\beta}\right)\right\}.\end{aligned} \tag{17}$$

Lemma 1. *Let ψ be a FSG of G. Then, for any $A \in \mathcal{F}(G)$,*

(i) $\underline{F}(A) \subseteq A$

(ii) $A \subseteq \overline{F}(A)$

Proof

(i) For any $r \in G$, let $\underline{F}(A)(r) = \beta$, then $r \in \underline{F}_{1-\beta}(A_{\beta^+})$. So, $F_{1-\beta}(r) \subseteq A_{\beta^+}$. Now, $F(x)(x) = 1 \geq 1 - \beta$ shows that $r \in F_{1-\beta}(x)$. Hence, $r \in A_{\beta^+}$, i.e., $A(r) > \beta = \underline{F}(A)(r)$. This shows $\underline{F}(A) \subseteq A$.

(ii) For any $r \in G$, let $A(r) = \beta$, then $r \in A_\beta$. On the other hand, $F(r)(r) = \psi(rr^{-1}) = \psi(e) = 1 \geq \beta$ shows that $r \in F_\alpha(r)$.

Hence, $r \in A_\beta \cap F_\beta$, i.e., $r \in \overline{F_\beta}(A_\beta)$. Now by Definition 5, $\overline{F}(A)(r) \geq \beta = A(r)$; hence, $A \subseteq \overline{F}(A)$. □

Remark 1. If in Definition 3 $\varphi(r) = 0$, for any $r \in G$, then, according to Definition 2, we have $\underline{F}(\varphi) = 0$.

Definition 6. Let ψ be a FSG of G and φ be a CFSS of ψ. For CFG $K = \text{Cay}\,F(G, \psi, \varphi)$, a pair of LAs and UAs, $\underline{K}$ and $\overline{K}$, are defined by

$$\begin{aligned}\underline{K} &= \text{Cay}\,F\left(G, \psi, \underline{F}(\varphi)\right), \\ \overline{K} &= \text{Cay}\,F\left(G, \psi, \overline{F}(\varphi)\right).\end{aligned} \tag{18}$$

Theorem 6. *Two FGs $\underline{K}$ and $\overline{K}$ are CFGs.*

Proof. We show that $\underline{K}$ and $\overline{K}$ hold the conditions of Definition 3.

$$\begin{aligned}\underline{F}(\varphi)(r) &= \vee\left\{\beta \in I; r \in \underline{F}_{1-\beta}\left(\varphi_{\beta^+}\right)\right\} \\ &= \vee\left\{\beta \in I; F_{1-\beta}(r) \subseteq \left(\varphi_{\beta^+}\right)\right\} \\ &= \vee\left\{\beta \in I; \forall p \in GR(r, p) = \psi\left(rp^{-1}\right) \geq 1 - \beta \Rightarrow \varphi(p) > \alpha\right\} \\ &= \vee\left\{\beta \in I; \forall p \in GR\left(r^{-1}, p\right) = \psi\left(r^{-1}p^{-1}\right) \geq 1 - \beta \Rightarrow \varphi(y) > \beta\right\} \\ &= \underline{F}(\varphi)\left(r^{-1}\right).\end{aligned} \tag{19}$$

Similarly we can prove $\overline{F}(\varphi)(r) = \overline{F}(\varphi)(r^{-1})$.

Since $\varphi \leq \psi$, then $\varphi_{\beta^+} \subseteq \psi_{\beta^+}$. Therefore, for any $r \in G$,

$$\begin{aligned}\underline{F}(\varphi)(r) &= \vee\left\{\beta \in I; r \in \underline{F}_{1-\beta}\left(\varphi_{\beta^+}\right)\right\} \\ &= \vee\left\{\beta \in I; F_{1-\beta}(r) \subseteq \varphi_{\beta^+}\right\} \\ &\leq \vee\left\{\beta \in I; F_{1-\beta}(r) \subseteq \psi_{\beta^+}\right\} \\ &= \underline{F}(\psi)(r).\end{aligned} \tag{20}$$

According to Lemma 1, since $\underline{F}(\psi) \leq \psi$, so $\underline{F}(\varphi) \leq \psi$.

Now, for any $r \in G$,

$$\begin{aligned}\overline{F}(\varphi)(r) &= \vee\left\{\beta \in I; r \in \overline{F}_{\beta}\left(\varphi_{\beta}\right)\right\} \\ &= \vee\left\{\beta \in I; F_{\beta}(r) \cap \varphi_{\beta} \neq \varnothing\right\} \\ &= \vee\{\beta \in I; \exists p \in GR(r, p) \geq \beta \text{ and } \varphi(p) \geq \beta\} \\ &= \vee\left\{\beta \in I; \exists p \in G\psi\left(rp^{-1}\right) \geq \beta \text{ and } \varphi(p) \geq \beta\right\}.\end{aligned} \tag{21}$$

Suppose $\overline{F}(\varphi)(r) = \beta_0$. Then, $\exists p \in G$ so that $\psi(rp^{-1}) \geq \beta_0$ and $\varphi(p) \geq \beta_0$. Since ψ is an FSG and $\psi(p) \geq \varphi(p)$, we have

$$\psi(r) = \psi\left(rp^{-1}p\right) \geq \psi\left(rp^{-1}\right) \wedge \psi(p)) \geq \beta_0. \tag{22}$$

Then, $\psi(r) \geq \overline{F}(\varphi)(r)$, so $\overline{F}(\varphi) \leq \psi$. Therefore, $\underline{K}$ and $\overline{K}$ are CFGs. □

Example 3. Consider $G = Z_4$ is the additive group of integers modulo 4. ψ: $Z_4 \longrightarrow [0,1]$ is defined by $\psi(0) = 1$, $\psi(1) = \psi(3) = 0.7$, and $\psi(2) = 0.9$. Let $\varphi(0) = 0.5$, $\varphi(2) = 0$, and $\varphi(1) = \varphi(3) = 0.6$. So, we have

$$\begin{aligned} &\underline{F}(\varphi)(r) = 0.5, \\ &\overline{F}(\varphi)(r) = 0.6, \quad \text{for all } r \in G. \end{aligned} \tag{23}$$

Then, $K = \text{Cay}\, F(Z_4, \psi, \varphi)$, $\underline{K}$, and $\overline{K}$ are given in Figure 2.

Theorem 7. *Let ψ, ψ_1 and ψ_2 be FSGs of G. Let $K = Cay\, F(G, \psi, \varphi)$, $K_1 = Cay\, F(G, \psi_1, \varphi_1)$, and $K_2 = Cay\, F(G, \psi_2, \varphi_2)$ be CFGs. Then, we have*

(1) $\underline{K} \subseteq K \subseteq \overline{K}$

(2) (a) $\underline{K_1 \cap K_2} = \underline{K_1} \cap \underline{K_2}$, *(b)* $\underline{K_1 \cup K_2} \supseteq \underline{K_1} \cup \underline{K_2}$, *if* $\psi_1 \subseteq \psi_2$

(3) (a) $\overline{K_1 \cup K_2} = \overline{K_1} \cup \overline{K_2}$, *if* $\psi_1 \subseteq \psi_2$ *or* $\psi_2 \subseteq \psi_1$, *(b)* $\overline{K_1 \cap K_2} \subseteq \overline{K_1} \cap \overline{K_2}$

(4) $K_1 \subseteq K_2 \Rightarrow \underline{K_1} \subseteq \underline{K_2}$ *and* $\overline{K_1} \subseteq \overline{K_2}$

Proof

(1) It follows from Theorem 4 and Lemma 1.

(2) (a) By Theorem 1 (e) and Theorem 3 (2), we have

$$\begin{aligned} \underline{K_1} \cap \underline{K_2} &= \text{Cay}\, F(G, \psi_1, \underline{F}(\varphi_1)) \cap \text{Cay}\, F(G, \psi_2, \underline{F}(\varphi_2)) \\ &= \text{Cay}\, F(G, \psi_1 \cap \psi_2, \underline{F}(\varphi_1)) \cap \underline{F}(\varphi_2)), \end{aligned} \tag{24}$$

and on the other hand, we have

$$\underline{K_1 \cap K_2} = \text{Cay}\, F\left(G, \psi_1 \cap \psi_2, \underline{F}(\varphi_1 \cap \varphi_2)\right). \tag{25}$$

Theorem 1 (e) implies $\underline{F}(\varphi_1 \cap \varphi_2) = \underline{F}(\varphi_1) \cap \underline{F}(\varphi_2)$. Therefore, $\underline{K_1 \cap K_2} = \underline{K_1} \cap \underline{K_2}$.

(b) Theorem 1 (i) implies $\underline{F}(\varphi_1 \cup \varphi_2) \supseteq \underline{F}(\varphi_1) \cup \underline{F}(\varphi_1)$. Hence, by Theorem 3 (1), we have

$$\begin{aligned} \underline{K_1 \cup K_2} &= \text{Cay}\, F\left(G, \psi_1 \cup \psi_2, \underline{F}(\varphi_1 \cup \varphi_2)\right) \\ &\supseteq \text{Cay}\, F\left(G, \psi_1 \cup \psi_2, \underline{F}(\varphi_1) \cup \underline{F}(\varphi_2)\right) \\ &= \text{Cay}\, F\left(G, \psi_1, \underline{F}(\varphi_1)\right) \cup \text{Cay}\, F\left(G, \psi_2, \underline{F}(\varphi_2)\right) \\ &= \underline{K_1} \cup \underline{K_2}. \end{aligned} \tag{26}$$

(3) By Theorems 1 (f) and (i), the proof is similar to (2).

(4) Suppose that $K_1 \subseteq K_2$, since $\varphi_1 \subseteq \varphi_2$, then $\underline{F}(\varphi_1) \subseteq \underline{F}(\varphi_2)$. Hence, $\underline{K_1} \subseteq \underline{K_2}$.

Similarly, we can prove $\overline{K_1} \subseteq \overline{K_2}$. □

Theorem 8. *Let $K = (G, \psi, \varphi)$ be CFG. If K is CCFG, then $\overline{K}$ is complete.*

Proof. Suppose that K is a CCFG. By Theorems 2 and Lemma 1, we have

$$\begin{aligned} &\psi\left(rp^{-1}\right) = \psi(r) \wedge \psi(p), \quad \forall r, p \in G, \\ &\overline{F}(\varphi)(r) \subseteq \psi(r) = \varphi(r) \subseteq \overline{F}(\varphi)(r), \quad \forall r \in G. \end{aligned} \tag{27}$$

So $\overline{F}(\varphi)(r) = \psi(r)$; hence, $\overline{K}$ is complete. □

Example 4. Consider $G = Z_4$ is the additive group of integers modulo 4 and ψ: $Z_4 \longrightarrow [0,1]$ is defined by $\psi(0) = 1$, $\psi(1) = \psi(3) = 0.7$, and $\psi(2) = 0.9$. Let $\varphi(0) = 1$, $\varphi(2) = 0.9$, and $\varphi(1) = \varphi(3) = 0.7$. By straight calculation, we have $\overline{F}(\varphi)(0) = 1$, $\overline{F}(\varphi)(1) = \overline{F}(\varphi)(3) = 0.9$, and $\overline{F}(\varphi)(2) = 0.9$. Then, $\overline{K}$ is complete.

Definition 7. Let $K = \text{Cay}\, F(G, \psi, \varphi)$ and $\underline{K}$ and $\overline{K}$ be LA and UA of K. The complement of K is $K^c = (\underline{K}^c, \overline{K}^c)$, where

$$\begin{aligned} \underline{K}^c &= \left(G, \psi^c, \underline{F}(\varphi)^c\right), \\ \overline{K}^c &= \left(G, \psi^c, \overline{F}(\varphi)^c\right), \end{aligned} \tag{28}$$

such that for all $r, p \in G$, we have

(a) $\psi^c(r) = \psi(r)$

(b) $\underline{F}(\varphi)^c(rp^{-1}) = (\psi(r) \wedge \psi(p)) - \underline{F}(\varphi)(rp^{-1})$

(c) $\overline{F}(\varphi)^c(rp^{-1}) = (\psi(r) \wedge \psi(p)) - \overline{F}(\varphi)(rp^{-1})$

Example 5. Suppose that hypothesis of Example 3 and group $G = Z_4$ are the group congruence modulo 4 integral number Z. Hence, according to Definition 7, $K^c = (G, \psi^c, \varphi^c)$, $\underline{K}^c = (G, \psi^c, \underline{F}(\varphi)^c)$, and $\overline{K}^c = (G, \psi^c, \overline{F}(\varphi)^c)$ are given in Figure 3.

5. Rough Pseudo-Cayley Graphs

Definition 8. Let ψ be a FSG of G and τ be a FSS of ψ so that $\tau(r) = \tau(r^{-1})$, $r \in G$. For the PCFG $K = PCay\, F(G, \tau, \varphi)$, a pair of LAs and UAs, $\underline{K'}$ and $\overline{K'}$, are defined by

$$\begin{aligned} \underline{K'} &= PCay\, F\left(G, \underline{F}(\tau), \varphi\right), \\ \overline{K'} &= PCay\, F(G, \overline{F}(\tau) \cap \psi, \varphi). \end{aligned} \tag{29}$$

Theorem 9. *Two FGs $\underline{K'}$ and $\overline{K'}$ are PCFGs.*

Proof. According to the Definition 5, for each $r \in G$,

$$\begin{aligned} \underline{F}(\tau)(r) &= \vee\left\{\beta \in I; r \in \underline{F}_{1-\beta}(\tau_{\alpha+})\right\} \\ &= \vee\left\{\beta \in I; F_{1-\beta}(r) \subseteq (\tau_{\beta+})\right\} \\ &= \vee\left\{\beta \in I; \forall p \in GR(r,p) = \psi\left(rp^{-1}\right) \geq 1 - \beta \Rightarrow \tau(p) > \alpha\right\} \\ &= \vee\left\{\beta \in I; \forall p \in GR\left(r^{-1}, p\right) = \psi\left(r^{-1}p^{-1}\right) \geq 1 - \beta \Rightarrow \tau(p) > \beta\right\} \\ &= \underline{F}(\tau)\left(r^{-1}\right). \end{aligned} \tag{30}$$

Similarly, we can prove $\overline{F}(\tau)(r) = \overline{F}(\tau)(r^{-1})$, $\forall r \in G$; hence,

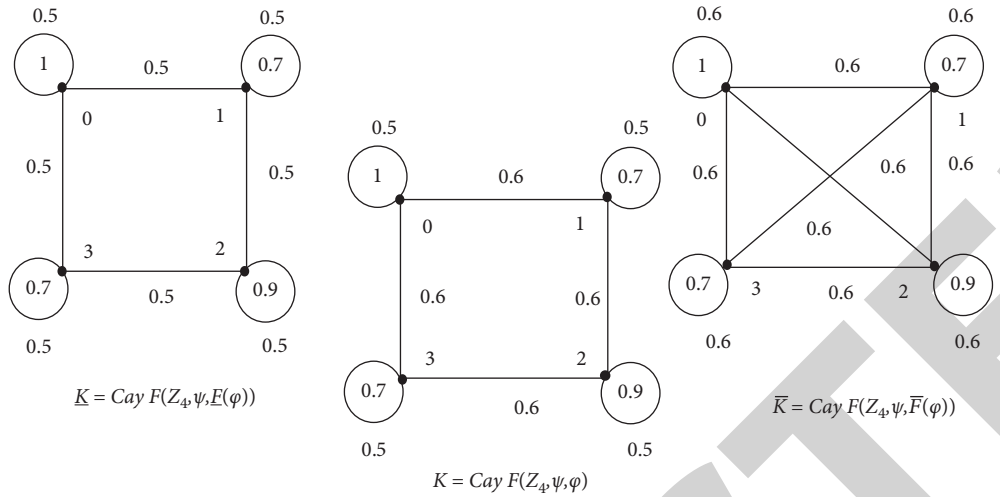

Figure 2: $K = \mathrm{Cay}\, F(Z_4, \psi, \varphi)$, $\underline{K}$ and $\overline{K}$.

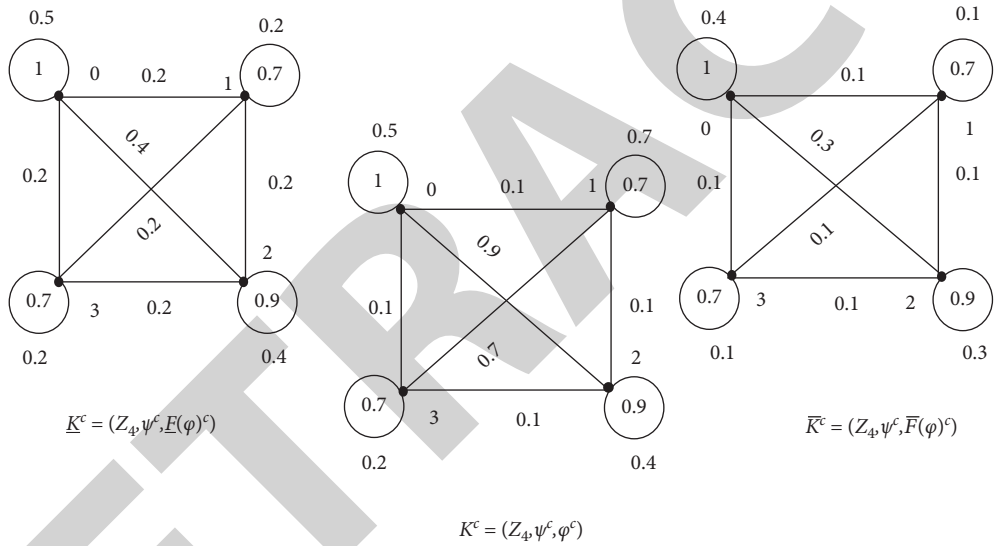

Figure 3: $K^c = (Z_4, \psi^c, \varphi^c)$, $\underline{K}^c$, and $\overline{K}^c$.

$$\begin{aligned}(\overline{F}(\tau)\cap\psi)(r) &= \overline{F}(\tau)(r)\wedge\psi(r) = \overline{F}(\tau)\left(r^{-1}\right)\wedge\psi\left(r^{-1}\right)\\ &= (\overline{F}(\tau)\cap\psi)\left(r^{-1}\right).\end{aligned} \tag{31}$$

On the other hand, since $\overline{F}(\tau)\cap\psi\subseteq\psi$ and $\underline{F}(\tau)\subseteq\tau\subseteq\psi$, $\underline{K'}$ and $\overline{K'}$ are PCFGs. □

Theorem 10. *Let ψ be a FSG of G, and $K = PCay\, F(G, \tau, \varphi)$, $K_1 = PCay\, F(G, \tau_1, \varphi_1)$. and $K_2 = PCay\, F(G, \tau_2, \varphi_2)$ are PCFGs. Then, we have*

(1) $\underline{K}' \subseteq K \subseteq \overline{K}'$

(2) *(a)* $(K_1\cap K_2)' = \underline{K_1}'\cap\underline{K_2}'$, *(b)* $(\underline{K_1\cup K_2})\prime\supseteq \underline{K_1}'\cup\underline{K_2}'$, *if* $\tau_1\subseteq\tau_2$

(3) *(a)* $(\overline{K_1\cup K_2})\prime = \overline{K_1}\prime\cup\overline{K_2}\prime$, *if* $\tau_1\subseteq\tau_2$ *or* $\tau_2\subseteq\tau_1$, *(b).* $(\overline{K_1\cap K_2})\prime\subseteq\overline{K_1}\prime\cap\overline{K_2}\prime$

(4) $K_1\subseteq K_2\Rightarrow \underline{K_1}\prime\subseteq\underline{K_2}\prime$ *and* $\overline{K_1}\prime\subseteq\overline{K_2}\prime$

Proof

(1) Since $\underline{F}(\tau)\subseteq\tau$, $\tau\subseteq\overline{F}(\tau)$, and $\tau\subseteq\psi$, $\underline{F}(\tau)\subseteq\tau\subseteq\overline{F}(\tau)\cap\psi$. Now, Theorem 4 shows $\underline{K}'\subseteq K\subseteq\overline{K}'$.

(2) (a) We have

$$\begin{aligned}\left(\underline{K_1\cap K_2}\right)\prime &= PCayF(G, \underline{F}(\tau_1\cap\tau_2), \varphi_1\cap\varphi_2)\\ &= PCayF(G, \underline{F}(\tau_1)\cap\underline{F}(\tau_2), \varphi_1\cap\varphi_2)\\ &= PCayF(G, \underline{F}(\tau_1), \varphi_1)\cap PCayF(G, \underline{F}(\tau_2), \varphi_2)\\ &= \underline{K_1'}\cap\underline{K_2'}.\end{aligned} \tag{32}$$

(b) Theorem 1 (i) implies $\underline{F}(\tau_1\cup\tau_2)\supseteq\underline{F}(\tau_1)\cup\underline{F}(\tau_1)$. Hence,

$$\begin{aligned}\left(\underline{K_1\cup K_2}\right)\prime &= PCayF(G, \underline{F}(\tau_1\cup\tau_2), \varphi_1\cup\varphi_2)\\ &\supseteq PCayF(G, \underline{F}(\tau_1)\cup\underline{F}(\tau_2), \varphi_1\cup\varphi_2)\\ &= PCayF(G, \underline{F}(\tau_1), \varphi_1\cup PCayF(G, \underline{F}(\tau_2), \varphi_2)\\ &= \underline{K_1'}\cup\underline{K_2'}.\end{aligned} \tag{33}$$

(3) (a) We have

$$\begin{aligned}(\overline{K_1 \cup K_2})\prime &= PCayF(G, \overline{F}(\tau_1 \cup \tau_2) \cap \psi, \varphi_1 \cup \varphi_2)\\ &= PCayF(G, (\overline{F}(\tau_1) \cap \psi) \cup (\overline{F}(\tau_2) \cap \psi), \varphi_1 \cup \varphi_2)\\ &= PCayF(G, \overline{F}(\tau_1) \cap \psi, \varphi_1) \cup PCayF(G, \overline{F}(\tau_2) \cap \psi, \varphi_2)\\ &= \overline{K_1'} \cup \overline{K_2'}.\end{aligned} \tag{34}$$

(b)

$$\begin{aligned}(\overline{K_1 \cap K_2})\prime &= PCayF(G, \overline{F}(\tau_1 \cap \tau_2) \cap \psi, \varphi_1 \cap \varphi_2)\\ &\subseteq PCayF(G, (\overline{F}(\tau_1) \cap \psi) \cap (\overline{F}(\tau_2) \cap \psi), \varphi_1 \cap \varphi_2)\\ &= PCayF(G, \overline{F}(\tau_1) \cap \psi, \varphi_1) \cap PCayF(G, \overline{F}(\tau_2) \cap \psi, \varphi_2)\\ &= \overline{K_1'} \cap \overline{K_2'}.\end{aligned} \tag{35}$$

(4) Assume $K_1 \subseteq K_2$. Then, $\tau_1 \subseteq \tau_1$ and $\varphi_1 \subseteq \varphi_2$. So, $\underline{F}(\tau_1) \subseteq \underline{F}(\tau_2)$ and hence $\underline{K_1}\prime \subseteq \underline{K_2}\prime$. Similarly, we can prove $\overline{K_1}\prime \subseteq \overline{K_2}\prime$. □

Example 6. Consider $G = Z_5$ is the additive group of integers modulo 5 and ψ: $Z_5 \longrightarrow [0, 1]$ is defined by $\psi(0) = 1$ and $\psi(1) = \psi(2) = \psi(3) = \psi(4) = 0.8$. Let $\varphi(r) = 0.5$, $\forall r$ in Z_4 and τ be an FSSs of ψ so that $\tau(0) = 0.7$, $\tau(1) = \tau(4) = 0.6$, and $\tau(2) = \tau(3) = 0.5$. So we have

$$\begin{aligned}&\underline{F}(\tau)(r) = 0.5,\\ &\overline{F}(\tau)(r) = 0.7, \quad \text{for } r \in G.\end{aligned} \tag{36}$$

Then, $K = PCayF(Z_5, \tau, \varphi)$, $\underline{K'}$, and $\overline{K'}$ are given in Figure 4.

Definition 9. For the PCFG $K = PCayF(G, \tau, \varphi)$, a pair of LAs and UAs, $\underline{K''}$ and $\overline{K''}$, are defined by

$$\begin{aligned}\underline{K''} &= PCayF(G, \underline{F}(\tau), \underline{F}(\varphi)),\\ \overline{K''} &= PCayF(G, \overline{F}(\tau) \cap \psi, \overline{F}(\varphi)).\end{aligned} \tag{37}$$

Theorem 11. *Two FGs $\underline{K''}$ and $\overline{K''}$ are PCFGs.*

Proof. According to Theorem 9, $(\overline{F}(\tau) \cap \psi) \subseteq \psi$, $\underline{F}(\tau) \subseteq \tau \subseteq \psi$, $\underline{F}(\tau)(r) = \underline{F}(\tau)(r^{-1})$ and $(\overline{F}(\tau) \cap \psi)(r) = (\overline{F}(\tau) \cap \psi)(r^{-1})$, we show that $\underline{K''}$ and $\overline{K''}$ satisfy the conditions of Definition 4. For any $r \in G$, we have

$$\begin{aligned}\overline{F}(\varphi)(r) &= \vee\{\beta \in I; r \in \overline{F}_\beta(\varphi_\beta)\}\\ &= \vee\{\beta \in I; F_\beta(r) \subseteq (\varphi_\beta)\}\\ &= \vee\{\beta \in I; \exists p \in GR(r, p) = \psi(rp^{-1}) \geq \beta \Rightarrow \varphi(p) \geq \beta\}\\ &= \vee\{\beta \in I; \exists p \in GR(r^{-1}, p) = \psi(r^{-1}p^{-1}) \geq \beta \Rightarrow \varphi(p) \geq \beta\}\\ &= \overline{F}(\varphi)(r^{-1}).\end{aligned} \tag{38}$$

Similarly, we can prove $\underline{F}(\varphi)(r) = \underline{F}(\varphi)(r^{-1})$, $\forall r \in G$. □

Example 7. Consider $G = Z_3$ is the additive group of integers modulo 3 and ψ: $Z_3 \longrightarrow [0, 1]$ is defined by $\psi(0) = 1$, $\psi(1) = \psi(2) = 0.9$. Let $\varphi(0) = 0.4$ and $\varphi(1) = \varphi(2) = 0.5$. Let τ be a FSS of ψ so that $\tau(0) = 0.8$, $\tau(1) = \tau(2) = 0.6$. So we have

$$\begin{aligned}&\underline{F}(\tau)(r) = 0.6,\\ &\overline{F}(\tau)(r) = 0.8, \quad \text{for } r \in G,\\ &\underline{F}(\varphi)(r) = 0.4,\\ &\overline{F}(\varphi)(r) = 0.5, \quad \text{for } r \in G,\\ &(\overline{F}(\tau) \cap \psi)(r) = 0.8.\end{aligned} \tag{39}$$

Then, $K = PCay(Z_3, \tau, \varphi)$, $\underline{K''}$, and $\overline{K''}$ are given in Figure 5.

Theorem 12. *Let ψ be a FSG of G. Let $K = PCayF(G, \tau, \varphi)$, $K_1 = PCayF(G, \tau_1, \varphi_1)$, and $K_2 = PCayF(G, \tau_2, \varphi_2)$ are PCFGs. Then, we have*

(1) $\underline{K''} \subseteq K \subseteq \overline{K''}$

(2) $(\underline{K_1 \cap K_2})'' = \underline{K_1}'' \cap \underline{K_2}''$

(3) $K_1 \subseteq K_2 \Rightarrow \underline{K_1}'' \subseteq \underline{K_2}''$

(4) $K_1 \subseteq K_2 \Rightarrow \overline{K_1}'' \subseteq \overline{K_2}''$

(5) $(\overline{K_1 \cap K_2})'' \subseteq \overline{K_1}'' \cap \overline{K_2}''$

Proof

(1) We have

$$\begin{aligned}\underline{K''} &= PCay\,F(G, \underline{F}(\tau), \underline{F}(\varphi))\\ &\subseteq PCay\,F(G, \tau, \varphi) = K\\ &\subseteq PCay\,F(G, \overline{F}(\tau) \cap \psi, \overline{F}(\varphi))\\ &= \overline{K''}.\end{aligned} \tag{40}$$

(2) We have

$$\begin{aligned}(\underline{K_1 \cap K_2})'' &= PCay\,F(G, \underline{F}(\tau_1 \cap \tau_2), \underline{F}(\varphi_1 \cap \varphi_2))\\ &= PCay\,F(G, \underline{F}(\tau_1) \cap \underline{F}(\tau_2), \underline{F}(\varphi_1) \cap \underline{F}(\varphi_2))\\ &= PCay\,F(G, \underline{F}(\tau_1), \underline{F}(\varphi_1)) \cap PCay\,F(G, \underline{F}(\tau_2), \underline{F}(\varphi_2))\\ &= \underline{K_1''} \cap \underline{K_2''}.\end{aligned} \tag{41}$$

(3) Assume $K_1 \subseteq K_2$. Then, $\tau_1 \subseteq \tau_1$ and $\varphi_1 \subseteq \varphi_2$. So, $\underline{F}(\tau_1) \subseteq \underline{F}(\tau_2)$ and $\underline{F}(\varphi_1) \subseteq \underline{F}(\varphi_2)$. Hence, $\underline{K_1''} \subseteq \underline{K_2''}$.

(4) By Theorem 1 (h), the proof is similar to (3).

(5) We have

$$\begin{aligned}(\overline{K_1 \cap K_2})'' &= PCay\,F(G, \overline{F}(\tau_1 \cap \tau_2) \cap \psi, \overline{F}(\varphi_1 \cap \phi_2))\\ &\subseteq PCay\,F(G, (\overline{F}(\tau_1) \cap \overline{F}(\tau_2))\\ &\cap \psi, (\overline{F}(\varphi_1) \cap \overline{F}(\varphi_2))\\ &= PCay\,F(G, \overline{F}(\tau_1) \cap \psi, \overline{F}(\varphi_1))\\ &\quad \cap PCay\,F(G, \overline{F}(\tau_2) \cap \psi, \overline{F}(\varphi_2))\\ &= \overline{K_1''} \cap \overline{K_2''}.\end{aligned} \tag{42}$$

□

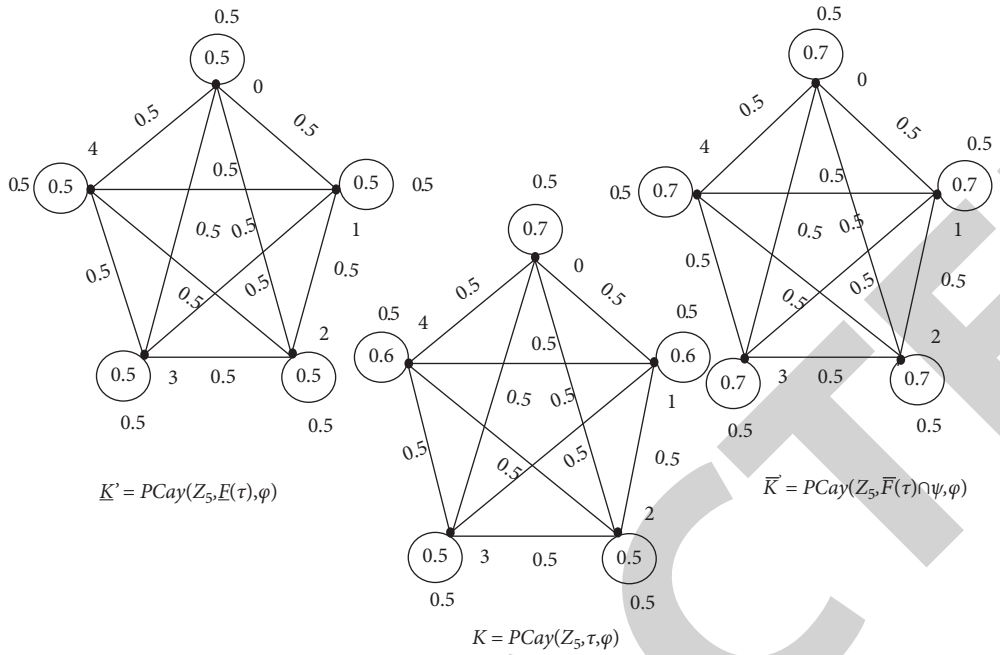

Figure 4: $K = P\text{Cay}F(Z_5, \tau, \varphi), \underline{K'}$, and $\overline{K'}$.

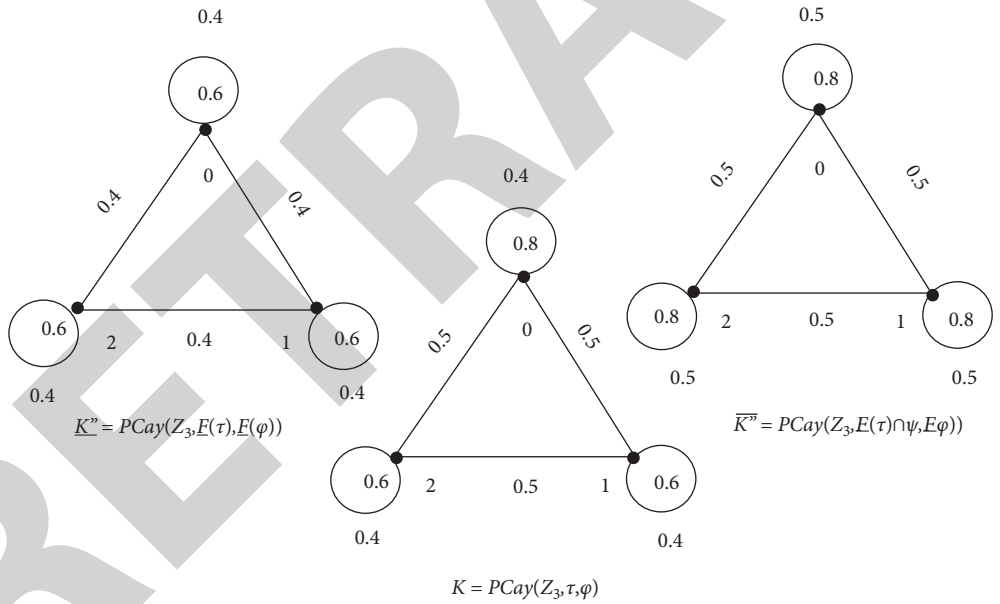

Figure 5: $K = P\text{Cay}(Z_3, \tau, \varphi), \underline{K''}$, and $\overline{K''}$.

6. Application

Example 8. Water and water resources are critical in maintaining adequate food resources and a productive environment for all living organisms. Demand for fresh water in the world is growing rapidly as the population grows and economies grow. The negative effects of global population growth, the effects of climate change, and lifestyle changes on our vital water resources are putting increasing pressure, which in turn is leading to widespread water tensions in many countries. As a result, there is an urgent need for water conservation. Water is the fluid of life because it has a strong impact on living standards and public health, although water is unevenly distributed around the world. Liquid water is very important and its existence is necessary to maintain vital human activities such as blood circulation, excretion, and reproduction. Water is also a place to live and one of the main constituents of the living environment. Population growth along with increasing water consumption not only leads to a sharp decline in water for all but also causes stress on biodiversity throughout the global ecosystem. Other important factors that limit the

availability of water are rainfall rate, soil quality, and vegetation type. In addition, there are currently serious problems with the equitable allocation of freshwater resources in the world and between and within countries. Reports indicate that water consumption has increased seven times more than that of the last century. The world's drinking water resources, unsustainable urbanization, overpopulation, water pollution, water loss, rising greenhouse gases, and overindustrialization are increasingly damaging and degrading the water resources.

Therefore, considering that water is one of the most valuable elements on the planet and that we should try to use it properly and manage it better, it is necessary to have experienced and literate people who have sufficient mastery in the use of cyberspace to advance this.

Suppose K is a CFG on the group $G = Z_6 = \{0, 1, 2, 3, 4, 5\}$ is the additive group of integers modulo 6, where the nodes and edges are expressed as follows.

The nodes (Table 2) represent the employees of the Water and Sewerage Company which correspond to the members of the group Z_6. Edges (Table 3) are the degree of people mastering the authorized space (WhatsApp, Facebook, Instagram, etc.) to improve in this organization.

Figure 6 shows that financial expert has 70% awareness to guide people on how to save water. Education and the use of technology are directly related. For example, the use of technology between the manager and the deputy is 70% that is more than other edges. As we can see, the manager has the highest impact on other officials in terms of the use of technology, so the manager is the most effective person in this office.

Example 9. Football in Iran has become the most popular sport in this country. The Iranian football team won the championship at the highest level in Asia in several years and first qualified for the 1978 FIFA World Cup. The main infrastructure of the football industry includes clubs that play a major role in the economic development of the industry. Using their equipment and facilities, these clubs have turned skilled and specialized manpower and effective football management into a money-making industry. The better the situation of the clubs, the more developed the football of that country will be. Therefore, considering this issue, to improve the quality of matches in the national league, the use of refereeing facilities (video check cameras, etc.) in these matches is of special importance. And the stronger the teams, the more sensitive this will be. In the following, we will review 8 clubs that won the first to eighth place in 2021. Suppose K is a CFG on the group $G = Z_8 = \{0, 1, 2, 3, 4, 5, 6, 7\}$ with the group congruence modulo 8 integral number$Z$, where the nodes and edges are expressed as follows:

(a) The nodes (Table 4) represent the names of the clubs and their weight. The quality of the game of these teams during the league which correspond to the members of group Z_8

Table 2: The staff education rate.

Employees	Label	Education rate
Manager	0	0.9
Deputy	1	0.9
Financial expert	2	0.9
Billing expert	3	0.8
Responsible for subscriber affairs	4	0.8
Services	5	0.7

Table 3: The use of technology corresponding to Figure 5.

	0	1	2	3	4	5
0	0	0.6	0.5	0.4	0.5	0.6
1	0.6	0	0.6	0.5	0.4	0.5
2	0.5	0.6	0	0.6	0.5	0.4
3	0.4	0.5	0.6	0	0.6	0.5
4	0.5	0.4	0.5	0.6	0	0.6
5	0.6	0.5	0.4	0.5	0.6	0

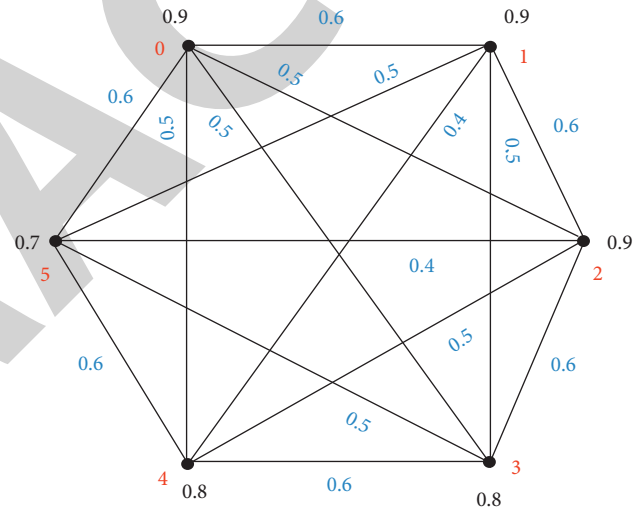

Figure 6: CFG.

Table 4: Ranking of the country's football clubs.

Team names	Label	Game quality
Esteghlal	0	0.9
Perspolis	1	0.9
Sepahan	2	0.9
Gol Gohar	3	0.8
Foolad	4	0.8
Mes Rafsanjan	5	0.8
Aluminium Arak	6	0.7
Zob Ahan	7	0.7

(b) The edges (Table 5) of the matches between these clubs and their weight are the importance of refereeing facilities about these matches

As we know, the match between the teams of the country's premier league is much more sensitive than other leagues. For example, according to Figure 7, the sensitivity of Esteghlal and Persepolis games and the sensitivity of

Table 5: Referee's sensitivity to matches according to Figure 7.

	0	1	2	3	4	5	6	7
0	0	0.6	0.5	0.4	0.4	0.4	0.5	0.6
1	0.6	0	0.6	0.5	0.4	0.4	0.4	0.5
2	0.5	0.6	0	0.6	0.5	0.4	0.4	0.4
3	0.4	0.5	0.6	0	0.6	0.5	0.4	0.4
4	0.4	0.4	0.5	0.6	0	0.6	0.5	0.4
5	0.4	0.4	0.4	0.5	0.6	0	0.6	0.5
6	0.5	0.4	0.4	0.4	0.5	0.6	0	0.6
5	0.6	0.5	0.4	0.4	0.4	0.5	0.6	0

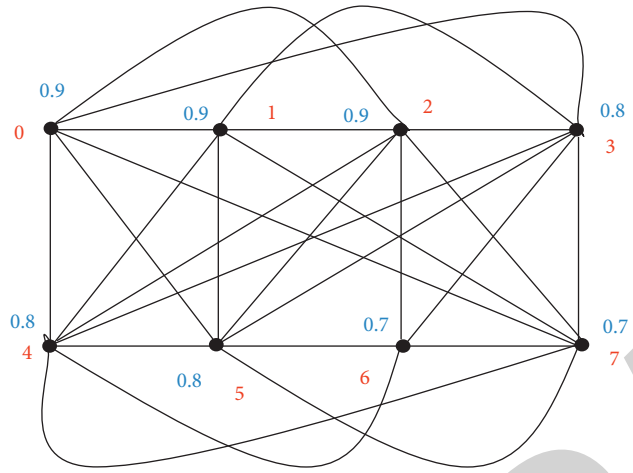

Figure 7: The CFG for the matches of 8 teams in the country's premier league.

Aluminum Arak and Zobahan are on the same level. Therefore, using a variety of refereeing facilities (video check camera, use of yellow and red cards, experienced referee and assistant referee, etc.) can change the fate of the game.

7. Conclusion

The fuzzy rough models are very important in FG problems and they give more integrity, flexibility, and suitability to the system. CFG has a wide bound of applications in the field of psychological sciences as well as the reconnoiter of individuals founded on oncological behaviors. So, in this survey, we have introduced two new algebraic definitions called CFGs and PCFGs and studied their rough approximations with several examples. Likewise, some properties of fuzzy rough sets (FRSs) in CFGs and PCFGs have been investigated. Finally, two applications are presented using CFG, in one of which the most effective and literate person in cyberspace technology in the Water and Sewerage Organization is identified, and in the other, the sensitivity of refereeing facilities in the country's Premier Football League is shown. It means we showed that the use of refereeing facilities is more among the teams that are at the top of the table than other teams.

Data Availability

No data were used to support this study.

Conflicts of Interest

The authors declare that they have no conflicts of interest.

Acknowledgments

This work was supported by the National Key R and D Program of China (Grant 2018YFB1005100), the National Natural Science Foundation of China (no. 62172116), and the Guangzhou Academician and Expert Workstation (no. 20200115-9).

References

[1] A. Rosenfeld, "Fuzzy graphs," in *Fuzzy Sets and Their Applications to Cognitive and Decision Processes*, L. A. Zadeh, K. S. Fu, and M. Shimura, Eds., pp. 77–95, Academic Press, New York, NY, USA, 1975.

[2] L. A. Zadeh, "Fuzzy sets," *Information and ControlInformation and Control*, vol. 8, no. 3, pp. 338–353, 1965.

[3] N. O. Alshehri and M. Akram, "Cayley bipolar fuzzy graphs," *The Scientific World Journal*, vol. 2013, Article ID 156786, 8 pages, 2013.

[4] N. M. Namboothiri, V. A. Kumar, and P. T. Ramachandran, "Cayley fuzzy graphs," *Far East Journal of Mathematical Sciences*, vol. 73, pp. 1–15, 2013.

[5] M. Akram, M. G. Karunambigal, and O. K. Kaluivani, "Cayley intutionistic fuzzy graphs," *Journal of Appllied Mathematics and Informatics*, vol. 32, no. 5-6, pp. 827–842, 2014.

[6] R. A. Borzooei and H. Rashmanlou, "Cayley interval-valued fuzzy graphs," *UPB Scientific Bulletin, Series A: Applied Mathematics and Physics*, vol. 78, no. 3, pp. 83–94, 2016.

[7] Z. Pawlak, "Rough sets," *International Journal of Computer & Information Sciences*, vol. 11, no. 5, pp. 341–356, 1982.

[8] A. Skowron and L. Polkowski, *Rough Sets in Knowledge Discovery*, Springer-Verlag, Berlin, Germany, 1998.

[9] W. P. Ziarko, "Rough sets, fuzzy sets and knowledge discovery," in *Proceedings of the International Workshop on Rough Sets and Knowledge Discovery*, London, UK, October 1994.

[10] R. Biswas and S. Nanda, "Rough groups and rough subgroups," *Bulletin of the Polish Academy of Sciences - Mathematics*, vol. 42, pp. 251–254, 1994.

[11] N. Kuroki and J. N. Moderson, "Structures of rough sets and rough groups," *Journal of Fuzzy Mathematics*, vol. 5, no. 1, pp. 183–191, 1997.

[12] T. He and K. Shi, "Rough graph and its structure," *Journal of Shandong University*, vol. 41, no. 6, pp. 46–50, 2006.

[13] M. H. Shahzamanian, M. Shirmohammadi, and B. Davvaz, "Roughness in Cayley graphs," *Information Sciences*, vol. 180, no. 17, pp. 3362–3372, 2010.

[14] K. Chakrabarty, R. Biswas, and S. Nanda, "Fuzziness in rough sets," *Fuzzy Sets and Systems*, vol. 110, no. 2, pp. 247–251, 2000.

[15] W. Wu, M. Ju-Sheng, and W.-X. Zhang, "Generalized fuzzy rough sets," *Information Sciences*, vol. 151, pp. 263–282, 2003.

[16] R. Mahapatra, S. Samanta, M. Pal, and Q. Xin, "Link prediction in social networks by neutrosophic graph," *International Journal of Computational Intelligence Systems*, vol. 13, no. 1, pp. 1699–1713, 2020.

[17] R. Mahapatra, S. Samanta, and M. Pal, "Generalized neutrosophic planar graphs and its application," *Journal of Applied Mathematics and Computing*, vol. 65, no. 1-2, pp. 693–712, 2020.

Hindawi
Journal of Mathematics
Volume 2023, Article ID 9838794, 1 page
https://doi.org/10.1155/2023/9838794

Retraction

Retracted: On Some Classes of Estimators Derived from the Positive Part of James–Stein Estimator

Journal of Mathematics

Received 19 December 2023; Accepted 19 December 2023; Published 20 December 2023

This article has been retracted by Hindawi following an investigation undertaken by the publisher [1]. This investigation has uncovered evidence of one or more of the following indicators of systematic manipulation of the publication process:

(1) Discrepancies in scope

(2) Discrepancies in the description of the research reported

(3) Discrepancies between the availability of data and the research described

(4) Inappropriate citations

(5) Incoherent, meaningless and/or irrelevant content included in the article

(6) Manipulated or compromised peer review

The presence of these indicators undermines our confidence in the integrity of the article's content and we cannot, therefore, vouch for its reliability. Please note that this notice is intended solely to alert readers that the content of this article is unreliable. We have not investigated whether authors were aware of or involved in the systematic manipulation of the publication process.

Wiley and Hindawi regrets that the usual quality checks did not identify these issues before publication and have since put additional measures in place to safeguard research integrity.

We wish to credit our own Research Integrity and Research Publishing teams and anonymous and named external researchers and research integrity experts for contributing to this investigation.

The corresponding author, as the representative of all authors, has been given the opportunity to register their agreement or disagreement to this retraction. We have kept a record of any response received.

References

[1] A. Hamdaoui, A. Benkhaled, M. Alshahrani, M. Terbeche, W. Almutiry, and A. Alahmadi, "On Some Classes of Estimators Derived from the Positive Part of James–Stein Estimator," *Journal of Mathematics*, vol. 2023, Article ID 5221061, 12 pages, 2023.

Hindawi
Journal of Mathematics
Volume 2023, Article ID 5221061, 12 pages
https://doi.org/10.1155/2023/5221061

Research Article

On Some Classes of Estimators Derived from the Positive Part of James–Stein Estimator

Abdenour Hamdaoui,[1,2] **Abdelkader Benkhaled**,[3,4] **Mohammed Alshahrani**,[5] **Mekki Terbeche**,[1,6] **Waleed Almutiry**,[7] **and Amani Alahmadi**[8]

[1]*Department of Mathematics, University of Sciences and Technology, Mohamed Boudiaf, Oran, Algeria*
[2]*Laboratory of Statistics and Random Modelisations of University About Bekr Belkaid (LSMA), Tlemcen, El Mnaouar, BP 1505, Bir El Djir 31000, Oran, Algeria*
[3]*Department of Biology, University of Mascara, Mascara, Algeria*
[4]*Laboratory of Stochastic Models, Statistics and Applications, University Tahar Moulay of Saïda, Mascara 29000, Algeria*
[5]*Department of Mathematics, College of Science and Humanities in Al-Kharj, Prince Sattam Bin Abdulaziz University, Al-Kharj 11942, Saudi Arabia*
[6]*Laboratory of Analysis and Application of Radiation (LAAR), USTO-MB, El Mnaouar, BP 1505, Bir El Djir 31000, Oran, Algeria*
[7]*Department of Mathematics, College of Science and Arts in Ar Rass, Qassim University, Buryadah 52571, Saudi Arabia*
[8]*Department of Mathematics, College of Science and Humanities in Ad Dawadmi, Shaqra University, Shaqra, Saudi Arabia*

Correspondence should be addressed to Abdenour Hamdaoui; abdenour.hamdaoui@univ-usto.dz

Received 24 April 2022; Revised 18 June 2022; Accepted 22 June 2022; Published 8 April 2023

Academic Editor: Naeem Jan

This work consists of developing shrinkage estimation strategies for the multivariate normal mean when the covariance matrix is diagonal and known. The domination of the positive part of James–Stein estimator (PPJSE) over James–Stein estimator (JSE) relative to the balanced loss function (BLF) is analytically proved. We introduce a new class of shrinkage estimators which ameliorate the PPJSE, and then we construct a series of polynomial shrinkage estimators which improve the PPJSE; also, any estimator of this series can be ameliorated by adding to it a new term of higher degree. We end this paper by simulation studies which confirm the performance of the suggested estimators.

1. Introduction

The minimax approach has received the most extensive development in the estimation of the mean parameter of a random vector $Y \sim N_d(\nu, \sigma^2 I_d)$. It has been known since Stein [1] that if $d < 3$, the maximum likelihood estimator (MLE) Y is minimax and admissible. Namely, the MLE is minimax and it is considered to bethe best estimator of the mean δ under the quadratic loss function. However, when $d > 2$, Stein [1] and James and Stein [2] showed that the shrinkage estimator $\delta_a = (1 - (a/\|Y\|^2))Y$ with the shrinkage function $\phi_a = (1 - (a/\|Y\|^2))$ which shrinks the components of the vector Y to zero has a quadratic risk inferior to the MLE for specific values of the real parameter a. This explains the inadmissibility of the MLE for $d > 2$. The better estimator in the class of estimator δ_a is called the JSE.

Several studies have been interested in constructing new shrinkage estimators that improve both the MLE and the JSE, for example, Lindley [3], Bhattacharya [4], Berger [5], Stein [6], Norouzirad and Arashi [7], Cheng and Chaturvedi [8], and Kashani et al. [9]. Other studies developed the shrinkage estimators under the Bayesian framework, and we cite, for example, Strawderman [10], Lindley [11], Efron and Morris [12], Hudson [13], and Hamdaoui et al. [14].

As the shrinkage real function can take negative values which can affect it by losing its target of reducing the compounds of the MLE to 0, Baranchik [15] introduced the PPJSE estimator $\delta_a^+ = (1 - (a/\|Y\|^2))^+ Y$ which can take only positive values,

where $(1-(a/\|Y\|^2))^+ = \max(0; 1-(a/\|Y\|^2))$. Baranchik [15] shows that under the quadratic loss function, the PPJSE dominates the MLE and it also ameliorates the JSE. The shrinkage estimators in all of the above cited studies were based on the quadratic loss function.

Zellner [16] extended the problem of estimating the multivariate normal mean in large dimension, and then he suggested the BLF that generalizes the quadratic loss function. The published papers in this direction include Sanjari Farsipour and Asgharzadeh [17], Selahattin and Issam [18], Nimet and Selahattin [19], Lahoucine et al. [20], Karamikabir and Afsahri [21], and Karamikabir et al. [22].

PPJSE is one of the best estimators that significantly improves the JSE under the quadratic loss function. Benmansour and Hamdaoui [23] and Hamdaoui and Benmansour [24] have proved this in the simulation section in their studies. Hamdaoui [25] also proposed a class of shrinkage estimators derived from the MLE and improved the PPJSE under the quadratic loss function. Therefore, in this work, we generalize the results obtained in Hamdaoui [25] by using the BLF instead of the quadratic loss function in the comparison between two different estimators. That is, we deal with the model $Y \sim N_d(\nu, I_d)$. The main goal is to estimate the parameter ν by shrinkage estimators derived from the MLE. To determine the quality of each considered estimator, we use the risk function that is based on the BLF.

This paper is arranged as follows. In Section 2, we give details of the shrinkage estimators and recall some important published results. Also, we introduce a class of estimators that improve the PPJSE. In Section 3, we construct a series of shrinkage polynomial type estimators derived from the PPJSE and prove the domination and performance properties of these estimators between them. We end this work by simulation results followed by the conclusion.

2. A New Class of Estimators That Improve the PPJSE

First, we consider the model that has the random variable Y to follow the multivariate normal distribution with a mean vector ν and identity covariance matrix I_d. In this model, we will focus on estimating the mean parameters ν using the shrinkage estimators that are based on the BLF. For the quality comparison of any estimator T of ν, we incorporate the BLF in the calculation of its risk function as defined in Hamdaoui et al. [26].

$$\ell_\omega(T,\nu) = \omega\|T-T_0\|^2 + (1-\omega)\|T-\nu\|^2, \quad 0 \le \omega < 1. \tag{1}$$

Then, based on equation (1), the risk function is defined as

$$R_\omega(T,\nu) = \mathbb{E}(\ell_\omega(T,\nu)). \tag{2}$$

In this case, the MLE is $Y := T_0$, its risk function is equal to $(1-\omega)d$, and the classical estimator that dominates the MLE under the BLF given in equation (1) is the following JSE:

$$T_{JS}(Y) = \left(1-\frac{\alpha}{\|Y\|^2}\right)Y, \tag{3}$$

where $\alpha = (1-w)(d-2)$. Its risk function under the BLF is

$$R_\omega\left(T_{JS}(Y),\nu\right) = (1-\omega)d - (1-w)^2(d-2)^2\mathbb{E}\left(\frac{1}{\|Y\|^2}\right). \tag{4}$$

Also, the classical estimator that improves the JSE is the PPJSE defined as

$$T_{JS+}(Y) = \left(1-\alpha\frac{1}{\|Y\|^2}\right)^+ Y = \left(1-\alpha\frac{1}{\|Y\|^2}\right)\mathbb{I}_{(\alpha/\|Y\|^2)\le 1}Y, \tag{5}$$

where $(1-\alpha(1/\|Y\|^2))^+ = \max(0, 1-\alpha(1/\|Y\|^2))$ and $\mathbb{I}_{(\alpha/\|Y\|^2)\le 1}$ is the indicator function of $\{(\alpha/\|Y\|^2)\le 1\}$. Hamdaoui et al. [26] demonstrated that its risk function is defined as

$$R_\omega\left(T_{JS+}(Y),\nu\right) = R_\omega\left(T_{JS}(Y),\nu\right) + \mathbb{E}\left[\left(\|Y\|^2 + \frac{(1-\omega)^2(d-2)^2}{\|Y\|^2} - 2(1-\omega)d\right)\mathbb{I}_{(\alpha/\|Y\|^2)\ge 1}\right]. \tag{6}$$

They also proved that, based on the BLF, $T_{JS+}(Y)$ dominates $T_{JS}(Y)$.

Now, we will construct a simple class of estimators that improves $T_{JS+}(Y)$ under the BLF. We add a term of the form $\beta(1/\|Y\|^2)^2\mathbb{I}_{(\alpha/\|Y\|^2)\le 1}Y$ to the PPJSE estimator $T_{JS+}(Y)$. That is, we consider the following estimator:

$$T^{(2)}_{\beta,JS+}(Y) = T_{JS+}(Y) + \beta\left(\frac{1}{\|Y\|^2}\right)^2\mathbb{I}_{(\alpha/\|Y\|^2)\le 1}Y, \tag{7}$$

where the constant β can be related to d and ω.

Proposition 1. *Based on the BLF, the risk function of the estimator $T^{(2)}_{\beta,JS+}(Y)$ given in equation (7) can be expressed as*

$$R_\omega\left(T^{(2)}_{\beta,JS+}(Y),\nu\right) = R_\omega\left(T_{JS+}(Y),\nu\right) + \beta^2\mathrm{IE}\left(\frac{1}{\|Y\|^6}\mathbb{I}_{(\alpha/\|Y\|^2)\le 1}\right) - 4\beta(1-\omega)\mathrm{IE}\left(\frac{1}{\|Y\|^4}\mathbb{I}_{(\alpha/\|Y\|^2)\le 1}\right). \tag{8}$$

Proof. As

$$
\begin{aligned}
R_{\omega}\left(T^{(2)}_{\beta,JS+}(Y),\nu\right) &= \omega\mathbb{E}\left(\left\|T_{JS+}(Y)+\beta\frac{1}{\left(\|Y\|^2\right)^2}\mathbb{I}_{\left(\alpha/\|Y\|^2\right)\le 1}Y-Y\right\|^2\right)\\
&\quad+(1-\omega)\mathbb{E}\left(\left\|T_{JS+}(Y)+\beta\frac{1}{\left(\|Y\|^2\right)^2}\mathbb{I}_{\left(\alpha/\|Y\|^2\right)\le 1}Y-\nu\right\|^2\right)\\
&= R_{\omega}\left(T_{JS+}(Y),\nu\right)+\beta^2\mathbb{E}\left(\frac{1}{\left(\|Y\|^2\right)^3}\mathbb{I}_{\left(\alpha/\|Y\|^2\right)\le 1}\right)\\
&\quad+2\omega\beta\mathbb{E}\left(\left\langle T_{JS+}(Y)-Y,\frac{1}{\left(\|Y\|^2\right)^2}\mathbb{I}_{\left(\alpha/\|Y\|^2\right)\le 1}Y\right\rangle\right)\\
&\quad+2(1-\omega)\beta\mathbb{E}\left(\left\langle T_{JS+}(Y)-\nu,\frac{1}{\left(\|Y\|^2\right)^2}\mathbb{I}_{\left(\alpha/\|Y\|^2\right)\le 1}Y\right\rangle\right),
\end{aligned}
\tag{9}
$$

then

$$
\begin{aligned}
R_{\omega}\left(T^{(2)}_{\beta,JS+}(Y),\nu\right) &= R_{\omega}\left(T_{JS+}(Y),\nu\right)+\beta^2\mathbb{E}\left(\frac{1}{\left(\|Y\|^2\right)^3}\mathbb{I}_{\left(\alpha/\|Y\|^2\right)\le 1}\right)\\
&\quad+2\omega\beta\mathbb{E}\left(\left\langle T_{JS+}(Y)-Y,\frac{1}{\left(\|Y\|^2\right)^2}\mathbb{I}_{\left(\alpha/\|Y\|^2\right)\le 1}Y\right\rangle\right)\\
&\quad+2(1-\omega)\beta E\left(\left\langle T_{JS+}(Y)-Y+Y-\nu,\frac{1}{\left(\|Y\|^2\right)^2}\mathbb{I}_{\left(\alpha/\|Y\|^2\right)\le 1}Y\right\rangle\right).
\end{aligned}
\tag{10}
$$

Thus,

$$
\begin{aligned}
R_{\omega}\left(T^{(2)}_{\beta,JS+}(Y),\nu\right) &= R_{\omega}\left(T_{JS+}(Y),\nu\right)+\beta^2\mathbb{E}\left(\frac{1}{\left(\|Y\|^2\right)^3}\mathbb{I}_{\left(\alpha/\|Y\|^2\right)\le 1}\right)\\
&\quad+2\beta\mathbb{E}\left(\left\langle T_{JS+}(Y)-Y,\frac{1}{\left(\|Y\|^2\right)^2}\mathbb{I}_{\left(\alpha/\|Y\|^2\right)}Y\right\rangle\right)\\
&\quad+2(1-\omega)\beta\mathbb{E}\left(\left\langle Y-\nu,\frac{1}{\left(\|Y\|^2\right)^2}\mathbb{I}_{\left(\alpha/\|Y\|^2\right)}Y\right\rangle\right).
\end{aligned}
\tag{11}
$$

The second expectation of equation (11) can be expressed as

$$\mathbb{E}\left(\left\langle T_{JS+}(Y)-Y,\frac{1}{\left(\|Y\|^2\right)^2}\mathbb{I}_{\left(\alpha/\|Y\|^2\right)\le 1}Y\right\rangle\right)=\mathbb{E}\left(\left\langle -\frac{\alpha}{\left(\|Y\|^2\right)^2}\mathbb{I}_{\left(\alpha/\|Y\|^2\right)\le 1}Y,\frac{1}{\left(\alpha/\|Y\|^2\right)\le 1}\mathbb{I}_{\left(\alpha/\|Y\|^2\right)\le 1}Y\right\rangle\right)=-\alpha\mathbb{E}\left(\frac{1}{\|Y\|^4}\mathbb{I}_{\left(\alpha/\|Y\|^2\right)\le 1}\right). \tag{12}$$

Also, based on Lemma 2.1 of Shao and Strawderman [27], the third expectation of equation (11) can be expressed as

$$\begin{aligned}&\mathbb{E}\left(\left\langle Y-\nu,\frac{1}{\left(\|Y\|^2\right)^2}\mathbb{I}_{\left(\alpha/\|Y\|^2\right)\le 1}Y\right\rangle\right)\\&=(d-4)\mathbb{E}\left(\frac{1}{\|Y\|^4}\mathbb{I}_{\left(\alpha/\|Y\|^2\right)\le 1}\right).\end{aligned} \tag{13}$$

Then, according to equations (11), (12), and (13), we obtain the desired result. □

Theorem 1. *For $d>4$ and based on the BLF, a sufficient condition for which the estimator $T^{(2)}_{\beta,JS+}(Y)$ dominates $T_{JS+}(Y)$ is*

$$0\le\beta\le 4(1-\omega)^2(d-2). \tag{14}$$

Proof. As

$$\begin{aligned}\mathbb{E}\left(\frac{1}{\|Y\|^6}\mathbb{I}_{\left(\alpha/\|Y\|^2\right)\le 1}\right)&=\mathbb{E}\left(\frac{1}{\|Y\|^2}\frac{1}{\|Y\|^4}\mathbb{I}_{\left(\alpha/\|Y\|^2\right)\le 1}\right)\\&\le\mathbb{E}\left(\frac{1}{\alpha}\frac{1}{\|Y\|^4}\mathbb{I}_{\left(\alpha/\|Y\|^2\right)\le 1}\right)\\&=\frac{1}{(1-\omega)(d-2)}\mathbb{E}\left(\frac{1}{\|Y\|^4}\mathbb{I}_{\left(\alpha/\|Y\|^2\right)\le 1}\right),\end{aligned} \tag{15}$$

we can deduce from Proposition 1 that

$$\begin{aligned}R_\omega\left(T^{(2)}_{\beta,JS+}(Y),\nu\right)&\le R_\omega\left(T_{JS+}(Y),\nu\right)\\&\quad+\beta\left(\frac{\beta}{(1-\omega)(d-2)}-4(1-\omega)\right)\\&\quad\mathbb{E}\left(\frac{1}{\|Y\|^4}\mathbb{I}_{\left(\alpha/\|Y\|^2\right)\le 1}\right).\end{aligned} \tag{16}$$

Consequently, a sufficient condition for which the estimator $T^{(2)}_{\beta,JS+}(Y)$ dominates $T_{JS+}(Y)$ is

$$\frac{\beta}{(1-\omega)(d-2)}-4(1-\omega)\le 0, \tag{17}$$

which is equivalent to

$$0\le\beta\le 4(1-\omega)^2(d-2). \tag{18}$$

From the convexity of the right hand side of inequality (16) with respect to β and taking its first derivative, we can deduce that this term takes its minimum value when

$$\widehat{\beta}=2(1-\omega)^2(d-2), \tag{19}$$

and if we substitute β by $\widehat{\beta}$, we obtain the domination of $T^{(2)}_{\widehat{\beta},JS+}(Y)$ over $T_{JS+}(Y)$, as shown below:

$$\begin{aligned}R_\omega\left(T^{(2)}_{\widehat{\beta},JS+}(Y),\nu\right)&\le R_\omega\left(T_{JS+}(Y),\nu\right)\\&\quad-4(1-\omega)^3(d-2)\mathbb{E}\left(\frac{1}{\|Y\|^4}\mathbb{I}_{\left(\alpha/\|Y\|^2\right)\le 1}\right)\\&\le R_\omega\left(T_{JS+}(Y),\nu\right).\end{aligned} \tag{20}$$

□

3. The Performance of Some Derived Shrinkage Estimators from the PPJSE

In Section 2, we note that when a term of the form $\beta(1/\|Y\|^2)^2\mathbb{I}_{(\alpha/\|Y\|^2)\le 1}Y$ is added to the $T_{JS+}(Y)$, we obtain estimators that have smaller risk than the risk of $T_{JS+}(Y)$. Therefore, following this effect, the main idea of this section is to construct new classes of estimators deduced by modifying $T_{JS+}(Y)$. We add recursively a term of the form $c(1/\|Y\|^2)^m\mathbb{I}_{(\alpha/\|Y\|^2)\le 1}Y$, where m is an integer parameter and c is a constant that can be related to d and ω. Consequently, we build a series of estimators of polynomial type with the indeterminate $(1/\|Y\|^2)\mathbb{I}_{(\alpha/\|Y\|^2)\le 1}Y$ such as if we increase the degree of the polynomial, we obtain a best estimator. Now, consider the estimator

$$\begin{aligned}T^{(3)}_{\gamma,JS+}(Y)&=T^{(2)}_{\widehat{\beta},JS+}(Y)+\gamma\left(\frac{1}{\|Y\|^2}\right)^3\mathbb{I}_{\left(\alpha/\|Y\|^2\right)\le 1}Y\\&=\left(1-\alpha\frac{1}{\|Y\|^2}+\widehat{\beta}\left(\frac{1}{\|Y\|^2}\right)^2+\gamma\left(\frac{1}{\|Y\|^2}\right)^3\right)\mathbb{I}_{\left(\alpha/\|Y\|^2\right)\le 1}Y,\end{aligned} \tag{21}$$

where $\widehat{\beta}$ is defined in equation (19) and the positive real parameter γ can be related to d and ω.

Proposition 2. *Based on the BLF ℓ_ω, the risk function of $T^{(3)}_{\gamma,JS+}(Y)$ given in equation (21) is*

$$\begin{aligned}R_\omega\left(T^{(3)}_{\gamma,JS+}(Y),\nu\right)&=R_\omega\left(T^{(2)}_{\widehat{\beta},JS+}(Y),\nu\right)\\&\quad+\gamma^2\mathbb{E}\left(\frac{1}{\|Y\|^{10}}\mathbb{I}_{\left(\alpha/\|Y\|^2\right)\le 1}\right)\\&\quad+4\gamma(1-\omega)(d-6)\mathbb{E}\left(\frac{1}{\|Y\|^8}\mathbb{I}_{\left(\alpha/\|Y\|^2\right)\le 1}\right)\\&\quad-8\gamma(1-\omega)\mathbb{E}\left(\frac{1}{\|Y\|^6}\mathbb{I}_{\left(\alpha/\|Y\|^2\right)\le 1}\right).\end{aligned} \tag{22}$$

Proof.

$$
\begin{aligned}
R_{\omega}\left(T^{(3)}_{\gamma,JS+}(Y),\nu\right) &= \omega\mathbb{E}\left(\left\|T^{(2)}_{\widehat{\beta},JS+}(Y)+\gamma\left(\frac{1}{\|Y\|^2}\right)^3\mathbb{I}_{(\alpha/\|Y\|^2)\le 1}Y-Y\right\|^2\right)\\
&\quad+(1-\omega)\mathbb{E}\left(\left\|T^{(2)}_{\widehat{\beta},JS+}(Y)+\gamma\left(\frac{1}{\|Y\|^2}\right)^3\mathbb{I}_{(\alpha/\|Y\|^2)\le 1}Y-\nu\right\|^2\right)\\
&= R_{\omega}\left(T^{(2)}_{\widehat{\beta},JS+}(Y),\nu\right)+\gamma^2\mathbb{E}\left(\frac{1}{\left(\|Y\|^2\right)^5}\mathbb{I}_{(\alpha/\|Y\|^2)\le 1}\right)+2\gamma\omega\mathbb{E}\left(\left\langle T^{(2)}_{\widehat{\beta},JS+}(Y)-Y,\frac{1}{\left(\|Y\|^2\right)^3}\mathbb{I}_{(\alpha/\|Y\|^2)\le 1}Y\right\rangle\right)\\
&\quad+2c(1-\omega)\mathbb{E}\left(\left\langle T^{(2)}_{\widehat{\beta},JS+}(Y)-\nu,\frac{1}{\left(\|Y\|^2\right)^3}\mathbb{I}_{(\alpha/\|Y\|^2)\le 1}Y\right\rangle\right)\\
&= R_{\omega}\left(T^{(2)}_{\widehat{\beta},JS+}(Y),\nu\right)+\gamma^2\mathbb{E}\left(\frac{1}{\left(\|Y\|^2\right)^5}\mathbb{I}_{(\alpha/\|Y\|^2)\le 1}\right)+2\gamma\omega\mathbb{E}\left(\left\langle T^{(2)}_{\widehat{\beta},JS+}(Y)-Y,\frac{1}{\left(\|Y\|^2\right)^3}\mathbb{I}_{(\alpha/\|Y\|^2)\le 1}Y\right\rangle\right)\\
&\quad+2\gamma(1-\omega)\mathbb{E}\left(\left\langle T^{(2)}_{\widehat{\beta},JS+}(Y)-Y+Y-\nu,\frac{1}{\left(\|Y\|^2\right)^3}\mathbb{I}_{(\alpha/\|Y\|^2)\le 1}Y\right\rangle\right)\\
&= R_{\omega}\left(T^{(2)}_{\widehat{\beta},JS+}(Y),\nu\right)+\gamma^2 IE\left(\frac{1}{\left(\|Y\|^2\right)^5}\mathbb{I}_{(\alpha/\|Y\|^2)\le 1}\right)+2\gamma\mathbb{E}\left(\left\langle T^{(2)}_{\widehat{\beta},JS+}(Y)-Y,\frac{1}{\left(\|Y\|^2\right)^3}\mathbb{I}_{(\alpha/\|Y\|^2)\le 1}Y\right\rangle\right)\\
&\quad+2\gamma(1-\omega)\mathbb{E}\left(\left\langle Y-\nu,\frac{1}{\left(\|Y\|^2\right)^3}\mathbb{I}_{(\alpha/\|Y\|^2)\le 1}Y\right\rangle\right).
\end{aligned}
\tag{23}
$$

As

$$
\begin{aligned}
\mathbb{E}\left(\left\langle \mathbb{T}^{(2)}_{\widehat{\beta},JS+}(Y)-Y,\frac{1}{\left(\|Y\|^2\right)^3}\mathbb{I}_{(\alpha/\|Y\|^2)\le 1}Y\right\rangle\right) &= \mathbb{E}\left(\left\langle\left(1-\frac{\alpha}{\|Y\|^2}+\frac{\widehat{\beta}}{\|Y\|^4}\right)\mathbb{I}_{(\alpha/\|Y\|^2)\le 1}Y-Y,\frac{1}{\|Y\|^6}\mathbb{I}_{(\alpha/\|Y\|^2)\le 1}Y\right\rangle\right)\\
&= \mathbb{E}\left(-\alpha\frac{1}{\|Y\|^6}\mathbb{I}_{(\alpha/\|Y\|^2)\le 1}+\widehat{\beta}\frac{1}{\|Y\|^8}\mathbb{I}_{(\alpha/\|Y\|^2)\le 1}\right),
\end{aligned}
\tag{24}
$$

by applying Lemma 2.1 of Shao and Strawderman [27], we obtain

$$
\begin{aligned}
&\mathbb{E}\left\langle Y-\nu,\frac{1}{\|Y\|^6}\mathbb{I}_{(\alpha/\|Y\|^2)\le 1}Y\right\rangle\\
&\quad=(d-6)\mathbb{E}\left(\frac{1}{\|Y\|^6}\mathbb{I}_{(\alpha/\|Y\|^2)\le 1}\right).
\end{aligned}
\tag{25}
$$

From equations (23), (24), and (25), we get the desired result. □

Theorem 2. *For $d>6$ and based on the BLF, a sufficient condition for which the estimator $T^{(3)}_{\gamma,JS+}(Y)$ dominates $T^{(2)}_{\widehat{\beta},JS+}(Y)$ is*

$$
0\le\gamma\le 4(1-\omega)^3(d-2)^2. \tag{26}
$$

Proof. As

$$\mathbb{E}\left(\frac{1}{\|Y\|^{10}}\mathbb{I}_{(\alpha/\|Y\|^2)\le 1}\right)=\mathbb{E}\left(\frac{1}{\|Y\|^4}\frac{1}{\|Y\|^6}\mathbb{I}_{(\alpha/\|Y\|^2)\le 1}\right)$$
$$\le \mathbb{E}\left(\frac{1}{\alpha^2}\frac{1}{\|Y\|^6}\mathbb{I}_{(\alpha/\|Y\|^2)\le 1}\right) \quad (27)$$
$$=\frac{1}{\alpha^2}\mathbb{E}\left(\frac{1}{\|Y\|^6}\mathbb{I}_{(\alpha/\|Y\|^2)\le 1}\right),$$

and

$$\mathbb{E}\left(\frac{1}{\|Y\|^8}\mathbb{I}_{(\alpha/\|Y\|^2)\le 1}\right)=\mathbb{E}\left(\frac{1}{\|Y\|^2}\frac{1}{\|Y\|^6}\mathbb{I}_{(d-2/\|Y\|^2)\le 1}\right)$$
$$\le \mathbb{E}\left(\frac{1}{\alpha}\frac{1}{\|Y\|^6}\mathbb{I}_{(\alpha/\|Y\|^2)\le 1}\right) \quad (28)$$
$$=\frac{1}{\alpha}\mathbb{E}\left(\frac{1}{\|Y\|^6}\mathbb{I}_{(\alpha/\|Y\|^2)\le 1}\right),$$

by using equations (27) and (28) and Proposition 2, we obtain

$$R_\omega\left(T^{(3)}_{\gamma,JS+}(Y),\nu\right)\le R_\omega\left(T^{(2)}_{\widehat{\beta},JS+},\nu\right)$$
$$+\gamma^2\frac{1}{\alpha^2}\mathbb{E}\left(\frac{1}{\|Y\|^6}\mathbb{I}_{(\alpha/\|Y\|^2)\le 1}\right)$$
$$+2\gamma\frac{\widehat{\beta}}{\alpha}\mathbb{E}\left(\frac{1}{\|Y\|^6}\mathbb{I}_{(\alpha/\|Y\|^2)\le 1}\right)$$
$$-8\gamma(1-\omega)\mathbb{E}\left(\frac{1}{\|Y\|^6}\mathbb{I}_{(\alpha/\|Y\|^2)\le 1}\right) \quad (29)$$
$$=R_\omega\left(T^{(2)}_{\widehat{\beta}}(Y),\nu\right)$$
$$+\gamma\left(\frac{\gamma}{(1-\omega)^2(d-2)^2}-4(1-\omega)\right)$$
$$\mathbb{E}\left(\frac{1}{\|Y\|^6}\mathbb{I}_{(\alpha/\|Y\|^2)\le 1}\right).$$

Then, a sufficient condition for which the estimator $T^{(3)}_{\gamma,JS+}(\|Y\|^2)$ dominates $\delta^{(2)}_{\widehat{\beta},JS+}$ is

$$\frac{\gamma}{(1-\omega)^2(d-2)^2}-4(1-\omega)\le 0, \quad (30)$$

which can be expressed as

$$0\le\gamma\le 4(1-\omega)^3(d-2)^2. \quad (31)$$

The value of γ that minimizes the right hand side of inequality (29) is

$$\widehat{\gamma}=2(1-\omega)^3(d-2)^2. \quad (32)$$

Then, by substituting $\gamma=\widehat{\gamma}$ in inequality (29), we get

$$R_\omega\left(T^{(3)}_{\gamma,JS+}(Y),\nu\right)\le R_\omega\left(T^{(2)}_{\widehat{\beta},JS+}(Y),\nu\right)$$
$$-4(1-\omega)^4(d-2)^2\mathbb{E}\left(\frac{1}{\|Y\|^6}\mathbb{I}_{(\alpha/\|Y\|^2)\le 1}\right) \quad (33)$$
$$\le R_\omega\left(T^{(2)}_{\widehat{\beta},JS+}(Y),\nu\right).$$

Now, we consider the new estimator that dominates $T^{(3)}_{\gamma,JS+}(Y)$ that is defined as

$$T^{(4)}_{\delta,JS+}\left(\|Y\|^2\right)=T^{(3)}_{\widehat{\gamma},JS+}(Y)+\delta\left(\frac{1}{\|Y\|^2}\right)^4\mathbb{I}_{(\alpha/\|Y\|^2)\le 1}Y$$
$$=\left(1-\alpha\frac{1}{\|Y\|^2}+\widehat{\beta}\left(\frac{1}{\|Y\|^2}\right)^2+\widehat{\gamma}\left(\frac{1}{\|Y\|^2}\right)^3\right. \quad (34)$$
$$\left.+\delta\left(\frac{1}{\|Y\|^2}\right)^4\right)\mathbb{I}_{(\alpha/\|Y\|^2)\le 1}Y,$$

where $\widehat{\beta}$ and $\widehat{\gamma}$ are defined in equations (19) and (32), respectively, and the parameter δ behaves like γ in equation (21). The analogous technique used in the proof of Proposition 2 leads to the following proposition. □

Proposition 3. *Based on the BLF ℓ_ω, the risk function of $T^{(4)}_{\delta,JS+}$ given in equation (34) is*

$$R_\omega\left(T^{(4)}_{\delta,JS+}(Y),\nu\right)=R_\omega\left(T^{(3)}_{\widehat{\gamma},JS+}(Y),\nu\right)$$
$$+\delta^2\mathbb{E}\left(\frac{1}{\|Y\|^{14}}\mathbb{I}_{(\alpha/\|Y\|^2)\le 1}\right)$$
$$+2\delta\widehat{\gamma}\mathbb{E}\left(\frac{1}{\|Y\|^{12}}\mathbb{I}_{(\alpha/\|Y\|^2)\le 1}\right) \quad (35)$$
$$+2\delta\widehat{\beta}\mathbb{E}\left(\frac{1}{\|Y\|^{10}}\mathbb{I}_{(\alpha/\|Y\|^2)\le 1}\right)$$
$$-12\delta(1-\omega)\mathbb{E}\left(\frac{1}{\|Y\|^8}\mathbb{I}_{(\alpha/\|Y\|^2)\le 1}\right).$$

Theorem 3. *For $d>8$ and based on the BLF ℓ_ω, a sufficient condition for which the estimator $T^{(4)}_{\delta,JS+}(Y)$ dominates $T^{(3)}_{\widehat{\gamma},JS+}(Y)$ is*

$$0\le\delta\le 4(1-\omega)^4(d-2)^3. \quad (36)$$

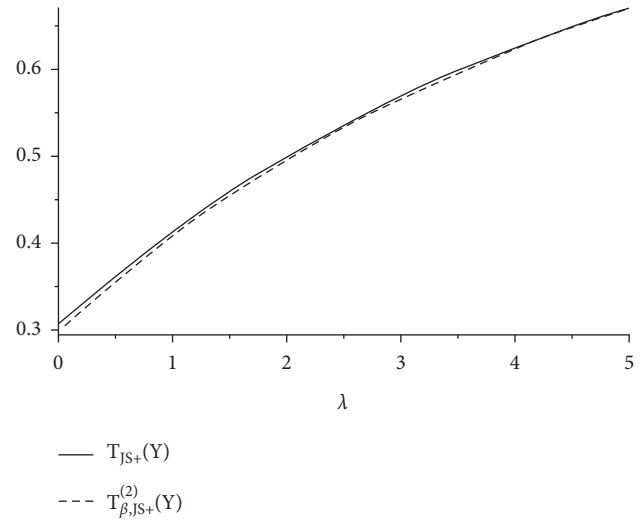

Figure 1: Curves of $R_\omega(T_{JS+}(Y),\nu)/R_\omega(Y,\nu)$ and $R_\omega(T^{(2)}_{\widehat{\beta},JS+}(Y),\nu)/R_\omega(Y,\nu)$ as functions of λ for $d=6$ and $\omega=0.1$.

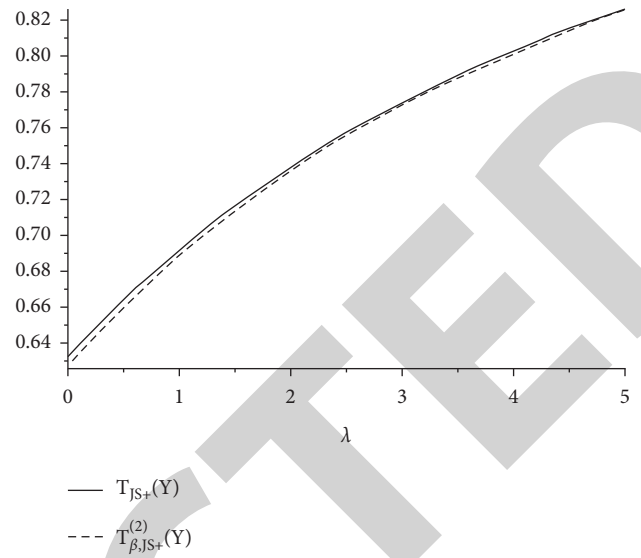

Figure 2: Curves of $R_\omega(T_{JS+}(Y),\nu)/R_\omega(Y,\nu)$ and $R_\omega(T^{(2)}_{\widehat{\beta},JS+}(Y),\nu)/R_\omega(Y,\nu)$ as functions of λ for $d=6$ and $\omega=0.5$.

Proof. As

$$\begin{aligned}\mathbb{E}\left(\frac{1}{\|Y\|^{14}}\mathbb{I}_{(\alpha/\|Y\|^2)\le 1}\right) &= \mathbb{E}\left(\frac{1}{\|Y\|^{6}}\frac{1}{\|Y\|^{8}}\mathbb{I}_{(\alpha/\|Y\|^2)\le 1}\right)\\ &\le \mathbb{E}\left(\frac{1}{\alpha^3}\frac{1}{\|Y\|^{8}}\mathbb{I}_{(\alpha/\|Y\|^2)\le 1}\right)\\ &= \frac{1}{\alpha^3}\mathbb{E}\left(\frac{1}{\|Y\|^{8}}\mathbb{I}_{(\alpha/\|Y\|^2)\le 1}\right),\end{aligned} \tag{37}$$

$$\begin{aligned}\mathbb{E}\left(\frac{1}{\|Y\|^{12}}\mathbb{I}_{(\alpha/\|Y\|^2)\le 1}\right) &= \mathbb{E}\left(\frac{1}{\|Y\|^{4}}\frac{1}{\|Y\|^{8}}\mathbb{I}_{(\alpha/\|Y\|^2)\le 1}\right)\\ &\le \mathbb{E}\left(\frac{1}{\alpha^2}\frac{1}{\|Y\|^{8}}\mathbb{I}_{(\alpha/\|Y\|^2)\le 1}\right)\\ &= \frac{1}{\alpha^2}\mathbb{E}\left(\frac{1}{\|Y\|^{8}}\mathbb{I}_{(\alpha/\|Y\|^2)\le 1}\right),\end{aligned} \tag{38}$$

and

$$\begin{aligned}\mathbb{E}\left(\frac{1}{\|Y\|^{10}}\mathbb{I}_{(\alpha/\|Y\|^2)\le 1}\right) &= \mathbb{E}\left(\frac{1}{\|Y\|^{2}}\frac{1}{\|Y\|^{8}}\mathbb{I}_{(\alpha/\|Y\|^2)\le 1}\right)\\ &\le \mathbb{E}\left(\frac{1}{\alpha}\frac{1}{\|Y\|^{8}}\mathbb{I}_{(\alpha/\|Y\|^2)\le 1}\right)\\ &= \frac{1}{\alpha}\mathbb{E}\left(\frac{1}{\|Y\|^{8}}\mathbb{I}_{(\alpha/\|Y\|^2)\le 1}\right),\end{aligned} \tag{39}$$

by using equations (37), (38), and (39) and Proposition 3, we have

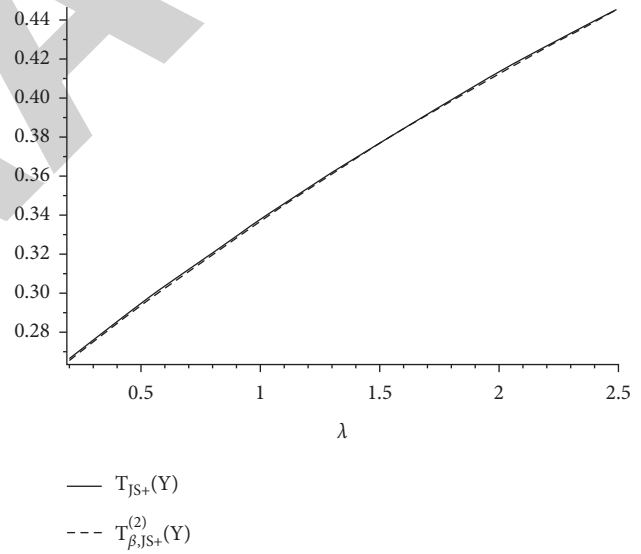

Figure 3: Curves of $R_\omega(T_{JS+}(Y),\nu)/R_\omega(Y,\nu)$ and $R_\omega(T^{(2)}_{\widehat{\beta},JS+}(Y),\nu)/R_\omega(Y,\nu)$ as functions of λ for $d=8$ and $\omega=0.1$.

$$\begin{aligned}R_\omega\left(T^{(4)}_{\delta,JS+}(Y),\nu\right) &\le R_\omega\left(T^{(3)}_{\widehat{\gamma},JS+}(Y),\nu\right)\\ &\quad+\delta\left(\frac{\gamma}{\alpha^3}-4(1-\omega)\right)\\ &\quad\mathbb{E}\left(\frac{1}{\|Y\|^{8}}\mathbb{I}_{(\alpha/\|Y\|^2)\le 1}\right).\end{aligned} \tag{40}$$

Then, a sufficient condition for which the estimator $T^{(4)}_{\delta,JS+}(Y)$ dominates $T^{(3)}_{\widehat{\gamma},JS+}(Y)$ is

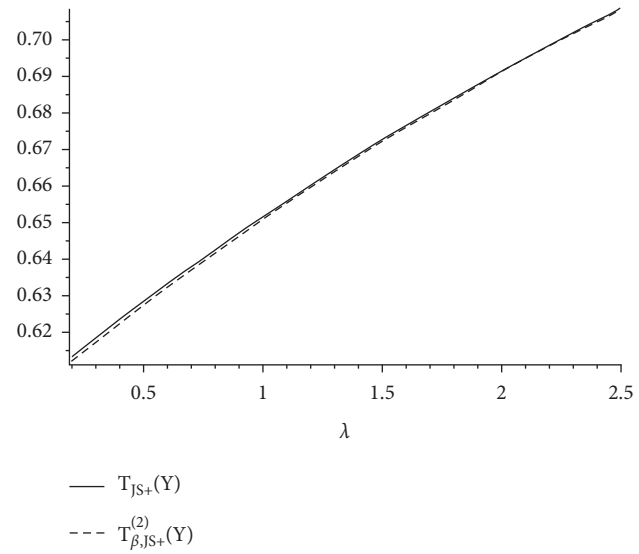

Figure 4: Curves of $R_\omega(T_{JS+}(Y),\nu)/R_\omega(Y,\nu)$ and $R_\omega(T^{(2)}_{\widehat{\beta},JS+}(Y),\nu)/R_\omega(Y,\nu)$ as functions of λ for $d=8$ and $\omega=0.5$.

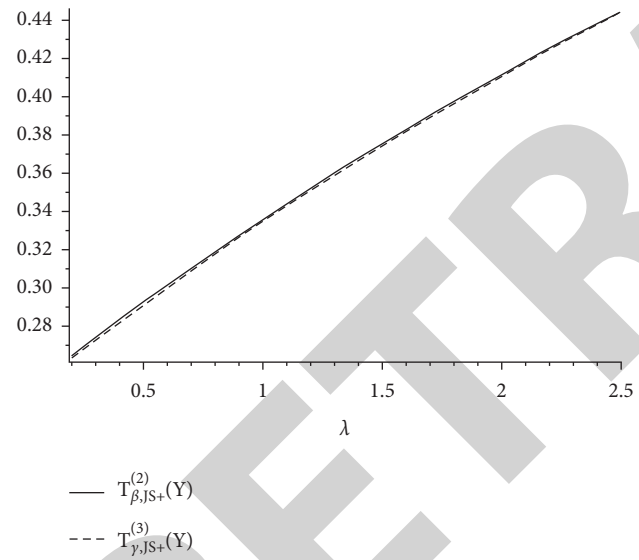

Figure 5: Curves of $R_\omega(T^{(2)}_{\widehat{\beta},JS+}(Y),\nu)/R_\omega(Y,\nu)$ and $R_\omega(T^{(3)}_{\widehat{\gamma},JS+}(Y),\nu)/R_\omega(Y,\nu)$ as functions of λ for $d=8$ and $\omega=0.1$.

$$0\le\delta\le 4(1-\omega)^4(d-2)^3, \tag{41}$$

and the optimal value for δ that minimizes the right hand side of equation (40) is

$$\widehat{\delta}=2(1-\omega)^4(d-2)^3. \tag{42}$$

If we take $\delta=\widehat{\delta}$, the inequality in equation (40) becomes

$$R_\omega\left(T^{(4)}_{\delta,JS+}(Y),\nu\right)\le R_\omega\left(\delta^{(3)}_{\widehat{\gamma},JS+}(Y),\nu\right) - 4(1-\omega)^4(d-2)^3\mathbb{E}\left(\frac{1}{\|Y\|^8}\right) \le R\left(T^{(3)}_{\widehat{\gamma},JS+}(Y),\nu\right). \tag{43}$$

□

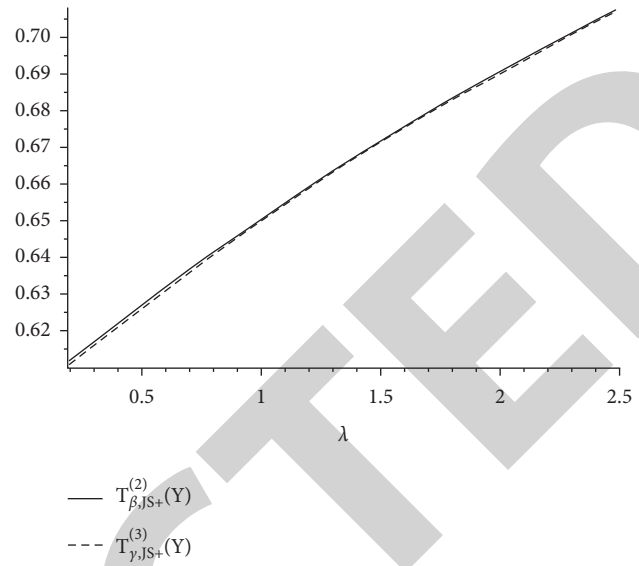

Figure 6: Curves of $R_\omega(T^{(2)}_{\widehat{\beta},JS+}(Y),\nu)/R_\omega(Y,\nu)$ and $R_\omega(T^{(3)}_{\widehat{\gamma},JS+}(Y),\nu)/R_\omega(Y,\nu)$ as functions of λ for $d=8$ and $\omega=0.5$.

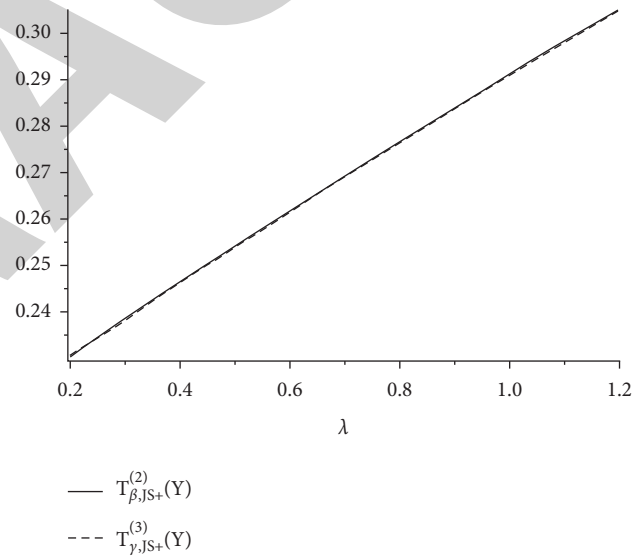

Figure 7: Curves of $R_\omega(T^{(2)}_{\widehat{\beta},JS+}(Y),\nu)/R_\omega(Y,\nu)$ and $R_\omega(T^{(3)}_{\widehat{\gamma},JS+}(Y),\nu)/R_\omega(Y,\nu)$ as functions of λ for $d=10$ and $\omega=0.1$.

4. Simulation Studies

In this section, we present figures and tables that show the values of the risk ratios of the estimators $T_{JS+}(Y)$, $T^{(2)}_{\widehat{\beta},JS+}(Y)$, $T^{(3)}_{\widehat{\gamma},JS+}(Y)$, and $T^{(4)}_{\widehat{\delta},JS+}(Y)$, to the MLE. We recall that $T_{JS+}(Y)$ is defined in equation (5) and its risk function under the BLF ℓ_ω is given in equation (6), and the estimators $T^{(2)}_{\widehat{\beta},JS+}(Y)$, $T^{(3)}_{\widehat{\gamma},JS+}(Y)$, and $T^{(4)}_{\widehat{\delta},JS+}(Y)$ are defined, respectively, in equations (7), (21), and (34) with $\beta=\widehat{\beta}=(1-\omega)(d-6)$, $\gamma=\widehat{\gamma}=(1-\omega)(d-10)^2$, and $\delta=\widehat{\delta}=2(1-\omega)(d^2-28p+188)(d-14)$. Their risk functions under ℓ_ω are obtained by

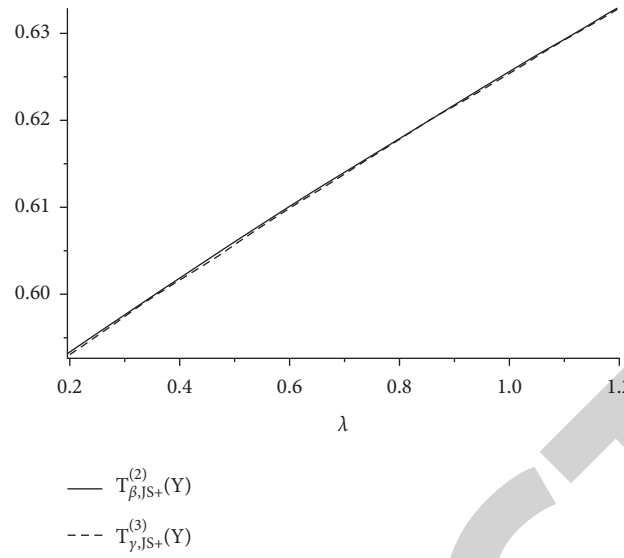

FIGURE 8: Curves of $R_\omega(T^{(2)}_{\widehat{\beta},JS+}(Y),\nu)/R_\omega(Y,\nu)$ and $R_\omega(T^{(3)}_{\widehat{\gamma},JS+}(Y),\nu)/R_\omega(Y,\nu)$ as functions of λ for $d = 10$ and $\omega = 0.5$.

TABLE 1: Values of risk ratios $R_\omega(T_{JS+}(Y),\nu)/R_\omega(Y,\nu)$ (top), $R_\omega(T^{(2)}_{\widehat{\beta},JS+}(Y),\nu)/R_\omega(Y,\nu)$ (middle), and $R_\omega(T^{(3)}_{\widehat{\gamma},JS+}(Y),\nu)/R_\omega(Y,\nu)$ (bottom) for $d = 8$ and different values of ω and $\lambda = \|\nu\|^2$.

λ	ω					
	0.0	0.1	0.2	0.5	0.7	0.9
	0.2800	0.3567	0.4341	0.6619	0.8030	0.9353
1.2418	0.2785	0.3552	0.4327	0.6608	0.8024	0.9352
	0.2769	0.3537	0.4312	0.6599	0.8020	0.9351
	0.3775	0.4455	0.5131	0.7083	0.8289	0.9435
2.4948	0.3764	0.4445	0.5121	0.7076	0.8286	0.9435
	0.3753	0.4433	0.5111	0.7069	0.8283	0.9435
	0.5221	0.5749	0.6266	0.7739	0.8661	0.9556
5.0019	0.5215	0.5743	0.6261	0.7735	0.8659	0.9555
	0.5209	0.5738	0.6256	0.7733	0.8658	0.9555
	0.6944	0.7267	0.7585	0.8507	0.9107	0.9702
10.4311	0.6942	0.7266	0.7584	0.8506	0.9106	0.9702
	0.6941	0.7265	0.7583	0.8506	0.9106	0.9702
	0.7721	0.7954	0.8185	0.8869	0.9322	0.9774
15.4110	0.7720	0.7954	0.8184	0.8869	0.9322	0.9774
	0.7720	0.7953	0.8184	0.8869	0.9322	0.9774
	0.8150	0.8337	0.8522	0.9077	0.9446	0.9815
20.0000	0.8150	0.8337	0.8522	0.9077	0.9446	0.9815
	0.8150	0.8337	0.8522	0.9077	0.9446	0.9815

substituting β by $\widehat{\beta}$, γ by $\widehat{\gamma}$, and δ by $\widehat{\delta}$ in Propositions 1, 2, and 3, respectively. We denote the risk ratios of the above estimators as $R_\omega(T_{JS+}(Y),\nu)/R_\omega(Y,\nu)$, $R_\omega(T^{(2)}_{\widehat{\beta},JS+}(Y),\nu)/R_\omega(Y,\nu)$, $R_\omega(T^{(3)}_{\widehat{\gamma},JS+}(Y),\nu)/R_\omega(Y,\nu)$, and $R_\omega(T^{(4)}_{\widehat{\delta},JS+}(Y),\nu)/R_\omega(Y,\nu)$, respectively. First, for selected values of d and ω, we graph $R_\omega(T_{JS+}(Y),\nu)/R_\omega(Y,\nu)$, $R_\omega(T^{(2)}_{\widehat{\beta},JS+}(Y),\nu)/R_\omega(Y,\nu)$, and $R_\omega(T^{(3)}_{\widehat{\gamma},JS+}(Y),\nu)/R_\omega(Y,\nu)$ as functions of $\lambda = \|\nu\|^2$. In the second part, we give two types of tables. The first one includes the values of $R_\omega(T_{JS+}(Y),\nu)/R_\omega(Y,\nu)$, $R_\omega(T^{(2)}_{\widehat{\beta},JS+}(Y),\nu)/R_\omega(Y,\nu)$, and $R_\omega(T^{(3)}_{\widehat{\gamma},JS+}(Y),\nu)/R_\omega(Y,\nu)$ for fixes values of d and ω at different values of $\lambda = \|\nu\|^2$. The second table shows the values of $R_\omega(T^{(3)}_{\widehat{\gamma},JS+}(Y),\nu)/R_\omega(Y,\nu)$ and $R_\omega(T^{(4)}_{\widehat{\delta},JS+}(Y),\nu)/R_\omega(Y,\nu)$ for fixed values of d and ω at different values of $\lambda = \|\nu\|^2$.

Figures 1–8 show that $R_\omega(T_{JS+}(Y),\nu)/R_\omega(Y,\nu)$, $R_\omega(T^{(2)}_{\widehat{\beta},JS+}(Y),\nu)/R_\omega(Y,\nu)$, and $R_\omega(T^{(3)}_{\widehat{\gamma},JS+}(Y),\nu)/R_\omega(Y,\nu)$ are less than one which indicate that the estimators $T_{JS+}(Y)$, $T^{(2)}_{\widehat{\beta},JS+}(Y)$, and $T^{(3)}_{\widehat{\gamma},JS+}(\|Y\|^2)$ are better than the MLE

Table 2: Values of risk ratios $R_\omega(T_{JS+}(Y),\nu)/R_\omega(Y,\nu)$ (top), $R_\omega(T^{(2)}_{\widehat{\beta},JS+}(Y),\nu)/R_\omega(Y,\nu)$ (middle), and $R_\omega(T^{(3)}_{\widehat{\gamma},JS+}(Y),\nu)/R_\omega(Y,\nu)$ (bottom) for $d = 10$ and different values of ω and $\lambda = \|\nu\|^2$.

λ	ω					
	0.0	0.1	0.2	0.5	0.7	0.9
1.2418	0.2261	0.3083	0.3914	0.6349	0.7855	0.9290
	0.2257	0.3078	0.3910	0.6346	0.7853	0.9289
	0.2252	0.3073	0.3905	0.6342	0.7852	0.9289
2.4948	0.3121	0.3868	0.4612	0.6756	0.8084	0.9364
	0.3118	0.3865	0.4609	0.6754	0.8083	0.9364
	0.3114	0.3861	0.4605	0.6751	0.8083	0.9364
5.0019	0.4462	0.5070	0.5666	0.7364	0.8432	0.9478
	0.4460	0.5068	0.5664	0.7363	0.8431	0.9478
	0.4458	0.5066	0.5662	0.7362	0.8431	0.9478
10.4311	0.6210	0.6610	0.7003	0.8145	0.8889	0.9630
	0.6208	0.6610	0.7003	0.8145	0.8889	0.9630
	0.6208	0.6609	0.7003	0.8145	0.8889	0.9630
15.4110	0.7075	0.7375	0.7671	0.8549	0.9129	0.9710
	0.7075	0.7375	0.7671	0.8549	0.9129	0.9710
	0.7075	0.7375	0.7671	0.8549	0.9129	0.9710
20.0000	0.7581	0.7825	0.8068	0.8793	0.9276	0.9759
	0.7581	0.7825	0.8068	0.8793	0.9276	0.9759
	0.7581	0.7825	0.8068	0.8793	0.9276	0.9759

Table 3: Values of risk ratios $R_\omega(T^{(3)}_{\widehat{\gamma},JS+}(Y),\nu)/R_\omega(Y,\nu)$ (top) and $R_\omega(T^{(4)}_{\widehat{\delta},JS+}(\|Y\|^2),\nu)/R_\omega(Y,\nu)$ (bottom) for $d = 10$ and different values of ω and $\lambda = \|\nu\|^2$.

λ	ω					
	0.0	0.1	0.2	0.5	0.7	0.9
1.2418	0.2252	0.3073	0.3905	0.6342	0.7852	0.9289
	0.2246	0.3068	0.3900	0.6340	0.7851	0.9289
2.4948	0.3114	0.3861	0.4605	0.6751	0.8083	0.9364
	0.3110	0.3857	0.4602	0.6750	0.8082	0.9364
5.0019	0.4458	0.5066	0.5662	0.7362	0.8431	0.9478
	0.4456	0.5046	0.5660	0.7361	0.8431	0.9478
10.4311	0.6208	0.6609	0.7003	0.8145	0.8889	0.9630
	0.6208	0.6609	0.7002	0.8144	0.8889	0.9630
15.4110	0.7075	0.7375	0.7671	0.8549	0.9129	0.9710
	0.7075	0.7375	0.7671	0.8548	0.9129	0.9710
20.0000	0.7581	0.7825	0.8068	0.8793	0.9276	0.9759
	0.7581	0.7825	0.8068	0.8793	0.9276	0.9759

Y for the different values of d and ω, and thus they are minimax. We remark that $T^{(2)}_{\widehat{\beta},JS+}(Y)$ dominates $T_{JS+}(Y)$ and $T^{(3)}_{\widehat{\gamma},JS+}(Y)$ dominates $T^{(2)}_{\widehat{\beta},JS+}(Y)$ for the chosen values of d and ω. We also note that the improvement increases when ω value is close to zero and decreases as ω approaches one. Tables 1 and 2 confirm this remark. In these tables, we started with chosen values of d and ω to compute $R_\omega(T_{JS+}(Y),\nu)/R_\omega(Y,\nu)$, $R_\omega(T^{(2)}_{\widehat{\beta},JS+}(Y),\nu)/R_\omega(Y,\nu)$, and $R_\omega(T^{(3)}_{\widehat{\gamma},JS+}(Y),\nu)/R_\omega(Y,\nu)$ at different values of λ. So, when the values of ω and $\lambda = \|\nu\|^2$ are small, we have got significant improvement of $R_\omega(T_{JS+}(Y),\nu)/R_\omega(Y,\nu)$, $R_\omega(T^{(2)}_{\widehat{\beta},JS+}(Y),\nu)/R_\omega(Y,\nu)$, and $R_\omega(T^{(3)}_{\widehat{\gamma},JS+}(Y),\nu)/R_\omega(Y,\nu)$. As ω and λ increase, the improvement decreases towards zero, and then a small improvement is obtained. For fixed value of ω, an indication of better improvement is deduced when the value of d increases. We conclude that the improvement of the estimators can be significant when the value of d is large, λ is small, and ω tends to be close to zero. Therefore, the improvement of the risks ratios is clearly affected by the combination of the different values of d, ω, and λ.

Tables 3 and 4 show the risk ratios $R_\omega(T^{(3)}_{\widehat{\gamma}}(Y),\nu)/R_\omega(Y,\nu)$ and $R_\omega(T^{(4)}_{\widehat{\delta}}(Y),\nu)/R_\omega(Y,\nu)$ for the selected values of d and ω at different values of λ. In these tables, we observe small improvement of $T^{(4)}_{\widehat{\delta},JS+}(Y)$ to $T^{(3)}_{\widehat{\gamma},JS+}(Y)$ in comparison

Table 4: Values of risk ratios $R_\omega(T^{(3)}_{\widehat{\gamma},JS+}(Y),\nu)/R_\omega(Y,\nu)$ (top) and $R_\omega(T^{(4)}_{\widehat{\delta},JS+}(\|Y\|^2),\nu)/R_\omega(Y,\nu)$ (bottom) for $d=12$ and different values of ω and $\lambda=\|\nu\|^2$.

λ	ω					
	0.0	0.1	0.2	0.5	0.7	0.9
1.2418	0.1893	0.2751	0.3619	0.6157	0.7729	0.9246
	0.1891	0.2749	0.3618	0.6156	0.7729	0.9246
2.4948	0.2658	0.3450	0.4241	0.6518	0.7935	0.9313
	0.2656	0.3449	0.4240	0.6517	0.7934	0.9313
5.0019	0.3893	0.4560	0.5214	0.7079	0.8258	0.9420
	0.3893	0.4560	0.5214	0.7079	0.8258	0.9420
10.4311	0.5612	0.6077	0.6531	0.7850	0.8712	0.9571
	0.5612	0.6077	0.6531	0.7850	0.8712	0.9571
15.4110	0.6526	0.6883	0.7235	0.8276	0.8966	0.9655
	0.6526	0.6883	0.7235	0.8276	0.8966	0.9655
20.0000	0.7082	0.7377	0.7670	0.8545	0.9127	0.9709
	0.7082	0.7377	0.7670	0.8545	0.9127	0.9709

with the improvement of $T^{(2)}_{\beta,JS+}(Y)$ to $T_{JS+}(Y)$ or the improvement of $T^{(3)}_{\widehat{\gamma},JS+}(Y)$ to $T^{(2)}_{\widehat{\beta},JS+}(Y)$ that appeared in Tables 1 and 2. We also notice that d, ω, and λ have similar effect to the risks ratios as in Tables 1 and 2.

5. Conclusion

In this article, we investigated the estimation of the mean ν of the random vector $Y\sim N_d(\nu,I_d)$. The risk associated to the BLF is the adopted criterion to determine the quality of the considered estimators. We introduced a class of estimators $T^{(2)}_{\beta,JS+}(Y)=T_{JS+}(Y)+\beta(1/\|Y\|^2)^2Y\mathbb{I}_{(\alpha/\|Y\|^2)\le 1}$. We gave a sufficient condition on β, so that $\mathrm{T}^{(2)}_{\beta,JS+}(\|Y\|^2)$ dominates $\mathrm{T}_{JS+}(\|Y\|^2)(\|Y\|^2)$. Then, we suggested the estimators of polynomial type with the indeterminate $(1/\|Y\|^2)\mathbb{I}_{(\alpha/\|Y\|^2)\le 1}$. That is, we added recursively the term $\gamma(1/\|Y\|^2)^m\mathbb{I}_{(\alpha/\|Y\|^2)\le 1}Y$. Then, at each time, we got estimators that improve those estimators defined previously. Therefore, we obtained a series of polynomial form's estimators with the indeterminate $(1/\|Y\|^2)\mathbb{I}_{(\alpha/\|Y\|^2)\le 1}$ and proved that if we increase the degree of the polynomial, we can build a best estimator from the one given previously. A point that should be considered is that increasing the degree of the of the polynomial has to accompany with having large dimension space of the parameter in order to satisfy the domination conditions. However, more difficult computation of the risk of the estimators can be observed which can lead to difficulties in determining the sufficiency conditions of the domination. Further investigation of this point can be considered as future work to determine the optimal degree of the polynomial form that provides the ultimate best estimator.

As an extension of this work, we can look for analogous results and examine the performance of estimators of the type $\mathrm{T}_{JS+}(Y)+\beta(1/\|Y\|^2)^r\mathbb{I}_{(\alpha/\|Y\|^2)\le 1}Y$, using the general BLF $\ell_{\omega,\rho}(T,\nu)=\omega\rho(\|T-T_0\|^2)+(1-\omega)\rho(\|T-\nu\|^2),\quad 0\le\omega<1$, where $\rho(\cdot)$ is an arbitrary positive real function. This work can also be investigated under the Bayesian framework.

Data Availability

The numerical dataset used to support the findings of this study is available from the corresponding author upon request.

Conflicts of Interest

The authors declare that they have no conflicts of interest.

References

[1] C. Stein, "Inadmissibilty of the usual estimator for the mean of a multivariate normal distribution," in *Proceedings of the Third Berkeley Symposium on Mathematical Statistics and Probability*, University of California Press, Berkeley, CA, USA, 1956.

[2] W. James and C. Stein, "Estimation with quadratic loss," in *Proceedings of the Fourth Berkeley Symposium on Mathematical Statistics and Probability*, University of California Press, Berkeley, CA, USA, 1961.

[3] D. Lindley, "Discussion on professor Stein's paper," *Journal of the Royal Statistical Society: Series B*, vol. 24, pp. 285–287, 1962.

[4] P. K. Bhattacharya, "Estimating the mean of a multivariate normal population with general quadratic loss function," *The Annals of Mathematical Statistics*, vol. 37, no. 6, pp. 1819–1824, 1966.

[5] J. O. Berger, "Admissible minimax estimation of a multivariate normal mean with arbitrary quadratic loss," *Annals of Statistics*, vol. 4, no. 1, pp. 223–226, 1976.

[6] C. M. Stein, "Estimation of the mean of a multivariate normal distribution," *Annals of Statistics*, vol. 9, no. 6, pp. 1135–1151, 1981.

[7] M. Norouzirad and M. Arashi, "Preliminary test and Stein-type shrinkage ridge estimators in robust regression," *Statistical Papers*, vol. 60, no. 6, pp. 1849–1882, 2019.

[8] C. L. Cheng, A. Chaturvedi, and A. Chaturvedi, "Goodness of fit for generalized shrinkage estimation," *Theory of Probability and Mathematical Statistics*, vol. 100, pp. 191–214, 2020.

[9] M. Kashani, MR. Rabiei, and M. Arashi, "An integrated shrinkage strategy for improving efficiency in fuzzy regression modeling," *Soft Computing*, vol. 25, no. 13, pp. 8095–8107, 2021.

Hindawi
Journal of Mathematics
Volume 2023, Article ID 7767936, 14 pages
https://doi.org/10.1155/2023/7767936

Research Article

The Approximation of a Modified Baskakov Operator

Ma Yingdian[1] **and Wang Weimeng**[2]

[1]*School of Finance and Mathematics, Huainan Normal University, Huainan 232038, China*
[2]*Aeronautical Research Institute, Singapore University of Technology and Design, Singapore*

Correspondence should be addressed to Ma Yingdian; wangyunhong@hnnu.edu.cn

Received 6 May 2022; Revised 15 June 2022; Accepted 20 June 2022; Published 1 March 2023

Academic Editor: Naeem Jan

Because of their simple form and high quality, linear arithmetical operators, particularly linear positive operators, are very popular. The number of in-depth studies on linear operator approximation is extensive, and the majority of the published material falls into four categories: types and structures of operators, approximation of operators, order of approximation and the converse theorem of operators, and operator saturation. The Baskakov operator will be transformed in the same way to explore its approximation characteristics as well as the approximation theorem and converse theorem.

1. Introduction and Background

1.1. Background. The famous Korovkin theorem [1], back in 1952, was a great boost to the studies of the positive linear arithmetic approximation. The results of the studies focusing on the problems with the order of approximation and the saturation of linear arithmetic were concluded in Devore's book in 1972 [2]. In that same year, Berens and Lorentz [3] solved the converse theorem of the approximation problem of the Bernstein operator, and the converse theorem and its equivalence theorems have become a research hotspot since then. The subsequent development of the modulus of smoothness and the Korovkin-functionals, as well as some other qualified linear arithmetic, drew a large number of research studies and applications. Ditzian and Totik's paper from 1987 [4] detailed the key findings.

Many academics have developed tweaks and revisions to various well-known operators to speed up the approximation process [5]. Integral transform, generalisation, weighting, combinatorics, and applying probability approaches are some of the methods for making such alterations and corrections [6].

We know that the Bernstein operator is linear, so there is

$$B_n(e_i;x) = x^i,\ i = 0, 1. \tag{1}$$

Here, $e_i = t^i$. However, the Bernstein Operator does not have its retention with quadratic function,

$$B_n(e_2;x) = x^2 + \frac{x(1-x)}{n} \neq e_2. \tag{2}$$

In order to keep the quadratic function constant, a transformation was applied to the Bernstein operator in the reference literature [7].

$$B_n^*(f,x) = \sum_{k=0}^{n} f\left(\frac{k}{n}\right)\binom{n}{k}\left(r_n^*(x)\right)^k\left(1-r_n^*(x)\right)^{n-k}. \tag{3}$$

Here,

$$r_n^*(x) = \begin{cases} x^2, & n = 1, \\ -\dfrac{1}{2(n-1)} + \sqrt{\dfrac{n}{n-1}x^2 + \dfrac{1}{4(n-1)^2}}, & n = 2, 3, \cdots. \end{cases} \tag{4}$$

Thus,

$$\begin{aligned} B_n^*(e_i;x) &= x^i,\ i = 0, 2, \\ B_n^*(e_1;x) &= r_n^*(x). \end{aligned} \tag{5}$$

Other literature [8, 9] have done similar transformations to the Meyer-König and Zeller operators; we will perform the same transformation to the Baskakov operator to study its approximation properties, the approximation theorem, and the converse theorem.

1.2. Modulus of Smoothness and the K-Functional. Assume $f \in L_p[0,+\infty)(1 \le P \le +\infty)$ (asquare-integrable function on $[0,+\infty)$, written as $L_\infty[0,+\infty) \triangleq C[0,+\infty)$)), $\phi(x) = \sqrt{x(1+x)}$, $0 \le \lambda \le 1$, so the R^{th} order modulus of smoothness is defined as

$$\omega^r_{\phi^\lambda}(f,t)_p = \sup_{0<h\le t} \left\| \Delta^r_{h\phi^\lambda} f \right\|_p. \tag{6}$$

With

$$\Delta^r_{h\varphi^\lambda} f(x) = \begin{cases} \sum_{k=0}^{r} (-1)^k \binom{r}{k} f\left(x + \left(\frac{r}{2} - k\right) h\varphi^\lambda(x)\right), & x \pm \frac{r}{2} h\varphi^\lambda(x) \in [0,\infty), \\ 0, & \text{other.} \end{cases} \tag{7}$$

When $\lambda = 0$ in specific, it is called the classical modulus of smoothness; and when $\lambda = 1$, it is called the Ditzian–Totik modulus of smoothness. The R^{th} order K-functional of f is defined as

$$K^r_{\phi^\lambda}(f,t)_p = \inf_{g^{(r-1)} \in AC_{\text{loc}}} \left\{ \|f-g\|_p + t^r \left\| \varphi^{r\lambda} g^{(r)} \right\|_p \right\}. \tag{8}$$

Here, $A.C_{\text{loc}}$ is defined to be a sum set of absolute continuous functions on $[0,+\infty)$. Based on our reference literature [10], we know $K^r_{\varphi^\lambda}(f,t^r)_p$ is equivalent to $\omega^r_{\phi^\lambda}(f,t)_p$, which means there exists a constant $c > 0, t_0 > 0$, so that when $0 < t < t_0$:

$$C^{-1} \omega^r_{\phi^\lambda}(f,t)_p \le K^r_{\varphi^\lambda}\left(f,t^r\right)_p \le C\omega^r_{\phi^\lambda}(f,t)_p. \tag{9}$$

Note: when $p = \infty$, we use $\omega^r_{\varphi^\lambda}(f,t)_\infty = \omega^r_{\varphi^\lambda}(f,t)$; $K^r_{\varphi^\lambda}(f,t)_\infty = K^r_{\varphi^\lambda\ (f,t)}$; $\|f\|_\infty = \|f\|$ for convenience.

1.3. Baskakov Operator. For $f \in C[0,\infty)$, the famous Baskakov operator is defined as

$$V_n(f,x) = \sum_{k=0}^{\infty} v_{n,k}(x) f\left(\frac{k}{n}\right). \tag{10}$$

Where $x \in [0,\infty)$, $v_{n,k}(x) = \binom{n+k-1}{k} x^k (1+x)^{-n-k}$. Calculation shows

$$V_n(1,x) = 1; V_n(t,x) = x; V_n\left(t^2,x\right) = x^2 + \frac{\phi^2(x)}{n}. \tag{11}$$

This demonstrates that the Baskakov operator preserves the function's linearity but not its quadratic function [11]. There have been several in-depth studies on the approximation of the Baskakov operator, the results of which are documented in the literature [12–19]. When we apply the procedure described in [2] to the Baskakov operator, we can easily get an approximation result using the first-order classical modulus of smoothness as follows:

Theorem 1. *If $\delta > 0$, $f \in C[0,\infty)$, then*

$$\left|V_n(f,x) - f(x)\right| \le \omega(f,\delta)\left[1 + \frac{1}{\delta}\sqrt{\frac{x(1+x)}{n}}\right], \quad x \in [0,\infty). \tag{12}$$

Literature [19] used the generalized modulus of smoothness $\omega^2_{\phi^\lambda}(f,t)$ to study the approximation theorem and its reverse theorem of $V_n(f,x)$ and has gotten

$$\left|V_n(f,x) - f(x)\right| \le C\omega^2_{\varphi^\lambda}\left(f; n^{-1/2}\varphi^{1-\lambda}(x)\right),\ x \in [0,\infty). \tag{13}$$

Theorem 2. *Let $f \in C_B[0,+(\infty)$, $0 \le \lambda \le 1$, then*

Theorem 3. *Let $f \in C_B[0,+\infty)$, $0 \le \lambda \le 1$; $0 \le \alpha \le 1$, then*

$$\left|V_n(f,x) - f(x)\right| \le C\left(n^{-1/2}\varphi^{1-\lambda}(x)\right)^\alpha \Longrightarrow \omega^2_{\varphi^\lambda}(f;t) = O\left(t^\alpha\right). \tag{14}$$

Here, Theorems 2 and 3 have unified the results of the classic modulus of smoothness and the Ditzian–Totik modulus correspondingly.

1.4. The Structure of the Modified Baskakov Operator. Literature [4] has addressed the linear combination to increase the order of approximation of the Baskakov operator, and this thesis will execute the following adjustment to the Baskakov operator:

$$V_n^*(f,x) =: V_n\left(f, r_n^*(x)\right) = \sum_{k=0}^{\infty} v_{n,k}\left(r_n^*(x)\right) f\left(\frac{k}{n}\right), \quad (15)$$

where $v_{n,k}(x)$ keeps the same,

$$r_n^*(x) = \begin{cases} x^2, & n = 1, \\ -\dfrac{1}{2(n+1)} + \sqrt{\dfrac{n}{n+1}x^2 + \dfrac{1}{4(n+1)^2}}, & n = 2, 3, \cdots. \end{cases} \quad (16)$$

Obviously, $r_n^*(x) \geq 0$, $x \in [0, +\infty) n = 1, 2, \ldots\ldots$ Here we know that V_n^* is linear positive operator on $C([0,\infty))$.

$$V_n^*\left(e_i\right)(x) = x^i,\ i = 0, 2 \text{ while } V_n^*\left(e_1, x\right) = r_n^*(x). \quad (17)$$

This means this operator remains constant to function 1 and x^2.

1.5. Conclusion. For the modified Baskakov operator $V_n^*(f,x)$, we have the following conclusions:

Theorem 4. *Assume $f \in C[0,\infty)$,and there exists $tM_f > 0$, $l \geq 0$, which let*

$$|f(t)| \leq M_f\left(1 + t^2\right)\left(t^l + 1\right)^{1/2}, t \in [0,\infty). \quad (18)$$

So,

$$\lim_{n\longrightarrow\infty} \left\|V_n^*(f) - f\right\|_{C(D)} = 0, \quad (19)$$

where $D = [\alpha, \beta]$, $\subset [0,\infty)$ (any closed interval).

Theorem 5. *Assume $f \in C[0,\infty)$, $x \in [0,\infty)$, $\delta > 0$, so*

$$\left|V_n^*(f,x) - f(x)\right| \leq \omega(f;\delta)\left(1 + \frac{1}{\delta}\sqrt{2x\left(x - r_n^*(x)\right)}\right). \quad (20)$$

Where $r_n^*(x)$ is the same with expression (16)

Theorem 6. *Assume $f \in C[0,\infty)$, $0 \leq \lambda \leq 1$, so*

$$\leq C\left|V_n^*(f,x) - f(x)\right| \leq C\omega_{\phi^\lambda}^1\left(f, n^{-1/2}\phi^{1-\lambda}(x)\right). \quad (21)$$

Theorem 7. *Assume $f \in C[0,\infty)$, $0 \leq \lambda \leq 1$, $0 < \alpha < 1$, so*

$$\left|V_n^*(f,x) - f(x)\right| = O\left(\left(n^{-1/2}\phi^{1-\lambda}(x)\right)^\alpha\right) \Longleftrightarrow \omega_{\phi^\lambda}^1(f,t) = O\left(t^\alpha\right). \quad (22)$$

The approximation features of the modified Baskakov operator will be discussed in Chapter II (Theorems 4 and 5). The approximation theorem and its reverse theorem will be discussed in Chapter III (Theorems 6 and 7).

Let us restate the important notations that will be used:

(1) $A = O(B)$ means there is constant C that makes $|A| \leq C|B|$;

(2) $\phi(x) = \sqrt{x(1+x)}$;

(3) $\|f\|_p =: (\int_0^1 |f(x)|^p \mathrm{d}x)^{1/p}$, $\|f\|_\infty = \sup_{x\in[0,+\infty)}|f(x)|$;

(4) N means the positive integer set, $N_0 = N \cup \{0\}$;

(5) $A.C_{\mathrm{loc}}$ is defined as an absolute continuous function space on $[0, +\infty)$;

(6) C means a constant, it refers to different values according to the situation.

2. The Approximation of the Modified Baskakov Operator

First of all, let us introduce the Korovkin theorem built by Ditzian for the local convergence of linear positive operators. Let $T(-\infty, +\infty)$ or $[0,\infty)$, $\mu(t) \in C(T)$ and $\mu(t) \geq 1\ (t \in T)$. Written as follows:

$$C_\mu(T) = \left\{f \in C(T) | f(t) \leq M_f\left(1 + t^2\right)\mu(t),\ t \in T\right\}, \quad (23)$$

where M_f is a positive constant related to f.

Theorem 8 (see [20]). *Let $\{L_n\}_{n\in N}$ be a linear positive operator sequence on $C(T)$, and $D = [\alpha, \beta] \subset T$ applies to the following conditions:*

(1) For $k = 0, 1, 2$, there's $\lim_{n\longrightarrow\infty}\|L_n(e_i) - e_i\|_{C(D)} = 0$,

(2) $\lim_{n\longrightarrow\infty}\max_{x\in D}|L_n((t-x)^2\mu(t),x)|=0.$

Then, for every $f\in C_\mu(T)$, there is

$$\lim_{n\longrightarrow\infty}\left\|L_n(f)-f\right\|_{C(D)}=0. \tag{24}$$

Apply this theorem to operator V_n^*, and we can get

Theorem 9. *Let $f\in C[0,\infty)$, and there exists $M_f>0$, $l\geq 0$ that makes: $|f(t)|\leq M_f(1+t^2)(t^l+1)^{1/2}t\in[0,\infty)$,*

Thus, there is

$$\lim_{n\longrightarrow\infty}\left\|V_n^*(f)-f\right\|_{C(D)}=0, \tag{25}$$

where $D=[\alpha,\beta]$, $\subset[0,\infty)$ (any closed interval).

Proof. Make $r\in N$, then there is

$$\begin{aligned}V_n^*(e_{r+1};x)&=\sum_{k=0}^{\infty}\left(\frac{k}{n}\right)^{r+1}v_{n,k}(r_n^*(x))\\&=\sum_{k=0}^{\infty}\left(\frac{k}{n}+\frac{1}{n}\right)^{r}\frac{n+k}{n}v_{n,k}(r_n^*(x))\frac{r_n^*(x)}{1+r_n^*(x)}\\&=\frac{r_n^*(x)}{1+r_n^*(x)}\sum_{j=0}^{r}\binom{r}{j}\left(\frac{1}{n}\right)^{r-j}V_n^*(e_j;x)+\frac{r_n^*(x)}{1+r_n^*(x)}\sum_{j=0}^{r}\binom{r}{j}\left(\frac{1}{n}\right)^{r-j}V_n^*(e_{j+1};x).\end{aligned} \tag{26}$$

Therefore, a recurrence relation exists

$$\begin{aligned}&V_n^*(e_{r+1};x)=\frac{r_n^*(x)}{n^r}V_n^*(e_0;x)+r_n^*(x)\sum_{j=1}^{r}\left[\binom{r}{j}\left(\frac{1}{n}\right)^{r-j}+\binom{r}{j-1}\left(\frac{1}{n}\right)^{r-j+1}\right]V_n^*(e_j;x),\\&V_n^*(e_0;x)=1;V_n^*(e_1;x)=r_n^*(x);V_n^*(e_2;x)=x^2.\end{aligned} \tag{27}$$

Therefore,

$$\begin{aligned}V_n^*(e_3;x)&=r_n^*(x)\left(x^2+\frac{2(x^2+r_n^*(x))}{n}+\frac{1+r_n^*(x)}{n^2}\right),\\V_n^*(e_4;x)&=r_n^{*2}(x)x^2+\frac{r_n^*(x)}{n}\left[3x^2+(5x^2+2r_n^*(x))r_n^*(x)\right]\\&\quad+\frac{r_n^*(x)}{n^2}\left[3x^2+2(2+3x^2)r_n^*(x)+7r_n^{*2}(x)\right]\\&\quad+\frac{r_n^*(x)}{n^3}(1+4r_n^*(x)+3r_n^{*2}(x)).\end{aligned} \tag{28}$$

Written as

$$T_{n,r}(x) = V_n^*\left((t-x)^r; x\right) r = 0, 1, \cdots. \tag{29}$$

So,

$$\begin{aligned}
T_{n,0}(x) &= 1;\\
T_{n,1}(x) &= r_n^*(x) - x;\\
T_{n,2}(x) &= 2x\left(x - r_n^*(x)\right);\\
T_{n,3}(x) &= -4x^3 + 4x^2 r_n^*(x) + \frac{2r_n^*(x)\left(x^2 + r_n^*(x)\right)}{n} + \frac{r_n^*(x)\left(1 + r_n^*(x)\right)}{n^2},\\
T_{n,4}(x) &= 7x^4 - 8x^3 r_n^*(x) + x^2 r_n^{*2}(x) + \frac{r_n^*(x)}{n}\left[-8x^3 + 3x^2 + \left(5x^2 - 8x + 2r_n^*(x)\right)r_n^*(x)\right]\\
&\quad + \frac{r_n^*(x)}{n^2}\left[3x^2 - 4x + 2\left(2 - 2x + 3x^2\right)r_n^*(x) + 7r_n^{*2}(x)\right].
\end{aligned} \tag{30}$$

When $x \in D = [\alpha, \beta]$, there is

$$r_n^*(x) = x - \frac{1+x}{2n} + \frac{4x^2 + 4x + 1}{8xn^2} + o\left(\frac{1}{n^2}\right). \tag{31}$$

Substitute this back into $T_{n,4}(x)$, we get

$$T_{n,4}(x) = \frac{9/4x^4 + 6x^3 + 3x^2}{n^2} + o\left(\frac{1}{n^2}\right). \tag{32}$$

Therefore,

$$\left\|T_{n,4}\right\|_{C(D)} = \max_{x\in D} V_n^*\left((t-x)^4; x\right) \le \frac{M(D)}{n^2}, \tag{33}$$

where $M(D)$ is a positive constant dependent on $D = [\alpha, \beta]$. Please note that

$$\left|r_n^*(x) - x\right| \le \frac{1+x}{n+1}. \tag{34}$$

So for $k = 0, 1$, there is

$$\begin{aligned}
\lim_{n\longrightarrow\infty}\left\|V_n^*(e_k) - e_k\right\|_{C(D)} &= 0,\\
\lim_{n\longrightarrow\infty}\left\|V_n^*\left(e^k\right) - e^k\right\|_{C(D)} &= 0.
\end{aligned} \tag{35}$$

Take the following values: $\mu(t) = (t^l + 1)^{1/2}, t \in [0, \infty)$ (l is any determinate, nonnegative integer), then for any $x \in D$, based on the Schwarz inequality, we can get:

$$V_n^*\left((t-x)^2\mu(t); x\right) \le \left(V_n^*\left((t-x)^4; x\right)\right)^{1/2}\left(V_n^*\left(\left(t^l + 1\right); x\right)\right)^{1/2} \le \left(\frac{M(D)}{n^2}\right)^{1/2}\left(M_l(D) + 1\right)^{1/2}. \tag{36}$$

Thus,

$$\lim_{n\longrightarrow\infty}\max_{x\in D} V_n^*\left((t-x)^2\mu(t); x\right) = 0. \tag{37}$$

From Theorem 8, we know that for $f \in C[0, \infty)$ and $|f(t)| \le M_f(1 + t^2)(t^l + 1)^{1/2} t \in [0, \infty)$, there is

$$\lim_{n\longrightarrow\infty}\left\|V_n^*(f) - f\right\|_{C(D)} = 0. \tag{38}$$

Theorem proven.

Now assume $f \in C[0, \infty)$, then for any positive integer δ, there is

$$\begin{aligned}\left|V_n^*(f,x)-f(x)\right| &\le \left|V_n^*(|f(t)-f(x)|;x)\right| + |f(x)|\left|V_n^*(1;x)-1\right| \\ &\le V_n^*(\omega(f,|t-x|);x) \\ &\le \omega(f,\delta)V_n^*\left(1+\frac{|t-x|}{\delta};x\right) \\ &\le \omega(f,\delta)\left[V_n^*(1;x)+\frac{1}{\delta}V_n^*(|t-x|;x)\right] \\ &\le \omega(f,\delta)\left[1+\frac{1}{\delta}V_n^{*\,1/2}\left((t-x)^2;x\right)\right] \\ &\le \omega(f,\delta)\left[1+\frac{1}{\delta}\sqrt{2x\left(x-V_n^*(e_1)(x)\right)}\right].\end{aligned} \tag{39}$$

Note that $V_n^*(e_1)(x) = r_n^*(x)$, thus we have □

Theorem 10. *Assume* $f \in C[0,\infty)$, $x \in [0,\infty)$, $\delta > 0$, *so*

$$\left|V_n^*(f;x)-f(x)\right| \le \omega(f;\delta)\left(1+\frac{1}{\delta}\sqrt{2x\left(x-r_n^*(x)\right)}\right). \tag{40}$$

Note: because

$$2x\left(x-r_n^*(x)\right) \le \frac{x(1+x)}{n}. \tag{41}$$

Based on this, we can tell the operator V_n^* has a better performance in the order of approximation than the classic Baskakov operator V_n. In fact,

$$2x\left(x-r_n^*(x)\right) \le \frac{x(1+x)}{n}, \tag{42}$$

is equivalent with

$$r_n^*(x) \ge \frac{2n-1}{2n}x - \frac{1}{2n}, \tag{43}$$

because

$$\frac{n}{n+1}x^2 + \frac{1}{4(n+1)^2} - \frac{(2n-1)^2}{4n^2}x^2 = \frac{3n-1}{4n^2(n+1)}x^2 + \frac{1}{4(n+1)^2} \ge 0, \tag{44}$$

which is

$$\sqrt{\frac{n}{n+1}x^2 + \frac{1}{4(n+1)^2}} \ge \frac{2n-1}{2n}x. \tag{45}$$

Thus, we can get

$$r_n^*(x) \ge \frac{2n-1}{2n}x - \frac{1}{2n}, x \in [0,\infty). \tag{46}$$

3. Theorem and the Converse Theorem of the Modified Baskakov Operator

3.1. Theorem of Approximation. To build the approximation theorem of the operator, we need to introduce a few following theorems first:

Lemma 1. *Assume* $n \in N$, *then* $V_n^*((t-x)^2,x) \le 4n^{-1}\phi^2(x)$.

Proof. We note that

$$\begin{aligned}V_n^*\left((t-x)^2,x\right) &= V_n^*\left(t^2,x\right) - 2xV_n^*(t,x) + x^2V_n^*(1,x) \\ &= 2\left(x--r_n^*(x)\right).\end{aligned} \tag{47}$$

When $n = 1$, there is

$$x - r_n^*(x) = x - x^2 \le x \le 1 + x, \tag{48}$$

when $n \ge 2$, there is

$$\begin{aligned}x - r_n^*(x) &= x + \frac{1}{2(n+1)} - \sqrt{\frac{n}{n+1}x^2 + \frac{1}{4(n+1)}} \\ &\le \frac{x^2+x}{(n+1)x} \le \frac{2(1+x)}{n}.\end{aligned} \tag{49}$$

Lemma proven. □

Lemma 2. *Assume* $g \in A.C._{loc}$, *then*

$$\left|V_n^*(R_1(g,t,x),x)\right| \le Cn^{-1/2}\phi^{1-\lambda}(x)\left\|\phi^\lambda g'\right\|, \tag{50}$$

where $R_1(g,t,x)=\int_x^t g'(u)du$.

Proof. From

$$\begin{aligned}\left|R_1(g,t,x)\right| &= \left|\int_x^t g'(u)\mathrm{d}u\right| \le \left|\int_x^t \left|g'(u)\right|\mathrm{d}u\right| \\ &\le \left\|\varphi^{\lambda}g'\right\|\left|\int_x^t \varphi^{-\lambda}(u)\mathrm{d}u\right|.\end{aligned} \tag{51}$$

we can get

$$\begin{aligned}\left|V_n^*(R_1(g,t,x);x)\right| &\le V_n^*\left(\left|R_1(g,t,x)\right|,x\right) \\ &\le \left\|\phi^{\lambda}g'\right\|V_n^*\left(\left|\int_x^t \varphi^{-\lambda}(u)\mathrm{d}u\right|;x\right) \\ &\le \left\|\phi^{\lambda}g'\right\|\sum_{k=0}^{\infty}v_{n,k}(r_n^*(x))\left|\int_x^{k/n}\phi^{-\lambda}(u)\mathrm{d}u\right|.\end{aligned} \tag{52}$$

Now we estimate $|\int_x^{k/n}\phi^{-\lambda}(u)\mathrm{d}u|$

When $k=0$, there is

$$\begin{aligned}\left|\int_x^0 \phi^{-\lambda}(u)\mathrm{d}u\right| &= \int_0^x u^{-\lambda/2}(1+u)^{-\lambda/2}\mathrm{d}u \\ &= \phi^{-\lambda}(x)\int_0^x\left[\frac{x(1+x)}{u(1+u)}\right]^{\lambda/2}\mathrm{d}u \\ &\le \phi^{-\lambda}(x)\int_0^x\left(\frac{x}{u}\right)^{\lambda}\mathrm{d}u \\ &\le \varphi^{-\lambda}(x)x^{\lambda}\int_0^x u^{-\lambda}\mathrm{d}u \\ &\le C\varphi^{-\lambda}(x)x^{\lambda}x^{-\lambda+1} \\ &= C\varphi^{-\lambda}(x)x.\end{aligned} \tag{53}$$

When $k\ge 1$, there is

$$\begin{aligned}\left|\int_x^{k/n}\phi^{-\lambda}(u)\mathrm{d}u\right| &= \left|\int_x^{k/n}u^{-\lambda/2}(1+u)^{-\lambda/2}\mathrm{d}u\right| \\ &\le \left[(1+x)^{-\lambda/2}+\left(1+\frac{k}{n}\right)^{-\lambda/2}\right]\left|\int_x^{k/n}u^{-\lambda/2}\mathrm{d}u\right| \\ &\le \left[(1+x)^{-\lambda/2}+\left(1+\frac{k}{n}\right)^{-\lambda/2}\right]\left|\int_x^{k/n}u^{-1/2}du\right|^{\lambda}\left|\int_x^{k/n}1\ du\right|^{1-\lambda} \\ &\le C\left[(1+x)^{-\frac{\lambda}{2}}+\left(1+\frac{k}{n}\right)^{-\lambda/2}\right]\left|\sqrt{\frac{k}{n}}-\sqrt{x}\right|^{\lambda}\left|\frac{k}{n}-x\right|^{1-\lambda} \\ &\le C\left[(1+x)^{-\lambda/2}+\left(1+\frac{k}{n}\right)^{-\lambda/2}\right]\frac{|k/n-x|}{x^{\lambda/2}} \\ &\le C\left(\left|\frac{k}{n}-x\right|\varphi^{-\lambda}(x)+\frac{|k/n-x|}{(1+k/n)^{\lambda/2}x^{\lambda/2}}\right).\end{aligned} \tag{54}$$

Therefore,

$$\begin{aligned}\left|V_n^*(R_1(g,t,x);x)\right| &\le C\left\|\varphi^{\lambda}g'\right\|\left\{v_{n,0}(r_n^*(x))\frac{x}{\varphi^{\lambda}(x)}+\sum_{k=1}^{\infty}\left[\frac{|k/n-x|}{\varphi^{\lambda}(x)}+\frac{|k/n-x|}{(1+k/n)^{\lambda/2}x^{\lambda/2}}\right]v_{n,k}(r_n^*(x))\right\} \\ &\le C\left\|\varphi^{\lambda}g'\right\|\left(\sum_{k=0}^{\infty}v_{n,k}(r_n^*(x))\frac{|k/n-x|}{\varphi^{\lambda}(x)}+\sum_{k=1}^{\infty}\frac{|k/n-x|}{(1+k/n)^{\lambda/2}x^{\lambda/2}}v_{n,k}(r_n^*(x))\right) \\ &C\left\|\varphi^{\lambda}g'\right\|\left(\frac{V_n^*(|t-x|;x)}{\varphi^{\lambda}(x)}+\sum_{k=1}^{\infty}\frac{|k/n-x|}{(1+k/n)^{\lambda/2}x^{\lambda/2}}v_{n,k}(r_n^*(x))\right).\end{aligned} \tag{55}$$

The first item within the bracket in the above equation is as follows:

$$\begin{aligned} V_n^*(|t-x|;x)\phi^{-\lambda}(x) &\le \phi^{-\lambda}(x)V_n^{*1/2}\left((t-x)^2;x\right)V_n^{*1/2}(1;x) \\ &\le \phi^{-\lambda}(x)V_n^{*1/2}\left((t-x)^2;x\right) \\ &\le Cn^{-1/2}\varphi^{1-\lambda}(x). \end{aligned} \tag{56}$$

The second item within the bracket in the above equation is as follows:

$$\begin{aligned} &\sum_{k=1}^{\infty}\frac{|k/n-x|}{(1+k/n)^{\lambda/2}x^{\lambda/2}}v_{n,k}(r_n^*(x)) \\ &\le \left(\sum_{k=1}^{\infty}v_{n,k}(r_n^*(x))(1+k/n)^{-\lambda}\right)^{1/2}x^{-\lambda/2}\left(\sum_{k=1}^{\infty}v_{n,k}(r_n^*(x))|k/n-x|^2\right)^{1/2} \\ &\le x^{-\lambda/2}\left(\sum_{k=1}^{\infty}v_{n,k}(r_n^*(x))|k/n-x|^2\right)^{1/2}\left(\sum_{k=0}^{\infty}v_{n,k}(r_n^*(x))(1+k/n)^{-1}\right)^{\lambda/2}, \end{aligned} \tag{57}$$

and

$$\begin{aligned} \sum_{k=0}^{\infty}v_{n,k}(r_n^*(x))\left(1+\frac{k}{n}\right)^{-1} &= \frac{1}{1+r_n^*(x)}\sum_{k=0}^{\infty}v_{n-1,k}(r_n^*(x))\frac{n(n+k-1)}{(n-1)(n+k)} \\ &\le \frac{C}{1+r_n^*(x)}. \end{aligned} \tag{58}$$

When $x \ge 1$,

$$\begin{aligned} \frac{1+x}{1+r_n^*(x)} &= \frac{1+x}{1-1/2(n+1)+\sqrt{n/n+1x^2+1/4(n+1)^2}} \le \frac{1+x}{x\sqrt{n/n+1}} \\ &\le 2\sqrt{2}. \end{aligned} \tag{59}$$

When $0 \le x < 1$,

$$\frac{1+x}{1+r_n^*(x)} \le \frac{2}{1-1/2(n+1)+\sqrt{1/4(n+1)^2}} = 2. \tag{60}$$

Thus, we have

$$\frac{1}{1+r_n^*(x)} \le \frac{C}{1+x}. \tag{61}$$

Substitute back to (58), we get

$$\sum_{k=0}^{\infty}v_{n,k}(r_n^*(x))\left(1+\frac{k}{n}\right)^{-1} \le \frac{C}{1+x}. \tag{62}$$

Substitute equation (62) and the result of Lemma 1 into (57), we get

$$\sum_{k=1}^{\infty}\frac{|k/n-x|}{(1+k/n)^{\lambda/2}x^{\lambda/2}}v_{n,k}(r_n^*(x))\le Cx^{-\lambda/2}n^{-1/2}\phi(x)(1+x)^{-\lambda/2}\le Cn^{-1/2}\phi^{1-\lambda}(x). \tag{63}$$

Substitute this equation and (56) back into (55) we get

$$\left|V_n^*(R_1(g,t,x),x)\right|\le Cn^{-1/2}\phi^{1-\lambda}(x)\left\|\phi^{\lambda}g'\right\|. \tag{64}$$

Thus, Lemma 2 is proven.

With Lemma 1 and Lemma 2, we can build the approximation theorem of operator V_n^* under the generalized modulus of smoothness as follows: □

Theorem 11. *Assume* $f\in C[0,\infty)$, $0\le\lambda\le 1$, *then*

$$\left|V_n^*(f;x)-f(x)\right|\le C\omega_{\varphi^{\lambda}}\left(f,n^{-1/2}\varphi^{1-\lambda}(x)\right)\le C. \tag{65}$$

Proof. Based on the definition of $K_{\phi^{\lambda}}(f,t)$, we can select the $g_n\in A.C._{\mathrm{loc}}$ that makes

$$\left\|f-g_n\right\|+n^{-1/2}\phi^{1-\lambda}(x)\left\|\phi^{\lambda}g_n'\right\|\le C\omega_{\varphi^{\lambda}}\left(f,n^{-1/2}\varphi^{1-\lambda}(x)\right). \tag{66}$$

Apply Lemma 2, we get

$$\begin{aligned}\left|V_n^*(f;x)-f(x)\right|&\le\left|V_n^*(f-g_n;x)-(f(x)-g_n(x))\right|+\left|V_n^*(g_n;x)-g_n(x)\right|\\&\le C\left\|f-g_n\right\|+\left|V_n^*(R_1(g_n,t,x);x)\right|\\&\le C\left(\left\|f-g_n\right\|+n^{-1/2}\varphi^{1-\lambda}(x)\left\|\varphi^{\lambda}g_n'\right\|\right)\\&\le C\omega_{\phi^{\lambda}}^{1}\left(f,n^{-1/2}\phi^{1-\lambda}(x)\right).\end{aligned} \tag{67}$$

Theorem proven. □

3.2. The Reverse Theorem of Approximation. Let us now construct the opposite theorem of approximation of the operator's equivalent form V_n^*. First and foremost, certain important theorems must be introduced in order to prepare.

Lemma 3. *Assume* $f\in A.C._{loc}$, $0\le\lambda\le 1$, *then*

$$\left|\varphi^{\lambda}(x)V_n^{*'}(f,x)\right|\le C\left\|\phi^{\lambda}f'\right\|(n\ge 2). \tag{68}$$

Proof. When $n\ge 2$,

$$v_{n,k}'(x)=\begin{cases}-nv_{n+1,0}(x), & k=0,\\ n\left(v_{n+1,k-1}(x)-v_{n+1,k}(x)\right), & k\ge 1,\end{cases}\qquad (r_n^*(x))'=\frac{n/n+1x}{\sqrt{n/n+1x^2+1/4(n+1)^2}}. \tag{69}$$

Thus, there is

$$\begin{aligned}V_n^{*'}(f,x)&=n\left[\sum_{k=1}^{\infty}f\left(\frac{k}{n}\right)v_{n+1,k-1}(r_n^*(x))-\sum_{k=0}^{\infty}v_{n+1,k}(r_n^*(x))f\left(\frac{k}{n}\right)\right]\\&=(r_n^{*'}(x))\\&=n\left[\sum_{k=0}^{\infty}f\left(\frac{k+1}{n}\right)v_{n+1,k}(r_n^*(x))-\sum_{k=0}^{\infty}f\left(\frac{k}{n}\right)v_{n+1,k}(r_n^*(x))\right](r_n^{*'}(x))\\&=n\sum_{k=0}^{\infty}\left[f\left(\frac{k+1}{n}\right)-f\left(\frac{k}{n}\right)\right]v_{n+1,k}(r_n^*(x))\frac{n/n+1x}{\sqrt{n/n+1x^2+1/4(n+1)^2}}.\end{aligned} \tag{70}$$

Now we estimate $|f(k+1/n) - f(k/n)|$

When $k = 0$,

$$\begin{aligned}\left|f\left(\frac{1}{n}\right) - f(0)\right| &= \left|\int_0^{1/n} f'(u)\mathrm{d}u\right| \le \int_0^{1/n}\left|f'(u)\right|\mathrm{d}u \\ &\le \left\|\phi^{\lambda} f'\right\| \int_0^{1/n} \phi^{-\lambda}(u)\mathrm{d}u \\ &\le \left\|\phi^{\lambda} f'\right\| \int_0^{1/n} u^{-\lambda/2}\mathrm{d}u \\ &\le n^{-1+\lambda/2}\left\|\phi^{\lambda} f'\right\|.\end{aligned} \tag{71}$$

When $k \ge 1$,

$$\begin{aligned}\left|f\left(\frac{k+1}{n}\right) - f\left(\frac{k}{n}\right)\right| &= \left|\int_0^{1/n} f'\left(\frac{k}{n}+u\right)\mathrm{d}u\right| \le \int_0^{1/n}\left|f'\left(\frac{k}{n}+u\right)\right|\mathrm{d}u \\ &\le \left\|\phi^{\lambda} f'\right\| \int_0^{1/n} \phi^{-\lambda}\left(\frac{k}{n}+u\right)\mathrm{d}u \\ &\le \left\|\phi^{\lambda} f'\right\| \frac{1}{n}\left(\frac{k}{n}\right)^{-\lambda/2}\left(1+\frac{k}{n}\right)^{-\lambda/2}.\end{aligned} \tag{72}$$

So we can get

$$\begin{aligned}\left|\varphi^{\lambda}(x) V_n^{'*}(f,x)\right| &\le \phi^{\lambda}(x) n \sum_{k=0}^{\infty}\left|f\left(\frac{k+1}{n}\right) - f\left(\frac{k}{n}\right)\right| v_{n+1,k}\left(r_n^*(x)\right) \\ &\quad \cdot \frac{n/n+1x}{\sqrt{n/n+1x^2 + 1/4(n+1)^2}} \\ &\le C\left\|\phi^{\lambda} f'\right\| \phi^{\lambda}(x)\left[\sum_{k=1}^{\infty}\left(\frac{n}{k}\right)^{\lambda/2}\left(\frac{n}{n+k}\right)^{\lambda/2} v_{n+1,k}\left(r_n^*(x)\right) + n^{\lambda/2} v_{n+1,0}\left(r_n^*(x)\right)\right] \\ &\quad \cdot \frac{n/n+1x}{\sqrt{n/n+1x^2 + 1/4(n+1)^2}}.\end{aligned} \tag{73}$$

For the summarized equation in the square bracket above, based on the Holder inequality, we get

$$\begin{aligned}\sum_{k=1}^{\infty}\left(\frac{n}{k}\right)^{\lambda/2}\left(\frac{n}{n+k}\right)^{\lambda/2}v_{n+1,k}\left(r_n^*(x)\right) &\le \left(\sum_{k=1}^{\infty}\frac{n^2}{k(k+n)}v_{n+1,k}\left(r_n^*(x)\right)\right)^{\lambda/2}\\ &= \phi^{-\lambda}\left(r_n^*(x)\right)\left(\sum_{k=1}^{\infty}\frac{n^2}{k(n+k)}\,\frac{(n+k)(k+1)}{n(n-1)}v_{n-1,k+1}\left(r_n^*(x)\right)\right)^{\lambda/2}\\ &\le C\phi^{-\lambda}\left(r_n^*(x)\right)\left(\sum_{k=1}^{\infty}v_{n-1,k+1}\left(r_n^*(x)\right)\right)^{\lambda/2}\\ &\le C\phi^{-\lambda}\left(r_n^*(x)\right).\end{aligned} \tag{74}$$

For the second item in the above square bracket, because $v_{n+1,0}\left(r_n^*(x)\right) \le 1$, so there is

$$\begin{aligned}n^{\lambda/2}v_{n+1,0}\left(r_n^*(x)\right) &\le \left(nv_{n+1,0}\left(r_n^*(x)\right)\right)^{\lambda/2}\\ &= \varphi^{-\lambda}\left(r_n^*(x)\right)\left(\frac{n}{n-1}v_{n-1,1}\left(r_n^*(x)\right)\right)^{\lambda/2}\\ &\le C\phi^{-\lambda}\left(r_n^*(x)\right).\end{aligned} \tag{75}$$

From equations (73), (74), and (75), we get

$$\begin{aligned}\left|\varphi^{\lambda}(x)V_n^{'*}(f,x)\right| &\le C\left\|\varphi^{\lambda}f\right\|\varphi^{\lambda}(x)\varphi^{-\lambda}\left(r_n^*(x)\right)\\ &\cdot\frac{n/n+1x}{\sqrt{n/n+1x^2+1/4(n+1)^2}}.\end{aligned} \tag{76}$$

Because when $n \ge 2$, $0 \le r_n^*(x) \le x$, so,

$$\begin{aligned}r_n^*(x) &= -\frac{1}{2(n+1)}+\sqrt{\frac{n}{n+1}x^2+\frac{1}{4(n+1)^2}}\\ &\ge \frac{n/n+1x^2}{2\sqrt{n/n+1x^2+1/4(n+1)^2}}.\end{aligned} \tag{77}$$

Thus,

$$\begin{aligned}&\phi^{\lambda}(x)\phi^{-\lambda}\left(r_n^*(x)\right)\frac{n/n+1x}{\sqrt{n/n+1x^2+1/4(n+1)^2}}\\ &= x^{\lambda/2}(1+x)^{\lambda/2}\left(r_n^*(x)\right)^{-\lambda/2}\left(1+r_n^*(x)\right)^{-\lambda/2}\cdot\frac{n/n+1x}{\sqrt{n/n+1x^2+1/4(n+1)^2}}\\ &= \left(\frac{1+x}{1+r_n^*(x)}\right)^{\lambda/2}\left(\frac{x}{r_n^*(x)}\right)^{\lambda/2}\frac{n/n+1x}{\sqrt{n/n+1x^2+1/4(n+1)^2}}.\end{aligned} \tag{78}$$

From Lemma 2, we have

$$\frac{1+x}{1+r_n^*(x)} \le C. \tag{79}$$

When $x > 1/2(n+1)$,

$$\frac{x}{r_n^*(x)} \le \frac{2\sqrt{n/n+1x^2+1/4(n+1)^2}}{n/n+1x} \le C. \tag{80}$$

For any $x \in [0,\infty)$,

$$\frac{n/n+1x}{\sqrt{n/n+1x^2+1/4(n+1)^2}} \le C. \tag{81}$$

So when $x > 1/2(n+1)$, there is

$$\left(\frac{x}{r_n^*}\right)^{\lambda/2}\frac{n/n+1x}{\sqrt{n/n+1x^2+1/4(n+1)^2}} \le C. \tag{82}$$

When $x \le 1/2(n+1)$, based on equation (77), there is

$$\left(\frac{x}{r_n^*(x)}\right)^{\lambda/2}\frac{n/n+1x}{\sqrt{n/n+1x^2+1/4(n+1)^2}}\le Cx^{1-\lambda/2}\left(\sqrt{\frac{n}{n+1}x^2+\frac{1}{4(n+1)^2}}\right)^{\lambda/2-1}$$
$$\le Cx^{1-\lambda/2}\left(\sqrt{\frac{n}{n+1}x^2+x^2}\right)^{\lambda/2-1}$$
$$= Cx^{1-\lambda/2}\left(\sqrt{\frac{n}{n+1}+1}\right)^{\lambda/2-1}x^{\lambda/2-1}$$
$$\le C. \tag{83}$$

After all, we get

$$\phi^{\lambda}(x)\phi^{-\lambda}\left(r_n^*(x)\right)\frac{n/n+1x}{\sqrt{n/n+1x^2+1/4(n+1)^2}}\le C. \tag{84}$$

In summary,

$$\left|\varphi^{\lambda}(x)V_n^{'*}(f,x)\right|\le C\left\|\phi^{\lambda}f'\right\|(n\ge 2). \tag{85}$$

Lemma 3 proven. □

Lemma 4. *Assume* $f\in C[0,\infty)$, $0\le\lambda\le 1$,

$$\left|V_n^{'*}(f,x)\right|\le Cn^{1/2}\phi^{-1}(x)\|f\|. \tag{86}$$

Proof. Use

$$v_{n,k}^{'}(x)=n\phi^{-2}(x)\left(\frac{k}{n}-x\right)v_{n,k}(x). \tag{87}$$

We can get

$$\left|\phi^{\lambda}(x)V_n^{'*}(f,x)\right|=\left|\varphi^{\lambda}(x)\sum_{k=0}^{\infty}n\varphi^{-2}\left(r_n^*(x)\right)\left(\frac{k}{n}-r_n^*(x)\right)v_{n,k}\left(r_n^*(x)\right)f\left(\frac{k}{n}\right)r_n^{'*}(x)\right|$$
$$\le\phi^{\lambda-1}(x)\|f\|n\phi(x)\phi^{-2}\left(r_n^*(x)\right)\sum_{k=0}^{\infty}\left|\frac{k}{n}-r_n^*(x)\right|v_{n,k}\left(r_n^*(x)\right)\frac{n/n+1x}{\sqrt{n/n+1x^2+1/4(n+1)^2}}$$
$$\le C\phi^{\lambda-1}(x)\|f\|n\phi(x)\phi^{-2}\left(r_n^*(x)\right)\left(\sum_{k=0}^{\infty}\left|\frac{k}{n}-r_n^*(x)\right|^2v_{n,k}\left(r_n^*(x)\right)\right)^{1/2}\frac{n/n+1x}{\sqrt{n/n+1x^2+1/4(n+1)^2}}$$
$$\le Cn\phi^{\lambda-1}(x)\|f\|\phi(x)\phi^{-2}\left(r_n^*(x)\right)n^{-1/2}\phi\left(r_n^*(x)\right)\frac{n/n+1x}{\sqrt{n/n+1x^2+1/4(n+1)^2}}$$
$$\le Cn^{1/2}\phi^{\lambda-1}(x)\|f\|\phi(x)\phi^{-1}\left(r_n^*(x)\right)\frac{n/n+1x}{\sqrt{n/n+1x^2+1/4(n+1)^2}}$$
$$\le Cn^{1/2}\phi^{\lambda-1}(x)\|f\|. \tag{88}$$

The last inequality has used the result of (84), and now Lemma 4 is proven. □

Lemma 5. *For* $0<t<1/8$, $x\ge t/2$, $0\le\beta\le 1$, *there is*

$$\int_{-t/2}^{t/2}\varphi^{-\beta}(x+u)\mathrm{d}u\le 4t\varphi^{-\beta}(x). \tag{89}$$

Proof. When $\beta=0$, it is clear that the equation holds. Now we move to the proof for $\beta=1$. For $0<\beta<1$, the Holder inequality gives us the following:

When $x\ge t/2$, $-t/2\le u\le t/2$, there is

$$\frac{1}{2}\sqrt{1+x}\le\sqrt{1+x+u}, \tag{90}$$

so

$$\begin{aligned}\int_{-(t/2)}^{(t/2)}\varphi^{-1}(x+u)\mathrm{d}u &\le \frac{2}{\sqrt{1+x}}\int_{-(t/2)}^{(t/2)}\frac{1}{\sqrt{x+u}}\mathrm{d}u\\ &= \frac{4}{\sqrt{1+x}}\left(\sqrt{x+\frac{t}{2}}-\sqrt{x-\frac{t}{2}}\right)\le \frac{4}{\sqrt{1+x}}\frac{t}{\sqrt{x+t/2}+\sqrt{x-(t/2)}}\le 4t\varphi^{-1}(x).\end{aligned} \tag{91}$$

□

Theorem 12. *Assume* $f\in C[0,\infty)$, $0\le\lambda\le 1$, $0<\alpha<1$,

$$\left|V_n^*(f,x)-f(x)\right|\le C\left(n^{-(1/2)}\phi^{1-\lambda}(x)\right)^{\alpha}\Longleftrightarrow\omega_{\phi^\lambda}^1(f,t)=\mathrm{O}(t^{\alpha}). \tag{92}$$

Proof. Theorem 11 gives us its sufficiency directly, so now we try to prove its necessity. Since $\phi^{\alpha(1-\lambda)}(x)$ is a convex function, we can get

$$\begin{aligned}\left|\Delta_{t\varphi^\lambda}^1 f(x)\right| &\le \left|\Delta_{t\varphi^\lambda}^1\left(f(x)-V_n^*(f,x)\right)\right|+\left|\Delta_{t\phi^\lambda}^1 V_n^*(f,x)\right|\\ &\le \sum_{j=0}^{1}\binom{1}{j}\left|V_n^*\left(f,x+\left(j-\frac{1}{2}\right)t\phi^\lambda(x)\right)-f\left(x+\left(j-\frac{1}{2}\right)t\phi^\lambda(x)\right)\right|\left|\Delta_{t\phi^\lambda}^1 V_n^*(f,x)\right|\\ &\le \sum_{j=0}^{1}\binom{1}{j}\left(n-\frac{1}{2}\phi^{1-\lambda}\left(x+\left(j-\frac{1}{2}\right)t\phi^\lambda(x)\right)\right)^{\alpha}+\left|\Delta_{t\phi^\lambda}^1 V_n^*(f,x)\right|\le C\left(n^{-(1/2)}\phi^{1-\lambda}(x)\right)^{\alpha}+\left|\Delta_{t\phi^\lambda}^1 V_n^*(f,x)\right|.\end{aligned} \tag{93}$$

We can select a g_n that satisfies

$$\|f-g_n\|+n^{-(1/2)}\phi^{1-\lambda}(x)\left\|\phi^\lambda g_n'\right\|\le C\omega_{\varphi^\lambda}\left(f,n^{-(1/2)}\varphi^{1-\lambda}(x)\right). \tag{94}$$

Apply, Lemmas 3–5

$$\begin{aligned}\left|\Delta_{t\phi^\lambda}^1 V_n^*(f,x)\right| &= \left|\int_{-\left(t\varphi^\lambda(x)/2\right)}^{t\varphi^\lambda(x)/2} V_n^{*'}(f,x+u)\mathrm{d}u\right|\\ &\le \left|\int_{-\left(t\varphi^\lambda(x)/2\right)}^{\left(t\varphi^\lambda(x)/2\right)} V_n^{*'}(f-g_n,x+u)\mathrm{d}u\right|+\left|\int_{-\left(t\varphi^\lambda(x)/2\right)}^{\left(t\varphi^\lambda(x)/2\right)} V_n^{*'}(g_n,x+u)\mathrm{d}u\right|\\ &\le C n^{1/2}\|f-g_n\|\int_{-\left(t\varphi^\lambda(x)/2\right)}^{\left(t\varphi^\lambda(x)/2\right)}\phi^{-1}(x+u)\mathrm{d}u+C\left\|\varphi^\lambda g_n'\right\|\int_{-\left(t\varphi^\lambda(x)/2\right)}^{\left(t\varphi^\lambda(x)/2\right)}\phi^{-\lambda}(x+u)\mathrm{d}u\\ &\le C\left(tn^{1/2}\varphi^{\lambda-1}(x)\|f-g_n\|+t\left\|\varphi^\lambda g_n'\right\|\right)\\ &\le C\,tn^{1/2}\phi^{\lambda-1}(x)\left(\|f-g_n\|+n^{-1/2}\phi^{1-\lambda}(x)\left\|\phi^\lambda g_n'\right\|\right)\\ &\le C\,tn^{1/2}\phi^{\lambda-1}(x)\omega_{\phi^\lambda}^1\left(f,n^{-1/2}\phi^{1-\lambda}(x)\right).\end{aligned} \tag{95}$$

From equations (93) and (95), we have

$$\left|\Delta^1_{t\phi^\lambda(x)} f(x)\right| \le C\left(\left(n^{-(1/2)}\varphi^{1-\lambda}(x)\right)^\alpha + \frac{t}{n^{-(1/2)}\varphi^{1-\lambda}(x)}\omega^1_{\varphi^\lambda}\left(f, n^{-(1/2)}\varphi^{1-\lambda}(x)\right)\right). \tag{96}$$

For any fixed $0 < \delta < (1/8)$ and all $x \in [0, \infty)$, use a sufficiently great n that makes the following equation stand:

$$n^{-(1/2)}\phi^{1-\lambda}(x) \le \delta \le 2\left(n^{-(1/2)}\phi^{1-\lambda}(x)\right). \tag{97}$$

Now we have

$$\left|\Delta^1_{t\phi^\lambda(x)} f(x)\right| \le C\left(\delta^\alpha + \frac{t}{\delta}\omega^1_{\varphi^\lambda}(f, \delta)\right). \tag{98}$$

Thus,

$$\omega^1_{\phi^\lambda}(f, t) \le C\left(\delta^\alpha + \frac{t}{\delta}\omega^1_{\varphi^\lambda}(f, \delta)\right) \tag{99}$$

Use lemma Lorenz-Hermann (literature [20] P_{199}), then we can get

$$\omega^1_{\phi^\lambda}(f, t) = O\left(t^\alpha\right). \tag{100}$$

Theorem 12 proven. □

Data Availability

The data used to support the findings of this study are included within the article.

Conflicts of Interest

The authors declare that they have no conflicts of interest.

References

[1] P. P. Korovkin, *Linear Operators and Approximation Theory*, Hindustan Publishing Corporation, New Delhi, India, 1960.

[2] R. Devore, "The approximation of continuous functions by positive linear operators," *Lecture Notes in Math*, vol. 293, Springer-Verlag, New York, NY, USA, 1972.

[3] H. Berens and G. Lorentz, "Inverse theorems for Bernstein polynomials," *Indiana University Mathematics Journal*, vol. 21, no. 8, pp. 693–708, 1972.

[4] Z. Ditzian and V. Totik, *Moduli of Smoothness*, Springer-Verlag, New York, NY, USA, 1987.

[5] S. M. Ferguson, "Partnering with the NIH: now part of the "value proposition" for start-ups," *Journal of Commercial Biotechnology*, vol. 18, no. 2, pp. 60–67, 2012.

[6] M. Heilmann, "Direct and converse results for operators of baskakov-durrmeyer type," *Approximation Theory and Its Apptlcation5*, no. 1, pp. 105–127, 1989.

[7] J. P. King, "Positive linear operators which preserve," *Acta Mathematica Hungarica*, vol. 99, no. 3, pp. 203–208, 2003.

[8] X. Pei-cai, "Weighted approximation of Baskakov type operators," *Acta Mathematica Hungarica*, vol. 133, pp. 614–624, 1995.

[9] J. D. L Cal and L. . Francisco, "A note on limiting properties of some bernstein-type operators," *Math. Anal. Appl.*vol. 184, pp. 585–593, 1994.

[10] C. P. May, "Saturation and inverse theorems for combinations of a class of exponential-type operators," *Canadian Journal of Mathematics*, vol. 28, no. 6, pp. 1224–1250, 1976.

[11] G. Ladds, "The roles and responsibilities of the EU qualified person for pharmacovigilance under Volume IXa March 2007," *Journal of Commercial Biotechnology*, vol. 13, no. 4, pp. 259–262, 1969.

[12] O. Duman and M. A. Özarslan, "Szász–Mirakjan type operators providing a better error estimation," *Applied Mathematics Letters*, vol. 20, no. 12, pp. 1184–1188, 2007.

[13] Z. Walczak, "On certain positive linear operators in polynomial weight spaces," *Acta Mathematica Hungarica*, vol. 101, no. 3, pp. 179–191, 2003.

[14] M. A. özarslan and O. Duman, "MKZ type operators providing a better estimation on [1/2, 1)," *Canadian Mathematical Bulletin*, vol. 50, no. 3, pp. 434–439, 2007.

[15] N. Deo, "Pointwise estimate for modified Baskakov type operators," *Lobachevskii Journal of Mathematics*, vol. 31, no. 1, pp. 36–42, 2010.

[16] S.-sheng Guo and Z.-jie Song, "Pointwise approximation of baskakov-durrmeyer," *Mathematical research and review*, vol. 3, 2001.

[17] S.-qin Wang and P.-hua Wang, "Pointwise approximation of modified Baskakov type operators," *Journal of Quanzhou Normal University*, vol. 6, 2004.

[18] J.-bin Li, "Approximation of modified Baskakov type operators," *Journal of Ningxia Normal University (Natural Science edition)*, no. 12, 2008.

[19] S.-sheng Guo, L. I. Cui-xiang, and G.-sheng Zhang, "Pointwise estimate for Baskakov operators, northeast," *The Mathematica Journal*, vol. 17, no. 2, pp. 133–137, 2001.

[20] C. Wen-zhong, *Operator Approximation Theory*, Xiamen University Press, Fujian, China, 1989.

Hindawi
Journal of Mathematics
Volume 2023, Article ID 9843601, 1 page
https://doi.org/10.1155/2023/9843601

Retraction

Retracted: Novel Concepts in Bipolar Fuzzy Graphs with Applications

Journal of Mathematics

Received 25 November 2022; Accepted 25 November 2022; Published 11 January 2023

Journal of Mathematics has retracted the article titled "Novel Concepts in Bipolar Fuzzy Graphs with Applications" [1] due to concerns that the peer review process has been compromised.

Following an investigation conducted by the Hindawi Research Integrity team [2], significant concerns were identified with the peer reviewers assigned to this article; the investigation has concluded that the peer review process was compromised. We therefore can no longer trust the peer review process, and the article is being retracted with the agreement of the Chief Editor.

The authors do not agree to the retraction.

References

[1] C. Wan, F. Deng, S. Li, S. Omidbakhsh Amiri, A. A. Talebi, and H. Rashmanlou, "Novel Concepts in Bipolar Fuzzy Graphs with Applications," *Journal of Mathematics*, vol. 2022, Article ID 8162474, 9 pages, 2022.

[2] L. Ferguson, "Advancing Research Integrity Collaboratively and with Vigour," 2022, https://www.hindawi.com/post/advancing-research-integrity-collaboratively-and-vigour/.

Hindawi
Journal of Mathematics
Volume 2023, Article ID 9874714, 1 page
https://doi.org/10.1155/2023/9874714

Retraction

Retracted: International Chinese Education Expert System Based on Artificial Intelligence and Machine Learning Algorithms

Journal of Mathematics

Received 10 October 2023; Accepted 10 October 2023; Published 11 October 2023

This article has been retracted by Hindawi following an investigation undertaken by the publisher [1]. This investigation has uncovered evidence of one or more of the following indicators of systematic manipulation of the publication process:

(1) Discrepancies in scope

(2) Discrepancies in the description of the research reported

(3) Discrepancies between the availability of data and the research described

(4) Inappropriate citations

(5) Incoherent, meaningless and/or irrelevant content included in the article

(6) Peer-review manipulation

The presence of these indicators undermines our confidence in the integrity of the article's content and we cannot, therefore, vouch for its reliability. Please note that this notice is intended solely to alert readers that the content of this article is unreliable. We have not investigated whether authors were aware of or involved in the systematic manipulation of the publication process.

Wiley and Hindawi regrets that the usual quality checks did not identify these issues before publication and have since put additional measures in place to safeguard research integrity.

We wish to credit our own Research Integrity and Research Publishing teams and anonymous and named external researchers and research integrity experts for contributing to this investigation.

The corresponding author, as the representative of all authors, has been given the opportunity to register their agreement or disagreement to this retraction. We have kept a record of any response received.

References

[1] L. Shen and F. Latif, "International Chinese Education Expert System Based on Artificial Intelligence and Machine Learning Algorithms," *Journal of Mathematics*, vol. 2022, Article ID 2160289, 12 pages, 2022.

Hindawi
Journal of Mathematics
Volume 2022, Article ID 2160289, 12 pages
https://doi.org/10.1155/2022/2160289

Research Article

International Chinese Education Expert System Based on Artificial Intelligence and Machine Learning Algorithms

Lin Shen[1] and Faiza Latif[2]

[1]*College of Foreign Languages, Guizhou University, Guiyang 550025, China*
[2]*Department of Business, University of Central Punjab Lahore, Lahore, Pakistan*

Correspondence should be addressed to Faiza Latif; faiza_latif@ucp.edu.pk

Received 9 April 2022; Revised 16 May 2022; Accepted 24 May 2022; Published 18 July 2022

Academic Editor: Naeem Jan

This study builds an international Chinese education expert system based on artificial intelligence and machine learning algorithms, introduces interval intuition fuzzy sets to express expert evaluation information, and uses the entropy weight method to determine the weight of evaluation attributes in order to improve the effect of international Chinese teaching and learning. The group utility value, personal regret value, and comprehensive evaluation value of each system are then calculated in this study. At the same time, this study introduces the degree of closeness and satisfaction to improve the decision-making process and finally determines the optimal solution. In addition, this study constructs an intelligent system based on the improved algorithm. The research shows that the international Chinese education expert system based on artificial intelligence and machine learning algorithm proposed in this study has a very good effect.

1. Introduction

Compared with physical spaces such as traditional classrooms and multimedia classrooms, online Chinese learning spaces have unique environmental metaphors. Moreover, cyberspace stores a large number of Chinese learning resources such as pictures, texts, audio, and video, and is a treasure trove of knowledge for Chinese learners. The creation of a network resource database allows for the integration of multiple dispersed resources, making it easier for individuals to search and analyze them. There are no limits and uniform time schedules in the online Chinese learning environment. All Chinese learners may use the internet to study Chinese at any time and from any location, and they can choose their own material and learning techniques. Furthermore, the online Chinese learning environment offers Chinese students a free, autonomous, resource-integrated, and convenient Chinese learning environment.

The interactive function of the online Chinese learning space is a distinctive feature that is different from the traditional Chinese learning space. Students can send requests to the platform system according to their own needs, and the system can feed back the corresponding information and related module content after retrieval. In the process of human-computer interaction, online Chinese learning can effectively improve students' autonomy and self-control, enabling Chinese learners to participate and control the Chinese learning process independently. The online Chinese learning space can break through the limitations of time and space, making it possible for flipped classrooms and cross-regional collaborative Chinese learning. On the one hand, online Chinese learning can break through the time limit, and the construction of online classrooms makes teaching activities not limited to classroom time. Teachers turn the course content into videos for students to watch Chinese learning at any time, breaking away from traditional classroom teaching and time constraints. On the other hand, online Chinese learning can break through space constraints. Through real-time transmission technology, different schools can form teaching alliances, integrate their own high-quality teaching resources, provide the best-quality teaching content to all students in the alliance, and maximize the utilization of high-quality teaching resources.

Space resources include various forms of multimedia materials, courseware, texts, and other materials that require learners to browse independently. The learner's way of learning is acceptance learning, and the way of knowledge construction is individual construction. The live teaching space relies on real-time video tools and voice communication software to achieve real-time dialogue, which is the reproduction of real classrooms in cyberspace. Learners and teachers communicate, leave messages, vote, etc., through the interactive area of the screen. The learning method is acceptance learning, and the knowledge construction method is group construction [1]. In the learning community space, learners or teachers and students can interact and communicate, and any account subject can post or leave messages, comments, and likes independently. The learning method is discovery learning, and the knowledge construction method is group construction. In the role-playing space, learners or teachers select virtual characters representing their own images according to the role settings. Moreover, they complete tasks through autonomous exploration, group cooperation, or teacher-student cooperation in a virtual situation. The learning method is discovery learning, and the knowledge construction method may be individual construction or group construction [2]. The course service space relies on the course platform to provide course selection, teaching, learning support services, etc. The learning method is acceptance learning, and the knowledge construction method may be individual construction or group construction [3].

In order to improve the effect of international Chinese teaching and learning, this study constructs an international Chinese education expert system based on artificial intelligence and machine learning algorithms to improve the intelligent development effect of international Chinese education.

2. Related Work

Online learning theory research covers computer science, psychology, communication, education, and other disciplines and related interdisciplinary subjects, with multiple theoretical backgrounds. Literature [4] believes that online learning is the product of the combination of education and network technology, and the process of online learning is the process of knowledge increment, transmission, exchange, and generation, emphasizing the active construction of learners and the interaction of the learning process, widely recognized and widely used in academia. Literature [5] believes that online learning can help learners to independently control the learning content, progress, and time, and rely on the learner's own experience to achieve learning goals. Scholars in the field of educational technology pay attention to the technical support means related to online learning, including learning system design, software development, and application [6]. Literature [7] proposes the definition of online learning, and points out that the four key elements of online learning are teachers, learners, courses, and technology, which is an earlier and more complete analysis of online learning in China. The technical research related to online learning mainly covers the design and support services of learning system components and platforms. The research in the field of application focuses on the teaching mode, teaching strategy, and teaching application of online learning, and the literature [8] studies the design process of the contextual experience course. At present, the evaluation system and management research of online learning are relatively small, and it rarely involves the funds, market operation, and management of the online learning system. Research trends in the field of online learning are increasingly focused on how to enable learners to experience personalized learning and deep learning, and how to sustain learners' interest in learning. The application of virtual technology and artificial intelligence technology will change the form of learning places, bring a new interactive participation experience, and improve the convenience of teacher-student interaction and student-student interaction [9].

The macrolevel study seeks to build the digital and ecological environments of online learning, and give a fundamental framework guide for the system [10]. The digital and ecological environments for e-learning are carefully designed in literature [11]. The research at the mesolevel is rather large and in-depth, based on the number of papers published, and the research hotspot is the design, development, and effective communication techniques of external learning websites and platforms. The two publications on the building of network teaching platforms heavily rely on literature [12]. This study analyzes the learners' needs for the construction of learning network teaching platforms and the specific application strategies of social interaction in language teaching platforms. The construction of the teaching platform provides a literature. Literature [13] proposed the conceptual model, structure, and function of the remote visual external teaching platform. The visual teaching platform focuses on interactivity and the analysis of learners' needs. Research at the microlevel mainly focuses on online learning behavior, learning strategies, and the compilation of teaching courseware [14]. Literature [15] proposes a dual-class teaching model that combines real classrooms and virtual classrooms based on cloud platforms, and points out that the dual-class teaching mode is helpful to improve the practical problems of insufficient teaching hours in real classrooms, low level of participatory learning, and resource sharing.

Literature [16] constructed the basic framework of "everyone in cyberspace" and pointed out that the development of technical specifications can ensure the effective implementation of the framework. Literature [17] summarizes the general design principles of online learning spaces and focuses on analyzing the value demands of individual learning spaces. Literature [18] discusses the developmental goals and value positioning of the online learning space platform in detail, and summarizes the construction strategy of the online learning space platform. Literature [19] summarizes the network learning space into five types and proposes the enlightenment of the classification to the practice field.

3. Expert Data Processing System Based on Machine Learning and Artificial Intelligence

In order to describe the ambiguity of information, a language-intuitive fuzzy set, which reflects people's uncertainty preference, is proposed.

Definition 1. We set $X = \{x_1, x_2, x_3\}$ as a nonempty universe and define an intuitionistic fuzzy set A on any element in the following form:

$$A = \left\{\left(x, \mu_A(x)^0, \nu_A(x)^0\right) | x \in X\right\}. \tag{1}$$

Definition 2. We call $\pi_A(x) = 1 - \mu_A(x) - \nu_A(x)$ the hesitation degree of the x element in A, which represents the uncertainty degree of whether x belongs to the set A or not. Obviously, there is $0 \le \pi_A(x) \le 1$.

Due to the complexity and uncertainty of the decision-making environment, it is difficult for experts to express the values of $\mu_A(x)^0$ and $\pi_A(x)$ with exact real numbers in the actual scoring, but it is more suitable to express them in the form of interval numbers. For this reason, the membership degree and nonmembership degree of the intuitionistic fuzzy set can be improved to the interval number, so that it becomes the interval intuitionistic fuzzy set.

As an information expression, fuzzy numbers can reflect the fuzziness of decision-making information. Compared with the previous intuitionistic fuzzy set, the interval intuitionistic fuzzy set expresses the membership degree and nonmembership degree of the intuitionistic fuzzy set as interval values, so as to better show the psychological hesitation state of decision-makers. Atanassovl et al. extended the intuitionistic fuzzy set and proposed the definition of interval intuitionistic fuzzy set.

Definition 3. x is set to be a nonempty set, and the interval intuitionistic fuzzy set A is expressed as follows:

$$A = \{(x, \mu_A(x), \nu_A(x)) | x \in X\}. \tag{2}$$

Among them, there is $\mu_A(x) \subseteq [0,1], \nu_A(x) \subseteq [0,1]$, and the condition $\sup\mu_A(x) + \sup\mu_A(x) \le 1$ is satisfied. $u(x)$ is the membership function of A, and $v(x)$ is the nonmembership function of A. The upper and lower bounds of $u_a(x)$ are denoted as $u_t(x)$ and $p(x)$, respectively, and the upper and lower bounds of $v_a(x)$ are denoted as $v_A(x)$, respectively. Formula (2) can also be expressed as follows:

$$A = \left\{x, \left(\left[\mu_A^L(x), \mu_A^R(x)\right]\right), \left[\nu_A^L(x), \nu_A^R(x)\right] | x \in X\right\}. \tag{3}$$

Then, the hesitation degree of A is expressed as follows:

$$\begin{aligned}\pi_A(x) &= 1 - \mu_A(x) - \nu_A(x) \\ &= \left[1 - \nu_A^R(x) - \mu_A^R(x), 1 - \mu_A^L(x) - \nu_A^L(x)\right].\end{aligned} \tag{4}$$

For the convenience of description, the interval intuitionistic fuzzy number is denoted as $\alpha = (\mu_\alpha, \nu_\alpha) = ([\mu_\alpha^L, \mu_\alpha^R], [\nu_\alpha^L, \nu_\alpha^R])$, and the hesitation degree of α is denoted as $\pi_\alpha(x) = [\pi_\alpha^L, \pi_\alpha^R]$. Among them, there is $\mu_\alpha \subseteq [0,1], \nu_\alpha \subseteq [0,1], \mu_\alpha^R + \nu_\alpha^R \le 1$.

Definition 4. We set a set of interval intuitionistic fuzzy numbers. IIFWA is an interval intuitionistic fuzzy weighted operator, and the formula is as follows:

$$\mathrm{IIFWA}_\omega(r_1, r_2, \ldots, r_z) = \left(\left[1 - \prod_{j=1}^{n}\prod n\left(1 - \mu_j^L\right)^{\omega_j}, 1 - \prod_{j=1}^{n}\left(1 - \mu_j^R\right)^{\omega_j}\right], \left[\prod_{j=1}^{n}\left(\mu_j^L\right)^{\omega_j}, \prod_{j=1}^{n}\left(\mu_j^R\right)^{\omega_j}\right]\right). \tag{5}$$

The Euclidean distance between the two can be used to represent the difference between the two interval intuitionistic fuzzy numbers, which is similar to calculating the distance between the two intuitionistic fuzzy numbers.

$$d(\gamma_{ab}, \gamma_{c\,d}) = \sqrt{\frac{1}{4}\left[\left(\mu_{ab}^L - \mu_{c\,d}^L\right)^2 + \left(\mu_{ab}^R - \mu_{c\,d}^R\right)^2 + \left(\nu_{ab}^L - \nu_{c\,d}^L\right)^2 + \left(\nu_{ab}^R - \nu_{c\,d}^R\right)^2\right]}. \tag{6}$$

For any two real numbers m, n[0,1], the Einstein product is represented by $T(m,n)$, and the Einstein sum is represented by $S(m,n)$. Einstein's algorithm is as follows:

$$\begin{aligned}T(m,n) &= \frac{mn}{1 + (1-m)(1-n)}, \\ S(m,n) &= \frac{m+n}{1+mn}.\end{aligned} \tag{7}$$

We set the sum of interval intuitionistic fuzzy sets as $B = \{(x, \mu_B(x), v_B(x))|x \in X\}$ and $A = \{(x, \mu_A(x), v_A(x))| x \in X\}$. Based on the Einstein algorithm given by formula (7), Wang et al. proposed the following interval intuitionistic fuzzy set algorithm as follows:

$$
\begin{aligned}
&(1)A^c = \{\{(x, v_A(x), \mu_A(x))|x \in X\}\},\\
&(2)A \oplus B = \left\{\left[S\left(\left[\mu_A^L(x), \mu_A^L(x)\right]\right), S\left[v_A^R(x), v_A^R(x)\right]\right], T\left(\left[v_A^L(x), v_B^L(x)\right]\right), T\left[v_A^R(x), v_B^R(x)\right]\right\}\\
&\quad = \left\{\left[\frac{\mu_A^L(x) + \mu_B^L(x)}{1 + \mu_A^L(x)\mu_B^L(x)}, \frac{\mu_A^R(x) + \mu_B^R(x)}{1 + \mu_A^R(x)\mu_B^R(x)}\right], \left[\frac{v_A^L(x), v_B^L(x)}{1 + \left(1 - v_A^L(x)\right)\left(1 - v_B^L(x)\right)}\right], \frac{v_A^R(x), v_B^R(x)}{1 + \left(1 - v_A^R(x)\right)\left(1 - v_B^R(x)\right)}\right\},\\
&(3)A \otimes B = \left\{\left[T\left(\left[\mu_A^L(x), \mu_A^L(x)\right]\right), T\left[v_A^R(x), v_A^R(x)\right]\right], S\left(\left[v_A^L(x), v_B^L(x)\right]\right), S\left[v_A^R(x), v_B^R(x)\right]\right\}\\
&\quad = \left\{\left[\frac{\mu_A^R(x) + \mu_B^R(x)}{1 + \left(1 - \mu_A^R(x)\right)\left(1 - \mu_B^R(x)\right)}, \frac{\mu_A^R(x), \mu_B^R(x)}{1 + \left(1 - \mu_A^R(x)\right)\left(1 - \mu_B^R(x)\right)}\right], \left[\frac{v_A^L(x) + v_B^L(x)}{1 + v_A^L(x)v_B^L(x)}, \frac{v_A^R(x) + v_B^R(x)}{1 + v_A^R(x)v_B^R(x)}\right]\right\},\\
&(4)A^\epsilon = \left\{\left[\frac{2\left(\mu_A^L(x)\right)^\epsilon}{\left(2 - \mu_A^L(x)\right)^\epsilon + \left(\mu_A^L(x)\right)^\epsilon}, \frac{2\left(\mu_A^R(x)\right)^\epsilon}{\left(2 - \mu_A^R(x)\right)^\epsilon + \left(\mu_A^R(x)\right)^\epsilon}\right],\right.\\
&\quad \left.\cdot \left[\frac{\left(1 + v_A^R(x)\right)^\epsilon - \left(1 - v_A^R(x)\right)^\epsilon}{\left(1 + v_A^L(x)\right)^\epsilon + \left(1 - v_A^L(x)\right)^\epsilon}, \frac{\left(1 + v_A^R(x)\right)^\epsilon - \left(1 - v_A^R(x)\right)^\epsilon}{\left(1 + v_A^R(x)\right)^\epsilon + \left(1 - v_A^R(x)\right)^\epsilon}\right]\right\}, \quad \epsilon > 0.
\end{aligned}
\tag{8}
$$

Among them, A^C represents the complement of A.

For any $A = \{(x, \mu_A(x), v_A(x))|x \in X\}$ and $B = \{(x, \mu_B(x), v_B(x))|x \in X\}$, the mapping is as follows:

(1) $\mu_A^L(x) = \mu_A^R(x) = 0$, $\mu_A^L(x) = \mu_A^R(x) = 1, v_A^L(x) = v_A^R(x) = 0$;

(2) $E(A) = 1$ holds if and only if $[\mu_A^L(x), \mu_A^R(x)] = [v_A^L(x), v_A^R(x)]$;

(3) $E(A) = E(A^C)$, and there is $A^C = \{(x, \mu_A(x), v_A(x))|x \in X\}$;

(4) If there is $v_x \in X$, when there is $u_n(x) \geq v$: (x), and there is $u_a(x) \geq u_s(x)$ and $v_a(x) \leq v_g(x)$ or when there is $4 = (X) \leq v_s(x)$, and there is $u_g(x) \leq u_z(x)$ and $v_a(x) \geq V$: (x), then there is $E(A) \leq E(B)$. Then, $E(A)$ is the interval intuitionistic fuzzy entropy.

The interval intuitionistic fuzzy entropy $E(A)$ can be defined as follows:

$$
E_A = \frac{1}{n}\sum \frac{4 - \left[\left|\mu_A^L(x_i) - v_A^L(x_i)\right| + \left|\mu_A^u(x_i) - v_A^u(x_i)\right|\right]^2 + \left[\pi_A^L(x_i) - \pi_A^v(x_i)\right]^2}{8}. \tag{9}
$$

It can be seen from formula (9) that the entropy formula not only includes the interval membership degree and interval nonmembership degree, but also includes the interval hesitation degree, which makes the information of interval intuition fuzzy entropy more complete. Thus, formula (9) completely contains the entropy information of interval intuitionistic fuzzy sets.

A typical multiattribute decision-making approach is the simple linear weighting method. When using the SWA approach, it is important to remember that the decision-maker must standardize the decision matrix such that all signs are positive. Because of its easy decision-making processes, the SWA approach is often utilized for dealing with multiattribute decision-making situations. The basic steps of this method include the following points:

(a) First, the attribute weights of the alternatives are determined, and the weight vectors of several attributes are set as follows:

$$
\omega = (\omega_1, \omega_2, \ldots, \omega_n)^T. \tag{10}
$$

(b) The standard matrix $X = (x_{ij})_{n \times m}$ is obtained, and m is the number of alternatives.

(c) The linear weighted average value of each alternative is obtained, as shown by the following formula:

$$\mu_j = \sum_{j=1}^{m} \omega_j x_{ij}, \quad 1, 2, \ldots, n. \tag{11}$$

(d) The linear weighted average is calculated by formula (11), and the optimal solution is selected according to the principle of u maximization, which is shown by the following formula:

$$U(P^*) = \max_{1 \le i \le n} \sum_{j=1}^{m} \omega_j x_{ij}. \tag{12}$$

As a common and simple decision-making method, the AHP has been widely studied and applied by various scholars. This approach is distinguished by the use of numbers to indicate the connection between the influencing elements, and it is used to evaluate decision-making possibilities, method plans, and so on. The concept is to arrange the things to be approximately examined according to their advantages and disadvantages before evaluating and selecting them one by one in the order of sorting. The issue is then separated into three layers: the goal layer, criteria layer, and indication layer. The upper-level factors have a dominant effect on the lower-level factors, and at the same time, it can divide multiple research objects into multiple factors. For simple system properties, the two are compared in pairs. After the comparison, the importance of the relevant indicators is obtained, so as to rank the alternatives, and provide a theoretical basis for decision-makers from the perspective of qualitative and quantitative conversion. The calculation sequence is shown in Figure 1.

Because the AHP decomposes the decision-making problem into the multilevel target level, criterion level, and index level. Therefore, its weight determination principle is to simulate the logical relationship of the human brain, with great human subjectivity. It cannot make use of existing data, cannot convince people, and goes against the idea of objective science.

We set $F: R^n \longrightarrow R$, and there is the following:

$$F_w(x_1, x_2, \ldots, x_n) = \sum_{j=1}^{n} \omega_j y_j. \tag{13}$$

Among them, $\omega = (\omega_1, \omega_2, \ldots, \omega_n)^T$ and F are related to each other, and ω_j satisfies the following conditions. Among them, there is $\sum_{j=1}^{n} \omega_j = 1 (j \in N), 0 \le \omega_j \le 1$.

The ordered weighted average method is based on the range of the index weight given by the decision-maker and uses the linear programming method to establish a mathematical model to obtain an index weight. Compared with the analytic hierarchy process, the ordered weighted average method has obvious advantages in objective science. However, its operation process is more complicated, and it still retains the limitation of a simple linear weighting method for decision-making of complex problems.

We assume a decision problem with m alternatives and n attributes. Among them, the evaluation value of the scheme the TOPSIS method is calculated as follows:

Step 1. The decision matrix $R = (r_{ij})_{n \times m}$ is standardized and transformed to obtain a standardized decision matrix:

$$F = \left(f_{ij}\right)_{n \times m}, f_{ij} = \frac{r_{ij}}{\sqrt{\sum_{i=1}^{m} \left(r_{ij}\right)^2}}, \quad i = 1, 2 \ldots, m; j = 1, 2, \ldots, n. \tag{14}$$

Step 2. The following formula is adopted for the decision matrix $Y = (y_{ij}) m \times n$.

$$y_{ij} = \omega_j \times f_{ij}, \quad i = 1, 2, \ldots, m, j = 1, 2, \ldots, n. \tag{15}$$

Among them, $\omega_j = (j = 1, 2, \ldots, n)$ is the weight of attribute c_j.

Step 3. The positive-ideal solution y^+ and the negative-ideal solution y of the scheme are calculated.

Among them, for the benefit index, there is the following:

$$\begin{aligned} y_i^+ &= \max_{1 \le i \le m} \left\{y_{ij}\right\}, \\ y_i^- &= \min_{1 \le i \le m} \left\{y_{ij}\right\}. \end{aligned} \tag{16}$$

Second, for cost metrics, there is the following:

$$\begin{aligned} y_i^+ &= \min_{1 \le i \le m} \left\{y_{ij}\right\}, \\ y_i^- &= \max_{1 \le i \le m} \left\{y_{ij}\right\}. \end{aligned} \tag{17}$$

Step 4. The distances from scheme $A_i (i = 1,2, \ldots, m)$ to the positive-ideal solution and the negative-ideal solution are calculated.

$$\begin{aligned} d_i^+ &= \sqrt{\sum_{j=1}^{n} \left(y_{ij} - y_j^+\right)^2}, \quad i = 1, 2, \ldots, m, \\ d_i^- &= \sqrt{\sum_{j=1}^{n} \left(y_{ij} - y_j^-\right)^2}, \quad i = 1, 2, \ldots, m. \end{aligned} \tag{18}$$

Step 5. The approximation coefficient of scheme A_i $(i = 1, 2, \ldots, m)$ and the positive-ideal solution is calculated.

$$T_i = \frac{di^-}{di^+ + di^-}, \quad i = 1, 2, \ldots, m. \tag{19}$$

Step 6. According to the value of the closeness coefficient T_i $(i = 1,2, \ldots, m)$, the alternatives are sorted from large to small, so as to select the scheme. The larger the program is, the better the program is.

In recent years, the multiattribute decision-making approach based on fuzzy theory has become a hotspot for study in decision-making methods. Numerous researchers have been experimenting with and developing the VIKOR

multiattribute decision-making approach, which is extensively utilized in many domains. VIKOR has an advantage over the TOPSIS in that it can modify the effect of group utility value and individual regret value on program ranking. It compensates for TOPSIS' impact on solution ordering, which solely examines the distance between alternatives and positive- and negative-ideal solutions.

Step 1. The positive- and negative-ideal solutions Y^+ and Y^+ of each scheme in the alternative scheme are calculated, which is the same as the TOPSIS method.

Step 2. The group utility value s_i and the individual regret value R_i of each alternative are calculated by the following formula:

$$S_i = \sum_{j=1}^{n} \omega_j \frac{\left(f^+ - f_{ij}\right)}{\left(f^+ - f_j^-\right)}, \quad 1 \le i \le m,$$
$$R_i = \max_j \omega_j \frac{\left(f^+ - f_{ij}\right)}{\left(f^+ - f_j^-\right)}, \quad 1 \le i \le m. \tag{20}$$

In the formula, ω_j represents the weight of the indicator.

Step 3. The following formula is used to calculate the degree of proximity between each scheme and the ideal solution, that is, the comprehensive evaluation value Q_i.

$$Q_i = x\frac{\left(s^+ - s_{ij}\right)}{\left(s^+ - s_j^-\right)} + (1-x)\frac{\left(R^+ - R_{ij}\right)}{\left(R^+ - R_j^-\right)}. \tag{21}$$

Among them, when x is greater than 0.5, the group utility value has a greater impact on the outcome of the program. When x is less than 0.5, the personal regret value has a greater impact on the program results. When x is equal to 0.5, the group utility value and the individual regret value have an equal impact on the program outcome. For problems in real life, we generally set $x = 0.5$ to achieve a more reasonable purpose.

Step 4. According to the calculated three evaluation values S_t, R, and Q, the multiple attribute sequence of the alternatives is performed. At the same time, the most compromised solution is selected according to the following two conditions. When the two conditions are satisfied at the same time, the compromise solution that needs to be arranged according to the value of Q is the best solution. The smaller the Q, the better the solution [20].

Condition 1. The acceptable advantage is $Q(A^2) - Q(A^1) \ge (1/(m-1))A$.

Condition 2. Acceptable stability in the decision-making process is as follows: when sorted according to S and R, the stability requirement is met when A is still ranked first.

3.1. The Comprehensive Fuzzy Decision Matrix Is Calculated. We set $U_k\,(k = 1, 2, \ldots, l)$ as the kth expert, and the expert weight $\lambda_k\,(0 \le k \le 1)$ through the subjective weighting method satisfies $\sum_{k=1}^{1} \lambda_k = 1, \lambda_k \ge 0$. The attribute evaluation value is an interval intuitionistic fuzzy number. We set $A = \{A_i, A_2, \ldots, A_m\}$ as the scheme set and $C = \{C, c, \ldots, C\}$ as the attribute set. $D = \left\{D, D_2, \ldots, D_g\right\}$ (k represents k decision-makers or k time periods) represents a set of group decision matrices. Then, D_x (the k^{th} decision matrix in the group decision matrix) is the decision matrix about the solution set A on the attribute set c as follows:

$$D_k = \begin{bmatrix} \gamma_{11}^k & \gamma_{12}^k & \cdots & \gamma_{1n}^k \\ \gamma_{21}^k & \gamma_{22}^k & \cdots & \gamma_{2n}^k \\ \vdots & \vdots & \ddots & \vdots \\ \gamma_{m1}^k & \gamma_{m2}^k & \cdots & \gamma_{mn}^k \end{bmatrix}. \tag{22}$$

Among them, $\gamma_{ij}^k = ([\mu_{ij}^{kL}, \mu_{ij}^{kR}], [\nu_{ij}^{kL}, \nu_{ij}^{kR}])$ $(i = 1, 2, \ldots, m;\ j = 1, 2, \ldots, n)$ is the interval intuition fuzzy representation of the attribute C of the k^{th} decision-maker on scheme A.

The expert weight is used as a weighting factor; formula (22) is used to collect the evaluation value matrix of each attribute of each decision-making expert about the scheme; and the synthetic fuzzy decision matrix is obtained as follows:

$$D = \begin{bmatrix} \gamma_{11} & \gamma_{12} & \cdots & \gamma_{1n} \\ \gamma_{21} & \gamma_{22} & \cdots & \gamma_{2n} \\ \vdots & \vdots & \ddots & \vdots \\ \gamma_{m1} & \gamma_{m2} & \cdots & \gamma_{mn} \end{bmatrix}. \tag{23}$$

The positive- and negative-ideal schemes A^+ and A^- can be directly obtained from the comprehensive fuzzy decision matrix.

$$A^+ = \left(r_{ij}^+\right) = \max_{i=1} r_{ij} = \left(\left[\max_{i=1} \mu_{ij}^L, \max_{i=1} \mu_{ij}^R\right], \left[\max_{i=1} \nu_{ij}^L, \max_{i=1} \nu_{ij}^R\right]\right),$$
$$A^- = \left(r_{ij}^-\right) = \min_{i=1} r_{ij} = \left(\left[\min_{i=1} \mu_{ij}^L, \min_{i=1} \mu_{ij}^R\right], \left[\min_{i=1} \nu_{ij}^L, \min_{i=1} \nu_{ij}^R\right]\right). \tag{24}$$

The entropy weight method is objective, scientific, and accurate. Moreover, it does not require decision-makers to provide subjective evaluation information of weights and can directly use the collected data to obtain more objective attribute weights. Based on the analysis of interval intuitionistic fuzzy theory, this study chooses the entropy weight

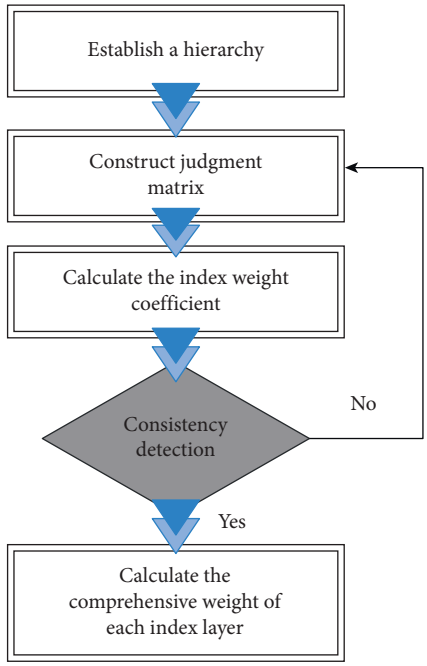

Figure 1: AHP calculation sequence.

method with strong objectivity to determine the attribute weight. It can eliminate the influence of subjectivity on weights to a certain extent, and make the analysis process objective and fair. The weight o of each attribute can be obtained as follows:

$$\omega_i = \frac{1 - e_i}{\sum_{p=1}^{n} (1 - e_p)}, \quad i = 1, 2, \ldots, m. \tag{25}$$

3.2. Proximity T_{ij} and Satisfaction φ_{ij} Are Calculated. To avoid that when the distance between the alternatives and the positive- and negative-ideal schemes is used to determine the pros and cons of the schemes, several alternatives and the positive-ideal scheme have the same distance value, making it impossible to sort case, and several alternatives and the positive-ideal scheme have the same distance value. Here, the following definitions of closeness and satisfaction are introduced according to the concepts related to the VIKOR method, and the distance formula of formula (6) is used to solve the following:

$$T_{ij} = \frac{d\left(r_{ij}^{-}, r_{ij}\right)}{\left(d\left(r_{ij}^{+}, r_{ij}\right) + d\left(r_{j}^{-}, r_{ij}\right)\right)}, \quad 1 \le i \le m. \tag{26}$$

Typically, T_i is between 0 and 1. The closeness of the decision experts to the evaluation value of the plan and the ideal point of the group evaluation is expanded into a group closeness matrix as follows:

$$T = \begin{bmatrix} T_{11} & T_{12} & \cdots & T_{1n} \\ T_{21} & T_{22} & \cdots & T_{2n} \\ \vdots & \vdots & \ddots & \vdots \\ T_{m1} & T_{m2} & \cdots & T_{mn} \end{bmatrix}. \tag{27}$$

According to the decision satisfaction function, the threshold for measuring the decision satisfaction is set for the transformation of the closeness matrix. The decision satisfaction function is defined as follows:

$$\varphi_{ij} = \begin{cases} 1, & T_i > 0.5, \\ 0, & \text{other}. \end{cases} \tag{28}$$

According to formula (28), the group closeness matrix T is converted into a 0-1 matrix, and the group satisfaction matrix p is obtained as follows:

$$\varphi_{ij} = \begin{bmatrix} \varphi_{11} & \varphi_{12} & \cdots & \varphi_{1n} \\ \varphi_{21} & \varphi_{22} & \cdots & \varphi_{2n} \\ \vdots & \vdots & \ddots & \vdots \\ \varphi_{m1} & \varphi_{m2} & \cdots & \varphi_{mn} \end{bmatrix}. \tag{29}$$

According to the group satisfaction matrix op, the ratio of the number of elements 1 in the matrix to the number of matrix elements is calculated, that is, the group satisfaction. The indicator GSI is as follows:

$$\mathrm{GSI} = \frac{1}{mn}\left(\sum_{i}^{m}\sum_{j}^{n}\varphi_{ij}\right). \tag{30}$$

When the decision-making group satisfaction index GSI meets the set group satisfaction threshold GSIO (GSI ≥ GSIO), the group decision-making activities can proceed.

3.3. Group Utility Value S and Individual Regret Value R_t Are Calculated. Interval intuitionistic fuzzy set Definition 4 is combined with formula (6), which can be transformed into the following:

$$\begin{aligned} S_i &= \sum_{j=1}^{n} \omega_j \frac{d\left(r_j^{+}, r_{ij}\right)}{d\left(r_j^{+}, r_j^{-}\right)}, \quad 1 \le i \le m, \\ R_i &= \max_j \omega_j \frac{d\left(r_j^{+}, r_{ij}\right)}{d\left(r_j^{+}, r_j^{-}\right)}, \quad 1 \le i \le m. \end{aligned} \tag{31}$$

3.4. The Comprehensive Evaluation Value Q_i Is Calculated.

$$Q_i = x\frac{\left(s_i - s^{-}\right)}{\left(s^{+}, s^{-}\right)} + (1 - x)\frac{d\left(R^{+} - R_{ij}\right)}{d\left(R^{+} - R_j^{-}\right)}, \tag{32}$$

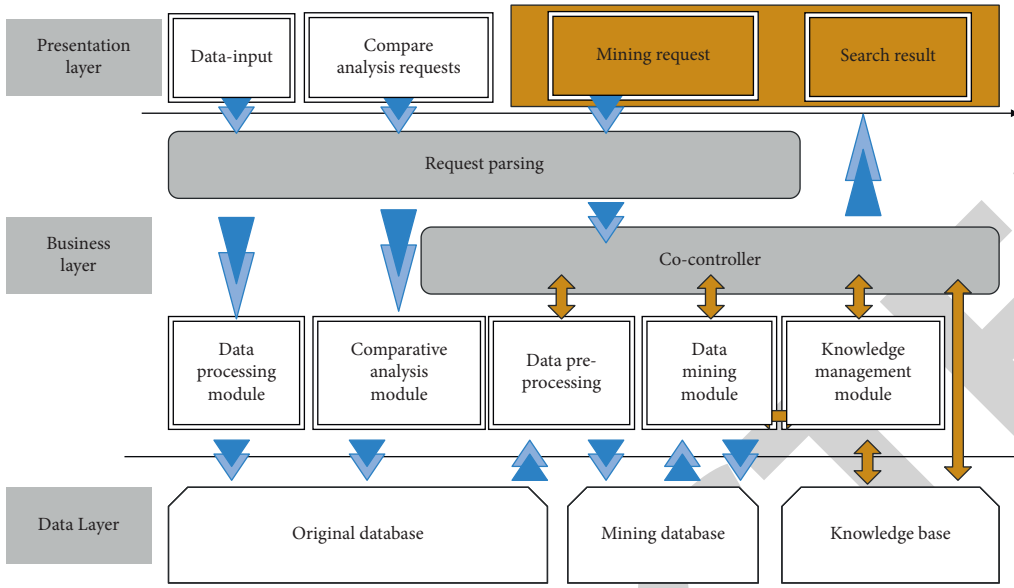

Figure 2: The three-layer structure of the international Chinese education expert system.

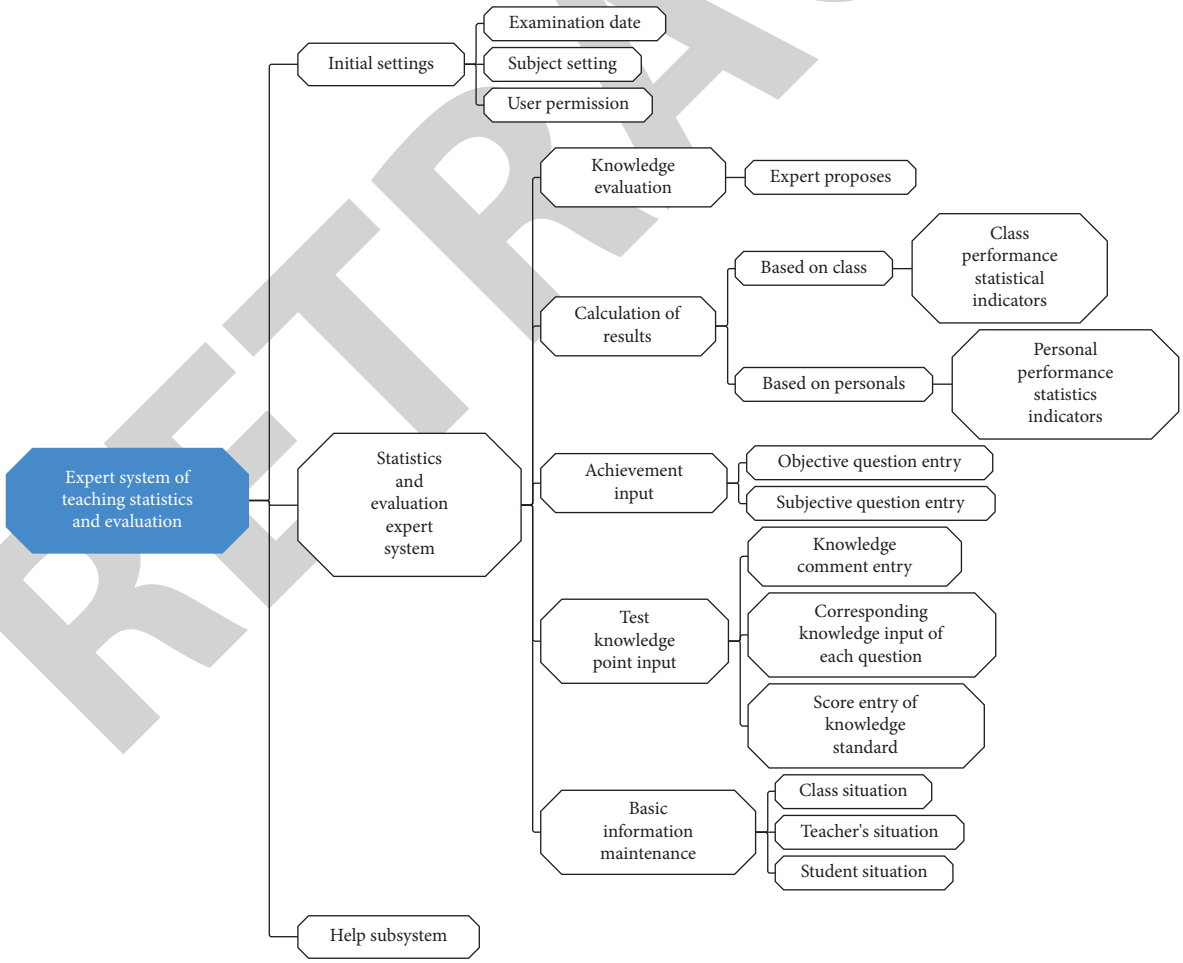

Figure 3: Exploded view of system function modules.

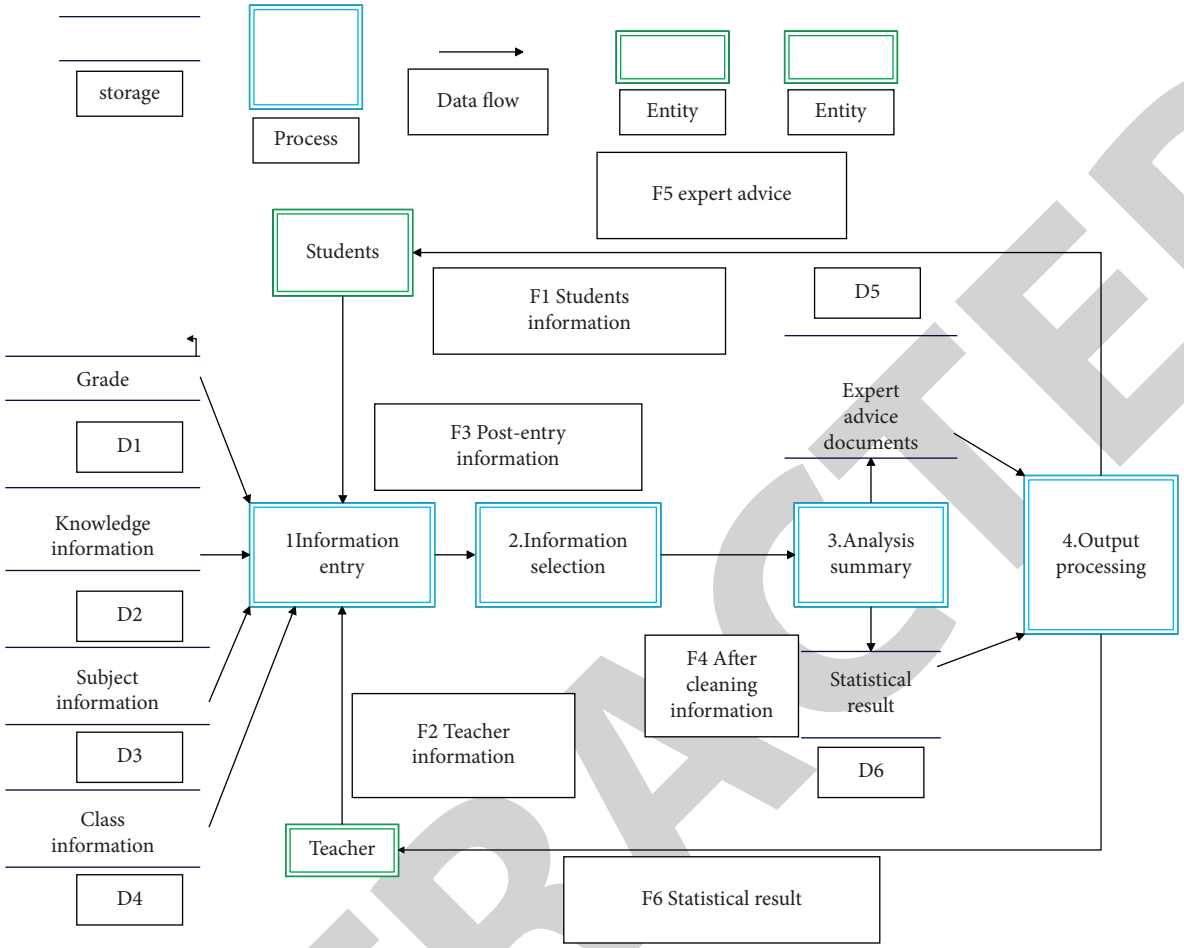

Figure 4: Top-level data-flow diagram.

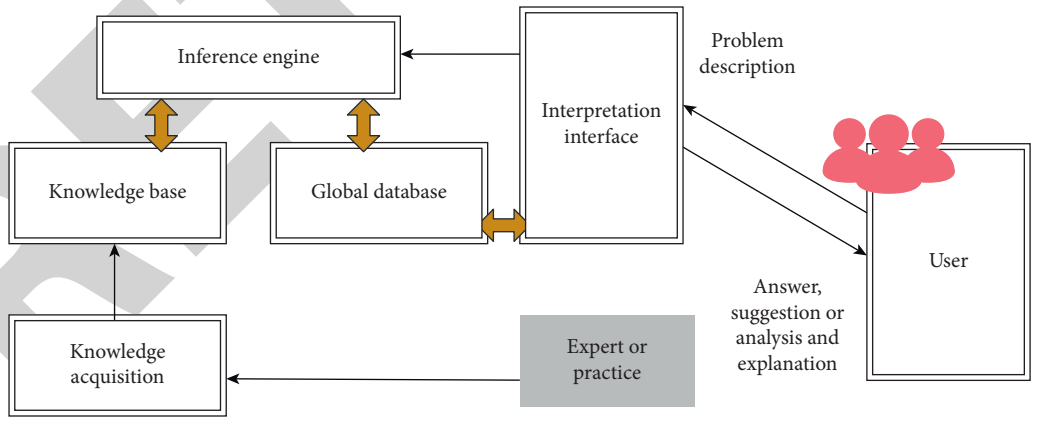

Figure 5: General structure of the international Chinese education expert system.

where x is a compromise coefficient, which reflects the subjective preference of decision-makers. When there is $x > 0.5$, it means that the decision-makers formulate strategies according to the opinions of the majority, that is, in a way that maximizes the group benefit. When there is $x < 0.5$, it means that it formulates a strategy based on the objection, that is, in a way that minimizes the weight of individual regrets. When there is $x = 0.5$, it means that both group

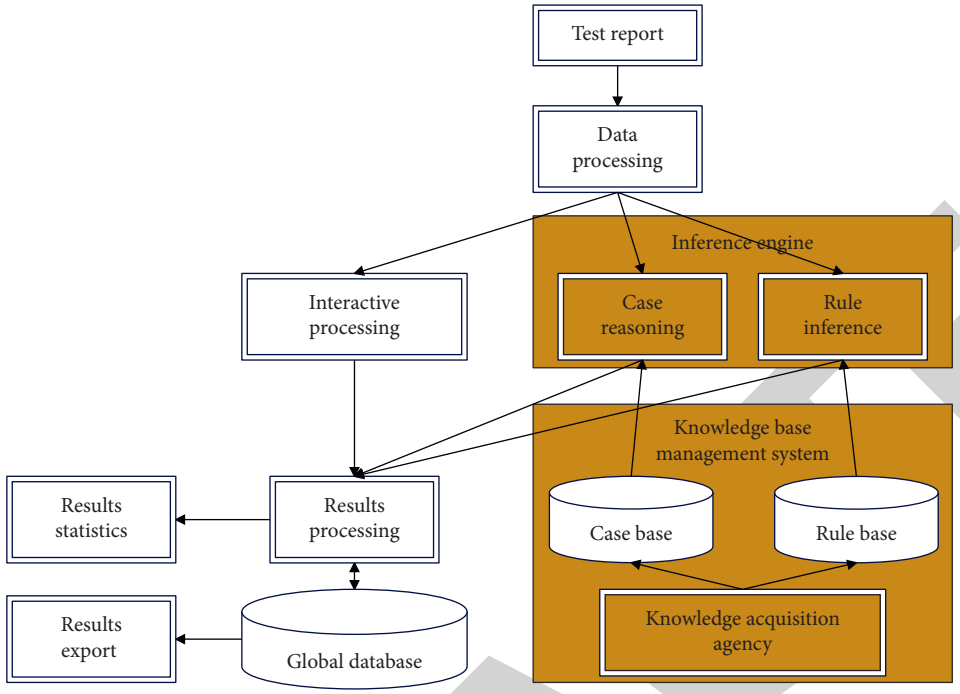

Figure 6: Overall model diagram of the international Chinese education expert system.

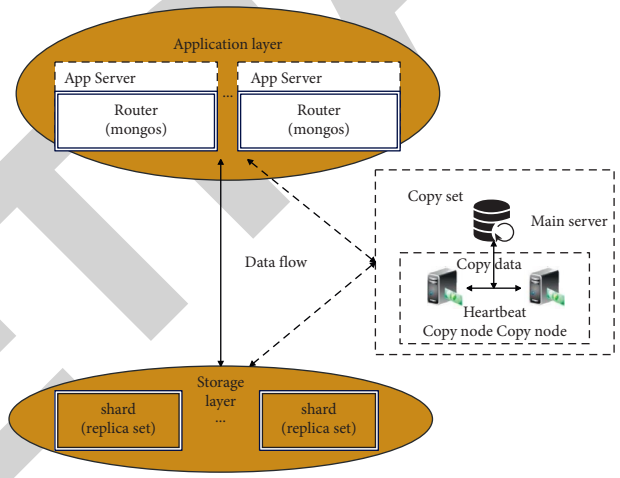

Figure 7: Cluster architecture diagram.

benefit and individual regret are considered, and strategies are formulated according to the equilibrium situation. Usually, $x = 0.5$ is taken.

4. International Chinese Education Expert System Based on Artificial Intelligence and Machine Learning Algorithms

The overall system architecture diagram is as shown in Figure 2.

On the basis of subsystem division, the corresponding subsystems are further decomposed into functional modules with clear meaning and single function, so as to obtain the functional module decomposition diagram of the system, as shown in Figure 3.

The data-flow analysis method is adopted to obtain the business process and the business and data connection from the description, and the analysis result is represented by a data-flow diagram (data-flow diagram, DFD), as shown in Figure 4.

The structure of the international Chinese education expert system includes a knowledge base, an inference engine, a comprehensive database, a human-machine interface, an interpreter, and a knowledge acquisition program, as shown in Figure 5.

On the basis of the core model design of the system, the overall model design of the system needs to be completed. In

Table 1: Chinese teaching effect of international Chinese education expert system based on artificial intelligence and machine learning algorithm.

Number	Teaching effect	Number	Teaching effect	Number	Teaching effect
1	81.16	25	87.75	49	84.67
2	85.39	26	77.03	50	83.19
3	79.26	27	88.30	51	81.50
4	78.36	28	82.83	52	89.37
5	80.12	29	85.04	53	84.87
6	81.66	30	79.97	54	83.43
7	82.68	31	86.90	55	85.77
8	88.11	32	83.16	56	88.60
9	81.71	33	85.09	57	83.69
10	78.72	34	79.07	58	89.69
11	77.70	35	84.17	59	87.35
12	82.05	36	80.61	60	81.87
13	87.69	37	88.90	61	82.02
14	89.33	38	83.75	62	83.27
15	77.32	39	88.04	63	85.77
16	77.59	40	86.15	64	89.67
17	82.65	41	84.09	65	85.25
18	89.10	42	88.11	66	87.56
19	81.77	43	84.38	67	86.31
20	88.58	44	87.31	68	84.94
21	77.19	45	81.65	69	79.72
22	84.03	46	79.36	70	79.80
23	83.21	47	87.14	71	82.29
24	86.65	48	89.74	72	85.03

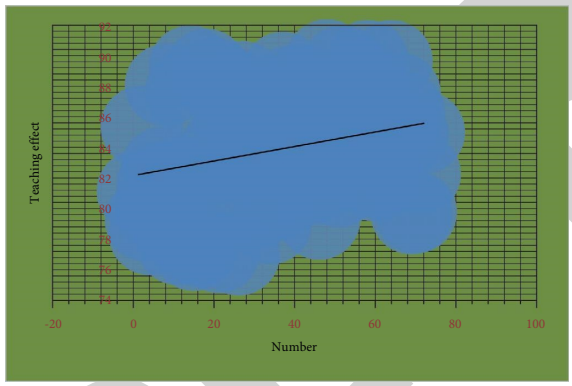

Figure 8: Chinese teaching clustering in the international Chinese education expert system based on artificial intelligence and machine learning algorithms.

addition to the design of the knowledge base and inference engine, the key modules included in the system are data processing, knowledge acquisition, comprehensive database management, and report import and export. Figure 6 is the overall model diagram of the system.

MongoDB has been extensively addressed in the structural design as a core data management tool for big data processing to assure data availability and consistency, parallel efficiency of data processing, and scalability of enormous data storage. The sharded cluster design following MongoDB 3.0 is seen in Figure 7. MongoDB created the replica set and sharded cluster functionalities to address the issues of big data volumes, high expansion, high performance, high availability, and a flexible data model. The replica set selects the master server using the bully method, ensuring the cluster's high availability. The main server stores metadata information, and the application layer interacts with the main server to obtain the storage address of the slice server where the data actually exist and then interacts with the slice storage layer to access data. In order to ensure high performance under large concurrency, the primary and secondary nodes of the replica set adopt a read-write separation strategy. Slice storage is to divide and expand collections horizontally, and perform distributed storage according to the data copy strategy. Moreover, MongoDB supports big data basic storage platforms such as HDFS and S3.

On the basis of the above research, the effect of the international Chinese education expert system based on artificial intelligence and machine learning algorithm is verified; the Chinese teaching effect is calculated; and the results shown in Table 1 and Figure 8 are obtained.

It can be seen from the above research that the international Chinese education expert system based on artificial intelligence and machine learning algorithm proposed in this study has a very good effect.

5. Conclusions

There are also some drawbacks in the online Chinese learning space, which adversely affect the effect of independent Chinese learning and Chinese learning experience. Online Chinese learning space resources have a large capacity and various forms. Because Chinese students must explore, evaluate, and compare many materials, they set higher standards for Chinese learning capacity and media

Hindawi
Journal of Mathematics
Volume 2022, Article ID 9073944, 7 pages
https://doi.org/10.1155/2022/9073944

Research Article

The Role of Soft θ-Topological Operators in Characterizing Various Soft Separation Axioms

Zanyar A. Ameen,[1] **Tareq M. Al-shami**,[2] **Abdelwaheb Mhemdi**,[3] **and Mohammed E. El-Shafei**[4]

[1]*Department of Mathematics, College of Science, University of Duhok, Duhok 42001, Iraq*
[2]*Department of Mathematics, Sana'a University, Sana'a, Yemen*
[3]*Department of Mathematics, College of Sciences and Humanities in Aflaj, Prince Sattam Bin Abdulaziz University, Riyadh, Saudi Arabia*
[4]*Department of Mathematics, Faculty of Science, Mansoura University, Mansoura, Egypt*

Correspondence should be addressed to Tareq M. Al-shami; tareqalshami83@gmail.com

Received 5 May 2022; Accepted 3 June 2022; Published 7 July 2022

Academic Editor: Naeem Jan

This manuscript begins with an introduction to a soft θ-kernel operator. Then, the main properties and connections of this soft topological operator with other known soft topological operators are examined. We show that soft θ-kernel operator is weaker than soft kernel operator but stronger than soft θ-closure. Both soft θ-closure and soft θ-kernel operators are equivalent on soft compact sets. Furthermore, the stated operators are utilized to obtain several new characterizations of soft R_i-topologies and soft T_j-topologies, for $i = 0, 1$ and $j = 0, 1, 2$.

1. Introduction

The majority of real-world problems in engineering, medicine, economics, the environment, and other professions are fraught with uncertainty. Molodtsov [1] presented the soft set theory in 1999 as a mathematical model for reducing uncertainty. This is freed of the drawbacks of prior theories such as fuzzy set theory [2], rough set theory [3], and so on. The nature of parameter sets, particularly those connected to soft sets, provides a consistent foundation for modeling uncertain data. This leads to the rapid growth of soft set theory in a short amount of time, as well as a wide range of real-world applications of soft sets.

Influenced by the standard postulates of ordinary topological space, Shabir and Naz [4], and Çağman et al. [5], separately, established another branch of topology known as "soft topology," which is a mixture of soft set theory and topology. It focuses on the development of the system of all soft sets. The study in [4, 5], in particular, was essential in building the subject of soft topology. Following these works, researchers have been discussed the topological concepts via soft topological spaces such as soft bases [6] and soft compactness [7]. In [8], the authors applied some soft operators to generate soft topologies.

The separation axioms are simply axioms in the sense that these criteria could be added as additional hypotheses to the definition of topological space to create a more restricted description of what a topological space is. These axioms have a great role in developing (classical) topology. Correspondingly, soft separation axioms are a significant aspect in the late development of soft topology; see for example [9, 10] for soft T_j-separation axioms and [11] for soft R_i-separation axioms. Despite the fact that intensive studies have been conducted on these axioms, however, significant contributions can indeed be made. Hence, we characterize both soft T_j and soft T_i-separation axioms in terms of the discussed soft topological operators. It should be noted that some amendments for a number of properties of separation axioms in soft settings were given in [12, 13].

The following is how the paper's body is organized: we provide an overview of the literature on soft set theory and soft topology in Section 2. The essential points of a soft θ-kernel operator and its link to the associated soft topological operators are discussed in Section 3. Sections 4 and 5 use soft operators provided in Section 3 to characterize soft R_i and soft T_j topologies for $i = 0, 1$ and $j = 0, 1, 2$, respectively. A brief summary and conclusions conclude Section 6 of our paper.

2. Preliminaries

Let X be a domain set, 2^X be the set of all subsets of X, and E be a set of parameters. A pair $(F, E) = \{(e, F(e)): e \in E\}$ is said to be a soft set over X, where F: $E \longrightarrow 2^X$ is a set-valued mapping. The set of all soft sets over X parameterized by E is identified by $S_E(X)$. We call a soft set (F, E) over X a soft point [14, 15], denoted by x_e, if $F(e) = \{x\}$ and $F(e') = \varnothing$ for every $e' \in E$ with $e' \neq e$, where $e \in E$ and $x \in X$. An argument $x_e \in (F, E)$ means that $x \in F(e)$. The set of all soft points over X is denoted by $P_E(X)$. A soft set $(X, E) - (F, E)$ (or simply $(F, E)^c$) is the complement of (F, E), where F^c: $E \longrightarrow 2^X$ is given by $F^c(e) = X - F(e)$ for every $e \in E$. If $(F, E) \in S_E(X)$, it is denoted by Φ if $F(e) = \varnothing$ for every $e \in E$ and is denoted by $\widetilde{X}$ if $F(e) = X$ for every $e \in E$. Evidently, $\widetilde{X}^c = \Phi$ and $\Phi^c = \widetilde{X}$. A soft set (F, E) is called degenerate if $(F, E) = \{x_e\}$ or $(F, E) = \Phi$. It is said that (A, E_1) is a soft subset of (B, E_2) (written by $(A, E_1)\widetilde{\subseteq}(B, E_2)$, [16]) if $E_1 \subseteq E_2$ and $A(e) \subseteq B(e)$ for every $e \in E_1$, and $(A, E_1) = (B, E_2)$ if $(A, E_1)\widetilde{\subseteq}(B, E_2)$ and $(B, E_2)\widetilde{\subseteq}(A, E_1)$. The union of soft sets $(A, E), (B, E)$ is represented by $(F, E) = (A, E)\widetilde{\cup}(B, E)$, where $F(e) = A(e) \cup B(e)$ for every $e \in E$, and intersection of soft sets $(A, E), (B, E)$ is given by $(F, E) = (A, E)\widetilde{\cap}(B, E)$, where $F(e) = A(e) \cap B(e)$ for every $e \in E$ (see, [17]).

Definition 1 (see [4, 5]). A collection $\mathcal{T}$ of $S_E(X)$ is said to be a soft topology on X if it satisfies the following axioms:

(T.1) $\Phi, \widetilde{X} \in \mathcal{T}$.

(T.2) If $(F_1, E), (F_2, E) \in \mathcal{T}$, then $(F_1, E)\widetilde{\cap}(F_2, E) \in \mathcal{T}$.

(T.3) If $\{(F_i, E): i \in I\}\widetilde{\subseteq}\mathcal{T}$, then $\widetilde{\cup}_{i\in I}(F_i, E) \in \mathcal{T}$.

Terminologically, we call $(X, \mathcal{T}, E)$ a soft topological space on X. The elements of $\mathcal{T}$ are called soft open sets. The complements of every soft open or elements of $\mathcal{T}^c$ are called soft closed sets. The lattice of all soft topologies on X is referred to $T_E(X)$ (see, [18]).

Definition 2 (see [4, 19]). Let $(B, E) \in S_E(X)$ and $\mathcal{T} \in T_E(X)$.

(1) The soft closure of (B, E) is $cl(B, E)$: $= \widetilde{\cap}\{(F, E): (B, E)\widetilde{\subseteq}(F, E), (F, E) \in \mathcal{T}^c\}$.

(2) The soft interior of (B, E) is $\text{int}(B, E)$: $= \widetilde{\cup}\{(F, E): (F, E)\widetilde{\subseteq}(B, E), (F, E) \in \mathcal{T}\}$.

(3) The soft kernel of (B, E) is $\ker(B, E)$: $= \widetilde{\cap}\{(G, E): (B, E)\widetilde{\subseteq}(G, E), (G, E) \in \mathcal{T}\}$.

Definition 3. [5] Let $(B, E) \in S_E(X)$ and $\mathcal{T} \in T_E(X)$. A point $x_e \in P_E(X)$ is called a soft limit point of (B, E) if $(G, E)\widetilde{\cap}(B, E) - \{x_e\} \neq \Phi$ for all $(G, E) \in \mathcal{T}$ with $x_e \in (G, E)$. The set of all soft limit points is symbolized by $\text{der}(B, E)$. Then, $\text{cl}(F, E) = (F, E)\widetilde{\cup}\text{der}(F, E)$ (see, Theorem 5 in [5])

Definition 4 (see [20]). Let $\mathcal{T} \in T_E(X)$. A set $(A, E) \in S_E(X)$ is called soft locally closed if there exist $(G, E) \in \mathcal{T}$ and $(F, E) \in \mathcal{T}^c$ such that $(A, E) = (G, E)\widetilde{\cap}(F, E)$. The family of all soft locally closed sets over X is referred to $LC(X)$.

Definition 5. [21] Let $\mathcal{T} \in T_E(X)$. A set $(A, E) \in S_E(X)$ is called soft θ-open if for every $x_e \in (A, E)$, there exists $(G, E) \in \mathcal{T}$ such that $x_e \in (G, E)\widetilde{\subseteq}\text{cl}(G, E)\widetilde{\subseteq}(A, E)$. The set of all soft θ-open sets forms a soft topology on X and denoted by $\mathcal{T}_\theta$. The complement of soft θ-open sets are soft θ-closed and their family is denoted by $\mathcal{T}_\theta^c$.

Remark 1. One can easily check that $\mathcal{T}_\theta\widetilde{\subseteq}\mathcal{T}$.

Definition 6 (see [21]). Let $(B, E) \in S_E(X)$ and $\mathcal{T} \in T_E(X)$.

(1) The soft θ-interior of (B, E) is $\text{int}_\theta(B, E)$: $= \widetilde{\cup}\{(F, E): (F, E)\widetilde{\subseteq}(B, E), (F, E) \in \mathcal{T}_\theta\}$.

(2) The soft θ-closure of (B, E) is $\text{cl}_\theta(B, E)$: $= \widetilde{\cap}\{(F, E): (B, E)\widetilde{\subseteq}(F, E), (F, E) \in \mathcal{T}_\theta^c\}$.

Lemma 1 (see [19, 21]). *Let $(B, E) \in S_E(X)$ and $\mathcal{T} \in T_E(X)$. Then,*

(1) $(B, E) \in \mathcal{T}_\theta^c$ whenever $cl_\theta(B, E) = (B, E)$.

(2) $cl(B, E)\widetilde{\subseteq}cl_\theta(B, E)$.

(3) $cl_\theta(B, E) \in \mathcal{T}^c$.

(4) $cl(B, E) = cl_\theta(B, E)$ whenever $(B, E) \in \mathcal{T}$.

(5) $ker(B, E) = \{x_e \in P_E(X): cl(\{x_e\})\widetilde{\cap}(B, E) \neq \Phi\}$

Definition 7 (see [19]). For $x_e \in P_E(X)$ and $\mathcal{T} \in T_E(X)$, we define

(1) the soft derived set of x_e as $\text{der}(\{x_e\})$: $= \text{cl}(\{x_e\}) - \{x_e\}$.

(2) the soft shell of x_e as $\text{shel}(\{x_e\})$: $= \ker(\{x_e\}) - \{x_e\}$.

(3) the soft set $\langle x_e\rangle$: $= \text{cl}(\{x_e\})\widetilde{\cap}\ker(\{x_e\})$.

Lemma 2 (see [19]). *The following properties are valid for every $x_e, y_{e'} \in P_E(X)$ and $\mathcal{T} \in T_E(X)$:*

(1) $y_{e'} \in ker(\{x_e\}) \Leftrightarrow x_e \in cl(\{y_{e'}\})$.

(2) $y_{e'} \in shel(\{x_e\}) \Leftrightarrow x_e \in der(\{y_{e'}\})$.

(3) $y_{e'} \in cl(\{x_e\}) \Rightarrow cl(\{y_{e'}\})\widetilde{\subseteq}cl(\{x_e\})$.

(4) $y_{e'} \in ker(\{x_e\}) \Rightarrow ker(\{y_{e'}\})\widetilde{\subseteq}ker(\{x_e\})$.

(5) $shel(\{x_e\})$ is degenerate iff for every $y_{e'} \in P_E(X)$ with $y_{e'} \neq x_e$, $der(\{x_e\})\widetilde{\cap}der(\{y_{e'}\}) = \Phi$.

(6) $der(\{x_e\})$ is degenerate iff for every $y_{e'} \in P_E(X)$ with $y_{e'} \neq x_e$, $shel(\{x_e\})\widetilde{\cap}shel(\{y_{e'}\}) = \Phi$.

(7) If $y_{e'} \in \langle x_e \rangle$, then $\langle y_{e'} \rangle = \langle x_e \rangle$.

(8) Either $\langle y_{e'} \rangle = \langle x_e \rangle$ or $\langle y_{e'} \rangle \widetilde{\cap} \langle x_e \rangle = \Phi$.

Definition 8 (see [11, 22]). A soft space $(X, E, \mathcal{T})$ (or simply soft topology $\mathcal{T} \in T_E(X)$) is called

(1) soft T_0 if for every $x_e, y_{e'} \in P_E(X)$ with $x_e \neq y_{e'}$, there exist $(U, E), (V, E) \in \mathcal{T}$ such that $x_e \in (U, E)$, $y_{e'} \notin (U, E)$ or $y_{e'} \in (V, E)$, $x_e \notin (V, E)$.

(2) soft T_1 if for every $x_e, y_{e'} \in P_E(X)$ with $x_e \neq y_{e'}$, there exist $(U, E), (V, E) \in \mathcal{T}$ such that $x_e \in (U, E)$, $y_{e'} \notin (U, E)$ and $y_{e'} \in (V, E)$, $x_e \notin (V, E)$.

(3) soft T_2 if for every $x_e, y_{e'} \in P_E(X)$ with $x_e \neq y_{e'}$, there exist $(U, E), (V, E) \in \mathcal{T}$ such that $x_e \in (U, E)$, $y_{e'} \in (V, E)$, and $(U, E) \widetilde{\cap} (V, E) = \Phi$.

(4) soft R_0 if for every $x_e \in P_E(X)$ and every $(U, E) \in \mathcal{T}$ with $x_e \in (U, E)$, we have $\mathrm{cl}(\{x_e\}) \widetilde{\subseteq} (U, E)$.

(5) soft R_1 if for every $x_e, y_{e'} \in P_E(X)$ with $\mathrm{cl}(\{x_e\}) \neq \mathrm{cl}(\{y_{e'}\})$, there exist $(U, E), (V, E) \in \mathcal{T}$ such that $\mathrm{cl}(\{x_e\}) \in (U, E)$, $\mathrm{cl}(\{y_{e'}\}) \in (V, E)$ and $(U, E) \widetilde{\cap} (V, E) = \Phi$.

Lemma 3 (see [22], Theorem 4.1). *Let $\mathcal{T} \in T_E(X)$. Then, $\mathcal{T}$ is soft T_1 iff $cl(\{x_e\}) = \{x_e\}$ for every $x_e \in P_E(X)$.*

Theorem 1 (see [11], Theorem 3.5). *Let $\mathcal{T} \in T_E(X)$. The following properties are equivalent:*

(1) *$\mathcal{T}$ is soft R_0.*

(2) *Either $cl(\{x_e\}) = cl(\{y_{e'}\})$ or $cl(\{x_e\}) \widetilde{\cap} cl(\{y_{e'}\}) = \Phi$ for every $x_e, y_{e'} \in P_E(X)$ with $x_e \neq y_{e'}$.*

(3) *For every $x_e \in P_E(X)$ and every $(F, E) \in \mathcal{T}^c$ with $x_e \notin (F, E)$, $cl(\{x_e\}) \widetilde{\cap} (F, E) = \Phi$.*

(4) *For every $x_e \in P_E(X)$ and every $(F, E) \in \mathcal{T}^c$ with $x_e \notin (F, E)$, there is $(G, E) \in \mathcal{T}$ such that $(F, E) \widetilde{\subseteq} (G, E)$ and $x_e \notin (G, E)$.*

Theorem 2 (see [11], Theorem 3.13). *Let $\mathcal{T} \in T_E(X)$. The following properties are equivalent:*

(1) *$\mathcal{T}$ is soft R_0.*

(2) *If $(F, E) \in \mathcal{T}^c$, then $ker(F, E) = (F, E)$.*

(3) *If $x_e \in (F, E) \in \mathcal{T}^c$, then $ker(\{x_e\}) \widetilde{\subseteq} (F, E)$.*

(4) *$ker(\{x_e\}) \widetilde{\subseteq} cl(\{y_{e'}\})$ for every $x_e \in P_E(X)$.*

Lemma 4 (see [11], Proposition 3.18). *Let $\mathcal{T} \in T_E(X)$. Then, $\mathcal{T}$ is soft T_1 iff it soft T_0 and soft R_0.*

3. Some Soft Topological Operators

In this section, we define "soft θ-kernel" and "soft θ-derived set" as soft topological operators. Then, the connections between soft θ-kernel, soft kernel, soft closure, soft θ-derived set, and soft derived set operators are obtained. The results of the present part will be used to characterize several soft separation axioms.

Definition 9. Let $(F, E) \in S_E(X)$ and let $\mathcal{T} \in T_E(X)$. The soft θ-kernel of (F, E) is defined by

$$\ker_\theta(F, E) := \widetilde{\cap}\{(G, E) : (G, E) \in \mathcal{T}_\theta, (F, E) \widetilde{\subseteq} (G, E)\}. \quad (1)$$

Definition 10. For $x_e \in P_E(X)$ and $\mathcal{T} \in T_E(X)$, we define the soft θ-derived set of x_e as $\mathrm{der}_\theta(\{x_e\}) := \mathrm{cl}_\theta(\{x_e\}) - \{x_e\}$.

Lemma 5. *Let $(F, E), (G, E) \in S_E(X)$ and $\mathcal{T} \in T_E(X)$. The following properties are valid:*

(1) *$(F, E) \widetilde{\subseteq} ker_\theta(F, E)$.*

(2) *$ker_\theta(F, E) \widetilde{\subseteq} ker_\theta(ker_\theta(F, E))$.*

(3) *$(F, E) \widetilde{\subseteq} (G, E) \Rightarrow ker_\theta(F, E) \widetilde{\subseteq} ker_\theta(G, E)$.*

(4) *$ker_\theta[(F, E) \widetilde{\cap} (G, E)] \widetilde{\subseteq} ker_\theta(F, E) \widetilde{\cap} ker_\theta(G, E)$.*

(5) *$ker_\theta[(F, E) \widetilde{\cup} (G, E)] = ker_\theta(F, E) \widetilde{\cup} ker_\theta(G, E)$.*

Proof. Standard.

Recall that a soft space $(X, \mathcal{T}, E)$ is called soft compact [23] if every soft open cover of $\tilde{X}$ possesses a finite subcover. □

Lemma 6. *The following properties are valid for every $(F, E) \in P_E(X)$ and $\mathcal{T} \in T_E(X)$:*

(1) *$ker_\theta(F, E) = \{x_e \in P_E(X) : cl_\theta(\{x_e\}) \widetilde{\cap} (F, E) \neq \Phi\}$.*

(2) *$ker(F, E) \widetilde{\subseteq} ker_\theta(F, E) \widetilde{\subseteq} cl_\theta(F, E)$.*

(3) *If (F, E) is soft compact, then $cl_\theta(F, E) = ker_\theta(F, E)$.*

Proof

(1) Let $x_e \in \ker_\theta(F, E)$. If $\mathrm{cl}_\theta(\{x_e\}) \widetilde{\cap} (F, E) = \Phi$, then one can find $(G, E) \in \mathcal{T}_\theta$ such that it contains (F, E) but not x_e, a contradiction.

Conversely, if $x_e \notin \ker_\theta(F, E)$ but $\mathrm{cl}_\theta(\{x_e\}) \widetilde{\cap} (F, E) \neq \Phi$, then there is $(G, E) \in \mathcal{T}_\theta$ such that $(F, E) \widetilde{\subseteq} (G, E)$ but $x_e \notin (G, E)$ and $y_{e'} \in \mathrm{cl}_\theta(\{x_e\}) \widetilde{\cap} (F, E)$. Therefore, $\tilde{X} - (G, E) \in \mathcal{T}_\theta^c$ including x_e but not $y_{e'}$. However, this contradicts to $y_{e'} \in \mathrm{cl}_\theta(\{x_e\}) \widetilde{\cap} (F, E)$. Thus, $x_e \in \ker_\theta(F, E)$.

(2) It follows from the fact that $\mathcal{T}_\theta \widetilde{\subseteq} \mathcal{T}$ and $\mathrm{cl}_\theta(F, E) = \{x_e \in P_E(X) : \mathrm{cl}(G, E) \widetilde{\cap} (F, E) \neq \Phi, (G, E) \in \mathcal{T}, x_e \in (G, E)\}$. That is, $\mathrm{cl}_\theta(F, E)$ can be seen as the intersection of the soft closure of every soft open set (G, E) that includes (F, E). Equivalently, it is a soft closed set including $\ker(F, E)$.

(3) From (2), it suffices to prove that $\mathrm{cl}_\theta(F, E) \widetilde{\subseteq} \ker_\theta(F, E)$. Suppose (F, E) is a soft compact set. If $x_e \notin \ker_\theta(F, E)$, then $\mathrm{cl}_\theta(\{x_e\}) \widetilde{\cap} (F, E) = \Phi$. Therefore, there exist $(G_{y_{e'}}, E)$, $(H_{y_{e'}}, E) \in \mathcal{T}$ such that $x_e \in (G_{y_{e'}}, E)$, $y_{e'} \in (H_{y_{e'}}, E)$, and $(G_{y_{e'}}, E) \widetilde{\cap} (H_{y_{e'}}, E) = \Phi$ for every $y_{e'} \in (F, E)$. Thus, $\mathcal{H} = \{(H_{y_{e'}}, E) : y_{e'} \in (F, E)\}$

forms a soft open cover of (F,E). Then, there is a finite subclass $\{y_{e'}^1, y_{e'}^2, \ldots, y_{e'}^n\}$ of $\mathscr{H}$ such that $(F,E)\widetilde{\subseteq}\widetilde{\cup}_{i=1}^{n}(H_{y^i},E)$. Set $(A,E)=\widetilde{\cap}_{i=1}^{n}(G_{y^i},E)$ and $(B,E)=\widetilde{\cup}_{i=1}^{n}(H_{y^i},E)$. Therefore, (A,E), $(B,E)\in\mathscr{T}$ such that $x_e\widetilde{\in}(A,E)$, $(F,E)\widetilde{\subseteq}(B,E)$, and $(A,E)\widetilde{\cap}(B,E)=\Phi$. This means that $x_e\notin \mathrm{cl}_\theta(F,E)$. We are done. □

Lemma 7. *The following properties are valid for every $x_e, y_{e'}\in P_E(X)$ and $\mathscr{T}\in T_E(X)$:*

(1) $\langle x_e\rangle=\langle y_{e'}\rangle\Leftrightarrow\ker(\{x_e\})=\ker(\{y_{e'}\})\Leftrightarrow cl(\{x_e\})=cl(\{y_{e'}\})$.

(2) $x_e\in cl_\theta(\{y_{e'}\})\Leftrightarrow y_{e'}\in cl_\theta(\{x_e\})$.

(3) $\ker_\theta(\{x_e\})=cl_\theta(\{x_e\})$.

(4) $cl(\langle x_e\rangle)=cl(\{x_e\})$.

(5) $cl_\theta(\langle x_e\rangle)=cl_\theta(\{x_e\})$.

(6) $ker(\langle x_e\rangle)=ker(\{x_e\})$.

(7) If $(F,E)\in\mathscr{T}\widetilde{\cup}\mathscr{T}^c$ *and* $x_e\in(F,E)$, *then* $\langle x_e\rangle\widetilde{\subseteq}(F,E)$.

Proof

(1) It is enough to show that $\ker(\{x_e\})=\ker(\{y_{e'}\})\Leftrightarrow\mathrm{cl}(\{x_e\})=\mathrm{cl}(\{y_{e'}\})$. If $\ker(\{x_e\})\neq\ker(\{y_{e'}\})$, then one can find $z_{e^*}\in\ker(\{x_e\})$ but $z_{e^*}\notin\ker(\{y_{e'}\})$. From $z_{e^*}\in\ker(\{x_e\})$, we get $x_e\in\mathrm{cl}(\{z_{e^*}\})$ and then $\mathrm{cl}(\{x_e\})\widetilde{\subseteq}\mathrm{cl}(\{z_{e^*}\})$. Since $z_{e^*}\notin\ker(\{y_{e'}\})$, by Lemma 2. (1), $\mathrm{cl}(\{z_{e^*}\})\widetilde{\cap}y_{e'}=\Phi$. Therefore, $\mathrm{cl}(\{z_{e^*}\})\widetilde{\cap}y_{e'}=\Phi$ implies $y_{e'}\notin\mathrm{cl}(\{x_e\})$. Hence, $\mathrm{cl}(\{y_{e'}\})\neq\mathrm{cl}(\{x_e\})$.

(2) If $x_e\notin\mathrm{cl}_\theta(\{y_{e'}\})$, then there are (G,E), $(H,E)\in\mathscr{T}$, respectively, containing x_e, $y_{e'}$ such that $(G,E)\widetilde{\cap}(H,E)=\Phi$. This implies that $y_{e'}\notin\mathrm{cl}_\theta(\{x_e\})$.

(3) It follows from Lemma 6 (3) as every $\{x_e\}$ is soft compact.

(4) Since $x_e\in\langle x_e\rangle$, so $\mathrm{cl}(\langle x_e\rangle)\widetilde{\subseteq}\mathrm{cl}(\{x_e\})$. On the other hand, $\mathrm{cl}(\langle x_e\rangle)=\mathrm{cl}(\mathrm{cl}(\{x_e\}))\ \widetilde{\cap}\,\mathrm{cl}(\ker(\{x_e\}))\widetilde{\subseteq}\mathrm{cl}(\{x_e\})$. Hence, $\mathrm{cl}(\langle x_e\rangle)=\mathrm{cl}(\{x_e\})$.

Other parts are similar or simple. □

4. Characterizations of Soft R_i-Spaces, $i\in\{0,1\}$

In this part, we obtain some characterizations of soft R_0 and soft R_1-spaces via certain soft topological operators.

Theorem 3. *Let $\mathscr{T}\in T_E(X)$. Then, $\mathscr{T}$ is soft R_0 iff $cl_\theta(\{x_e\})-cl(\{x_e\})$ is a union of soft closed sets for every $x_e\in P_E(X)$.*

Proof. Given $x_e\in P_E(X)$. W.l.o.g, we let $\mathrm{cl}_\theta(\{x_e\})-\mathrm{cl}(\{x_e\})\neq\Phi$, otherwise, the conclusion is trivially true. Suppose $y_{e'}\in\mathrm{cl}_\theta(\{x_e\})-\mathrm{cl}(\{x_e\})$. Then, $\mathrm{cl}(\{y_{e'}\})\widetilde{\subseteq}\mathrm{cl}_\theta(\{x_e\})$. Since $\mathscr{T}$ is soft R_0, by Theorem 1, $\mathrm{cl}(\{y_{e'}\})\widetilde{\cap}\mathrm{cl}(\{x_e\})=\Phi$. Thus, $\mathrm{cl}(\{y_{e'}\})\widetilde{\subseteq}\mathrm{cl}_\theta(\{x_e\})-\mathrm{cl}(\{x_e\})$ and so $\mathrm{cl}_\theta(\{x_e\})-\mathrm{cl}(\{x_e\})$ is a union of soft closed sets.

Conversely, let $x_e, y_{e'}\in P_E(X)$. Suppose $\mathrm{cl}_\theta(\{x_e\})-\mathrm{cl}(\{x_e\})=\widetilde{\cup}\{(F,E)\colon (F,E)\in\mathscr{T}^c\}$. In order to prove that $\mathscr{T}$ is soft R_0, we study the following cases:

(i) Assume $y_{e'}\in\mathrm{cl}_\theta(\{x_e\})-\mathrm{cl}(\{x_e\})$. Then, there is $(F,E)\in\mathscr{T}^c$ such that $(F,E)\widetilde{\subseteq}\mathrm{cl}_\theta(\{x_e\})-\mathrm{cl}(\{x_e\})$ and $y_{e'}\in(F,E)$. Therefore, $\mathrm{cl}(\{y_{e'}\})\widetilde{\subseteq}(F,E)$. This implies that $\mathrm{cl}(\{y_{e'}\})\widetilde{\cap}\mathrm{cl}(\{x_e\})=\Phi$.

(ii) Assume $y_{e'}\in\mathrm{cl}(\{x_e\})$. Clearly, $y_{e'}\in\mathrm{cl}_\theta(\{x_e\})$ and $x_e\in\mathrm{cl}_\theta(\{y_{e'}\})$. If $x_e\notin\mathrm{cl}(\{y_{e'}\})$, then $x_e\in\mathrm{cl}_\theta(\{y_{e'}\})-\mathrm{cl}(\{y_{e'}\})$. By (i), $\mathrm{cl}(\{y_{e'}\})\widetilde{\cap}\mathrm{cl}(\{x_e\})=\Phi$, which is a contradiction. Therefore, we must have $x_e\in\mathrm{cl}(\{y_{e'}\})$ and so $\mathrm{cl}(\{x_e\})=\mathrm{cl}(\{y_{e'}\})$.

(iii) Assume $y_{e'}\notin\mathrm{cl}_\theta(\{x_e\})$. Suppose if possible $\mathrm{cl}(\{x_e\})\widetilde{\cap}\mathrm{cl}(\{y_{e'}\})\neq\Phi$, then there is $z_{e^*}\in\mathrm{cl}(\{x_e\})$ and $z_{e^*}\in\mathrm{cl}(\{y_{e'}\})$. By (ii), $\mathrm{cl}(\{x_e\})=\mathrm{cl}(\{y_{e'}\})=\mathrm{cl}(\{z_{e^*}\})$. Therefore, $y_{e'}\in\mathrm{cl}(\{x_e\})$, a contradiction. Hence, $\mathrm{cl}(\{x_e\})\widetilde{\cap}\mathrm{cl}(\{y_{e'}\})=\Phi$.

In conclusion, we have shown that for every $x_e, y_{e'}\in P_E(X)$, either $\mathrm{cl}(\{x_e\})=\mathrm{cl}(\{y_{e'}\})$ or $\mathrm{cl}(\{x_e\})\widetilde{\cap}\mathrm{cl}(\{y_{e'}\})=\Phi$. Thus, $\mathscr{T}$ is soft R_0. □

Proposition 1. *Let $\mathscr{T}\in T_E(X)$. Then, $\mathscr{T}$ is soft R_1 iff $\langle x_e\rangle=cl_\theta(\{x_e\})$ for every $x_e\in P_E(X)$.*

Proof. Suppose $\mathscr{T}$ is soft R_1. The first direction is simple. That is $\langle x_e\rangle=\mathrm{cl}(\{x_e\})\widetilde{\cap}\ker(\{x_e\})\widetilde{\subseteq}\mathrm{cl}(\{x_e\})\widetilde{\subseteq}\mathrm{cl}_\theta(\{x_e\})$, see Lemma 2 (2). For the reverse, let $y_{e'}\notin\langle x_e\rangle$. By Lemma 2 (7), $\langle x_e\rangle\neq\langle y_{e'}\rangle$. By Lemma 7 (1), $\mathrm{cl}(\{x_e\})\neq\mathrm{cl}(\{y_{e'}\})$. Since $\mathscr{T}$ is soft R_1, there are (G,E), $(H,E)\in\mathscr{T}$ such that $x_e\in(G,E)$, $y_{e'}\in(H,E)$, and $(G,E)\widetilde{\cap}(H,E)=\Phi$. This implies $y_{e'}\notin\mathrm{cl}_\theta(\{x_e\})$, and hence, $\mathrm{cl}_\theta(\{x_e\})\widetilde{\subseteq}\langle x_e\rangle$. Thus, $\langle x_e\rangle=cl_\theta(\{x_e\})$.

The converse can be proved similarly. □

Proposition 2. *Let $\mathscr{T}\in T_E(X)$. Then, $\mathscr{T}$ is soft R_1 iff $\langle x_e\rangle\in\mathscr{T}_\theta^c$ for every $x_e\in P_E(X)$.*

Proof. Suppose $\mathscr{T}$ is soft R_1. It suffices to show that $\mathrm{cl}_\theta(\langle x_e\rangle)\widetilde{\subseteq}\langle x_e\rangle$. Let $y_{e'}\in\mathrm{cl}_\theta(\langle x_e\rangle)$. By Lemma 7 (5), $\mathrm{cl}_\theta(\langle x_e\rangle)=\mathrm{cl}_\theta(\{x_e\})$, and so $y_{e'}\in\mathrm{cl}_\theta(\{x_e\})$. This means that for all (G,E), $(H,E)\in\mathscr{T}$ containing $x_e, y_{e'}$, respectively, $(G,E)\widetilde{\cap}(H,E)=\Phi$. We must have $\mathrm{cl}(\{x_e\})=\mathrm{cl}(\{y_{e'}\})$, otherwise, we get a contradiction as $\mathrm{cl}(\{x_e\})$ and $\mathrm{cl}(\{y_{e'}\})$ can be separated by two disjoint soft open. Hence, $y_{e'}\in\langle x_e\rangle$.

Assume $\langle x_e\rangle\in\mathscr{T}_\theta^c$ for every $x_e\in P_E(X)$. That is, $\mathrm{cl}_\theta(\langle x_e\rangle)=\langle x_e\rangle$. Since $\langle x_e\rangle\widetilde{\subseteq}\ker(\{x_e\})$ and $\mathrm{cl}(\{x_e\})\widetilde{\subseteq}\mathrm{cl}_\theta(\{x_e\})=\mathrm{cl}_\theta(\langle x_e\rangle)$, then we obtain that $\langle x_e\rangle=\mathrm{cl}(\{x_e\})=\mathrm{cl}_\theta(\{x_e\})=\ker(\{x_e\})$. For $x_e, y_{e'}\in P_E(X)$, if $\mathrm{cl}(\{x_e\})\neq\mathrm{cl}(\{y_{e'}\})$, then $y_{e'}\notin\langle x_e\rangle$. Therefore, there are (G,E), $(H,E)\in\mathscr{T}$ containing $x_e, y_{e'}$, respectively, $(G,E)\widetilde{\cap}(H,E)=\Phi$. Obviously, $\mathrm{cl}(\{x_e\})\widetilde{\subseteq}(G,E)$ and $\mathrm{cl}(\{y_{e'}\})\widetilde{\subseteq}(H,E)$ as $\mathrm{cl}(\{x_e\})=\ker(\{x_e\})$, $\mathrm{cl}(\{y_{e'}\})=\ker(\{y_{e'}\})$. Hence, $\mathscr{T}$ is soft R_1. □

Proposition 3. *Let $\mathcal{T} \in T_E(X)$. The following properties are equivalent:*

(1) $\mathcal{T}$ is soft R_1.

(2) $cl_\theta(\{x_e\}) = cl(\{x_e\})$ for every $x_e \in P_E(X)$.

(3) $cl_\theta(\{x_e\}) = ker(\{x_e\})$ for every $x_e \in P_E(X)$.

(4) $cl(\{x_e\}) \in \mathcal{T}_\theta^c$ for every $x_e \in P_E(X)$.

(5) $ker(\{x_e\}) \in \mathcal{T}_\theta^c$ for every $x_e \in P_E(X)$.

Proof. If $\mathcal{T}$ is soft R_1, by Proposition 2, $\mathrm{cl}_\theta(\langle x_e\rangle) = \langle x_e\rangle$. Since $\langle x_e\rangle \widetilde{\subseteq} \ker(\{x_e\})$ and $\mathrm{cl}(\{x_e\}) \widetilde{\subseteq} \mathrm{cl}_\theta(\{x_e\}) = \mathrm{cl}_\theta(\langle x_e\rangle)$, then we obtain that $\langle x_e\rangle = \mathrm{cl}(\{x_e\}) = \ker(\{x_e\}) = \mathrm{cl}_\theta(\{x_e\})$. The equivalence of these statements can be easily concluded. □

Proposition 4. *Let $\mathcal{T} \in T_E(X)$. The following properties are equivalent:*

(1) $\mathcal{T}$ is soft R_1.

(2) If $(F,E) \in \mathcal{T}^c$ and $x_e \in (F,E)$, then $cl_\theta(\{x_e\}) \widetilde{\subseteq} (F,E)$.

(3) If $(G,E) \in \mathcal{T}$ and $x_e \in (G,E)$, then $cl_\theta(\{x_e\}) \widetilde{\subseteq} (G,E)$.

Proof. It follows from Lemma 7 (7) and Proposition 1. □

Proposition 5. *Let $\mathcal{T} \in T_E(X)$. Then, $\mathcal{T}$ is soft R_1 iff either $\langle x_e\rangle = \langle y_{e'}\rangle$ or $cl_\theta(\{x_e\}) \widetilde{\cap} cl_\theta(\{y_{e'}\}) = \Phi$, for every $x_e, y_{e'} \in P_E(X)$.*

Proof. Assume $\mathcal{T}$ is soft R_1. Given $x_e, y_{e'} \in P_E(X)$, then either $\mathrm{cl}(\{x_e\}) = \mathrm{cl}(\{y_{e'}\})$ or $\mathrm{cl}(\{x_e\}) \neq \mathrm{cl}(\{y_{e'}\})$. If $\mathrm{cl}(\{x_e\}) = \mathrm{cl}(\{y_{e'}\})$, then by Lemma 7 (1), $\langle x_e\rangle = \langle y_{e'}\rangle$. If $\mathrm{cl}(\{x_e\}) \neq \mathrm{cl}(\{y_{e'}\})$, since $\mathcal{T}$ is soft R_1, then there exist disjoint $(U,E), (V,E) \in \mathcal{T}$ such that $\mathrm{cl}(\{x_e\}) \widetilde{\subseteq} (U,E)$ and $\mathrm{cl}(\{y_{e'}\}) \widetilde{\subseteq} (V,E)$. By Proposition 3 (2), $\mathrm{cl}_\theta(\{x_e\}) \widetilde{\cap} \mathrm{cl}_\theta(\{y_{e'}\}) = \Phi$.

Conversely, let $x_e, y_{e'} \in P_E(X)$ such that $\mathrm{cl}(\{x_e\}) \neq \mathrm{cl}(\{y_{e'}\})$. Since $\mathrm{cl}(\{x_e\}) \widetilde{\subseteq} \mathrm{cl}_\theta(\{x_e\})$, by assumption, $\mathrm{cl}(\{x_e\}) \widetilde{\cap} \mathrm{cl}(\{y_{e'}\}) = \Phi$. Set $(U,E) = \widetilde{X} - \mathrm{cl}(\{y_{e'}\})$ and $(V,E) = \widetilde{X} - \mathrm{cl}(\{x_e\})$. Therefore, $(U,E), (V,E) \in \mathcal{T}$ such that $\mathrm{cl}(\{x_e\}) \widetilde{\subseteq} (U,E)$ and $\mathrm{cl}(\{y_{e'}\}) \widetilde{\subseteq} (V,E)$. Hence, $\mathcal{T}$ is soft R_1. □

Proposition 6. *Let $\mathcal{T} \in T_E(X)$. The following properties are equivalent:*

(1) $\mathcal{T}$ is soft R_1.

(2) For every $x_e, y_{e'} \in P_E(X)$, either there exists $(G,E) \in \mathcal{T}$ such that $x_e \in (G,E)$ iff $y_{e'} \in (G,E)$ or there exist disjoint sets $(U,E), (V,E) \in \mathcal{T}$ containing them.

(3) For every $x_e, y_{e'} \in P_E(X)$ with $cl(\{x_e\}) \neq cl(\{y_{e'}\})$, there exist $(F,E), (D,E) \in \mathcal{T}^c$ such that $x_e \in (F,E)$, $y_{e'} \in (D,E)$, and $\widetilde{X} = (F,E) \widetilde{\cup} (D,E)$.

Proof. It follows from the definition of a soft R_1-space and Proposition 5.

When all of the preceding propositions are added together, the following result arises: □

Theorem 4. *Let $\mathcal{T} \in T_E(X)$. The following properties are equivalent:*

(1) $\mathcal{T}$ is soft R_1.

(2) For every $x_e \in P_E(X)$, $\langle x_e\rangle = cl_\theta(\{x_e\})$.

(3) For every $x_e \in P_E(X)$, $\langle x_e\rangle = cl_\theta(\langle x_e\rangle)$.

(4) For every $x_e \in P_E(X)$, $cl_\theta(\{x_e\}) = cl(\{x_e\})$.

(5) For every $x_e \in P_E(X)$, $cl_\theta(\{x_e\}) = ker(\{x_e\})$.

(6) For every $x_e \in P_E(X)$, $cl(\{x_e\}) \in \mathcal{T}_\theta^c$.

(7) For every $x_e \in P_E(X)$, $ker(\{x_e\}) \in \mathcal{T}_\theta^c$.

(8) If $(F,E) \in \mathcal{T}^c$ and $x_e \in (F,E)$, then $cl_\theta(\{x_e\}) \widetilde{\subseteq} (F,E)$.

(9) If $(G,E) \in \mathcal{T}$ and $x_e \in (G,E)$, then $cl_\theta(\{x_e\}) \widetilde{\subseteq} (G,E)$.

(10) For every $x_e, y_{e'} \in P_E(X)$, either $\langle x_e\rangle = \langle y_{e'}\rangle$ or $cl_\theta(\{x_e\}) \widetilde{\cap} cl_\theta(\{y_{e'}\}) = \Phi$.

(11) For every $x_e, y_{e'} \in P_E(X)$ with $cl(\{x_e\}) \neq cl(\{y_{e'}\})$, there exist $(F,E), (D,E) \in \mathcal{T}^c$ such that $x_e \in (F,E)$, $y_{e'} \in (D,E)$, and $\widetilde{X} = (F,E) \widetilde{\cup} (D,E)$.

Theorem 5. *For $\mathcal{T} \in T_E(X)$, the following properties are equivalent:*

(1) $\mathcal{T}$ is soft R_1.

(2) $\ker_\theta(F,E) = \ker(F,E)$ for every $(F,E) \in S_E(X)$.

(3) $\ker_\theta(F,E) = cl(F,E)$ for every soft compact $(F,E) \in S_E(X)$.

(4) $cl_\theta(F,E) = cl(F,E)$ for every soft compact $(F,E) \in S_E(X)$.

Proof

(1) ⇒ (2) Suppose $\mathcal{T}$ is soft R_1. By Theorem 4 (4), we have $\ker_\theta(F,E) = \{x_e \in P_E(X)\colon \mathrm{cl}_\theta(\{x_e\}) \widetilde{\cap} (F,E) \neq \Phi\} = \{x_e \in P_E(X)\colon \mathrm{cl}(\{x_e\}) \widetilde{\cap} (F,E) \neq \Phi\} = \ker(F,E)$.

(2) ⇒ (3) Given a soft compact set (F,E), by (2) and Lemma 6 (3), $\mathrm{cl}_\theta(F,E) = \ker_\theta(F,E) = \ker(F,E)$. Since $\mathrm{cl}(F,E) \widetilde{\subseteq} \mathrm{cl}_\theta(F,E)$, so $\mathrm{cl}(F,E) \widetilde{\subseteq} \ker_\theta(F,E)$. By Theorem 2, $\ker(A) \widetilde{\subseteq} \mathrm{cl}(F,E)$. Therefore, $\ker_\theta(A) \widetilde{\subseteq} \mathrm{cl}(F,E)$. Hence, (3).

(3) ⇒ (4) It derives from Lemma 6 (3).

(4) ⇒ (1) It concludes from Theorem 4 (4). □

5. Characterizations of Soft T_i-Spaces, $i \in \{0,1,2\}$

In this section, we give characterizations of soft T_0, soft T_1, and soft T_2-spaces via the soft topological operators mentioned in Section 3.

Theorem 6 (see [19]). *Let $\mathcal{T} \in T_E(X)$. Then, $\mathcal{T}$ is soft T_0 iff der$(\{x_e\})$ is a union of soft closed sets for every $x_e \in P_E(X)$.*

Using the soft θ-derived set operator, a conclusion similar to the above can be established for soft T_1 topologies.

Theorem 7. *Let $\mathcal{T} \in T_E(X)$. Then, $\mathcal{T}$ is soft T_1 iff $\text{der}_\theta(\{x_e\})$ is a union of soft closed sets for every $x_e \in P_E(X)$.*

Proof. Suppose $\mathcal{T}$ is soft T_1. By Lemma 4, $\mathcal{T}$ is soft T_0 and soft R_0. By Theorems 3 and 6, we can easily conclude that $\text{der}_\theta(\{x_e\})$ is a union of soft closed sets for every $x_e \in P_E(X)$.

Conversely, given $x_e \in P_E(X)$. If $y_{e'} \in \text{der}(\{x_e\})$, then $y_{e'} \in \text{der}_\theta(\{x_e\})$ and $x_e \in \text{der}_\theta(\{y_{e'}\})$. Therefore, there exists $(F, E) \in \mathcal{T}^c$ with $(F, E) \widetilde{\subseteq} \text{der}_\theta(\{y_{e'}\})$ such that $x_e \in (F, E)$. Thus, $\text{cl}(\{x_e\}) \widetilde{\subseteq} \text{der}_\theta(\{y_{e'}\})$. This implies that $y_{e'} \notin \text{cl}(\{x_e\})$ and hence $\text{der}(\{x_e\}) = \text{cl}(\{x_e\}) - \{x_e\} = \Phi$. This proves that $\mathcal{T}$ is soft T_1. □

Theorem 8. *Let $\mathcal{T} \in T_E(X)$. Then, $\mathcal{T}$ is soft T_2 iff $cl_\theta(\{x_e\}) = \{x_e\}$ for every $x_e \in P_E(X)$.*

Proof. Suppose $\mathcal{T}$ is soft T_2. Given $x_e \in P_E(X)$. Then, for every $y_{e'} \in P_E(X)$ with $y_{e'} \neq x_e$, there are $(G, E), (H, E) \in \mathcal{T}$ such that $x_e \in (G, E)$, $y_{e'} \in (H, E)$, and $(G, E) \widetilde{\cap} (H, E) = \Phi$. Therefore, $(G, E) \widetilde{\cap} \text{cl}(H, E) = \Phi$. This means that $y_{e'} \notin \text{cl}_\theta(\{x_e\})$. Hence, $\text{cl}_\theta(\{x_e\}) = \{x_e\}$.

Conversely, suppose $\text{cl}_\theta(\{x_e\}) = \{x_e\}$ for every $x_e \in P_E(X)$. For any $y_{e'} \in P_E(X)$ with $y_{e'} \neq x_e$, $y_{e'} \notin \text{cl}_\theta(\{x_e\})$. This implies that there are disjoint $(G, E), (H, E) \in \mathcal{T}$ such that $x_e \in (G, E)$, $y_{e'} \in (H, E)$. Thus, $\mathcal{T}$ is soft T_2.

The next result is an immediate consequence of the above theorem: □

Corollary 1. *Let $\mathcal{T} \in T_E(X)$. Then, $\mathcal{T}$ is soft T_2 iff $\mathcal{T}_\theta$ is soft T_1 iff $\mathcal{T}_\theta$ is soft T_0.*

Theorem 9. *For $\mathcal{T} \in T_E(X)$, the following properties are equivalent:*

(1) $\mathcal{T}$ is soft T_2.

(2) $cl_\theta(\{x_e\}) \widetilde{\cap} cl_\theta(\{y_{e'}\}) = \Phi$ for every $x_e, y_{e'} \in P_E(X)$ with $x_e \neq y_{e'}$.

(3) $\ker_\theta(F, E) = (F, E)$ for every $(F, E) \in S_E(X)$.

(4) $\ker_\theta(F, E) = (F, E)$ for every soft compact $(F, E) \in S_E(X)$.

(5) $cl_\theta(F, E) = (F, E)$ for every soft compact $(F, E) \in S_E(X)$.

Proof

(1) ⇒ (2) Let $x_e, y_{e'} \in P_E(X)$ with $x_e \neq y_{e'}$. By (1) and Theorem 8, there exist disjoint $(G, E), (H, E) \in \mathcal{T}$ such that $\text{cl}_\theta(\{x_e\}) \widetilde{\subseteq} (G, E)$ and $\text{cl}_\theta(\{y_{e'}\}) \widetilde{\subseteq} (H, E)$. Hence, $\text{cl}_\theta(\{x_e\}) \widetilde{\cap} \text{cl}_\theta(\{y_{e'}\}) = \Phi$.

(2) ⇒ (3) By Lemma 6 (1), $\ker_\theta(F, E) = \{x_e : \text{cl}_\theta(\{x_e\}) \widetilde{\cap} (F, E) \neq \Phi\}$. Since for every $x_e \in (F, E)$ and for every $y_{e'} \neq x_e$, $\text{cl}_\theta(\{x_e\}) \widetilde{\cap} \text{cl}_\theta(\{y_{e'}\}) = \Phi$ and $x_e \in \text{cl}_\theta(\{x_e\})$. We must have that $\ker_\theta(F, E) = (F, E)$.

(3) ⇒ (4) Evident.

(4) ⇒ (1) Since each $\{x_e\}$ is soft compact, by Theorem 8, $\mathcal{T}$ is soft T_2. □

6. Conclusion

Soft separation axioms are collections of conditions for classifying a system of soft topological spaces according to particular soft topological properties. These axioms are usually described in terms of soft open or soft closed sets in a topological space. In this paper, we propose soft θ-kernel and soft θ-derived set operators and make find their relationships with other soft topological operators. Then, the mentioned operators are used to characterize various soft separation axioms. We see that soft θ-kernel, soft θ-closure, and soft θ-derived set operators behave better than their corresponding soft operators for characterizing soft T_i and soft R_j-spaces, where $i = 0, 1, 2$ and $j = 0, 1$ (*c.f.* [19]).

Data Availability

No data were used to support this study.

Conflicts of Interest

The authors declare that they have no competing interests.

References

[1] D. Molodtsov, "Soft set theory—first results," *Computers & Mathematics with Applications*, vol. 37, no. 4-5, pp. 19–31, 1999.

[2] L. Zadeh, "Fuzzy sets," *Information and Control*, vol. 8, no. 3, pp. 338–353, 1965.

[3] Z. Pawlak, "Rough sets," *International Journal of Computer & Information Sciences*, vol. 11, no. 5, pp. 341–356, 1982.

[4] M. Shabir and M. Naz, "On soft topological spaces," *Computers & Mathematics with Applications*, vol. 61, no. 7, pp. 1786–1799, 2011.

[5] N. Çağman, S. Karataş, and S. Enginoglu, "Soft topology," *Computers & Mathematics with Applications*, vol. 62, no. 1, pp. 351–358, 2011.

[6] J. C. R. Alcantud, "Soft open bases and a novel construction of soft topologies from bases for topologies," *Mathematics*, vol. 8, no. 5, p. 672, 2020.

[7] T. Hida, "A comprasion of two formulations of soft compactness," *Annals of Fuzzy Mathematics and Informatics*, vol. 8, no. 4, pp. 511–524, 2014.

[8] A. A. Azzam, Z. A. Ameen, T. M. Al-shami, and M. E. El-Shafei, "Generating soft topologies via soft set operators," *Symmetry*, vol. 14, no. 5, p. 914, 2022.

[9] T. M. Al-shami and A. Mhemdi, "Two families of separation axioms on infra soft topological spaces," *Filomat*, vol. 36, no. 4, pp. 1143–1157, 2022.

[10] W. K. Min, "A note on soft topological spaces," *Computers & Mathematics with Applications*, vol. 62, no. 9, pp. 3524–3528, 2011.

[11] A. B. Khalaf, N. K. Ahmed, and Q. H. Hamko, "Soft separation axioms and functions with soft closed graphs," *Proyecciones (Antofagasta)*, vol. 41, no. 1, pp. 177–195, 2022.
[12] T. M. Al-shami, "Comments on some results related to soft separation axioms," *Afrika Matematika*, vol. 31, no. 7-8, pp. 1105–1119, 2020.
[13] A. Singh and N. S. Noorie, "Remarks on soft axioms," *Annals of Fuzzy Mathematics and Informatics*, vol. 14, no. 5, pp. 503–513, 2017.
[14] A. Allam, T. H. Ismail, and R. Muhammed, "A new approach to soft belonging," *Journal of Annals of Fuzzy Mathematics and Informatics*, vol. 13, no. 1, pp. 145–152, 2017.
[15] S. Nazmul and S. Samanta, "Neighbourhood properties of soft topological spaces," *Annals of Fuzzy Mathematics and Informatics*, vol. 6, no. 1, pp. 1–15, 2013.
[16] P. K. Maji, R. Biswas, and A. R. Roy, "Soft set theory," *Computers & Mathematics with Applications*, vol. 45, no. 4-5, pp. 555–562, 2003.
[17] M. I. Ali, F. Feng, X. Liu, W. K. Min, and M. Shabir, "On some new operations in soft set theory," *Computers & Mathematics with Applications*, vol. 57, no. 9, pp. 1547–1553, 2009.
[18] S. Al Ghour and Z. A. Ameen, "Maximal soft compact and maximal soft connected topologies," *Applied Computational Intelligence and Soft Computing*, vol. 2022, Article ID 9860015, 7 pages, 2022.
[19] T.M. Al-shami, Z. A. Ameen, A. Azzam, and M. E. El-Shafei, Soft separation axioms via soft topological operators, submitted, vol. 7, no. 8, pp. 15107–15119, 2022.
[20] A. H. Kocaman and N. Tozlu, "Soft locally closed sets and decompositions of soft continuity," *Annals of Fuzzy Mathematics and Informatics*, vol. 11, no. 2, pp. 173–181, 2016.
[21] D. Georgiou, A. Megaritis, and V. Petropoulos, "On soft topological spaces," *Applied Mathematics & Information Sciences*, vol. 7, no. 5, pp. 1889–1901, 2013.
[22] S. Bayramov and C. Gunduz, "A new approach to separability and compactness in soft topological spaces," *TWMS Journal of Pure and Applied Mathematics*, vol. 9, no. 21, pp. 82–93, 2018.
[23] A. Aygünoğlu and H. Aygün, "Some notes on soft topological spaces," *Neural Computing & Applications*, vol. 21, no. S1, pp. 113–119, 2012.

Hindawi
Journal of Mathematics
Volume 2023, Article ID 9878505, 1 page
https://doi.org/10.1155/2023/9878505

Retraction

Retracted: Classical and Bayesian Inference of Marshall-Olkin Extended Gompertz Makeham Model with Modeling of Physics Data

Journal of Mathematics

Received 10 October 2023; Accepted 10 October 2023; Published 11 October 2023

This article has been retracted by Hindawi following an investigation undertaken by the publisher [1]. This investigation has uncovered evidence of one or more of the following indicators of systematic manipulation of the publication process:

(1) Discrepancies in scope

(2) Discrepancies in the description of the research reported

(3) Discrepancies between the availability of data and the research described

(4) Inappropriate citations

(5) Incoherent, meaningless and/or irrelevant content included in the article

(6) Peer-review manipulation

The presence of these indicators undermines our confidence in the integrity of the article's content and we cannot, therefore, vouch for its reliability. Please note that this notice is intended solely to alert readers that the content of this article is unreliable. We have not investigated whether authors were aware of or involved in the systematic manipulation of the publication process.

Wiley and Hindawi regrets that the usual quality checks did not identify these issues before publication and have since put additional measures in place to safeguard research integrity.

We wish to credit our own Research Integrity and Research Publishing teams and anonymous and named external researchers and research integrity experts for contributing to this investigation.

The corresponding author, as the representative of all authors, has been given the opportunity to register their agreement or disagreement to this retraction. We have kept a record of any response received.

References

[1] R. A. H. Mohamed, A. A. Al-Babtain, I. Elbatal, E. M. Almetwally, and H. M. Almongy, "Classical and Bayesian Inference of Marshall-Olkin Extended Gompertz Makeham Model with Modeling of Physics Data," *Journal of Mathematics*, vol. 2022, Article ID 2528583, 14 pages, 2022.

Hindawi
Journal of Mathematics
Volume 2022, Article ID 2528583, 14 pages
https://doi.org/10.1155/2022/2528583

Research Article

Classical and Bayesian Inference of Marshall-Olkin Extended Gompertz Makeham Model with Modeling of Physics Data

Rania A. H. Mohamed,[1] Abdulhakim A. Al-Babtain,[2] I. Elbatal,[3] Ehab M. Almetwally,[4,5] and Hisham M. Almongy[6]

[1]*Department of Statistics Mathematics and Insurance, Faculty of Commerce, Port Said University, Port Fuad 42526, Egypt*
[2]*Department of Statistics and Operations Research, King Saud University, Riyadh 11362, Saudi Arabia*
[3]*Department of Mathematics and Statistics-College of Science, Imam Mohammad Ibn Saud Islamic University (IMSIU), Riyadh 11362, Saudi Arabia*
[4]*Department of Statistics, Faculty of Business Administration, Delta University of Science and Technology, Gamasa 11152, Egypt*
[5]*The Scientific Association for Studies and Applied Research, Al Manzalah, Egypt*
[6]*Department of Applied Statistics and Insurance, Faculty of Commerce, Mansoura University, Mansoura 35516, Egypt*

Correspondence should be addressed to Ehab M. Almetwally; ehabxp_2009@hotmail.com

Received 20 April 2022; Revised 21 May 2022; Accepted 25 May 2022; Published 5 July 2022

Academic Editor: Naeem Jan

The purpose of this study is to present the Marshall- Olkin extended Gompertz Makeham (MOEGM) lifetime distribution, which has four parameters. As a result, we will describe some of the structural elements that are introduced for this model. The maximum likelihood approach is used to estimate the model parameters, and it is well known that likelihood estimators for unknown parameters are not always available. As a result, we examine the prior distributions, which allow for prior dependence among the components of the parameter vector, as well as the Bayesian estimators derived with respect to the squared error loss function. A Monte Carlo simulation research is carried out to examine the performance of the likelihood estimators and the Bayesian technique. Finally, we demonstrate the significance of the new model. And to conclude, we illustrate the importance of the new model by exploring some of the empirical applications of physics to show it's flexibility and potentiality of a new model.

1. Introduction

Gompertz distribution has been obtained by Gompertz [1]. It is critical in the analysis of survival periods in several areas, including marketing, gerontology, biology, and computer science. It was used to characterize human mortality, develop growth models, and create actuarial tables. The Gompertz distribution's hazard rate function (hrf) is an increasing function used by actuaries and demographers to characterize the distribution of adult life lengths. Makeham [2] looked at the Gompertz distribution's fit to actuarial data and found that by modifying it, he could enhance the fit. This change is now known as the Gompertz- Makeham (GM) distribution. The Gompertz - Makeham (GM) distribution studied by Bailey et al. [3]. The GM distribution has been frequently utilised in actuarial tables and growth models to describe human mortality.

Missov and Lenart [4] discovered closed-form solutions to the life-expectancy integral in homogeneous and gamma-heterogeneous populations, as well as in the presence or absence of the Makeham factor. Chukwu and Ogunde [5] introduced Kumaraswamy Gompertz-Makeham, a five-parameter generalized version of the GM with decreasing, rising, and bathtub-shaped failure rate functions. For the GM model, Wrycza [6] developed a straightforward formulation of life table entropy.

The cumulative distribution function (c.d.f.) of the Gompertz- Makeham (GM) distribution is given by

$$G_{\mathrm{GM}}(x,\theta,\alpha,\lambda) = 1 - e^{-\theta x-(\alpha/\lambda)\left(e^{\lambda x}-1\right)}, \quad x>0, \tag{1}$$

where $\lambda > 0$ is a scale parameter, $\theta > 0$ and $\alpha > 0$ are shape parameters.The corresponding probability density function (p.d.f) and hrf are given by

$$g_{GM}(x,\theta,\alpha,\lambda) = \left(\alpha e^{\lambda x} + \theta\right) e^{-\theta x - (\alpha/\lambda)\left(e^{\lambda x}-1\right)},$$

$$h_{GM}(x,\theta,\alpha,\lambda) = \frac{g_{GM}(x,\theta,\alpha,\lambda)}{\overline{G}_{GM}(x,\theta,\alpha,\lambda)} = \alpha e^{\lambda x} + \theta, \tag{2}$$

respectively.

There has lately been a resurgence of interest in developing innovative generators for univariate continuous distributions by introducing one or more additional shape factors into the baseline model. This parameter induction has been demonstrated to be useful in analyzing tail characteristics and increasing the goodness-of-fit of the recommended generator family. These asymmetric distributions were formed by adding new parameters to a baseline c.d.f., resulting in a new family of more analytically flexible asymmetric distributions. In the statistical literature, several classes have been proposed for constructing new distributions by adding one or more parameters. The beta-G by Eugene et al. [7], Kumaraswamy-G by Cordeiro and de Castro [8], new extended cosine-G distributions by Muhammad et al. [9], new truncated muth generated family by Almarashi et al. [10], odd Perks-G class by Elbatal et al. [11], and the Zografos-Balakrishnan-G family by Nadarajah et al. [12] are just a few examples of well-known generators.

Marshall and Olkin [13] suggested a general approach for adding a new positive shape parameter to a baseline distribution, resulting in the Marshall-Olkin family of distributions (abbreviated as "MO" for short). The baseline distribution is included in this family as a fundamental instance, and some distributions have more flexibility for representing diverse types of data. The proportional odds family with tilt parameter are other names for the MO family of distributions (Marshall and Olkin [14]). The Marshall and Olkin family's c.d.f. is defined as:

$$F(x,\gamma) = \frac{G(x)}{1-\overline{\gamma}\overline{G}(x)}, \quad x > 0,\ \gamma > 0. \tag{3}$$

The survival function $\overline{F}(x,\gamma)$ is given by

$$\overline{F}(x,\gamma) = \frac{\gamma\overline{G}(x)}{1-\overline{\gamma}\overline{G}(x)}, \tag{4}$$

where $\overline{\gamma} = (1-\gamma)$, for $\gamma = 1$, we get the baseline distribution, i.e., $\overline{F}(x) = \overline{G}(x)$, where the shape parameter γ is called tilt parameter, since the hazard rate function $h(x;\gamma)$ of the transformed distribution is shifted below when $\gamma \geq 1$ or shifted below when $0 < \gamma \leq 1$ from the baseline hazard rate function $h_G(x)$. In fact, $h(x;\gamma) \leq h_G(x)$ when $\gamma \geq 1$ and $h(x;\gamma) \geq h_G(x)$ when $0 < \gamma \leq 1$. The corresponding p.d.f becomes

$$f(x,\gamma) = \frac{\gamma g(x)}{[1-\overline{\gamma}\overline{G}(x)]^2}, \tag{5}$$

the hrf is given by

$$h(x,\gamma) = \frac{f(x,\gamma)}{\overline{F}(x,\gamma)} = \frac{\gamma g(x)}{\overline{G}(x)[1-\overline{\gamma}\overline{G}(x)]}. \tag{6}$$

In recent years, several authors have used this method to extend well-known distributions. A few examples include Ghitany et al. [15] presented censored scheme of MO extended Weibull distribution, Jayakumar and Mathew [16] introduced on a generalization to MO with application of Burr type XII distribution, Pérez-Casany and Casellas [17] presented MO extended Zipf Distribution, Krishna et al. [18] proposed the MO Fréchet distribution, Gui [19] introduced the MO power log - normal distribution and and its applications to survival data, Idika et al. [20] introduced the MO generalized Erlange - truncated exponential distribution, MirMostafaee et al. [21] represented the MO extended generalized Rayleigh distribution, among others. The aim of this paper is to propose a new class of lifetime distributions called "The MO extended Gompertz-Makeham" distribution, as referred to as (MOEGM).

In this paper, the Marshall- Olkin extended Gompertz Makeham (MOEGM) lifetime distribution has been presented, which has four parameters. As a result, we will describe some of the structural properties that are introduced for this model. The maximum likelihood approach is used to estimate the model parameters, and it is well known that likelihood estimators for unknown parameters are not always available. As a result, we examine the prior distributions, which allow for prior dependence among the components of the parameter vector, as well as the Bayesian estimators derived with respect to the squared error loss function. A Monte Carlo simulation and two real data sets are carried out to examine the performance of the model and likelihood estimators and the Bayesian technique.

The rest of the paper is organized as follows: The Marshall-Olkin extended Gompertz Makeham distribution and its technique are defined in Section 2. Section 3 introduces and investigates numerous structural characteristics properties of the MOEGM distribution. Section 4 shows the likelihood estimates for the unknown parameters. Section 5 shows the Bayesian estimates of the unknown parameters. Simulation results are carried out in Section 6. Section 7 depicts two real-world data applications. Finally, we demonstrate the significance of this study's closing remarks.

2. The MOEGM Model

In this section, we introduce the four parameter Marshall-Olkin extended Gompertz-Makeham (MOEGM) distribution. Using equations (1), (3) and (4) shown in the previous section, the c.d.f. and survival function can be written as follows,

$$F(x;\theta,\alpha,\lambda,\gamma)=\frac{G(x)}{1-\overline{\gamma}\overline{G}(x)}=\frac{1-e^{-\theta x-(\alpha/\lambda)\left(e^{\lambda x}-1\right)}}{1-\overline{\gamma}e^{-\theta x-(\alpha/\lambda)\left(e^{\lambda x}-1\right)}},$$
$$\overline{F}(x,\theta,\alpha,\lambda,\gamma)=\frac{\overline{G}(x)}{1-\overline{\gamma}\overline{G}(x)}=\frac{e^{-\theta x-(\alpha/\lambda)\left(e^{\lambda x}-1\right)}}{1-\overline{\gamma}e^{-\theta x-(\alpha/\lambda)\left(e^{\lambda x}-1\right)}}, \tag{7}$$

respectevely. The corresponding p.d.f given by

$$f(x;\theta,\alpha,\lambda,\gamma)=\frac{\gamma\left(\alpha e^{\lambda x}+\theta\right)e^{-\theta x-(\alpha/\lambda)\left(e^{\lambda x}-1\right)}}{\left[1-\overline{\gamma}e^{-\theta x-(\alpha/\lambda)\left(e^{\lambda x}-1\right)}\right]^2}. \tag{8}$$

Henceforth, Let $X\sim \mathrm{MOEGM}(\varphi)$, having p.d.f. (8) where $\varphi=(\theta,\alpha,\lambda,\gamma)$. Figure 1 display some plots of the p.d.f. of MOEGM model for some different parameter values.

The failure (hazard) rate function in event time analysis quantifies the current likelihood of failure for the population that has not yet failed. The hrf is essential when dealing with lifetime data in reliability analysis, survival analysis, and demography, as well as when building and creating models. The hrf for the Marshall-Olkin extended Gompertz-Makeham distribution is as follows in Figure 2. Figure 2 display some plots of the hrf of MOEGM model for some different parameter values.

$$h(x,\varphi)=\frac{f(x;\varphi)}{\overline{F}(x;\varphi)}=\frac{\gamma\left(\alpha e^{\lambda x}+\theta\right)}{1-\overline{\gamma}e^{-\theta x-(\alpha/\lambda)\left(e^{\lambda x}-1\right)}}. \tag{9}$$

2.1. Expansion of p.d.f. In this subsection, we present the expansion of the *MOEGM* density function in terms of an infinite linear combination of Gompertz-Makeham distribution. using the power series expansion

$$(1-z)^{-n}=\sum_{i=0}^{\infty}\frac{\Gamma(n+i)}{\Gamma(n)i!}z^i,\quad n>0,\ |z|<1. \tag{10}$$

We get

$$\left[1-\overline{\gamma}e^{-\theta x-(\alpha/\lambda)\left(e^{\lambda x}-1\right)}\right]^{-2}=\sum_{i=0}^{\infty}(i+1)\overline{\gamma}^i e^{-i\left[\theta x+(\alpha/\lambda)\left(e^{\lambda x}-1\right)\right]}, \tag{11}$$

substituting equation (11) into equation (8), we get

$$f(x;\varphi)=\gamma\sum_{i=0}^{\infty}(i+1)\overline{\gamma}^i\left(\alpha e^{\lambda x}+\theta\right)e^{-(i+1)\left[\theta x+(\alpha/\lambda)\left(e^{\lambda x}-1\right)\right]}. \tag{12}$$

Using the series expansion of $e^{-(i+1)e^{\lambda x}}$ as follows

$$e^{-(i+1)(\alpha/\lambda)e^{\lambda x}}=\sum_{j=0}^{\infty}\frac{(-1)^j(i+1)^j(\alpha/\lambda)^j}{j!}e^{\lambda jx}, \tag{13}$$

thus after some algebra (12) can be written as

$$f(x;\varphi)=\sum_{k=0}^{\infty}\delta_k\left(\alpha(j+1)^k+\theta j^k\right)x^k e^{-(i+1)\theta x}, \tag{14}$$

where

$$\delta_k=\sum_{i,j=0}^{\infty}\frac{\gamma(i+1)^{j+1}(-1)^{j+k}\overline{\gamma}^i e^{(i+1)(\alpha/\lambda)}(\alpha/\lambda)^j\lambda^k}{j!k!}. \tag{15}$$

3. Statistical Features

3.1. Quantile Function. For a random variable X has c.d.f. of Marshall- Olkin power generalized Weibull distribution, the quantile function $Q(p)$ is given by the relation

$$\theta x_p+\frac{\alpha}{\lambda}\left(e^{\lambda x_p}-1\right)+\log\left[\frac{1-p}{1-p\overline{\gamma}}\right]=0,\quad p\in(0,1). \tag{16}$$

By equation (16), in addition to using the qf to obtain the Bowley's skewness and the Moors' kurtosis, is highly useful for generating MOEGM random variate and can be simply applied. Bowley's skewness is based on quartiles, as described by Kenney and Keeping [22], it's given by

$$B_S=\frac{Q(3/4)-2Q(2/4)+Q(1/4)}{Q(3/4)-Q(1/4)}, \tag{17}$$

and the Moor's kurtosis, see Moors [23], is given by

$$M_k=\frac{Q(7/8)-Q(5/8)+Q(3/8)-Q(1/8)}{Q(6/8)-Q(2/8)}, \tag{18}$$

where $Q(\cdot)$ is the quantile function given by equation (16).

3.2. Moments. The r_{th} moment of the MOEGM distribution is discussed in this subsection. In any statistical analysis, especially in applications, moments are crucial and important. It can be used to investigate a distribution's most essential properties and qualities (e.g., tendency, dispersion, skewness and kurtosis).

3.3. Theorem Quantile Function. If X has $X\sim\mathrm{MOEGM}(\varphi)$, where $\varphi=(\theta,\alpha,\lambda,\gamma)$ then the r_{th} moment of X is given by

$$\mu_r'(x)=\sum_{k=0}^{\infty}\delta_k\left(\alpha(j+1)^k+\theta j^k\right)\frac{\Gamma(r+k+1)}{[(i+1)\theta]^{r+k+1}}. \tag{19}$$

Proof. Let X be a random variable with the distribution MOEGM. The well-known formula can be used to calculate the r_{th} ordinary moment.

$$\begin{aligned}\mu_r'(x)&=\int_0^{\infty}x^r f(x,\varphi)\mathrm{d}x\\&=\sum_{k=0}^{\infty}\delta_k\left(\alpha(j+1)^k+\theta j^k\right)\int_0^{\infty}x^{r+k}e^{-(i+1)\theta x}\mathrm{d}x,\end{aligned} \tag{20}$$

setting $y=(i+1)\theta x$, after some algebra, the r_{th} ordinary moment can be written as

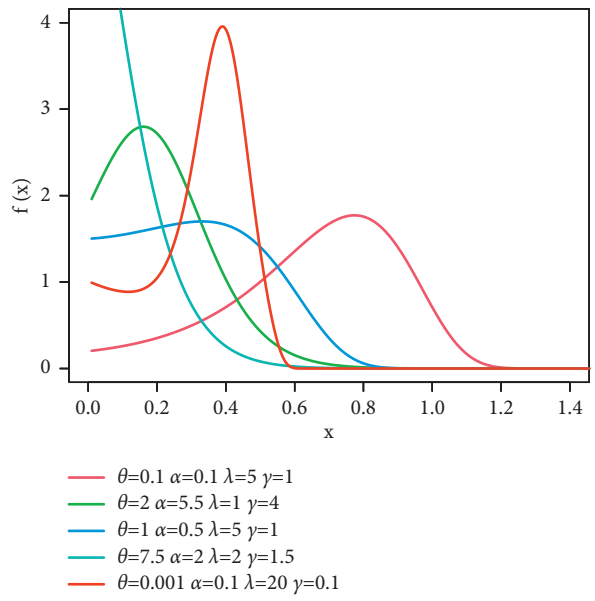

Figure 1: The p.d.f. plot for the MOEGM model.

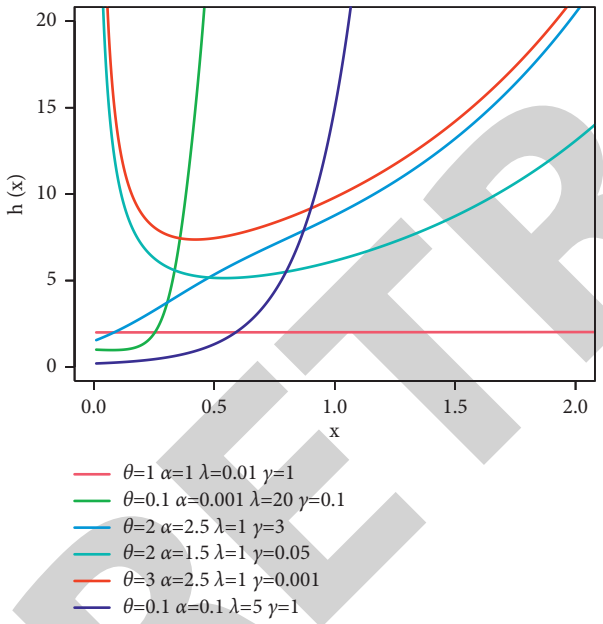

Figure 2: The hrf plot for the MOEGM model.

$$\mu_r'(x) = \sum_{k=0}^{\infty} \delta_k\left(\alpha(j+1)^k + \theta j^k\right) \frac{\Gamma(r+k+1)}{[(i+1)\theta]^{r+k+1}}, \tag{21}$$

where $\Gamma(n) = \int_0^{\infty} x^{n-1}e^{-x}\mathrm{d}x$ denotes the gamma function. □

3.4. Moment Generating Function. Moment generating functions are helpful for a variety of reasons, one of which being their usage in sums of random variables analysis. When compared to working directly with the probability function or c.d.f. of a random variable, it provides the foundation for an alternative approach to analytic solutions.

Theorem 1. *If X has the MOEGM$(\theta, \alpha, \lambda, \gamma)$, then the the moment generating function (mgf) of X is given as follows*

$$M_X(t) = \sum_{k=0}^{\infty} \delta_k\left(\alpha(j+1)^k + \theta j^k\right) \frac{\Gamma(k+1)}{[\theta(i+1) - t]^{k+1}}. \tag{22}$$

Proof. We begin with the well-known simplification of the moment generating function, which is as follows:

$$\begin{aligned} M_X(t) &= E\left(e^{tX}\right) \\ &= \int_0^{\infty} e^{tx} f(x)\mathrm{d}x \\ &= \sum_{k=0}^{\infty} \delta_k\left(\alpha(j+1)^k + \theta j^k\right) \int_0^{\infty} x^k e^{-[(i+1)\theta - t]x}\mathrm{d}x \\ &= \sum_{k=0}^{\infty} \delta_k\left(\alpha(j+1)^k + \theta j^k\right) \frac{\Gamma(k+1)}{[\theta(i+1) - t]^{k+1}}, \end{aligned} \tag{23}$$

which completes the proof. □

3.5. Conditional Moments. The s_{th} lower incomplete moment of MOEGM distribution is

$$\begin{aligned} \eta_s(t) &= \int_0^t x^s f(x)\mathrm{d}x \\ &= \sum_{k=0}^{\infty} \delta_k\left(\alpha(j+1)^k + \theta j^k\right) \int_0^t x^{s+k} e^{-(i+1)\theta x}\mathrm{d}x \\ &= \sum_{k=0}^{\infty} \delta_k\left(\alpha(j+1)^k + \theta j^k\right) \frac{\gamma(s+k+1, \theta(i+1)t)}{[\theta(i+1)]^{s+k+1}}, \end{aligned} \tag{24}$$

where $\gamma(s,t) = \int_0^t x^{s-1}e^{-x}\mathrm{d}x$ is the lower incomplete gamma function. The first incomplete moment of X, denoted by, $\eta_1(t)$, is computed using equation (24) by setting $s = 1$ as

$$\eta_1(t) = \sum_{k=0}^{\infty} \delta_k\left(\alpha(j+1)^k + \theta_j^k\right) \frac{\gamma(k+2, \theta(i+1)t)}{[\theta(i+1)]^{k+2}}. \tag{25}$$

Similarly, the s_{th} upper incomplete moment of MOEGM distribution is

$$\begin{aligned} \xi_s(t) &= \int_t^{\infty} x^s f(x)\mathrm{d}x \\ &= \sum_{k=0}^{\infty} \delta_k\left(\alpha(j+1)^k + \theta j^k\right) \int_t^{\infty} x^{s+k} e^{-(i+1)\theta x}\mathrm{d}x \\ &= \sum_{k=0}^{\infty} \delta_k\left(\alpha(j+1)^k + \theta j^k\right) \frac{\Gamma(s+k+1, \theta(i+1)t)}{[\theta(i+1)]^{s+k+1}}, \end{aligned} \tag{26}$$

where $\Gamma(s,t) = \int_t^{\infty} x^{s-1}e^{-x}\mathrm{d}x$ is the upper incomplete gamma function.

The mean residual lifespan (MRL) has a diverse set of uses and applications see Lai and Xie [24]. The expected

extended life length for a unit alive at age t is represented by the MRL (or life expectancy at age t). The MRL is given by

$$\mu(t) = E(X|X > t) = \frac{\xi_1(t)}{\overline{F}(t)} - t, \tag{27}$$

where $\xi_1(t)$ is the first incomplete moment of X and by setting $s = 1$ in equation (26), we get

$$\mu(t) = \frac{1}{\overline{F}(t)} \sum_{k=0}^{\infty} \delta_k \left(\alpha(j+1)^k + \theta j^k\right) \frac{\Gamma(k+2, \theta(i+1)t)}{[\theta(i+1)]^{k+2}} - t. \tag{28}$$

In addition, the mean inactivity time (MIT) shows the amount of time that has passed after an item has failed, assuming that the failure happened in $(0; t)$. For $t > 0$, the MIT of X is defined by

$$\tau(t) = E(X|X < t) = t - \frac{\eta_1(t)}{F(t)} = t - \frac{1}{F(t)} \sum_{k=0}^{\infty} \delta_k \left(\alpha(j+1)^k + \theta j^k\right) \frac{\gamma(k+2, \theta(i+1)t)}{[\theta(i+1)]^{k+2}}. \tag{29}$$

4. Estimation and Inference

Only full samples are used to calculate the maximum likelihood estimates (MLEs) of the parameters of the MOEGM distribution in this section. Let $X_1, \ldots, X_n$ be a random sample of size n from MOEGM(φ) where $\varphi = (\theta, \alpha, \lambda, \gamma)$. Let $\varphi = (\theta, \alpha, \lambda, \gamma)^T$ be the parameter vector. The log-likelihood function for the vector of parameters $\varphi = (\theta, \alpha, \lambda, \gamma)$ can be written as

$$\log L(\varphi) = n \log(\gamma) + \sum_{i=1}^{n} \log\left(\alpha e^{\lambda x_i} + \theta\right) - \theta \sum_{i=1}^{n} x_i - \frac{\alpha}{\lambda} \sum_{i=1}^{n} \log\left(e^{\lambda x_i} - 1\right) - 2 \sum_{i=1}^{n} \log\left[1 - \overline{\gamma} e^{-\theta x_i - (\alpha/\lambda)\left(e^{\lambda x_i} - 1\right)}\right]. \tag{30}$$

The following is the associated score function:

$$U_n(\varphi) = \left[\frac{\partial L(\varphi)}{\partial \theta}, \frac{\partial L(\varphi)}{\partial \alpha}, \frac{\partial L(\varphi)}{\partial \lambda}, \frac{\partial L(\varphi)}{\partial \gamma}\right]^T. \tag{31}$$

Either directly or by solving the nonlinear likelihood equations derived by differentiating equation (30), the log-likelihood can be maximized. The score vector's components of likelihood are as follows:

$$\begin{aligned}
\frac{\partial \log L(\varphi)}{\partial \theta} &= \sum_{i=1}^{n} \frac{1}{\alpha e^{\lambda x_i} + \theta} - \sum_{i=1}^{n} x_i - 2 \sum_{i=1}^{n} \frac{\overline{\gamma} x_i e^{-\theta x_i - (\alpha/\lambda)\left(e^{\lambda x_i} - 1\right)}}{1 - \overline{\gamma} e^{-\theta x_i - (\alpha/\lambda)\left(e^{\lambda x_i} - 1\right)}}, \\
\frac{\partial \log L(\varphi)}{\partial \alpha} &= \sum_{i=1}^{n} \frac{e^{\lambda x_i}}{\alpha e^{\lambda x_i} + \theta} - \frac{1}{\lambda} \sum_{i=1}^{n} \log\left(e^{\lambda x_i} - 1\right) - \frac{2}{\lambda} \sum_{i=1}^{n} \frac{\overline{\gamma} e^{-\theta x_i - (\alpha/\lambda)\left(e^{\lambda x_i} - 1\right)} \left(e^{\lambda x_i} - 1\right)}{1 - \overline{\gamma} e^{-\theta x_i - (\alpha/\lambda)\left(e^{\lambda x_i} - 1\right)}}, \\
\frac{\partial \log L(\varphi)}{\partial \lambda} &= \sum_{i=1}^{n} \frac{\alpha x_i e^{\lambda x_i}}{\alpha e^{\lambda x_i} + \theta} - \alpha \sum_{i=1}^{n} \left(\frac{x_i e^{\lambda x_i}}{\lambda} - \frac{e^{\lambda x_i} - 1}{\lambda^2}\right) \\
&\quad + \frac{2\alpha}{\lambda^2} \sum_{i=1}^{n} \frac{\overline{\gamma} e^{-\theta x_i - (\alpha/\lambda)\left(e^{\lambda x_i} - 1\right)} \left(\lambda x_i e^{\lambda x_i} - e^{\lambda x_i} + 1\right)}{1 - \overline{\gamma} e^{-\theta x_i - (\alpha/\lambda)\left(e^{\lambda x_i} - 1\right)}}, \\
\frac{\partial \log L(\varphi)}{\partial \gamma} &= \frac{n}{\gamma} - 2 \sum_{i=1}^{n} \frac{e^{-\theta x_i - (\alpha/\lambda)\left(e^{\lambda x_i} - 1\right)}}{1 - \overline{\gamma} e^{-\theta x_i - (\alpha/\lambda)\left(e^{\lambda x_i} - 1\right)}}.
\end{aligned} \tag{32}$$

The maximum likelihood estimation (MLE) of φ, say $\widehat{\varphi}$, is obtained by solving the nonlinear system $U_n(\varphi) = 0$.

5. Bayesian Estimation

The Bayesian technique deals with the parameters because random and parameter uncertainties are represented by a previous joint distribution that was formed before the failure data was collected. The flexibility of the Bayesian technique to incorporate past knowledge into research makes it particularly useful in the study of reliability, as one of the major challenges with reliability analysis is a lack of data. Prior gamma distributions are used in the θ, λ, α and γ parameters of the MOEGM distribution, where θ, λ, α, and γ are non-negative values. As separate joint prior density functions, the θ, λ, α, and γ parameters as follows:

$$\prod(\theta, \lambda, \alpha, \gamma) \propto \theta^{q_1 - 1} \lambda^{q_2 - 1} \alpha^{q_3 - 1} \gamma^{q_4 - 1} e^{-\left(w_1 \theta + w_2 \lambda + w_3 \alpha + w_4 \gamma\right)}. \tag{33}$$

The likelihood function of the MOEGM distribution and joint prior density (30) are used to produce the joint posterior density function of θ, λ, α, and γ.

$$\pi(\theta,\lambda,\alpha,\gamma|\underline{x}) = \frac{L(\underline{x}|\theta,\lambda,\alpha,\gamma)\prod(\theta,\lambda,\alpha,\gamma)}{\int_\theta\int_\lambda\int_\alpha\int_\gamma L(\underline{x}|\theta,\lambda,\alpha,\gamma)\prod(\theta,\lambda,\alpha,\gamma)\mathrm{d}\theta\mathrm{d}\lambda\mathrm{d}\alpha\mathrm{d}\gamma},$$

$$\propto L(\underline{x}|\theta,\lambda,\alpha,\gamma)\prod(\theta,\lambda,\alpha,\gamma),\ \propto \theta^{q_1-1}\lambda^{q_2-1}\alpha^{q_3-1}\gamma^{n+q_4-1}e^{-\theta\left(w_1+\sum_{i=1}^{n}x_i\right)-\alpha\left[w_3+\left(\sum_{i=1}^{n}(e^{\lambda x_i}-1)/\lambda\right)\right]}\times \tag{34}$$

$$\prod_{i=1}^{n}\frac{e^{-w_4\gamma\left(\alpha e^{-\lambda(w_2-x_i)}+\theta e^{-w_2\lambda}\right)}}{\left[1-\overline{\gamma}e^{-\theta x_i-\alpha/\lambda\left(e^{\lambda x_i}-1\right)}\right]^2}.$$

The majority of Bayesian inference algorithms are based on symmetric loss functions. A prominent symmetric loss function is the squared-error loss function (SELF). The Bayesian estimators of θ, λ, α, and γ, say $(\widetilde{\theta}_B,\widetilde{\lambda}_B,\widetilde{\alpha}_B,\widetilde{\gamma}_B)$ based on SELF.

$$\begin{aligned}\widetilde{\theta} &= E(\theta\,|\,\alpha,\lambda,\gamma,\underline{x}),\\ \widetilde{\lambda} &= E(\lambda\,|\,\alpha,\theta,\gamma,\underline{x}),\\ \widetilde{\alpha} &= E(\alpha\,|\,\theta,\lambda,\gamma,\underline{x}),\\ \widetilde{\gamma} &= E(\gamma\,|\,\theta,\lambda,\alpha,\underline{x}).\end{aligned} \tag{35}$$

It should be noted that the integrals supplied by equation (35) cannot be deduced clearly. As a result, we use Markov-Chain-Monte-Carlo (MCMC) to approximate the value of expectations in equation (35).

An observation was made that the integrals are given by equation (35) are not possible to derive explicitly. As a result, we employ the MCMC technique to approximate the value of integrals in equation (35). Many of studies used MCMC technique such as Al-Babtain et al. [25], Tolba et al. [26, 27], and Bantan et al. [28].

In Gibbs samplers, more general Metropolis algorithms are important subclasses of MCMC algorithms. Two of the most prevalent MCMC methodologies are the Metropolis-Hastings (MH) and Gibbs sampling methods. The MH technique, like acceptance-rejection sampling, assumes that each algorithm iteration can yield a candidate value from a proposal distribution. We apply the MH in the Gibbs sampling phases to get random samples of conditional posterior densities from the MOEGM distribution:

$$\begin{aligned}\pi(\theta|\lambda,\alpha,\gamma,\underline{x}) &\propto \theta^{n+q_1-1}e^{-\theta\left(w_1+\sum_{i=1}^{n}x_i\right)}\prod_{i=1}^{n}\frac{1}{\left[1-\overline{\gamma}e^{-\theta x_i-(\alpha/\lambda)\left(e^{\lambda x_i}-1\right)}\right]^2},\\ \pi(\lambda|\theta,\alpha,\gamma,\underline{x}) &\propto \lambda^{q_2-1}e^{-\left(\alpha\sum_{i=1}^{n}(e^{\lambda x_i}-1)/\lambda\right)}\prod_{i=1}^{n}\frac{e^{-\lambda(w_2-x_i)}+\theta e^{-w_2\lambda}}{\left[1-\overline{\gamma}e^{-\theta x_i-(\alpha/\lambda)\left(e^{\lambda x_i}-1\right)}\right]^2},\\ \pi(\alpha|\theta,\lambda,\gamma,\underline{x}) &\propto \alpha^{q_3-1}e^{-\alpha w_3}\prod_{i=1}^{n}\frac{\alpha}{\left[1-\overline{\gamma}e^{-\theta x_i-(\alpha/\lambda)\left(e^{\lambda x_i}-1\right)}\right]^2},\\ \pi(\gamma|\theta,\lambda,\alpha,\underline{x}) &\propto \gamma^{n+q_4-1}\prod_{i=1}^{n}\frac{e^{-w_4\gamma}}{\left[1-\overline{\gamma}e^{-\theta x_i-(\alpha/\lambda)\left(e^{\lambda x_i}-1\right)}\right]^2}.\end{aligned} \tag{36}$$

6. Simulation

The Monte-Carlo simulation approach is used in this section to compare the likelihood estimation method with the Bayesian estimation method. The *R* language is used to estimate MOEGM distribution parameters using MLE and a Bayesian estimation approach based on MCMC under SELF. Monte-Carlo experiments are carried out using 10000 randomly generated MOEGM distribution samples, where x represents the MOEGM lifetime for various parameter actual values and sample sizes n: (30, 70, 150, and 200). The best estimator approaches could be described as minimizing estimator bias ($A1$) and mean squared error ($A2$). The MOEGM distribution's true parameters have been determined.

Tables 1–3 describe the simulation results of the approaches presented in this paper for point estimate. In order to do the essential comparison between various point

estimating methods, we examine the A1 and A2 values. As a result, the following conclusions were drawn:

(1) For parameters of the MOEGM distribution, the $A1$ and $A2$ decrease as sample size n grows.
(2) The best estimating method is Bayesian estimation.
(3) The $A1$ and $A2$ for all parameters diminish as γ increases.
(4) The $A1$ and $A2$ for all parameters increase as θ increases.

7. Applications of Physics

In this section, two real-world data applications are used to demonstrate the significance of the MOEGM distribution. We employ the Akaike information criterion measures (AICM), Bayesian information criterion measures (BICM), Consistent Akaike information Criterion (AICCM), Kolmogorov-Smirnov statistics (KSS), and the PVKSS test to compare the models. Smaller values of these statistical metrics equate to a better fit to the data set. The maximum likelihood approach is used to estimate the parameters of each distribution, while the Bayesian estimation method is used to estimate the parameters of the *MOEGM* distribution.

7.1. First Real Data of Flood Peaks. In this subsection, the first application of real data set is employed to illustrate the importance of the MOEGM distribution. This data set represents 72 excrescences of flood peaks for the years 1958–1984 (rounded to one decimal place) of flood peaks (in m^3/s) of the Wheaton River near Carcross in Yukon Territory, Canada. The first data set is: "1.7, 2.5, 27.4, 1.0, 27.1, 2.2, 22.9, 1.7, 0.1, 1.1, 14.4, 1.1, 0.4, 20.6, 5.3, 0.7, 1.9, 13.0, 12.0, 9.3, 1.4, 18.7, 8.5, 25.5, 11.6, 21.5, 27.6, 36.4, 2.7, 14.1, 22.1, 1.1, 2.5, 14.4, 1.7, 37.6, 0.6, 2.2, 39.0, 0.3, 15.0, 11.0, 7.3, 0.6, 9.0, 1.7, 7.0, 20.1, 0.4, 2.8, 14.1, 9.9, 10.4, 10.7, 30.0, 3.6, 5.6, 30.8, 13.3, 4.2, 25.5, 3.4, 11.9, 64.0, 1.5, 20.2, 16.8, 5.3, 9.7, 27.5, 2.5 and 7.0." The fit of the proposed model are compared with the transmuted Gompertz-Makeham (TGM) (Abd El-Bar [29]), beta generalized Gompertz (BGG) (Benkhelifa [30]), kumaraswamy gompertz makeham (KGM) (Chukwu and Ogunde [5]), Gompertz Lomax (GL) (Oguntunde et al. [31]), exponentiated generalized Weibull-Gompertz (EGWG) (El-Bassiouny et al. [32]), generalized Gompertz (GG) (El-Gohary et al. [33]) and Gompertz models.

Table 4 presents the MLEs with standard error (SE) of the model parameters for the first data set. The values of AICM, BICM, AICCM, HQICM, KSS and the PVKS are presented for the MOEGM model and the other models.

From Table 4, we conclude that the MOEGM model gives the best fit, where the values of AICM, BICM, AICCM, HQICM, and KSS are smaller and the PVKS is higher for the MOEGM model when compared with those values of the other models. Figures 3(a), 3(b) illustrate the p.d.f., empirical c.d.f.s and probability plots, respectively, of the comparative models to show the over fitting of the MOEGM distribution. Figures 3(a)–3(c) illustrate estimated p.d.f. with histogram, estimated c.d.f. with empirical c.d.f., and Q-Q plot of the MOEGM distribution, respectively. Figures 4 and 5 clarify probability plots of the comparative models to show the over fitting of the MOEGM distribution.

Based on the results in Table 4 and Figures 3 and 4, we conclude that the MOEGM distribution is a better fit than comparative models for this data set.

Table 5 discussed MLE and Bayesian estimation methods comparing by SE, we note that the Bayesian estimation has smaller SE than MLE. The trace plots and the convergence plots of parameters by MCMC results of the MOEGM distribution are obtained in right and left Figure 6. The posterior density of MCMC findings for each parameter is shown in the center of Figure 6, which indicates a symmetric normal distribution comparable to the proposed distribution.

7.2. Second Real Data of Stochastic Processes. In this subsection, we discuss data set of stochastic processes which was first introduced by Aarset [34] and represents the lifetimes of 50 devices (in weeks). This data set, also reported in Benkhelifa [30] BGG distribution, and Abd El-Bar [29] to discuss TGM distribution, is: "0.1, 0.2, 1, 1, 1, 67, 67, 67, 72, 75, 79, 1, 1, 2, 3, 6, 7, 11, 60, 63, 63, 12, 18, 18, 85, 85, 85, 18, 18, 18, 21, 32, 36, 40, 45, 46, 47, 50, 55, 67, 82, 82, 83, 84, 84, 84, 85, 85, 86, 86." The TGM distribution is better than Gompertz, shifted Gompertz, transmuted Lindley, Gompertz Makeham, transmuted Burr type III, transmuted Gompertz, transmuted exponentiated exponential, and transmuted generalized linear exponential distributions, for more details see Abd El-Bar [29]. The BGG distribution is better than Gompertz, beta generalized exponential, generalized exponential, beta Gompertz, exponential, beta exponential, and GG, for more details see Benkhelifa [30].

Table 6 presents the MLEs of the model parameters for the stochastic processes data set. The values of AICM, BICM, AICCM, HQICM, KSS and the PVKS are presented for the MOEGM model and the TGM, and the BGG distribution.

From Table 6, we conclude that the MOEGM model gives the best fit, where the values AICM, BICM, AICCM, HQICM, and KSS are smaller for MOEFM distribution than TGM and BGG distribution, and the PVKS is higher for the MOEGM model than TGM and BGG distribution. Figures 7(a), 7(b) illustrate the p.d.f.s, empirical c.d.f.s and probability plots, respectively, of the comparative models to show the over fitting of the MOEGM distribution.

Table 1: $A1$ and $A2$ of MOEGM parameters by MLE, and Bayesian when. $\alpha = 0.5$, $\lambda = 0.5$.

			$\gamma = 0.75$				$\gamma = 3$			
$\alpha = 0.5, \lambda = 0.5$			MLE		Bayesian		MLE		Bayesian	
θ	n		$A1$	$A2$	$A1$	$A2$	$A1$	$A2$	$A1$	$A2$
0.75	30	θ	0.0663	0.2090	−0.0105	0.0807	0.1024	0.1833	−0.0064	0.0839
		α	0.2976	2.6962	−0.0118	0.0642	−0.0389	0.3818	0.0092	0.0688
		λ	0.5169	2.1535	−0.0483	0.0773	0.4304	1.0915	−0.0201	0.0679
		γ	0.6221	5.1127	−0.0147	0.0593	0.2325	3.3815	−0.0333	0.1281
	70	θ	0.0361	0.1570	−0.0009	0.0252	0.1016	0.1289	0.0094	0.0244
		α	0.0892	1.0049	−0.0178	0.0238	−0.0932	0.1873	0.0020	0.0174
		λ	0.3333	1.1596	−0.0219	0.0284	0.3409	0.4543	−0.0251	0.0271
		γ	0.2307	1.4412	−0.0108	0.0224	−0.0001	1.3741	−0.0164	0.0293
	150	θ	0.0413	0.1089	0.0009	0.0204	0.0643	0.0681	−0.0001	0.0187
		α	−0.0081	0.3685	−0.0046	0.0162	−0.0659	0.1047	0.0050	0.0119
		λ	0.2005	0.5740	−0.0189	0.0251	0.2062	0.2413	−0.0174	0.0172
		γ	0.0851	0.5711	−0.0052	0.0172	0.0176	0.6182	0.0087	0.0219
	200	θ	0.0605	0.0764	0.0019	0.0056	0.0504	0.0349	−0.0053	0.0051
		α	−0.0431	0.0853	−0.0059	0.0048	−0.0346	0.0603	0.0026	0.0045
		λ	0.1002	0.2251	−0.0083	0.0062	0.1023	0.1092	−0.0004	0.0045
		γ	0.0373	0.1438	−0.0064	0.0049	0.0306	0.4561	−0.0045	0.0064
3	30	θ	−0.6898	1.7822	−0.0026	0.1054	−0.4916	1.0311	−0.0101	0.1357
		α	0.9339	10.4192	−0.0348	0.0685	0.5875	5.2078	−0.0263	0.0934
		λ	1.5259	10.5863	−0.0581	0.1057	0.9608	5.9980	−0.0252	0.0891
		γ	0.3771	2.7854	0.0451	0.0909	0.8456	9.9552	−0.0161	0.1125
	70	θ	−0.6936	1.3025	−0.0004	0.0283	−0.4240	0.7049	−0.0079	0.0323
		α	0.5995	5.5597	−0.0336	0.0319	0.7208	4.3036	−0.0227	0.0276
		λ	0.8973	4.5855	−0.0218	0.0362	0.4344	3.7110	−0.0188	0.0314
		γ	0.0863	0.9616	−0.0041	0.0221	0.7759	9.5984	0.0030	0.0353
	150	θ	−0.4045	0.7562	−0.0024	0.0246	−0.2864	0.4528	−0.0088	0.0243
		α	0.5395	3.1483	−0.0043	0.0252	0.5922	2.7309	−0.0113	0.0204
		λ	0.3132	2.7684	−0.0180	0.0268	0.1767	2.6308	−0.0174	0.0270
		γ	0.1129	0.6149	0.0007	0.0130	0.5947	5.4817	0.0037	0.0255
	200	θ	−0.3160	0.4131	0.0007	0.0060	−0.1378	0.2110	0.0019	0.0070
		α	0.2804	0.8734	−0.0102	0.0067	0.2864	0.9394	−0.0035	0.0055
		λ	0.1636	1.3895	−0.0075	0.0081	0.0428	1.4592	−0.0057	0.0072
		γ	0.0105	0.1054	0.0013	0.0043	0.2357	2.0228	−0.0033	0.0065

Table 2: $A1$, and $A2$ of MOEGM parameters by MLE, and Bayesian when.$\alpha = 2$, $\lambda = 0.75$.

			$\gamma = 0.75$				$\gamma = 3$			
$\alpha = 2, \theta = 0.75$			MLE		Bayesian		MLE		Bayesian	
λ	n		$A1$	$A2$	$A1$	$A2$	$A1$	$A2$	$A1$	$A2$
0.5	30	θ	0.2234	1.3192	−0.0571	0.1101	0.1057	0.5171	−0.0292	0.0957
		α	0.2155	8.8678	0.0025	0.1119	−0.2657	2.6640	0.0056	0.1101
		λ	0.7288	6.6163	−0.0177	0.0883	0.6797	2.8948	−0.0474	0.0687
		γ	0.5717	5.5573	0.0139	0.0535	0.6411	9.8986	−0.0285	0.1085
	70	θ	0.0565	0.9048	−0.0155	0.0298	0.0954	0.3111	−0.0119	0.0304
		α	0.0168	3.6365	−0.0194	0.0301	−0.1759	1.2053	−0.0051	0.0262
		λ	0.2718	2.7239	−0.0203	0.0316	0.3094	1.1250	−0.0149	0.0300
		γ	0.2262	1.9272	0.0014	0.0197	0.3733	7.0686	−0.0003	0.0335
	150	θ	0.0826	0.6743	−0.0187	0.0269	0.0326	0.1921	−0.0013	0.0216
		α	0.1547	3.0759	−0.0044	0.0227	−0.2055	0.4865	−0.0038	0.0205
		λ	0.0107	1.8665	−0.0170	0.0246	0.2044	0.4764	−0.0012	0.0200
		γ	0.2081	1.3476	−0.00001	0.0155	−0.0034	2.7353	0.0001	0.0258
	200	θ	0.0121	0.3445	0.00004	0.0064	0.0015	0.0763	−0.0033	0.0063
		α	−0.0127	0.9029	−0.0012	0.0058	−0.1218	0.2391	0.0017	0.0059
		λ	0.0517	0.6778	−0.0063	0.0066	0.1161	0.1799	−0.0056	0.0053
		γ	0.0401	0.3068	0.0013	0.0043	−0.0460	1.2654	−0.0002	0.0059

Table 2: Continued.

			$\gamma = 0.75$				$\gamma = 3$			
$\alpha = 2, \theta = 0.75$			MLE		Bayesian		MLE		Bayesian	
λ	n		$A1$	$A2$	$A1$	$A2$	$A1$	$A2$	$A1$	$A2$
3	30	θ	0.5940	2.3168	−0.0579	0.1390	0.1581	1.38285	−0.0576	0.11203
		α	0.0865	5.9463	−0.0084	0.0992	−0.2814	2.56117	0.0197	0.10938
		λ	0.9393	9.0583	−0.0141	0.1159	1.1403	5.1957	−0.0045	0.1068
		γ	0.5021	3.3756	0.0013	0.0544	0.2552	9.34188	−0.0265	0.12716
	70	θ	0.4157	1.2562	−0.0165	0.0327	0.1110	0.45985	−0.0051	0.03112
		α	0.0020	3.1157	−0.0081	0.0297	−0.1964	1.6083	−0.0062	0.0274
		λ	0.4155	3.8968	−0.0107	0.0295	0.6467	2.39636	−0.0168	0.02602
		γ	0.2856	1.5833	−0.0040	0.0207	0.1558	4.69425	−0.0031	0.03366
	150	θ	0.2229	0.6404	−0.0268	0.0249	0.1088	0.1939	−0.0139	0.0266
		α	−0.1318	1.2423	0.0052	0.0212	−0.1068	0.99542	0.0015	0.02033
		λ	0.3486	2.0025	−0.0055	0.0249	0.3275	1.06376	−0.0004	0.02312
		γ	0.1034	0.6022	0.0004	0.0142	0.1821	2.7484	−0.0116	0.0256
	200	θ	0.0952	0.2498	−0.0003	0.0058	0.0622	0.06397	−0.0057	0.00671
		α	−0.1570	0.5557	−0.0010	0.0061	−0.0534	0.58078	−0.0028	0.00549
		λ	0.2533	0.7987	0.0012	0.0061	0.1733	0.5270	−0.0043	0.0058
		γ	0.0112	0.1641	0.0020	0.0042	0.1292	1.52845	−0.0012	0.00647

Table 3: $A1$ and $A2$ of MOEGM parameters by MLE, and Bayesian when.$\alpha = 1.5$, $\lambda = 2$.

			$\gamma = 0.75$				$\gamma = 3$			
$\theta = 1.5, \lambda = 2$			MLE		Bayesian		MLE		Bayesian	
α	n		$A1$	$A2$	$A1$	$A2$	$A1$	$A2$	$A1$	$A2$
2	30	θ	0.3758	2.0520	−0.0504	0.1184	0.1751	1.3836	−0.0540	0.1333
		α	0.1679	7.5009	−0.0406	0.1219	−0.0944	3.4698	−0.0152	0.1037
		λ	1.2045	10.8415	−0.0046	0.1205	1.0588	6.0416	0.0114	0.1023
		γ	0.4812	3.8034	0.0184	0.0523	0.8747	9.6510	−0.0330	0.1342
	70	θ	0.1450	1.1987	−0.0010	0.0338	0.2552	0.7051	−0.0007	0.0292
		α	−0.1459	2.9704	−0.0025	0.0295	−0.1261	1.7495	−0.0012	0.0275
		λ	0.7292	5.2783	−0.0206	0.0307	0.5441	2.7962	−0.0113	0.0273
		γ	0.0962	0.7837	0.0040	0.0190	0.5367	7.7801	−0.0064	0.0333
	150	θ	0.1380	0.7847	0.0020	0.0247	0.1120	0.2308	−0.0063	0.0263
		α	−0.0373	1.3426	−0.0046	0.0252	−0.1260	0.9165	−0.0007	0.0208
		λ	0.2790	2.4414	−0.0041	0.0288	0.3392	1.2381	−0.0091	0.0231
		γ	0.0879	0.4284	0.0054	0.0142	0.2194	3.2863	−0.0066	0.0243
	200	θ	0.0384	0.3915	−0.0017	0.0065	0.0734	0.1321	−0.0037	0.0061
		α	−0.1123	0.4354	0.0009	0.0069	−0.0612	0.5020	0.0042	0.0064
		λ	0.2016	0.9034	−0.0012	0.0064	0.1647	0.5829	−0.0015	0.0059
		γ	0.0069	0.1181	−0.0038	0.0046	0.1241	1.5795	0.0004	0.0066
4	30	θ	0.2236	3.2384	−0.0636	0.1240	0.2958	2.5922	−0.0100	0.1290
		α	−0.1682	7.2254	−0.0192	0.1180	−0.6578	7.8654	−0.0266	0.1177
		λ	1.1611	9.1960	−0.0561	0.1317	1.5862	9.9355	0.0020	0.1226
		γ	0.2173	1.4663	0.0239	0.0529	0.9513	9.4847	−0.0503	0.1214
	70	θ	0.2432	2.8862	−0.0067	0.0291	0.2506	1.9412	−0.0095	0.0343
		α	0.0337	5.1864	−0.0036	0.0326	−0.5213	4.9119	−0.0199	0.0336
		λ	0.3411	6.1987	−0.0065	0.0278	0.8382	5.8843	−0.0292	0.0346
		γ	0.1539	0.7071	0.0074	0.0197	0.4678	10.9169	−0.0150	0.0357
	150	θ	0.0727	1.3884	−0.0028	0.0246	0.0395	0.9230	−0.0098	0.0262
		α	−0.1128	1.7539	−0.0143	0.0257	−0.3259	2.2341	0.0030	0.0261
		λ	0.2263	2.2326	−0.0131	0.0249	0.4201	2.2449	−0.0039	0.0222
		γ	0.0540	0.2351	0.0067	0.0117	0.0980	3.8122	−0.0031	0.0239
	200	θ	0.0722	0.9579	0.0036	0.0074	0.0215	0.6763	0.0000	0.0060
		α	−0.0290	1.1019	−0.0035	0.0062	−0.2542	1.3980	−0.0041	0.0062
		λ	0.0586	1.4141	0.0012	0.0065	0.2818	1.1992	−0.0040	0.0073
		γ	0.0331	0.1423	0.0021	0.0043	0.0397	2.1774	0.0021	0.0069

Table 4: MLEs of the models parameters with SE and different measures for fitting: flood peaks data.

		MLEs	SE	KSS	PVKS	CVMS	ADS	AICM	AICCM	BICM	HQICM
MOEGM	θ	0.0141	0.0569	0.0985	0.4873	0.1014	0.5756	506.9077	507.5047	516.0144	510.5331
	α	0.0185	0.0379								
	λ	0.0319	0.0382								
	γ	0.2966	0.3969								
GL	θ	1.7323	3.7299	0.0999	0.4691	0.1193	0.6709	507.6678	508.2648	516.7744	511.2931
	α	0.4989	3.6786								
	λ	1.2268	5.6233								
	γ	0.1877	0.6431								
Gompertz	λ	0.0013	0.0081	0.1463	0.0918	0.1120	0.6459	508.2565	508.429	518.8094	512.8534
	α	0.0852	0.0148								
EGWG	θ	1.6924	19.7580	0.1026	0.4351	0.1027	0.6039	509.3512	510.2603	520.7345	513.8829
	λ	0.4178	4.5617								
	α	0.1118	4.4805								
	γ	0.5656	3.0847								
	β	0.3331	0.4674								
BGG	λ	0.0123	0.0191	0.0998	0.4799	0.4754	0.5876	508.5600	509.4691	519.9433	513.0917
	α	0.0331	0.0851								
	γ	0.5632	1.6298								
	θ	1.4283	4.6792								
	β	1.6742	3.1784								
KGM	λ	0.0229	0.0442	0.1034	0.4251	0.1102	0.5928	508.7930	509.7020	520.1763	513.3247
	α	0.0160	0.0508								
	γ	0.0399	0.0788								
	a	0.7910	0.1410								
	b	1.1351	0.9661								
TGM	λ	0.0036	0.0596	0.1290	0.1821	0.1112	0.6376	508.4915	509.0885	517.5982	512.1169
	α	0.0655	0.0499								
	θ	0.0053	0.0060								
	γ	0.2544	0.4056								

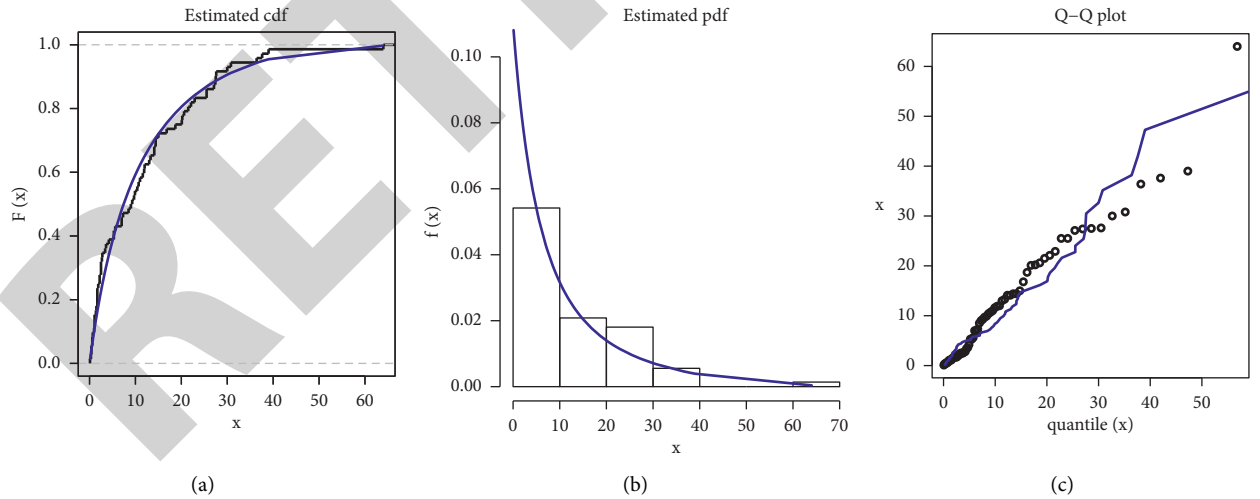

Figure 3: (a) Histogram and estimated p.d.f., (b) Estimated c.d.f. and the empirical c.d.f., (c) generate qunatile and data: flood peaks data.

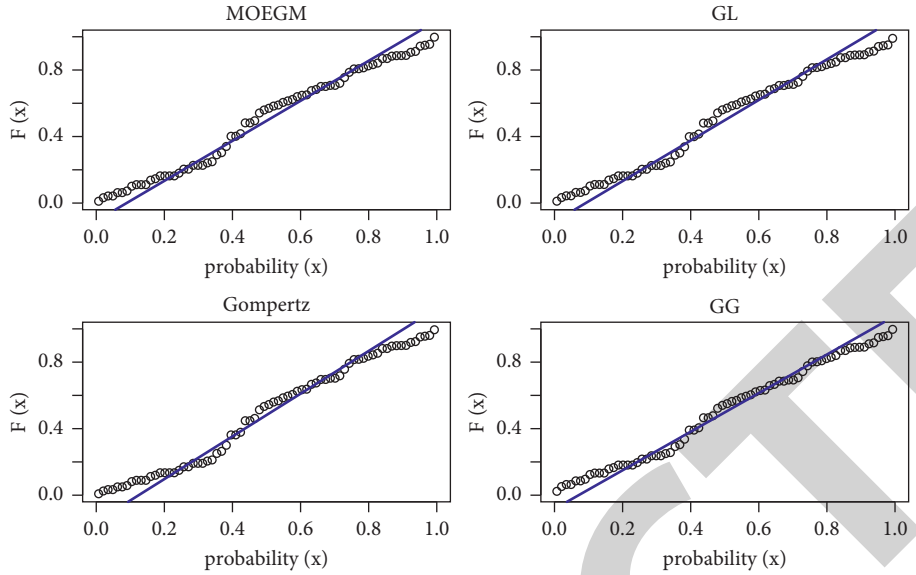

Figure 4: PP plot for different models.

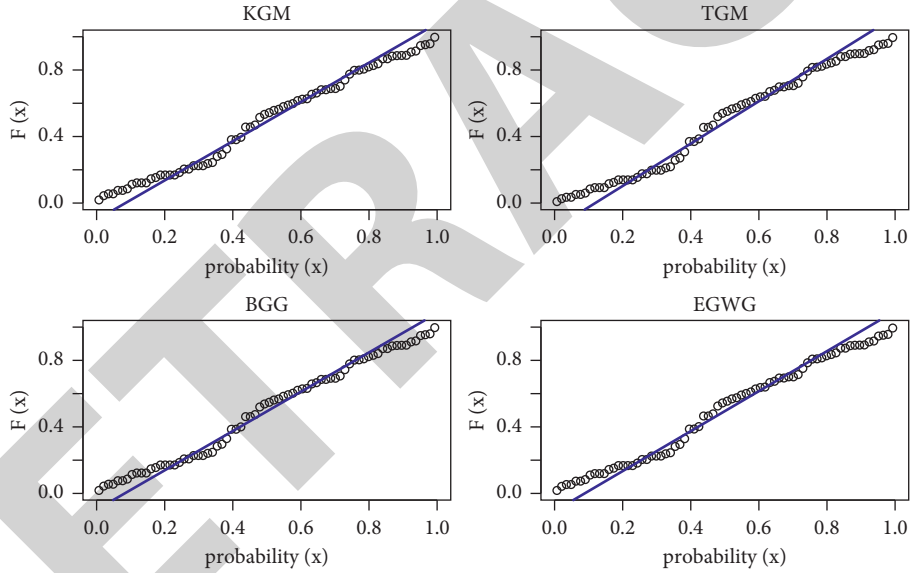

Figure 5: PP plot for different models.

Table 5: MLE and Bayesian estimation methods comparing by SE: flood peaks data.

	MLE		Bayesian	
	Estimates	SE	Estimates	SE
θ	0.0141	0.0569	0.014041	0.003221
α	0.0185	0.0379	0.018479	0.001432
λ	0.0319	0.0382	0.031859	0.001461
γ	0.2966	0.3969	0.294978	0.148231

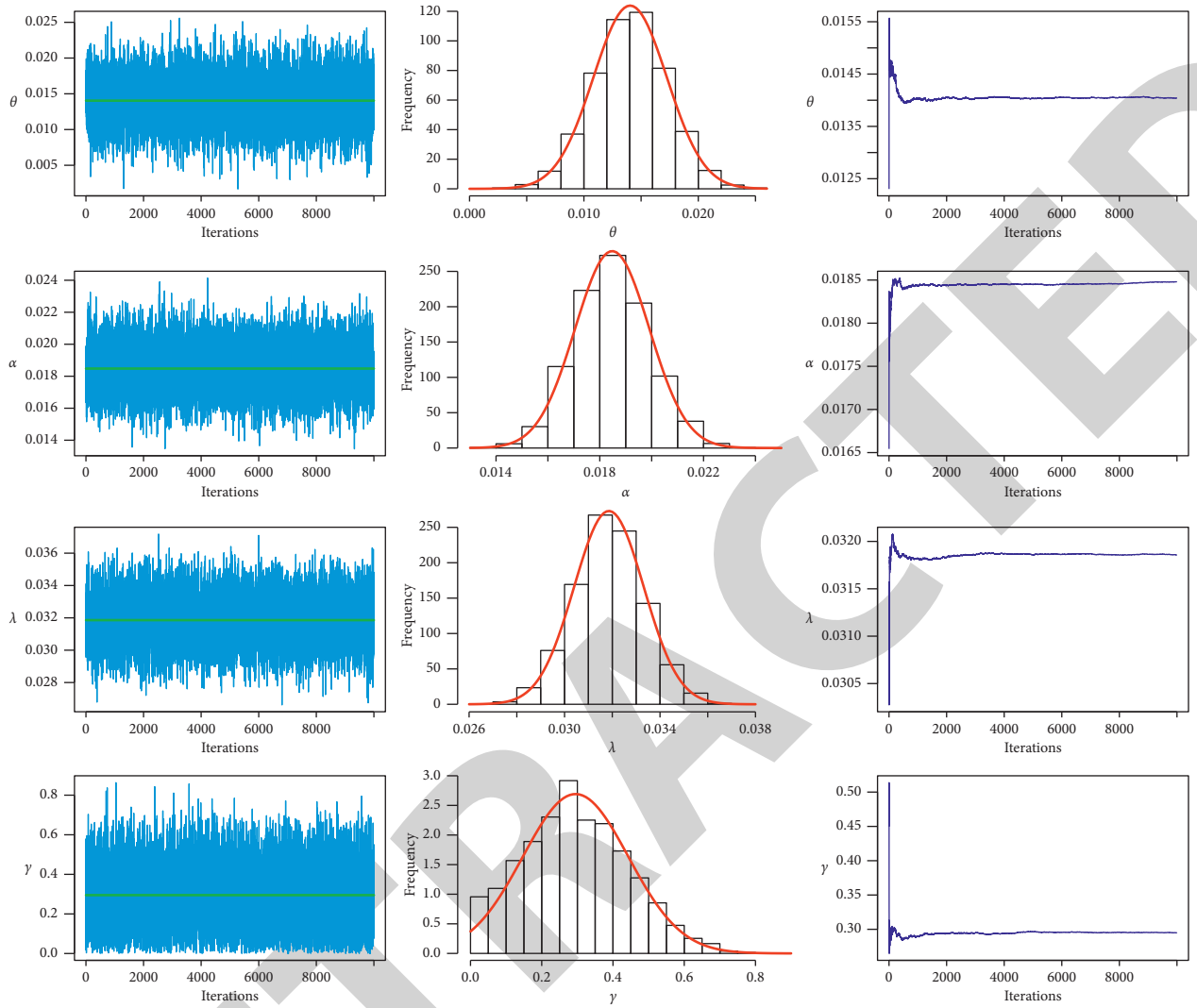

Figure 6: The trace plots, posterior density and the convergence for parameters θ, α, λ and γ: flood peaks data.

Table 6: Comparison between MOEGM, BGG and TGM distributions:stochastic processes data.

	θ	α	λ	γ	b	KSS
MOEGM	0.0096	$1.593E-10$	0.2511	0.5168		0.1265
TGM	0.0998	0.0003	0.0115	0.1280		0.1517
BGG	0.0638	0.0029	1.3644	0.1198	0.1776	0.1266
	CVMS	AICM	AICCM	BICM	HQICM	PVKS
MOEGM	0.1214	440.6824	441.5713	448.3305	443.5948	0.4003
TGM	0.2751	454.0590	454.9480	461.7070	456.9710	0.2002
BGG	0.157543	461.0024	462.366	470.5625	464.6429	0.3871

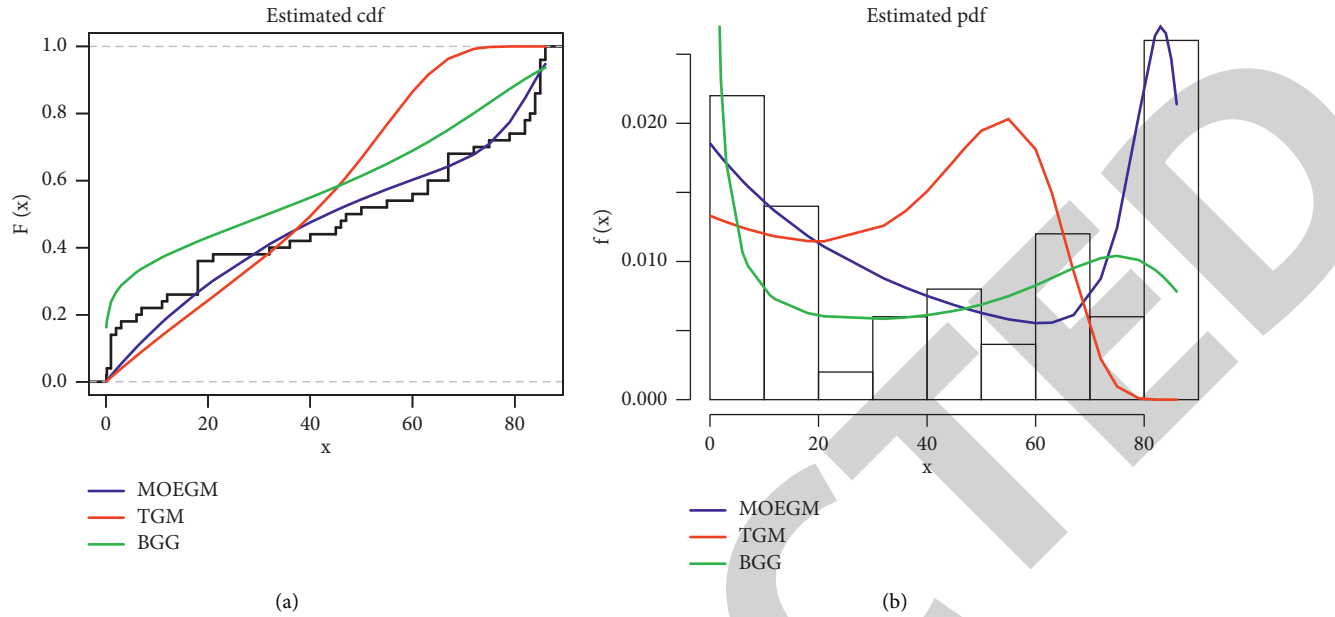

Figure 7: (a) Histogram and estimated p.d.f., (b) Estimated c.d.f. and the empirical c.d.f.: stochastic processes data.

Table 7: MLE and Bayesian estimation methods comparing by SE: stochastic processes data.

	MLE		Bayesisna	
	Estimates	SE	Estimates	SE
θ	0.0096	0.3547	0.4195	0.2138
α	$1.593E-10$	$8.680E-07$	$3.34E-09$	$4.13E-09$
λ	0.2511	0.0945	0.2514	0.0338
γ	0.5168	0.0568	0.5015	0.0191

Table 7 discussed MLE and Bayesian estimation methods comparing by SE, we note Bayesian estimation has smaller SE than MLE.

8. Conclusion

Based on Marshall and Olkin approach, a new four-parameter extended Gompertz Makeham distribution was developed, the Marshall-Olkin extended Gompertz Makeham distribution. It includes special models, the Marshall-Olkin extended Makeham, Marshall-Olkin Gompertz Makeham, Gompertz Makeham, and Makeham distributions. Depending on the shape parameters, the MOEGM density function can take on a variety of shapes. Furthermore, depending on the design parameters, its hazard rate function might take on various shapes. We have included some statistical features. The method of likelihood and Bayesian estimation methods are used to estimate the unknown parameters of the proposed distribution. An MCMC technique is used to give a comparison for the estimated parameters. These comparisons were made using bias and MSE as criteria. The MSE and Bias of the Bayesian-based SELF are superior to both MLE in our simulation case. Real data sets were observed and it was noted that the MOEGM distribution resulted in the best fit. To summaries, the MOEGM distribution may provide a relatively flexible mechanism for fitting a wide range of positive real-world data sets. The novel distribution may be a feasible alternative to existing models now available in the literature for modeling actual data in domains like as engineering, survival analysis, hydrology, economics, and others.

Data Availability

The data used to corroborate the study's conclusions is supplied in the paper.

Conflicts of Interest

The authors declare no conflicts of interest.

Acknowledgments

The authors would like to thank their universities. The authors would also like to thank everyone who helped in improving the paper. This project is supported by Researchers Supporting Project number (RSP-2021/156), King Saud University, Riyadh, Saudi Arabia.

References

[1] B. Gompertz, "On the nature of the function expressive of the law of human mortality, and on a new mode of determining the value of life contingencies," *Philosophical Transactions of the Royal Society of London*, vol. 115, pp. 513–583, 1825.

[2] W. M. Makeham, "On the law of mortality and the construction of annuity tables," *The Assurance Magazine and Journal of the Institute of Actuaries*, vol. 8, no. 6, pp. 301–310, 1860.

[3] R. C. Bailey, L. D. Homer, and J. P. Summe, "A proposal for the analysis of kidney graft survival," *Transplantation*, vol. 24, pp. 309–15, 1977.

Hindawi
Journal of Mathematics
Volume 2023, Article ID 9806481, 1 page
https://doi.org/10.1155/2023/9806481

Retraction

Retracted: A New Four-Parameter Inverse Weibull Model: Statistical Properties and Applications

Journal of Mathematics

Received 10 October 2023; Accepted 10 October 2023; Published 11 October 2023

This article has been retracted by Hindawi following an investigation undertaken by the publisher [1]. This investigation has uncovered evidence of one or more of the following indicators of systematic manipulation of the publication process:

(1) Discrepancies in scope

(2) Discrepancies in the description of the research reported

(3) Discrepancies between the availability of data and the research described

(4) Inappropriate citations

(5) Incoherent, meaningless and/or irrelevant content included in the article

(6) Peer-review manipulation

The presence of these indicators undermines our confidence in the integrity of the article's content and we cannot, therefore, vouch for its reliability. Please note that this notice is intended solely to alert readers that the content of this article is unreliable. We have not investigated whether authors were aware of or involved in the systematic manipulation of the publication process.

Wiley and Hindawi regrets that the usual quality checks did not identify these issues before publication and have since put additional measures in place to safeguard research integrity.

We wish to credit our own Research Integrity and Research Publishing teams and anonymous and named external researchers and research integrity experts for contributing to this investigation.

The corresponding author, as the representative of all authors, has been given the opportunity to register their agreement or disagreement to this retraction. We have kept a record of any response received.

References

[1] N. Yahia and N. Alsadat, "A New Four-Parameter Inverse Weibull Model: Statistical Properties and Applications," *Journal of Mathematics*, vol. 2022, Article ID 5936783, 6 pages, 2022.

Hindawi
Journal of Mathematics
Volume 2022, Article ID 5936783, 6 pages
https://doi.org/10.1155/2022/5936783

Research Article

A New Four-Parameter Inverse Weibull Model: Statistical Properties and Applications

Nagla Yahia [1,2] **and Najwan Alsadat** [3]

[1]*Cairo University, Faculty of Economics and Political Sciences, Department of Statistics, Giza, Egypt*
[2]*Department of Statistics, Faculty of Science, Al-Faisaliah Campus, University of Jeddah, Jeddah 21438, Saudi Arabia*
[3]*King Saud University, College of Business Administration, Department of Quantitative Analysis, Riyadh, Saudi Arabia*

Correspondence should be addressed to Nagla Yahia; naglayehia1966@cu.edu.eg

Received 15 March 2022; Revised 15 April 2022; Accepted 5 May 2022; Published 13 June 2022

Academic Editor: Naeem Jan

A four-parameter Type II Topp Leone generalized inverse Weibull (TIITLGINW) model is suggested. The reliability study of the new model is provided. Quantiles, moments, moment generating function, and probability weighted moment are some of the mathematical properties being researched. The maximum likelihood (ML) estimate is employed for TIITLGINW parameters. A simulation study is conducted to estimate the model parameters of the TIITLGINW model. A single real-world collection of data is used to analyze TIITLGINW's significance and accessibility.

1. Introduction

Because of its failure rate, the inverse Weibull (INW) model has a broader applicability in the field of dependability and biological investigations. Keller and Kanath [1] proposed the INW model to investigate the form of the density function (pdf) and hazard rate function (FUN) (hrf). The INW model fits numerous datasets through terms of the time required for an insulated fluid to decompose, the topic of which led to the action of continuous tension. Nelson and Jiang et al. [2, 3] presented Weibull (W) and INW mixing models [4]. Models with two INW models were examined [5]. The flexibility of the INW model was investigated [6]. Bayesian and maximum likelihood estimates of the INW parameters with progressive type-II censoring were examined.

The probability density function (pdf) and cumulative FUN (cdf) of the generalized INW (GINW) model are given by [7]

$$f(z;\mu,\eta,\gamma)=\frac{\gamma\eta\mu^{\eta}}{z^{\eta+1}}e^{-\gamma(\mu/z)^{\eta}},\quad z,\mu,\eta,\ \gamma>0, \tag{1}$$

and

$$F(z;\mu,\eta,\gamma)=e^{-\gamma(\mu/z)^{\eta}},\quad z,\mu,\eta,\ \gamma>0. \tag{2}$$

The INW model has recently been introduced in statistical theory literature [8]. A modified INW model was suggested, while Shahbaz et al. [9] proposed the Kumaraswamy INW model. Hanook et al. [10] developed the beta INW model, whereas Khan et al. [11] investigated features of the transmuted INW model [12]. The Topp Leone (TL) INW model was presented [13]. The beta generalized INW geometric model was investigated. Alkarni et al. [14] proposed the extended INW model. Even power weighted generalized INW distribution was studied by Mutlk and Al-Dubaicy [15], Algarni et al. [16] proposed classical and Bayesian estimation of the INW distribution under progressive type-I censoring scheme, Al-Moisheer et al. [17] discussed the odd inverse power generalized Weibull generated family of distributions, and Ahmadini et al. [18] studied estimation of the constant stress partially accelerated life test for INW distribution with type-I censoring.

Ahmadini et al. [18] investigated the Type II TL class (TIITL) class of models. In addition, Elgarhy et al. [19] developed a three-parameter TIITLINW model. The TIITL class cdf is supplied via

$$F(z;\ \mu,\ \omega)=1-\left[1-[G(x;\omega)]^{2}\right]^{\mu}. \tag{3}$$

The equivalent pdf to (3) is produced via

$$f(z;\mu,\omega) = 2\mu g(z;\omega)G(z;\omega) \cdot \left[1-[G(z;\omega)]^2\right]^{\mu-1}, \quad z \in R,\ \mu > 0. \tag{4}$$

The main goal of this study is as follows:

To introduce a new four-parameter model which is called Type II Topp Leone generalized inverse Weibull model

The suggested model is very flexible and contains many submodels

The suggested model has closed form of quantile

The pdf of the suggested model can be unimodal and right skewness. Also, the hazard rate function can be increasing and J-shaped.

The following is how this document is structured. The Section 2 defines the new model (which is a broad model). The Section 3 investigates the linear formulation of the TIITLGINW model's pdf. Section 4 investigates statistical characteristics. In the Section 5, the ML estimation approach is used to generate the estimates of the TIITLGINW parameters. In Section 6, a simulation study is carried out to determine the model parameters of the TIITLGINW model. Section 7 employs the study of a single real-world data collection. Section 8 has concluding observations.

2. The New Model

Inside this section, we develop the TIITLGINW model, a novel lifespan model. The cdf of the TIITLGINW model with set of parameters $\varphi = (\mu, \eta, \rho, \gamma)$ is computed by inserting (2) into (3) as follows:

$$G(z;\varphi) = 1-\left[1-e^{-2\gamma(\mu/z)^{\eta}}\right]^{\rho}. \tag{5}$$

Inserting (1) and (2) into (4) yields the matching pdf to (5):

$$g(z;\varphi) = 2\rho\gamma\eta\mu^{\eta}z^{-\eta-1}e^{-2\gamma(\mu/z)^{\eta}} \cdot \left[1-e^{-2\gamma(\mu/z)^{\eta}}\right]^{\rho-1}, \quad z,\rho,\mu,\eta,\gamma > 0, \tag{6}$$

where μ and γ are the scale parameters and ρ, η are the two shape parameters.

The TIITLGINW model is a highly adaptable model that contains several additional models. The submodels of the TIITLGINW model are given in Table 1.

Figure 1 shows different TIITLGINW pdf graphs for appropriate parameter combinations.

X's survival FUN (sf), hrf, inverted hrf, and cumulative hrf are described as follows:

$$R(z;\varphi) = \left[1-e^{-2\gamma(\mu/z)^{\eta}}\right]^{\rho}, \quad z,\rho,\mu,\eta,\gamma > 0, \tag{7}$$

$$h(z;\varphi) = \frac{2\rho\gamma\eta\mu^{\eta}z^{-\eta-1}e^{-2\gamma(\mu/z)^{\eta}}}{1-e^{-2\gamma(\mu/z)^{\eta}}}, \tag{8}$$

$$\tau(z;\varphi) = \frac{2\rho\gamma\eta\mu^{\eta}z^{-\eta-1}e^{-2\gamma(\mu/z)^{\eta}}\left[1-e^{-2\gamma(\mu/z)^{\eta}}\right]^{\rho-1}}{1-\left[1-e^{-2\gamma(\mu/z)^{\eta}}\right]^{\rho}}, \tag{9}$$

$$H(z;\varphi) = -\ln\left[1-e^{-2\gamma(\mu/z)^{\eta}}\right]^{\rho}. \tag{10}$$

Figure 2 shows different TIITLGINW hrf graphs for appropriate parameter combinations.

3. Useful Expansion

Inside this part, we propose two useful pdf and cdf expansions for the TIITLGINW model. Now, examine the binomial series:

$$(1-a)^n = \sum_{k=0}^{\infty}(-1)^k\binom{a}{k}a^k, \quad 0 < a < 1. \tag{11}$$

As a result of using (11), the accompanying phrase within (6) can be indicated:

$$\left(1-e^{-2\gamma\left(\mu/z_i\right)^{\eta}}\right)^{\rho-1} = \sum_{i=0}^{\infty}(-1)^i\binom{\rho-1}{i}e^{-2\gamma\left(\mu/z_i\right)^{\eta}}. \tag{12}$$

After several simplifications, we arrive at

$$f(z) = \eta\mu^{\eta}\sum_{i=0}^{\infty}W_i z^{-\eta-1}e^{-2(i+1)\gamma\left(\mu/z_i\right)^{\eta}}, \tag{13}$$

where $w_i = 2(-1)^i\binom{\rho-1}{i}\rho\gamma$.

Also, the expansion of cdf can be expressed as follows:

$$[F(z)]^h = \left[1-\left(1-e^{-2\gamma\left(\mu/z_i\right)^{\eta}}\right)^{\rho}\right]^h. \tag{14}$$

Then,

$$[F(z)]^h = \sum_{k=0}^{\infty}W_k e^{-2k\gamma\left(\mu/z_i\right)^{\eta}}, \tag{15}$$

where $w_k = \sum_{j=0}^{h}(-1)^{j+k}\binom{h}{j}\binom{\rho j}{k}$.

4. Fundamental Mathematical Features

Numerous statistical features of the TIITLGINW model are obtained in this section.

4.1. Quantile Function. The quantile FUN of Z, denoted by Z_u, is determined via

$$Zu = \mu\left(\frac{-1}{\gamma}ln\sqrt{1-(1-u)^{1/\rho}}\right)^{(-1/\eta)}. \tag{16}$$

Table 1: Submodels of the TIITLGINW model.

	Model	ρ	μ	η	γ	cdf	Author
1	TIITLGINR	—	—	—	1	$F(z;\rho,\mu,\gamma) = 1-[1-e^{-2\gamma(\mu/z)^2}]^{\rho}$	New
2	TIITLGINE	—	—	—	2	$F(z;\rho,\mu,\gamma) = 1-[1-e^{-(2\gamma\mu/z)}]^{\rho}$	New
3	TIITLINW	—	1	—	—	$F(z;\rho,\mu) = 1-[1-e^{-2(\mu/z)^2}]^{\rho}$	New
4	TIITLINR	—	1	—	1	$F(z;\rho,\mu) = 1-[1-e^{-2(\mu/z)^2}]^{\rho}$	New
5	TIITLINE	—	1	—	2	$F(z;\rho,\mu) = 1-[1-e^{-(2\mu/z)}]^{\rho}$	New

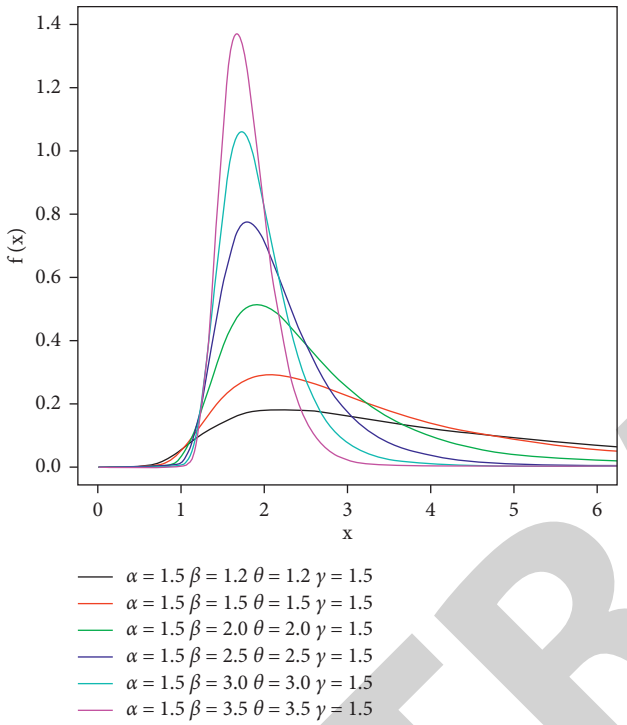

Figure 1: TIITLGINW pdf graphs for appropriate parameter combinations.

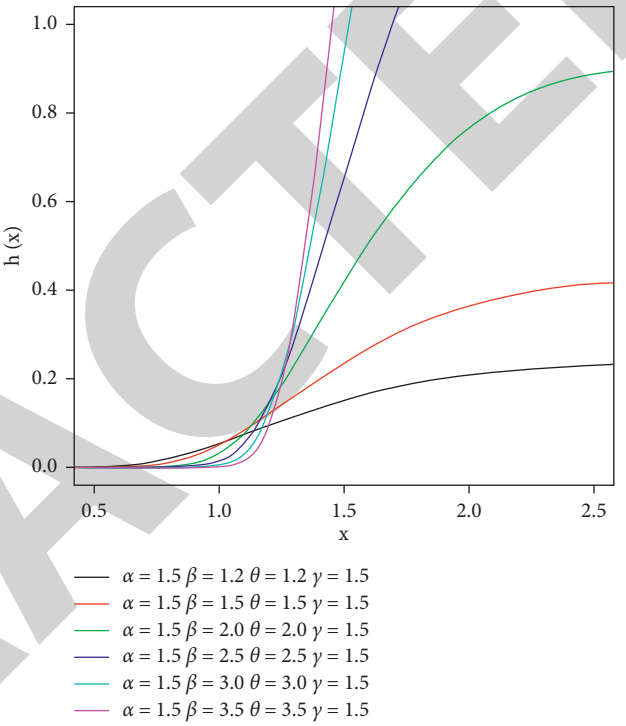

Figure 2: TIITLGINW hrf graphs for appropriate parameter combinations.

4.2. Different Types of Moments. The r^{th} moment (Mom) of Z may be determined utilizing relation.

$$\mu_r' = E(Z^r) = \int_{-\infty}^{\infty} z^r g(z;\varphi)dz. \tag{17}$$

Simply replacing (13) within (17) results in

$$\mu_r' = \sum_{i=0}^{\infty} W_i \int_0^{\infty} z^{r-\eta-1} e^{-2(i+1)\gamma(\mu/z_i)^{\eta}} dz. \tag{18}$$

Suppose $y = (\mu/z_i)^{\eta}$; after that,

$$\mu_r' = \mu^r \sum_{i=0}^{\infty} W \int_i^{\infty} y e^{-2(i+1)\gamma y} dy. \tag{19}$$

Then, μ_r' becomes

$$\mu_r' = \mu^r \sum_{i=0}^{\infty} W_i \frac{\Gamma(1-(r/\eta))}{(2(i+1)\gamma)^{(1-(r/\eta))}}, \quad \frac{r}{\eta} < 1. \tag{20}$$

The TIITLGINW model's Mom generating FUN is provided by

$$M_Z(t) = \sum_{r=0}^{\infty} \frac{t^r}{r!} E(Z^r) = \sum_{r,i=0}^{\infty} \frac{t^r}{r!} \frac{w_i \Gamma(1-(r/\beta))}{[2(i+1)\gamma]^{(1-(r/\beta))}}, \quad r/\beta < 1. \tag{21}$$

The probability weighted Mom (PrWMs) may be computed as follows:

$$\tau_{r,s} = E[Z^r G(z)^s] = \int_{-\infty}^{\infty} x^r g(z)(G(z))^s dz. \tag{22}$$

Trying to insert (13) and (6) within (22), we get

$$\tau_{r,s} = \sum_{i,k=0}^{\infty} W_i W_k \int_0^{\infty} z^{r-\eta-1} e^{-2(i+k+1)\gamma(\mu/z_i)^{\eta}} dz. \tag{23}$$

As a result, the PrWM of the TIITLGINW model looks like

$$\tau_{r,s} = \mu^r \sum_{i,k=0}^{\infty} W_i W_k \frac{\Gamma(1-(r/\eta))}{(2(i+k+1)\gamma)^{(1-(r/\eta))}}, \quad \frac{r}{\eta} < 1. \tag{24}$$

Table 2: Numerous numerical values of MLEs and C1 of the TIITLGINW model.

n	Par	MLE	C1	MLE	C1
		Set 1: (0.5, 0.5, 0.5, 0.5)		Set 2: (0.5, 0.5, 0.5, 0.5)	
30	μ	0.4870	0.0071	0.4991	0.0042
	η	0.4711	0.0212	1.5740	0.2106
	ρ	0.4664	0.0163	0.5386	0.0424
	γ	0.3743	0.0329	0.8978	0.5204
50	μ	0.5217	0.0031	0.4917	0.0030
	η	0.4862	0.0102	1.5609	0.1372
	ρ	0.5095	0.0071	0.5054	0.0227
	γ	0.3871	0.0245	0.7790	0.3332
200	μ	0.5007	0.0011	0.5021	0.0016
	η	0.4889	0.0033	1.5440	0.0447
	ρ	0.5078	0.0027	0.5155	0.0117
	γ	0.4073	0.0127	0.7120	0.0856
		Set 3: (0.5, 0.5, 0.5, 0.3)		Set 4: (0.5, 1.5, 0.5, 0.3)	
30	μ	0.5410	0.0162	0.5118	0.0136
	η	0.5525	0.0512	1.8293	0.6032
	ρ	0.5455	0.0332	1.0048	2.5698
	γ	0.4392	0.1288	0.4504	0.2833
50	μ	0.5526	0.0097	0.5280	0.0082
	η	0.5478	0.0276	1.7470	0.2578
	ρ	0.5551	0.0173	0.6603	0.1249
	γ	0.3953	0.0391	0.3532	0.0251
200	μ	0.4849	0.0012	0.4809	0.0017
	η	0.4405	0.0061	1.6474	0.0560
	ρ	0.4713	0.0028	0.4649	0.0086
	γ	0.2932	0.0028	0.2548	0.0042
		Set 5: (0.3, 0.8, 0.3, 0.5)		Set 6: (0.3, 0.5, 0.3, 0.3)	
30	μ	0.2961	0.0030	0.3516	0.0106
	η	0.8937	0.2663	0.4791	0.0338
	ρ	0.3563	0.0362	0.4123	0.0572
	γ	0.5952	0.5313	0.1735	0.6286
50	μ	0.2888	0.0010	0.3049	0.0021
	η	0.6398	0.0470	0.3800	0.0218
	ρ	0.2708	0.0048	0.3028	0.0061
	γ	0.2629	0.0633	0.1901	0.4063
200	μ	0.3048	0.0005	0.3041	0.0003
	η	0.7341	0.0092	0.3934	0.0131
	ρ	0.3122	0.0017	0.3094	0.0014
	γ	0.3184	0.0354	0.4173	0.0356

5. ML Method of Approach

The ML estimates (MLEs) of the unknown parameters for such TIITLGINW model are produced using complete samples. Assume $Z_1, \ldots, Z_n$ be seen from the TIITLGINW model with something like a certain number of parameters $\varphi = (\mu, \eta, \rho, \gamma)^T$. The total log-likelihood (LL) FUN for the vector of parameters φ may be phrased as

$$\begin{aligned}\ln L(\varphi) = {} & n \ln 2\ \rho + n \ln \gamma + n \ln \eta + n\eta \ln \mu \\ & - (\eta + 1) \sum_{i=1}^{n} \ln z_i - 2\gamma \sum_{i=1}^{n} \left(\frac{\mu}{z_i}\right)^{\eta} \\ & + (\rho - 1) \sum_{i=1}^{n} \ln\left[1 - e^{-2\gamma (\mu/z_i)^{\eta}}\right]. \end{aligned} \tag{25}$$

The scoring FUN $U(\varphi) = (U_\mu, U_\eta, U_\rho, U_\gamma)$ elements are specified by

$$\begin{aligned} U_\mu = {} & \frac{n\eta}{\mu} - 2\gamma\eta\mu^{\eta-1} \sum_{i=1}^{n} z_i^{-\eta} \\ & + 2\gamma\eta\mu^{\eta-1} (\rho - 1) \sum_{i=1}^{n} \frac{z_i^{-\eta} e^{-2\gamma (\mu/z_i)^{\eta}}}{1 - e^{-2\gamma (\mu/x_i)^{\eta}}}, \end{aligned} \tag{26}$$

$$\begin{aligned} U_\eta = {} & \frac{n}{\eta} - n \ln \mu - \sum_{i=1}^{n} \ln z_i - 2\gamma \sum_{i=1}^{n} \left(\frac{\mu}{z_i}\right)^{\eta} \ln\left(\frac{\mu}{z_i}\right) \\ & + (\rho - 1) \sum_{i=1}^{n} \frac{2\gamma (\mu/z_i)^{\eta} \ln(\mu/z_i) e^{-2\gamma (\mu/z_i)^{\eta}}}{1 - e^{-2\gamma (\mu/z_i) z_i^{\eta}}}, \end{aligned} \tag{27}$$

Table 3: MLEs, C2, C3, C4, and C5 for the dataset.

Model	MLE and C2				C3	C4	C5
TIITLGINW (μ, η, ρ, γ)	1.494 (195300)	3.724 (2.265)	1.146 (1.21)	0.664 (323200)	30.8	0.09702	0.99177
TIITLGIR (μ, ρ, γ)	1.112 (333800)	3.61 (1.334)	2.204 (1323000)		31.736	0.12642	0.90655
GINW (μ, β, γ)	1.868 (282500)	4.017 (0.697)	0.489 (296900)		30.817	0.10195	0.98545
GIR (μ, γ)	1.953 (244100)	0.724 (181000)			42.365	0.25659	0.14358
TIITLIE (μ, ρ)	3.086 (0.543)	20.766 (10.928)			34.209	0.15423	0.72826
IE (μ)	1.725 (0.386)				65.337	0.38725	0.00497

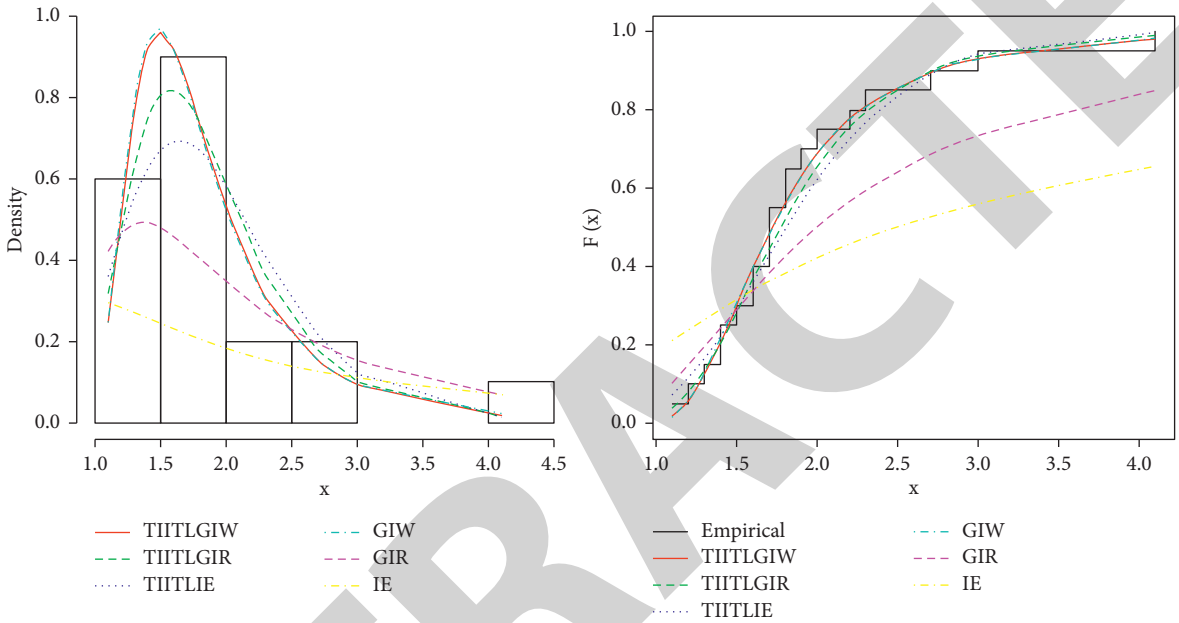

Figure 3: The empirical pdf and empirical cdf of the TIITLGINW model.

$$U_\rho = \frac{n}{\rho} + \sum_{i=1}^{n} \ln\left[1 - e^{-2\gamma(\mu/z_i)^\eta}\right], \tag{28}$$

$$U_\gamma = \frac{n}{\gamma} - 2\sum_{i=1}^{n}\left(\frac{\mu}{z_i}\right)^\eta + 2(\rho-1)\sum_{i=1}^{n}\frac{(\mu/z_i)^\eta e^{-2\gamma(\mu/z_i)^\eta}}{1 - e^{-2\gamma(\mu/z_i)^\eta}}. \tag{29}$$

The MLEs of the φ parameters are then produced via assigning $U(\varphi) = 0$ and calculating them.

6. Numerical Outcomes

Comparing the theoretical performances of alternative estimators MLE for the TIITLGINW model is extremely challenging. Mathematica 9 software is used to do a numerical analysis. The experiments take into account different sample sizes of $n = 30$, 50, and 200, and furthermore, the various values of the φ parameters.

The study will indeed be repeated 5000 times in total. In each experiment, ML estimation techniques will be utilized to provide parameter estimates. As a consequence of these experiments, the MLEs and mean square errors (C1) for the various estimators will be reported.

7. Modelling

Throughout this section, we test the adaptability of the TIITLGINW model by applying it to a real-world data collection. The TIITLGINW model is compared to the TIITLGIR, TIITLIE, GINW, GIR, and IE models.

The used data are reported in [20], and it is 2.7, 4.1, 1.8, 1.5, 1.1, 1.4, 1.8, 1.6, 2.2, 1.7, 1.2, 1.4, 3, 1.3, 1.7, 1.9, 1.7, 2.3, 1.6, 2.

Tables 2 and 3 provide the ML estimates as well as the standard errors (C2) of the model parameters. Analytical metrics such as 2LL (C3), Kolmogorov–Smirnov (C4), and p value (C5) are included in the identical tables.

The numerical values of MLEs, C2, C3, C4, and C5 are given in Table 3.

The fits of the TIITLGINW model to the TIITLGIR, TIITLIE, GINW, GIR, and IE models are compared and given in Table 3. The statistics in these tables demonstrate that the

Hindawi
Journal of Mathematics
Volume 2023, Article ID 9783969, 1 page
https://doi.org/10.1155/2023/9783969

Retraction

Retracted: The Application of the Internet of Things Framework in the Ideological and Political Teaching System

Journal of Mathematics

Received 13 September 2023; Accepted 13 September 2023; Published 14 September 2023

This article has been retracted by Hindawi following an investigation undertaken by the publisher [1]. This investigation has uncovered evidence of one or more of the following indicators of systematic manipulation of the publication process:

(1) Discrepancies in scope

(2) Discrepancies in the description of the research reported

(3) Discrepancies between the availability of data and the research described

(4) Inappropriate citations

(5) Incoherent, meaningless and/or irrelevant content included in the article

(6) Peer-review manipulation

The presence of these indicators undermines our confidence in the integrity of the article's content and we cannot, therefore, vouch for its reliability. Please note that this notice is intended solely to alert readers that the content of this article is unreliable. We have not investigated whether authors were aware of or involved in the systematic manipulation of the publication process.

Wiley and Hindawi regrets that the usual quality checks did not identify these issues before publication and have since put additional measures in place to safeguard research integrity.

We wish to credit our own Research Integrity and Research Publishing teams and anonymous and named external researchers and research integrity experts for contributing to this investigation.

The corresponding author, as the representative of all authors, has been given the opportunity to register their agreement or disagreement to this retraction. We have kept a record of any response received.

References

[1] B. Qiu and P. Ikram, "The Application of the Internet of Things Framework in the Ideological and Political Teaching System," *Journal of Mathematics*, vol. 2022, Article ID 2846103, 9 pages, 2022.

Hindawi
Journal of Mathematics
Volume 2022, Article ID 2846103, 9 pages
https://doi.org/10.1155/2022/2846103

Research Article

The Application of the Internet of Things Framework in the Ideological and Political Teaching System

Bei Qiu[1] and Pakiza Ikram[2]

[1]*School of Marxism, Jiangsu Agri-Animal Husbandry Vocational College, Taizhou City, Jiangsu 215300, China*
[2]*Department of Computer Science, Superior University Lahore, Lahore, Pakistan*

Correspondence should be addressed to Pakiza Ikram; pakizaikram01@gmail.com

Received 9 April 2022; Revised 16 May 2022; Accepted 23 May 2022; Published 10 June 2022

Academic Editor: Naeem Jan

This study uses Internet of Things technology to build a smart system for ideological and political education in order to remove several flaws in present ideological and political teaching. Furthermore, to achieve intelligent monitoring of the ideological and political classroom, this research uses a technique based on IGHT edge feature matching and the ideological and political classroom monitoring image monitoring calculation formula to compute the image light reflection angle. In addition, this paper adopts the method of adaptively obtaining segmentation threshold (OTSU algorithm) to binarize the differenced image. After constructing the smart teaching system, this paper conducts a systematic evaluation based on the simulation experiment. The research results show that the ideological and political teaching system based on the Internet of Things technology proposed in this paper has a good simulation teaching effect, and the system can be used in the follow-up ideological and political teaching to improve the teaching effect.

1. Introduction

Information technology with computer multimedia and computer network as the core has changed all aspects of social life and has also had a profound impact on the ideological and political teaching system. Generally speaking, the four elements of ideological and political teaching resources, such as teachers, students, ideological and political teaching content, and ideological and political teaching media, constitute a static ideological and political teaching system, and the ideological and political teaching process is the movement form of the system. Moreover, ideological and political teaching resources are the material basis of the ideological and political teaching process, and different material bases constitute different ideological and political teaching processes and their teacher-student (social) relationships.

Instructors continue to teach information and skills, and pupils progressively attain the same cognitive understanding as teachers as a result of frequent stimulation [1]. The "central" and "authority" position of instructors in the educational process are the most visible manifestations of the teacher-student interaction [2]. Instructors' words and acts infect pupils quietly in the face-to-face education process, and teachers' expertise and charisma have earned students' respect and adoration. Teachers' teaching, educating, answering inquiries, and resolving doubts functions, as well as their leadership position in the teaching process, may be thoroughly shown at this time. The teaching process oriented on student learning has progressively become a reality as information technology has advanced, resulting in a new "learning-centered teaching system model" and a new teacher-student interaction [3].

Information technology not only changes the content, methods, and means of ideological and political teaching, but also affects the structural model of the entire ideological and political teaching system, centered system model. The two ideological and political teaching system models have their own advantages and disadvantages: systematic academic education, especially the ideological and political

teaching of knowledge with strong logic and abstract concepts, requires an ideological and political teaching system centered on teacher teaching, while vocational education and adult continuing education are suitable. An ideological and political teaching system centered on student learning: In particular, the advantages of the ideological and political teaching system model centered on teacher teaching in the basic functions of teaching and educating people and the high-efficiency overall ideological and political teaching make the information technology so developed today; the traditional ideological and political teaching system model still dominates, mainstream. The two ideological and political teaching models have their own merits. For the same ideological and political teaching resources, people can adopt different organizational forms to implement different ideological and political teaching processes; the two ideological and political teaching models complement each other and penetrate each other. Only then can we adapt to the information age and vigorously develop education for all. The education career of lifelong education: it is necessary to expand quality skills, but also to systematically learn professional knowledge; it is necessary to develop vocational skills education, but also to improve the quality of professional academic education. The ideological and political teaching system is a large system dominated by people. Although different ideological and political teaching system models have their own strengths, the final ideological and political teaching effect is determined by the joint action of teachers and students.

This paper combines the Internet of Things technology to construct an ideological and political teaching system, improve the intelligence of ideological and political teaching, and promote the interactive teaching of teachers and students.

2. Related Work

The teaching information mining system based on the Internet of Things technology is an important part of building a smart campus, and there are many related studies. The use of invisible methods to collect students' classroom attendance information instead of the traditional teacher's roll call and the current card swiping method fully respects the students' privacy. Through the smart camera, not only the face information of a single student can be collected and compared with the student information stored in the database to accurately identify the student's identity, but also the image of the entire classroom scene can be collected to identify the attendance rate of the students in the classroom [4]. Literature [5] only makes big data statistics of classroom student attendance, and the results are presented in the form of percentage and overall data.

Using the images collected by the smart camera, the attendance rate of students in a certain course in a certain period of time can be counted. There is a lot of information hidden behind the big data of attendance [6]. The changes in the attendance of students in the whole semester of the course can reflect the changes in the quality of teachers' teaching, the degree of attraction of the course to students in different chapters, and the test scores of the students in the course, and so on [7].

Using the images collected by the smart camera, it is convenient to count the occupancy of the seats in the study room and push it to the students in a variety of ways to help the students reasonably arrange and utilize the resources of the study room [8].

It is possible to determine the pace at which pupils glance up in class, as well as their tiredness condition, using photos acquired by smart cameras (such as whether they are dozing off or sleeping). The teacher's authority over the whole classroom and the appeal of the course material to the students are reflected in the student rise rate. Students' tiredness levels might be connected to their work and rest environments. These data may be connected and excavated by comparing them to other educational material. Provide a wealth of relevant information and provide some positive recommendations for the school's teaching management efforts [9]. Design a user-interactive information service software, which can run on mobile phones, PCs, and public information query terminals, so that students, teachers, and managers can query relevant information and data, efficiently share campus resources, and enrich campus culture [10]. Infrared photoelectric through-beam sensors are widely used in public transportation systems to count the number of passengers. Although this method is simple to install and has a low cost, it requires a certain length of the detection channel, which has low accuracy and is easily affected by pedestrians staying and carrying items. Infrared photoelectric through-beam sensors cannot record images, which brings difficulties to real-time on-site observation. The false detection rate is high, and only rough traffic statistics can be performed. The method of reading student cards is more accurate. The biggest problem is that this method needs to obtain the personal information of classmates. In essence, like signing in by name, it will leak the privacy of students, which is not conducive to the development of teaching management [11]. The multicamera stereo vision people counting system accomplishes the task of people counting by segmenting the pedestrians present in the image. This method requires the application of a stereo depth algorithm to calculate the depth map of the scene, and the stereo vision people counting system in the depth map is suitable for cross-sectional and regional environments [12]. Due to the use of three-dimensional depth information, the multicamera is less affected by the mutual occlusion of pedestrians, and the segmentation of pedestrians in the image is accurate. However, the multicamera stereo vision system uses multiple accurately calibrated cameras, which is bulky and expensive. The single-camera people counting system is applicable to the cross-sectional and regional environments as well as the stereo vision system, and computer vision and artificial intelligence methods are also applied [13]. The main features of this technology are high accuracy, easy installation, and seamless compatibility with existing monitoring systems in classrooms. During installation, the camera can be adjusted to an angle close to vertical downward, with less occlusion, improving statistical accuracy, making the task of people counting easier, and

greatly reducing system costs [14]. Considering factors such as cost, accuracy, information security, and students' personal privacy, this design finally selects a single-camera people counting method. The video-based people counting algorithm and program built into the smart camera can obtain the accurate number of people at the scene [15]. Currently, surveillance cameras are installed in classrooms, and the basic lines of surveillance cameras can be borrowed. The surveillance cameras only need to be updated to smart cameras with the function of counting people based on video images and capturing the rate of student head-up. A well-performing people counting system can be used in cameras [16]. Accurate counting in the case of vertical angles: In addition, when the width of the human body is less than 30 pixels, it is difficult to distinguish pedestrians one by one when there are many occlusions by the crowd. Using an optical zoom camera can magnify the size of the target on the screen and obtain more accurate data. Another advantage of smart cameras is that they can reduce the computational pressure and communication pressure on the background server [17]. The traditional camera directly transmits the picture to the background server with stronger computing power, and the server runs the algorithm to process the image information, but this method has high requirements on the communication link; it requires a large bandwidth to transmit the picture information, and requires a large number of pictures. The image data of the data brings great pressure to the background computer [18].

3. Ideological and Political Teaching Monitoring Algorithm Based on Internet of Things Framework

In this paper, two methods based on IGHT edge feature matching and ideological and political classroom monitoring image monitoring calculation formula are used to calculate the image light reflection angle. These two methods cooperate with each other to achieve the purpose of accurately measuring the reflection angle of image light.

The steps of the edge feature matching algorithm are shown in Figure 1.

First, the algorithm performs median adaptive filtering on the collected color images to filter out noise. The programme then turns the color picture to a grayscale image by grayscaling it. The programme then extracts the edge characteristics of the monitoring image string in the ideological and political classroom by performing interframe difference and binarization processing on three successive frames of pictures. The algorithm then matches the local features of the ideological and political classroom monitoring image string to the edge feature template of the ideological and political classroom monitoring image string recorded in the database using the invariant generalised Hough transform. Finally, the algorithm calculates the image light reflection angle of the ideological and political classroom monitoring image string by determining the coordinates of both ends of the ideological and political classroom monitoring image string. Due to the different climate and weather conditions and the acquisition of images in different time periods, false edges may be generated during edge extraction, which reduces the detection accuracy of edges. Taking into account the difference of image characteristics between different locations, we filter the image with an adaptive median filter that can change the window size according to the image characteristics of the filtered area.

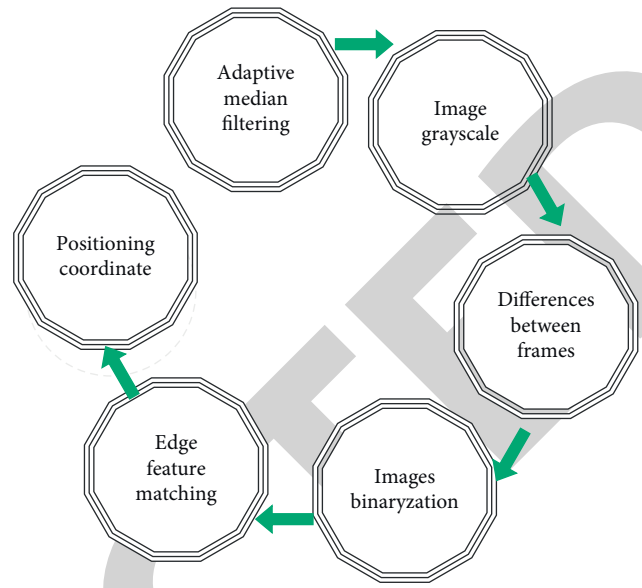

Figure 1: Steps of edge feature matching algorithm.

The image collected by the tower is a color image. If the color image is directly processed, the R, G, and B components need to be processed separately, which greatly increases the complexity and time of processing the image. Therefore, according to formula (1), the RGB image is converted into a grayscale image as follows:

$$Y = 0.299 * R + 0.587 * G + 0.114 * B. \quad (1)$$

Among them, Y is the brightness, that is, the gray value of the grayscale image pixel, and R, G, and B are the red, green, and blue components of the color image, respectively.

In this paper, the interframe difference method is used to extract the edge feature information of the monitoring image string in the ideological and political classroom. The interframe difference method is a fast, low-computation, and easy-to-implement algorithm, which can effectively adapt to changes in external conditions such as illumination. The main idea of using the interframe difference method in this paper is to use the adjacent three frames of images in the buccal frame as a group to perform symmetric difference. This method is more complete than the traditional frame difference method to detect the edge feature information of moving objects. The specific algorithm is described as follows:

Three consecutive frames of images $f_{k-1}(x, y)$, $f_k(x, y)$, and $f_{k+1}(x, y)$ are selected, where $f_{k-1}(x, y)$ represents the k-th frame image, and $D_k(x, y)$ represents the difference result of the k–1, k, and k+1-th frame images.

$$D_k(x,y) = f_{k-1}(x,y) - f_k(x,y) + f_{k+1}(x,y) - f_k(x,y),$$
$$D_k(x,y) = f_{k-1}(x,y) + f_{k+1}(x,y) - 2f_k(x,y). \tag{2}$$

In this paper, the method of adaptively obtaining segmentation threshold (OTSU algorithm) is used to binarize the differenced image, and the algorithm can automatically calculate the optimal segmentation reading value. The pixels whose gray value of the edge image is greater than the optimal threshold are white, otherwise they are black, and the image is converted into a binary image to obtain the target edge feature. The specific algorithm is as follows:

The gray level $G = \{0, 1, ..., L-1\}, t \in G$ is the selected segmentation threshold. Among them, $R_k(x,y)$ is the image after binarizing $D_k(x,y)$, and the expression is shown in formula

$$R_k(x,y) = \begin{cases} 0, & R_k(x,y) < t \\ 1, & R_k(x,y) \geq t. \end{cases} \tag{3}$$

If the number of pixels with gray level i is assumed to be N_i, the total number of pixels in a frame of image is

$$M = \sum_{i=0}^{L-1} N_i. \tag{4}$$

The probability of occurrence of a pixel with gray level i is

$$P_i = \frac{N_i}{M},$$
$$\sum_{i=0}^{L-1} P_i = 1. \tag{5}$$

Taking the segmentation threshold t as the boundary, the gray level is divided into two categories: background area {0.1,...,t} and target area {t+1,t+2...,L−1}. Then, the ratio of background pixels is P($t = c$), and the average gray levels of the background and target objects are, respectively,

$$u_0 = \frac{\sum_{i=0}^{t} iP_i}{P(t)},$$
$$u_1 = \frac{\sum_{i=t+1}^{L-1} iP_i}{1 - P(t)}. \tag{6}$$

The variance between the background and the target object is

$$\sigma^2 = P(t)(1 - p(t))(u_1 - u_0). \tag{7}$$

When the variance σ^2 takes the maximum value, the variable t is the optimal threshold value.

The invariant generalised Hough transform is used in this study to match the edge features of the monitoring image string in the ideological and political classroom. The method is simpler than the extended Hough transform and is invariant in translation, scaling, and rotation. When the feature rotation varies, utilizing the invariant generalised Hough transform to find the picture provides substantial benefits. The implementation steps of this algorithm are as follows:

(1) The algorithm determines the index angle β and ω_j of the edge point ω_i.

The algorithm assumes point ω_i and a fixed characteristic angle α, then the point ω_j can be determined, and then the angle β between the tangent at ω_j and the tangent connecting point ω_j can be determined. Here, α takes the element $\pi/4$, as shown in Figure 2.

(2) The algorithm selects the eigenvalues of the edge point ω_i.

To locate the center point $b = (x_0, y_0)$, the algorithm calculates the distance d from ω_i to the location point b and defines the angle k as the difference between the angle ϕ_i' of point ω_i and the slope ϕ_i'' of the straight line formed by edge points ω_i and b, that is, $k = \phi_i' - \phi_i''$. It is independent of rotation, where ϕ_i'' is expressed as the slope of the straight line (8), as shown in Figure 3.

$$y_0 = \phi_i''(x_0 - \omega_{xi}) + \omega_{yi}. \tag{8}$$

(3) Store eigenvalues.

The algorithm repeats steps (1) and (2) and determines the eigenvalues (β, k, d) of each edge point ω_i one by one and stores them to construct an invariant R-table.

Since the monitoring image string in the ideological and political classroom will bend and deform when the wind deflection occurs, the geometric features in Figure 4 are very unique. The ideological and political classroom monitoring image string can be replaced by the feature information shown in Figure 4, and the amount of calculation can be greatly reduced. Therefore, we only establish the invariant R-table of the local features of the ideological and political classroom monitoring image string shown in Figure 4 to match the ideological and political classroom monitoring image string, where (x, y) are the coordinate points to be located.

For each edge point ω_j' in the processed image, the algorithm obtains the corresponding edge angle ω_j' according to the given characteristic angle $\alpha = \pi/4$ and then calculates the corresponding index angle β'. The algorithm then indexes the corresponding eigenvalues k, d in the invariant R-table according to the index angle. Then, the algorithm collects evidence according to the definition of these eigenvalues according to the straight line defined by formula (6) and calculates the voting point of the edge point ω_j' in the two-dimensional cumulative space. This procedure is repeated until all edge points have voted. Finally, discover the local extreme points whose votes surpass the threshold in the voted Hough space. The number and location of local extreme points in the picture signify the number and location of target matches. There are two matching points in the image to be detected. After the coordinates of the two matching points are determined, a geometric analysis of the image light reflection angle is performed on them, as shown in Figure 5.

As shown in Figure 5, the coordinates of the pixel positions at both ends of the ideological and political

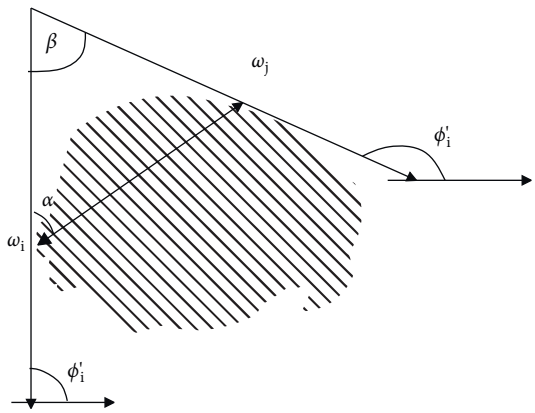

Figure 2: Invariant generalised Hough transform displacement vector.

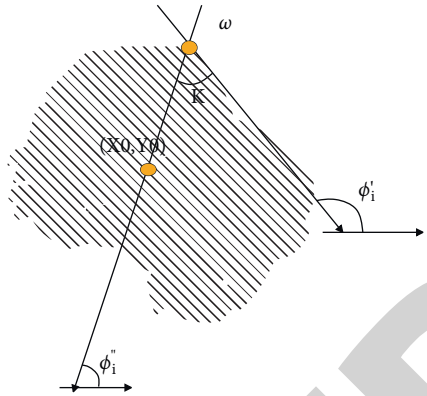

Figure 3: Invariant generalised Hough transform angle definition.

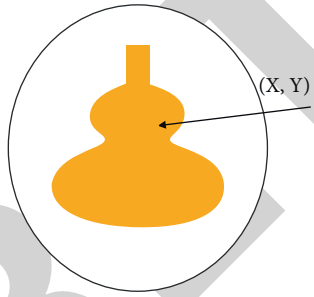

Figure 4: Local features of monitoring image strings in ideological and political classrooms.

classroom monitoring image string are (x_1, y_1) and (x_2, y_2), respectively, and d is the offset of the ideological and political classroom monitoring image string. Then, the calculation formula of the image light reflection angle of the monitoring image string in the ideological and political classroom is

$$\theta = \arctan\left(\frac{(x_1 - x_2)}{(y_1 - y_2)}\right). \tag{9}$$

Now, the more mature wind deflection calculation is based on the force diagram of the ideological and political classroom monitoring image string shown in Figure 6. From

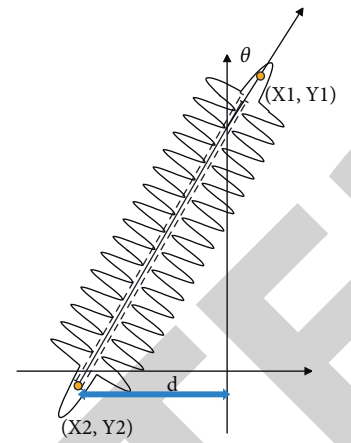

Figure 5: Geometric analysis of image ray reflection angle calculation.

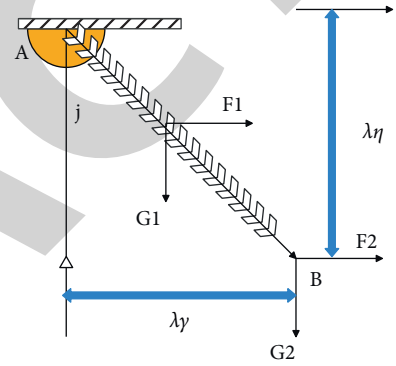

Figure 6: The force diagram of the monitoring image string in the ideological and political classroom.

the figure, the formula for the image light reflection angle can be obtained:

$$\theta = \arctan\left(\frac{0.5F_1 + F_2}{0.5G_1 + G_2}\right). \tag{10}$$

In the formula, F1 is the wind load of the ideological and political classroom monitoring image string, F2 is the wind load of the wire, G1 is the vertical load and gravity of the ideological and political classroom monitoring image string, and G2 is the vertical load of the wire. Among them,

$$F_1 = 9.80665v^2/16, \tag{11}$$

$$F_2 = \alpha K A F_0 \sin^2\theta, \tag{12}$$

$$F_0 = pv^2/2, \tag{13}$$

$$G_2 = Lqn. \tag{14}$$

The image light reflection angle is

$$\varphi = \arctan\left(\frac{0.5 \times 9.80665Sv^2 + \alpha p v^2 K A \sin^2\theta/2}{0.5G_1 + Lqn}\right). \tag{15}$$

The formula for density is

$$\rho = \frac{1.29305 \times (p - 0.3779h)}{(1 + 0.00367T) \times 1013.25}. \quad (16)$$

In formula (15), S is the cross-sectional area of the hanging ideological and political classroom monitoring image string perpendicular to the wind direction. Generally, after the model of the monitoring image string in the ideological and political classroom is determined, S is the determined value. α is the wind pressure uneven coefficient, generally taken as 0.61. K is the shape coefficient of the wire. When the diameter of the wire is less than 17 mm or covered with ice, $K = 1.2$, and in other cases, $K = 1.1$. A is the cross-sectional area of the wire connecting the hanging ideological and political classroom monitoring image string perpendicular to the wind direction, and L is the vertical span of the hanging ideological and political classroom monitoring image string. q is the gravity per unit length of the wire connecting the hanging ideological and political classroom monitoring image string, n is the number of wires in each phase, which determines the image light reflection angle of the hanging ideological and political classroom monitoring image string, and A, L, and q are the determined values. V is the wind speed around the hanging ideological and political classroom monitoring image string at that time. θ is the angle between the wire connecting the hanging ideological and political classroom monitoring image string and the wind direction, and v and v can be measured by the wind speed and direction sensor installed on the tower. p is the atmospheric pressure of the air around the hanging ideological and political classroom monitoring image string, which can be measured by the atmospheric pressure sensor WJ-3A installed on the tower. T is the atmospheric temperature of the air around the hanging ideological and political classroom monitoring image string; h is the atmospheric humidity of the air surrounding the hanging ideological and political classroom monitoring image string, which can be measured by the temperature and humidity sensor SHT11 installed on the tower. p is the density of the air around the monitoring image string of the hanging ideological and political classroom. After p, h, and T are measured, they can be calculated by formula (16). Therefore, to calculate the image light reflection angle p, we only need to measure the wind speed v, wind direction, atmospheric pressure p, temperature T, and humidity h.

4. Ideological and Political Teaching System Based on Internet of Things System

The course management module provides the foundation for other modules such as course selection, course layout, and grade management. As illustrated in Figure 7, the whole process includes creating a semester teaching plan, maintaining course information, querying course information, and scheduling teaching responsibilities throughout the semester. The system administrator is in charge of the teaching plan formulation module. In colleges and universities, system administrators may determine grades, departments, majors, courses, and other information and build public professional and quality plans based on student-created training plans. The system administrator also controls the course information administration module, which includes establishing course start and finish times, appointing professors, determining course hours and credits, and so on. The class scheduling management module is the most functional and complex module in the system, as shown in Figure 8. The administrators in this module are divided into academic administrators and department administrators. Among them, the academic administrator can manage the courses of the whole school in a unified way and can divide the course arrangement campus, course arrangement time period, and course arrangement teachers according to the information of the college. Department administrators can only participate in the scheduling tasks of their own courses. After the course arrangement is completed, both students and teachers can log in to the system to view the course arrangement results. If the teacher role needs to adjust the timetable for special reasons and needs to fill in the application for class adjustment, partial adjustments can be made after the system administrator approves; otherwise the teacher role has no authority to operate the class scheduling system.

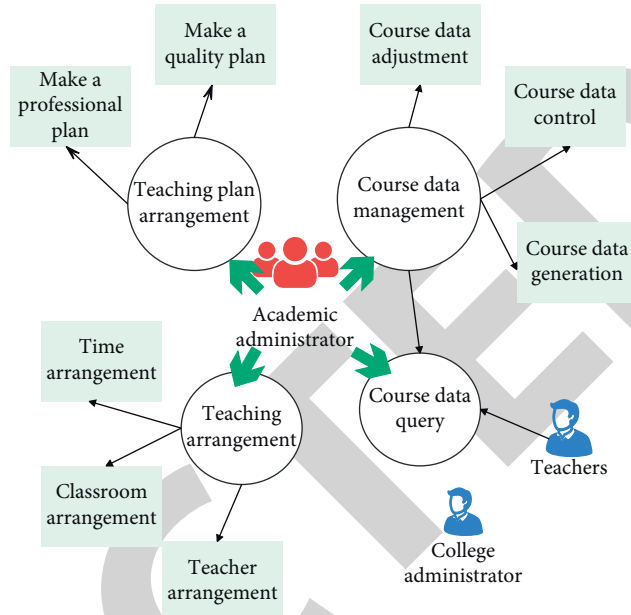

Figure 7: Use case diagram of course management module.

The edge network for smart classroom big data applications should be designed as shown in Figure 9. The control node in the edge network uses SDN/NFV technology to manage and control the resources of the global network and process user requests from outside the edge network. The controller corresponding to the connection to N6 in Figure 9 is C1. Moreover, a corresponding control server is also deployed on the network node closest to the user's access, which manages and controls the terminal equipment and data flow within the range of the access point. Corresponding to the connection with N1 : N2:N3 in Figure 9 are C2 : C3:C4, respectively. It is worth noting that C1, C2, C3, and C4 are logical controllers with nodes in the network, not necessarily directly connected to the corresponding network

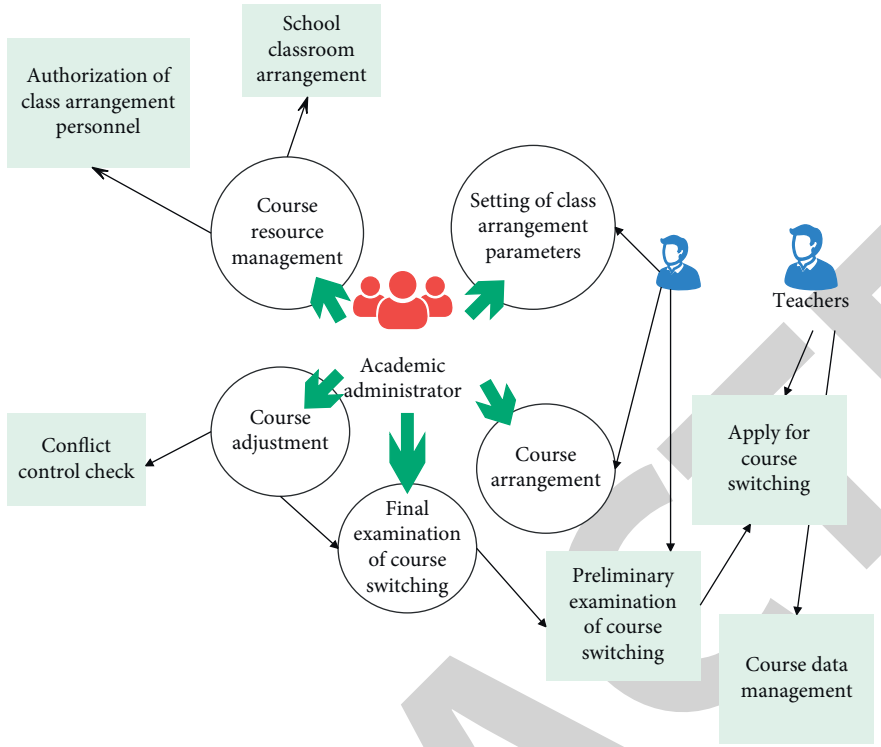

Figure 8: Use case diagram of course scheduling management module.

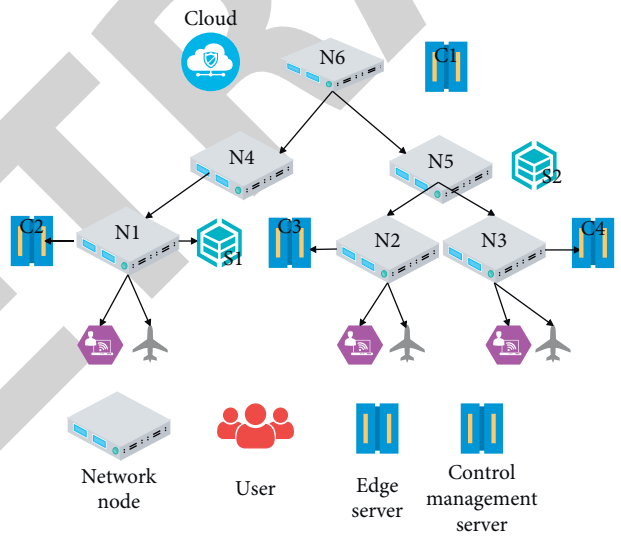

Figure 9: Design of edge network for smart classrooms.

nodes. On the other hand, S1 and S2 in Figure 9 are edge servers, which provide computing power for edge big data applications.

Figure 10 shows the simulation diagram of the ideological and political teaching system based on the Internet of Things framework, which is also the structure of the smart classroom. In this paper, Matlab is used to simulate the ideological and political teaching system based on the Internet of Things technology to explore its simulation teaching effect. The evaluation results are shown in Table 1.

From the above research, it can be seen that the ideological and political teaching system based on the Internet of Things technology proposed in this paper has a good simulation teaching effect, and the system can be used in

Figure 10: Simulation of ideological and political teaching based on the Internet of Things.

Table 1: Simulation evaluation of ideological and political teaching system based on Internet of Things technology.

Num	Simulation teaching	Num	Simulation teaching	Num	Simulation teaching
1	89.5	19	85.8	37	88.7
2	92.6	20	87.2	38	84.5
3	91.2	21	84.9	39	92.2
4	92.6	22	86.9	40	90.6
5	90.7	23	92.4	41	90.3
6	89.0	24	92.2	42	87.5
7	92.1	25	90.4	43	92.2
8	87.3	26	87.3	44	86.2
9	88.6	27	87.7	45	86.9
10	87.7	28	88.6	46	91.2
11	86.4	29	86.3	47	89.3
12	92.1	30	86.3	48	91.3
13	90.0	31	88.8	49	90.7
14	92.3	32	91.8	50	88.6
15	89.9	33	86.9	51	84.9
16	88.6	34	91.9	52	87.9
17	86.3	35	85.5	53	89.2
18	84.6	36	85.3	54	85.4

subsequent ideological and political teaching to improve the teaching effect.

5. Conclusion

On the contrary, under the premise of not violating the constraints of ideological and political teaching resources on the ideological and political teaching process, different organizational forms and ideological and political teaching processes for ideological and political teaching resources exist, depending on different ideological and political teaching goals. With the backward ideological and political teaching medium developed by humans for a long period, the traditional ideological and political teaching mode based on teachers' teaching is the most coordinated and efficient ideological and political teaching system. It is supported by the learning theory of behaviorism, the system resources are configured around teachers' ideological and political teaching, and the ideological and political teaching process is designed around teachers' teaching. The systematic ideological and political teaching resources and the ideological and political teaching process are completely controlled by teachers, while the students, who are the cognitive subjects, are in the position of passive acceptance. This paper combines the Internet of Things technology to construct a smart system for ideological and political teaching. Moreover, this paper adopts the method based on IGHT edge feature matching and the ideological and political classroom monitoring image monitoring calculation formula to calculate the image light reflection angle to realize the intelligent monitoring of the ideological and political classroom. It can be seen that the ideological and political teaching system based on the Internet of Things technology proposed in this paper has a good simulation teaching effect, and the

Hindawi
Journal of Mathematics
Volume 2022, Article ID 1786221, 12 pages
https://doi.org/10.1155/2022/1786221

Research Article

An Enhanced Fermatean Fuzzy Composition Relation Based on a Maximum-Average Approach and Its Application in Diagnostic Analysis

P. A. Ejegwa,[1] G. Muhiuddin,[2] E. A. Algehyne,[2] J. M. Agbetayo,[1] and D. Al-Kadi[3]

[1]*Department of Mathematics, University of Agriculture, P.M.B. 2373, Makurdi, Nigeria*
[2]*Department of Mathematics, Faculty of Science, University of Tabuk, P.O. Box 741, Tabuk 71491, Saudi Arabia*
[3]*Department of Mathematics and Statistic, College of Science, Taif University, P.O. Box 11099, Taif 21944, Saudi Arabia*

Correspondence should be addressed to G. Muhiuddin; chishtygm@gmail.com

Received 6 February 2022; Revised 4 April 2022; Accepted 6 April 2022; Published 30 May 2022

Academic Editor: Lazim Abdullah

The idea of composition relations on Fermatean fuzzy sets based on the maximum-extreme values approach has been investigated and applied in decision making problems. However, from the perspective of the measure of central tendency, this approach is not reliable because of the information loss occasioned by the use of extreme values. Based on this limitation, we introduce an enhanced Fermatean fuzzy composition relation with a better performance rating based on the maximum-average approach. An easy-to-follow algorithm based on this approach is presented with numerical computations. An application of Fermatean fuzzy composition relations is discussed in diagnostic analysis where diseases and patients are mirrored as Fermatean fuzzy pairs characterized with some related symptoms. To ascertain the veracity of the novel Fermatean fuzzy composition relation, a comparative analysis is presented to showcase the edge of this novel Fermatean fuzzy composition relation over the existing Fermatean fuzzy composition relation.

1. Introduction

Diagnostic analysis of patients' medical samples is a delicate assignment enmeshed with vagueness and hesitation. Many approaches have been posited to ameliorate this problem, like the introduction of fuzzy sets [1]. Though the fuzzy set seems to be promising in tackling uncertainties, it is unreliable because it considers the membership degree Υ (MD) of the case under consideration without minding the possibility of hesitation. Sequel to this weakness, some generalized varieties of fuzzy sets have been put forward such as the intuitionistic fuzzy set (IFS) [2], the Pythagorean fuzzy set (PFS) [3, 4], and the Fermatean fuzzy set (FFS) [5, 6]. By including nonmembership degree Φ (NMD) to Υ of fuzzy set, the idea of IFSs was proposed and applied in numerous applicative areas. Boran and Akay [7] explored pattern recognition using a biparametric similarity measure. Some techniques of similarity measures and distance measures of IFSs have been used to handle pattern recognition problems [8–10]. In [11], a medical diagnosis was carried out based on composite relations. Similarly, in [12, 13], a diagnostic analysis was done based on a similarity measure approach.

The noticeable inadequacy of IFSs is that it only handles the scenario where the summation of membership degree Υ (MD) and nonmembership degree Φ (NMD) is not more than unity. Because of this drawback, intuitionistic fuzzy set of second type (IFSST) was proposed [3, 14], which is widely called Pythagorean fuzzy sets (PFSs) [4]. In PFS, the parameters Υ and Φ are characterized by $\Upsilon + \Phi \geq 1$ such that $\Upsilon^2 + \Phi^2 \leq 1$. PFS has been applied to solve some hands-on problems such as medical diagnosis based on composite relation [15] and other sundry problems [16, 17]. A method for undertaking multi-attribute decision-making (MADM) under interval-valued Pythagorean fuzzy linguistic information was deliberated in [18]. A number of aggregation operators using Einstein t-conorm, Einstein operator, and

Einstein t-norm under the Pythagorean fuzzy environment for decision-making were deliberated in [19, 20]. A new extension of the TOPSIS (technique for order preference by similarity to ideal solution) approach for multiple criteria decision-making (MCDM) with hesitant PFSs was discussed in [21]. Wang and Garg [22] developed some aggregation operators for PFS based on interactive Archimedean norm processes with application to MADM. In [23], a Choquet integral based interval type-2 trapezoidal fuzzy approach was applied in MCDM involving sustainable selection of supplier. A group decision-making approach was discussed in a dynamic feedback mechanism with an attitudinal consensus threshold for minimum adjustment cost [24].

In the same way as IFSs, the construct of PFSs is limited to handle a situation when $\Upsilon = \sqrt[3]{6}/2$ and $\Phi = 1/2$. In a quest to resolve this brainteaser, the intuitionistic fuzzy set of third type (IFSTT) also known as the Fermatean fuzzy set (FFS) was introduced [5, 6]. FFS has a broader scopes include $\Upsilon + \Phi \geq 1$, $\Upsilon^2 + \Phi^2 \geq 1$ and $\Upsilon^3 + \Phi^3 \leq 1$ with the ability to certainly handle indeterminate information in decision making. A number of operators on FFSs were elaborated in [25], and differential calculus of Fermatean fuzzy functions have been introduced [26]. A number of applications of FFSs in MCDM problems based on TOPSIS method, distance measures and certain weighted aggregated operators have been explored [6, 27–29]. Sari et al. [30] studied interval-valued Fermatean fuzzy sets and applied them to capital budgeting techniques. Jeevaraj [31] imposed ordering on interval-valued FFSs with application. A novel decision-making method based on Fermatean fuzzy WASPAS (weighted aggregated sum product assessment) for green construction supplier evaluation was discussed in [32]. In [33], some TOPSIS techniques via Fermatean fuzzy soft sets were discussed with application. Sahoo [34] presented certain score functions on FFSs with application to bride selection. Aydin [35] discussed a fuzzy MCDM method using Fermatean fuzzy theories, and Zhou et al. [36] applied the Fermatean fuzzy ELECTRE (Elimination Et Choix Traduisant la Realite) method to tackle multiple-criteria group decision making. Shahzadi et al. [37] discussed MADM via Fermatean fuzzy Hamacher interactive geometric operators.

The applications of FFSs based on TOPSIS and MCDM methods have been discussed in [33–37]. Some applications of FFSs in the selection of COVID-19 testing centres using aggregation operators, the SAW (simple additive weighting) approach, the VIKOR (VIekriterijumsko KOmpromisno Rangiranje) approach, and the ARAS (additive ratio assessment) approach were considered in [38, 39]. The concept of Fermatean fuzzy composition relations has been studied based on maximum-extreme values with application to diagnostic analysis using simulated data [40].

The idea of composition relation has been presented in intuitionistic fuzzy settings [11], Pythagorean fuzzy setting [41] and Fermatean fuzzy settings [40] based on the maximum-extreme values approach with applications. This approach, though presented in different frameworks, cannot be reliable because it makes use of only minimum and maximum values. This present work puts forward a new composition relation under the Fermatean fuzzy domain based on the maximum-average approach. To express the applicability of the new Fermatean fuzzy composition relation, a case of diagnostic analysis is considered via the approach where diseases and patients are viewed as Fermatean fuzzy pairs. More concepts related to this study have been studied in [42–45].

The specific objectives of the work are to (i) reiterate the max-min-max approach of composition relation [11, 40, 41] in a Fermatean fuzzy setting, (ii) present an enhanced Fermatean fuzzy composition relation based on the max-average approach, (iii) numerically demonstrate the max-min-max approach in conjunction with the new Fermatean fuzzy composition relation, (iv) decide patients' medical status in a Fermatean fuzzy environment based on Fermatean fuzzy composition relations via max-min-max approach and maximum-average approach, respectively, and (v) present a comparative analysis to showcase the edge of the new Fermatean fuzzy composition relation over the approach in [11, 40, 41]. The summary of the paper follows: Section 2 presents the basis of FFSs and the existing Fermatean fuzzy composition relation [40], Section 3 discusses the new Fermatean fuzzy composition relation via the maximum-average approach, Section 4 dwells on diagnostic analysis of patients' medical status where diseases and patients are presented as Fermatean fuzzy values, and Section 5 synopses the paper with recommendations for future work.

2. Fermatean Fuzzy Sets

Some fundamentals of FFSs have been presented in [6, 28, 29, 40]. Let $S \neq \varnothing$ designates a fixed set for this work.

Definition 1. A FFS X in S is a generalized fuzzy set of the form

$$X = \{\langle s, \Upsilon_X(s), \Phi_X(s)\rangle | s \in S\}, \tag{1}$$

where $\Upsilon_X, \Phi_X: S \longrightarrow [0,1]$ define MD and NMD of $s \in S$ for $0 \leq \Upsilon_X^3(s) + \Phi_X^3(s) \leq 1$. For a FFS X in S,

$$\Psi_X(s) \in [0,1] = \sqrt[3]{1 - \Upsilon_X^3(s) - \Phi_X^3(s)}, \tag{2}$$

represents the FFS index or hesitation margin of X.

In an IFS, $0 \leq \Upsilon + \Phi \leq 1$, $\Psi = 1 - \Upsilon - \Phi$ and $\Upsilon + \Phi + \Psi = 1$. For PFS, $0 \leq \Upsilon^2 + \Phi^2 \leq 1$, $\Psi = \sqrt{1 - \Upsilon^2 - \Phi^2}$ and $\Upsilon^2 + \Phi^2 + \Psi^2 = 1$. For the case of FFS, we have $0 \leq \Upsilon^3 + \Phi^3 \leq 1$, $\Psi = \sqrt[3]{1 - \Upsilon^3 - \Phi^3}$ and $\Upsilon^3 + \Phi^3 + \Psi^3 = 1$.

Now, some properties of FFSs are presented including equality, inclusion, complement, union, and intersection.

Definition 2. Suppose X and Y in S are FFSs, then

(i) $\overline{X} = \{\langle s, \Phi_X(s), \Upsilon_X(s)\rangle | s \in S\}$

(ii) $X = Y$ iff $\Upsilon_X(s) = \Upsilon_Y(s)$, $\Phi_X(s) = \Phi_Y(s), \forall s \in S$

(iii) $X \subseteq Y$ iff $\Upsilon_X(s) \leq \Upsilon_Y(s)$, $\Phi_X(s) \geq \Phi_Y(s), \forall s \in S$

(iv) $X \prec Y$ iff $\Upsilon_X(s) \leq \Upsilon_Y(s)$, $\Phi_X(s) \leq \Phi_Y(s), \forall s \in S$

(v) $X \cup Y =$
$\{\langle s, \max(\Upsilon_X(s), \Upsilon_Y(s)), \min(\Phi_X(s), \Phi_Y(s))\rangle | s \in S\}$

(vi) $X \cap Y = \{\langle s, \min(\Upsilon_X(s), \Upsilon_Y(s)), \max(\Phi_X(s), \Phi_Y(s))\rangle | s \in S\}$

Now, we present a Fermatean fuzzy pairs (FFPs) thus

Definition 3. FFP is designated by $\langle \alpha, \beta \rangle$ such that $\alpha^3 + \beta^3 \leq 1$ where $\alpha, \beta \in [0, 1]$. A FFP evaluates the FFS for which the components (α and β) are interpreted as MD and NMD.

For simplicity sake, we write a FFS $X = \{\langle s, \Upsilon_X(s), \Phi_X(s)\rangle | s \in S\}$ as $X = (\Upsilon_X(s), \Phi_X(s))$.

2.1. Fermatean Fuzzy Composite Relation. Composite relation has been established under IFS, PFS, and FFS [11, 40, 41] to enhance the applications of IFSs, PFSs, and FFSs in decision making. Suppose S_1 and S_2 are two sets. A Fermatean fuzzy relation (FFR) Δ from S_1 to S_2 is a FFS in $S_1 \times S_2$ comprises of MD Υ_Δ and NMD Φ_Δ. A FFR from S_1 to S_2 is denoted by $\Delta(S_1 \longrightarrow S_2)$ or $\Delta \in S_1 \times S_2$.

Definition 4. Suppose Δ_1 and Δ_2 are FFRs in $S_1 \times S_2$ and $S_2 \times S_3$, which can also be written as $\Delta_1(S_1 \longrightarrow S_2)$ and $\Delta_2(S_2 \longrightarrow S_3)$. Then, the Fermatean fuzzy composite relation (FFCR) $\Delta = \Delta_1 \circ \Delta_2$ of $S_1 \times S_3$ is defined by

$$\breve{\Delta} = \left\{\langle\langle(s_1, s_3), \Upsilon_{\breve{\Delta}}(s_1, s_3), \Phi_{\breve{\Delta}}(s_1, s_3)\rangle | (s_1, s_3) \in S_1 \times S_3\rangle\right\}, \tag{3}$$

where

$$\begin{aligned} \Upsilon_{\breve{\Delta}}(s_1, s_3) &= \max\left(\min\left(\Upsilon_{\Delta_1}(s_1, s_2), \Upsilon_{\Delta_2}(s_2, s_3)\right)\right) \\ \Phi_{\breve{\Delta}}(s_1, s_3) &= \min\left(\max\left(\Phi_{\Delta_1}(s_1, s_2), \Phi_{\Delta_2}(s_2, s_3)\right)\right), \end{aligned} \tag{4}$$

$\forall (s_1, s_2) \in S_1 \times S_2$ and $(s_2, s_3) \in S_2 \times S_3$.

Using Definition 4, the FFCR $\Delta = \Delta_1 \circ \Delta_2$ is computed by

$$\breve{\Delta} = \Upsilon_{\breve{\Delta}}(s_1, s_3) - \Phi_{\breve{\Delta}}(s_1, s_3)\Psi_{\breve{\Delta}}(s_1, s_3), \quad \forall (s_1, s_3) \in S_1 \times S_3. \tag{5}$$

The composite relation presented in [11, 40, 41] uses the extreme values, i.e., the maximum of the minimum of the membership degrees and the minimum of the maximum of the nonmembership degrees. The result from this approach is not reliable, judging from the knowledge of the measure of central tendency. Because of this limitation, we modify the technique in [11, 40, 41] based on the maximum-average approach.

3. Enhanced Fermatean Fuzzy Composite Relation

This section presents a FFCR based on the maximum of the mean values of membership degrees, and the minimum of the mean values of nonmembership degrees to enhance better performance.

Definition 5. Let Δ_1 and Δ_2 be FFRs of $S_1 \times S_2$ and $S_2 \times S_3$, which can also be written as $\Delta_1(S_1 \longrightarrow S_2)$ and $\Delta_2(S_2 \longrightarrow S_3)$. Then, the FFCR $\breve{\Pi} = \Delta_1 \circ \Delta_2$ of $S_1 \times S_3$ is defined by

$$\breve{\Pi} = \left\{\langle(s_1, s_3), \Upsilon_{\breve{\Pi}}(s_1, s_3), \Phi_{\breve{\Pi}}(s_1, s_3)\rangle | (s_1, s_3) \in S_1 \times S_3\rangle\right\}, \tag{6}$$

where

$$\begin{aligned} \Upsilon_{\breve{\Pi}}(s_1, s_3) &= \max\left(\text{average}\left(\Upsilon_{\Delta_1}(s_1, s_2), \Upsilon_{\Delta_2}(s_2, s_3)\right)\right) \\ \Phi_{\breve{\Pi}}(s_1, s_3) &= \min\left(\text{average}\left(\Phi_{\Delta_1}(s_1, s_2), \Phi_{\Delta_2}(s_2, s_3)\right)\right), \end{aligned} \tag{7}$$

for $0 \leq \Upsilon^3_{\breve{\Pi}}(s_1, s_3) + \Phi^3_{\breve{\Pi}}(s_1, s_3) \leq 1, \forall (s_1, s_3) \in S_1 \times S_3$. Certainly,

$$\Psi_{\breve{\Pi}}(s_1, s_3) = \sqrt[3]{1 - \Upsilon^3_{\breve{\Pi}}(s_1, s_3) - \Phi^3_{\breve{\Pi}}(s_1, s_3)}. \tag{8}$$

From Definition 5, the new FFCR $\breve{\Pi}$ is computed by

$$\breve{\Pi} = \Upsilon_{\breve{\Pi}}(s_1, s_3) - \Phi_{\breve{\Pi}}(s_1, s_3)\Psi_{\breve{\Pi}}(s_1, s_3), \quad \forall (s_1, s_3) \in S_1 \times S_3. \tag{9}$$

Definition 6. Suppose Δ is a FFR in $S_1 \times S_2$, then the inverse of Δ denoted as Δ^{-1} in $(S_2 \times S_1)$ is defined by

$$\Upsilon_{\Delta^{-1}}(s_2, s_1) = \Upsilon_\Delta(s_1, s_2), \Phi_{\Delta^{-1}}(s_2, s_1) = \Phi_\Delta(s_1, s_2), \quad \forall (s_1, s_2) \in S_1 \times S_2. \tag{10}$$

Definition 7. Suppose Δ_1 and Δ_2 are FFRs in $S_1 \times S_2$, then

(i) $\Delta_1 \leq \Delta_2$ iff $\Upsilon_{\Delta_1}(s_1, s_2) \leq \Upsilon_{\Delta_2}(s_1, s_2)$ and $\Phi_{\Delta_1}(s_1, s_2) \geq \Phi_{\Delta_2}(s_1, s_2), \forall (s_1, s_2) \in S_1 \times S_2$

(ii) $\Delta_1 \prec \Delta_2$ iff $\Upsilon_{\Delta_1}(s_1, s_2) \leq \Upsilon_{\Delta_2}(s_1, s_2)$ and $\Phi_{\Delta_1}(s_1, s_2) \leq \Phi_{\Delta_2}(s_1, s_2), \forall (s_1, s_2) \in S_1 \times S_2$

(iii) $\Delta_1 \wedge \Delta_2 = \{\langle (s_1, s_2), \min(\Upsilon_{\Delta_1}(s_1, s_2), \Upsilon_{\Delta_2}(s_1, s_2)), \max(\Phi_{\Delta_1}(s_1, s_2), \Phi_{\Delta_2}(s_1, s_2))\rangle\}$

(iv) $\Delta_1 \vee \Delta_2 = \{\langle (s_1, s_2), \max(\Upsilon_{\Delta_1}(s_1, s_2), \Upsilon_{\Delta_2}(s_1, s_2)), \min(\Phi_{\Delta_1}(s_1, s_2), \Phi_{\Delta_2}(s_1, s_2))\rangle\}$

(v) $\overline{\Delta_1} = \left\{\langle (s_1, s_2), \Phi_{\Delta_1}(s_1, s_2), \Upsilon_{\Delta_1}(s_1, s_2)\rangle\right\}$, $\overline{\Delta_2} = \left\{\langle (s_1, s_2), \Phi_{\Delta_2}(s_1, s_2), \Upsilon_{\Delta_2}(s_1, s_2)\rangle\right\}$

Theorem 1. *If Δ_1, Δ_2 and Δ_3 are FFRs in $S_1 \times S_2$, then*

(i) $\Delta_1 \leq \Delta_2 \Rightarrow \Delta_1^{-1} \leq \Delta_2^{-1}$

(ii) $(\Delta_1 \vee \Delta_2)^{-1} = \Delta_1^{-1} \vee \Delta_2^{-1}$

(iii) $(\Delta_1 \wedge \Delta_2)^{-1} = \Delta_1^{-1} \wedge \Delta_2^{-1}$

(iv) $(\Delta_1^{-1})^{-1} = \Delta_1$

(v) $\Delta_1 \wedge (\Delta_2 \vee \Delta_3) = (\Delta_1 \wedge \Delta_2) \vee (\Delta_1 \wedge \Delta_3)$

(vi) $\Delta_1 \vee (\Delta_2 \wedge \Delta_3) = (\Delta_1 \vee \Delta_2) \wedge (\Delta_1 \vee \Delta_3)$

(vii) if $\Delta_1 \geq \Delta_2$ *and* $\Delta_1 \geq \Delta_3$ *then* $\Delta_1 \geq \Delta_2 \vee \Delta_3$

(viii) if $\Delta_1 \leq \Delta_2$ *and* $\Delta_1 \leq \Delta_3$ *then* $\Delta_1 \leq \Delta_2 \wedge \Delta_3$

(ix) If $\Delta_1 \wedge \Delta_2 \leq \Delta_1$ *then* $\Delta_1 \wedge \Delta_2 \leq \Delta_2$

(x) If $\Delta_1 \vee \Delta_2 \geq \Delta_1$ then $\Delta_1 \vee \Delta_2 \geq \Delta_2$

Proof. (i) Assume $\Delta_1 \leq \Delta_2$, then

$$\Upsilon_{\Delta_1^{-1}}(s_2, s_1) = \Upsilon_{\Delta_1}(s_1, s_2) \leq \Upsilon_{\Delta_2}(s_1, s_2) = \Upsilon_{\Delta_2^{-1}}(s_2, s_1), \quad (11)$$

and similarly we have

$$\Phi_{\Delta_1^{-1}}(s_2, s_1) = \Phi_{\Delta_1}(s_1, s_2) \geq \Phi_{\Delta_2}(s_1, s_2) = \Phi_{\Delta_2^{-1}}(s_2, s_1), \quad \forall (s_1, s_2) \in S_1 \times S_2. \quad (12)$$

To prove (ii), we have

$$\begin{aligned} \Upsilon_{(\Delta_1 \vee \Delta_2)^{-1}}(s_2, s_1) &= \Upsilon_{\Delta_1 \vee \Delta_2}(s_1, s_2) \\ &= \max\left(\Upsilon_{\Delta_1}(s_1, s_2), \Upsilon_{\Delta_2}(s_1, s_2)\right) \\ &= \max\left(\Upsilon_{\Delta_1^{-1}}(s_2, s_1), \Upsilon_{\Delta_2^{-1}}(s_2, s_1)\right) \\ &= \Upsilon_{\Delta_1^{-1} \vee \Delta_2^{-1}}(s_2, s_1), \quad \forall (s_1, s_2) \in S_1 \times S_2. \end{aligned} \quad (13)$$

Similarly, we have

$$\begin{aligned} \Phi_{(\Delta_1 \vee \Delta_2)^{-1}}(s_2, s_1) &= \Phi_{\Delta_1 \vee \Delta_2}(s_1, s_2) \\ &= \min\left(\Phi_{\Delta_1}(s_1, s_2), \Phi_{\Delta_2}(s_1, s_2)\right) \\ &= \min\left(\Phi_{\Delta_1^{-1}}(s_2, s_1), \Phi_{\Delta_2^{-1}}(s_2, s_1)\right) \\ &= \Phi_{\Delta_1^{-1} \vee \Delta_2^{-1}}(s_2, s_1), \quad \forall (s_1, s_2) \in S_1 \times S_2. \end{aligned} \quad (14)$$

The proof of (iii) is similar to (ii). The proof of (iv) follows:

$$\Upsilon_{(\Delta_1^{-1})^{-1}}(s_2, s_1) = \Upsilon_{\Delta_1^{-1}}(s_1, s_2) = \Upsilon_{\Delta_1}(s_2, s_1) = \Upsilon_{\Delta_1}(s_1, s_2). \quad (15)$$

Similarly, $\Phi_{(\Delta_1^{-1})^{-1}}(s_2, s_1) = \Phi_{\Delta_1}(s_1, s_2)$.
Now, we prove (v) as follows:

$$\begin{aligned} \Upsilon_{\Delta_1 \wedge (\Delta_2 \vee \Delta_3)}(s_1, s_2) &= \min\left(\Upsilon_{\Delta_1}(s_1, s_2), \max\left(\Upsilon_{\Delta_2}(s_1, s_2), \Upsilon_{\Delta_3}(s_1, s_2)\right)\right) \\ &= \max\left(\min\left(\Upsilon_{\Delta_1}(s_1, s_2), \Upsilon_{\Delta_2}(s_1, s_2)\right), \min\left(\Upsilon_{\Delta_1}(s_1, s_2), \Upsilon_{\Delta_3}(s_1, s_2)\right)\right) \\ &= \max\left(\Upsilon_{\Delta_1 \wedge \Delta_2}(s_1, s_2), \Upsilon_{\Delta_1 \wedge \Delta_3}(s_1, s_2)\right) = \Upsilon_{(\Delta_1 \wedge \Delta_2) \vee (\Delta_1 \wedge \Delta_3)}(s_1, s_2), \\ &\forall (s_1, s_2) \in S_1 \times S_2. \end{aligned} \quad (16)$$

Similarly, by using Definition 7 we have

$$\Phi_{\Delta_1 \wedge (\Delta_2 \vee \Delta_3)}(s_1, s_2) = \Phi_{(\Delta_1 \wedge \Delta_2) \vee (\Delta_1 \wedge \Delta_3)}(s_1, s_2), \quad \forall (s_1, s_2) \in S_1 \times S_2. \quad (17)$$

The proofs of (vi)–(x) are straightforward. □

Theorem 2. *Suppose we have two FFRs Δ_1 in $S_1 \times S_2$ and Δ_2 in $S_2 \times S_3$, respectively, then $(\Delta_1 \circ \Delta_2)^{-1} = \Delta_1^{-1} \circ \Delta_2^{-1}$.*

Proof. Firstly, we show the result with respect to the membership degree. Then,

$$\begin{aligned} \Upsilon_{(\Delta_1 \circ \Delta_2)^{-1}}(s_3, s_1) &= \Upsilon_{\Delta_1 \circ \Delta_2}(s_1, s_3) \\ &= \max\left(\text{average}\left(\Upsilon_{\Delta_1}(s_1, s_2), \Upsilon_{\Delta_2}(s_2, s_3)\right)\right) \\ &= \max\left(\text{average}\left(\Upsilon_{\Delta_1^{-1}}(s_2, s_1), \Upsilon_{\Delta_2^{-1}}(s_3, s_2)\right)\right) \\ &= \max\left(\text{average}\left(\Upsilon_{\Delta_2^{-1}}(s_3, s_2), \Upsilon_{\Delta_1^{-1}}(s_2, s_1)\right)\right) \\ &= \Upsilon_{\Delta_1^{-1} \circ \Delta_2^{-1}}(s_3, s_1), \quad \forall (s_3, s_1) \in S_3 \times S_1. \end{aligned} \quad (18)$$

Similarly, we have

$$\begin{aligned}\Phi_{(\Delta_1\circ\Delta_2)^{-1}}(s_3,s_1) &= \Phi_{\Delta_1\circ\Delta_2}(s_1,s_3)\\ &= \min\left(\text{average}\left(\Phi_{\Delta_1}(s_1,s_2),\Phi_{\Delta_2}(s_2,s_3)\right)\right)\\ &= \min\left(\text{average}\left(\Phi_{\Delta_1^{-1}}(s_2,s_1),\Phi_{\Delta_2^{-1}}(s_3,s_2)\right)\right)\\ &= \min\left(\text{average}\left(\Phi_{\Delta_2^{-1}}(s_3,s_2),\Phi_{\Delta_1^{-1}}(s_2,s_1)\right)\right)\\ &= \Phi_{\Delta_1^{-1}\circ\Delta_2^{-1}}(s_3,s_1),\quad \forall(s_3,s_1)\in S_3\times S_1.\end{aligned} \tag{19}$$

□

Theorem 3. *Suppose Δ is a FFR in $S_1\times S_2$, and Δ_1 is a FFR in $S_2\times S_3$ and $\Delta_2\le\Delta_1$. Then,*

(i) $\Delta_1\circ\Delta=\Delta^{\circ}\Delta_1$

(ii) $(\Delta_2\circ\Delta_1)\circ\Delta=\Delta_2\circ(\Delta_1\circ\Delta)$

Proof. (i) We show that the FFRs are commutative as follows:

$$\begin{aligned}\Upsilon_{\Delta_1\circ\Delta}(s_1,s_3) &= \max\left(\text{average}\left(\Upsilon_{\Delta}(s_1,s_2),\Upsilon_{\Delta_1}(s_2,s_3)\right)\right)\\ &= \max\left(\text{average}\left(\Upsilon_{\Delta_1}(s_2,s_3),\Upsilon_{\Delta}(s_1,s_2)\right)\right)\\ &= \Upsilon_{\Delta^{\circ}\Delta_1}(s_1,s_3),\quad \forall(s_1,s_3)\in S_1\times S_3.\end{aligned} \tag{20}$$

Similarly,

$$\begin{aligned}\Phi_{\Delta_1\circ\Delta}(s_1,s_3) &= \min\left(\text{average}\left(\Phi_{\Delta}(s_1,s_2),\Phi_{\Delta_1}(s_2,s_3)\right)\right)\\ &= \min\left(\text{average}\left(\Phi_{\Delta_1}(s_2,s_3),\Phi_{\Delta}(s_1,s_2)\right)\right)\\ &= \Phi_{\Delta^{\circ}\Delta_1}(s_1,s_3),\quad \forall(s_1,s_3)\in S_1\times S_3.\end{aligned} \tag{21}$$

(ii) Now, we proof the associativity as the FFRs as follows:

$$\begin{aligned}\Upsilon_{(\Delta_2\circ\Delta_1)\circ\Delta}(s_1,s_3) &= \max\left(\text{average}\left(\Upsilon_{\Delta}(s_1,s_2),\Upsilon_{\Delta_2\circ\Delta_1}(s_2,s_3)\right)\right)\\ &= \max\left(\text{average}\left(\Upsilon_{\Delta}(s_1,s_2),\ \max\left(\text{average}\left(\Upsilon_{\Delta_1}(s_2,s_3),\Upsilon_{\Delta_2}(s_2,s_3)\right)\right)\right)\right)\\ &= \max\left(\text{average}\left(\max\left(\text{average}\left(\Upsilon_{\Delta}(s_1,s_2),\Upsilon_{\Delta_1}(s_2,s)\right)\right),\Upsilon_{\Delta_2}(s,s_3)\right)\right)\\ &= \max\left(\text{average}\left(\Upsilon_{\Delta_1\circ\Delta}(s_1,s),\Upsilon_{\Delta_2}(s,s_3)\right)\right)=\Upsilon_{\Delta_2\circ(\Delta_1\circ\Delta)}(s_1,s_3),\end{aligned} \tag{22}$$

for all $(s_1,s_3)\in S_1\times S_3$.

On the contrary, we get

$$\begin{aligned}\Phi_{(\Delta_2\circ\Delta_1)\circ\Delta}(s_1,s_3) &= \min\left(\text{average}\left(\Phi_{\Delta}(s_1,s_2),\Phi_{\Delta_2\circ\Delta_1}(s_2,s_3)\right)\right)\\ &= \min\left(\text{average}\left(\Phi_{\Delta}(s_1,s_2),\ \min\left(\text{average}\left(\Phi_{\Delta_1}(s_2,s_3),\Phi_{\Delta_2}(s_2,s_3)\right)\right)\right)\right)\\ &= \min\left(\text{average}\left(\min\left(\text{average}\left(\Phi_{\Delta}(s_1,s_2),\Phi_{\Delta_1}(s_2,s)\right)\right),\Phi_{\Delta_2}(s,s_3)\right)\right)\\ &= \min\left(\text{average}\left(\Phi_{\Delta_1\circ\Delta}(s_1,s),\Phi_{\Delta_2}(s,s_3)\right)\right)=\Phi_{\Delta_2\circ(\Delta_1\circ\Delta)}(s_1,s_3),\end{aligned} \tag{23}$$

for all $(s_1,s_3)\in S_1\times S_3$. □

Theorem 4. *Let Δ_1 and Δ_2 be FFRs of $S_1\times S_2$, and Δ_3 and Δ_4 be FFRs of $S_2\times S_3$, then we have the following properties:*

(i) $\Delta_1\le\Delta_2\Rightarrow\Delta_1\circ\Delta^*\le\Delta_2\circ\Delta^*$ *for every FFR* Δ^* *in* $S_2\times S_3$

(ii) $\Delta_3\le\Delta_4\Rightarrow\Delta_*\circ\Delta_3\le\Delta_*\circ\Delta_4$ *for every FFR* Δ_* *in* $S_1\times S_2$

(iii) $\Delta_1\prec\Delta_2\Rightarrow\Delta_1\circ\Delta^*\prec\Delta_2\circ\Delta^*$ *for every FFR* Δ^* *in* $S_2\times S_3$

(iv) $\Delta_3\prec\Delta_4\Rightarrow\Delta_*\circ\Delta_3\prec\Delta_*\circ\Delta_4$ *for every FFR* Δ_* *in* $S_1\times S_2$

(v) $\Delta_*\le\Delta^*\Rightarrow\Delta_*\circ\Delta_*\le\Delta^*\circ\Delta^*$ *if* Δ_* *and* Δ^* *are FFRs in* $S_1\times S_1$

Proof. (i) Assume $\Delta_1\le\Delta_2$. Then, $\Upsilon_{\Delta_1}(s_1,s_2)\le\Upsilon_{\Delta_2}(s_1,s_2)$ and $\Phi_{\Delta_1}(s_1,s_2)\ge\Phi_{\Delta_2}(s_1,s_2)$. Now, we have

$$\begin{aligned}\Upsilon_{\Delta_1\circ\Delta^*}(s_1,s_3) &= \max\left(\text{average}\left(\Upsilon_{\Delta^*}(s_1,s_2),\Upsilon_{\Delta_1}(s_2,s_3)\right)\right)\\ &\le \max\left(\text{average}\left(\Upsilon_{\Delta^*}(s_1,s_2),\Upsilon_{\Delta_2}(s_2,s_3)\right)\right)\\ &= \Upsilon_{\Delta_2\circ\Delta^*}(s_1,s_3).\end{aligned} \tag{24}$$

Similarly,

$$\begin{aligned}\Phi_{\Delta_1\circ\Delta^*}(s_1,s_3) &= \min\left(\text{average}\left(\Phi_{\Delta^*}(s_1,s_2),\Phi_{\Delta_1}(s_2,s_3)\right)\right)\\ &\ge \min\left(\text{average}\left(\Phi_{\Delta^*}(s_1,s_2),\Phi_{\Delta_2}(s_2,s_3)\right)\right)\\ &= \Phi_{\Delta_2\circ\Delta^*}(s_1,s_3).\end{aligned} \tag{25}$$

The proofs of (ii)–(iv) are similar.

(v) If $\Delta_* \le \Delta^*$, then $\Upsilon_{\Delta_*}(s_1,s_1) \le \Upsilon_{\Delta^*}(s_1,s_1)$ and $\Phi_{\Delta_*}(s_1,s_2) \ge \Phi_{\Delta^*}(s_1,s_2)$. Then,

$$\begin{aligned}\Upsilon_{\Delta_*\circ\Delta_*}(s_1,s_1) &= \max\left(\text{average}\left(\Upsilon_{\Delta_*}(s_1,s_1),\Upsilon_{\Delta_*}(s_1,s_1)\right)\right)\\ &\le \max\left(\text{average}\left(\Upsilon_{\Delta^*}(s_1,s_1),\Upsilon_{\Delta^*}(s_1,s_1)\right)\right)\\ &= \Upsilon_{\Delta^*\circ\Delta^*}(s_1,s_1).\end{aligned} \tag{26}$$

Similarly,

$$\begin{aligned}\Phi_{\Delta_*\circ\Delta_*}(s_1,s_1) &= \min\left(\text{average}\left(\Phi_{\Delta_*}(s_1,s_1),\Phi_{\Delta_*}(s_1,s_1)\right)\right)\\ &\ge \min\left(\text{average}\left(\Phi_{\Delta^*}(s_1,s_1),\Phi_{\Delta^*}(s_1,s_1)\right)\right)\\ &= \Phi_{\Delta^*\circ\Delta^*}(s_1,s_1).\end{aligned} \tag{27}$$

□

Theorem 5. *Let Δ_1, Δ_2 be FFRs in $S_2 \times S_3$, and Δ be FFR in $S_1 \times S_2$. Then, we have*

(i) $(\Delta_1 \vee \Delta_2)\circ\Delta \ge (\Delta_1\circ\Delta)\vee(\Delta_2\circ\Delta)$

(ii) $(\Delta_1 \wedge \Delta_2)\circ\Delta \le (\Delta_1\circ\Delta)\wedge(\Delta_2\circ\Delta)$

Proof. By Theorem 1, we have $\Delta_1 \vee \Delta_2 \ge \Delta_1$ and $\Delta_1 \vee \Delta_2 \ge \Delta_2$. Thus, $(\Delta_1 \vee \Delta_2)\circ\Delta \ge (\Delta_1\circ\Delta)$ and $(\Delta_1 \vee \Delta_2)\circ\Delta \ge (\Delta_2\circ\Delta)$. Hence, we get $(\Delta_1 \vee \Delta_2)\circ\Delta \ge (\Delta_1\circ\Delta)\vee(\Delta_2\circ\Delta)$, which proves (i). The proof of (ii) is similar. □

Theorem 6. *Suppose Δ_1, Δ_2 are FFRs in $S_2 \times S_3$, and Δ is a FFR in $S_1 \times S_2$. Then, we have*

(i) $(\Delta_1 \vee \Delta_2)\circ\Delta = (\Delta_1\circ\Delta)\vee(\Delta_2\circ\Delta)$

(ii) $(\Delta_1 \wedge \Delta_2)\circ\Delta = (\Delta_1\circ\Delta)\wedge(\Delta_2\circ\Delta)$

Proof. We first proof (i) as follows:

$$\begin{aligned}\Upsilon_{(\Delta_1\vee\Delta_2)\circ\Delta}(s_1,s_3) &= \max\left(\text{averge}\left(\Upsilon_{\Delta}(s_1,s_2)\Upsilon_{\Delta_1\vee\Delta_2}(s_2,s_3)\right)\right)\\ &= \max\left(\text{averge}\left(\Upsilon_{\Delta}(s_1,s_2),\Upsilon_{\Delta_1}(s_2,s_3)\right),\text{averge}\left(\Upsilon_{\Delta}(s_1,s_2),\Upsilon_{\Delta_2}(s_2,s_3)\right)\right)\\ &= \max\left(\Upsilon_{\Delta^\circ\Delta_1}(s_1,s_3),\Upsilon_{\Delta^\circ\Delta_2}(s_1,s_3)\right) = \Upsilon_{(\Delta_1\circ\Delta)\vee(\Delta_2\circ\Delta)}(s_1,s_3).\end{aligned} \tag{28}$$

Similarly, we obtain

$$\begin{aligned}\Phi_{(\Delta_1\vee\Delta_2)\circ\Delta}(s_1,s_3) &= \min\left(\text{averge}\left(\Phi_{\Delta}(s_1,s_2),\Phi_{\Delta_1\vee\Delta_2}(s_2,s_3)\right)\right)\\ &= \min\left(\text{averge}\left(\Phi_{\Delta}(s_1,s_2),\Phi_{\Delta_1}(s_2,s_3)\right),\text{averge}\left(\Phi_{\Delta}(s_1,s_2),\Phi_{\Delta_2}(s_2,s_3)\right)\right)\\ &= \min\left(\Phi_{\Delta^\circ\Delta_1}(s_1,s_3),\Phi_{\Delta^\circ\Delta_2}(s_1,s_3)\right) = \Phi_{(\Delta_1\circ\Delta)\vee(\Delta_2\circ\Delta)}(s_1,s_3).\end{aligned} \tag{29}$$

The proof of (ii) is similar. □

3.1. Numerical Illustration of FFCRs. An example is given to show the supremacy of the new FFCR over the existing FFCR [11, 40, 41].

Given that X and Y are FFSs in $S = \{s_1, s_2, s_3\}$ defined by

$$\begin{aligned}X &= \{\langle s_1, 0.6, 0.2\rangle, \langle s_2, 0.4, 0.6\rangle, \langle s_3, 0.5, 0.3\rangle\},\\ Y &= \{\langle s_1, 0.8, 0.1\rangle, \langle s_2, 0.7, 0.3\rangle, \langle s_3, 0.6, 0.1\rangle\}.\end{aligned} \tag{30}$$

Using the existing FFCR $\breve{\Delta}$, the minimum of the membership degrees between FFSs X and Y for s_1, s_2, s_3 are $0.6, 0.4, 0.5$ implying that

$$\Upsilon_{\breve{\Delta}}(s) = \max(0.6, 0.4, 0.5) = 0.6. \tag{31}$$

Similarly, the maximum of the nonmembership degrees between FFSs X and Y for s_1, s_2, s_3 are $0.2, 0.6, 0.3$, implying that

$$\Phi_{\breve{\Delta}}(s) = \min(0.2, 0.6, 0.3) = 0.2. \tag{32}$$

Now, the FFCR between X and Y is $\breve{\Delta} = 0.6 - (0.2 \times 0.9189) = 0.4162$.

Using the new FFCR $\breve{\Pi}$ in Definition 5, the mean values of the membership degrees between FFSs X and Y for s_1, s_2, s_3 are $0.7, 0.55, 0.55$. Thus,

$$\Upsilon_{\breve{\Pi}}(s) = \max(0.7, 0.55, 0.55) = 0.7. \tag{33}$$

Again, the mean values of the nonmembership degrees between FFSs X and Y for s_1, s_2, s_3 are $0.15, 0.45, 0.2$. Thus,

$$\Phi_{\breve{\Pi}}(s) = \min(0.15, 0.45, 0.2) = 0.15. \tag{34}$$

Again, the mean values of the nonmembership degrees between FFSs X and Y for s_1, s_2, s_3 are $0.15, 0.45, 0.2$. Thus,

$$\Phi_{\breve{\Pi}}(s) = \min(0.15, 0.45, 0.2) = 0.15. \tag{35}$$

The new FFCR between FFSs X and Y is $\breve{\Pi} = 0.7 - (0.15 \times 0.8678) = 0.5698$.

From the results, it is certain that the new FFCR is better than the approach in [11, 40, 41] because the FFCR between X and Y is greater for the new approach (i.e., while the existing

approach yields 0.4162, the new approach yields 0.5698). This justifies the advantage of taking the mean values of the parameters of FFS over taking the extreme values.

4. Fermatean Fuzzy Composite Relation in Determination of Patients' Medical Status

This section discusses an application of FFCRs in diagnosis analysis of a patient's medical status using a simulated database of disease diagnosis. For the sake of simulation, take $\mathcal{S}$ as a set of symptoms, $\mathcal{D}$ as a set of diseases, and $\mathcal{P}$ as a set of patients. Then, we represent a medical knowledge in Fermatean fuzzy pairs based on a FFR Δ from $\mathcal{S}$ to $\mathcal{D}$ indicated by $\mathcal{S} \times \mathcal{D}$ to bespeak the grades of association and otherwise between $\mathcal{S}$ and $\mathcal{D}$. In the Fermatean fuzzy medical diagnostic process, the symptoms of the diseases are determined, the medical knowledge of the patients based on Fermatean fuzzy values is formulated, and the diagnosis on the basis of the composition using the existing FFCR and the new FFCR are determined.

4.1. New FFCR between Patients and Diseases. Suppose the medical condition of a patient $\mathcal{P}$ is described in terms of a set of symptoms $\mathcal{S}$, then $\mathcal{P}$ is taken to be assigned a diagnosis based on $\breve{\Pi}$ via a FFR Δ_1 from $\mathcal{S}$ to $\mathcal{D}$ designated as $\mathcal{S} \longrightarrow \mathcal{D}$ as simulated by medical knowledge in terms of degrees of association and otherwise.

We construct a FFR Δ_2 from $\mathcal{P}$ to $\mathcal{S}$ represented by $\mathcal{P} \longrightarrow \mathcal{S}$ as Δ_1. Then, the FFCR $\breve{\Pi}$ of Δ_1 and Δ_2 (i.e., $\breve{\Pi} = \Delta_1 \circ \Delta_2$) signifies the medical condition of the patients with regards to the ailments given by the MD and NMD in equation (36).

$$\begin{aligned} \Upsilon_{\breve{\Pi}}(p,d) &= \max\Big(\text{average}\Big(\Upsilon_{\Delta_2}(p,s), \Upsilon_{\Delta_1}(s,d)\Big)\Big), \\ \Phi_{\breve{\Pi}}(p,d) &= \min\Big(\text{average}\Big(\Phi_{\Delta_2}(p,s), \Phi_{\Delta_1}(s,d)\Big)\Big), \end{aligned} \tag{36}$$

for all the patients and ailments.

The result for which $\breve{\Pi} = \Upsilon_{\breve{\Pi}}(p,d) - \Phi_{\breve{\Pi}}(p,d)\Psi_{\breve{\Pi}}(p,d)$ is the greatest determines the diagnosis of the patient P. For easy computation of the FFCR, the algorithm which describes the step-to-step computational processes of the composite relation between the patients and the diseases is given as follows:

Step 1: Institute a relation between $\mathcal{S}$ and $\mathcal{D}$ as FFPs

Step 2: Institute a relation between $\mathcal{P}$ and $\mathcal{S}$ as FFPs

Step 3: Find MD and NMD of $\Delta_1 \circ \Delta_2$ between the patients and diseases with respect to the clinical symptoms

Step 4: Calculate FFCR $\breve{\Pi}$ between the patients and diseases using the information from Step 3

Step 5: Decide the diagnosis on the basis of the relation for which the FFCR Π is maximum

The algorithm can be represented as a flowchart.

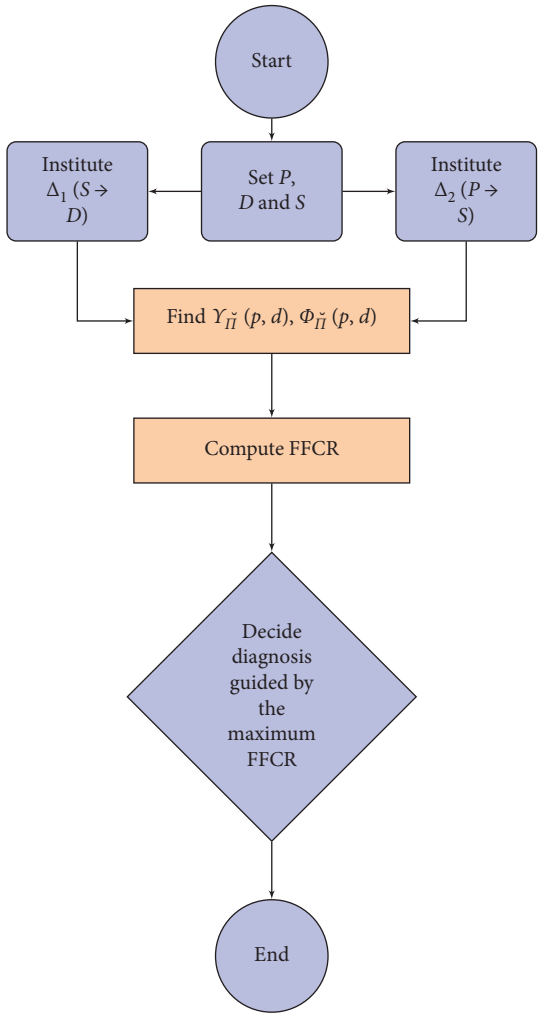

4.2. Application Example. Assume patients $\mathcal{P} = \{\mathcal{P}_1, \mathcal{P}_2, \mathcal{P}_3, \mathcal{P}_4\}$ visit a medical lab to ascertain their health conditions. After the vital signs of the patients were collected, the following symptoms $\mathcal{S}$, namely, high temperature, headache, stomach pain, cough, and chest pain were observed. From medical knowledge of the consultation, we simulate FFR $\Delta_2(\mathcal{P} \longrightarrow \mathcal{S})$, as shown in Table 1.

After the medical consultations guided by the vital signs, the patients are suspected to be infected by viral fever (V), malaria (M), typhoid fever (T), stomach problem (S), and heart problem (H). Similarly, FFR $\Delta_1(\mathcal{S} \longrightarrow \mathcal{D})$ is given in Table 2. The simulated data in Tables 1 and 2 were used in [11] (S. K. De, R. Biswas, A. R. Roy (2001) An application of intuitionistic fuzzy sets in medical diagnosis, Fuzzy Sets and Systems 117(2) 209–213) to demonstrate the application of IFSs in medical diagnosis. However, the data are extended to Fermatean fuzzy values in this work.

Table 1: $\Delta_2(\mathscr{P} \longrightarrow \mathscr{S})$.

Δ_2	Temp	Headache	Stomach pain	Cough	Chest pain
$\Upsilon_{\mathscr{P}_1}$	0.8000	0.6000	0.2000	0.6000	0.1000
$\Phi_{\mathscr{P}_1}$	0.1000	0.1000	0.8000	0.1000	0.6000
$\Upsilon_{\mathscr{P}_2}$	0.0000	0.4000	0.6000	0.1000	0.1000
$\Phi_{\mathscr{P}_2}$	0.8000	0.4000	0.1000	0.7000	0.8000
$\Upsilon_{\mathscr{P}_3}$	0.8000	0.8000	0.0000	0.2000	0.0000
$\Phi_{\mathscr{P}_3}$	0.1000	0.1000	0.6000	0.7000	0.5000
$\Upsilon_{\mathscr{P}_4}$	0.6000	0.5000	0.3000	0.7000	0.3000
$\Phi_{\mathscr{P}_4}$	0.1000	0.4000	0.4000	0.2000	0.4000

Table 2: $\Delta_1(\mathscr{S} \longrightarrow \mathscr{D})$.

Δ_1	Temp	Headache	Stomach pain	Cough	Chest pain
Υ_V	0.4000	0.3000	0.1000	0.4000	0.1000
Φ_V	0.0000	0.5000	0.7000	0.3000	0.7000
Υ_M	0.7000	0.2000	0.0000	0.7000	0.1000
Φ_M	0.0000	0.6000	0.9000	0.0000	0.8000
Υ_T	0.3000	0.6000	0.2000	0.2000	0.1000
Φ_T	0.3000	0.1000	0.7000	0.6000	0.9000
Υ_S	0.1000	0.2000	0.8000	0.2000	0.2000
Φ_S	0.7000	0.4000	0.0000	0.7000	0.7000
Υ_H	0.1000	0.0000	0.2000	0.2000	0.8000
Φ_H	0.8000	0.8000	0.8000	0.8000	0.1000

Table 3: MD and NMD for FFCR $\breve{\Pi}$.

$\mathscr{P}$ vs $\mathscr{D}$	V	M	T	S	H
$\mathscr{P}_1$	0.6000	0.7500	0.6000	0.5000	0.4500
	0.0500	0.0500	0.1000	0.2500	0.3500
$\mathscr{P}_2$	0.3500	0.4000	0.5000	0.7000	0.4500
	0.4000	0.3500	0.2500	0.0500	0.4500
$\mathscr{P}_3$	0.6000	0.7500	0.7000	0.5000	0.4500
	0.0500	0.0500	0.1000	0.2500	0.3000
$\mathscr{P}_4$	0.5500	0.7000	0.5500	0.5500	0.5500
	0.0500	0.0500	0.2000	0.2000	0.2500

Table 4: MD and NMD for FFCR $\breve{\Delta}$.

$\mathscr{P}$ vs $\mathscr{D}$	V	M	T	S	H
$\mathscr{P}_1$	0.4000	0.7000	0.6000	0.2000	0.2000
	0.1000	0.1000	0.1000	0.4000	0.6000
$\mathscr{P}_2$	0.3000	0.2000	0.4000	0.6000	0.2000
	0.5000	0.6000	0.4000	0.1000	0.8000
$\mathscr{P}_3$	0.4000	0.7000	0.6000	0.2000	0.2000
	0.1000	0.1000	0.1000	0.4000	0.5000
$\mathscr{P}_4$	0.4000	0.7000	0.5000	0.3000	0.3000
	0.1000	0.1000	0.3000	0.4000	0.4000

By applying our new approach, we get the parameters MD and NMD, as shown in Table 3.

By applying the approach of [11] in a Fermatean fuzzy setting, the parameters MD and NMD of FFCR $\breve{\Delta}$ are computed, as shown in Table 4.

After calculating the indexes of the FFPs, the results for FFCRs using the existing approach [11] are contained in the following matrix:

$$\begin{matrix} \text{V} & \text{M} & \text{T} & \text{S} & \text{H} & \\ \begin{bmatrix} 0.3022 & 0.6131 & 0.5078 & -0.1902 & -0.3513 \\ -0.1733 & -0.3513 & 0.0178 & 0.5078 & -0.4264 \\ 0.3022 & 0.6131 & 0.5078 & -0.1902 & -0.2768 \\ 0.3022 & 0.6131 & 0.2161 & -0.0875 & -0.0875 \end{bmatrix} & \begin{matrix} \mathcal{P}_1 \\ \mathcal{P}_2 \\ \mathcal{P}_3 \\ \mathcal{P}_4 \end{matrix} \end{matrix}. \tag{37}$$

From the matrix, the following diagnosis are deduced:

(i) Patient $\mathscr{P}_1$ is diagnosed with malaria fever with a reasonable proportion of typhoid fever

(ii) Patient $\mathscr{P}_2$ is diagnosed with stomach problem

(iii) Patient $\mathscr{P}_3$ is diagnosed with malaria fever with a reasonable proportion of typhoid fever

(iv) Patient $\mathscr{P}_4$ is diagnosed with malaria fever

None of the patient is suffering from viral fever and heart problem. $\mathscr{P}_1$ has negative relation with stomach problem and heart problem; $\mathscr{P}_2$ has negative relation with viral fever, malaria fever, and heart problem; $\mathscr{P}_3$ has negative relation with stomach problem and heart problem; and $\mathscr{P}_4$ also has negative relation with stomach problem and heart problem. From the analysis, it is sensible the physician administers the same treatment to patients $\mathscr{P}_1$ and $\mathscr{P}_3$ because they have the same infection load of malaria fever and typhoid fever.

Similarly, the results using the new FFCR $\breve{\Pi}$ are contained in the following matrix:

$$\begin{matrix} \text{V} & \text{M} & \text{T} & \text{S} & \text{H} & \\ \begin{bmatrix} 0.5539 & 0.7084 & 0.5078 & 0.2623 & 0.1164 \\ -0.0352 & -0.0352 & 0.2623 & 0.6565 & 0.0292 \\ 0.5539 & 0.7084 & 0.6131 & 0.2623 & 0.1623 \\ 0.5029 & 0.6584 & 0.3624 & 0.3624 & 0.3162 \end{bmatrix} & \begin{matrix} \mathcal{P}_1 \\ \mathcal{P}_2 \\ \mathcal{P}_3 \\ \mathcal{P}_4 \end{matrix} \end{matrix}. \tag{38}$$

From the matrix, we obtain the following diagnosis:

(i) Patient $\mathscr{P}_1$ is suffering from malaria fever with a reasonable proportion of viral fever and typhoid fever

(ii) Patient $\mathscr{P}_2$ is suffering from stomach problem only

(iii) Patient $\mathscr{P}_3$ is suffering from malaria fever with a reasonable proportion of typhoid fever and viral fever

(iv) Patient $\mathscr{P}_4$ is suffering from malaria fever with a reasonable proportion of viral fever

In order to show the edge of FFSs over IFSs and PFSs in terms of the ability to restrict uncertainties based on the new composition approach, we make use of the data in Tables 1–3 to compute the composite relation between each patients and diseases. By using the data as intuitionistic fuzzy data, we get the results in the matrix that follows:

$$\begin{matrix} \text{V} & \text{M} & \text{T} & \text{S} & \text{H} & \\ \begin{bmatrix} 0.5825 & 0.7400 & 0.5700 & 0.4375 & 0.3800 \\ 0.5825 & 0.3125 & 0.4375 & 0.6875 & 0.4050 \\ 0.5825 & 0.7400 & 0.6800 & 0.4375 & 0.3750 \\ 0.5300 & 0.6875 & 0.5000 & 0.5000 & 0.5000 \end{bmatrix} & \begin{matrix} \mathcal{P}_1 \\ \mathcal{P}_2 \\ \mathcal{P}_3 \\ \mathcal{P}_4 \end{matrix} \end{matrix}. \tag{39}$$

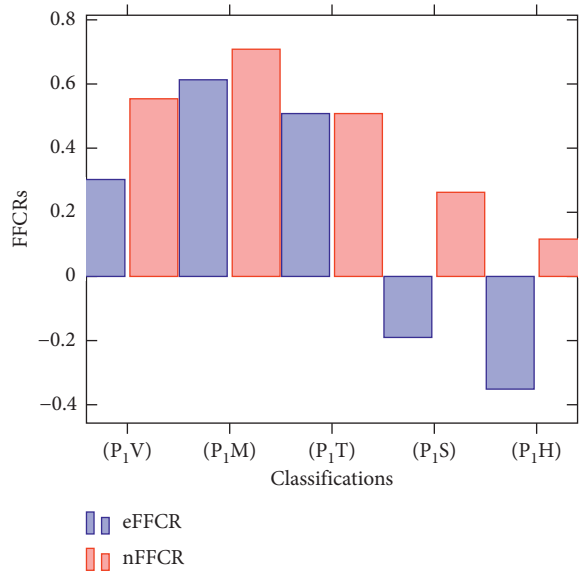

Figure 1: P_1 vs diseases.

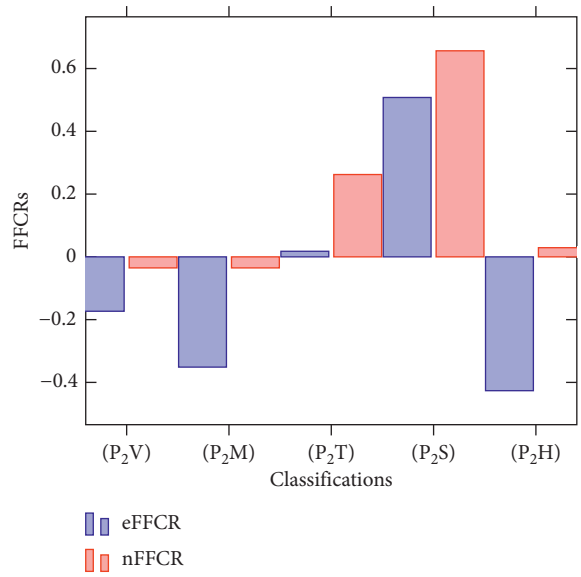

Figure 2: P_2 vs diseases.

From the results using intuitionistic fuzzy data, the following diagnoses are given: patient $\mathscr{P}_1$ is suffering from the same disease as given by our approach; patient $\mathscr{P}_2$ is suffering from stomach problem with a reasonable proportion of viral fever, which is different from the diagnosis of our approach (because of the inability of IFS to reasonably curb uncertainties); patient $\mathscr{P}_3$ is suffering from the same diseases as given by our approach; patient $\mathscr{P}_4$ is suffering from malaria fever with a reasonable proportion of viral fever, and equal proportion of typhoid fever, stomach problem, and heart problem (different from the diagnoses of our approach due to the inability of IFS to reasonably curb uncertainties). Though the values of the composite relation using intuitionistic fuzzy data are greater than our approach, it is certainly because of the inability of IFS to reasonably restrict the uncertainties in the process of diagnosis.

In addition, by using the data as Pythagorean fuzzy data, we get the following results:

$$\begin{array}{c} \begin{matrix} \text{V} & \text{M} & \text{T} & \text{S} & \text{H} \end{matrix} \\ \begin{bmatrix} 0.5601 & 0.7170 & 0.5206 & 0.2927 & 0.1624 \\ 0.0112 & 0.1035 & 0.2927 & 0.6644 & 0.1029 \\ 0.5601 & 0.7170 & 0.6293 & 0.2927 & 0.1977 \\ 0.5083 & 0.6644 & 0.3878 & 0.3878 & 0.3508 \end{bmatrix} \begin{matrix} \mathscr{P}_1 \\ \mathscr{P}_2 \\ \mathscr{P}_3 \\ \mathscr{P}_4 \end{matrix} \end{array}. \tag{40}$$

Because the concept of PFSs is better than IFSs in terms of the ability to control uncertainties, the diagnoses gotten from the Pythagorean fuzzy data using our approach are the same as with our new Fermatean fuzzy composite relation approach. Though the values of the composite relation using

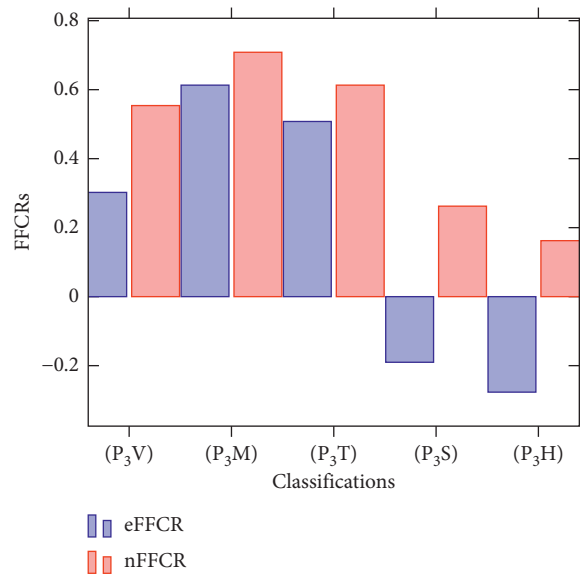

Figure 3: P_3 vs diseases.

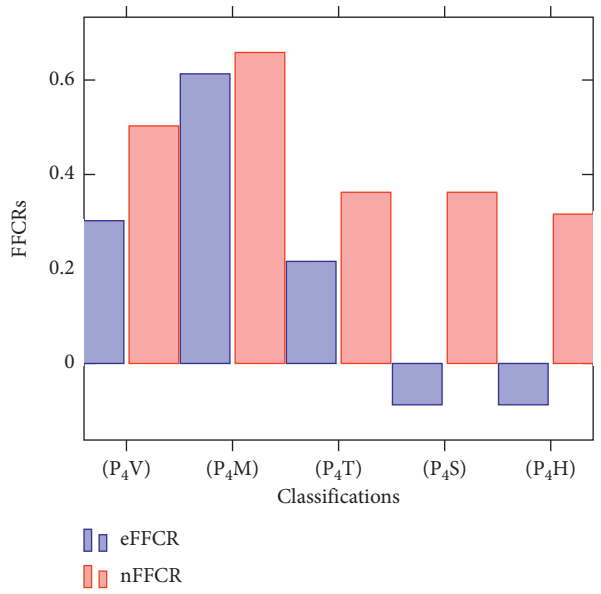

Figure 4: P_4 vs diseases.

Table 5: Comparative table.

$\mathscr{P}$ vs $\mathscr{D}$	V	M	T	S	H
$\mathscr{P}_1$	0.3022	0.6131	0.5078	−0.1902	−0.3513
	0.5539	**0.7084**	**0.5078**	**0.2623**	**0.1164**
$\mathscr{P}_2$	−0.1733	−0.3513	0.0178	0.5078	−0.4264
	−0.0352	**−0.0352**	**0.2623**	**0.6565**	**0.0292**
$\mathscr{P}_3$	0.3022	0.6131	0.5078	−0.1902	−0.2768
	0.5539	**0.7084**	**0.6131**	**0.2623**	**0.1623**
$\mathscr{P}_4$	0.3022	0.6131	0.2161	−0.0875	−0.0875
	0.5029	**0.6584**	**0.3624**	**0.3624**	**0.3162**

Pythagorean fuzzy data based on our approach are slightly greater than our Fermatean fuzzy data approach, it is certainly because of the failure of PFSs to reasonably restrain the uncertainties of the diagnostic process.

4.3. Comparative Analysis of the FFCRs. To establish the superiority of the new FFCR (nFFCR) over the existing FFCR (eFFCR) [11, 40, 41], a comparative analysis is presented in Figures 1–4 and Table 5.

From Figures 1–4 and Table 5, the new FFCR is superior to the existing FFCR because it provides better relation between the patients and ailments, and thus will guide physician on the suitable treatment. The existing FFCR uses extreme values (the max-min-max approach), whereas the new FFCR uses the maximum-average approach to augment the performance rating. The diagnostic analysis derived from the existing FFCR and the new FFCR are the same, although the new FFCR shows more additional diagnosis with grade of severities. In fact, while the approach in [11, 40, 41] shows that patients $\mathscr{P}_1$ and $\mathscr{P}_3$ should be treated for malaria fever and typhoid fever only, the new approach suggested treatment for viral fever for the patients in addition to malaria fever and typhoid fever. Similarly, while the existing FFCR suggested that patient $\mathscr{P}_4$ should be treated for malaria fever, the new approach included treatment for viral fever.

5. Conclusion

tIn this paper, we have introduced an enhanced FFCR with a better performance rating and applied it in determining the medical diagnosis of certain patients. The modified FFCR was introduced to promote the application of FFSs in decision-making. An algorithm for the modified FFCR was presented to ease computation. To validate the advantage of the new FFCR over the existing approach [11, 40, 41], a comparative analysis was presented in Table 5, from which the modified FFCR approach outperformed the existing approach. Diagnostic analysis on some patients wasconducted based on the modified FFCR where the patients and ailments were presented in FFPs. The medical diagnosis via the modified FFCR will improve suitable drug administration and therapy. The new FFCR will foster further application of FFSs in practical areas of decision making. Although the proposed method enhances reliability with a better performance rating compared to the extreme values method, it has some limitations, which include the following: (i) it cannot be used to model cases involving picture fuzzy information and spherical fuzzy information because it only admits three parameters, and (ii) the maximum-average approach of composite relation cannot be determined by mere inspection like the maximum-extreme values approach.

Data Availability

No data were used to support this study.

Conflicts of Interest

The authors declare that there are no conflicts of interest.

Acknowledgments

This work was supported by the Taif University Researchers Supporting Project (TURSP-2020/246), Taif University, Taif, Saudi Arabia.

References

[1] L. A. Zadeh, "Fuzzy sets," *Information and Control*, vol. 8, no. 3, pp. 338–353, 1965.

[2] K. T. Atanassov, "Intuitionistic fuzzy sets," *Fuzzy Sets and Systems*, vol. 20, no. 1, pp. 87–96, 1986.

[3] K. T. Atanassov, *Intuitionistic Fuzzy Sets: Theory and Applications*, Physica-Verlag, Heidelberg, Germany, 1999.

[4] R. R. Yager, "Pythagorean membership grades in multicriteria decision making," Technical Report MII-3301 Machine Intelligence Institute, Iona College, New Rochelle, NY, USA, 2013.

[5] S. S. Begum and R. Srinivasan, "Some properties on intuitionistic fuzzy sets of third type," *Ann Fuzzy Math Inform*, vol. 10, no. 5, pp. 799–804, 2015.

[6] T. Senapati and R. R. Yager, "Fermatean fuzzy sets," *Journal of Ambient Intelligence and Humanized Computing*, vol. 11, no. 2, pp. 663–674, 2020.

[7] F. E. Boran and D. Akay, "A biparametric similarity measure on intuitionistic fuzzy sets with applications to pattern recognition," *Information Sciences*, vol. 255, no. 10, pp. 45–57, 2014.

[8] S.-M. Chen and C.-H. Chang, "A novel similarity measure between Atanassov's intuitionistic fuzzy sets based on transformation techniques with applications to pattern recognition," *Information Sciences*, vol. 291, pp. 96–114, 2015.

[9] S. M. Chen and Y. Randyanto, "A novel similarity measure between intuitionistic fuzzy sets and its applications," *International Journal of Pattern Recognition and Artificial Intelligence*, vol. 27, no. 7, Article ID 1350021, 2013.

[10] A. G. Hatzimichailidis, G. A. Papakostas, and V. G. Kaburlasos, "A novel distance measure of intuitionistic fuzzy sets and its application to pattern recognition problems," *International Journal of Intelligent Systems*, vol. 27, no. 4, pp. 396–409, 2012.

[11] S. K. De, R. Biswas, and A. R. Roy, "An application of intuitionistic fuzzy sets in medical diagnosis," *Fuzzy Sets and Systems*, vol. 117, no. 2, pp. 209–213, 2001.

[12] E. Szmidt and J. Kacprzyk, "Medical diagnostic reasoning using a similarity measure for intuitionistic fuzzy sets," *Note IFS*, vol. 10, no. 4, pp. 61–69, 2004.

[13] E. Szmidt and J. Kacprzyk, "Intuitionistic fuzzy sets in some medical applications," *Note IFS*, vol. 7, no. 4, pp. 58–64, 2001.

[14] R. Parvathi and N. Palaniappan, "Some operations on IFSs of second type," *Note IFS*, vol. 10, no. 2, pp. 1–19, 2004.

[15] P. A. Ejegwa, "Improved composite relation for Pythagorean fuzzy sets and its application to medical diagnosis," *Granular Computing*, vol. 5, no. 2, pp. 277–286, 2020.

[16] R. R. Yager and A. M. Abbasov, "Pythagorean membership grades, complex numbers, and decision making," *International Journal of Intelligent Systems*, vol. 28, no. 5, pp. 436–452, 2013.

[17] W. Zeng, D. Li, and Q. Yin, "Distance and similarity measures of Pythagorean fuzzy sets and their applications to multiple criteria group decision making," *International Journal of Intelligent Systems*, vol. 33, no. 11, pp. 2236–2254, 2018.

[18] Y. Du, F. Hou, W. Zafar, Q. Yu, and Y. Zhai, "A novel method for multiattribute decision making with interval-valued Pythagorean fuzzy linguistic information," *International Journal of Intelligent Systems*, vol. 32, no. 10, pp. 1085–1112, 2017.

[19] H. Garg, "A new generalized Pythagorean fuzzy information aggregation using Einstein operations and its application to decision making," *International Journal of Intelligent Systems*, vol. 31, no. 9, pp. 886–920, 2016.

[20] H. Garg, "Generalized pythagorean fuzzy geometric aggregation operators using einsteint-norm andt-conorm for multicriteria decision-making process," *International Journal of Intelligent Systems*, vol. 32, no. 6, pp. 597–630, 2017.

[21] D. Liang and Z. Xu, "The new extension of TOPSIS method for multiple criteria decision making with hesitant Pythagorean fuzzy sets," *Applied Soft Computing*, vol. 60, pp. 167–179, 2017.

[22] L. Wang and H. Garg, "Algorithm for multiple attribute decision-making with interactive Archimedean norm operations under Pythagorean fuzzy uncertainty," *International Journal of Computational Intelligence Systems*, vol. 14, no. 1, pp. 503–527, 2021.

[23] Y. Xing, M. Cao, Y. Liu, M. Zhou, and J. Wu, "A Choquet integral based interval Type-2 trapezoidal fuzzy multiple attribute group decision making for Sustainable Supplier Selection," *Computers & Industrial Engineering*, vol. 165, Article ID 107935, 2022.

[24] Q. Sun, J. Wu, F. Chiclana, H. Fujita, and E. Herrera-Viedma, "A dynamic feedback mechanism with attitudinal consensus threshold for minimum adjustment cost in group decision making," *IEEE Transactions on Fuzzy Systems*, vol. 30, no. 5, pp. 1287–1301, 2021.

[25] I. Silambarasan, "New operators for Fermatean fuzzy sets," *Ann Commun Math*, vol. 3, no. 2, pp. 116–131, 2020.

[26] Z. Yang, H. Garg, and X. Li, "Differential calculus of Fermatean fuzzy functions: continuities, derivatives, and differentials," *International Journal of Computational Intelligence Systems*, vol. 14, no. 1, pp. 282–294, 2021.

[27] D. Liu, Y. Liu, and X. Chen, "Fermatean fuzzy linguistic set and its application in multicriteria decision making," *International Journal of Intelligent Systems*, vol. 34, no. 5, pp. 878–894, 2019.

[28] T. Senapati and R. R. Yager, "Fermatean fuzzy weighted averaging/geometric operators and its application in multicriteria decision-making methods," *Engineering Applications of Artificial Intelligence*, vol. 85, pp. 112–121, 2019.

[29] T. Senapati and R. R. Yager, "Some new operations over Fermatean fuzzy numbers and application of Fermatean fuzzy WPM in multiple criteria decision making," *Informatica*, vol. 30, no. 2, pp. 391–412, 2019.

[30] S. D. Sari, I. Ucal, and S. Tapan, "Extension of capital budgeting techniques using interval-valued Fermatean fuzzy sets," *Journal of Intelligent and Fuzzy Systems*, vol. 42, 2021.

[31] S. Jeevaraj, "Ordering of interval-valued Fermatean fuzzy sets and its applications," *Expert Systems with Applications*, vol. 185, 2021.

[32] K. G. Mehdi, A. Maghsoud, H. T. Mohammad, K. Z. Edmundas, and K. Arturas, "A new decision-making approach based on Fermatean fuzzy sets and WASPAS for green construction supplier evaluation," *Mathematics*, vol. 8, 2020.

[33] V. Salsabeela and S. J. John, "TOPSIS techniques on fermatean fuzzy soft sets," *AIP Conference Proceedings*, vol. 2336, Article ID 040022, 2021.

[34] L. Sahoo, "Some score functions on Fermatean fuzzy sets and its application to bride selection based on TOPSIS method,"

International Journal of Fuzzy System Applications, vol. 11, no. 1, 2022.

[35] S. Aydin, "A fuzzy MCDM method based on new Fermatean fuzzy theories," *International Journal of Information Technology and Decision Making*, vol. 20, no. 3, pp. 881–902, 2021.

[36] L. P. Zhou, S. P. Wan, and J. Y. Dong, "A Fermatean fuzzy ELECTRE method for multi-criteria group decision-making," *Informatica*, vol. 33, 2021.

[37] G. Shahzadi, F. Zafar, and M. A. Alghamdi, "Multiple-attribute decision-making using Fermatean fuzzy Hamacher interactive geometric operators," *Mathematical Problems in Engineering*, vol. 2021, Article ID 5150933, 20 pages, 2021.

[38] H. Garg, G. Shahzadi, and M. Akram, "Decision-making analysis based on Fermatean fuzzy Yager aggregation operators with application in COVID-19 testing facility," *Mathematical Problems in Engineering*, vol. 2020, Article ID 7279027, 16 pages, 2020.

[39] S. Gul, "Fermatean fuzzy set extensions of SAW, ARAS, and VIKOR with applications in COVID-19 testing laboratory selection problem," *Expert Systems*, vol. 38, 2021.

[40] P. A. Ejegwa, K. N. Nwankwo, M. Ahmad, T. M. Ghazal, and M. A. Khan, "Composite relation under Fermatean fuzzy context and its application in disease diagnosis," *Informatica*, vol. 32, no. 10, pp. 87–101, 2021.

[41] P. A. Ejegwa, "Pythagorean fuzzy set and its application in career placements based on academic performance using max-min-max composition," *Complex & Intelligent Systems*, vol. 5, no. 2, pp. 165–175, 2019.

[42] G. Shahzadi, G. Muhiuddin, M. Arif Butt, and A. Ashraf, "Hamacher interactive hybrid weighted averaging operators under fermatean fuzzy numbers," *Journal of Mathematics*, vol. 2021, Article ID 5556017, 17 pages, 2021.

[43] C. Jana, G. Muhiuddin, and M. Pal, "Multi-criteria decision making approach based on SVTrN Dombi aggregation functions," *Artificial Intelligence Review*, vol. 54, no. 5, pp. 3685–3723, 2021.

[44] C. Jana, G. Muhiuddin, and M. Pal, "Multiple-attribute decision making problems based on SVTNH methods," *Journal of Ambient Intelligence and Humanized Computing*, vol. 11, no. 9, pp. 3717–3733, 2020.

[45] C. Jana, G. Muhiuddin, and M. Pal, "Some Dombi aggregation of Q-rung orthopair fuzzy numbers in multiple-attribute decision making," *International Journal of Intelligent Systems*, vol. 34, no. 12, pp. 3220–3240, 2019.

Hindawi
Journal of Mathematics
Volume 2023, Article ID 9760174, 1 page
https://doi.org/10.1155/2023/9760174

Retraction

Retracted: Optimized CNN-Based Recognition of District Names of Punjab State in Gurmukhi Script

Journal of Mathematics

Received 19 December 2023; Accepted 19 December 2023; Published 20 December 2023

This article has been retracted by Hindawi following an investigation undertaken by the publisher [1]. This investigation has uncovered evidence of one or more of the following indicators of systematic manipulation of the publication process:

(1) Discrepancies in scope

(2) Discrepancies in the description of the research reported

(3) Discrepancies between the availability of data and the research described

(4) Inappropriate citations

(5) Incoherent, meaningless and/or irrelevant content included in the article

(6) Manipulated or compromised peer review

The presence of these indicators undermines our confidence in the integrity of the article's content and we cannot, therefore, vouch for its reliability. Please note that this notice is intended solely to alert readers that the content of this article is unreliable. We have not investigated whether authors were aware of or involved in the systematic manipulation of the publication process.

Wiley and Hindawi regrets that the usual quality checks did not identify these issues before publication and have since put additional measures in place to safeguard research integrity.

We wish to credit our own Research Integrity and Research Publishing teams and anonymous and named external researchers and research integrity experts for contributing to this investigation.

The corresponding author, as the representative of all authors, has been given the opportunity to register their agreement or disagreement to this retraction. We have kept a record of any response received.

References

[1] S. Sharma, S. Gupta, D. Gupta et al., "Optimized CNN-Based Recognition of District Names of Punjab State in Gurmukhi Script," *Journal of Mathematics*, vol. 2022, Article ID 6580839, 10 pages, 2022.

Hindawi
Journal of Mathematics
Volume 2022, Article ID 6580839, 10 pages
https://doi.org/10.1155/2022/6580839

Research Article

Optimized CNN-Based Recognition of District Names of Punjab State in Gurmukhi Script

Sandhya Sharma,[1] **Sheifali Gupta**,[2] **Deepali Gupta**,[2] **Sapna Juneja**,[3] **Hamza Turabieh**,[4] **Lokesh Sharma**,[5] **and Zelalem Kiros Bitsue**[6]

[1]*Chitkara University Institute of Engineering and Technology, Chitkara University, Baddi, Himachal Pradesh, India*
[2]*Chitkara University Institute of Engineering and Technology, Chitkara University, Rajpura, Punjab, India*
[3]*KIET Group of Institutions, Delhi NCR, Ghaziabad, India*
[4]*Department of Information Technology, College of Computing and Information Technology, Taif University, P.O. Box 11099, Taif 21944, Saudi Arabia*
[5]*Bennett University, Noida, Uttar Pradesh, India*
[6]*United States of African Health Organization, Addis Ababa, Ethiopia*

Correspondence should be addressed to Zelalem Kiros Bitsue; bitsue.zelalem29@gmail.com

Received 27 January 2022; Revised 16 February 2022; Accepted 5 May 2022; Published 28 May 2022

Academic Editor: Naeem Jan

Automation of Postal systems has the major research scope in the field of automation. To create Postal Automation set-up for countries like India is a tedious task if compared with other countries because of India's multiscript and multilingual behavior. This work will help in recognizing the "Gurmukhi" handwritten district names of the State Punjab. To recognize the district names, a CNN-based architecture is proposed by employing a Holistic approach. For this, an image database of 22000 samples is prepared having 1000 sample images for every district name which is collected from 500 different writers. Maximum accuracy on validation data achieved by the proposed Model is 99%.

1. Introduction

Artificial Intelligence (AI) is bridging the gap between the capabilities of humans and computers. One such area is Computer Vision [1]. The primary aim of this field is to make the computers behave as humans, perceive it in the same manner, and also use the knowledge for various tasks like for image recognition, image analysis, image classification, natural language processing (NLP), and so on. Similarly, Recognition of text can be done using Deep Learning which is the subset of AI. In this, automatic feature extraction and classification is done [1]. District names recognition helps in the automation of the postal system. To develop a postal automation system for the nation India is a tedious task as almost every state has its own script [2]. In this proposed work, Gurmukhi Script is considered as Government of Punjab has declared this as the official language. The address on all the official documents which are to be posted is usually written in the Gurmukhi Script only.

For the recognition, a Holistic approach is used instead of Analytical approach [3]. In the Holistic approach, word for the recognition is not divided into individual characters instead a complete word is recognized whereas in Analytical approach, segmentation of word into characters is done [4]. As Gurmukhi being the cursive handwriting and characters in the word are usually written close to each other, recognition of such words using Analytical approach does not generate good recognition results.

This work will help in automatically reading the district name of the State Punjab. This Script has 35 characters, 6 consonants, and 9 vowels. Its writing style is from left to right [3]. Aim of this work is to produce a system that can allow successful recognition of such handwritten words

without their segmentation. In this article, the major contribution of the author is as follows:

(a) 22000 images of handwritten dataset are created for the districts of the state Punjab in which 500 writers contributed

(b) Deep learning-based model is developed which can help to automate the postal system of the State Punjab

(c) Results which are obtained by the proposed model have been compared with those obtained by other state–of-the-art models

Paper is structured as follows. In Section 2, work related to the postal automation is given, in Section 3, research methodology of the work done is given. Results and Analysis are introduced in Section 4 of the manuscript, and Conclusion is given in Section 5.

This manuscript has been presented as thesis in Shodhganga, a reservoir of Indian theses according to the link: https://shodhganga.inflibnet.ac.in/handle/10603/347820 which is the work of the author itself, and thesis is titled as "CNN-Based Recognition of District Names of Punjab State in Gurmukhi Script."

2. Related Work

In this section, literature survey for the work done in the field of postal automation is presented. There are numerous fields which are present on the postal document like digits for address or pin code, city names, street names, and country names. Address or pin code may include numerals while word letters represent the city name, street name, or country name. Sharma et al. [5] have presented a work for the postal automation. The CNN model to recognize and detect the pin codes is introduced. Model has been implemented on 2300 handwritten English and Bangla written pin code digits. Different architectural networks are employed like Zeiler and Ferges, Visual geometry group (16), and VGG_M. Considerable results to recognize the pin codes are obtained by using VGG_M with the employment of the recurrent convolutional neural network model. Pincode box is also recognized using Zeiler and Ferges with an accuracy of 88%. 56% accuracy is obtained for the detection of pin code regions using VGG_M. 87% accuracy is obtained using VGG16 for the recognition of complete address region.

To determine the 18000 handwritten city names which are written in Gurmukhi, Bansal et al. [6] have proposed a method. A dataset is collected from 60 different writers, and each writer has created 30 samples of each city name. From the total created dataset, 16200 are used to make the network model able to learn and rest to analyze the network model. Preprocessing on the collected dataset is also done like Binarization of the images, normalization, and also thinning operation. Diagonal tree extraction technique is employed on the preprocessed images so that various features can be extracted. Classifiers like K-nearest neighbor (KNN) and support vector machines (SVMs) are imposed. Highest recognition accuracy of 90.8% is obtained with the help of SVM classifier. Similarly, Thadchanamorthy et al. [7] have introduced a technique to recognize city names which are written in Tamil Script. Database having 265 Tamil handwritten city names is created first. Recognition is carried out on individual characters after the segmentation of words. Various features of the segmented characters are computed with the help of modified quadratic discriminant function (MQDF). Achieved accuracy is 96.89%. Pal et al. [8] have also developed a model to recognize the city names which are written in different scripts. To correct the slanted handwritten text, slant correction technique is employed. Next step is to segment them into characters. The model has been tested on 161321 handwritten city names with the accuracy of 92.25%. Similarly, Pal et al. [9] have also developed a technique for the identification and classification of the handwritten city names, written in Bangla.

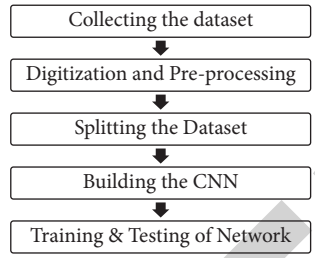

Figure 1: Research methodology.

Wen et al. [10] elaborated the method for the identification of handwritten numerals which are represented in Bangla Script. In the preprocessing step for the recognition of numerals, firstly the location of the numeral which is written on postcode is located so that it can be segmented. Features are extracted after the completion of the preprocessing step. Two different approaches are employed to recognize the Bangla numerals. In one approach, image reconstruction is carried out, and in the other approaches, feature extraction is carried out which is further combined with the principal component analysis (PCA) approach. Average accuracy obtained for the purpose of recognition is 95.6%. Nurseitov et al. [11] have also developed the two CNN model networks for identifying the handwritten names of the cities. The initial model works on CNN while the second one used the recurrent neural network (RNN). For the decoding, the connectionist temporal classification algorithm is implemented. Dataset used has 21000 images with 42 different categories of the city names which are written by 500 writers. Accuracy obtained the first model is 55.3%, and accuracy obtained by the other model is 75.1%. Sahoo et al. [12] have introduced a method to recognize the Bangla handwritten city names. A Holistic approach is used. Recognition is carried out on 50 popular city names of Bengal where each city has 150 samples. Once the features are extracted, then various classifiers like multilayer perceptron (MLP) and sequential minimal optimization (SMO) are used for the classification of images.

So, in this section, an effort has been made to present the work that has been done in the field of postal automation.

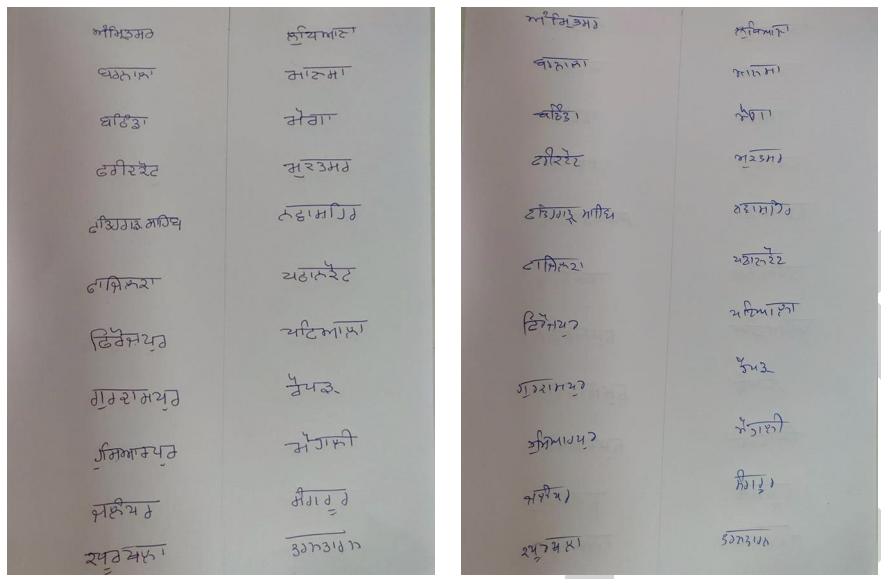

(a) (b)

Figure 2: Handwritten sheets: (a) written by "Writer 1" and (b) written by"Writer 2."

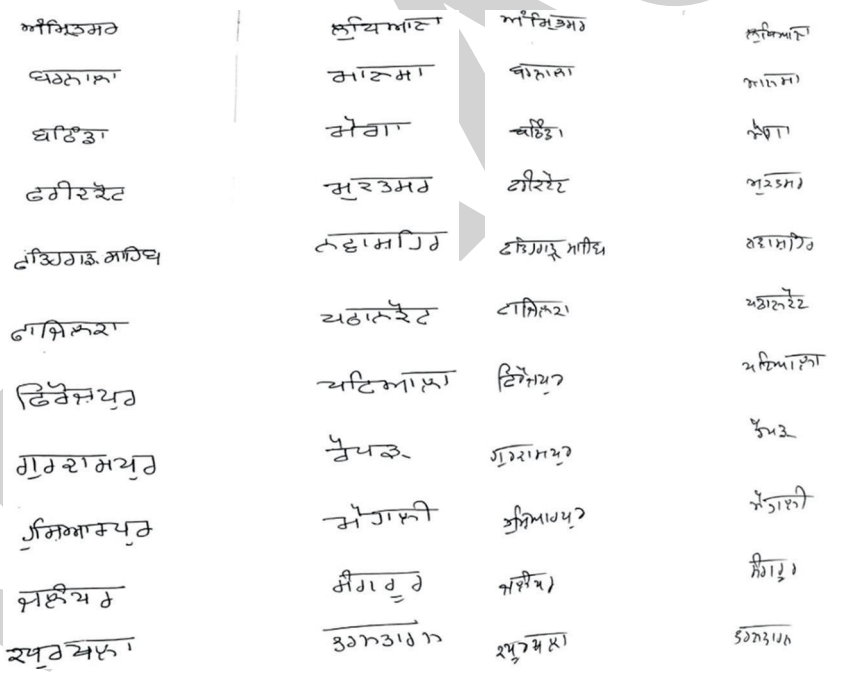

(a) (b)

Figure 3: Scanned handwritten sheets: (a) scanned image "Sample 1" and (b) scanned image "Sample 2."

3. Proposed Research Methodology

The methodology of the research work is presented in Figure 1.

Research methodology is developed to identify the district names of the Punjab State. Here, a Holistic approach is used for the purpose in which the segmentation of the words is not carried out. All the operations are employed on the whole word. The CNN model is trained and tested on Python platform using keras and Tensorflow libraries. To prepare the dataset, Adobe Photoshop is used.

3.1. Dataset. Firstly, the dataset is required to be collected on which the CNN model can be imposed for the purpose of recognition. As recognition is carried out on the 22 district names, 22000 Gurmukhi handwritten dataset images are created, whereas 1000 dataset image samples for every district name are created.

Table 1: Districts names written with their corresponding prepared samples.

S. no.	Districts names	Sample 1	Sample 2	Sample 3
1	Amritsar	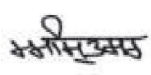	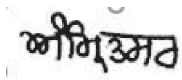	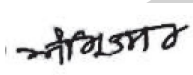
2	Barnala	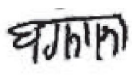	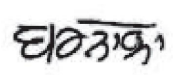	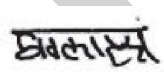
3	Bathinda	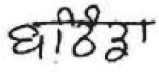	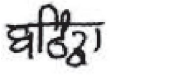	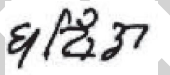
4	Faridkot	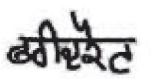	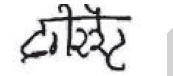	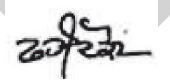
5	Fatehgarh		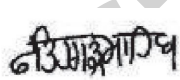	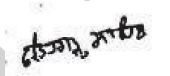
6	Firozpur	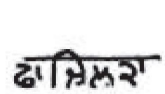	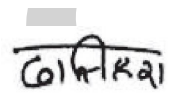	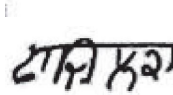
7	Fazilka	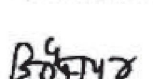	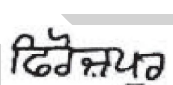	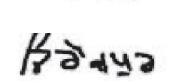
8	Gurdaspur	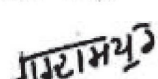	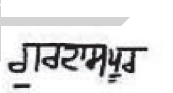	
9	Hoshiarpur	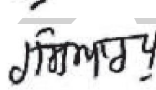	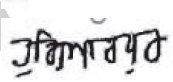	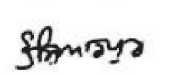
10	Jalandhar	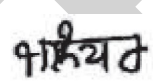	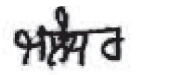	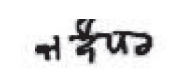
11	Kapurthala	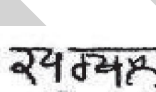		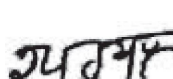
12	Ludhiana	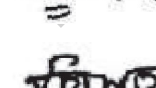	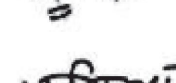	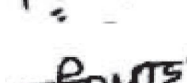
13	Mansa	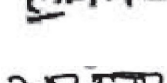	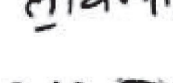	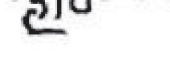
14	Moga			
15	Muktsar			
16	Nawanshahr			

Table 1: Continued.

S. no.	Districts names	Sample 1	Sample 2	Sample 3
17	Pathankot	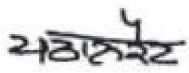	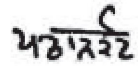	
18	Patiala	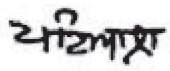	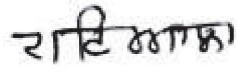	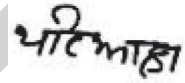
19	Ropar			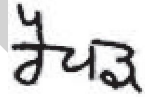
20	Mohali	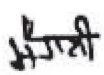	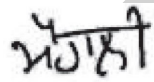	
21	Sangrur		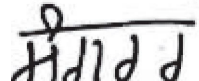	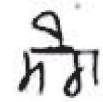
22	Taran taaran	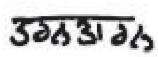	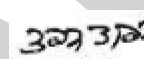	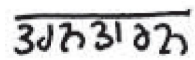

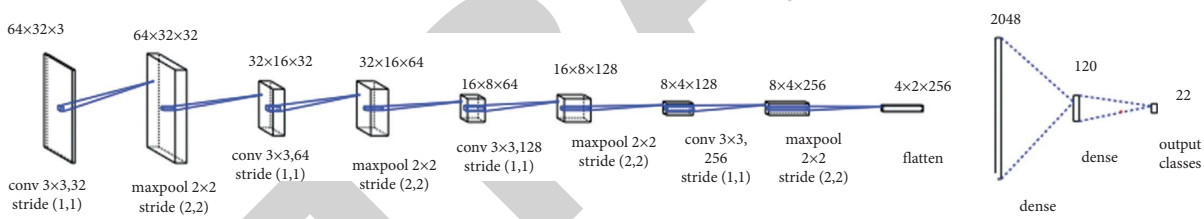

Figure 4: Architecture of the CNN model.

For the creation of dataset of Gurmukhi handwritten words, the handwritten dataset samples are collected from 500 different writers which are selected on the basis of different age groups, different educational, and professional backgrounds. Sample sheets written by the writers are shown in Figure 2.

3.2. Digitization and Preprocessing. After the collection of handwritten sheets, each sheet is digitized using the scanner which was set at the 300 dpi resolution. Scanned images obtained are shown in Figure 3.

Next, to upgrade the quality of scanned sheets, some preprocessing techniques are employed. For the purpose of preprocessing, Adobe Photoshop has been used. For the preprocessing, Brightness, pixel intensity, and Contrast values are adjusted. Later, the words are cropped from the entire sheet. Table 1 is showing a few images of the prepared dataset.

3.3. Splitting the Dataset. Next step after the preparation of the dataset is to divide it into an 80 : 20 ratio. 200 images of each district name will be kept for the purpose of validation while some extra unseen images will be used to test the model.

Table 2: Simulation parameters.

S. no.	Parameter	Value
1.	Optimizer used	ADAM
2.	Total layers in the model	12
3.	Number of training images	17600
4.	Number of validation images	4400
5.	Total layers of the model	12.0
6.	Batch size (BS) of the training images	4.0
7.	LR used	0.001
8.	Steps/Epoch	3000

3.4. Building the Proposed CNN Model. A CNN model is created to identify the district names. The model network will foretell the accuracy, loss, recall, and precision. The model consists of three layers: (a) "convolution," "max-pooling," and "flattening" layer.

Table 3: Results obtained with the proposed CNN model.

Epoch	Training loss	Validation loss	Validation accuracy (%)	Validation recall	Validation precision
1	2.62	0.87	77.0	0.65	0.88
2	1.17	1.04	74.0	0.68	0.84
3	0.78	2.34	60.0	0.56	0.68
4	0.57	0.68	89.0	0.80	0.84
5	0.43	0.18	95.0	0.95	0.96
12	0.17	0.37	97.0	0.97	0.97
13	0.17	0.14	97.0	0.98	0.98
32	0.07	0.19	98.0	0.98	0.98
33	0.06	0.10	98.0	0.98	0.98
34	0.07	0.10	98.0	0.98	0.98
35	0.06	0.14	98.0	0.98	0.98
36	0.06	0.08	98.0	0.98	0.98
37	0.07	0.15	98.0	0.98	0.98
41	0.06	0.40	97.0	0.97	0.97
42	0.05	0.08	98.0	0.98	0.98
43	0.06	0.35	98.0	0.98	0.98
44	0.05	0.08	98.0	0.98	0.99
45	0.05	0.08	99.0	0.99	0.99
Average values	**0.20**	**0.29**	**95.6**	**0.95**	**0.96**

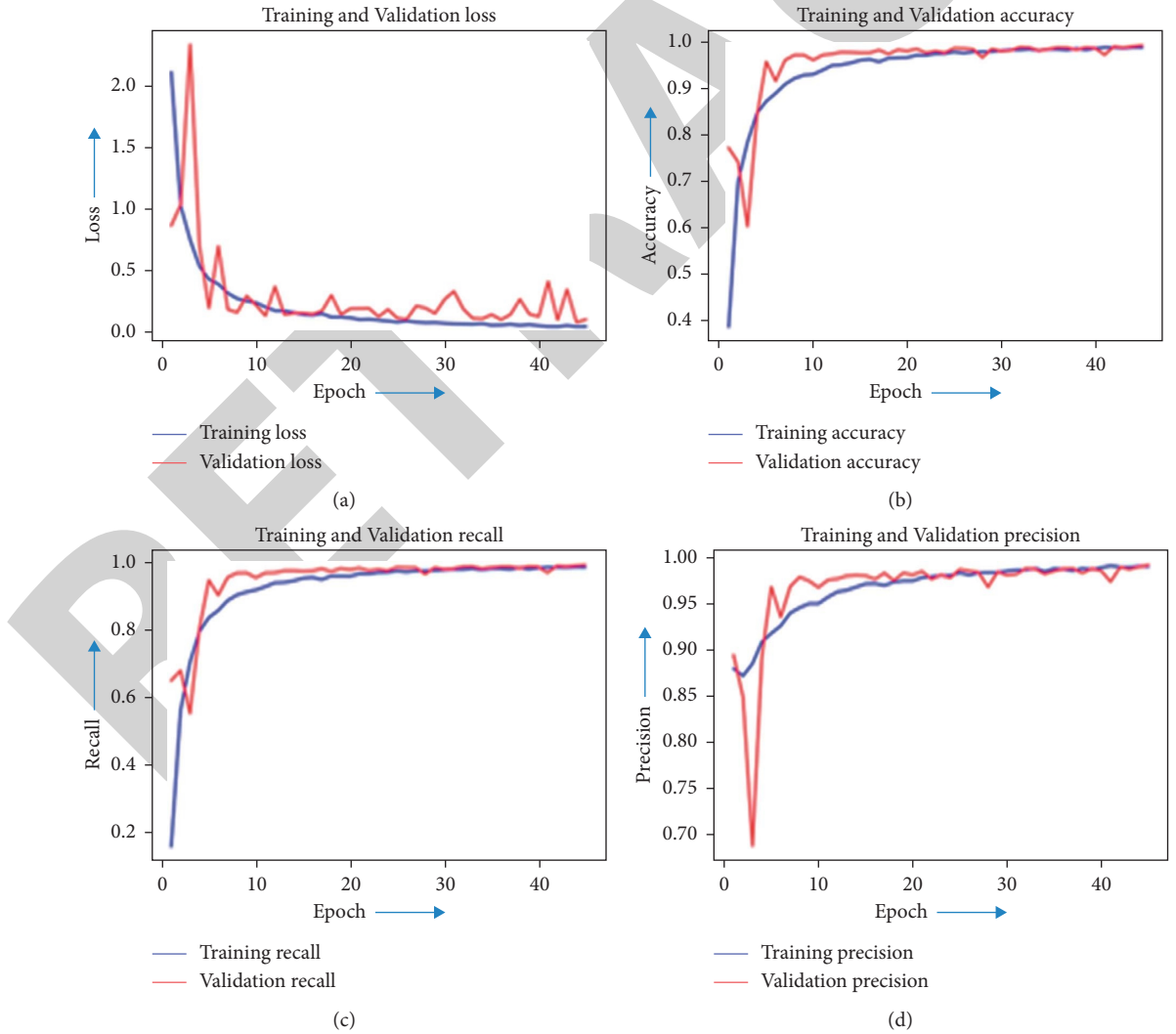

Figure 5: Plot curve obtained for the training and validation dataset using ADAM optimizer with a LR of 0.001 and 45 Epochs, (a) loss, (b) accuracy, (c) recall, and (d) precision.

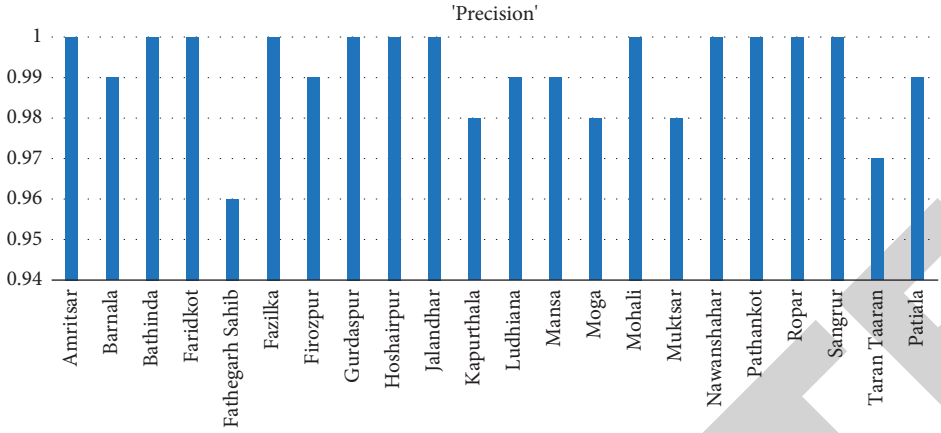

Figure 6: Precision for each district.

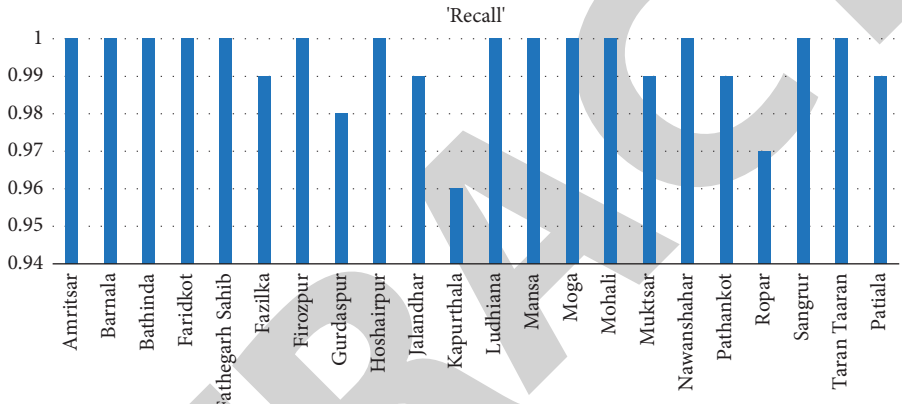

Figure 7: Recall for each district.

Layers, i.e., convolution and pooling help to preserve the important features of the given data images. The obtained features are converted into a column with the help of flattening layer so that they can be easily fed to the last layer of the model which helps to classify the output. The architecture network of the suggested CNN model is given in Figure 4. This model has 12 layers, having 4 pairs of convolution and pooling layers, followed by 1 fattening layer, 2 dense layers, and 1 output layer. Filter size is 3×3 while the number of filters used in the different convolution layers is 32 filters in the first layer, 64 filters in the second, 128 filters in the third layer, and 256 filters are used in the last layer. All the max pooling layers have a size of 2×2.

3.5. Training and Testing of the Network. The suggested CNN network model is now trained and tested on the developed dataset. The specifications like accuracy [13], recall, loss, and precision are calculated. Calculation is done using the discrete metrics of the confusion matrix (CM). Parameters used to simulate the model are shown in Table 2. The model performed at its best by employing the combinations of the values given in Table 2. On changing any of the values, the model's performance either deteriorated or remained the same [14]. On further adding the number of layers in the model, the accuracy obtained remained the same but the time taken for the training of the model increased [15].

4. Results and Analysis

In this part, various results are obtained on the training as well as the validation dataset. Results are seen in Table 3. Value obtained for the minimum training loss is 0.05 which is obtained on the 45th Epoch. On the validation dataset, loss obtained is 0.08, accuracy is 99.0%, and recall and precision obtained are 0.99 on the last epoch. From the proposed model, the highest obtained validation accuracy is 99%.

Figure 5 presents the plot curve of the values which are attained in Table 3. Figure 5(a) shows that the maximum validation loss of 2.3 is obtained on the 3rd epoch. From the 4th epoch onwards, the loss curve for the validation dataset is almost reducing with fluctuations while the curve of training loss is linearly reducing. In Figure 5(b), for validation accuracy, the accuracy is lowest on the 3rd epoch but from the 4th epoch onwards it is also increasing while the curve for the training loss is a linearly changing its value. Plots for the validation dataset using recall and precision parameters are shown in Figures 5(c) and 5(d). Curve for the training dataset is approximating close to 0.99.

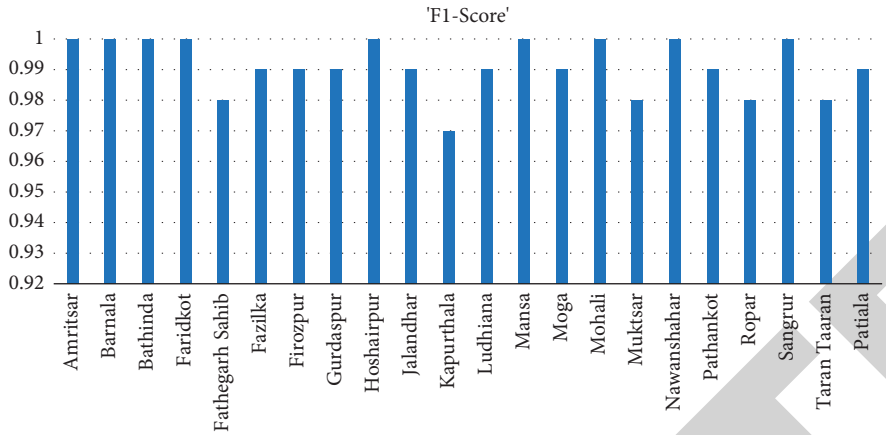

Figure 8: F1-score for each district.

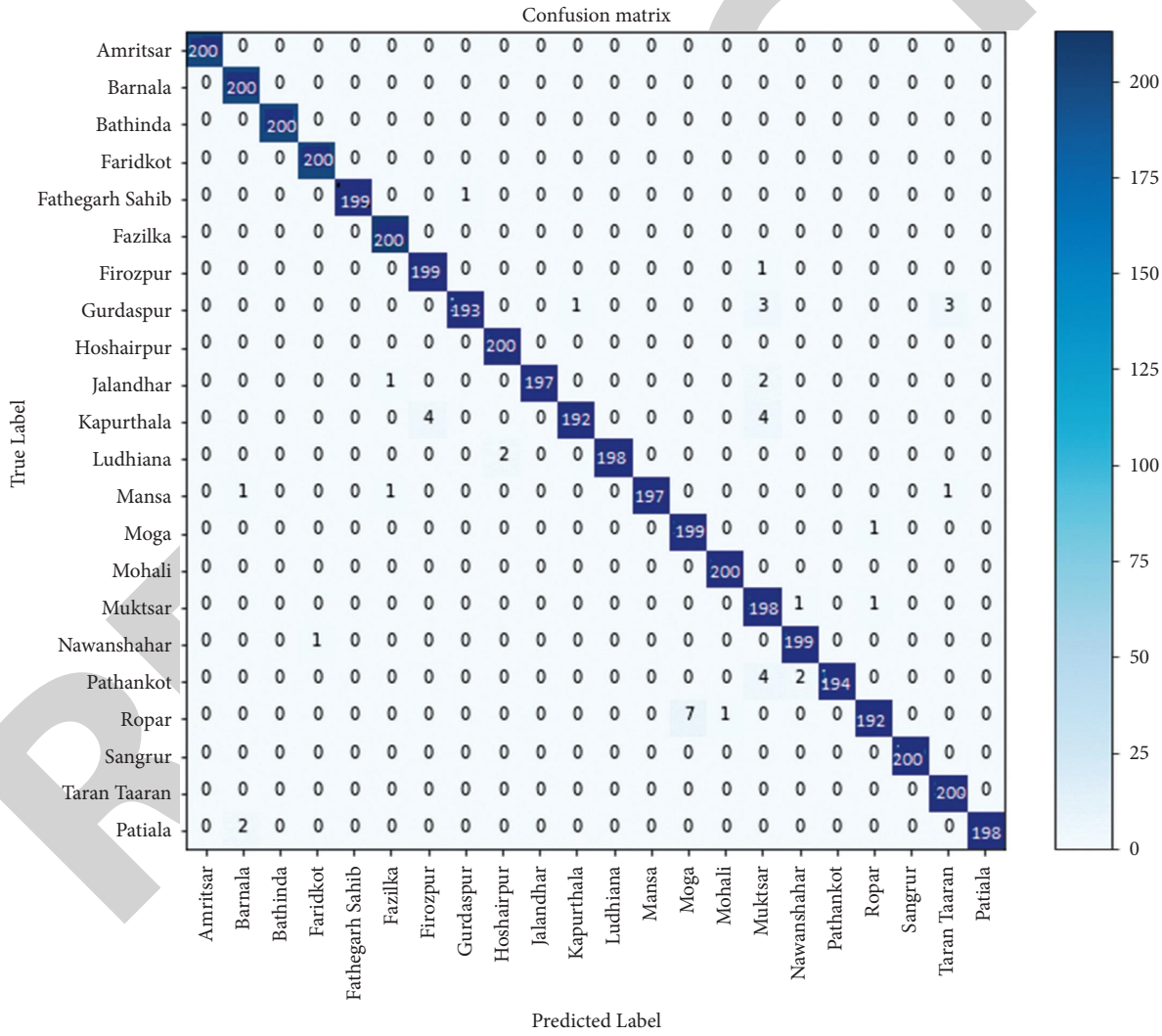

Figure 9: Confusion matrix.

Precision value, F1 score value, and recall value are also computed for each of the district name as shown in Figures 6–8. Figure 6 shows that the implemented model is 100% précised for the recognition of the given districts. Bathinda, Amritsar, Fazilka, Jalandhar, Hoshiarpur, Gurdaspur, Mohali, Sangrur, Nawanshahr, and Ropar as the precision value have reached 1 while lowest value of 0.96 is achieved for the districts: "Fathegarh Sahib." In Figure 7,

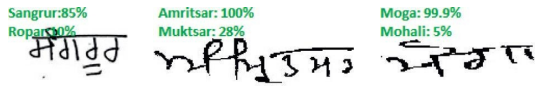

(a) (b) (c)

Figure 10: Testing of few dataset images: (a) Sangrur; (b) Amritsar; (c) Moga.

Table 4: Comparison of the work with state-of-the-art techniques.

Ref no./year	Worked on	Script	Technique used	Accuracy obtained (%)
Reference [16], 2021	City names	Bangla	CNN	98.86
Reference [11], 2019	City and country names	Russian and Kazzak	CNN	55.3
Reference [17], 2017	District names	Malayalam	NN SVM Random forest	94.59 97 87.83
Reference [8], 2012	City names	English, Hindi, and Bangla	Manual feature extraction and dynamic programming	92.5
Reference [7], 2013	City names	Tamil	Manual feature extraction and modified quadratic discriminant function	96.89
Reference [18], 2009	City names	Bangla	Manual feature extraction followed by hidden Markov model	86.44
Reference [19], 2021	UNHD handwritten words	Urdu	Resnet18	86
Reference [20], 2021	Handwritten words	Manipuri	CNN	98.70
Reference [21], 2016	Handwritten words	Bengali	CNN combined with a recurrent model	86.96
Reference [22], 2012	UNIPEN handwritten database	English	CNN	92.20
Reference [23], 2019	Handwritten words	Bangla	Feature extraction: elliptical, vertical, and tetragonal pixel density histogram Classification: MLP and SVM	83.64
Proposed work	District names	Gurmukhi	CNN	99

value for recall is 1 or 100% for "Amritsar," "Bathinda," "Barnala," "Fathegarh Sahib," "Mansa," and "Hoshiarpur" and the minimum value is obtained by the district "Kapurthala." Figure 8 shows the F1-score; 100% value is obtained for the districts "Amritsar," "Bathinda," "Faridkot," "Mohali," and so on, and the lowest score is obtained for the district "Kapurthala."

CM for the proposed CNN model is given in Figure 9. As it is already mentioned, 80% of the images from each of the district names are kept for the purpose of training and 20% are kept for the purpose of testing. It means 800 images of each district are used to train and the remaining 200 to test the model. Figure 9 shows that the model has correctly speculated all districts: "Amritsar," "Faridkot," "Bathinda," and "Fazilka."

4.1. Testing of Images. Here, testing the few images from the prepared dataset is done using the proposed model, and results are presented in Figure 10. In Figure 10(a), district name "Sangrur" is 85% correctly tested.

Similarly, the district name "Amritsar" is 100% correctly predicted, and it is predicted 28% as "Muktsar" also in Figure 10(b). So, it can be declared as district name "Amritsar." Figure 10(c) shows that the district name "Moga" is 99.9% predicted correctly.

4.2. Comparative Analysis with Available Models. Table 4 shows the comparison of the proposed work with the previous available approaches. Table 4 represents accuracy parameter results obtained using various scripts.

5. Conclusion

In this paper, a CNN model is developed to recognize the 22 district names of Punjab. So, a dataset has been generated by different writers for the recognition which are handwritten in Gurmukhi Script. Recognition of Punjab's district names is an application area of postal automation, which will help in the automatic sorting of mails at the post office. This work is also helpful to recognize the handwritten Gurmukhi words without dividing them into individual characters as well as this model has also eliminated the need of manual feature extraction which are required to train the model. The implemented CNN model has obtained a validation

Hindawi
Journal of Mathematics
Volume 2023, Article ID 9893017, 1 page
https://doi.org/10.1155/2023/9893017

Retraction

Retracted: Research on the Flow Space Planning Model of a Classical Garden Based on an Ant Colony Optimization Algorithm

Journal of Mathematics

Received 10 October 2023; Accepted 10 October 2023; Published 11 October 2023

This article has been retracted by Hindawi following an investigation undertaken by the publisher [1]. This investigation has uncovered evidence of one or more of the following indicators of systematic manipulation of the publication process:

(1) Discrepancies in scope
(2) Discrepancies in the description of the research reported
(3) Discrepancies between the availability of data and the research described
(4) Inappropriate citations
(5) Incoherent, meaningless and/or irrelevant content included in the article
(6) Peer-review manipulation

The presence of these indicators undermines our confidence in the integrity of the article's content and we cannot, therefore, vouch for its reliability. Please note that this notice is intended solely to alert readers that the content of this article is unreliable. We have not investigated whether authors were aware of or involved in the systematic manipulation of the publication process.

Wiley and Hindawi regrets that the usual quality checks did not identify these issues before publication and have since put additional measures in place to safeguard research integrity.

We wish to credit our own Research Integrity and Research Publishing teams and anonymous and named external researchers and research integrity experts for contributing to this investigation.

The corresponding author, as the representative of all authors, has been given the opportunity to register their agreement or disagreement to this retraction. We have kept a record of any response received.

References

[1] Y. Tang and Z. Madina, "Research on the Flow Space Planning Model of a Classical Garden Based on an Ant Colony Optimization Algorithm," *Journal of Mathematics*, vol. 2022, Article ID 2001084, 8 pages, 2022.

Hindawi
Journal of Mathematics
Volume 2022, Article ID 2001084, 8 pages
https://doi.org/10.1155/2022/2001084

Research Article

Research on the Flow Space Planning Model of a Classical Garden Based on an Ant Colony Optimization Algorithm

YuLu Tang[1] **and Zamira Madina**[2]

[1]*School of Art Design, Gingko College of Hospitality Management, Chengdu 610042, China*
[2]*The Department of Industrial Engineering, International Ataturk Alatoo University, Bishkek, Kyrgyzstan*

Correspondence should be addressed to Zamira Madina; prof.zamira@mail.cu.edu.kg

Received 21 January 2022; Revised 21 April 2022; Accepted 25 April 2022; Published 27 May 2022

Academic Editor: Naeem Jan

The traditional spatial planning model has a large error and poor spatial planning effect, which cannot adapt to the construction of classical gardens. The flow spatial planning model of classical gardens based on an ant colony optimization algorithm is designed. The aim of the study is to perform the following: Analysis of classical garden flow space scale, quantifying the spatial flow scale of classical gardens, modifying classical garden spatial sequence based on the ant colony optimization algorithm, and constructing the flow space planning model of classical garden. By means of a comparison experiment, the error of the new model is small, and the effect of spatial planning is increased, which is of great popularization value.

1. Introduction

Systematic planning of the mutual "relations" existing in garden flow space configuration extends the 2-dimensional or 2.5-dimensional flow design thinking to 3-dimensional or even high-dimensional, providing a guide and reference for designers in the design of space configuration. The modern landscape space is ever-changing, the study and analysis of the relationships among the various landscape flow spatial configurations can better sort out and summarize, and form an accurate and clear understanding in the face of various spatial configurations [1]. It offers a new way of looking at landscape assessment by taking into account the structural relationships between landscape spaces in terms of landscape space arrangement. Traditional research explains the landscape configuration and analysis based on the researchers' result that can be wrong or incomplete. Using a computer to analyze the botanical garden area on a large scale, entering the world of quantitative analysis, and pushing the computer strategy of landscape design.

First of all, Chinese classical gardens are China's precious traditional cultural heritage, which have been repeatedly studied and explored by countless scholars for hundreds of years. However, in the vast majority of research materials, gardens are only the description of superficial phenomena, or the summary and induction of ancient garden literature [2–4]. Although these materials are of great help to our understanding of gardens, they neglect the research and exploration on how to express and inherit the spatial characteristics and design techniques of classical gardens in modern architectural design. Therefore, we should not only understand the garden but also know how to use and develop the garden.

Second, the modernist architectural issue highlights the loss of humanity in a merely logical setting. Humanized space experience, on the other hand, is lavished to the extreme in Chinese classical gardens with hundreds of years of history. Despite the fact that Chinese classical gardens have become historical and cultural landmarks, history does not imply a return to the past [5]. The personal care and inventive design concepts found in Chinese classical gardens, on the other hand, are precisely what the modernist architectural school of thinking lacks. As a result, studying from the ancients and extracting lessons from them is a valuable reflection and inspiration for present architectural design processes.

However, the Chinese classical garden is an inclusive philosophy, history, culture, aesthetics, architecture, and other disciplines of the comprehensive art. All of the disciplines have a myriad of links, the lack of any aspect of the garden cannot be called Chinese classical garden. However, the Chinese classical garden is comprehensive, extensive, and profound, and any knowledge contained therein is worth our long-term study and research [6]. In a book or paper, it seems to be an impossible task to thoroughly consider all aspects of Chinese classical gardens. In fact, there is no senior scholar to do this. So, it is inevitable to choose the content of the garden itself. Therefore, based on the practical and guiding significance of Chinese classical gardens to modern architectural design, the study of Chinese classical gardens should pay more attention to the common points and converge between Chinese classical gardens and modern architectural design [7, 8].

Everything in the world operates according to its own set of laws. Are there inherent laws in landscape phenomena, such as the genetic sequence that controls the emergence of living organisms or the principles of note generation in a musical tune, if we consider landscape to be an art of making space? The most significant fundamental talent of a landscape architect is spatial organization, which is the advanced stage of flowing space. Flow space, with its interpersonal, spatial experience, and ecological efficiency benefit, is moving the heart of every designer in the twentieth century. Even then, no thorough systematic investigation has been done on the flow of "confused a century" space. In this paper, we will examine the flow space subset of classical gardens, comb, conclude, and summarize, and try to quantify, the botanical garden space for digital processing, this concept landscape flow space organization, in order to pursue the essence of the phenomena, find out what is hidden in the order, and reveal the nature of flow space more design methods and rules [9].

2. Design of the Classical Garden Flow Space Planning Model Based on the Ant Colony Optimization Algorithm

2.1. Analysis of the Classical Garden Flow Space Scale. Space is the basic material form of garden, and the size and form of space are determined by the scale of its elements and the proportion between them. Scale and proportion are two concepts about the relationship between quantity. Proportion is to achieve a harmonious relationship between the building itself, while scale is to pursue the relative relationship between the building and people's visual and physical feelings, as well as the harmonious relationship between the building and the surrounding environment. Ultimately, they are all about creating a harmonious visual order. The space of gardens needs to be processed into a realistic material space that is "expected, feasible, accessible, and habitable" through certain artistic means, so as to achieve the perfect integration of artistic realm and real life [10–12]. It is the most important task for gardens to organize abundant and appropriate flow space. We can learn about the configuration of the spatial prototype by studying it in the space above, and we can summarize and evaluate the organizational form and law of the garden flow space by quantifying the size of the spatial prototype. There is a spatial link between the ratio of the distance from the human perspective to the building and the height of the building in the study of the interior space scale [13]. The interior space of the Chinese traditional garden architecture comes in a variety of shapes and sizes, with the height of the interior space determined by the building's roof. Internal height constraints, for example, are formed by the tops of various kinds of structures, such as Ming Chui, Cao Pai, and Xuan ceilings. Even the same type and scale of buildings give people different space feelings. The DH ratio between building distance (depth) and building height ranges from 0 to 4, which can be divided into five types, as shown in Table 1.

As shown in Table 1, $D/H = 1$, the vertical angle of view of people is 45°, although the interior of the building still feels cramped. However, there is some equalization between the building distance and height. The ratio of distance to height of interior buildings is mostly $1 < DH < 2$. Within the range, people's vertical perspective is within the range of 30°–40°, with relatively open and comfortable space scale. When $2 < D/H < 3$, the vertical angle of view is within the range of 20°–25°, and the internal space is relatively open. And so on, when $D/H > 3$, the vertical angle of view is about 15°, the internal space is open and empty, and the sense of space isolation and security is reduced [14].

The size of anything in relation to a reference standard or other things is referred to as scale, which makes it easier for individuals to do different measurements. The size of anything in relation to a reference standard or another item is called scale. A proper or harmonic connection between one component and another part or total is defined as proportion [15]. This link might be about more than just significance; it could also be about quantity and rank. By measuring, we mean the relationship between absolute dimensions and various proportions, which are largely dictated by the relevant functions, particularly the human body's size. The link between the impression and the true size of an item may be determined by investigating the perceived size of the thing as a whole or in pieces. The dimensional scale is the ratio that each component amount affects; it is relative and does not include particular dimensions. Scale, on the other hand, refers to actual measurements and dimensions. The scale refers to the connection between an element's perceived size impression and its genuine size, rather than the element's true size. The fundamental control scale of "shape" and "form" had been well established by the ancients. Shape, often within 100 feet, but non-mustard shape with a 1,000-foot rate, but not too far or too huge potential. The primary control scale of the plane (depth and breadth), elevation (height), and viewing distance of space composition is "one thousand feet is potential, one hundred feet is form" [16]. 100 feet is about 2335 meters, while 1000 feet is approximately 230350 meters. The monomer's form is one hundred feet, which regulates the space enclosing size, and the monomer's far viewing distance is less than one thousand feet.

Table 1: Types of classical garden buildings.

The internal space	Distance D/m	High H/m	D/H	Vertical angle (°)
Mingse house and Hanbishan house	6.35	6.40	D/H = 1	45°
West building of the Quxi building	3.26	2.70	1 < DH < 2	30°–40°
Yuan lake	7.00	2.70	2 < D/H < 3	20°–25°

2.2. Quantifying the Spatial Flow Scale of Classical Gardens. The highest achievement of classical garden space organization, although is a private garden, with a sample of the garden as a traditional garden set. Moreover, because the miller garden is a private garden, not to the verification of the stream of people, so the selection of Roosevelt memorial as a sample of modern flowing gardens. A comparative study of two typical samples was carried out using the configuration space syntax analysis. The reason why space syntax can provide reliable interpretation of landscape phenomena is that space syntax is "system-wide summing up" and exhausts all possibilities [17]. The scope of landscape explains the empirical study which explains the sampling method technique on the rule of basic possibilities as well as hidden rule of relationship with sampling data.

Buildings became a major feature of the classical garden landscape after the Qing Dynasty; thus, the size of architecture has a direct impact on the space arrangement and aesthetic mood of the whole garden. The architectural scale must be decreased to conform to the restricted site area of classical gardens and the tiny scale of landscape, particularly for scenery primarily for viewing; thus, greater attention is devoted to scale design. The use of the perspective concept of close big and distant tiny to reduce architectural scale not only adapts to the restricted site but also expands the depth of field. Suzhou ancient gardens are used as an example in this work, and the spatial flow scale quantification is provided in Table 2.

As can be seen from Table 2, the West building of Quxi building in the Lingering garden is located in the southeast of the central scenic spot. The west building on its north side is slightly backward, with a width of 13.86 meters and a depth of only 3.26 meters. However, there are smaller spaces in front of the Quxi building and at the junction of the West building to form a contrast. In addition, there are several large open windows on the west wall. The whole empty window faces the mountain pool, which is exactly perpendicular to the west corridor of the mountain pool, so there is no feeling of walking through the corridor after entering the Quxi building [18]. Two ends of entrance and exit in the end are clearly showing the wiggle room impact. Crossing the Quxi building and turning right to enter the West building, which is 8.26 meters wide and 5.28 meters deep. Here, the indoor floor level is slightly raised to make the space more amiable due to the low height. At the same time, the vertical space combination of elevation makes the overall scene plump and integrated, forming two floors, one front and one back, one long and one short, one high and one low, with a clear and unified main body, achieving the artistic effect of contrast between virtual and real. The landscape diagram of the lingering garden is shown in Figure 1.

With an area of 257.41 square meters, the Wufeng fairy hall is the largest building group in the eastern part of the garden, while Crane house, Shilin Hut, Jingzhong View, and Jizhou Feng Xuan are smaller buildings on the east side of the Wufeng fairy hall that have formed several small courtyards independently. We get to Shilin Cottage generation one via the large Wufeng Xianguan building, which has a discrete main and secondary area but is interconnected. As a result, Table 2 shows the garden flow quantification table.

As shown in Table 3, the space form of the Lingering garden changes from large to small and from simple to complex, interspersing, and switching with each other to form an artistic effect of integrating inside and outside space.

The opening, depth, and eave heights of the Culbite hill house and Minser house are 12.5 m, 6.35 m, and 3.8 m, respectively, and 5 m, 6.03 m, and 5.25 m, respectively. The external spatial pattern of the Culbite hill house and Minser house is shown in Figure 2.

Figure 2 shows the green mountain room, bright floor and volume as well as height in the stark contrast; it explained about the central scenic area of the space form and new part of the world, WenMuJi sweet in a group of buildings in photograph echo, and the difference can be seen from the data in the center area of architecture. Viewed from the opposite pavilion, it forms an organic whole with the surrounding lakes and forests, which is unique and harmonious. In traditional gardens, the walk is a fascinating and complicated structure. Architecture, scenery, and plant arrangement may be observed in the plane of classical gardens, but it is difficult to clearly define the garden walk since the road is disguised in these aspects [19]. As a result, the notion of a path in the garden encompasses not just outside passable paths but also all routes with traffic functions, implying that architecture is an essential aspect of the garden's complex path system. The true efficiency of the investigation may be assured by quantifying the traditional garden space flow scale.

2.3. Modification of the Classical Garden Spatial Sequence Based on the Ant Colony Optimization Algorithm. From different perspectives, the methods of structural dynamic modification can be roughly classified as follows: according to the classification of model modification objects, they can be divided into matrix and physical parameter methods. According to the scope of structural modification, it can be divided into the integral modification method and partial modification method. The global correction method is to modify the parameters of the whole structure or the whole system matrix, while the local correction method is only to modify the local parameters. In terms of calculation

Table 2: Quantification of building scale in the middle of Liu Yuan.

Building	Room/Side length (m)	Depth (m)	Eaves height (m)	Floor area (m^2)
Green mountain	12.5	6.35	3.8	32.69
Bright building	5	6.03	5.25	24.8
Green shade	5.23	3.55	2.8	18.76
The Quxi floor	13.86	3.26	5.29	40.77
City of putting	2.65	2.65	2.9	7.02
West wing	8.26	5.28	4.5	42
The wind pool pavilion	3.9	5.62	2.8	21.9
Far cui attic	8.4	7	5.9	58.8
Ke pavilion	1.74	—	2.8	7
Smell the sweet clover	5.02	4.89	3.1	24.9

Figure 1: Landscape diagram of Liu Yuan.

Table 3: Scale quantification of Liu Yuan East.

Building	Room/Side length (m)	Depth (m)	Eaves height (m)	Floor area (m^2)
Crane Suo	11.7	2.5	2.8	32.69
The stone forest cabin	3.62	2.53	3.1	8.67
Static medium	3.94	1.74	3.92	9.3
Renewed peak thin	8.13	3.96	3.85	32.14
This text fairy pavilion	20.11	13.16	4.2	257.41

methods, it can be divided into direct method, iterative method, and group method. The direct method is based on a certain mathematical relationship, a calculation to get the revised model. The iterative method means that the modified model can be obtained through several iterations. The grouping method means the combination of the above two methods. It may be split into incomplete space technique and practical full space method based on the completeness of the reference base internal modal space [20]. The measurement mode is only included in the incomplete space technique, but the practical full space method includes both the measurement mode and the comparable higher order theoretical mode. It may be separated into nondiagnostic and diagnostic methods based on the functional categorization. Nondiagnostic approaches can only supply changed models for response analysis later on. The diagnostic approach may be used in structural dynamic design to not only give a repair model but also to detect modeling errors. The dynamic identification approach based on dynamic test data might be dubbed dynamic finite element model modification, depending on the test information utilized in model modification. Static identification method using static test data can also be combined with static and dynamic test data for finite element correction. In order not to change the stiffness in the original spatial sequence and the original properties of the mass matrix, the revised

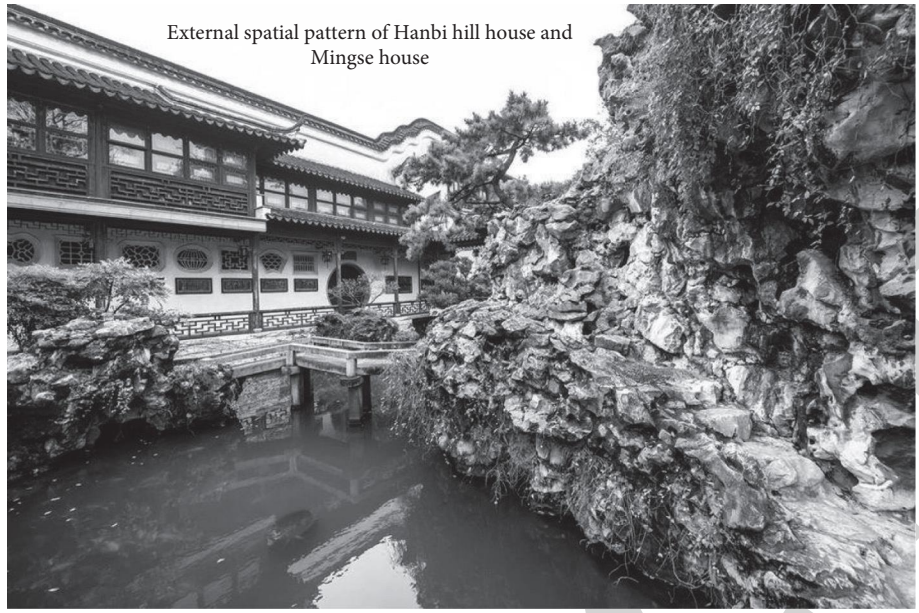

Figure 2: External spatial pattern of the Hanbishan house and Mingse building.

structural stiffness and mass matrix are expressed as follows:

$$K_U = \sum_{i=1}^{n_e} \alpha_i K_{ia}, \tag{1}$$

$$M_U = \sum_{i=1}^{n_e} \beta_i M_{ia}. \tag{2}$$

In formula (1) and (2), K_U and M_U are the structural stiffness and mass matrix of the spatial sequence of the garden in the initial state, respectively. K_{ia} and M_U are the structural stiffness and mass matrix of the i-th spatial sequence in the initial state, respectively. α_i and β_i are the correction coefficients of the structural stiffness and mass matrix of the i-th spatial sequence, respectively. n_e is the number of nodes in the initial spatial sequence. In the actual measurement, the number of sensor points is far less than the number of nodes in the analysis model, assuming that the number of measured points is m and the number of unmeasured points is 1. In order to distinguish measured points from unmeasured points, the dynamic equation of the modified model can be expressed as follows:

$$\left(\begin{bmatrix} K_{mm} & K_{ml} \\ K_{lm} & K_{ll} \end{bmatrix}_U - \lambda_s \begin{bmatrix} M_{mm} & M_{ml} \\ M_{lm} & M_{ll} \end{bmatrix}_U \right) \begin{Bmatrix} \Phi_m \\ \Phi_l \end{Bmatrix} = 0. \tag{3}$$

In formula (3), $\begin{bmatrix} K_{mm} & K_{ml} \\ K_{lm} & K_{ll} \end{bmatrix}_U$ is the U measurement data. $\begin{bmatrix} M_{mm} & M_{ml} \\ M_{lm} & M_{ll} \end{bmatrix}_U$ is the U-th data to be measured. λ_s is the S-th measured eigenvalue. Φ_m and Φ_l the mode components m of the measured points corresponding to the measured eigenvalues λ_s and l of the unmeasured points. K_{mm} is the spatial sequence stiffness of $m \times m$ dimension. K_{ml} is the spatial sequence stiffness of $m \times l$ dimension. K_{lm} is the spatial sequence stiffness of $l \times M$ dimension. K_{ll} is the spatial sequence stiffness of $l \times l$ dimension. M_{mm} is the quality of $m \times m$ dimensional spatial sequence. M_{ml} is the quality of $m \times l$ dimensional spatial sequence. M_{lm} is the spatial sequence quality of $l \times m$ dimension. M_{ll} is the spatial sequence quality of $l \times l$ dimension. Due to the unknown of Φ_m and Φ_l, the test points cannot correspond to the degrees of freedom of the analysis model one by one. Two approaches may be employed to compare the test mode expansion method and analytical condensation method related to the test points and degrees of freedom of analysis in order to directly compare the generated eigenvectors with the tested eigenvectors. The test mode expansion technique, which uses the ant colony algorithm to evaluate the stiffness and mass matrix of a spatial sequence and extract the mode components on the nodes of structural dynamic mode, is briefly described below.

$$\begin{aligned} \{\Phi\} &= \begin{Bmatrix} \Phi_m \\ \Phi_l \end{Bmatrix} = G(\lambda_s)\{\Phi_m\}, \\ G(\lambda_s) &= \begin{bmatrix} I_m \\ -P(\lambda_s)^{-1} Q(\lambda_s) \end{bmatrix}. \end{aligned} \tag{4}$$

In formula (4), I_m is the identity matrix of $m \times m$ dimension and $-P(\lambda_s)^{-1}$ is the inverse matrix of $l \times l$ dimension. $Q(\lambda_s)$ is $l \times m$ dimensional matrix. $P(\lambda_s)^{-1}$ and $Q(\lambda_s)$ can be obtained by the following formula:

$$\begin{aligned} P(\lambda_s)^{-1} &= K_{ll}^{-1} + \lambda_s K_{ll} - 1 M_{ll} K_{ll}^{-1}, \\ Q(\lambda_s) &= K_{lm}^{-1} - \lambda_s M_{lm}. \end{aligned} \tag{5}$$

In formula (5), the mass matrix $m \times m$ dimensions of the stiffness of the reduced analysis model that has been modified are as follows:

$$K(\lambda_s)_{UR} = G(\lambda_s)^T K_U G(\lambda_s),$$
$$M(\lambda_s)_{UR} = G(\lambda_s)^T M_U G(\lambda_s). \quad (6)$$

In formula (6), U, R and T are the test space Xue sequence parameters, respectively. At this point, the mass and stiffness matrices must satisfy the following canonical equation:

$$\Phi_m^T K(\lambda_s)_{UR} \Phi_m - \lambda_s = 0,$$
$$\Phi_m^T M(\lambda_s)_{UR} \Phi_m - I = 0. \quad (7)$$

In formula (7), $\Phi_m^T K(\lambda_s)_{UR} \Phi_m - \lambda_s$ is the measured eigenvalue of dimension and the corresponding measured mode of $t \times t$ dimension, and T is the total order of the measured eigenvalue, I is the vector parameter. Combining equations (1), (6), and (7), the correction coefficient α_i and β_i equation are obtained as follows:

$$\Phi^T \left(\sum_{i=1}^{n_e} \alpha_i K_{ia} \right) \Phi - \lambda_s = 0,$$
$$\Phi^T \left(\sum_{i=1}^{n_e} \beta_i M_{ia} \right) \Phi - I = 0. \quad (8)$$

In formula (8), since the vibration mode Φ and measured eigenvalue λ_s are known, the model correction coefficient α_i and β_i can be obtained by solving formula (7). In actual engineering, the number of unknown α_i and β_i is $2n_e$, far greater than that of formula (7), so there is no unique solution to formula (7). In this paper, the number of objectives is firstly determined, and the minimum objective function α_i and β_i is obtained by using different optimization algorithms such as genetic algorithm to solve the above equation. To ensure maximum correction effect of spatial sequence.

2.4. Constructing the Flow Space Planning Model of Classical Gardens. Buildings and courtyards form the overall landscape pattern. A group of courtyards have the main scenic spots and the best viewing points. The best viewing points are the stopping points, which basically exist in the form of buildings. The space types in gardens are divided into three types: interior space dominated by hall, hall, building, pavilion and porch, gray space dominated by pavilion and gallery structure, and external space dominated by landscape pattern. The gray space often connects internal and external spaces and plays an excessive role. If there is no excessive grey space, the spatial relationship is simple and stiff, which is closely related to its functional nature. The main function of residential houses is living, while the main function of gardens is recreation. Distinct functional requirements need different spatial forms and structures. On the structure, internal, external, and grey space can be used as an art technique in the relationship between black and white ash, as the black and white and grey relation expression object of light and shadow creates a stereo feeling, but only the structure of the relationship between surface and surface, and the internal, external, and grey space is space structure relations between black and white ash, is between 3 d and 3 d

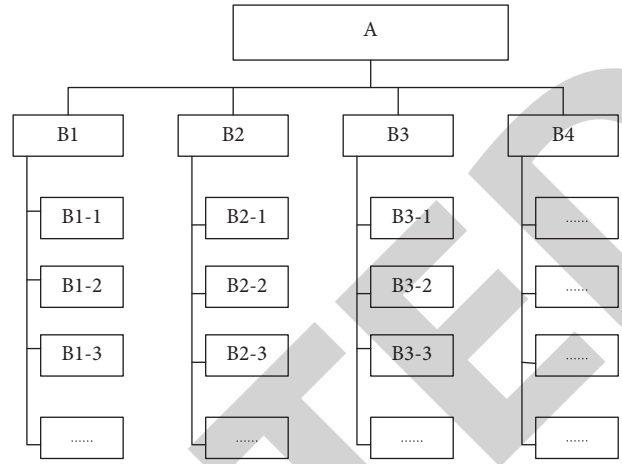

Figure 3: Flow space planning model of classical gardens.

dialogue, spatial organization form a complex, rich, and c As a result, the "image outside the scene and the scene outside the scene" impact of garden art is created. The number of measured points, natural frequencies, and modes for big structures are significantly smaller than the model freedom produced by the finite element technique. The data are far from full, even when measured in the same order as the modal vectors. The issue may be solved in two ways: the first is to minimize the free degree of the original analytical model, a process known as model condensation. The alternative option is to increase the measured mode's freedom degree, which is known as modal expansion. The measured mode of each order is the subject of modal extension. Interpolation techniques are used to achieve modal expansion, with the Berman and Farhat iterative interpolation approach and the optimum fitting method being two examples. In addition, for modal expansion, various model condensation techniques may be applied in reverse. As a result, this work uses the hierarchical technique to build the garden flow space planning model, which is displayed in Figure 3.

As shown in Figure 3, after the flow space planning model of classical gardens is constructed, the elements at the upper and lower levels form a membership relationship. The elements at the A level, $B1$, $B2$,..., Bn have a dominant relationship. Similarly, the elements of $B1$ layer have the same effect on the next layer $B1$-1, $B1$-2... has a dominant relationship. Pair-wise comparison of the same level of indicators can further reduce the error of spatial liquidity parameters and improve the effect of spatial planning.

3. Experimental Test

3.1. Experimental Preparation. The initial worry in the structural model modification problem is the evolution process of the objective function value, since this evolution process can be used to estimate the effectiveness of the adaptive ant colony algorithm and the influence of model modification. Many variables influence the search status of each parameter value in the ant colony optimization method. Figure 4 depicts the development of the worldwide volatility coefficient.

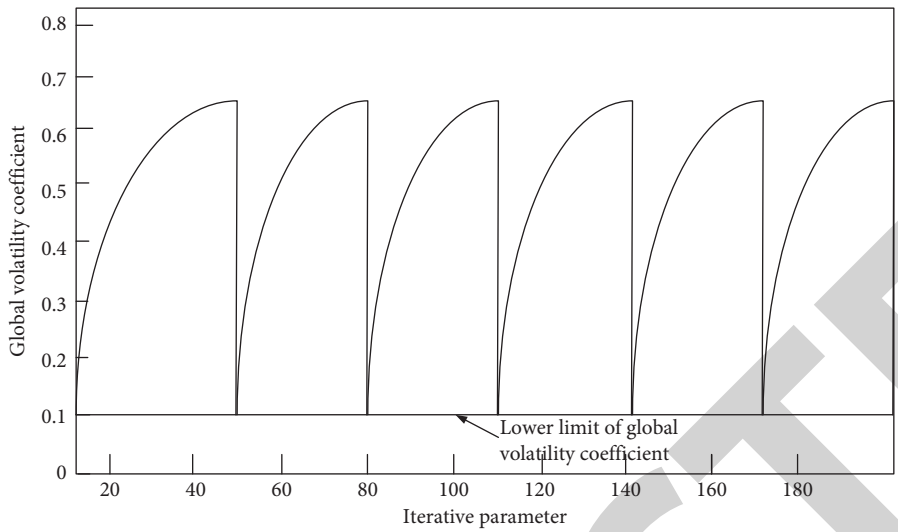

Figure 4: Evolution diagram of global volatilization coefficient.

As shown in Figure 4, in the ant colony system, there are two ways for ants to select paths: probabilistic search and path selection based on prior knowledge. The two search methods have their own advantages and disadvantages: the path selection based on prior knowledge has fast convergence speed, but easy to fall into local optimal. Probabilistic search can avoid falling into local optimum, but usually the convergence speed is slow. Therefore, good ant colony algorithms use some strategies to adjust the selection of search methods to take advantage of the advantages of both search methods. Adjusting the selection of search method and path in this iteration step in a probabilistic way. If the dispersity of garden space is low, it means that the route of ants from one garden space to another is concentrated in a few, and that the information is concentrated in these few pathways, which may easily lead to premature and stalling in the future search for the best solution. As a result, more paths should be chosen in order to diversify solutions. When the dispersity of garden space is greater, the dissemination of information from one garden space to another is more dispersed, making it harder to enhance the optimum information and resulting in a sluggish convergence rate. As a result, a smaller number of better pathways should be chosen with a higher probability in order to increase the positive feedback information.

3.2. Experimental Result. In the above experimental environment, the traditional spatial planning model was compared with the spatial planning model designed in this paper to verify the error effects of flow parameters (Ed, Rd, Ad, Id) of the two models. The results are shown in Table 4.

As shown in Table 4, the flow parameter error of the traditional spatial planning model is large, and the spatial planning effect is poor, which cannot adapt to the construction of classical gardens. The flow parameter error of the spatial planning model designed in this paper is small, and the spatial planning effect increases accordingly. It can adapt to the construction of classical gardens, create conditions for the planning of garden flow space, and meet the research purpose of this paper.

Table 4: Experimental results.

The flow parameters	Flow parameter error effect of traditional spatial programming model	The flow parameter error effect of spatial programming model is designed in this paper
Ed	0.132	0.013
Rd	0.245	0.014
Ad	0.356	0.016
Id	0.428	0.018

4. Conclusion

In the context of the rapid development of the global economy, modern and post-modern design trends are gradually pouring into the traditional design ideas and aesthetic concepts have a violent collision, but in the fast-paced urban life, traditional culture is gradually forgotten and ignored. Contemporary landscape designers are confused about this, whether to blindly pursue the western design concept, or adhere to the tradition, or carry out the eastern design philosophy. How to deal with the relationship between tradition and modern, modern landscape designers need to consider the problem. "Take the essence, discard the dross," absorb the western excellent design concept at the same time to carry out the traditional design methods, to realize the combination of geographical location, talent utilization and cultural deposits, and makes the contemporary landscape design can meet the requirements of the current generation of city life space, and can meet people's traditional aesthetic idea, potential shaping urban landscape with cultural characteristics, that is the shared vision of modern landscape designers.

Data Availability

The data used to support the findings of this study are deposited in a repository.

Hindawi
Journal of Mathematics
Volume 2023, Article ID 9865757, 1 page
https://doi.org/10.1155/2023/9865757

Retraction

Retracted: Dynamic Alterations and the Affecting Attributes of the Unbalanced Economic Development in the Basin of the Yellow River: Analysis Utilizing Population-Weighted Coefficient of Variation

Journal of Mathematics

Received 13 September 2023; Accepted 13 September 2023; Published 14 September 2023

This article has been retracted by Hindawi following an investigation undertaken by the publisher [1]. This investigation has uncovered evidence of one or more of the following indicators of systematic manipulation of the publication process:

(1) Discrepancies in scope
(2) Discrepancies in the description of the research reported
(3) Discrepancies between the availability of data and the research described
(4) Inappropriate citations
(5) Incoherent, meaningless and/or irrelevant content included in the article
(6) Peer-review manipulation

The presence of these indicators undermines our confidence in the integrity of the article's content and we cannot, therefore, vouch for its reliability. Please note that this notice is intended solely to alert readers that the content of this article is unreliable. We have not investigated whether authors were aware of or involved in the systematic manipulation of the publication process.

Wiley and Hindawi regrets that the usual quality checks did not identify these issues before publication and have since put additional measures in place to safeguard research integrity.

We wish to credit our own Research Integrity and Research Publishing teams and anonymous and named external researchers and research integrity experts for contributing to this investigation.

The corresponding author, as the representative of all authors, has been given the opportunity to register their agreement or disagreement to this retraction. We have kept a record of any response received.

References

[1] Z. Zhao, "Dynamic Alterations and the Affecting Attributes of the Unbalanced Economic Development in the Basin of the Yellow River: Analysis Utilizing Population-Weighted Coefficient of Variation," *Journal of Mathematics*, vol. 2022, Article ID 3549510, 8 pages, 2022.

Hindawi
Journal of Mathematics
Volume 2022, Article ID 3549510, 8 pages
https://doi.org/10.1155/2022/3549510

Research Article

Dynamic Alterations and the Affecting Attributes of the Unbalanced Economic Development in the Basin of the Yellow River: Analysis Utilizing Population-Weighted Coefficient of Variation

Ziqiang Zhao [1,2]

[1]*School of Mathematics and Statistics, Henan Finance University, Zhengzhou 450046, China*
[2]*Department of Management, Southern Federal University, Rostov-na-Donu, Russia*

Correspondence should be addressed to Ziqiang Zhao; zhaoziqiang@hafu.edu.cn

Received 20 March 2022; Revised 11 April 2022; Accepted 15 April 2022; Published 23 May 2022

Academic Editor: Naeem Jan

This paper employs a method called the population-weighted coefficient of variation (PWCV) to investigate the dynamic changes related to the imbalanced economic progression in the Yellow River Basin (YRB) between 2010 and 2020, and also analyzes the affecting attributes that are related to industry-specific and the spatial property of this change through the double decomposition of the PWCV method. The imbalanced economic progression in the YRB that tends to decline generally was found. The basin of the Yellow River, with three constituent regions, namely upper, middle, and lower streams of it, experiencing an imbalanced development has roots in the condition of the imbalanced economic progression in the YRB. However, since 2018, the imbalance ratio between regions has expanded. When the industrial decomposition is under consideration, the YRB experiences imbalanced economic development due to the dissimilarity between the industrial implementations, called the secondary and tertiary. Before 2018, the imbalance caused by the difference in the secondary industry accounted for more than 50%, while the imbalance led by the difference in the tertiary industry exceeded the imbalance caused by the secondary industry after 2018.

1. Introduction

Geographically, the basin is defined as a relatively narrow and long zone, and the economic operation and development of each section often present diversity. As the Yellow River Basin spans nine provinces, greater differences can be observed in the conditions of the natural resources, transportation infrastructures, education, science and technology levels, and economic policies, resulting in the increasingly prominent problem of the unbalanced development in the Yellow River Basin [1–5]. China's domestic research on the river basin economy has been mostly limited to the development and utilization of various resources; however, few research studies [6–9] lacks the perspective of regional economics, thus a mature theoretical system of the river basin economy has not been formed yet [10]. Moreover, the research related to the imbalanced economic development in the river basin has been still in its infancy, and more attention has been preferably paid to the basins of the Yangtze River, the Pearl River, and the Xijiang River like the early research studies [11, 12], or the empirical research studies [13, 14]. As for the relevant research on the basin of the Yellow River, insufficiency can be instantly observed. Besides, some research results were involved in the past, which are outdated and could not reflect the latest trend of the unbalanced economic progression in the YRB when time is under consideration. Moreover, this manuscript utilizes a method called the double decomposition approach of the PWCV proposed by a few studies [15–18] to gauge the degree of the unbalanced economic development and the new dynamic changes in the YRB. Therefore, it analyzes both spatial and industrial causes of this change within a

systematic framework to provide a reference for the theoretical construction of the basin economy and help the decision-making process for more comprehensive regional development.

The organization of the rest of the paper is constructed as follows. Section 2 portrays an overview of economic development in the YRB. Section 3 presents the research method. Section 4 exhibits the results in detail. Section 5 provides a comprehensive discussion. Section 6 finalizes the research with some suggestions.

2. Overviewing the Basin of the Yellow River concerning Its Economic Development

The second-largest in China is the Yellow River whose journey begins at the Bayabgla Mountain in Qinghai Province and streams through the Qinghai, Sichuan, Gansu, Ningxia, Inner Mongolia, Shanxi, Shaanxi, Henan, and Shandong provinces, and pours into the sea called Bohai near the city of Dongying in the province of Shandong. The length is 5464 km, and the total drop is about 4480 m. It spans some typical areas in the West, Middle, and East, respectively. The lower reaches of the basin are mainly concentrated in the Shandong Taohuayu section of Henan Province, including the famous Shandong peninsula area. The middle reaches are mainly distributed in Shanxi, Shaanxi, and Western Henan with a catchment area of $3.44 \times 10^5\,\mathrm{km}^2$. The upstream flow through Qinghai, Sichuan, Gansu, Ningxia, and Hekou town in Inner Mongolia, whose total length is 3472 km with a catchment area of $4.28 \times 10^5\,\mathrm{km}^2$ [19]. The YRB has a key function in the economic development of the nation, accounting for 27.3% of the country's area, carrying 23.3% of the country's population and 21.8% of the total economy. The proportion of the whole society's fixed-asset investment and the revenue of the local public budget were 23.8% and 17.8%, respectively, in the country. However, the YRB experiences a low-quality progression concerning the measurements of GDP [20–24], GDP per capita, fiscal revenue, tertiary industrial structure, and urbanization rate that fall behind the average figures of the whole population. The general status of the economic progress in the YRB was presented in Table 1.

The figures show that (1) the basin of the Yellow River experiences a level of economic development whose shape is called a "reverse altitude gradient" with "lower (downstream) high and upper (upstream) low," that is, upstream < midstream < downstream in order; (2) the trend of the distribution does not exclude the possibility of certain "variation" within each domain. For example, some economic indicators of Inner Mongolia are higher than those of Shanxi and Henan in the upstream domain, which are relatively downstream. This special situation may be related to the relatively small population and richer mineral resources in Inner Mongolia; (3) the reverse geographical gradient difference of the economic progression rank of the basin has been particularly obvious in the other related indicators of industrialization such as industrial structure, and the rate of the urbanization.

3. Research Method

3.1. The Measurement Method of the Imbalanced Economic Progression in the YRB. In this manuscript, the PWCV approach is used to gauge the imbalanced economic progression in the YRB. Suppose that there are m regions, and the region consists of $\sum_1^m x_i$ cities. For instance, for region i, $\overline{y}_{ij}$ represents the GDP per capita of city j, N_{ij} represents the total population of city j where N_i represents the total population in region i, Y_i represents the GDP, and $\overline{Y}_i = (Y_i/N_i)$ denotes the GDP per capita in the region i. The same procedure may be easily adapted to obtain a total $N = \sum_{i=1}^{m} \sum_{j=1}^{x_i} N_{ij}$ that represents the total population in the basin of the Yellow River. Similarly, $Y = \sum_{i=1}^{m} \sum_{j=1}^{x_i} N_{ij}\overline{y}_{ij}$ expresses the total GDP, and $\overline{Y} = (Y/N)$ designates the GDP per capita in the basin, respectively. Then, the degree of the imbalanced economic progression in the YRB could be measured by the square of the PWVC shown in equation (1),

$$CV(Y) = \frac{1}{\overline{Y}^2} \sum_{i=1}^{m} \sum_{j=1}^{x_i} \frac{N_{ij}}{N} \left(\overline{y}_{ij} - \overline{Y}\right)^2, \tag{1}$$

where $\mathbf{Y} = (Y_1, Y_2, \ldots, Y_m)$.

3.2. Decomposition Method of the Affecting Attributes of the Unbalanced Economic Progression in the YRB. We decompose the PWVC of GDP into the spatial and income sources and examine their affecting role on the unbalanced economic progression in the YRB. The spatial decomposition is firstly conducted. By doing so, the imbalanced economic development of the regions and the imbalanced inter-regional economic development are separated. The income sources are secondly decomposed and investigated concerning the effect of various income sources related to the unbalanced economic progression in the YRB. Wenchao (1) implies the imbalanced economic progression in the YRB, which has been decomposed into intraregional and inter-regional imbalances expressed by equation (2).

$$\begin{aligned} V(\mathbf{Y})^2 &= \frac{1}{\overline{Y}^2} \sum_{i=1}^{m} \left(\frac{N_i}{N}\right) \left(\frac{\overline{Y}_i}{\overline{\overline{Y}}}\right)^2 \mathrm{CV}(\mathbf{Y_i})^2 + \mathrm{CV}(\overline{Y})^2 \\ &= \mathrm{CV}_W + \mathrm{CV}_B, \end{aligned} \tag{2}$$

where $\mathrm{CV}(\mathbf{Y_i})^2 = (1/\overline{Y}_i^2) \sum_{j=1}^{x_i} (N_{ij}/N)(\overline{y}_{ij} - \overline{Y}_i)^2$ indicates the degree of the imbalance in the economic development in region i by (2), $\mathrm{CV}_W = \sum_{i=1}^{m} (N_i/N)(\overline{Y}_i/\overline{Y})^2 \mathrm{CV}(\mathbf{Y_i})^2$ indicates the degree of the imbalance in the economic development in m regions, $\mathrm{CV}(\mathbf{Y})^2 = (1/\overline{Y}^2) \sum_{i=1}^{m} (N_i/N)(\overline{Y}_i - \overline{Y})^2$ shows the imbalanced degree in economic development among m regions. Noted that the weighted mean is not represented by CV_W when the degree of the imbalance in the region is a concern, so the weights cannot be added.

If the GDP per capita of each prefecture-level city is composed, the formulas

Table 1: Comparison of the main economic indicators in both provinces and regions located at the YRB in 2019.

Indicators	Per capita GDP (yuan/person)	Urbanization rate (%)	Tertiary industry (%)
Qinghai	48981	55.52	7.1 : 41.9 : 51.0
Sichuan	55774	53.79	10.3 : 37.3 : 52.4
Gansu	32995	48.49	12.1 : 32.8 : 55.1
Ningxia	54217	59.86	10.2 : 39.1 : 50.7
Inner Mongolia	67852	63.37	10.8 : 39.6 : 49.6
Shanxi	45724	59.55	4.8 : 43.8 : 51.4
Shaanxi	66649	59.43	7.7 : 46.4 : 45.9
Henan	56388	53.21	8.5 : 43.5 : 48.0
Shandong	70653	61.51	7.2 : 39.8 : 53.0
China	70724	60.6	7.1 : 39.0 : 53.9

$$\begin{aligned}\overline{y}_{ij} &= \overline{y}_{ij1} + \overline{y}_{ij2} + \cdots + \overline{y}_{ijk},\\ \overline{Y}_i &= \overline{Y}_{i1} + \overline{Y}_{i2} + \cdots + \overline{Y}_{ik},\end{aligned} \tag{3}$$

are employed where $\overline{Y}_{ik} = (1/N_1)\sum_{j=1}^{x_i} N_{ij}\overline{y}_{ijk}$.

Then, the internal imbalance in this region can be further decomposed as follows:

$$\mathrm{CV}(\mathbf{Y_i})^2 = \sum_{k=1}^{K} z_{ik}\mathrm{COV}(\mathbf{Y_i}, \mathbf{Y_{ik}}). \tag{4}$$

$\mathrm{COV}(\mathbf{Y_i}, \mathbf{Y_{ik}}) = (1/\overline{Y}_i)(1/\overline{Y}_{ik})\sum_{j=1}^{x_i}(N_{ij}/N_i)\quad(\overline{y}_{ij} - \overline{Y}_i)(\overline{y}_{ijk} - \overline{Y}_{ik})$ represents the weighted covariance of the regional GDP per capita. $z_{ik} = (\overline{Y}_{ik}/\overline{Y}_i)$ indicates the share of region i concerning k-item income per capita in regional GDP where $\mathbf{Y_i} = (\overline{y}_{i1}, \overline{y}_{i2}, \ldots, \overline{y}_{ix_i})$, and $\mathbf{Y_{ik}} = (\overline{y}_{i1k}, \overline{y}_{i2k}, \ldots, \overline{y}_{ix_ik})$.

Similarly, the imbalance in the regional economic development can be decomposed as follows:

$$\mathrm{CV}(\overline{Y})^2 = \sum_{k=1}^{K} z_k \mathrm{COV}(\overline{Y}, \overline{Y}_{\mathbf{k}}). \tag{5}$$

$\mathrm{COV}(\overline{Y}, \overline{Y}_{\mathbf{k}}) = (1/\overline{Y})(1/\overline{Y}_{*k})\sum_{i=1}^{m}(N_i/N)(\overline{Y}_i - \overline{Y})\quad(\overline{Y}_{ik} - \overline{Y}_{*k})$ expresses the weighted covariance of GDP per capita in the YRB, and $z_k = (\overline{Y}_{*k}/\overline{Y})$ represents the share of kth item per capita income of GDP in the YRB. In this formula, the item could be described by $\overline{Y}_{\mathbf{k}} = (\overline{Y}_{1k}, \overline{Y}_{2k}, \ldots, \overline{Y}_{mk})$ and $\overline{Y}_{*k} = (\sum_{i=1}^{m} N_i\overline{Y}_{ik}/N)$.

Substituting (4) and (5) into (1) results in (6).

By dividing both sides of the equation,

$$1 = \sum_{i=1}^{m}\frac{N_i}{N}\left(\frac{\overline{Y}_i}{\overline{Y}}\right)^2 \sum_{k=1}^{K} z_{ik}s_{ik} + \sum_{k=1}^{K} z_k\overline{s}_k. \tag{6}$$

is obtained where $s_{ik} = (\mathrm{COV}(\mathbf{Y_i}, \mathbf{Y_{ik}})/\mathrm{CV}(\mathbf{Y})^2), \overline{s}_k = (\mathrm{COV}(\overline{Y}, \overline{Y}_{\mathbf{k}})/\mathrm{CV}(\mathbf{Y})^2)$.

Besides, $(N_i/N)(\overline{Y}_i/\overline{Y})^2\sum_{k=1}^{K} z_{ik}s_{ik}$ represents the contribution rate of k-item income in region i to the unbalanced economic progression in the YRB, and the product of $z_k\overline{s}_k$ represents the contribution rate of k-item income to the unbalanced economic development between regions.

3.3. Data Source and Its Processing. The manuscript studies the imbalance circumstance and the affecting attributes of the economic development in the YRB between 2010 through 2020 with the utilization of the 69 prefecture-level cities in the lower, middle, and upper sections of the YRB. By going through the spatial level and utilizing these areas as the spatial units in the double decomposition of the PWCV for the state of the economic development, the contribution of the imbalanced economic development in these three areas dealing with the regional imbalanced economic development, and the contribution of the imbalanced economic development between them dealing with the regional imbalanced economic development are studied in the YRB, respectively. This paper uses the data sets that were extracted from *The Statistical Yearbook of Chinese Cities* from 2011 to 2021 and the statistical book for both provinces and autonomous regions published annually.

4. Results

4.1. The Changing Process of the Unbalanced Economic Progression in the YRB. Figure 1 depicts the imbalanced economic development in the YRB. Even though the long-run trend was downward, the period between 2010 through 2020 had witnessed some ups and downs. However, the imbalanced economic progression in the YRB has designated a sharp downward trend since 2010. We summarized what happened between 2010 through 2016 and 2017 through 2020 as follows. The PWCV for the economic progression in the YRB decreased from 0.3836 to 0.3208 between 2010 through 2016 with an average annual decrease of 2.73%, and the fluctuation range of the imbalanced economic progression in the YRB during this period was small. On the other hand, the decline was particularly straightforward between 2017 through 2020. The PWCV for the economic progression in the YRB decreased from 0.3725 to 0.1816 with an average annual decrease of 17.08%.

4.2. The Spatial Decomposition of the Unbalanced Changes in the Economic Progression in the YRB. Utilizing the three areas in the YRB for comparison aims at studying the imbalanced economic development. Table 2 shows that the contribution of the imbalanced economic development in these regions to the regional imbalanced economic progression in the YRB changed between 75.54 through 89.48%, and the contribution of the imbalanced economic development among the three regions to the regional imbalanced economic progression in the YRB varied between 9.56

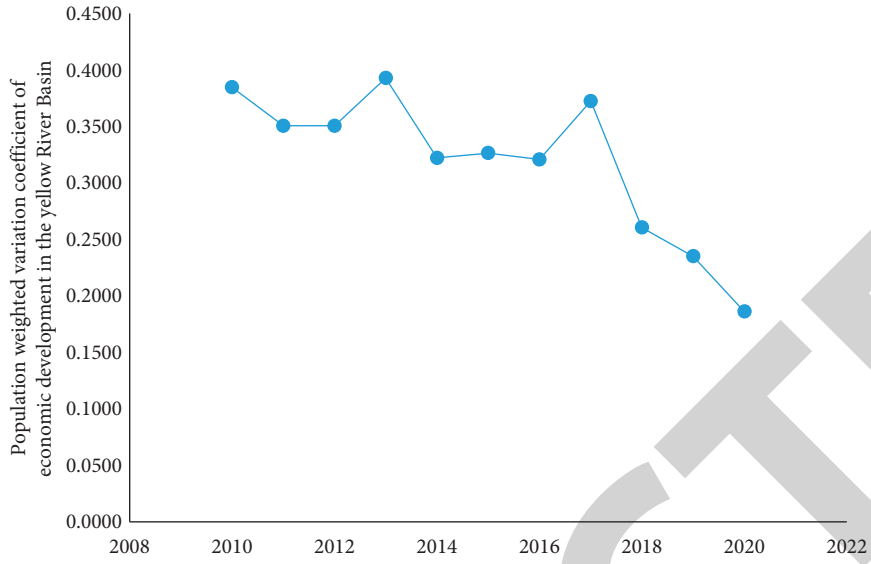

Figure 1: The process of the unbalanced economic progression in the YRB during 2010–2020.

Table 2: The spatial decomposition results of the unbalanced development changes in the YRB between 2010 and 2020.

Years	Regional internal imbalance		Imbalance between regions	
	PWCV	Proportion in regional imbalance (%)	PWCV	Proportion in regional imbalance (%)
2010	0.3310	86.0568	0.0536	13.9432
2011	0.3138	89.4846	0.0369	10.5154
2012	0.3131	89.2824	0.0335	9.5606
2013	0.3511	89.3736	0.0417	10.6264
2014	0.2828	87.7935	0.0393	12.2065
2015	0.2805	85.9385	0.0459	14.0615
2016	0.2718	84.7285	0.0490	15.2715
2017	0.3253	87.3299	0.0472	12.6701
2018	0.1968	75.5372	0.0637	24.4628
2019	0.1927	81.9731	0.0424	18.0269
2020	0.1516	81.4656	0.0345	18.5344

through 24.46%. Thus, the imbalanced economic development in the three regions was the main influencing factor for the imbalanced economic progression in the YRB. The mechanism worked as follows. The imbalanced economic situation in the region was mainly caused by the imbalanced economic development followed by the imbalanced economic progression between regions. Therefore, the imbalanced economic progression between regions tended to expand on a yearly basis.

Figure 2 depicts that the regional imbalanced economic progression in the YRB was characterized as a fluctuating downward inclination between 2010 and 2020. The year 2016 was used as a split point so the full period was divided into two subperiods, namely, between 2010 through 2016 and between 2016 through 2020. The PWCV for the economic progression in the YRB decreased from 0.3310 in 2010 to 0.2718 in 2016 with an average annual decline of 2.98%. Besides, the PWCV for the economic progression in the YRB decreased from 0.2718 in 2016 to 0.1516 in 2020 with an average annual decline of 11.06%. Thus, the imbalanced economic development in the YRB decreased significantly between 2016 and 2020. Therefore, it can be concluded that the degree of the imbalance within the economic development region of the YRB was generally high and volatile.

Figure 3 depicts that the imbalanced economic progression in the YRB between 2010 and 2020 had been constantly fluctuating. While the average annual decline of the PWCV among economic progression regions in the YRB was 6.5% between 2010 through 2012, the average annual decline of the PWCV among economic progression regions in the YRB was 4.7% between 2012 and 2018. On the other hand, the average annual decline of the PWCV among economic progression regions in the YRB was 15.28% between 2018 through 2020. It can be concluded that the degree of the imbalance among regions in the YRB was generally towering and changing.

4.3. The Industrial Decomposition of the Unbalanced Changes in the Economic Progression in the YRB. When GDP was decomposed concerning the classification of primary, secondary, and tertiary industries, this paper decomposed the unbalanced changes in the economic progression in the YRB. We select the years 2010, 2013, 2015, 2018, and 2020, which are significant, to investigate the effect of these three

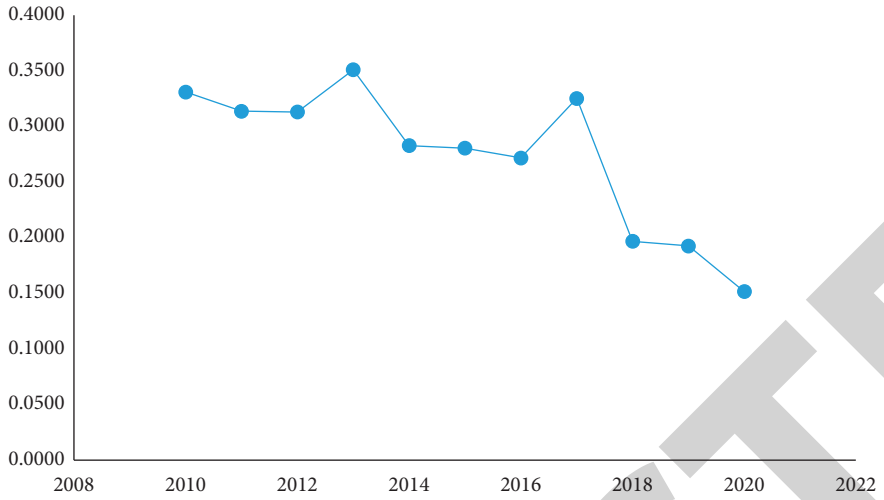

Figure 2: The unbalanced change process of the economic progress in the YRB between 2010 and 2020.

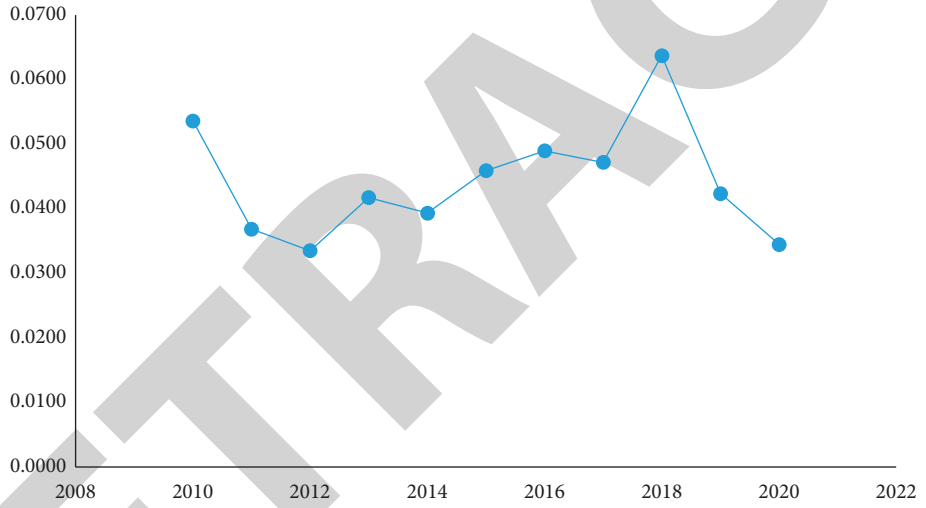

Figure 3: The change process of the regional imbalance of the economic progress in the YRB between 2010 and 2020.

Table 3: The industrial decomposition results of the unbalanced development in the YRB in 2010 (unit: %).

Regional imbalance	Regional internal imbalance	Internal imbalance in the upstream region	Internal imbalance in the middle reaches	Internal imbalance in downstream areas	Imbalance between regions	Total
Primary industry	0.56	0.14	0.31	0.11	0.83	1.39
Secondary industry	51.24	13.28	18.38	19.58	7.99	59.23
Tertiary industry	34.26	8.21	14.13	11.92	5.12	39.39
Total	86.06	21.63	32.81	31.62	13.94	100

industries on the unbalanced economic progression of the YRB. The results are presented in Tables 3–7.

Tables 3–7 firstly present that (1) the dissimilarity between the secondary and the tertiary industries is the most important factor leading to the unbalanced economic progression in the YRB among the industrial sources with the proportion reaching more than 98%. (2) The secondary industry contributing to the unbalanced economic progression in the YRB was more than 50% and decreased after 2018, and the last figure was 45.67% in 2020. (3) The tertiary industry contributing to the unbalanced economic progression in the YRB increased on a yearly basis, which changed from 39.39% to 55.62%. (4) However, its contribution to the regional imbalanced average income of the residing people in rural areas of China was marginally higher than that of the average wage in 1993, and its contribution

Table 4: The industrial decomposition results of the unbalanced development in the YRB in 2013 (unit: %).

Regional imbalance	Regional internal imbalance	Internal imbalance in the upstream region	Internal imbalance in the middle reaches	Internal imbalance in downstream areas	Imbalance between regions	Total
Primary industry	0.75	0.10	0.27	0.38	0.53	1.29
Secondary industry	50.23	11.77	18.33	20.12	5.40	55.63
Tertiary industry	38.39	8.46	14.62	15.31	4.69	43.09
Total	89.37	20.33	33.23	35.81	10.63	100

Table 5: The industrial decomposition results of the unbalanced development in the YRB in 2015 (unit: %).

Regional imbalance	Regional internal imbalance	Internal imbalance in the upstream region	Internal imbalance in the middle reaches	Internal imbalance in downstream areas	Imbalance between regions	Total
Primary industry	0.23	−0.08	0.38	−0.06	0.55	0.78
Secondary industry	44.98	10.11	19.00	15.88	7.06	52.04
Tertiary industry	40.72	9.07	18.01	13.65	6.45	47.17
Total	85.94	19.09	37.38	29.46	14.06	100

Table 6: The industrial decomposition results of the unbalanced development in the YRB in 2018 (unit: %).

Regional imbalance	Regional internal imbalance	Internal imbalance in the upstream region	Internal imbalance in the middle reaches	Internal imbalance in downstream areas	Imbalance between regions	Total
Primary industry	0.04	−0.14	0.26	−0.08	0.67	0.71
Secondary industry	37.56	5.08	13.19	19.29	11.81	49.37
Tertiary industry	37.94	6.26	12.05	19.64	11.98	49.92
Total	75.54	11.20	25.49	38.84	24.46	100

Table 7: The industrial decomposition results of the unbalanced development in the YRB in 2020 (unit: %).

Regional imbalance	Regional internal imbalance	Internal imbalance in the upstream region	Internal imbalance in the middle reaches	Internal imbalance in downstream areas	Imbalance between regions	Total
Primary industry	−0.88	−0.31	0.08	−0.65	0.09	−0.79
Secondary industry	38.11	6.35	15.63	16.13	7.56	45.67
Tertiary industry	45.13	6.75	12.34	26.04	10.49	55.62
Total	82.36	12.79	28.05	41.52	18.14	100

was also lower than that of the average wage in other years. In 2009, its contribution was 47.88%, which was lower than that of the average wage. The effect of the primary industry on the unbalanced economic progression in the YRB was very small, which was just less than 2%.

Secondly, the impact of the three major industries on the regional and inter-regional imbalances for the economic progression of the three regions in the YRB was consistent with the impact of the abovementioned imbalance in the economic progression in the YRB. The difference originated from the contribution to the regional imbalance that was significantly greater than that to the inter-regional imbalance. Moreover, except for the primary industry, the difference pertinent to the impact of the secondary and the tertiary industries on the region generally showed a downward trend, and the impact on the region showed a fluctuating upward trend. Specifically, the contribution difference between the tertiary industry and regions increased by 13.02% from 2010 to 2020, and the contribution difference between the secondary industry and the regions did not change a lot. Correspondingly, the contribution difference of the tertiary industry to the region increased by 10.87% from 2010 to 2020, and the contribution difference of the secondary industry to the region decreased by 13.13%.

Thirdly, the impact on the intraregional imbalance was greater than that on inter-regional imbalance when the overall impact of the industry on inter-regional imbalance and intraregional imbalance were under consideration. The gaps of this impact were 72.12%, 78.74%, 71.88%, 51.08%, and 64.22% in 2010, 2013, 2015, 2018, and 2020, respectively. However, the gap was generally decreasing.

Fourth, the impact of the imbalance of the internal economic development in the lower and middle sections was relatively large when the internal industrial difference impact of the regional imbalance was under consideration. The impact of the unbalanced economic progression in the middle sections on the regional imbalance accounted for 38.12%, 37.18%, 43.50%, 33.74%, and 34.06% in 2010, 2013,

2015, 2018, and 2020, respectively. The impact of the unbalanced economic development in downstream areas on the regional imbalance accounted for 36.74%, 40.07%, 34.28%, 51.42%, and 50.41% in 2010, 2013, 2015, 2018, and 2020, respectively, with an increasing trend in a yearly basis.

5. Findings

5.1. Building a New Development Layout for Both Urban and Rural Regions. A more comprehensive approach is needed to tackle the issues mentioned previously. Hence, providing a comprehensive perspective to determine the comparative advantages of the regions, promoting the slimming and fitness of megacities, and building large- and medium-sized cities in a way of orderly manner should be realized. Then, promoting the urbanization of county towns, eradicating the weaknesses, expanding and strengthening the county economy, thus comprehensively implementing the Rural Revitalization Strategy should be done. Eventually, devising a development layout concerning the characteristics of the subregions, urban and rural areas based on their respective positions, collaborative linkage, and organic mutual promotion is a key implementation that is highly required.

5.2. Utilization of Both Characteristics and Advantages to Building a Contemporary Industrial System. Relying on a strong domestic market, accelerating the structural reform of the supply side economy, investing more in both technological and scientific efforts and innovations, strengthening the characteristics of the industries according to regional resources, factor endowment, and development foundation are the first round of implementations that are needed. Besides, by focusing on areas with a strong industrial foundation along the lower and middle sections of the YRB, building a strategic cooperation platform that helps any industry appear with an effective connection between production and supply sides and collaborative cooperation among industries in the upstream, middle, and lower reaches of the region. Thus, a close connection between the industrial innovation chain and supply chain would be constructed that would promote the upgrading of the industrial system and the reconstruction of the basic capacity and hence would result in building industrial clusters with strong competitiveness. Therefore, acceleration and transformation of new and old driving forces would support the manufacturing industry aiming at reaching high-quality end products so the transformation of the resource-based industries would be realized, which would construct a contemporary system that would provide unique characteristics and advantages to the industry.

5.3. Improving the Realization of the Value and Compensation Instrument of the Ecofriendly Goods. To establish a mechanism of value realization based on ecological products in the YRB including the organic combination of both vertical and horizontal dimensions, government and market would need to take the stage that carries out the value accounting and measurement of ecological products, gradually promoting the standardization, and finally provide support for compensations. Besides, the marketization of comprehensive ecological compensation should be devised that make up for the economic losses caused by abandoning large-scale industrial infrastructures since they are the main functions in some areas of the YRB to protect the functionality of the area, and compensation should be provided with those areas with a low environmental carrying capacity that gives up development opportunities for ecological protection to reduce the imbalanced economic progression in the YRB.

6. Conclusions

The research concludes that the imbalanced economic progression in the YRB generically showed a downward trend between 2010 through 2020, especially in 2018, which was mainly due to the national poverty alleviation and rural revitalization plans. However, the degree of the imbalance in the region generally was still high. Besides, the difference between main cities and underdeveloped counties and townships in the region was the main factor that led to the outcomes. Moreover, the imbalanced economic progression in the YRB was mainly caused by the differences between the secondary and the tertiary industries whose contribution rate was more than 98%, and the contribution of the tertiary industry to the imbalanced economic progression tended to expand gradually. The aforementioned conclusion implies that the level of economic development in these three regions of the Yellow River was in obvious contrast. On the other hand, the Shandong Peninsula in the lower section of the YRB has become a dazzling wonderful flower in the YRB, China, and even in the world. However, the upper sections and their resources look like they were almost a forgotten corner. The accumulated economic gap in the basin has been still a very serious issue. Therefore, more serious measures should be taken and implemented in this regard.

Data Availability

The data will be provided upon request to authors.

Conflicts of Interest

The authors declare that they have no conflicts of interest.

References

[1] W. Wenchao, "Temporal and spatial evolution analysis of county economic development imbalance in the Yellow River Basin," *Statistics and decision making*, vol. 37, no. 21, pp. 132–135, 2021.

[2] G. Li, "Fang Xubing Temporal and spatial evolution characteristics of green development level in the Yellow River Basin," *China Desert*, vol. 41, no. 04, pp. 129–139, 2021.

[3] J. Xi, "Speech at the symposium on ecological protection and high-quality development in the Yellow River Basin," *Qiushi*, vol. 42, no. 20, pp. 1–5, 2019.

[4] W. Wu, "Analysis of the temporal and spatial evolution of the imbalance of county economic development in the Yellow River Basin," *Statistics and Decisions*, vol. 37, no. 21, pp. 132–135, 2021.

Hindawi
Journal of Mathematics
Volume 2023, Article ID 9793012, 1 page
https://doi.org/10.1155/2023/9793012

Retraction

Retracted: Fuzzy Intelligence in Physical Immersion Teaching System Based on Digital Simulation Technology

Journal of Mathematics

Received 10 October 2023; Accepted 10 October 2023; Published 11 October 2023

This article has been retracted by Hindawi following an investigation undertaken by the publisher [1]. This investigation has uncovered evidence of one or more of the following indicators of systematic manipulation of the publication process:

(1) Discrepancies in scope

(2) Discrepancies in the description of the research reported

(3) Discrepancies between the availability of data and the research described

(4) Inappropriate citations

(5) Incoherent, meaningless and/or irrelevant content included in the article

(6) Peer-review manipulation

The presence of these indicators undermines our confidence in the integrity of the article's content and we cannot, therefore, vouch for its reliability. Please note that this notice is intended solely to alert readers that the content of this article is unreliable. We have not investigated whether authors were aware of or involved in the systematic manipulation of the publication process.

Wiley and Hindawi regrets that the usual quality checks did not identify these issues before publication and have since put additional measures in place to safeguard research integrity.

We wish to credit our own Research Integrity and Research Publishing teams and anonymous and named external researchers and research integrity experts for contributing to this investigation.

The corresponding author, as the representative of all authors, has been given the opportunity to register their agreement or disagreement to this retraction. We have kept a record of any response received.

References

[1] A. Du, "Fuzzy Intelligence in Physical Immersion Teaching System Based on Digital Simulation Technology," *Journal of Mathematics*, vol. 2022, Article ID 3741475, 10 pages, 2022.

Hindawi
Journal of Mathematics
Volume 2022, Article ID 3741475, 10 pages
https://doi.org/10.1155/2022/3741475

Research Article

Fuzzy Intelligence in Physical Immersion Teaching System Based on Digital Simulation Technology

Aihui Du

School of Physics, Henan Normal University, Xinxiang, Henan 453007, China

Correspondence should be addressed to Aihui Du; 2020210805@mail.chzu.edu.cn

Received 23 March 2022; Revised 21 April 2022; Accepted 25 April 2022; Published 17 May 2022

Academic Editor: Naeem Jan

In order to improve the effect of physics teaching, this study combines digital simulation technology to construct a physical immersion teaching system to improve the effect of physics teaching in colleges and universities. Moreover, this study transforms abstract physical knowledge into recognizable digital physical images and realizes the idea of multifeature fusion through reasonable feature selection and the use of a classifier algorithm suitable for the subject of this paper. In addition, this study proposes a new algorithm based on the morphological features of geometric images, which combines the transformation detection method of cluster analysis to realize the intelligent processing of images. Finally, this study verifies the effectiveness of the physical immersion teaching system based on fuzzy intelligence and digital simulation technology through experimental research. The results show that the system can effectively improve the effect of physics teaching.

1. Introduction

Immersion theory relies on technological tools to provide a near-real learning environment for learners, enabling them to complete knowledge and theory creation in an immersed state. Immersion theory is one of the artificial intelligence ideas that has had the most influence on higher education so far. The early immersion theory proposed that, in order to keep users immersed, a balance of abilities and difficulties must be maintained, which may influence the occurrence of "learning behaviour" in users [1]. With the combination of computer technology and immersion theory, the theory's meaning has expanded to include human-computer interaction and scene-based learning, further strengthening the theoretical foundation of "immersion teaching" [2]. Immersion teaching is a real expression of immersion theory as a new educational paradigm. It offers immersion, intense engagement, and a flexible mode, all of which are beneficial to the development of creative and inventive new media abilities. Traditional media talent training at colleges and universities, on the contrary, has inherent flaws such as a lack of enthusiasm in learning, a single kind of practical training, limited learning involvement, and a lack of innovation potential. In the age of artificial intelligence, this will not be enough to address the training demands of applied and compound media professionals. The question of how to create an appropriate training model for media talent in colleges and universities based on "immersion teaching" has become a crucial issue worth investigating [3].

The modular education thinking is integrated into the training process of media talents in colleges and universities and is oriented to improve the professional skills of students. According to the different training goals and types of physics talents in colleges and universities, each module implements personalized "immersion teaching" according to the characteristics of the major and the requirements of practical training. In the talent training module, artificial intelligence technology, 3D real-time rendering technology, and motion capture and recognition technology are used to build a virtual studio with 3D graphics workstation, camera tracking system, etc. Moreover, students can use the platform to complete virtual training so that students can experience an alternative studio experience in the interweaving of reality and reality. Through the digital synthesis of three-dimensional scenes, moving images, and actual training processes, students' "immersion" is enhanced, knowledge and abilities

are more easily mastered, and a resource module system is formed.

This study combines digital simulation technology to construct a physical immersion teaching system, improve the effect of physics teaching in colleges and universities, and transform abstract physics knowledge into recognizable digital physics images to help students understand and improve the efficiency of physics teaching.

2. Related Work

The modular education thinking is integrated into the training process of media talents in colleges and universities and is guided by the improvement of students' professional skills. According to the different goals and types of media talents training in colleges and universities, the talent training process is divided into radio and television director talent-training modules, film and television photography and production majors' talent training module, and broadcasting and hosting professional talent-training module, and each module implements personalized "immersion teaching" according to different professional characteristics and training requirements [4]. Artificial intelligence technology, 3D real-time rendering technology, and motion capture and recognition technology are combined to create a virtual studio with a 3D graphics workstation, camera tracking system, and other features in the physics teaching talent training module. Students may utilise this platform to complete virtual instruction, allowing them to have a unique studio experience that combines reality and reality. The "immersion" of pupils is improved, and it is simpler to grasp information and talents, thanks to the digital synthesis of three-dimensional settings, moving visuals, and real training process [5], focuses on developing students' ability to comprehend various scenarios and environments, and can use virtual scene simulation technology to design simulation scene systems, integrating camera perspective roaming, subjective immersive browsing, interactive simulation experience, intelligent scene identification, and other functions, not only can design multiple simulation scene systems. The simulation scene is convenient for students to freely explore unknown scenes according to their personal cognitive situation, transform knowledge, and skills and can easily perform camera operations, compare the effects of different operation schemes, and enhance students' perception of the scene. [6].

Immersive virtual reality (immersiveVR) provides participants with a fully immersive experience so that users have a feeling of being in a virtual world, so it can best show virtual reality effects. Related equipment includes helmet-mounted displays, walking equipment, cave-style stereoscopic displays, devices, data gloves, and spatial position trackers [7]. The obvious characteristics of immersive virtual reality are the use of closed scenes and sound systems to isolate the user's visual and auditory from the outside world so that the user can be completely immersed in the computer-generated environment; it has a high sense of immersion, high real time, good system integration, and parallel processing capabilities [8]. At present, the common immersive virtual reality systems include helmet-type virtual reality systems, cockpit-type virtual reality systems, projection-type virtual reality systems, and cave-type virtual reality systems. Compared with desktop virtual reality and distributed virtual reality, immersive virtual reality will be one of the important contents in the application of virtual reality technology in college physics teaching in the future [9].

Immersive virtual experiment technology allows college professors to use novel and different teaching approaches. It offers several benefits in experimental education, including a high usage rate, excellent safety, and ease of maintenance. It is an active investigation in colleges and universities to promote "intelligence + education," and it will become a college, and universities rebuild the education ecosystem and create the essential link of intelligent education [10]. The greatest impediment to the use of immersive virtual reality in smart teaching in colleges and universities is its high cost. The cost of research and development and equipment acquisition, such as location tracking and location tracking, is greater, as it is the cost of repair and maintenance [11]. The problem that restricts the application of immersive virtual reality in smart teaching in colleges and universities is a technical problem of personnel. Compared with nonimmersive VR systems and semi-immersive VR systems, immersive VR systems have higher requirements for smart teaching administrators in colleges and universities [12]. Generally speaking, the operation of nonimmersive VR systems and semi-immersive VR systems is relatively simple. Smart teaching administrators in colleges and universities only need short-term training to achieve skilled operation. Immersive VR systems require a deep understanding of virtual reality technology. To ensure the long-term stable operation of the immersive VR system, not only professionals are required to operate the equipment but also professionals are required to perform repairs and maintenance [13]. In order to improve the reader's immersive and exchangeable experience of immersive VR systems, it also depends on the further improvement of visual scene generation technology. The panorama technology generally used in smart teaching in colleges and universities that use nonimmersive VR systems and semi-immersive VR systems can help readers find their favorite books in smart teaching in colleges and universities as much as possible. The technical cost requirements are lower, but the immersive and exchangeable experience is poor [14]. The 3D modeling technology generally used in the immersive VR system has the characteristics of good immersion and interactivity, but the construction process of complex models is relatively heavy and complicated, and the construction of an effective interactive virtual scene requires a large amount of programming and technology. The difficulty requirement is higher [15].

3. Digital Simulation Technology

As seen in Figure 1, the RGB model describes a colour by a point in three-dimensional space. Each pixel contains three components that indicate the pixel's colour's red, green, and

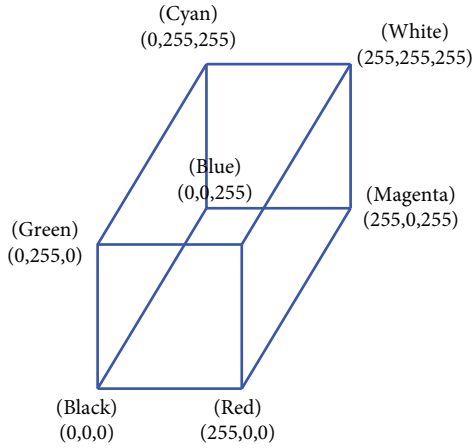

Figure 1: RGB model cube.

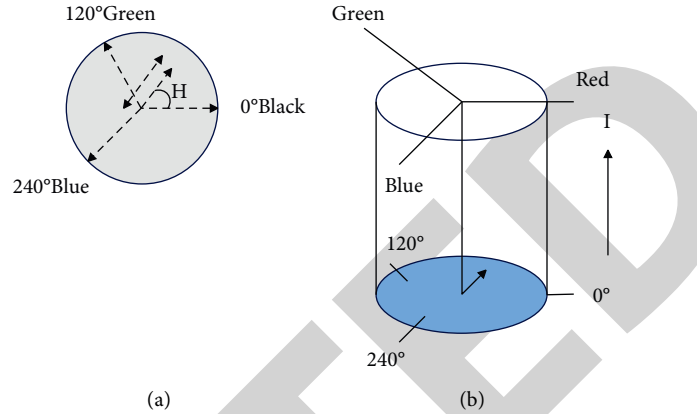

Figure 2: HSI colour model. (a) Color cycle and (b) Column color space.

blue brightness levels. The brightness value range for frequently used 24-bit colour digital photographs is normally a closed interval [0,255], which may represent more than one million colours. The RGB colour system is based on the idea that colours emit light. To put it in another way, it is like having three lights: red, green, and blue. The colours are blended when the lights of these three lamps are overlaid on each other, and the brightness equals the total of the two brightnesses. The greater the brightness is, the more blended it is, that is, additive mixing [16].

The hue circle in Figure 2(a) describes the two parameters, hue and saturation. The hue is expressed in angle, which reflects the wavelength of the light wave in the spectrum that the colour is closest to. Generally, 0° is defined as red, 120° as green, and 240″ as blue. Hue from 0° to 240° covers all colours of the visible spectrum in the physical sense, and hue between 240° and 300° is the nonspectral (purple) of the human eye courseware.

As illustrated in Figure 2, the three attribute parameters of the HSI model establish a three-dimensional circular three-dimensional space (b). The grayscale shadows go from black at the bottom to white at the top along the axis, with increasing brightness until the maximum point. Figure 2 shows that the colours with the highest saturation are found around the perimeter of the cylinder's top surface.

The formula for converting the RGB colour model to the I model is as follows.

For any three R, G, and B parameter values in the [0,255] closed interval, the calculation of the I, S, and H components in the corresponding HI model is as follows:

① $I = (1/3)(R + B + G)$

② $S = 1 - (3/(R + G + B))[\min(R, G, B)]$

③ $H = \arccos\{[(R - G) + (R - B)]/2/[(R - G)^2 + (R - B)(G - B)]^{1/2}\}$

The value range of H calculated by formula ② is [0°, 180°], corresponding to $G \geq B$.

The grayscale histogram of an image reflects the distribution of each grayscale pixel in the image and also reflects the grayscale in the image and the probability relationship of a certain grayscale. The scale of the abscissa represents the grayscale of the image, and the scale of the ordinate represents the number of pixels of a certain grayscale, or the number of pixels with a certain grayscale value in the image. The ratio of the total number of pixels in the image is shown in Figure 3 [17].

3.1. Gray Value Linear Transformation Method. In order to optimize the contrast of the image, we can use the method of redistributing the pixel value domain, and we can use the linear mapping method to expand the gray value range of the image, as shown in Figure 4.

The gray value of the image is f (x, y), the gray value range is $[m, M]$, and the gray value of the image after linear gray value transformation is g (x, y). The gray value range is extended to $[n, N]$, which is the value range of g (x, y). The gray value linear transformation enhancement formula is

$$g(x, y) = \frac{(N - n)[f(x, y) - m]}{(M - m) + n}, \quad (1)$$

where x and y represent the coordinate position of the pixel in the image.

3.2. Histogram Equalization. The gray value histogram of an image is to describe the image in the Cartesian coordinate system through a discrete function of gray level, which can be described as

$$H_s(s_k) = \frac{n_k}{n}, k = 0, 1, \ldots, N - 1, \quad (2)$$

where $H_s(s_k)$ represents the probability of occurrence of gray level k, n represents the total number of pixels in the image, and n_k represents the total number of pixels with gray level k in the digital image.

Histogram equalization is generally divided into the following steps:

① The algorithm computes a grayscale histogram from the original grayscale image: $H_s(s_k) = n_k/n$, $k = 0, 1, \ldots, N - 1$

② The algorithm calculates $r_k = \sum_{i=0}^{k} H_s(s_i) = \sum_{i=0}^{k} n_i/n$ to obtain the cumulative gray-level histogram of the original grayscale image

③ The algorithm determines the gray level t after histogram equalization processing according to the formula $t_k = \text{int}[(N-1)r_k + 0.5]$, where the symbol int represents the forensic value part and N is the number of gray levels in the original gray image

④ After determining the mapping relationship between the original grayscale image level from s_k to t_k, the algorithm converts the grayscale value of each pixel in the original grayscale image according to the relationship [18]

The degree to which an image is disturbed by noise can be expressed by the signal-to-noise ratio (SNR), which is also one of the most commonly used metrics we use to measure image quality:

$$\text{SNR} = -\log_{10}\frac{\sum_{x=0}^{N-1}\sum_{y=0}^{N-1}[f(x,y)-\overline{f(x,y)}]^2}{\sum_{x=0}^{N-1}\sum_{y=0}^{N-1}f(x,y)^2}. \quad (3)$$

For general images, in order to obtain a better recognition effect, we must filter and denoise the image.

3.2.1. Airspace Method Filtering and Noise Reduction. Neighborhood averaging filtering is an effective method for dealing with point-like noise. The filtering processing principle of the neighborhood average method is to first select a small block of the image, then average the gray levels of each pixel, and finally assign the gray value to the center point (x, y) of the small block as the pixel point. The new gray value $g(x, y)$ of the conversion formula is as follows:

$$g(x,y) = \frac{1}{M}\sum_{f\in s} f(x,y), \quad (4)$$

where $x, y = 0,1, \ldots, N\text{-}1$: M is the number of pixels included in the neighborhood and s is the set of points in the small neighborhood with (x, y) as the center point. The small neighborhood is also called the Box template. In the so-called Box template market value template, all the coefficients in the template go to the same value. Generally, 3×3, 5×5, or other square matrices are selected, as shown in Figure 5.

Neighborhoods are divided into two categories: four-neighborhood and eight-neighborhood. The higher, lower, left, and right points of the tiny block's center point are only considered in the four-neighborhood technique. The upper, lower, left, right, and four diagonal points of the tiny block's center point are included in the eight-neighborhood, as illustrated in Figure 6.

Usually, the eight-neighbor template is more commonly used, and the conversion formula for the processing images is

$$g(x,y) = \frac{1}{9}\sum_{i=1}^{9} f(x_i, y_i), \quad (5)$$

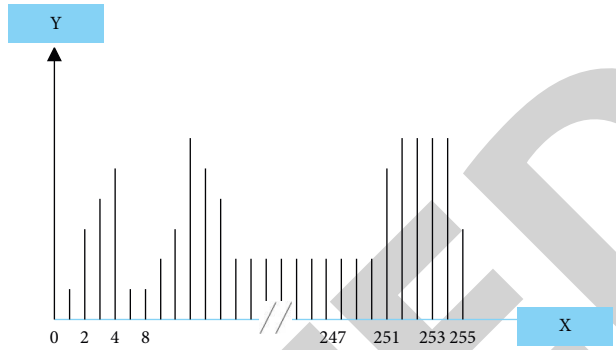

Figure 3: Image grayscale histogram.

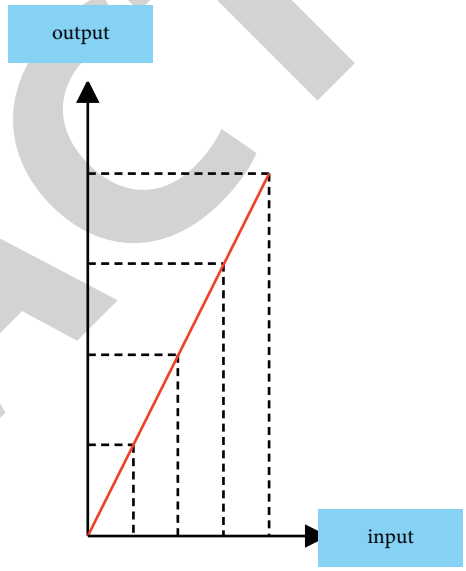

Figure 4: Grayscale linear transformation.

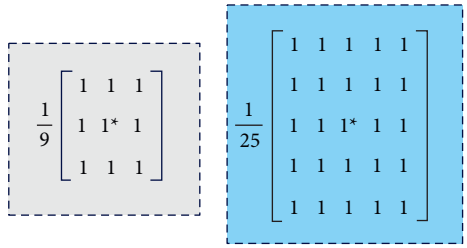

Figure 5: 3×3 and 5×5 templates.

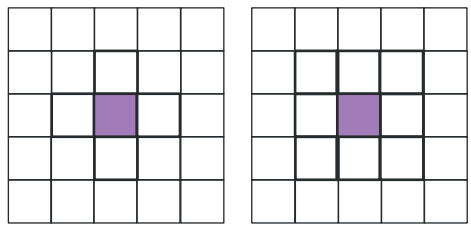

(a) (b)

Figure 6: Four-neighborhood (a). Eight-neighborhood (b).

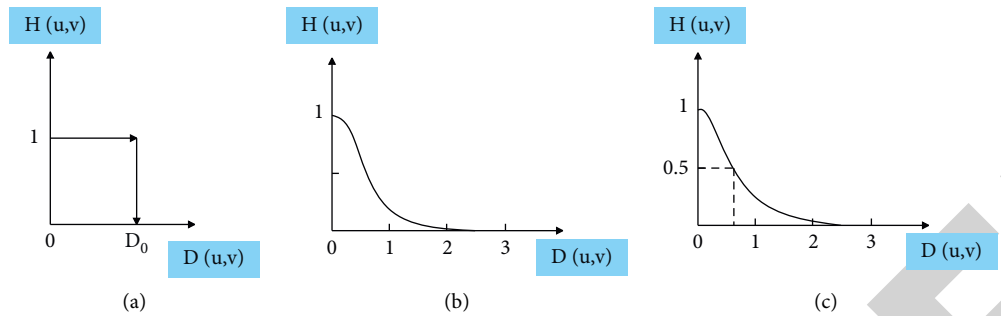

Figure 7: Characteristic curves of three types of low-pass filtering.

where $g(x, y)$ is the new gray value of the pixel point (x, y), and f (x, y) is the gray value of the point (x, y) in the original grayscale image.

Gaussian filter is a kind of filter commonly used in image smoothing processing, and this filter has ideal characteristics. The formula for the Gaussian smoothing filter is

$$G(x, y) = \frac{1}{\sqrt{2\pi}} \exp\left(-\frac{x^2 + y^2}{2\sigma^2}\right), \tag{6}$$

where (x, y) represents the position of the pixel in the image. If a uniform smoothing scale is used in all neighborhoods in the image, relative to the adaptive smoothing filter, its calculation formula is

$$w^{(t)}(x, y) = \exp\left(-\frac{\left(d^{(t)}(x, y)\right)^2}{2k^2}\right), \tag{7}$$

where t represents the number of iterations, the k-scale parameter is similar, and $d^{(t)}(x, y)$ is a metric function reflecting the image features, which determines the edge magnitudes that can be preserved during the smoothing process.

For the signal f (x, y) of the two-dimensional image, $d'(x, y)$ is defined as the gradient of f (x, y). For the above 3×3 two-dimensional Gaussian template, the gradient formula is

$$\left(\frac{\partial f^t(x, y)}{\partial x}, \frac{\partial f^t(x, y)}{\partial y}\right)^t = \left(f_x, f_y\right)^t. \tag{8}$$

The formula for calculating the amplitude is

$$d^t(x, y) = \sqrt{f_x^2 + f_y^2}. \tag{9}$$

Combining the above two formulas, we can obtain

$$w^{(t)}(x, y) = \exp\left(-\frac{f_x^2 + f_y^2}{2k^2}\right). \tag{10}$$

To sum up, we can get the smooth pixel value of the pixel point (x, y). The calculation formula is as follows:

$$f^{t+1}(x, y) = \frac{1}{\sum_{i=-1}^{1}\sum_{j=-1}^{1} w^{(t)}(x + i, y + j)} \sum_{i=-1}^{1}\sum_{j=-1}^{1} f^{(t)}(x + i, y + j) w^{(t)}(x + i, y + j). \tag{11}$$

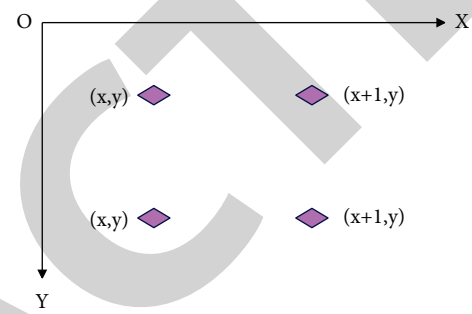

Figure 8: Pixel gray gradient.

3.2.2. Frequency-Domain Filtering and Noise Reduction. Three commonly used frequency-domain low-pass filters are ideal low-pass filter (ILPF), exponential low-pass filter (ELPF), and Butterworth low-pass filter (BLPF). The characteristic curves of these three low-pass filters are shown in Figure 7.

① The filter function of the ideal low-pass filter (ILPFE) is

$$H(u, v) = \begin{cases} 0, & d(u, v) \le d_0, \\ 1, & d(u, v) \le d_0. \end{cases} \tag{12}$$

② The filter function of the exponential low-pass filter (ELPFP) is

$$H(u, v) = e^{-0.374\left[d_0/d(u,v)\right]^n}. \tag{13}$$

③ The filter function of the Butterworth low-pass filter (BLPF) is

$$H(u, v) = \frac{1}{1 + \left[d_0/d(u, v)\right]^{2n}}. \tag{14}$$

In the above three formulas, d is the distance from the origin of the frequency plane to the cutoff frequency, and $d(u, v) = \sqrt{u^2 + v^2}$ is the distance from the point (u, v) to the origin of the frequency plane.

The method of calculating the gray gradient is shown in Figure 8.

The grayscale of the image is represented by f (x, y). For point P (x, y), the grayscale values of its adjacent pixels are f $(x + 1, y)$, f $(x, y + 1)$, and f $(x + 1, y + 1)$, respectively. The gray

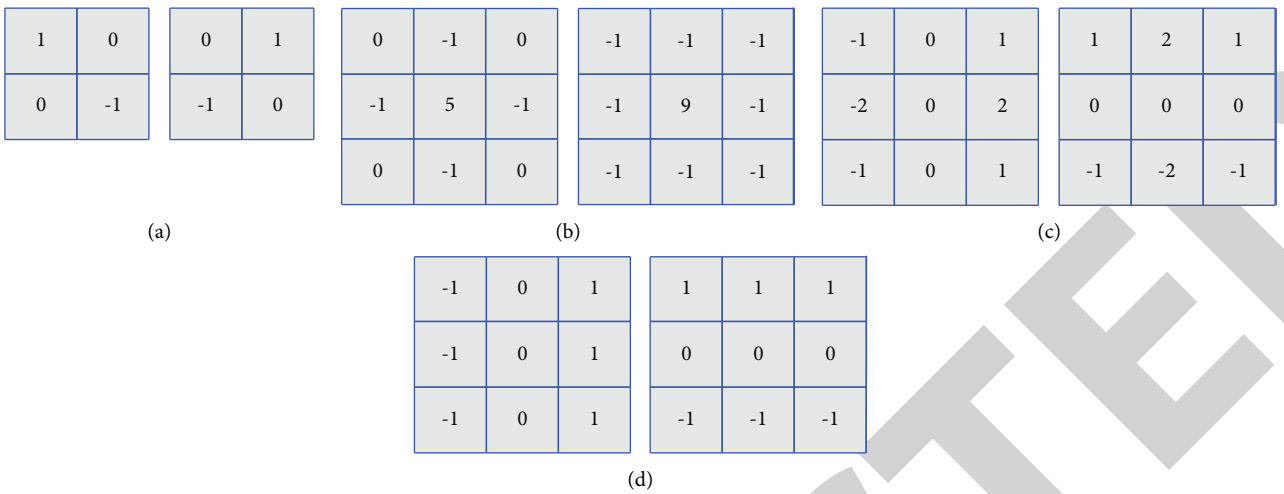

Figure 9: Commonly used edge sharpening templates.

value gradient of the point P can be calculated by the cross-difference method. The algorithm is divided into two steps.

① The grayscale gradients in the x and y directions are

$$G_x[f(x,y)] = |f(x+1,y) - f(x,y)|,$$
$$G_y[f(x,y)] = |f(x,y+1) - f(x,y)|. \quad (15)$$

② The gray value gradient of point P can be calculated by the cross-difference method:

$$G_x[f(x,y)] = \sqrt{G_x^2 + G_y^2}. \quad (16)$$

Then,

$$G_y[f(x,y)] \approx |f(x+1,y+1) - f(x,y)| + |f(x,y+1) - f(x+1,y)|. \quad (17)$$

Commonly used sharpening templates mainly include (a) Robert template, (b) Laplacian template, (c) Sobel template, and (d) Prewitt template, as shown in Figure 9.

We must segment the picture or extract the region matching to the object of interest in the image, in order to retrieve the information about the item of interest in the image. The most basic and often used the picture segmentation method is threshold segmentation. The following is how threshold segmentation is defined:

$$S = \{(x,y) \in R | g_{\min} \le f_{x,y} \le g_{\max}\}. \quad (18)$$

Reliability: a feature value of all objects in the same category should be as close as possible. The closer the eigenvalues within the class, the higher the reliability of the eigenvalues used to identify such objects. The reliability of a feature can be qualitatively measured with the following mathematical formula:

$$\sigma = \sqrt{\frac{1}{M}\sum_{i=1}^{N}(X_i - \mu_x)^2}. \quad (19)$$

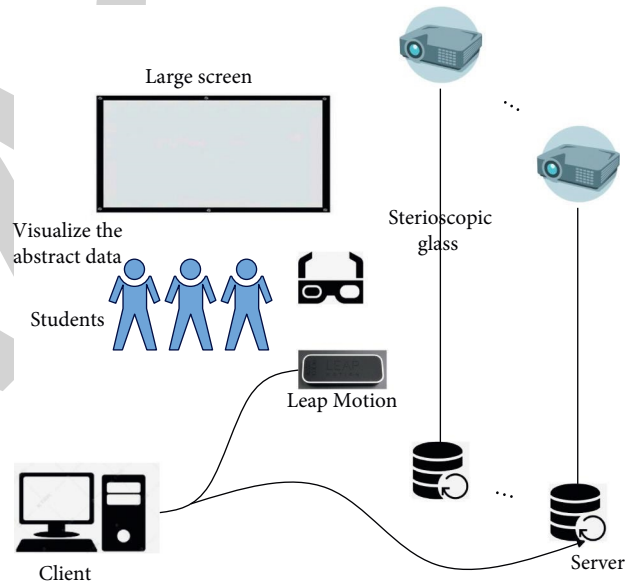

Figure 10: Schematic diagram of immersive VR physics teaching environment.

Among them, the eigenvalue of the ith sample is represented by X_i, u_i represents the mathematical expectation value of the sample eigenvalue of this category, and the number of samples in a certain category is represented by M. The smaller the feature standard deviation is, the closer the eigenvalues in the class are and the higher the reliability of this eigenvalue is.

The independence of features can be measured using the following formula:

$$\lambda_{xy} = \frac{1/M\sum_{i=1}^{M}(x_i - \mu_x)(y_i - \mu_y)}{\sqrt{\sigma_x^2\sigma_y^2}}. \quad (20)$$

The greater the difference between the feature values used to identify an object for objects of different categories, the higher the distinguishability of the feature

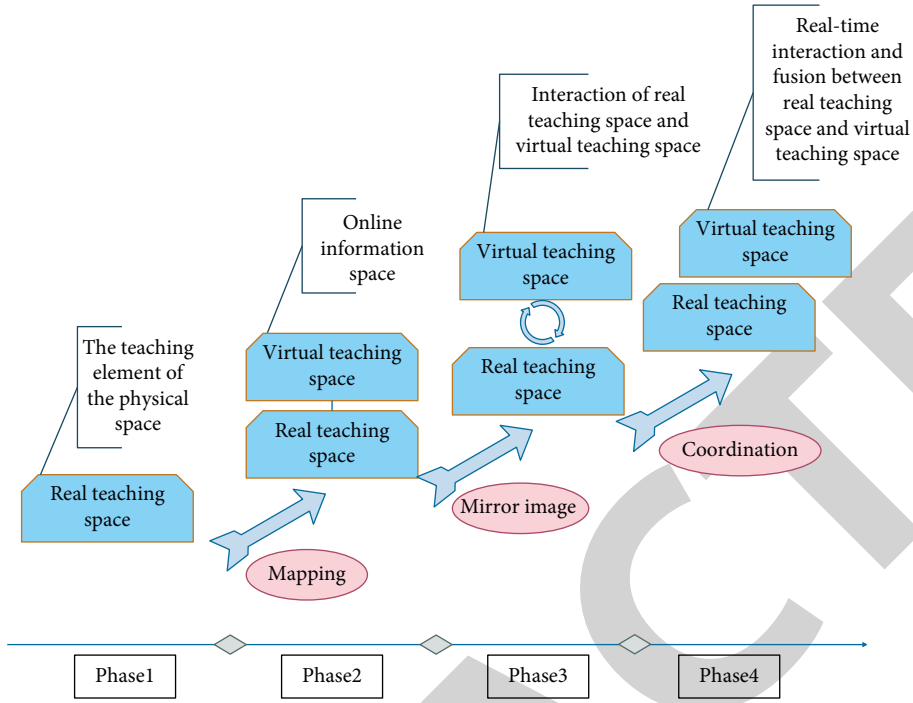

FIGURE 11: Framework of mapping, mirroring, and collaborative operation between physical reality teaching space and virtual teaching space.

for distinguishing different categories. The distinguishability of features can be measured using the following formula:

$$D_{xab} = \frac{|u_{xa} - u_{xb}|}{\sqrt{\sigma_{xa}^2 + \sigma_{xb}^2}}. \tag{21}$$

The calculation formula is as follows.

The first moment is Mean $= \sum_{i=1}^{N} p_i/N$.

The second moment is Variance $= \sqrt{\sum_{i=1}^{N} (p_i - \text{Mean})^2/N}$.

The third moment is Variance $= \sqrt{\sum_{i=1}^{N} (p_i - \text{Mean})^2}/N$.

Among them, p_i is the hue (He) value of the ith pixel in the image and N is the number of pixels.

The target coordinate y_t of the first segment chain code is $y_t = y_0 + \sum_{i=1}^{l} \Delta y_i$, and the calculation formula of the area is $A = \sum_{i=1}^{N} (y_{i-1}\ \Delta x_i + a)$.

Among them, $\Delta y_i = \begin{cases} -1, & \varepsilon_i = 5, 6, 7 \\ 0, & \varepsilon_i = 0, 4 \\ 1, & \varepsilon_i = 1, 2, 3 \end{cases}$, $\Delta x_i = \begin{cases} -1, & \varepsilon_i = 3, 4, 5 \\ 0, & \varepsilon_i = 2, 6 \\ 1, & \varepsilon_i = 0, 1, 7 \end{cases}$, $a = \begin{cases} -(1/2), & \varepsilon_i = 3, 7 \\ 0, & \varepsilon_i = 0, 2, 4, 6, \\ (1/2), & \varepsilon_i = 1, 5 \end{cases}$ and ε_i represents the ith symbol.

At present, there are four main methods for measuring the circularity of the shape of an object: density, boundary energy, circularity, and ratio of area to the square of the average distance. Among them, the density and boundary energy are more commonly used and effective.

The density C is the ratio of the square of the perimeter (P) to the area (S):

$$C = \frac{P^2}{S}. \tag{22}$$

A quantitative property used to quantify the shape complexity of an item is the format factor, which is a variant of density. The perimeter and area of the item are used to compute it, and the measurement's result is mapped in a (0.1) interval. The shape parameter's computation formula is as follows:

$$e = 4\pi \frac{S}{P^2}, \tag{23}$$

where S is the area and P is the perimeter. If it is assumed that the perimeter of a circle is 2nr, then its area is πr^2, and $e = 1.0$ is calculated by the above formula, indicating that the value of e is 1 when the object is a regular center. e takes a value in the interval (0, 1). When the value of e is larger and closer to 1, it means that the object is closer to a circle. On the contrary, when the value of e is smaller and closer to 0, it means that the graph is more complex and less like a circle.

Boundary energy is a curvature-based method to quantify the circularity of an object. For the point p on the boundary, the coordinates are (x, y). For digital images, the boundary energy calculation is discretized to obtain the calculation formula as follows:

$$E = \frac{1}{p} \sum_{i=0}^{P} |C(p_i)|, \tag{24}$$

where P is the length of the boundary, that is, the perimeter of the object, $C(p_i)$ is the instantaneous curvature of the ith

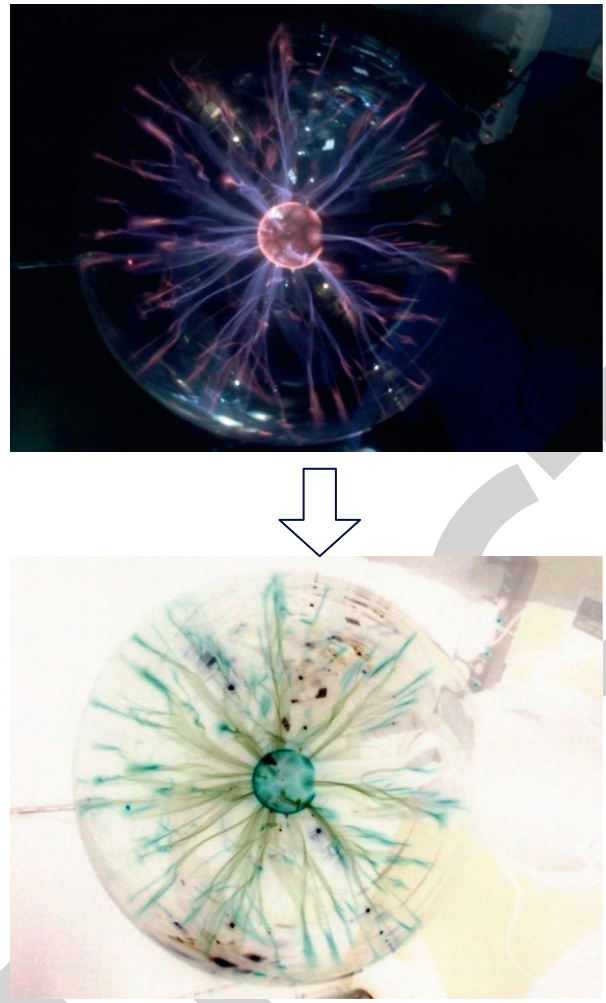

Figure 12: An example of a simulation image of physical immersion teaching based on digital simulation technology.

Table 1: Effect verification of physical immersion teaching system based on digital simulation technology.

Number	Teaching effect	Number	Teaching effect	Number	Teaching effect
1	83.20	21	81.68	41	77.74
2	81.07	22	85.38	42	76.42
3	79.27	23	79.71	43	83.35
4	75.76	24	77.29	44	86.76
5	84.12	25	77.31	45	75.72
6	82.02	26	80.17	46	79.93
7	81.60	27	81.01	47	83.31
8	83.43	28	79.12	48	80.17
9	79.95	29	81.59	49	77.77
10	81.19	30	78.24	50	80.26
11	83.20	31	80.72	51	75.66
12	75.28	32	79.74	52	86.29
13	86.66	33	75.10	53	75.80
14	80.45	34	84.11	54	80.05
15	76.99	35	79.69	55	85.34
16	84.49	36	86.21	56	78.41
17	80.91	37	84.98	57	85.53
18	77.80	38	85.48	58	77.26
19	84.24	39	79.03	59	84.66
20	80.47	40	83.75	60	84.19

The above research verifies the effectiveness of the physical immersion teaching system based on digital simulation technology, which can effectively improve the effect of physics teaching.

boundary point, that is, the radius $(r(p_i))^{-1}$ of the circle tangent to the boundary at the point p_i. When the object is a regular circle, the boundary energy obtains the minimum value $1/R^2$.

4. Physical Immersion Teaching System Based on Digital Simulation Technology

Immersive VR physics teaching environment, as shown in Figure 10, includes virtual reality hardware devices, such as large screens, projectors, servers, and three-dimensional interactive devices. The related software creates a highly open, interactive, and immersive learning environment for learners. The goal is to visualize scientific data or abstract concepts so that students can see and even "touch" the data interactively.

The connectivity and integration of actual teaching space and virtual teaching space is the foundation for the integration and application of virtual and real teaching space. The functional layer's key functions include the development of online learning elements as well as the integration and application of virtual and physical teaching venues. Its goal is to create a virtual and physical teaching area that can be mapped, mirrored, and collaborated on. Figure 11 depicts the unique operating structure.

Figure 12 shows the simulation image of Lightning Magic Globe, which can effectively improve the teaching effect of physical immersion teaching.

On the basis of the above research, the effect evaluation of the physical immersion teaching system based on digital simulation technology proposed in this study is carried out, and the evaluation effect shown in Table 1 is obtained.

5. Conclusion

In the training module of physics talents, it focuses on cultivating students' ability to grasp different scenarios and environments. The virtual scene simulation technology can be used to design a simulation scene system, integrating camera perspective roaming, subjective immersive browsing, interactive simulation experience, intelligent scene identification, and other functions. Students may freely explore unexpected settings and alter information and skills according to their particular cognitive condition by building different simulation scenarios. Furthermore, students may easily conduct experiments, evaluate the impacts of various operating schemes, enhance their perception of the picture, and create an interactive module system. This study combines digital simulation technology to construct a physical immersion teaching system to improve the effect of physics teaching in colleges and universities. The experimental research shows that the physical immersion teaching system based on digital simulation technology has certain effects.

Data Availability

The data used to support the findings of this study are included within the article.

Conflicts of Interest

The authors declare that they have no conflicts of interest.

References

[1] S. F. Alfalah, "Perceptions toward adopting virtual reality as a teaching aid in information technology," *Education and Information Technologies*, vol. 23, no. 6, pp. 2633–2653, 2018.

[2] G. Cooper, H. Park, Z. Nasr, L. P. Thong, and R. Johnson, "Using virtual reality in the classroom: preservice teachers' perceptions of its use as a teaching and learning tool," *Educational Media International*, vol. 56, no. 1, pp. 1–13, 2019.

[3] X. Ma, "Analysis on the application of multimedia-assisted music teaching based on AI technology," *Advances in Multimedia*, vol. 2021, Article ID 5728595, 12 pages, 2021.

[4] S. J. Bennie, K. E. Ranaghan, H. Deeks et al., "Teaching enzyme catalysis using interactive molecular dynamics in virtual reality," *Journal of Chemical Education*, vol. 96, no. 11, pp. 2488–2496, 2019.

[5] S. F. M. Alfalah, J. F. M. Falah, T. Alfalah, M. Elfalah, N. Muhaidat, and O. Falah, "A comparative study between a virtual reality heart anatomy system and traditional medical teaching modalities," *Virtual Reality*, vol. 23, no. 3, pp. 229–234, 2019.

[6] M. Reymus, A. Liebermann, and C. Diegritz, "Virtual reality: an effective tool for teaching root canal anatomy to undergraduate dental students–a preliminary study," *International Endodontic Journal*, vol. 53, no. 11, pp. 1581–1587, 2020.

[7] V. L. Dayarathna, S. Karam, R. Jaradat et al., "Assessment of the efficacy and effectiveness of virtual reality teaching module: a gender-based comparison," *International Journal of Engineering Education*, vol. 36, no. 6, pp. 1938–1955, 2020.

[8] O. Hernandez-Pozas and H. Carreon-Flores, "Teaching international business using virtual reality," *Journal of Teaching in International Business*, vol. 30, no. 2, pp. 196–212, 2019.

[9] V. Andrunyk, T. Shestakevych, and V. Pasichnyk, "The technology of augmented and virtual reality in teaching children with ASD," *Econtechmod: Scientific Journal*, vol. 7, no. 4, pp. 59–64, 2018.

[10] R. Mayne and H. Green, "Virtual reality for teaching and learning in crime scene investigation," *Science and Justice*, vol. 60, no. 5, pp. 466–472, 2020.

[11] M. Taubert, L. Webber, T. Hamilton, M. Carr, and M. Harvey, "Virtual reality videos used in undergraduate palliative and oncology medical teaching: results of a pilot study," *BMJ Supportive and Palliative Care*, vol. 9, no. 3, pp. 281–285, 2019.

[12] K. E. McCool, S. A. Bissett, T. L. Hill, L. A. Degernes, and E. C. Hawkins, "Evaluation of a human virtual-reality endoscopy trainer for teaching early endoscopy skills to veterinarians," *Journal of Veterinary Medical Education*, vol. 47, no. 1, pp. 106–116, 2020.

[13] X. Xu, P. Guo, J. Zhai, and X. Zeng, "Robotic kinematics teaching system with virtual reality, remote control and an on–site laboratory," *International Journal of Mechanical Engineering Education*, vol. 48, no. 3, pp. 197–220, 2020.

[14] P. W. Chang, B. C. Chen, C. E. Jones, K. Bunting, C. Chakraborti, and M. J. Kahn, "Virtual reality supplemental teaching at low-cost (VRSTL) as a medical education adjunct for increasing early patient exposure," *Medical Science Educator*, vol. 28, no. 1, pp. 3-4, 2018.

[15] J. Zhang and Y. Zhou, "Study on interactive teaching laboratory based on virtual reality," *International Journal of*

Hindawi
Journal of Mathematics
Volume 2023, Article ID 9843601, 1 page
https://doi.org/10.1155/2023/9843601

Retraction

Retracted: Novel Concepts in Bipolar Fuzzy Graphs with Applications

Journal of Mathematics

Received 25 November 2022; Accepted 25 November 2022; Published 11 January 2023

Journal of Mathematics has retracted the article titled "Novel Concepts in Bipolar Fuzzy Graphs with Applications" [1] due to concerns that the peer review process has been compromised.

Following an investigation conducted by the Hindawi Research Integrity team [2], significant concerns were identified with the peer reviewers assigned to this article; the investigation has concluded that the peer review process was compromised. We therefore can no longer trust the peer review process, and the article is being retracted with the agreement of the Chief Editor.

The authors do not agree to the retraction.

References

[1] C. Wan, F. Deng, S. Li, S. Omidbakhsh Amiri, A. A. Talebi, and H. Rashmanlou, "Novel Concepts in Bipolar Fuzzy Graphs with Applications," *Journal of Mathematics*, vol. 2022, Article ID 8162474, 9 pages, 2022.

[2] L. Ferguson, "Advancing Research Integrity Collaboratively and with Vigour," 2022, https://www.hindawi.com/post/advancing-research-integrity-collaboratively-and-vigour/.

Hindawi
Journal of Mathematics
Volume 2022, Article ID 8162474, 9 pages
https://doi.org/10.1155/2022/8162474

Research Article

Novel Concepts in Bipolar Fuzzy Graphs with Applications

Chang Wan,[1] Fei Deng,[2] Shitao Li,[3] S. Omidbakhsh Amiri,[4] A. A. Talebi,[4] and H. Rashmanlou[4]

[1]*Guangdong Polytechnic of Science and Technology, Guangzhou 510640, China*
[2]*College of Information Science and Technology, Chengdu University of Technology, Chengdu 610059, China*
[3]*Shenzhen Tourism College of Jinan University, Shenzhen 518053, China*
[4]*Department of Mathematics University of Mazandaran, Babolsar, Iran*

Correspondence should be addressed to Shitao Li; li_st@sz.jnu.edu.cn

Received 22 February 2022; Revised 25 March 2022; Accepted 31 March 2022; Published 9 May 2022

Academic Editor: Lazim Abdullah

Many problems of practical interest can be modeled and solved by using bipolar graph algorithms. Bipolar fuzzy graph (BFG), belonging to fuzzy graphs (FGs) family, has good capabilities when facing with problems that cannot be expressed by FGs. Hence, in this paper, we introduce the notion of (ϑ, δ)–homomorphism of BFGs and classify homomorphisms (HMs), weak isomorphisms (WIs), and co-weak isomorphisms (CWIs) of BFGs by (ϑ, δ)–HMs. Also, an application of homomorphism of BFGs has been presented by using coloring-FG. Universities are very important organizations whose existence is directly related to the general health of the society. Since the management in each department of the university is very important, therefore, we have tried to determine the most effective person in a university based on the performance of its staff.

1. Introduction

Graphs from ancient times to the present day have played a very important role in various fields, including computer science and social networks, so that with the help of the vertices and edges of a graph, the relationships between objects and elements in a social group can be easily introduced. However, there are some phenomena around our lives that have a wide range of complexities that make it impossible for us to express certainty. These complexities and ambiguities were reduced with the introduction of FSs by Zadeh [1]. The FS focuses on the membership degree of an object in a particular set. However, membership alone could not solve the complexities in different cases, so the need for a degree of membership was felt. To solve this problem, Zhang [2] defined the concept of bipolar fuzzy sets (BFSs) as a generalization of fuzzy sets (FSs). BFSs are an extension of FSs whose membership degree range is $[-1, 1]$. The first definition of FGs was proposed by Kafmann [3] in 1993, from Zade's fuzzy relations [4, 5]. However, Rosenfeld [6] introduced another elaborated definition including fuzzy vertex and fuzzy edges and several fuzzy analogs of graph theoretic concepts such as paths, cycles, connectedness, and so on. Akram et al. [7, 8] introduced BFGs and cayley-BFGs. Rashmanlou et al. [9] investigated categorical properties in intuitionistic fuzzy graphs. Bhattacharya [10] gave some remarks on FGs, and some operations of FGs were introduced by Mordeson and Peng [11]. The concept of weak isomorphism, co-weak isomorphism, and isomorphism between FGs was introduced by Bhutani in [12]. Liu [13] defined domination number in maximal outer planar graphs. Borzooei [14] introduced domination in vague graphs. Ghorai and Pal [15] studied some isomorphic properties of m-polar FGs. Krishna et al. [16] presented new concept in cubic graph. Shao et al. [17] investigated strong equality of roman and perfect roman domination in trees. Mordeson and Nair [18] introduced the concept of complement of fuzzy graph and studied some operations on fuzzy graphs. The complement of FGs was studied by Sunitha and Vijayakumar [19]. Nagoorgani and Malarvizhi [20] investigated isomorphism properties on FGs. Ezhilmaran et al. [21] studied morphism of bipolar intuitionistic

fuzzy graphs. Muhiuddin et al. [22, 23] introduced new concepts of cubic graphs. Rao et al. [24–26] presented dominating set, equitable dominating set, and isolated vertex of vague graphs. Telebi and Rashmanlou [27] described complement and isomorphism on bipolar fuzzy graphs. Shi et al. [28, 29] introduced total dominating set and global dominating set in product vague graphs. Kosari et al. [30] defined vague graph structure with an application in medical sciences. Kou et al. [31] investigated g-eccentric node and vague detour g-boundary nodes in vague graphs. Ramprasad et al. [32] introduced morphism of m-Polar fuzzy graph. Tahmasbpour et al. [33] presented f-morphism on bipolar fuzzy graphs.

A BFG is a generalized structure of an FG that provides more exactness, adaptability, and compatibility to a system when matched with systems run on FGs. Also, a BFG is able to concentrate on determining the uncertainty coupled with the inconsistent and indeterminate information of any real-world problems, where FGs may not lead to adequate results. With the help of BFGs, the most efficient person in an organization can be identified according to the important factors that can be useful for an institution. Homomorphisms provide a way of simplifying the structure of objects one wishes to study while preserving much of it that is of significance. It is not surprising that homomorphisms also appeared in graph theory, and that they have proven useful in many areas. Hence, in this paper, we defined the notion of (ϑ, δ)−homomorphism of BFGs and classify homomorphisms (HMs), weak isomorphisms (WIs), and co-weak isomorphisms (CWIs) of BFGs by (ϑ, δ)−HMs. Finally, we introduced the application of homomorphism of BFGs by using coloring-FG, and an application of bipolar fuzzy influence digraph has also been presented.

2. Preliminaries

In this section, we give some necessary concepts of bipolar fuzzy graphs and bipolar fuzzy subgroups.

Definition 1. Let V be a finite nonempty set. A graph $G = (V, E)$ on V consists of a vertex set V and an edge set E, where an edge is an unordered pair of distinct vertices of G. We will use xy rather than $\{x, y\}$ to denote an edge. If xy is an edge, then we say that x and y are adjacent. A graph is called complete if every pair of vertices is adjacent.

Definition 2. Let $G_1 = (V_1, E_1)$ and $G_2 = (V_2, E_2)$ be graphs. A mapping $g: V_1 \longrightarrow V_2$ is a homomorphism from G_1 to G_2 if $g(r)$ and $g(s)$ are neighbor whenever r and s are neighbor.

Definition 3. Two graphs $G_1 = (V_1, E_1)$ and $G_2 = (V_2, E_2)$ are isomorphic if $\exists$ a bijective mapping $\psi: V_1 \longrightarrow V_2$ so that r and s are neighbor in G_1 if and only if $\psi(r)$ and $\psi(s)$ are neighbor in G_2, ψ is named isomorphism from G_1 to G_2. An isomorphism from a graph G to itself is named an automorphism of G. The set of all automorphisms of G forms a group, which is called the automorphism group of G and denoted by $\mathrm{Aut}(G)$.

Definition 4 (see [2]). Let V be a nonempty set. A BFS B in V is an object having the form as follows:

$$B = \left\{\langle r, \mu_B^P(r), \mu_B^N(r)\rangle | r \in V\right\}, \tag{1}$$

where $\mu_B^P: V \longrightarrow [0, 1]$ and $\mu_B^N: V \longrightarrow [-1, 0]$ are mappings.

For the sake of simplicity, we shall use the symbol $B = (\mu_B^P, \mu_B^N)$ for the BFS.

$$B = \left\{\langle r, \mu_B^P(r), \mu_B^N(r)\rangle | r \in V\right\}. \tag{2}$$

The family of all BFSs on V is written as $BFS[V]$.

Definition 5. Let $P_* = \{(p, q): q \in [-1, 0], p \in [0, 1]\}$. For any $(q_1, p_1), (q_2, p_2) \in P_*$, the orders $\leq$ and $<$ on P_* are defined as

$$\begin{aligned}&(q_1, p_1) \leq (q_2, p_2) \Leftrightarrow q_1 \geq q_2 \text{ and } p_1 \leq p_2,\\ &(q_1, p_1) < (q_2, p_2) \Leftrightarrow (q_1, p_1) \leq (q_2, p_2) \text{ and } q_1 > q_2 \text{ or } p_1 < p_2.\end{aligned} \tag{3}$$

By Definition 5, it is easy to see that $(P_*, \leq)$ constitutes a complete lattice with minimum element $(0, 0)$ and maximum element $(1, -1)$.

Definition 6. Let $B = (\mu_B^P, \mu_B^N)$ be a BFS. For each $(p, q) \in P_*$, we describe

$$B_{(p,q)} = \left\{r \in V: \mu_B^P(r) \geq p, \mu_B^N(r) \leq q\right\}. \tag{4}$$

Then, $B_{(p,q)}$ is named (q, p)-level set. The set $\{r | r \in V, \mu_A^P(r) \neq 0, \mu_A^N(r) \neq 0\}$ is named the support A and is shown by A^*.

Let V be a finite nonempty set. Denote by $\widetilde{V}^2$ the set of all 2-element subsets of V. A graph on V is a pair (V, E) where $E \subseteq \widetilde{V}^2$, V and E are called vertex set and edge set, respectively.

Definition 7. Let V be a finite nonempty set, $A \in \mathrm{BFS}[V]$, and $B \in \mathrm{BFS}[\widetilde{V}^2]$. The triple $X = (V, A, B)$ is named a BFG on V, if for each $(r, s) \in \widetilde{V}^2$,

$$\mu_B^P(r, s) \leq \mu_A^P(r) \wedge \mu_A^P(s) \text{ and } \mu_B^N(r, s) \geq \mu_A^N(r) \vee \mu_A^N(s). \tag{5}$$

Definition 8. A BFG $X = (V, A, B)$ is called a strong bipolar fuzzy graph (SBFG) if for each $(r, s) \in \widetilde{V}^2$,

$$\mu_B^P(r, s) = \mu_A^P(r) \wedge \mu_A^P(s), \mu_B^N(r, s) = \mu_A^N(r) \vee \mu_A^N(s), \tag{6}$$

that $(\mu_B^P(r, s), \mu_B^N(r, s)) \neq (0, 0)$ and is called complete bipolar fuzzy graph (CBFG), if for each $(r, s) \in \widetilde{V}^2$, we have

$$\mu_B^P(r, s) = \mu_A^P(r) \wedge \mu_A^P(s) \text{ and } \mu_B^N(r, s) = \mu_A^N(r) \vee \mu_A^N(s). \tag{7}$$

A complete bipolar fuzzy graph $X = (V, A, B)$ with n nodes is shown by $K_{n,A}$.

If $X = (V, A, B)$ is a BFG, then it is easy to see that $X^* = (A^*, B^*)$ is a graph and it is called underlying graph of X.

The set of all BFG on V is denoted by $\mathrm{BFG}[V]$. For given $X = (V, A, B) \in \mathrm{BFG}[V]$, in this study, suppose that $A^* = V$.

Definition 9. Let $X_1 = (V_1, A_1, B_1)$ and $X_2 = (V_2, A_2, B_2)$ be two BFGs. Then,

(1) A mapping $\psi: V_1 \longrightarrow V_2$ is a homomorphism from X_1 to X_2 if

(i) $\mu^P_{A_1}(r) \leq \mu_A$
$^P_2(\psi(r)), \mu^N_{A_1}(r) \geq \mu^N_{A_2}(\psi(r)),$ for all $r \in V_1$
(ii) $\mu^P_{B_1}(rs) \leq \mu^P_{B_2}$ $(\psi(r)\psi(s)), \mu^N_{B_1}(rs)$
$\geq \mu^N_{B_2}(\psi(r)\psi(s)),$ for all $rs \in \widetilde{V}^2$

(2) A mapping $\psi: V_1 \longrightarrow V_2$ is a weak isomorphism from X_1 to X_2 if ψ is a bijective homomorphism from X_1 to X_2 and

$$\mu^P_{A_1}(r) = \mu^P_{A_2}(\psi(r)), \mu^N_{A_1}(r) = \mu^N_{A_2}(\psi(r)), \text{for all } r \in V_1. \tag{8}$$

(3) A mapping $\psi: V_1 \longrightarrow V_2$ is a co-weak isomorphism from X_1 to X_2 if ψ is a bijective homomorphism from X_1 to X_2 and

$$\mu^P_{B_1}(rs) = \mu^P_{B_2}(\psi(r)\psi(s)), \mu^N_{B_1}(rs) = \mu^N_{B_2}(\psi(r)\psi(s)), \text{for all } rs \in \widetilde{V}^2. \tag{9}$$

(4) An isomorphism from X_1 to X_2 is a bijective mapping $\psi: V_1 \longrightarrow V_2$ so that

(i) $\mu^P_{A_1}(r) = \mu^P_{A_2}(\psi(r)), \mu^N_{A_1}(r) =$
$\mu^N_{A_2}(\psi(r)),$ for all $r \in V_1$
(ii) $\mu^P_{B_1}(rs) = \mu^P_{B_2}(\psi(r)\psi(s)), \mu^N_{B_1}(rs) =$
$\mu^N_{B_2}(\psi(r)\psi(s)),$ for all $rs \in \widetilde{V}^2$

Definition 10. Suppose that $X = (V, A, B)$ and $Y = (V, A', B')$ be two BFGs. Then, X is a BFSG of Y if $A \subseteq A'$ and $B \subseteq B'$.

Definition 11. Let $X = (V, A, B)$ be a BFG and $W \subseteq V$. Then, the BFG $Y = (W, A', B')$ so that

$$\begin{aligned} &\mu^P_{A'}(r) = \mu^P_A(r), \mu^N_{A'}(r) = \mu^N_A(r), \text{for all } r \in W, \\ &\mu^P_{B'}(rs) = \mu^P_B(rs), \mu^N_{B'}(rs) = \mu^N_B(rs), \text{for all } rs \in \widetilde{W}^2, \end{aligned} \tag{10}$$

is called the induced BFSG by W and shown by $X[W]$.

Definition 12. A family $\Gamma = \{\mu_1, \mu_2, \ldots, \mu_k\}$ of BFSs on V is named a k-coloring of BFG $X = (V, A, B)$ if

(i) $\vee\Gamma = A$.
(ii) $\mu_i \wedge \mu_j = 0$, for $1 \leq i, j \leq k$.
(iii) For each strong edge rs of X, $\min\{\mu_i(r), \mu_i(s)\} = 0$, for $1 \leq i \leq k$. We say that a graph is k-colorable if it can be colored with k colors.

All the basic notations are shown in Table 1.

3. Homomorphisms and Isomorphisms of Bipolar Fuzzy Graphs

In this section, we discuss homomorphisms and isomorphisms of bipolar fuzzy graphs by homomorphism of level graphs in bipolar fuzzy graphs.

Theorem 1. *Let V be a finite nonempty set, $A \in BFS(V)$ and $B \in BFS(\widetilde{V}^2)$. Then, $X = (V, A, B) \in BFG(V)$ if and only if $X_{(\vartheta,\delta)} = (A_{(\vartheta,\delta)}, B_{(\vartheta,\delta)})$ is a graph, for all $(\vartheta, \delta) \in P_*$, $A_{(\vartheta,\delta)} \neq \varnothing$.*

Proof. Let $X = (V, A, B)$ be a BFG. For each $(\vartheta, \delta) \in P_*$, $A_{(\vartheta,\delta)} \neq \varnothing$, suppose that $rs \in B_{(\vartheta,\delta)}$. Then, $\mu^P_B(rs) \geq \vartheta$ and $\mu^N_B(rs) \leq \delta$. Because X is a BFG,

$$\vartheta \leq \mu^P_B(rs) \leq \mu^P_A(r) \wedge \mu^P_A(s) \text{ and } \delta \geq \mu^N_B(rs) \geq \mu^N_A(r) \vee \mu^N_A(s). \tag{11}$$

It follows that $r, s \in A_{(\vartheta,\delta)}$. Therefore, $(A_{(\vartheta,\delta)}, B_{(\vartheta,\delta)})$ is a graph.

Conversely, let $X_{(\vartheta,\delta)} = (A_{(\vartheta,\delta)}, B_{(\vartheta,\delta)})$ is a graph, for all $(\vartheta, \delta) \in P_*$, $A_{(\vartheta,\delta)} \neq \varnothing$. For each $rs \in \widetilde{V}^2$, let $\mu^P_B(rs) = \vartheta, \mu^N_B(rs) = \delta$. Then, $rs \in B_{(\vartheta,\delta)}$. Hence, $r, s \in A_{(\vartheta,\delta)}$. Thus, $\mu^P_A(r) \geq \vartheta, \mu^P_A(s) \geq \vartheta, \mu^N_A(r) \leq \delta,$ and $\mu^N_A(s) \leq \delta$. This implies that $\mu^P_A(r) \wedge \mu^P_A(s) \geq \vartheta = \mu^P_B(rs)$ and $\mu^N_A(r) \vee \mu^N_A(s) \leq \delta = \mu^N_B(rs)$. Therefore, $X = (V, A, B)$ is a BFG. □

Definition 13. Let $X = (V, A, B)$ and $Y = (W, A\imath, B\imath)$ be two BFGs, $g: V \longrightarrow W$ a mapping. Then, for any $(\vartheta, \delta) \in P_*$, $A_{(\vartheta,\delta)} \neq \varnothing$, if g is a homomorphism from $X_{(\vartheta,\delta)} = (A_{(\vartheta,\delta)}, B_{(\vartheta,\delta)})$ to $Y_{(\vartheta,\delta)} = (A_{(\vartheta,\delta)'}, B_{(\vartheta,\delta)'})$, g is named (ϑ, δ)–homomorphism mapping from X to Y.

Theorem 2. *Let $X = (V, A, B)$ and $Y = (W, A', B')$ be two BFGs. Then, $g: X \longrightarrow Y$ is a homomorphism from X to Y if and only if g is (ϑ, δ)–homomorphism from X to Y.*

Proof. Assume that $g: X \longrightarrow Y$ is a homomorphism from X to Y. Let $A_{(\vartheta,\delta)} \neq \varnothing$, $(\vartheta, \delta) \in P_*$. If $r \in A_{(\vartheta,\delta)}$, then

$$\mu^P_{A'}(g(r)) \geq \mu^P_A(r) \geq \vartheta, \mu^N_{A'}(g(r)) \leq \mu^N_A(r) \leq \delta. \tag{12}$$

Hence, $g(r) \in A_{(\vartheta,\delta)'}$ implying g is a mapping from $A_{(\vartheta,\delta)}$ to $A_{(\vartheta,\delta)'}$. For $r, s \in A_{(\vartheta,\delta)}$, let $rs \in B_{(\vartheta,\delta)}$. Then,

$$\begin{aligned} \mu^P_B(rs) &\geq \vartheta, \\ \mu^N_B(rs) &\leq \delta. \end{aligned} \tag{13}$$

Hence,

$$\mu^P_{B'}(g(r)g(s)) \geq \mu^P_B(rs) \geq \vartheta, \mu^N_{B'}(g(r)g(s)) \leq \mu^N_B(rs) \leq \delta, \tag{14}$$

which implies $g(r)g(s) \in B_{(\vartheta,\delta)'}$. Therefore, g is a homomorphism from $X_{(\vartheta,\delta)}$ to $Y_{(\vartheta,\delta)}$.

Table 1: Some basic notations.

Notation	Meaning
FG	Fuzzy graph
BFS	Bipolar fuzzy set
FS	Fuzzy set
BFG	Bipolar fuzzy graph
CBFG	Complete bipolar fuzzy graph
SBFG	Strong bipolar fuzzy graph
BM	Bijective mapping
HM	Homomorphism
WI	Weak isomorphism
CWI	Co-weak isomorphism
BH	Bijective homomorphism
SG	Subgraph
CG	Complete graph
BFSG	Bipolar fuzzy subgraph

Conversely, let $g: V \longrightarrow W$ be a (ϑ, δ)–homomorphism from X to Y. For arbitrary element $r \in X$, let $\mu_A^P(r) = c$, $\mu_A^N(r) = \mathrm{d}$. Then, $r \in A_{(c,d)}$. Hence, $g(r) \in A_{(c,d)}{}'$ because g is a homomorphism from $(A_{(c,d)}, B_{(c,d)})$ to $(A_{(c,d)}{}', B_{(c,d)}{}')$. It follows that

$$\mu_{A'}^P(g(r)) \geq c, \mu_{A'}^N(g(r)) \leq d, \tag{15}$$

that is,

$$\mu_{A'}^P(g(r)) \geq \mu_A^P(r), \mu_{A'}^N(g(r)) \leq \mu_A^N(r). \tag{16}$$

Now, for arbitraries $r, s \in V$, let $\mu_B^P(rs) = e$, $\mu_B^N(rs) = f$. Then,

$$\begin{aligned} e = \mu_B^P(rs) &\leq \mu_A^P(r) \wedge \mu_A^P(s), \\ f = \mu_B^N(rs) &\geq \mu_A^N(r) \vee \mu_A^N(s). \end{aligned} \tag{17}$$

Hence, $r, s \in A_{(e,f)}$ and $rs \in B_{(e,f)}$. Because g is a homomorphism from $X_{(e,f)} = (A_{(e,f)}, B_{(e,f)})$ to $Y_{(e,f)} = (A_{(e,f)}{}', B_{(e,f)}{}')$, we conclude that $g(r), g(s) \in A_{(e,f)}{}'$ and $g(r)g(s) \in B_{(e,f)}{}'$. Therefore,

$$\mu_{B'}^P(g(r)g(s)) \geq e = \mu_B^P(rs), \mu_{B'}^N(g(r)g(s)) \leq f = \mu_B^N(rs). \tag{18}$$

□

Theorem 3. *Let $X = (V, A, B)$ and $Y = (W, A', B')$ be two BFGs. Then, $g: V \longrightarrow W$ is a WI from X to Y if and only if g is a bijective (ϑ, δ)–homomorphism from X to Y and*

$$\mu_A^P(r) = \mu_{A'}^P(g(r)), \mu_A^N(r) = \mu_{A'}^N(g(r)) \text{ for all } r \in V. \tag{19}$$

Proof. Let f be a WI from X to Y. From the definition of homomorphism, g is a bijective homomorphism from X to Y. By Theorem 2, f is a bijective (ϑ, δ)–homomorphism from X to Y, and also by the definition of WI, we have

$$\mu_A^P(r) = \mu_{A'}^P(g(r)), \mu_A^N(r) = \mu_{A'}^N(g(r)) \text{ for all } r \in V. \tag{20}$$

Conversely, from hypothesis, $g: A_{(0,1)} = V \longrightarrow A_{(0,1)}{}' = W$ is a bijective mapping and

$$\mu_A^P(r) = \mu_{A'}^P(g(r)), \mu_A^N(r) = \mu_{A'}^N(g(r)) \text{ for all } r \in V. \tag{21}$$

For $r, s \in V$, let $\mu_B^P(rs) = e$, $\mu_B^N(rs) = f$. Then,

$$e = \mu_B^P(rs) \leq \mu_A^P(r) \wedge \mu_A^P(s), f = \mu_B^N(rs) \geq \mu_A^N(r) \vee \mu_A^N(s), \tag{22}$$

which implies $r, s \in A_{(e,f)}$ and $rs \in B_{(e,f)}$. Because g is a homomorphism from $(A_{(e,f)}, B_{(e,f)})$ to $(A_{(e,f)}{}', B_{(e,f)}{}')$, we have $g(r), g(s) \in A_{(e,f)}{}'$ and $g(r)g(s) \in B_{(e,f)}{}'$. Hence,

$$\mu_{B'}^P(g(r)g(s)) \geq e = \mu_B^P(rs), \mu_{B'}^N(g(r)g(s)) \leq f = \mu_B^N(rs), \tag{23}$$

which completes the proof. □

Theorem 4. *Let $X = (V, A, B)$ and $Y = (W, A', B')$ be two BFGs. Then, $g: V \longrightarrow W$ is a co-weak isomorphism from X to Y if and only if g is a bijective (ϑ, δ)–homomorphism from X to Y and*

$$\mu_B^P(rs) = \mu_{B'}^P(g(r)g(s)), \mu_B^N(rs) = \mu_{B'}^N(g(r)g(s)) \text{for all } rs \in \tilde{V}^2. \tag{24}$$

Proof. Let $g: V \longrightarrow W$ be a co-weak isomorphism from X to Y. Then, g is a bijective homomorphism from X to Y. By Theorem 2, f is a bijective (ϑ, δ)–homomorphism from X to Y. Also, by the definition of co-weak isomorphism,

$$\mu_B^P(rs) = \mu_{B'}^P(g(r)g(s)), \mu_B^N(rs) = \mu_{B'}^N(g(r)g(s)) \text{for all } rs \in \tilde{V}^2. \tag{25}$$

Conversely, from hypothesis, we know that $f: A_{(0,1)} = V \longrightarrow A_{(0,1)}{}' = W$ is a bijective mapping and

$$\mu_B^P(rs) = \mu_{B'}^P(g(r)g(s)), \mu_B^N(rs) = \mu_{B'}^N(g(r)g(s)). \tag{26}$$

For arbitrary element $r \in V$, suppose that $\mu_A^P(r) = c$, $\mu_A^N(r) = d$. Then, we have $r \in A_{(c,d)}$. Now, because g is a homomorphism from $(A_{(c,d)}, B_{(c,d)})$ to $(A'_{(c,d)}, B'_{(c,d)})$, $g(r) \in A'_{(c,db)}$. Thus, $\mu_{A'}^P(g(r)) \geq c = \mu_A^P(r)$ and $\mu_{A'}^N(g(r)) \leq d = \mu_A^N(r)$, which implies g is a co-weak isomorphism from X to Y. □

Corollary 1. *Let $X = (V, A, B) \in BFG(V)$, $Y = (W, A', B') \in BFG(W)$. If $g: V \longrightarrow W$ is a co-weak*

isomorphism from X to Y, then g is an injective homomorphism from $X_{(\vartheta,\delta)}$ to $Y_{(\vartheta,\delta)}$, for all $(\vartheta,\delta) \in P_*$, $A_{(\vartheta,\delta)} \neq \varnothing$.

From the following example, we conclude that the converse of Corollary 1 does not need to be true.

Example 1. Let $X = (V, A, B)$ and $Y = (W, A', B')$ be two BFGs as shown in Figure 1. Consider the mapping $g: V \longrightarrow W$, defined by $g(v_i) = w_i$, $1 \le i \le 4$. In view of the (ϑ,δ)–level graphs of X and Y in Figure 1, it is easy to see that if $A_{(\vartheta,\delta)} \neq \varnothing$, then g is an injective homomorphism from $X_{(\vartheta,\delta)}$ to $Y_{(\vartheta,\delta)}$, but g is not a co-weak isomorphism.

Theorem 5. *Let $X = (V, A, B) \in BFG(V)$, $Y = (W, A', B') \in BFG(W)$, and $g: V \longrightarrow W$ be a mapping. For each $(\vartheta,\delta) \in P_*$, $A_{(\vartheta,\delta)} \neq \varnothing$, if g is an isomorphism from $X_{(\vartheta,\delta)}$ to a subgraph of $Y_{(\vartheta,\delta)}$, then g is a co-weak isomorphism from X to an induced BFSG of Y.*

Proof. The mapping g is an isomorphism from $X_{(0,1)} = (V, B_{(0,1)})$ to a subgraph $Y_{(0,1)} = (W, B'_{(0,1)})$. So, $g: V \longrightarrow W$ is an injective mapping. For arbitrary $r \in V$, suppose that $\mu_A^P(r) = \vartheta$, $\mu_A^N(r) = \delta$. Then, $r \in A_{(\vartheta,\delta)}$, and so $g(r) \in A'_{(\vartheta,\delta)}$. Hence, $\mu_{A'}^P(g(r)) \ge \vartheta = \mu_A^P(r)$ and $\mu_{A'}^N(g(r)) \le \delta = \mu_A^N(r)$. For $r, s \in V$, let $\mu_B^P(rs) = \vartheta$ and $\mu_B^N(rs) = \delta$. Then, $\vartheta \le \mu_A^P(r)$, $\vartheta \le \mu_A^P(s)$, $\delta \ge \mu_A^N(r)$, $\delta \ge \mu_A^N(s)$, and $rs \in B_{(\vartheta,\delta)}$. Hence, $r, s \in A_{(\vartheta,\delta)}$ and $rs \in B_{(\vartheta,\delta)}$. Since g isomorphism from $X_{(\vartheta,\delta)}$ to $Y_{(\vartheta,\delta)}$, we get $g(r), g(s) \in A'_{(\vartheta,\delta)}$ and $g(r), g(s) \in B'_{(\vartheta,\delta)}$. Therefore,

$$\mu_{B'}^P(g(r)g(s)) \ge \vartheta = \mu_B^P(rs), \mu_{B'}^N(g(r)g(s)) \le \delta = \mu_B^N(rs). (I). \tag{27}$$

Now, let $\mu_{B'}^P(g(r)g(s)) = t$, $\mu_{B'}^N(g(r)g(s)) = s$. Then, $g(r)g(s) \in A_{(t,s)}$. Because g is injective and an isomorphism from $X_{(p,q)}$ to a subgraph of $Y_{(p,q)}$, we have $p, q \in A_{(p,q)}$ and $xy \in B_{(p,q)}$. Therefore,

$$\mu_B^P(s) \ge p = \mu_{B'}^P(g(r)g(s)), \mu_B^N(rs) \le q = \mu_{B'}^N(g(r)g(s)). (II). \tag{28}$$

Now, by (I) and (II), we conclude that

$$\mu_{B'}^P(g(r)g(s)) = \mu_B^P(rs), \mu_{B'}^N(g(r)g(s)) = \mu_B^N(rs). \tag{29}$$

□

Corollary 2. *Let $X = (V, A, B)$ and $Y = (W, A', B')$ be two BFGs with $|V| = |W|$, and $g: V \longrightarrow W$ a mapping. For $(\vartheta,\delta) \in P_*$, $A_{(\vartheta,\delta)} \neq \varnothing$, if g is an isomorphism from $X_{(\vartheta,\delta)}$ to a subgraph of $Y_{(\vartheta,\delta)}$, then g is a co-weak isomorphism from X to Y.*

Theorem 6. *Let $X = (V, A, B)$ and $Y = (W, A', B')$ be two BFGs, $f: V \longrightarrow W$ be a bijective mapping. If for each $(\vartheta,\delta) \in P_*$, g is an isomorphism from $X_{(\vartheta,\delta)}$ to $Y_{(\vartheta,\delta)}$ and then g is an isomorphism from X to Y.*

Proof. From hypothesis, $g^{-1}: W \longrightarrow V$ is a bijective mapping and an isomorphism from $Y_{(\vartheta,\delta)}$ to $X_{(\vartheta,\delta)}$. By Theorem 5, g is a co-weak isomorphism from X to Y and g^{-1} is a co-weak isomorphism from Y to X. Therefore, g is an isomorphism from X to Y. □

Corollary 3. *Let $X = (V, A, B)$ be a BFG and $g: V \longrightarrow V$ a bijective mapping. Then, g is an automorphism of X if and only if $f_{|A_{(\vartheta,\delta)}}$ is an automorphism of $X_{(\vartheta,\delta)}$, from an $(\vartheta,\delta) \in P_*$, $A_{(\vartheta,\delta)} \neq \varnothing$.*

Theorem 7. *Let $X = (V, A, B)$ be a BFG. Then, X is a complete bipolar fuzzy graph if and only if $X_{(\vartheta,\delta)} = (A_{(\vartheta,\delta)}, B_{(\vartheta,\delta)})$ is a complete graph (CG) for $(\vartheta,\delta) \in P_*$.*

Proof. Proof. If $X = (V, A, B)$ is a complete bipolar fuzzy graph and for $(\vartheta,\delta) \in P_*$, $A_{(\vartheta,\delta)} \neq \varnothing$, $r, s \in A_{(\vartheta,\delta)}$, then $\mu_A^P(r) \ge \vartheta$, $\mu_A^P(s) \ge \vartheta$, $\mu_A^N(r) \le \delta$, $\mu_A^N(s) \le \delta$, and so

$$\mu_B^P(rs) = \mu_A^P(r) \wedge \mu_A^P(s) \ge \vartheta, \mu_B^N(rs) = \mu_A^N(r) \vee \mu_A^N(s) \le \delta. \tag{30}$$

Hence, $rs \in B_{(\vartheta,\delta)}$. It follows that $X_{(\vartheta,\delta)}$ is a CG.

Conversely, suppose that $X = (V, A, B)$ is not a complete bipolar fuzzy graph. Then, there are $r, s \in V$ so that $\mu_B^P(rs) < \mu_A^P(r) \wedge \mu_A^P(s)$ or $\mu_B^P(rs) < \mu_A^P(r) \vee \mu_A^P(s)$. Let $\mu_B^P(rs) < \mu_A^P(r) \wedge \mu_A^P(s)$ and $\mu_A^P(r) \wedge \mu_A^P(s) = \vartheta$, for $\vartheta \in (0, 1]$. Then, $\mu_A^P(r) \ge \vartheta$ and $\mu_A^P(s) \ge \vartheta$. Hence, $r, s \in A_{(\vartheta,\delta)}$, for a $\delta \in [0, 1]$, but $rs \notin B_{(\vartheta,\delta)}$. This implies that $X_{(\vartheta,\delta)}$ is not a CG. For the case $\mu_B^N(rs) > \mu_A^N(r) \vee \mu_A^N(s)$, it follows similarly. □

Theorem 8. *Let $X = (V, A, B) \in BFG(V)$. Then, $X_{(\vartheta,\delta)}$ has not IV, for each $(\vartheta,\delta) \in P_*$, $A_{(\vartheta,\delta)} \neq \varnothing$ if and only if for each $r \in V$, there exists $s \in V$ so that $\mu_B^P(rs) = \mu_A^P(r)$ and $\mu_B^N(rs) = \mu_A^N(r)$.*

Proof. Suppose that for each $(\vartheta,\delta) \in P_*$, $A_{(\vartheta,\delta)} \neq \varnothing$, graph $X_{(\vartheta,\delta)}$ has not IV and there is a vertex $r \in V$ so that for each $s \in V$, $\mu_B^P(rs) < \mu_A^P(r)$ or $\mu_B^N(rs) > \mu_A^N(r)$. Let $\mu_B^P(rs) < \mu_A^P(r)$ and $\mu_A^P(r) = \vartheta$, $\mu_A^N(r) = \delta$, for $(\vartheta,\delta) \in P_*$. Then, $r \in A_{(\vartheta,\delta)}$ and for each $s \in V$, $s \neq r$, $rs \notin B_{(\vartheta,\delta)}$. Therefore, r is an IV in the graph $X_{(\vartheta,\delta)} = (A_{(\vartheta,\delta)}, B_{(\vartheta,\delta)})$, which is a contradiction.

Now, suppose that for $(\vartheta,\delta) \in P_*$, $A_{(\vartheta,\delta)} \neq \varnothing$, vertex $r \in A_{(\vartheta,\delta)}$ is an IV in $X_{(\vartheta,\delta)}$. If $s \notin A_{(\vartheta,\delta)}$, then $\mu_B^P(rs) \le \mu_A^P(s) < \vartheta \le \mu_A^P(r)$ or $\mu_B^N(rs) \ge \mu_A^N(s) > \delta \ge \mu_A^N(r)$, and if $s \in A_{(\vartheta,\delta)}$, it is trivial that $rs \notin B_{(\vartheta,\delta)}$. Hence, $\mu_B^P(rs) < \vartheta \le \mu_A^P(r)$ or $\mu_B^N(rs) > \delta \ge \mu_A^N(r)$. Therefore, for each $s \in V$, $\mu_B^P(rs) \neq \mu_A^P(r)$, $\mu_B^N(rs) \neq \mu_A^N(r)$. □

Theorem 9. *A BFG $X = (V, A, B)$ is r-colorable ⇔ there exists a homomorphism from X to $K_{r,A'}$.*

Proof. Assume that X be r-colorable with r colors labeled $\Gamma = \{\mu_1, \mu_2, \ldots, \mu_r\}$. Let $V_i = \{v \in V | \mu_i(v) \neq 0\}$. We define complete bipolar fuzzy graph $K_{r,A'}$ with vertices set $\{1, 2, \ldots, r\}$, so that the degree of positive membership vertex i is $\mu_{A'}^P(i) = \max\{\mu_A^P(v) | v \in V_i\}$ and the degree of negative membership vertex i is $\mu_{A'}^N(i) = \min\{\mu_A^N(v) | v \in V_i\}$. Now, the mapping $g: X \longrightarrow K_{r,A'}$ defined by $g(v) = i, v \in V_i$ is a graph homomorphism because for $v \in V_i$

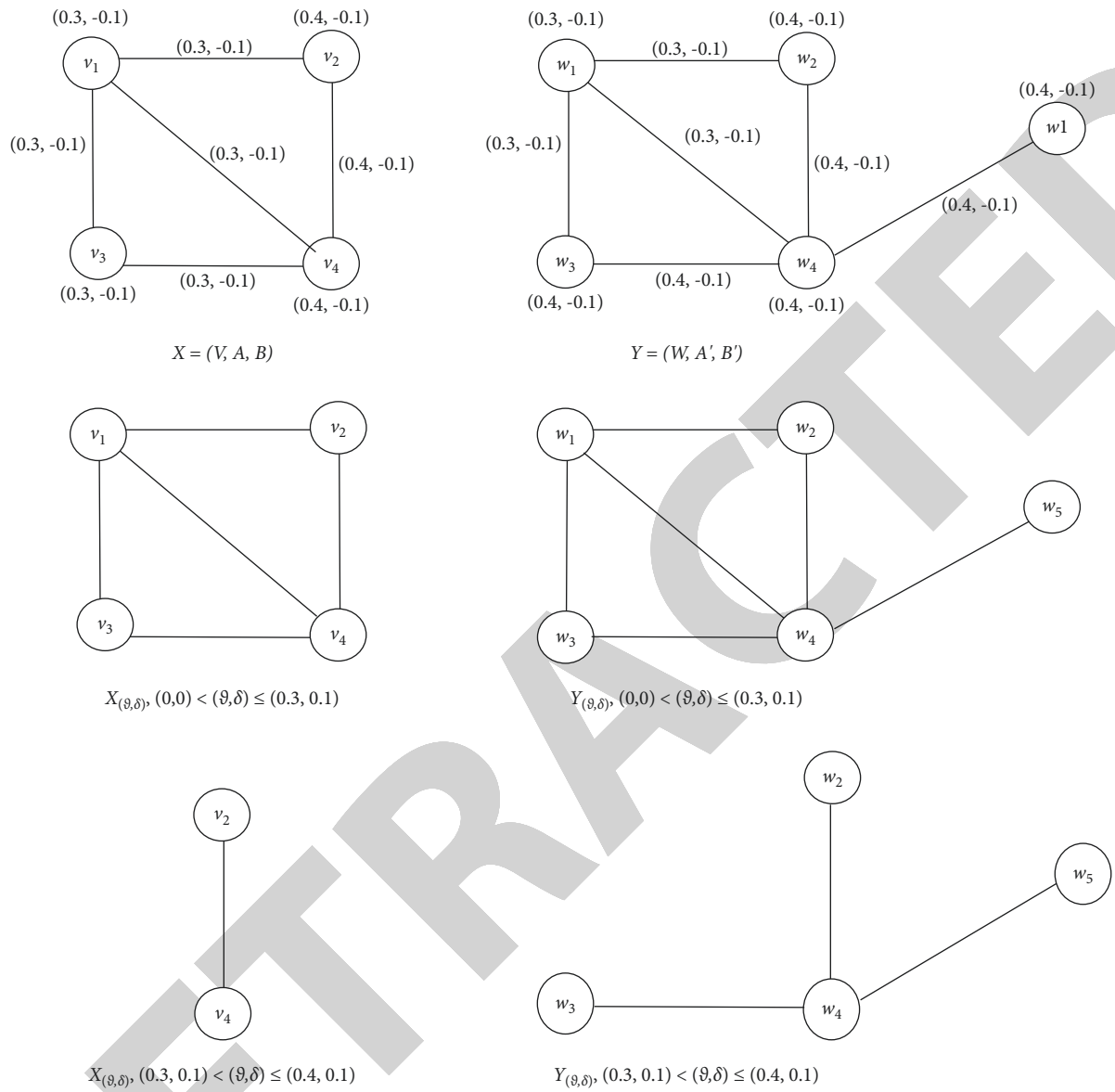

Figure 1: BFGs X, Y and the mapping g: $V_i \longrightarrow W_i$ which is not a co-weak isomorphism.

(i) $\mu_A^P(v) \leq \max\{\mu_A^P(w) | w \in V_i\} = \mu_{A'}^P(i) = \mu_{A'}^P(g(v))$,
$\mu_A^N(v) \geq \min\{\mu_A^N(w) | w \in V_i\} = \mu_{A'}^N(i) = \mu_{A'}^N(g(v))$. (31)

(ii) According to the definition of complete bipolar fuzzy graph, for $u \in V_i$ and $v \in V_j$, we have

$$\mu_B^P(uv) \leq \mu_A^P(u) \wedge \mu_A^P(v) \leq \mu_{A'}^P(i) \wedge \mu_{A'}^P(j) = \mu_{A'}^P(g(u)) \wedge \mu_{A'}^P(g(v)),$$
$$\mu_B^N(uv) \geq \mu_A^N(u) \vee \mu_A^N(v) \geq \mu_{A'}^N(i) \vee \mu_{A'}^N(j) = \mu_{A'}^N(g(u)) \vee \mu_{A'}^N(g(v)), \quad (32)$$

then $\mu_B^P(uv) \leq \mu_{B'}^P(g(u)g(v))$ and $\mu_B^N(uv) \geq \mu_{B'}^N(g(u)g((v)]$, for all $uv \in \widetilde{V}^2$.

Conversely, let g: $X \longrightarrow K_{r,A'}$ be a homomorphism. For a given $k \in V(K_{r,A'})$, define the set $g^{-1}(k) \subseteq V$ to be

$$g^{-1}(k) = \{x \in V | g(x) = k\}. \quad (33)$$

If $v \in g^{-1}(k)$, let $\mu_k(v) = (\mu_{\mu_k}^P(v), \mu_{\mu_k}(v)) = (t_A(v), f_A(v))$; otherwise, $\mu_k(v) = 0$. Therefore, the fuzzy bipolar graph X is r-colorable with coloring set $\{\mu_1, \mu_2, \ldots, \mu_r\}$. □

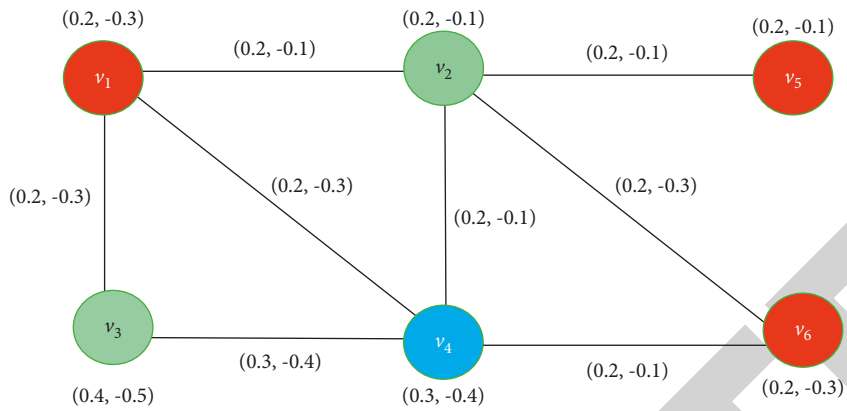

Figure 2: Bipolar fuzzy graph.$X = (V, A, B)$.

4. Application

Nowadays, the issue of coloring is very important in the theory of fuzzy graphs because it has many applications in controlling intercity traffic, coloring geographical maps, as well as finding areas with high population density. Therefore, in this section, we have tried to present an application of the coloring of vertices in a BFG.

Example 2. We obtain a BFG $X = (V, A, B)$ on the vertex set $\{v_1, v_2, v_3, v_4, v_5, v_6\}$ by joining two vertices with respect to the effect they have one another (see Figure 2). Let v_1v_2, v_1v_3, v_1v_4, v_2v_4, v_2v_6, v_2v_5, v_3v_4, and v_6v_4 be edges of graph X. The positive membership and negative membership values (μ_A^P, μ_A^N) of the vertices are the good and bad quality, respectively. Also, the positive membership and negative membership values (μ_B^P, μ_B^N) of the edges are compatible and incompatible materials, respectively. We want to see that how to put the materials in such a way that they do not have any effect on each other. Now, by Theorem 9, there is a homomorphism from X to CG with $n = 3$. Therefore, we need at least 3 parts (3-colors) to put the materials.

In the next example, we want to identify the most effective employee of a university with the help of a bipolar influence digraph.

Example 3. The emergence of science and knowledge is equal to the creation of man, and man has always sought to understand and comprehend. Science and knowledge have a special place in human life. The role of science in human life is to teach human beings the path to happiness, evolution, and construction. Science enables man to build the future the way he wants. Science is given as a tool at the will of man and makes nature as man wants and commands. Science and knowledge are two wings with which man can fly indefinitely. All the tools and instruments that we use today and cause the fundamental difference between past and present life are the result of effort and science and knowledge that man has discovered and used. Thanks to science and knowledge that many patients are saved from death, earthquake-proof buildings are built, and man can see the whole planet from above. Science and knowledge are the result of discovering hidden secrets in the heart of nature and secrets that human beings have endured many hardships to discover so that we can now easily use them. Although knowledge plays a very important role in human life and causes evolution and progress, sometimes it may also bring dangers to the human race, and this is if man uses what he has learned in the wrong way, science and knowledge need to know how to use it properly so that man is always on the right path. So, universities should hire the best teachers and staff to do the work of the students and provide the necessary conditions for their education. Therefore, in this section, we try to identify the most effective employees in a university according to their performance. Hence, we consider the vertices of the bipolar influence graph as the head of each ward of the university and the edges of the graph as the degree of interaction and influence of each other. For this university, the set of staff is B = {Alavi, Rasooli,
Tabari, Omrani, Razavi, Salehi, Taghavi}:

Table 2: Name of employees in a university and their services.

Name	Services
Alavi	Head of library
Rasooli	Head of postgraduate education
Tabari	Head of informatics department
Omrani	Head of security
Razavi	Head of university
Salehi	Head of welfare services
Taghavi	Head of research department

(a) Rasooli has been working with Omrani for 11 years and values his views on issues.

(b) Alavi has been the head of library for a long time, and not only Rasooli but also Omrani is very satisfied with Alavi's performance.

(c) In a university, preserving educational documents as well as taking care of university services is a very important task. Omrani is the most suitable person for this responsibility.

(d) Tabari and Salehi have a long history of conflict.

Table 3: The level of staff capability.

	Alavi	Rasooli	Tabari	Omrani	Razavi	Salehi	Taghavi
μ_B^P	0.4	0.9	0.6	0.7	0.8	0.9	0.5
μ_B^N	−0.4	−0.3	−0.2	−0.3	−0.2	−0.2	−0.4

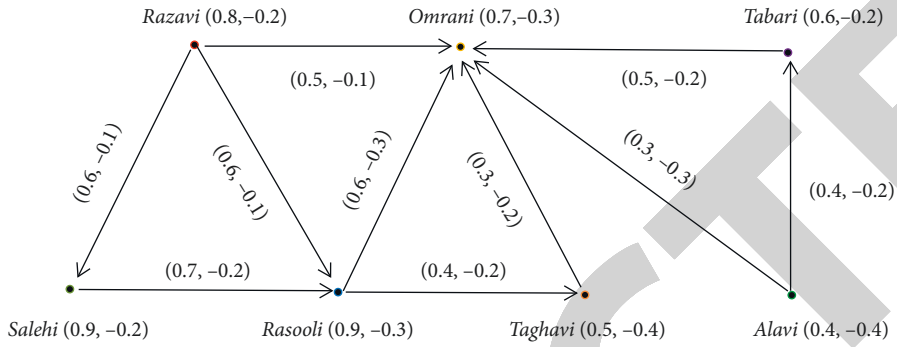

Figure 3: Bipolar influence digraph.

Table 4: Adjacency matrix corresponding to Figure 3.

	Alavi	Rasooli	Tabari	Omrani	Razavi	Salehi	Taghavi
Alavi	(0, 0)	(0, 0)	(0.4, −0.2)	(0.3, −0.3)	(0, 0)	(0, 0)	(0, 0)
Rasooli	(0, 0)	(0, 0)	(0, 0)	(0.6, −0.3)	(0, 0)	(0, 0)	(0.4, −0.2)
Tabari	(0, 0)	(0, 0)	(0, 0)	(0.5, −0.2)	(0, 0)	(0, 0)	(0, 0)
Omrani	(0, 0)	(0, 0)	(0, 0)	(0, 0)	(0, 0)	(0, 0)	(0, 0)
Razavi	(0, 0)	(0.6, −0.1)	(0, 0)	(0.5, −0.1)	(0, 0)	(0.6, −0.1)	(0, 0)
Salehi	(0, 0)	(0.7, −0.2)	(0, 0)	(0, 0)	(0, 0)	(0, 0)	(0, 0)
Taghavi	(0, 0)	(0, 0)	(0, 0)	(0.3, −0.2)	(0, 0)	(0, 0)	(0, 0)

(e) Tabari has an important role in the informatics department.

Given the above, we consider a bipolar influence graph. The vertices represent each of the university staff. Note that each staff member has the desired ability as well as shortcomings in the performance of their duties. Therefore, we use of BFS to express the weight of the vertices. The positive membership indicates the efficiency of the employee, and the negative membership shows the lack of management and shortcomings of each staff. However, the edges describe the level of relationships and friendships between employees that the positive membership shows a friendly relationship between both employees and the negative membership shows the degree of conflict between the two officials. Name of employees and level of staff capability are shown in Tables 2and 3. The adjacency matrix corresponding to Figure 3 is shown in Table 4.

Figure 3 shows that Salehi has 90% of the power needed to do the university work as the head of welfare services but does not have the 20% knowledge needed to be the boss. The directional edge Rasooli–Omrani shows that there is 60% friendship among these two employees, and unfortunately they have 30% conflict. Clearly, Razavi has dominion over both Salehi and Rasooli, and his dominance over both is 60%. It is clear that Razavi is the most influential employee of the university because he controls both the head of welfare services and head of postgraduate education, who have 90% of the power in the university.

5. Conclusion

BFGs have a wide range of applications in the field of psychological sciences as well as the identification of individuals based on oncological behaviors. With the help of BFGs, the most efficient person in an organization can be identified according to the important factors that can be useful for an institution. Hence, in this paper, we introduced the notion of (ϑ, δ)−homomorphism of BFGs and classify homomorphisms, weak isomorphisms, and co-weak isomorphisms of BFGs by (ϑ, δ)−homomorphisms. We also investigated the level graphs of BFGs to characterize some BFGs. Finally, we presented two applications of BFGs in coloring problem and also finding effective person in a university. In our future work, we will introduce new concepts of connectivity in BFGs and investigate some of their properties. Also, we will study new results of global dominating set, restrain dominating set, connected perfect

Hindawi
Journal of Mathematics
Volume 2023, Article ID 9829645, 1 page
https://doi.org/10.1155/2023/9829645

Retraction

Retracted: A Novel Multicriteria Decision-Making Approach for Einstein Weighted Average Operator under Pythagorean Fuzzy Hypersoft Environment

Journal of Mathematics

Received 10 October 2023; Accepted 10 October 2023; Published 11 October 2023

This article has been retracted by Hindawi following an investigation undertaken by the publisher [1]. This investigation has uncovered evidence of one or more of the following indicators of systematic manipulation of the publication process:

(1) Discrepancies in scope

(2) Discrepancies in the description of the research reported

(3) Discrepancies between the availability of data and the research described

(4) Inappropriate citations

(5) Incoherent, meaningless and/or irrelevant content included in the article

(6) Peer-review manipulation

The presence of these indicators undermines our confidence in the integrity of the article's content and we cannot, therefore, vouch for its reliability. Please note that this notice is intended solely to alert readers that the content of this article is unreliable. We have not investigated whether authors were aware of or involved in the systematic manipulation of the publication process.

Wiley and Hindawi regrets that the usual quality checks did not identify these issues before publication and have since put additional measures in place to safeguard research integrity.

We wish to credit our own Research Integrity and Research Publishing teams and anonymous and named external researchers and research integrity experts for contributing to this investigation.

The corresponding author, as the representative of all authors, has been given the opportunity to register their agreement or disagreement to this retraction. We have kept a record of any response received.

References

[1] P. Sunthrayuth, F. Jarad, J. Majdoubi, R. M. Zulqarnain, A. Iampan, and I. Siddique, "A Novel Multicriteria Decision-Making Approach for Einstein Weighted Average Operator under Pythagorean Fuzzy Hypersoft Environment," *Journal of Mathematics*, vol. 2022, Article ID 1951389, 24 pages, 2022.

Hindawi
Journal of Mathematics
Volume 2022, Article ID 1951389, 24 pages
https://doi.org/10.1155/2022/1951389

Research Article

A Novel Multicriteria Decision-Making Approach for Einstein Weighted Average Operator under Pythagorean Fuzzy Hypersoft Environment

Pongsakorn Sunthrayuth,[1] Fahd Jarad ,[2,3,4] Jihen Majdoubi,[5] Rana Muhammad Zulqarnain ,[6] Aiyared Iampan ,[7] and Imran Siddique[8]

[1]*Department of Mathematics and Computer Science, Faculty of Science and Technology, Rajamangala University of Technology Thanyaburi (RMUTT), Thanyaburi, Pathumthani 12110, Thailand*
[2]*Department of Mathematics, Cankaya University, Etimesgut, Ankara, Turkey*
[3]*Department of Mathematics, King Abdulaziz University, Jeddah, Saudi Arabia*
[4]*Department of Medical Research, China Medical University Hospital, China Medical University, Taichung, Taiwan*
[5]*Department of Computer Science, College of Science and Humanities at Alghat Majmaah University, Al-Majmaah 11952, Saudi Arabia*
[6]*Department of Mathematics, University of Management and Technology, Lahore, Sialkot Campus, Pakistan*
[7]*Department of Mathematics, School of Science, University of Phayao, Mae Ka, Mueang, Phayao 56000, Thailand*
[8]*Department of Mathematics, University of Management and Technology, Lahore, Pakistan*

Correspondence should be addressed to Fahd Jarad; fahd@cankaya.edu.tr

Received 12 January 2022; Revised 4 February 2022; Accepted 9 February 2022; Published 9 May 2022

Academic Editor: Lazim Abdullah

The experts used the Pythagorean fuzzy hypersoft set (PFHSS) in their research to discourse ambiguous and vague information in decision-making processes. The aggregation operator (AO) plays a prominent part in the sensitivity of the two forefront loops and eliminates anxiety from that perception. The PFHSS is the most influential and operative extension of the Pythagorean fuzzy soft set (PFSS), which handles the subparameterized values of alternatives. It is also a generalized form of Intuitionistic fuzzy hypersoft set (IFHSS) that provides better and more accurate assessments in the decision-making (DM) process. In this work, we present some operational laws for Pythagorean fuzzy hypersoft numbers (PFHSNs) and then formulate Pythagorean fuzzy hypersoft Einstein weighted average (PFHSEWA) operator based on developed operational laws. We discuss essential features such as idempotency, boundedness, and homogeneity for the proposed PFHSEWA operator. Furthermore, a DM approach has been developed based on the built-in operator to address multicriteria decision-making (MCDM) issues. A numerical case study of decision-making problems in real-life agricultural farming is considered to validate the settled technique's dominance and applicability. The consequences display that the planned model is more operative and consistent to handle inexact data based on PFHSS.

1. Introduction

In farming history, the subjugation of vegetations, wildlife, and the manufacturing and propagation methods used for high-yielding cultivation have been recorded. Farming started independently in numerous parts of the world, including a wide range of taxa. By 8000 BC, farming along the Nile was widely known. Around this time, farming developed autonomously in the Far East, most likely in China, and the main crop was rice instead of wheat. Modern agricultural practices result from an excessive water supply, extensive deforestation, and reduced soil fertility. Since there is lacking water to endure farming, it is compulsory to reexamine how to use essential water, land, and environmental resources to

raise crop vintages. Highlighting the importance of the ecosystem, considering the balances among the atmosphere and livings, and balancing the privileges and benefits of a range of manipulators may explain. The discriminations rising from these steps need to be addressed, such as the redeployment of water resources from the poor to the rich and clearing land to make room for more profitable farmland. Scientific development supports farmers with apparatuses and facilities to help them become more affluent. Maintenance farming is agricultural expertise that evades land loss due to deforestation, decreases water contamination, and rallies carbon impounding. It is a sample of scientific invention. Agriculture has not been a simple task to meet the rising mandate for nutrition and now requires more analysis and expertise. Statisticians, hydrologists, and agriculturalists met in California to progress a plan to diminish crop water ingesting while still generating profits for farmers and meeting market demand. Scientific representations use information, including plant growing features and water supplies, to regulate which yields and zones should not be planted. Farmers are gratified with the sensible use of their tools, while mathematicians work with professional specialists.

MCDM is considered the most appropriate technique for finding the most acceptable alternative from all possible options, following criteria or attributes. In real-life circumstances, most decisions are taken when the objectives and limitations are usually indefinite or ambiguous. To overcome such ambiguities and anxieties, Zadeh offered the idea of the fuzzy set (FS) [1], a prevailing tool to handle the obscurities and uncertainties in DM. Such a set allocates to all objects a membership value ranging from 0 to 1. Experts mainly consider membership and a nonmembership value in the DM process that FS cannot handle. Atanassov [2] introduced the generalization of the FS, the idea of the intuitionistic fuzzy set (IFS) to overcome the limitation mentioned above. Wang and Liu [3] presented numerous operations on IFS, such as Einstein product and Einstein sum, and constructed two aggregation operators (AOs). They also discussed some essential properties of these operators and utilized their proposed AO to resolve multiattribute decision making (MADM) for the IFS information. Atanassov [4] presented a generalized form of IFS in the light of ordinary interval values, called interval-valued intuitionistic fuzzy set (IVIFS). As a generalization of the IFS and IVIFS, Garg and Kaur [5] extended the concept of IFS and presented a novel idea of the cubic intuitionistic fuzzy set (CIFS). CIFS is a successful tool representing incomplete data by embedding IFS and IVIFS. They also discussed several desirable properties of CIFS.

The models mentioned above have been well-recognized by the specialists. Still, the existing IFS cannot handle the inappropriate and vague data because it is considered to envision the linear inequality between the membership and nonmembership grades. For example, if decision-makers choose membership and nonmembership values 0.7 and 0.6, respectively, then $0.7 + 0.6 \geq 1$. The IFS mentioned above theory cannot be applied to these data. To resolve the limitation described above, Yager [6] presented the idea of the Pythagorean fuzzy set (PFS) by amending the basic condition $a + b \leq 1$ to $a^2 + b^2 \leq 1$ and developed some results associated with score function and accuracy function. Ejegwa [7] extended the notion of PFS and presented a decision-making technique. Rahman et al. [8] formed the Einstein weighted geometric operator for PFS and presented a multiattribute group decision-making (MAGDM) methodology utilizing the proposed operator. Zhang and Xu [9] developed some basic operational laws and prolonged the technique for order preference by similarity to ideal solution (TOPSIS) method to resolve MCDM complications for PFS information. Pythagorean fuzzy power AOs along with essential characteristics were introduced by Wei and Lu [10]. They also recommended a DM technique to resolve MADM difficulties based on presented operators. Wang and Li [11] offered the interaction operational laws for PFNs and developed power Bonferroni mean operators under the PFS environment. They also discussed some definite cases of developed operators and discussed their basic characteristics. IIbahar et al. [12] offered the Pythagorean fuzzy proportional risk assessment technique to assess the professional health risk. Zhang [13] proposed a novel decision-making (DM) approach based on similarity measures to resolve multicriteria group decision-making (MCGDM) difficulties for the PFS.

Peng and Yang [14] introduced the division and subtraction operations for Pythagorean fuzzy numbers (PFNs), proved their basic properties, and presented a superiority and inferiority ranking approach under the PFS to overcome the MAGDM difficulties. Garg [15] introduced operational laws based on Einstein norms for PFNs, proposed generalized Pythagorean fuzzy Einstein average AOs, and then utilized these operators for DM. Garg [16] presented the generalized geometric AOs and established an MCDM approach based on developed operators. Garg [17] introduced logarithmic operational laws for the PFS and constructed various weighted operators based on presented logarithm operational laws. Gao et al. [18] developed numerous interaction aggregation operators under the PFS setting. Wang et al. [19] offered the interactive Hamacher operations for the PFS and settled a DM method to solve MCDM difficulties. Zulqarnain and Dayan [20] utilized the fuzzy TOPSIS to select the best alternative.

Peng and Yuan [21] explored some new inequalities of the Pythagorean fuzzy weighted average (PFWA) operator. They introduced some point operators under the PFS environment. They combined the Pythagorean fuzzy point operators with the generalized PFWA operator, developed a novel operator, and established a MADM methodology based on developed operators. Wang and Garg [22] presented the Archimedean-based interactive AOs for PFS and developed an algorithm to solve MADM problems. Rahman et al. [23] defined the interval-valued weighted AOs for interval-valued PFNs. They utilized the proposed operators to resolve the MADM issues under the interval-valued PFS. Wang and Li [24] used the interval-valued PFS, presented some novel PFS operators, and offered a DM approach to resolve the MCGDM complications. Arora and Garg [25]

presented basic operational laws and suggested several selected AOs for linguistic IFS. To examine the ranking of normal IFS and IVIFS, Garg [26] gave novel algorithms for solving the MADM problems. Ma and Xu [27] modified the existing score function and accuracy function for PFNs and defined novel Pythagorean fuzzy weighted geometric and Pythagorean fuzzy weighted averaging operators.

All the methods mentioned above have too many applications in many fields. However, due to their inefficiency, these methods have many limitations in terms of parameterization tools. Presenting the solution of this sort of obscurity and ambiguity, Molodtsov [28] introduced the basic notions of soft sets (SSs) and debated some elementary operations with their possessions. Maji et al. [29] prolonged the idea of SS. They defined several basic operations, and binary operations for Maji et al. [30] further applied the SS theory to solve the DM problems using rough mathematics. Moreover, Maji et al. [31] combined two prevailing notions, such as FS and SS, and developed the idea of FSS, which is a more robust and reliable tool. They also presented basic operations and established and applied this concept in the study by Maji et al. [32] who demonstrated the intuitionistic fuzzy soft set (IFSS) theory and offered some basic operations with their essential properties. Deli and Çağman [33] developed the intuitionistic fuzzy parameterized soft sets and DM methodology properties. Later on, Garg and Arora [34] presented Maclaurin symmetric mean operator for dual hesitant fuzzy soft numbers. Arora and Garg [35] developed the correlation coefficients and introduced an MCDM technique based on the generated correlation coefficients to measure the affiliation of two IFSS. In 2018, Garg and Arora [36] proposed generalized Maclaurin symmetric mean AOs based on Archimedean t-norm under the IFS environment. Garg and Arora [37] developed the TOPSIS concept and presented correlation measures based on previously constructed correlations. Wang and Liu [38] introduced the Maclaurin symmetric mean AOs based on Schweizer–Sklar operations for IFS and established the MAGDM technique to solve DM issues. Liu and Wang [39] presented the Bonferroni mean AOs for q-rung orthopair fuzzy sets and settled a MADM approach to solving DM complications.

Nowadays, the conception and application consequences of soft sets and the earlier-mentioned several research developments are evolving speedily. Peng et al. [40] developed the concept of PFSS by merging two existing models, PFS and SS. They also discussed some fundamental operations with their basic properties. Athira et al. [41] established entropy measures for the PFSS. They also offered Euclidean distance and hamming distance for the PFSS and utilized their methods for DM [42]. Naeem et al. [43] developed the TOPSIS and VIKOR methods for PFSS and presented an approach for the stock exchange investment problem. Zulqarnain et al. [44] introduced the AOs under the PFSS environment and presented an application for the green supplier chain management. Zulqarnain et al. [45] developed the interaction AOs for PFSS and constructed a DM technique to resolve the MCDM problems. Zulqarnain et al. [46-47] formed the Einstein weighted average and geometric AOs for PFSS. They also proposed the MAGDM techniques using their developed operators for sustainable supplier selection and a business to finance money. Siddique et al. [48] proposed a novel DM technique for PFSS using a score matrix. Zulqarnain et al. [49] introduced the TOPSIS method for PFSS based on the correlation coefficient.

Samarandche [50] proposed the idea of the hypersoft set (HSS), which penetrates multiple subattributes in the parameter function f, which is a characteristic of the Cartesian product with the n attribute. Compared with SS and other existing concepts, Samarandche HSS is the most suitable theory which handles the multiple subattributes of the considered parameters. Several HSS extensions and their decision-making methods have been proposed. Several researchers developed different hybrid structures HSS and presented several AOs with their DM techniques [51-60]. Deli [61] introduced several hybrid structures for other extensions by merging neutrosophic sets and HSS. PFHSS is a hybrid intellectual structure of PFSS. The AOs stated formerly are based on the elementary algebraic product and algebra sum, which is not the only operation that can model the intersection and union of PFHSS. Similarly, Einstein operations contain Einstein product and Einstein sum, an excellent alternate to algebraic product and algebra sum. Moreover, there appears to be some study on aggregation techniques using Einstein operations on PFHSS. Wang and Liu [62] proposed the average AOs under the IFS setting and constructed the MADM approach under their considered environment. Liu and Wang [63] developed a MADM method based on interaction Einstein AOs under the IFS setting.

An enhanced sorting approach fascinates investigators to crack baffling and inadequate information. Rendering to the investigation outcomes, PFHSS plays a vital role in DM by collecting numerous sources into a single value. According to the most generally known knowledge, the emergence of PFSS and hypersoft set (HSS) hybridization has not been combined with the PFSS background. PFHSS is a hybrid intellectual structure of PFSS. So, to encourage the modern exploration of PFHSS, we will state AOs based on rough data. The main intentions of the current study are given as follows:

(i) The PFHSS efficiently deals with the complex apprehensions seeing the multi-sub-attributes of the DM method's considered factors. To reserve this value in attention, we prolong Einstein operational laws for PFHSS and establish the Einstein AOs for PFHSS.

(ii) The Einstein AOs for PFHSS are well-known attractive evaluation AOs. It has been detected that the prevailing AOs feature is insensitive to scratch the exact outcome over the DM method in some states. To overcome these particular obstacles, these AOs need to be reviewed. We determine inventive Einstein operational laws for Pythagorean fuzzy hypersoft numbers (PFHSNs).

(iii) Pythagorean fuzzy hypersoft Einstein weighted average and geometric operators have presented

their essential properties expending advanced Einstein operational laws.

(iv) An innovative procedure was established on the intended operators to resolve the DM problem.

(v) Real-life agricultural farming is deliberated to endorse the developed method's supremacy and applicability. The significances show that the prearranged model is more operational and reliable to grip indefinite facts.

This study is systematized as follows. Basic knowledge of some important notions like SS, HSS, IFHSS, PFHSS, and Einstein norms are deliberated in section 2. Section 3 demarcated some basic operational laws for PFHSNs based on Einstein norms and established the PFHSEWA operator. Also, some dynamic properties of the planned operator have been debated in the same section. Section 4 also uses the agricultural example to explain several agricultural problems. The algorithm given in this section shows that it is realistic and appropriate. In Section 5, a comparison with some standing approaches is provided.

2. Preliminaries

This section remembers some fundamental notions such as soft set (SS), HSS, IFHSS, and PFHSS.

Definition 1 (see [28]). Let X and $\mathbb{N}$ be the universe of discourse and set of attributes, respectively. Let $\mathrm{P}(X)$ be the power set of X and $\mathscr{A}\subseteq\mathbb{N}$. A pair $(\Omega, \mathscr{A})$ is called a SS over X, and its mapping is expressed as follows:

$$\Omega : \mathscr{A} \longrightarrow \mathrm{P}(X). \tag{1}$$

Also, it can be defined as follows:

$$(\Omega, \mathscr{A}) = \{\Omega(e) \in \mathscr{P}(X): e \in \mathbb{N}, \Omega(e) = \varnothing \text{if } e \notin \mathscr{A}\}. \tag{2}$$

Definition 2 (see [50]). Let X be a universe of discourse and $\mathrm{P}(X)$ be a power set of X and $k = \{k_1, k_2, k_3, \ldots, k_n\}$, $(n \geq 1)$, and K_i represented the set of attributes and their corresponding subattributes such as $K_i \cap K_j = \varnothing$, where $i \neq j$ for each $n \geq 1$ and $i, j \in \{1,2,3, \ldots, n\}$. Assume $K_1 \times K_2 \times K_3 \times \ldots \times K_n = \dddot{\mathscr{A}} = \{d_{1h} \times d_{2k} \times \cdots \times d_{nl}\}$ is a collection of subattributes, where $1 \leq h \leq \alpha, 1 \leq k \leq \beta, 1 \leq l \leq \gamma$, and $\alpha\beta\gamma \in N$, Then, the pair $(\Omega, K_1 \times K_2 \times K_3 \times \ldots \times K_n) = (\Omega\dddot{\mathscr{A}})$ is known as HSS defined as follows:

$$\Omega: K_1 \times K_2 \times K_3 \times \ldots \times K_n = \dddot{\mathscr{A}} \longrightarrow \mathrm{P}(X). \tag{3}$$

It is also defined as

$$(\Omega, \dddot{\mathscr{A}}) = \left\{\breve{d}, \Omega_{\dddot{\mathscr{A}}}(\breve{d}): \breve{d} \in \dddot{\mathscr{A}}, \Omega_{\dddot{\mathscr{A}}}(\breve{d}) \in \mathrm{P}(X)\right\}. \tag{4}$$

Definition 3 (see [50]). Let X be a universe of discourse and $\mathrm{P}(X)$ be a power set of X and $k = \{k_1, k_2, k_3, \ldots k_n\}$, $(n \geq 1)$, and K_i represented the set of attributes and their corresponding subattributes such as $K_i \cap K_j = \varnothing$, where $i \neq j$ for each $n \geq 1$ and $i, j \in \{1,2,3, \ldots, n\}$. Assume $K_1 \times K_2 \times K_3 \times \ldots \times K_n = \dddot{\mathscr{A}} = \{d_{1h} \times d_{2k} \times \cdots \times d_{nl}\}$ is a collection of subattributes, where $1 \leq h \leq \alpha, 1 \leq k \leq \beta$ and $1 \leq l \leq \gamma$, and $\alpha\beta\gamma \in N$. And, IFS^X expresses the intuitionistic fuzzy power set over X. Then, the pair $(\Omega, K_1 \times K_2 \times K_3 \times \ldots \times K_n) = (\Omega\dddot{\mathscr{A}})$ is known as IFHSS defined as follows:

$$\Omega: K_1 \times K_2 \times K_3 \times \ldots \times K_n = \dddot{\mathscr{A}} \longrightarrow IFS^X. \tag{5}$$

It is also defined as

$$(\Omega, \dddot{\mathscr{A}}) = \left\{\left(\breve{d}, \Omega_{\dddot{\mathscr{A}}}(\breve{d})\right): \breve{d} \in \dddot{\mathscr{A}}, \Omega_{\dddot{\mathscr{A}}}(\breve{d}) \in IFS^X\right\}, \tag{6}$$

where $\Omega_{\dddot{\mathscr{A}}}(\breve{d}) = \left\{\left\langle \delta, a_{\Omega(\breve{d})}(\delta), b_{\Omega(\breve{d})}(\delta)\right\rangle: \delta \in X\right\}$, where $a_{\Omega(\breve{d})}(\delta)$ and $b_{\Omega(\breve{d})}(\delta)$ signify the membership value (Mem) and nonmembership value (NMem) of the subattributes:

$a_{\Omega(\breve{d})}(\delta), b_{\Omega(\breve{d})}(\delta), \in [0,1]$, and $0 \leq a_{\Omega(\breve{d})}(\delta) + b_{\Omega(\breve{d})}(\delta) \leq 1$.

Definition 4 (see [53]). Let X be a universe of discourse and $\mathrm{P}(X)$ be a power set of X and $k = \{k_1, k_2, k_3, \ldots k_n\}$, $(n \geq 1)$, and K_i represented the set of attributes and their corresponding subattributes such as $K_i \cap K_j = \varnothing$, where $i \neq j$ for each $n \geq 1$ and $i, j \in \{1,2,3, \ldots, n\}$. Assume $K_1 \times K_2 \times K_3 \times \ldots \times K_n = \dddot{\mathscr{A}} = \{d_{1h} \times d_{2k} \times \cdots \times d_{nl}\}$ is a collection of subattributes, where $1 \leq h \leq \alpha, 1 \leq k \leq \beta$, $1 \leq l \leq \gamma$ and $\alpha\beta\gamma \in N$. And, PFS^X expresses the Pythagorean fuzzy power set over X. Then, the pair $(\Omega, K_1 \times K_2 \times K_3 \times \ldots \times K_n) = (\Omega\dddot{\mathscr{A}})$ is known as PFHSS defined as follows:

$$\Omega: K_1 \times K_2 \times K_3 \times \ldots \times K_n = \dddot{\mathscr{A}} \longrightarrow PFS^X. \tag{7}$$

It is also defined as

$$(\Omega, \dddot{\mathscr{A}}) = \left\{\left(\breve{d}, \Omega_{\dddot{\mathscr{A}}}(\breve{d})\right): \breve{d} \in \dddot{\mathscr{A}}, \Omega_{\dddot{\mathscr{A}}}(\breve{d}) \in PFS^X\right\}, \tag{8}$$

where $\Omega_{\dddot{\mathscr{A}}}(\breve{d}) = \left\{\delta, a_{\Omega(\breve{d})}(\delta), b_{\Omega(\breve{d})}(\delta): \delta \in \mathscr{U}\right\}$, where $a_{\Omega(\breve{d})}(\delta)$ and $b_{\Omega(\breve{d})}(\delta)$ signify the Mem and NMem values of the attributes:

$a_{\Omega(\breve{d})}(\delta), b_{\Omega(\breve{d})}(\delta), \in [0,1]$, and $0 \leq (a_{\Omega(\breve{d})}(\delta))^2 + (b_{\Omega(\breve{d})}(\delta))^2 \leq 1$.

A Pythagorean fuzzy hypersoft number (PFHSN) can be stated as $\Omega = \left\{(a_{\Omega(\breve{d})}(\delta), b_{\Omega(\breve{d})}(\delta))\right\}$, where $0 \leq (a_{\Omega(\breve{d})}(\delta))^2 + (b_{\Omega(\breve{d})}(\delta))^2 \leq 1$.

Remark 1. If $(a_{\Omega(\breve{d})}(\delta))^2 + (b_{\Omega(\breve{d})}(\delta))^2$ and $a_{\Omega(\breve{d})}(\delta) + b_{\Omega(\breve{d})}(\delta) \leq 1$ both are holds, then PFHSS was reduced to IFHSS [58].

For readers' suitability, the PFHSN $\Omega_{\delta_i}(\breve{d}_j) = \left\{(a_{\Omega(\breve{d}_j)}(\delta_i), \mathrm{b}_{\Omega(\breve{d}_j)}(\delta_i))|\delta_i \in \mathscr{U}\right\}$ can be written as $\mathfrak{F}_{\breve{d}_{ij}} = a_{\Omega(\breve{d}_{ij})}, b_{\Omega(\breve{d}_{ij})}$. The score function [65] for $\mathfrak{F}_{\breve{d}_{ij}}$ is expressed as follows:

$$\mathbb{S}\left(\mathfrak{F}_{\breve{d}_{ij}}\right) = a^2_{\Omega\left(\breve{d}_{ij}\right)} - b^2_{\Omega\left(\breve{d}_{ij}\right)} \mathbb{S}\left(\mathfrak{F}_{\breve{d}_{ij}}\right) \in [-1,1], \tag{9}$$

However, in some cases, the above-defined score function cannot handle the scenario. For example, if we consider

two PFHSNs, such as $\mathfrak{F}_{\check{d}_{11}} = .4, .7$ and $\mathfrak{F}_{\check{d}_{12}} = .5, .8$. The score function cannot deliver relevant results to subtract the PFHSNs. So, in such situations, it is tough to achieve the most suitable alternative $\mathbb{S}(\mathfrak{F}_{\check{d}_{11}}) = .3 = \mathbb{S}(\mathfrak{F}_{\check{d}_{12}})$. To intimidated such problems, the accuracy function [65] had been developed.

$$H\left(\mathfrak{F}_{\check{d}_{ij}}\right)a^2_{\Omega\left(\check{d}_{ij}\right)} + b^2_{\Omega\left(\check{d}_{ij}\right)}H\left(\mathfrak{F}_{\check{d}_{ij}}\right) \in [0,1]. \tag{10}$$

The following comparison laws have been projected to compute two PFHSNs $\mathfrak{F}_{\check{d}_{ij}}$ and $\mathfrak{T}_{\check{d}_{ij}}$:

(1) If $\mathbb{S}(\mathfrak{F}_{\check{d}_{ij}}) > \mathbb{S}(\mathfrak{T}_{\check{d}_{ij}})$, then $\mathfrak{F}_{\check{d}_{ij}} > \mathfrak{T}_{\check{d}_{ij}}$
(2) If $\mathbb{S}(\mathfrak{F}_{\check{d}_{ij}}) = \mathbb{S}(\mathfrak{T}_{\check{d}_{ij}})$, then
(3) If $H(\mathfrak{F}_{\check{d}_{ij}}) > H(\mathfrak{T}_{\check{d}_{ij}})$, then $\mathfrak{F}_{\check{d}_{ij}} > \mathfrak{T}_{\check{d}_{ij}}$
(4) If $H(\mathfrak{F}_{\check{d}_{ij}}) = H(\mathfrak{T}_{\check{d}_{ij}})$, then $\mathfrak{F}_{\check{d}_{ij}} = \mathfrak{T}_{\check{d}_{ij}}$

Definition 5. Einstein sum $\oplus_\varepsilon$ and Einstein product $\oplus_\varepsilon$ are good alternatives of algebraic t-norm and t-conorm, respectively, given as follows:

$$a \oplus_\varepsilon b = \frac{a+b}{1+(a.b)} \text{ and } a \otimes_\varepsilon b = \frac{a.b}{1+(1-a).(1-b)}, \tag{11}$$

$$\forall (a,b) \in [0,1]^2.$$

Under the Pythagorean fuzzy environment, Einstein sum $\oplus_\varepsilon$ and Einstein product $\oplus_\varepsilon$ are defined as follows:

$$a \oplus_\varepsilon b = \sqrt{\frac{a^2+b^2}{1+\left(a^2.b^2\right)}},$$

$$a \otimes_\varepsilon b = \frac{a.b}{\sqrt{1+\left(1-a^2\right).\left(1-b^2\right)}}, \tag{12}$$

$$\forall (a,b) \in [0,1]^2,$$

where $a \oplus_\varepsilon b$ and $a \oplus_\varepsilon b$ are known as t-norm and t-conorm, respectively, satisfying the bounded, monotonicity, commutativity, and associativity properties.

3. Einstein Weighted Aggregation Operators for Pythagorean Fuzzy Hypersoft Set

This section will introduce a novel Einstein weighted AO such as the PFHSEWA operator for PFHSNs with essential properties.

3.1. Operational Laws for PFHSNs

Definition 6. Let $\mathfrak{F}_{\check{d}_k} = (a_{\check{d}_k}, b_{\check{d}_k})$, $\mathfrak{F}_{\check{d}_{11}} = (a_{\check{d}_{11}}, b_{\check{d}_{11}})$, and $\mathfrak{F}_{\check{d}_{12}} = (a_{\check{d}_{12}}, b_{\check{d}_{12}})$ represent the PFHSNs and ∂ is a positive real number. Then, operational laws for PFHSNs based on Einstein norms can be expressed as follows:

$$1\ \mathfrak{F}_{\check{d}_{11}} \oplus_\varepsilon \mathfrak{F}_{\check{d}_{12}} = \left(\sqrt{\left(1+a^2_{\check{d}_{12}}\right)-\left(1-a^2_{\check{d}_{12}}\right)} \Big/ \sqrt{\left(1+a^2_{\check{d}_{12}}\right)+\left(1-a^2_{\check{d}_{12}}\right)}\right), \left(\sqrt{2b^2_{\check{d}_{12}}} \Big/ \sqrt{\left(2-b^2_{\check{d}_{12}}\right)+b^2_{\check{d}_{12}}}\right)$$

$$\mathfrak{F}_{\check{d}_{11}} \otimes_\varepsilon \mathfrak{F}_{\check{d}_{12}} = \left(\frac{\sqrt{2\alpha^2_{\check{d}_{12}}}}{\sqrt{\left(2-\alpha^2_{\check{d}_{12}}\right)+\alpha^2_{\check{d}_{12}}}}, \frac{\sqrt{\left(1+b^2_{\check{d}_{12}}\right)-\left(1-b^2_{\check{d}_{12}}\right)}}{\sqrt{\left(1+b^2_{\check{d}_{12}}\right)+\left(1-b^2_{\check{d}_{12}}\right)}}\right) \tag{13}$$

$$2\ \partial\mathfrak{F}_{\check{d}_k} = \left(\sqrt{\left(1+a^2_{\check{d}_k}\right)^\partial-\left(1-a^2_{\check{d}_k}\right)^\partial} \Big/ \sqrt{\left(1+a^2_{\check{d}_k}\right)^\partial+\left(1-a^2_{\check{d}_k}\right)^\partial}\right),$$
$$\left(\sqrt{2\left(b^2_{\check{d}_k}\right)^\partial} \Big/ \sqrt{\left(2-b^2_{\check{d}_k}\right)^\partial+\left(b^2_{\check{d}_k}\right)^\partial}\right)$$

$$3\ \mathfrak{F}^\partial_{\check{d}_k} = \sqrt{2(a)^\partial} \Big/ \left(\sqrt{\left(1+b^2_{\check{d}_k}\right)^\partial-\left(1-b^2_{\check{d}_k}\right)^\partial} \Big/ \sqrt{\left(1+b^2_{\check{d}_k}\right)^\partial+\left(1-b^2_{\check{d}_k}\right)^\partial}\right), \sqrt{\left(2-a^2_{\check{d}_k}\right)^\partial+\left(a^2_{\check{d}_k}\right)^\partial},$$

Definition 7. Let $\mathfrak{F}_{\check{d}_{ij}} = (a_{\check{d}_{ij}}, b_{\check{d}_{ij}})$ be a collection of PFHSNs, then the PFHSEWA operator is defined as follows:

$$PFHSEWA = \left(\mathfrak{F}_{\check{d}_{11}}, \mathfrak{F}_{\check{d}_{12}}, \ldots, \mathfrak{F}_{\check{d}_{nm}}\right) \oplus^m_{\varepsilon j=1} \lambda_j \left(\oplus^n_{\varepsilon i=1} \theta_i \mathfrak{F}_{\check{d}_{ij}}\right), \tag{14}$$

where $(i = 1, 2, \ldots, n)$, $(j = 1, 2, \ldots, m)$, and θ_i and λ_j represent the weighted vectors such that $\theta_i > 0$, $\sum^n_{i=1} \theta_i = 1$, and $\lambda_j > 0$ and $\sum^n_{j=1} \lambda_j = 1$.

Theorem 1. *Let $\mathfrak{F}_{\check{d}_{jj}} = (a_{\check{d}_{ij}}, b_{\check{d}_{ij}})$ be a collection of PFHSNs, then the aggregated value attained by equation (3) given as*

$$PFHSEWA\left(\mathfrak{F}_{\check{d}_{11}}, \mathfrak{F}_{\check{d}_{12}}, \ldots, \mathfrak{F}_{\check{d}_{nm}}\right) = \oplus^m_{j=1} \lambda_j \left(\oplus^n_{i=1} \theta_i \mathfrak{F}_{\check{d}_{ij}}\right),$$

$$= \frac{\sqrt{\prod^m_{j=1}\left(\prod^n_{i=1}\left(1+\alpha^2_{\check{d}_{ij}}\right)^{\theta_i}\right)^{\lambda_j} - \prod^m_{j=1}\left(\prod^n_{i=1}\left(1-\alpha^2_{\check{d}_{ij}}\right)^{\theta_i}\right)^{\lambda_j}}}{\sqrt{\prod^m_{j=1}\left(\prod^n_{i=1}\left(1+\alpha^2_{\check{d}_{ij}}\right)^{\theta_i}\right)^{\lambda_j} + \prod^m_{j=1}\left(\prod^n_{i=1}\left(1-\alpha^2_{\check{d}_{ij}}\right)^{\theta_i}\right)^{\lambda_j}}}, \frac{\sqrt{2\prod^m_{j=1}\left(\prod^n_{i=1}\left(b^2_{\check{d}_{ij}}\right)^{\theta_i}\right)^{\lambda_j}}}{\sqrt{\prod^m_{j=1}\left(\prod^n_{i=1}\left(2-b^2_{\check{d}_{ij}}\right)^{\theta_i}\right)^{\lambda_j} + \prod^m_{j=1}\left(\prod^n_{i=1}\left(b^2_{\check{d}_{ij}}\right)^{\theta_i}\right)^{\lambda_j}}}, \tag{15}$$

where $(i = 1, 2, \ldots, n)$, $(j = 1, 2, \ldots, m)$ *and* θ_i *and* λ_j *represent the weight vectors such that* $\theta_i > 0$, $\sum_{i=1}^{n} \theta_i = 1$, *and* $\lambda_j > 0$, $\sum_{j=1}^{n} \lambda_j = 1$.

Proof. We will prove it by using mathematical induction.

For $n = 1$, we get $\theta_i = 1$

$$PFHSEWA = \left(\mathfrak{F}_{\breve{d}_{11}}, \mathfrak{F}_{\breve{d}_{12}}, \ldots, \mathfrak{F}_{\breve{d}_{nm}}\right) = \oplus_{j=1}^{m} \lambda_j \mathfrak{F}_{\breve{d}_{1j}}$$

$$= \left\langle \frac{\sqrt{\prod_{j=1}^{m}\left(1 + a_{\breve{d}_{1j}}^2\right)^{\lambda_j} - \prod_{j=1}^{m}\left(1 - a_{\breve{d}_{1j}}^2\right)^{\lambda_j}}}{\sqrt{\prod_{j=1}^{m}\left(1 + a_{\breve{d}_{1j}}^2\right)^{\lambda_j} + \prod_{j=1}^{m}\left(1 - a_{\breve{d}_{1j}}^2\right)^{\lambda_j}}}, \frac{\sqrt{2\prod_{j=1}^{m}\left(b_{\breve{d}_{1j}}^2\right)^{\lambda_j}}}{\sqrt{\prod_{j=1}^{m}\left(2 - b_{\breve{d}_{1j}}^2\right)^{\lambda_j} + \prod_{j=1}^{m}\left(b_{\breve{d}_{1j}}^2\right)^{\lambda_j}}} \right\rangle,$$

$$= \left\langle \frac{\sqrt{\prod_{j=1}^{m}\left(\prod_{i=1}^{1}\left(1 + a_{\breve{d}_{ij}}^2\right)^{\theta_i}\right)^{\lambda_j} - \prod_{j=1}^{m}\left(\prod_{i=1}^{1}\left(1 - a_{\breve{d}_{ij}}^2\right)^{\theta_i}\right)^{\lambda_j}}}{\sqrt{\prod_{j=1}^{m}\left(\prod_{i=1}^{1}\left(1 + a_{\breve{d}_{ij}}^2\right)^{\theta_i}\right)^{\lambda_j} + \prod_{j=1}^{m}\left(\prod_{i=1}^{1}\left(1 - a_{\breve{d}_{ij}}^2\right)^{\theta_i}\right)^{\lambda_j}}}, \frac{\sqrt{2\prod_{j=1}^{m}\left(\prod_{i=1}^{1}\left(b_{\breve{d}_{ij}}^2\right)^{\theta_i}\right)^{\lambda_j}}}{\sqrt{\prod_{j=1}^{m}\left(\prod_{i=1}^{1}\left(2 - b_{\breve{d}_{ij}}^2\right)^{\theta_i}\right)^{\lambda_j} + \prod_{j=1}^{m}\left(\prod_{i=1}^{1}\left(b_{\breve{d}_{ij}}^2\right)^{\theta_i}\right)^{\lambda_j}}} \right\rangle. \tag{16}$$

For $m = 1$, we get $\lambda_j = 1$.

$$PFHSEWA\left(\mathfrak{F}_{\breve{d}_{11}}, \mathfrak{F}_{\breve{d}_{12}}, \ldots, \mathfrak{F}_{\breve{d}_{nm}}\right) = \oplus_{i=1}^{n} \theta_i \mathfrak{F}_{\breve{d}_{i1}}$$

$$= \left\langle \frac{\sqrt{\prod_{i=1}^{n}\left(1 + a_{\breve{d}_{i1}}^2\right)^{\theta_i} - \prod_{i=1}^{n}\left(1 - a_{\breve{d}_{i1}}^2\right)^{\theta_i}}}{\sqrt{\prod_{i=1}^{n}\left(1 + a_{\breve{d}_{i1}}^2\right)^{\theta_i} + \prod_{i=1}^{n}\left(1 - a_{\breve{d}_{i1}}^2\right)^{\theta_i}}}, \frac{\sqrt{2\prod_{i=1}^{n}\left(b_{\breve{d}_{i1}}^2\right)^{\theta_i}}}{\sqrt{\prod_{i=1}^{n}\left(2 - b_{\breve{d}_{i1}}^2\right)^{\theta_i} + \prod_{i=1}^{n}\left(b_{\breve{d}_{i1}}^2\right)^{\theta_i}}} \right\rangle$$

$$= \left\langle \frac{\sqrt{\prod_{j=1}^{1}\left(\prod_{i=1}^{n}\left(1 + \alpha_{\breve{d}_{ij}}^2\right)^{\theta_i}\right)^{\lambda_j} - \prod_{j=1}^{1}\left(\prod_{i=1}^{n}\left(1 - \alpha_{\breve{d}_{ij}}^2\right)^{\theta_i}\right)^{\lambda_j}}}{\sqrt{\prod_{j=1}^{1}\left(\prod_{i=1}^{n}\left(1 + \alpha_{\breve{d}_{ij}}^2\right)^{\theta_i}\right)^{\lambda_j} + \prod_{j=1}^{1}\left(\prod_{i=1}^{n}\left(1 - \alpha_{\breve{d}_{ij}}^2\right)^{\theta_i}\right)^{\lambda_j}}}, \frac{\sqrt{2\prod_{j=1}^{1}\left(\prod_{i=1}^{n}\left(b_{\breve{d}_{ij}}^2\right)^{\theta_i}\right)^{\lambda_j}}}{\sqrt{\prod_{j=1}^{1}\left(\prod_{i=1}^{n}\left(2 - b_{\breve{d}_{ij}}^2\right)^{\theta_i}\right)^{\lambda_j} + \prod_{j=1}^{1}\left(\prod_{i=1}^{n}\left(b_{\breve{d}_{ij}}^2\right)^{\theta_i}\right)^{\lambda_j}}} \right\rangle. \tag{17}$$

So, equation (4) is true for $n = 1$ and $m = 1$.

Suppose that equation holds for $n = \delta_2$, $m = \delta_1 + 1$ and for $n = \delta_2 + 1$, $m = \delta_1$,

$$\oplus_{j=1}^{\delta_1+1} \lambda_j \left(\oplus_{i=1}^{\delta_2} \theta_i \mathfrak{F}_{\breve{d}_{ij}}\right) = \left\langle \frac{\sqrt{\prod_{j=1}^{\delta_1+1}\left(\prod_{i=1}^{\delta_2}\left(1 + \alpha_{\breve{d}_{ij}}^2\right)^{\theta_i}\right)^{\lambda_j} - \prod_{j=1}^{\delta_1+1}\left(\prod_{i=1}^{\delta_2}\left(1 - \alpha_{\breve{d}_{ij}}^2\right)^{\theta_i}\right)^{\lambda_j}}}{\sqrt{\prod_{j=1}^{\delta_1+1}\left(\prod_{i=1}^{\delta_2}\left(1 + \alpha_{\breve{d}_{ij}}^2\right)^{\theta_i}\right)^{\lambda_j} + \prod_{j=1}^{\delta_1+1}\left(\prod_{i=1}^{\delta_2}\left(1 - \alpha_{\breve{d}_{ij}}^2\right)^{\theta_i}\right)^{\lambda_j}}}, \frac{\sqrt{2\prod_{j=1}^{\delta_1+1}\left(\prod_{i=1}^{\delta_2}\left(b_{\breve{d}_{ij}}^2\right)^{\theta_i}\right)^{\lambda_j}}}{\sqrt{\prod_{j=1}^{\delta_1+1}\left(\prod_{i=1}^{\delta_2}\left(2 - b_{\breve{d}_{ij}}^2\right)^{\theta_i}\right)^{\lambda_j} + \prod_{j=1}^{\delta_1+1}\left(\prod_{i=1}^{\delta_2}\left(b_{\breve{d}_{ij}}^2\right)^{\theta_i}\right)^{\lambda_j}}} \right\rangle,$$

$$\oplus_{j=1}^{\delta_1} \lambda_j \left(\oplus_{i=1}^{\delta_2+1} \theta_i \mathfrak{F}_{\breve{d}_{ij}}\right) = \left\langle \frac{\sqrt{\prod_{j=1}^{\delta_1}\left(\prod_{i=1}^{\delta_2+1}\left(1 + \alpha_{\breve{d}_{ij}}^2\right)^{\theta_i}\right)^{\lambda_j} - \prod_{j=1}^{\delta_1}\left(\prod_{i=1}^{\delta_2+1}\left(1 - \alpha_{\breve{d}_{ij}}^2\right)^{\theta_i}\right)^{\lambda_j}}}{\sqrt{\prod_{j=1}^{\delta_1}\left(\prod_{i=1}^{\delta_2+1}\left(1 + \alpha_{\breve{d}_{ij}}^2\right)^{\theta_i}\right)^{\lambda_j} + \prod_{j=1}^{\delta_1}\left(\prod_{i=1}^{\delta_2+1}\left(1 - \alpha_{\breve{d}_{ij}}^2\right)^{\theta_i}\right)^{\lambda_j}}}, \frac{\sqrt{2\prod_{j=1}^{\delta_1}\left(\prod_{i=1}^{\delta_2+1}\left(b_{\breve{d}_{ij}}^2\right)^{\theta_i}\right)^{\lambda_j}}}{\sqrt{\prod_{j=1}^{\delta_1}\left(\prod_{i=1}^{\delta_2+1}\left(2 - b_{\breve{d}_{ij}}^2\right)^{\theta_i}\right)^{\lambda_j} + \prod_{j=1}^{\delta_1}\left(\prod_{i=1}^{\delta_2+1}\left(b_{\breve{d}_{ij}}^2\right)^{\theta_i}\right)^{\lambda_j}}} \right\rangle. \tag{18}$$

Now, we prove the equation for $m = \delta_1 + 1$ and $= n = \delta_2 + 1$:

$$\begin{aligned}
\oplus_{j=1}^{\delta_1+1}\lambda_j\left(\oplus_{i=1}^{\delta_2+1}\theta_i\mathfrak{F}_{\breve{d}_{ij}}\right) &= \oplus_{j=1}^{\delta_1+1}\lambda_j\left(\oplus_{i=1}^{\delta_2}\theta_i\mathfrak{F}_{\breve{d}_{ij}}\oplus\theta_{i+1}\mathfrak{F}_{\breve{d}_{(\delta_2+1)j}}\right)\\
&= \left(\oplus_{j=1}^{\delta_1+1}\oplus_{i=1}^{\delta_2}\theta_i\lambda_j\,\mathfrak{F}_{\breve{d}_{ij}}\right)\left(\oplus_{j=1}^{\delta_1+1}\lambda_j\theta_{i+1}\mathfrak{F}_{\breve{d}_{(\delta_2+1)j}}\right)\\
&= \left\langle \frac{\sqrt{\prod_{j=2}^{\delta_1+1}\left(\prod_{i=1}^{\delta_2}\left(1+\alpha_{\breve{d}_{ij}}^2\right)^{\theta_i}\right)^{\lambda_j}-\prod_{j=1}^{\delta_1+1}\left(\prod_{i=1}^{\delta_2}\left(1+\alpha_{\breve{d}_{ij}}^2\right)^{\theta_i}\right)^{\lambda_j}}}{\prod_{j=1}^{\delta_1+1}\left(\prod_{i=1}^{\delta_2}\left(1+\alpha_{\breve{d}_{ij}}^2\right)^{\theta_i}\right)^{\lambda_j}-\prod_{j=1}^{\delta_1+1}\left(\prod_{i=1}^{\delta_2}\left(1+\alpha_{\breve{d}_{ij}}^2\right)^{\theta_i}\right)^{\lambda_j}}\right.\\
&\quad \left.\frac{\sqrt{\prod_{j=1}^{\delta_1+1}\left(\left(1+\alpha_{\breve{d}_{(\delta_2+1)j}}^2\right)^{\theta\delta_2+1}\right)^{\lambda_j}-\prod_{j=1}^{\delta_1+1}\left(\left(1+\alpha_{\breve{d}_{(\delta_2+1)j}}^2\right)^{\theta\delta_2+1}\right)^{\lambda_j}}}{\sqrt{\prod_{j=1}^{\delta_1+1}\left(\left(1+\alpha_{\breve{d}_{(\delta_2+1)j}}^2\right)^{\theta\delta_2+1}\right)^{\lambda_j}+\prod_{j=1}^{\delta_1+1}\left(\left(1+\alpha_{\breve{d}_{(\delta_2+1)j}}^2\right)^{\theta\delta_2+1}\right)^{\lambda_j}}}\right.\\
&\quad \left.\frac{\sqrt{2\prod_{j=1}^{\delta_1+1}\left(\prod_{i=1}^{\delta_2}\left(b_{\breve{d}_{ij}}^2\right)^{\theta_i}\right)^{\lambda_j}}}{\sqrt{\prod_{j=1}^{\delta_1+1}\left(\prod_{i=1}^{\delta_2}\left(2+b_{\breve{d}_{ij}}^2\right)^{\theta_i}\right)^{\lambda_j}-\prod_{j=1}^{\delta_1+1}\left(\prod_{i=1}^{\delta_2}\left(b_{\breve{d}_{ij}}^2\right)^{\theta_i}\right)^{\lambda_j}}}\right.\\
&\quad \left.\oplus\frac{\sqrt{2\prod_{j=1}^{\delta_1+1}\left(\left(b_{\breve{d}_{(\delta_2+1)j}}^2\right)^{\theta\delta_2+1}\right)^{\lambda_j}}}{\sqrt{\prod_{j=1}^{\delta_1+1}\left(\left(2-b_{\breve{d}_{(\delta_2+1)j}}^2\right)^{\theta\delta_2+1}\right)^{\lambda_j}-\prod_{j=1}^{\delta_1+1}\left(\left(b_{\breve{d}_{(\delta_2+1)j}}^2\right)^{\theta\delta_2+1}\right)^{\lambda_j}}}\right\rangle\\
&= \left\langle \frac{\sqrt{\prod_{j=1}^{\delta_1+1}\left(\prod_{i=1}^{\delta_2+1}\left(1+\alpha_{\breve{d}_{ij}}^2\right)^{\theta_i}\right)^{\lambda_j}-\prod_{j=1}^{\delta_1+1}\left(\prod_{i=1}^{\delta_2+1}\left(1-\alpha_{\breve{d}_{ij}}^2\right)^{\theta_i}\right)^{\lambda_j}}}{\sqrt{\left(\prod_{j=1}^{\delta_1+1}\left(\prod_{i=1}^{\delta_2+1}\left(1+\alpha_{\breve{d}_{ij}}^2\right)\right)^{\theta_i}\right)^{\lambda_j}+\prod_{j=1}^{\delta_1+1}\left(\prod_{i=1}^{\delta_2+1}\left(1-\alpha_{\breve{d}_{ij}}^2\right)^{\theta_i}\right)^{\lambda_j}}},\right.\\
&\quad \left.\frac{\sqrt{2\prod_{j=1}^{\delta_1+1}\left(\prod_{i=1}^{\delta_2+1}\left(b_{\breve{d}_{ij}}^2\right)^{\theta_i}\right)^{\lambda_j}}}{\sqrt{\left(\prod_{j=1}^{\delta_1+1}\left(\prod_{i=1}^{\delta_2+1}\left(2-b_{\breve{d}_{ij}}^2\right)\right)^{\theta_i}\right)^{\lambda_j}+\prod_{j=1}^{\delta_1+1}\left(\prod_{i=1}^{\delta_2+1}\left(b_{\breve{d}_{ij}}^2\right)^{\theta_i}\right)^{\lambda_j}}}\right\rangle\\
&= \oplus_{j=1}^{\delta_1+1}\lambda_j\left(\oplus_{i=1}^{\delta_2+1}\theta_i\mathfrak{F}_{\breve{d}_{ij}}\right).
\end{aligned} \tag{19}$$

So, it is true for $m = \delta_1 + 1$ and $n = \delta_2 + 1$. □

3.2. Example. Let $\mathscr{R} = \{\mathscr{R}_1, \mathscr{R}_2, \mathscr{R}_3, \mathscr{R}_4\}$ be a set of experts with the given weight vector $\theta_i = (0.1, 0.3, 0.3, 0.3)^T$. The team of experts is going to describe the attractiveness of a house under-considered set of attributes $A = \{d_1 = \text{lawn}, d_2 = \text{security system}\}$ with their corresponding sub-attributes $\text{Lawn} d_1 = \{d_{11} = \text{with grass}, d_{12} = \text{without grass}\}$ and security system$d_2 = \{d_{21} = \text{guards}, d_{22} = \text{cameras}\}$. Let $\overset{\cdots}{\mathscr{A}} = d_1 \times d_2$ be a set of subattributes $\overset{\cdots}{\mathscr{A}} = d_1 \times d_2 = \{d_{11}, d_{12}\} \times \{d_{21}, d_{22}\} = \{(d_{11}, d_{21}), (d_{11}, d_{22}), (d_{12}, d_{21}), (d_{12}, d_{22})\}$.

$\overset{\cdots}{\mathscr{A}} = \{\breve{d}_1, \breve{d}_2, \breve{d}_3, \breve{d}_4\}$ represents the set subattributes with weights with weight vector $\lambda_j = (0.2, 0.2, 0.2, 0.4)^T$. The supposed rating values for all attributes in the form of PFSNs $(\mathscr{H}, \overset{\cdots}{\mathscr{A}}) = (a_{ij}, b_{ij})_{4\times 4}$ are given as follows:

$$(\mathscr{H}, \overset{\cdots}{\mathscr{A}}) = \begin{matrix} (0.5, 0.8) & (0.7, 0.5) & (0.4, 0.6) & (0.7, 0.4)\\ (0.5, 0.6) & (0.9, 0.1) & (0.3, 0.7) & (0.4, 0.5)\\ (0.4, 0.8) & (0.7, 0.5) & (0.4, 0.6) & (0.3, 0.5)\\ (0.3, 0.7) & (0.6, 0.5) & (0.5, 0.4) & (0.5, 0.7) \end{matrix} \tag{20}$$

As we know that

$$PFHSEWA\left(\mathfrak{F}_{\breve{d}_{11}}, \mathfrak{F}_{\breve{d}_{12}}, \ldots, \mathfrak{F}_{\breve{d}_{mn}}\right) = \left\langle \frac{\sqrt{\prod_{j=1}^{m}\left(\prod_{i=1}^{n}\left(1+\alpha_{\breve{d}_{ij}}^2\right)^{\theta_i}\right)^{\lambda_j}-\prod_{j=1}^{m}\left(\prod_{i=1}^{n}\left(1-\alpha_{\breve{d}_{ij}}^2\right)^{\theta_i}\right)^{\lambda_j}}}{\sqrt{\prod_{j=1}^{m}\left(\prod_{i=1}^{n}\left(1+\alpha_{\breve{d}_{ij}}^2\right)^{\theta_i}\right)^{\lambda_j}+\prod_{j=1}^{m}\left(\prod_{i=1}^{n}\left(1-\alpha_{\breve{d}_{ij}}^2\right)^{\theta_i}\right)^{\lambda_j}}}, \frac{\sqrt{2\prod_{j=1}^{m}\left(\prod_{i=1}^{n}\left(b_{\breve{d}_{ij}}^2\right)^{\theta_i}\right)^{\lambda_j}}}{\sqrt{\prod_{j=1}^{m}\left(\prod_{i=1}^{n}\left(2-b_{\breve{d}_{ij}}^2\right)^{\theta_i}\right)^{\lambda_j}+\prod_{j=1}^{m}\left(\prod_{i=1}^{n}\left(b_{\breve{d}_{ij}}^2\right)^{\theta_i}\right)^{\lambda_j}}}\right\rangle, \tag{21}$$

$$PFHSEWA\left(\mathfrak{F}_{\breve{d}_{11}}, \mathfrak{F}_{\breve{d}_{12}}, \ldots, \mathfrak{F}_{\breve{d}_{44}}\right) = \left\langle \frac{\sqrt{\prod_{j=1}^{4}\left(\prod_{i=1}^{4}\left(1+\alpha_{\breve{d}_{ij}}^2\right)^{\theta_i}\right)^{\lambda_j}-\prod_{j=1}^{4}\left(\prod_{i=1}^{n}\left(1-\alpha_{\breve{d}_{ij}}^4\right)^{\theta_i}\right)^{\lambda_j}}}{\sqrt{\prod_{j=1}^{4}\left(\prod_{i=1}^{4}\left(1+\alpha_{\breve{d}_{ij}}^2\right)^{\theta_i}\right)^{\lambda_j}+\prod_{j=1}^{4}\left(\prod_{i=1}^{4}\left(1-\alpha_{\breve{d}_{ij}}^2\right)^{\theta_i}\right)^{\lambda_j}}}, \frac{\sqrt{2\prod_{j=1}^{4}\left(\prod_{i=1}^{4}\left(b_{\breve{d}_{ij}}^2\right)^{\theta_i}\right)^{\lambda_j}}}{\sqrt{\prod_{j=1}^{4}\left(\prod_{i=1}^{4}\left(2-b_{\breve{d}_{ij}}^2\right)^{\theta_i}\right)^{\lambda_j}+\prod_{j=1}^{4}\left(\prod_{i=1}^{4}\left(b_{\breve{d}_{ij}}^2\right)^{\theta_i}\right)^{\lambda_j}}}\right\rangle$$

$$= \left\langle \frac{\sqrt{\begin{array}{l}\left\{(1.25)^{0.1}(1.25)^{0.3}(1.16)^{0.3}(1.09)^{0.3}\right\}^{0.2}\left\{(1.49)^{0.1}(1.81)^{0.3}(1.49)^{0.3}(1.36)^{0.3}\right\}^{0.2}\\ \left\{(1.16)^{0.1}(1.09)^{0.3}(1.16)^{0.3}(1.25)^{0.3}\right\}^{0.2}\left\{(1.49)^{0.1}(1.16)^{0.3}(1.09)^{0.3}(1.25)^{0.3}\right\}^{0.4}\\ -\\ \left[\left\{(0.75)^{0.1}(0.75)^{0.3}(0.84)^{0.3}(0.91)^{0.3}\right\}^{0.2}\left\{(0.51)^{0.1}(0.19)^{0.3}(0.51)^{0.3}(0.64)^{0.3}\right\}^{0.2}\right.\\ \left.\left\{(0.84)^{0.1}(0.91)^{0.3}(0.84)^{0.3}(0.75)^{0.3}\right\}^{0.2}\left\{(0.51)^{0.1}(0.84)^{0.3}(0.91)^{0.3}(0.75)^{0.3}\right\}^{0.4}\right]\end{array}}}{\sqrt{\begin{array}{l}\left\{(1.25)^{0.1}(1.25)^{0.3}(1.16)^{0.3}(1.09)^{0.3}\right\}^{0.2}\left\{(1.49)^{0.1}(1.81)^{0.3}(1.49)^{0.3}(1.36)^{0.3}\right\}^{0.2}\\ \left\{(1.16)^{0.1}(1.09)^{0.3}(1.16)^{0.3}(1.25)^{0.3}\right\}^{0.2}\left\{(1.49)^{0.1}(1.16)^{0.3}(1.09)^{0.3}(1.25)^{0.3}\right\}^{0.4}\\ +\\ \left[\left\{(0.75)^{0.1}(0.75)^{0.3}(0.84)^{0.3}(0.91)^{0.3}\right\}^{0.2}\left\{(0.51)^{0.1}(0.19)^{0.3}(0.51)^{0.3}(0.64)^{0.3}\right\}^{0.2}\right.\\ \left.\left\{(0.84)^{0.1}(0.91)^{0.3}(0.84)^{0.3}(0.75)^{0.3}\right\}^{0.2}\left\{(0.51)^{0.1}(0.84)^{0.3}(0.91)^{0.3}(0.75)^{0.3}\right\}^{0.4}\right]\end{array}}}, \frac{\sqrt{2\left[\left(\left\{(0.64)^{0.1}(0.36)^{0.3}(0.64)^{0.3}(0.49)^{0.3}\right\}^{0.2}\left\{(0.25)^{0.1}(0.01)^{0.3}(0.25)^{0.3}(0.25)^{0.3}\right\}^{0.2}\right.\right.}}{\sqrt{\left.\left.\left\{(0.36)^{0.1}(0.49)^{0.3}(0.36)^{0.3}(0.16)^{0.3}\right\}^{0.2}\left\{(0.16)^{0.1}(0.25)^{0.3}(0.25)^{0.3}(0.49)^{0.3}\right\}^{0.4}\right)\right]}} \right\rangle$$

$$= \left\langle \frac{\sqrt{\begin{array}{l}\left\{(1.36)^{0.1}(1.64)^{0.3}(1.36)^{0.3}(1.51)^{0.3}\right\}^{0.2}\left\{(1.75)^{0.1}(1.99)^{0.3}(1.75)^{0.3}(1.75)^{0.3}\right\}^{0.2}\\ \left\{(1.64)^{0.1}(1.51)^{0.3}(1.64)^{0.3}(1.84)^{0.3}\right\}^{0.2}\left\{(1.84)^{0.1}(1.75)^{0.3}(1.75)^{0.3}(1.51)^{0.3}\right\}^{0.4}\\ +\\ \left\{(0.64)^{0.1}(0.36)^{0.3}(0.64)^{0.3}(0.49)^{0.3}\right\}^{0.2}\left\{(0.25)^{0.1}(0.01)^{0.3}(0.25)^{0.3}(0.25)^{0.3}\right\}^{0.2}\\ \left\{(0.36)^{0.1}(0.49)^{0.3}(0.36)^{0.3}(0.16)^{0.3}\right\}^{0.2}\left\{(0.16)^{0.1}(0.25)^{0.3}(0.25)^{0.3}(0.49)^{0.3}\right\}^{0.4}\end{array}}}{\sqrt{\begin{array}{l}(1.0324)(1.0897)(1.0309)(1.0734)-\\ [(0.9616)(0.8350)(0.9638)(0.9105)]\end{array}}}, \frac{\sqrt{2\left[(0.8695)(0.6247)(0.7909)(0.6116)\right]}}{\sqrt{\begin{array}{l}(1.0822)(1.1270)(1.1061)(1.2313)+\\ (0.8695)(0.6247)(0.7909)(0.6116)\end{array}}} \right\rangle$$

$$= \left\langle \frac{\sqrt{\begin{array}{l}(1.0324)(1.0897)(1.0309)(1.0734)-\\ [(0.9616)(0.8350)(0.9638)(0.9105)]\end{array}}}{\sqrt{\begin{array}{l}(1.0324)(1.0897)(1.0309)(1.0734)+\\ [(0.9616)(0.8350)(0.9638)(0.9105)]\end{array}}}, \frac{\sqrt{2\left[(0.8695)(0.6247)(0.7909)(0.6116)\right]}}{\sqrt{\begin{array}{l}(1.0822)(1.1270)(1.1061)(1.2313)+\\ (0.8695)(0.6247)(0.7909)(0.6116)\end{array}}} \right\rangle$$

$$= 0.5263, 0.5225. \tag{22}$$

Lemma 1. *Let* $\mathfrak{F}_{\check{d}_{ij}} = a_{\check{d}_{ij}}, b_{\check{d}_{ij}}$, *where* $\theta_i > 0$, $\sum_{i=1}^{n} \theta_i = 1$, *and* $\lambda_j > 0$, $\sum_{j=1}^{n} \lambda_j = 1$, *then*

$$\prod_{j=1}^{m}\left(\prod_{i=1}^{n}\left(\mathfrak{F}_{\check{d}_{ij}}\right)^{\theta_i}\right)^{\lambda_j} = \sum_{j=1}^{m}\lambda_j\sum_{i=1}^{n}\theta_i\mathfrak{F}_{\check{d}_{ij}}. \tag{23}$$

Theorem 2. *Let* $\mathfrak{F}_{\check{d}_{ij}} = a_{\check{d}_{ij}}, b_{\check{d}_{ij}}$ *be a collection of PFHSNs, then*

$$PFHSWA\left(\mathfrak{F}_{\check{d}_{11}}, \mathfrak{F}_{\check{d}_{12}}, \ldots, \mathfrak{F}_{\check{d}_{nm}}\right) \geq PFHSEWA\left(\mathfrak{F}_{\check{d}_{11}}, \mathfrak{F}_{\check{d}_{12}}, \ldots, \mathfrak{F}_{\check{d}_{nm}}\right), \tag{24}$$

where $(i = 1, 2, \ldots, n)$, $(j = 1, 2, \ldots, m)$, *and* θ_i *and* λ_j *represent the weight vectors such as* $\theta_i > 0$, $\sum_{i=1}^{n} \theta_i = 1$, *and* $\lambda_j > 0$, $\sum_{j=1}^{n} \lambda_j = 1$.

Proof. As we know that

$$\sqrt{\prod_{j=1}^{m}\left(\prod_{i=1}^{n}\left(1+\alpha_{\breve{d}_{ij}}^{2}\right)^{\theta_i}\right)^{\lambda_j}+\prod_{j=1}^{m}\left(\prod_{i=1}^{n}\left(1-\alpha_{\breve{d}_{ij}}^{2}\right)^{\theta_i}\right)^{\lambda_j}}\leq\sqrt{\sum_{j=1}^{m}\lambda_j\sum_{i=1}^{n}\theta_i\left(1+a_{\breve{d}_{ij}}^{2}\right)+\sum_{j=1}^{m}\lambda_j\sum_{i=1}^{n}\theta_i\left(1-a_{\breve{d}_{ij}}^{2}\right)}$$

$$\sqrt{\sum_{j=1}^{m}\lambda_j\sum_{i=1}^{n}\theta_i\left(1+a_{\breve{d}_{ij}}^{2}\right)+\sum_{j=1}^{m}\lambda_j\sum_{i=1}^{n}\theta_i\left(1-a_{\breve{d}_{ij}}^{2}\right)}=\sqrt{2}$$

$$\sqrt{\prod_{j=1}^{m}\left(\prod_{i=1}^{n}\left(1+a_{\breve{d}_{ij}}^{2}\right)^{\theta_i)}\right)^{\lambda_j}+\prod_{j=1}^{m}\left(\prod_{i=1}^{n}\left(1-a_{\breve{d}_{ij}}^{2}\right)^{\theta_i}\right)^{\lambda_j}}\leq\sqrt{2} \tag{25}$$

$$\frac{\sqrt{\prod_{j=1}^{m}\left(\prod_{i=1}^{n}\left(1+a_{\breve{d}_{ij}}^{2}\right)^{\theta_i}\right)^{\lambda_j}-\prod_{j=1}^{m}\left(\prod_{i=1}^{n}\left(1-a_{\breve{d}_{ij}}^{2}\right)^{\theta_i}\right)^{\lambda_j}}}{\sqrt{\prod_{j=1}^{m}\left(\prod_{i=1}^{n}\left(1+a_{\breve{d}_{ij}}^{2}\right)^{\theta_i}\right)^{\lambda_j}+\prod_{j=1}^{m}\left(\prod_{i=1}^{n}\left(1-a_{\breve{d}_{ij}}^{2}\right)^{\theta_i}\right)^{\lambda_j}}}\leq\sqrt{1-\prod_{j=1}^{m}\left(\prod_{i=1}^{n}\left(1-a_{\breve{d}_{ij}}^{2}\right)^{\theta_i}\right)^{\lambda_j}},$$

again

$$\sqrt{\prod_{j=1}^{m}\left(\prod_{i=1}^{n}\left(2-b_{\breve{d}_{ij}}^{2}\right)^{\theta_i}\right)^{\lambda_j}+\prod_{j=1}^{m}\left(\prod_{i=1}^{n}\left(b_{\breve{d}_{ij}}^{2}\right)^{\theta_i}\right)^{\lambda_j}}\leq\sqrt{\sum_{j=1}^{m}\lambda_j\sum_{i=1}^{n}\theta_i\left(2-b_{\breve{d}_{ij}}^{2}\right)+\sum_{j=1}^{m}\lambda_j\sum_{i=1}^{n}\theta_i\left(b_{\breve{d}_{ij}}^{2}\right)}$$

$$\sqrt{\sum_{j=1}^{m}\lambda_j\sum_{i=1}^{n}\theta_i\left(2-b_{\breve{d}_{ij}}^{2}\right)+\sum_{j=1}^{m}\lambda_j\sum_{i=1}^{n}\theta_i\left(b_{\breve{d}_{ij}}^{2}\right)}\leq\sqrt{2}$$

$$\sqrt{\prod_{j=1}^{m}\left(\prod_{i=1}^{n}\left(2-b_{\breve{d}_{ij}}^{2}\right)^{\theta_i}\right)^{\lambda_j}+\prod_{j=1}^{m}\left(\prod_{i=1}^{n}\left(b_{\breve{d}_{ij}}^{2}\right)^{\theta_i}\right)^{\lambda_j}}\leq\sqrt{2} \tag{26}$$

$$\frac{\sqrt{2\prod_{j=1}^{m}\left(\prod_{i=1}^{n}\left(b_{\breve{d}_{ij}}^{2}\right)^{\theta_i}\right)^{\lambda_j}}}{\sqrt{\prod_{j=1}^{m}\left(\prod_{i=1}^{n}\left(2-b_{\breve{d}_{ij}}^{2}\right)^{\theta_i}\right)^{\lambda_j}+\prod_{j=1}^{m}\left(\prod_{i=1}^{n}\left(b_{\breve{d}_{ij}}^{2}\right)^{\theta_i}\right)\Big)^{\lambda_j}}}\geq\prod_{j=1}^{m}\left(\prod_{i=1}^{n}\left(b_{\breve{d}_{ij}}\right)^{\theta_i}\right)^{\lambda_j}.$$

Let $PFHSWA(\mathfrak{F}_{\breve{d}_{11}},\mathfrak{F}_{\breve{d}_{12}},\ldots,\mathfrak{F}_{\breve{d}_{nm}})=\mathfrak{F}_{\breve{d}_k}=(a_{\mathfrak{F}_{\breve{d}_k}},b_{\mathfrak{F}_{\breve{d}_k}})$ and PFHSEWA $(\mathfrak{F}_{\breve{d}_{11}},\mathfrak{F}_{\breve{d}_{12}},\ldots,\mathfrak{F}_{\breve{d}_{nm}})=\mathfrak{F}_{\breve{d}_k}^{\varepsilon}=(a_{\mathfrak{F}_{\breve{d}_k}^{\varepsilon}},b_{\mathfrak{F}_{\breve{d}_k}^{\varepsilon}})$. Then, inequalities (A) and (B) can be transformed into the forms $a_{\mathfrak{F}_{\breve{d}_k}}\geq a_{\mathfrak{F}_{\breve{d}_k}^{\varepsilon}}$ and $b_{\mathfrak{F}_{\breve{d}_k}}\leq b_{\mathfrak{F}_{\breve{d}_k}^{\varepsilon}}$ respectively. So, $S(\mathfrak{F}_{\breve{d}_k})=a_{\mathfrak{F}_{\breve{d}_k}}^{2}-b_{\mathfrak{F}_{\breve{d}_k}}^{2}\geq a_{\mathfrak{F}_{\breve{d}_k}^{\varepsilon}}^{2}-b_{\mathfrak{F}_{\breve{d}_k}^{\varepsilon}}^{2}=S(\mathscr{H}^{\varepsilon})$. Hence, $S(\mathfrak{F}_{\breve{d}_k})\geq S(\mathfrak{F}_{\breve{d}_k}^{\varepsilon})$.

If $SS(\mathfrak{F}_{\breve{d}_k})>S(\mathfrak{F}_{\breve{d}_k}^{\varepsilon})$, then $PFHSWA(\mathfrak{F}_{\breve{d}_{11}},\mathfrak{F}_{\breve{d}_{12}},\ldots,\mathfrak{F}_{\breve{d}_{nm}})>PFHSEWA(\mathfrak{F}_{\breve{d}_{11}},\mathfrak{F}_{\breve{d}_{12}},\ldots,\mathfrak{F}_{\breve{d}_{nm}})$ (C).

If $S(\mathfrak{F}_{\breve{d}_k})=S(\mathfrak{F}_{\breve{d}_k}^{\varepsilon})$, then $S(\mathfrak{F}_{\breve{d}_k})=a_{\mathfrak{F}_{\breve{d}_k}}^{2}-b_{\mathfrak{F}_{\breve{d}_k}}^{2}=a_{\mathfrak{F}_{\breve{d}_k}^{\varepsilon}}^{2}-b_{\mathfrak{F}_{\breve{d}_k}^{\varepsilon}}^{2}=S(\mathfrak{F}_{\breve{d}_k}^{\varepsilon})$.

So, $a_{\mathfrak{F}_{\breve{d}_k}}=a_{\mathfrak{F}_{\breve{d}_k}^{\varepsilon}}$ and $b_{\mathfrak{F}_{\breve{d}_k}}=b_{\mathfrak{F}_{\breve{d}_k}^{\varepsilon}}$; then, by accuracy function, $A(\mathfrak{F}_{\breve{d}_k})=a_{\mathfrak{F}_{\breve{d}_k}}^{2}+b_{\mathfrak{F}_{\breve{d}_k}}^{2}=a_{\mathfrak{F}_{\breve{d}_k}^{\varepsilon}}^{2}+b_{\mathfrak{F}_{\breve{d}_k}^{\varepsilon}}^{2}=A(\mathfrak{F}_{\breve{d}_k}^{\varepsilon})$. Thus, $PFHSWA(\mathfrak{F}_{\breve{d}_{11}},\mathfrak{F}_{\breve{d}_{12}},\ldots,\mathfrak{F}_{\breve{d}_{nm}})>PFHSEWA(\mathfrak{F}_{\breve{d}_{11}},\mathfrak{F}_{\breve{d}_{12}},\ldots,\mathfrak{F}_{\breve{d}_{nm}})$(D).

From (C) and (D), we get $PFHSWA(\mathfrak{F}_{\breve{d}_{11}},\mathfrak{F}_{\breve{d}_{12}},\ldots,\mathfrak{F}_{\breve{d}_{nm}})>PFHSEWA(\mathfrak{F}_{\breve{d}_{11}},\mathfrak{F}_{\breve{d}_{12}},\ldots,\mathfrak{F}_{\breve{d}_{nm}})$. □

3.3. Example. Using the data given in example 3.1,

$$PFHSWA\left(\mathfrak{F}_{\check{d}_{11}}, \mathfrak{F}_{\check{d}_{12}}, \ldots, \mathfrak{F}_{\check{d}_{44}}\right) = \left\langle \sqrt{1 - \prod_{j=1}^{4}\left(\prod_{i=1}^{4}\left(1-\alpha_{\check{d}_{ij}}^{2}\right)^{\theta_i}\right)^{\lambda_j}}, \prod_{j=1}^{4}\left(\prod_{i=1}^{4}\left(b_{\check{d}_{ij}}\right)^{\theta_i}\right)^{\lambda_j} \right\rangle$$

$$PFHSWA\left(\mathfrak{F}_{\check{d}_{11}}, \mathfrak{F}_{\check{d}_{12}}, \ldots, \mathfrak{F}_{\check{d}_{44}}\right) = \left\langle \sqrt{1 - \begin{bmatrix} \left\{(0.75)^{0.1}(0.75)^{0.3}(0.84)^{0.3}(0.91)^{0.3}\right\}^{0.2}\left\{(0.51)^{0.1}(0.19)^{0.3}(0.51)^{0.3}(0.64)^{0.3}\right\}^{0.2} \\ \left\{(0.84)^{0.1}(0.91)^{0.3}(0.84)^{0.3}(0.75)^{0.3}\right\}^{0.2}\left\{(0.51)^{0.1}(0.84)^{0.3}(0.91)^{0.3}(0.75)^{0.3}\right\}^{0.4} \end{bmatrix}}, \right.$$
$$\left. \begin{pmatrix} \left\{(0.8)^{0.1}(0.6)^{0.3}(0.8)^{0.3}(0.7)^{0.3}\right\}^{0.2}\left\{(0.5)^{0.1}(0.1)^{0.3}(0.5)^{0.3}(0.5)^{0.3}\right\}^{0.2} \\ \left\{(0.6)^{0.1}(0.7)^{0.3}(0.6)^{0.3}(0.4)^{0.3}\right\}^{0.2}\left\{(0.4)^{0.1}(0.5)^{0.3}(0.5)^{0.3}(0.7)^{0.3}\right\}^{0.4} \end{pmatrix} \right\rangle$$
$$= \left\langle \sqrt{1 - [(0.9616)(0.8350)(0.9638)(0.9105)]}, ((0.9324)(0.7904)(0.8893)(0.7820)) \right\rangle$$
$$= \langle 0.5404, 0.5125 \rangle. \tag{27}$$

Hence, from examples 3.1 and 3.2, it is proved that $PFHSWA(\mathfrak{F}_{\check{d}_{11}}, \mathfrak{F}_{\check{d}_{12}}, \ldots, \mathfrak{F}_{\check{d}_{nm}}) > PFHSEWA(\mathfrak{F}_{\check{d}_{11}}, \mathfrak{F}_{\check{d}_{12}}, \ldots, \mathfrak{F}_{\check{d}_{nm}})$.

3.4. Properties of PFHSEWA Operator

3.4.1. Idempotency. If $\mathfrak{F}_{\check{d}_{ij}} = \mathfrak{F}_{\check{d}_k} = (a_{\check{d}_{ij}}, b_{\check{d}_{ij}})$ $\forall i, j$, then PFHSEWA $(\mathfrak{F}_{\check{d}_{11}}, \mathfrak{F}_{\check{d}_{12}}, \ldots, \mathfrak{F}_{\check{d}_{nm}}) = \mathfrak{F}_{\check{d}_k}$.

Proof. We know that

$$PFHSEWA\left(\mathfrak{F}_{\check{d}_{11}}, \mathfrak{F}_{\check{d}_{12}}, \ldots, \mathfrak{F}_{\check{d}_{nm}}\right)$$
$$= \left\langle \frac{\sqrt{\prod_{j=1}^{m}\left(\prod_{i=1}^{n}\left(1+\alpha_{\check{d}_{ij}}^{2}\right)^{\theta_i}\right)^{\lambda_j} - \prod_{j=1}^{m}\left(\prod_{i=1}^{n}\left(1-\alpha_{\check{d}_{ij}}^{2}\right)^{\theta_i}\right)^{\lambda_j}}}{\sqrt{\prod_{j=1}^{m}\left(\prod_{i=1}^{n}\left(1+\alpha_{\check{d}_{ij}}^{2}\right)^{\theta_i}\right)^{\lambda_j} + \prod_{j=1}^{m}\left(\prod_{i=1}^{n}\left(1-\alpha_{\check{d}_{ij}}^{2}\right)^{\theta_i}\right)^{\lambda_j}}}, \frac{\sqrt{2\prod_{j=1}^{m}\left(\prod_{i=1}^{n}\left(b_{\check{d}_{ij}}^{2}\right)^{\theta_i}\right)^{\lambda_j}}}{\sqrt{\prod_{j=1}^{m}\left(\prod_{i=1}^{n}\left(2-b_{\check{d}_{ij}}^{2}\right)^{\theta_i}\right)^{\lambda_j} + \prod_{j=1}^{m}\left(\prod_{i=1}^{n}\left(b_{\check{d}_{ij}}^{2}\right)^{\theta_i}\right)^{\lambda_j}}} \right\rangle$$
$$= \left\langle \frac{\sqrt{\left(\left(1+\alpha_{\check{d}_{ij}}^{2}\right)^{\sum_{i=1}^{n}\theta_i}\right)^{\sum_{j=1}^{m}\lambda_j} - \left(\left(1-\alpha_{\check{d}_{ij}}^{2}\right)^{\sum_{i=1}^{n}\theta_i}\right)^{\sum_{j=1}^{m}\lambda_j}}}{\sqrt{\left(\left(1+\alpha_{\check{d}_{ij}}^{2}\right)^{\sum_{i=1}^{n}\theta_i}\right)^{\sum_{j=1}^{m}\lambda_j} + \left(\left(1-\alpha_{\check{d}_{ij}}^{2}\right)^{\sum_{i=1}^{n}\theta_i}\right)^{\sum_{j=1}^{m}\lambda_j}}}, \frac{\sqrt{2\left(\left(b_{\check{d}_{ij}}^{2}\right)^{\sum_{i=1}^{n}\theta_i}\right)^{\sum_{j=1}^{m}\lambda_j}}}{\sqrt{\left(\left(2-b_{\check{d}_{ij}}^{2}\right)^{\sum_{i=1}^{n}\theta_i}\right)^{\sum_{j=1}^{m}\lambda_j} + \left(\left(b_{\check{d}_{ij}}^{2}\right)^{\sum_{i=1}^{n}\theta_i}\right)^{\sum_{j=1}^{m}\lambda_j}}} \right\rangle$$
$$= \frac{\sqrt{\left(1+\alpha_{\check{d}_{ij}}^{2}\right) - \left(1-\alpha_{\check{d}_{ij}}^{2}\right)}}{\sqrt{\left(1+\alpha_{\check{d}_{ij}}^{2}\right) + \left(1-\alpha_{\check{d}_{ij}}^{2}\right)}}, \frac{\sqrt{2b_{\check{d}_{ij}}^{2}}}{\sqrt{\left(2-b_{\check{d}_{ij}}^{2}\right) + \left(b_{\check{d}_{ij}}^{2}\right)}}$$
$$= a_{\check{d}_{ij}}, b_{\check{d}_{ij}}$$
$$= \mathfrak{F}_{\check{d}_k}. \tag{28}$$

□

3.4.2. Boundedness. Let $\mathfrak{F}_{\check{d}_{ij}} = (a_{\check{d}_{ij}}, b_{\check{d}_{ij}})$ be a Collection PFHSNs and $\mathfrak{F}_{\min} = \min(\mathfrak{F}_{\check{d}_{ij}})\mathfrak{F}_{\max} = \max(\mathfrak{F}_{\check{d}_{ij}})$. Then, $\mathfrak{F}_{\min} \le PFHSEWA \le (\mathfrak{F}_{\check{d}_{11}}, \mathfrak{F}_{\check{d}_{12}}, \ldots, \mathfrak{F}_{\check{d}_{nm}}) \le \mathfrak{F}_{\max}$.

Proof. Let $g(y) = \sqrt{1 - y^2/1 + y^2}, y \in 0, 1]]$, then $(d/dy)(g(y)) = (-2y/(1+y^2)^2)\sqrt{1+y^2/1-y^2} < 0$ which shows that $g(y)$ is decreasing function on $0, 1]]$. So,

$a_{\min} \le a_{ij} \le a_{\max}, \forall i, j$. Hence, $g(a_{\max}) \le g(a_{\breve{d}_{ij}}) \le g(a_{\min}), \forall i, j$

$\Rightarrow \sqrt{1 - a_{\max}^2/1 + a_{\max}^2} \le \sqrt{1 - a_{\breve{d}_{ij}}^2/1 + a_{\breve{d}_{ij}}^2} \le \sqrt{1 - a_{\min}^2/1 + a_{\min}^2}$, $(i = 1, 2, \ldots, n)$ and $(j = 1, 2, \ldots, m)$.

Let θ_i and λ_j represent the weight vectors such as $\theta_i > 0$, $\sum_{i=1}^{n} \theta_i = 1$, and $\lambda_j > 0$, $\sum_{j=1}^{n} \lambda_j = 1$. We have

$$
\begin{aligned}
&\Leftrightarrow \sqrt{\prod_{j=1}^{m}\left(\prod_{i=1}^{n}\left(1 - a_{\max}^2/1 + a_{\max}^2\right)^{\theta_i}\right)^{\lambda_j}} \le \sqrt{\prod_{j=1}^{m}\left(\prod_{i=1}^{n}\left(1 - a_{\breve{d}_{ij}}^2/1 + a_{\breve{d}_{ij}}^2\right)^{\theta_i}\right)^{\lambda_j}} \le \sqrt{\prod_{j=1}^{m}\left(\prod_{i=1}^{n}\left(1 - a_{\min}^2/1 + a_{\min}^2\right)^{\theta_i}\right)^{\lambda_j}} \\
&\Leftrightarrow \sqrt{\left(\left(1 - a_{\max}^2/1 + a_{\max}^2\right)^{\sum_{i=1}^{n}\theta_i}\right)^{\sum_{j=1}^{m}\lambda_j}} \le \sqrt{\prod_{j=1}^{m}\left(\prod_{i=1}^{n}\left(1 - a_{\breve{d}_{ij}}^2/1 + a_{\breve{d}_{ij}}^2\right)^{\theta_i}\right)^{\lambda_j}} \le \sqrt{\left(\left(1 - a_{\min}^2/1 + a_{\min}^2\right)^{\sum_{i=1}^{n}\theta_i}\right)^{\sum_{j=1}^{m}\lambda_j}} \\
&\Leftrightarrow \sqrt{1 + \left(\frac{1 - a_{\max}^2}{1 + a_{\max}^2}\right)} \le \sqrt{1 + \prod_{j=1}^{m}\left(\prod_{i=1}^{n}\left(1 - a_{\breve{d}_{ij}}^2/1 + a_{\breve{d}_{ij}}^2\right)^{\theta_i}\right)^{\lambda_j}} \le \sqrt{1 + \left(\frac{1 - a_{\min}^2}{1 + a_{\min}^2}\right)} \\
&\Leftrightarrow \sqrt{\frac{2}{1 + a_{\max}^2}} \le \sqrt{1 + \prod_{j=1}^{m}\left(\prod_{i=1}^{n}\left(1 - a_{\breve{d}_{ij}}^2/1 + a_{\breve{d}_{ij}}^2\right)^{\theta_i}\right)^{\lambda_j}} \le \sqrt{\frac{2}{1 + a_{\min}^2}} \\
&\Leftrightarrow \sqrt{\frac{1 + a_{\min}^2}{2}} \le \left(\frac{1}{\sqrt{1 + \prod_{j=1}^{m}\left(\prod_{i=1}^{n}\left(1 - a_{\breve{d}_{ij}}^2/1 + a_{\breve{d}_{ij}}^2\right)^{\theta_i}\right)^{\lambda_j}}}\right) \le \sqrt{\frac{1 + a_{\max}^2}{2}} \\
&\Leftrightarrow \sqrt{1 + a_{\min}^2} \le \sqrt{\frac{2}{1 + \prod_{j=1}^{m}\left(\prod_{i=1}^{n}\left(1 - a_{\breve{d}_{ij}}^2/1 + a_{\breve{d}_{ij}}^2\right)^{\theta_i}\right)^{\lambda_j}}} \le \sqrt{1 + a_{\max}^2} \\
&\Leftrightarrow \sqrt{1 + a_{\min}^2 - 1} \le \sqrt{\frac{2}{1 + \prod_{j=1}^{m}\left(\prod_{i=1}^{n}\left(1 - a_{\breve{d}_{ij}}^2/1 + a_{\breve{d}_{ij}}^2\right)^{\theta_i}\right)^{\lambda_j}} - 1} \le \sqrt{1 + a_{\max}^2 - 1} \\
&\Leftrightarrow \sqrt{a_{\min}^2} \le \sqrt{\frac{2}{1 + \prod_{j=1}^{m}\left(\prod_{i=1}^{n}\left(1 - a_{\breve{d}_{ij}}^2/1 + a_{\breve{d}_{ij}}^2\right)^{\theta_i}\right)^{\lambda_j}} - 1} \le \sqrt{a_{\max}^2} \\
&\Leftrightarrow a_{\min} \le \sqrt{\frac{2}{1 + \prod_{j=1}^{m}\left(\prod_{i=1}^{n}\left(1 - a_{\breve{d}_{ij}}^2/1 + a_{\breve{d}_{ij}}^2\right)^{\theta_i}\right)^{\lambda_j}} - 1} \le a_{\max} \\
&a_{\min} \le \frac{\sqrt{\prod_{j=1}^{m}\left(\prod_{i=1}^{n}\left(1 + a_{\breve{d}_{ij}}^2\right)^{\theta_i}\right)^{\lambda_j} - \prod_{j=1}^{m}\left(\prod_{i=1}^{n}\left(1 - a_{\breve{d}_{ij}}^2\right)^{\theta_i}\right)^{\lambda_j}}}{\sqrt{\prod_{j=1}^{m}\left(\prod_{i=1}^{n}\left(1 + a_{\breve{d}_{ij}}^2\right)^{\theta_i}\right)^{\lambda_j} + \prod_{j=1}^{m}\left(\prod_{i=1}^{n}\left(1 - a_{\breve{d}_{ij}}^2\right)^{\theta_i}\right)^{\lambda_j}}} \le a_{\max}.
\end{aligned}
\tag{29}
$$

Let $f(x) = \sqrt{2 - x^2/x^2}$, $x \in 0, 1]]$, then $(d/dx)(f(x)) = (-2/x^3)\sqrt{x^2/2 - x^2} < 0$. So, $f(x)$ is decreasing function on $0, 1]]$. Since $b_{\min} \le b_{ij} \le b_{\max}$, $\forall i, j$, then $f(b_{\max}) \le f(b_{ij}) \le f(b_{\min})$. So, $\sqrt{(2 - b_{\max}^2/b_{\max}^2)} \le \sqrt{2 - b_{\breve{d}_{ij}}^2/b_{\breve{d}_{ij}}^2} \le \sqrt{(2 - b_{\min}^2/b_{\min}^2)}$, $(i = 1, 2, \ldots, n)$ and $(j = 1, 2, \ldots, m)$. Let θ_i and λ_j represent the weight vectors such as $\theta_i > 0$, $\sum_{i=1}^{n} \theta_i = 1$, and $\lambda_j > 0$, $\sum_{j=1}^{n} \lambda_j = 1$. We have

$$
\begin{aligned}
&\Leftrightarrow \sqrt{\prod_{j=1}^{m}\left(\prod_{i=1}^{n}\left(2 - b_{\max}^2/b_{\max}^2\right)^{\theta_i}\right)^{\lambda_j}} \le \sqrt{\prod_{j=1}^{m}\left(\prod_{i=1}^{n}\left(2 - b_{\breve{d}_{ij}}^2/b_{\breve{d}_{ij}}^2\right)^{\theta_i}\right)^{\lambda_j}} \le \sqrt{\prod_{j=1}^{m}\left(\prod_{i=1}^{n}\left(2 - b_{\min}^2/b_{\min}^2\right)^{\theta_i}\right)^{\lambda_j}} \\
&\Leftrightarrow \sqrt{\left(\left(2 - b_{\max}^2/b_{\max}^2\right)^{\sum_{i=1}^{n}\theta_i}\right)^{\sum_{j=1}^{m}\lambda_j}} \le \sqrt{\prod_{j=1}^{m}\left(\prod_{i=1}^{n}\left(2 - b_{\breve{d}_{ij}}^2/b_{\breve{d}_{ij}}^2\right)^{\theta_i}\right)^{\lambda_j}} \le \sqrt{\left(\left(2 - b_{min}^2/b_{min}^2\right)^{\sum_{i=1}^{n}\theta_i}\right)^{\sum_{j=1}^{m}\lambda_j}} \\
&\Leftrightarrow \sqrt{1 + \frac{2 - b_{\max}^2}{b_{\max}^2}} \le \sqrt{1 + \prod_{j=1}^{m}\left(\prod_{i=1}^{n}\left(2 - b_{\breve{d}_{ij}}^2/b_{\breve{d}_{ij}}^2\right)^{\theta_i}\right)^{\lambda_j}} \le \sqrt{1 + \frac{2 - b_{\min}^2}{b_{\min}^2}} \\
&\Leftrightarrow \sqrt{\frac{2}{b_{\max}^2}} \le \sqrt{1 + \prod_{j=1}^{m}\left(\prod_{i=1}^{n}\left(2 - b_{\breve{d}_{ij}}^2/b_{\breve{d}_{ij}}^2\right)^{\theta_i}\right)^{\lambda_j}} \le \sqrt{\frac{2}{b_{\min}^2}} \\
&\Leftrightarrow \sqrt{\frac{b_{\min}^2}{2}} \le \frac{1}{\sqrt{1 + \prod_{j=1}^{m}\left(\prod_{i=1}^{n}\left(2 - b_{\breve{d}_{ij}}^2/b_{\breve{d}_{ij}}^2\right)^{\theta_i}\right)^{\lambda_j}}} \le \sqrt{b_{\max}^2/2} \\
&\Leftrightarrow b_{\min} \le \sqrt{\frac{2}{1 + \prod_{j=1}^{m}\left(\prod_{i=1}^{n}\left(2 - b_{\breve{d}_{ij}}^2/b_{\breve{d}_{ij}}^2\right)^{\theta_i}\right)^{\lambda_j}}} \le b_{\max} \\
&b_{\min} \le \frac{\sqrt{2\prod_{j=1}^{m}\left(\prod_{i=1}^{n}\left(b_{\breve{d}_{ij}}^2\right)^{\theta_i}\right)^{\lambda_j}}}{\sqrt{\prod_{j=1}^{m}\left(\prod_{i=1}^{n}\left(2 - b_{\breve{d}_{ij}}^2\right)^{\theta_i}\right)^{\lambda_j} + \prod_{j=1}^{m}\left(\prod_{i=1}^{n}\left(b_{\breve{d}_{ij}}^2\right)^{\theta_i}\right)^{\lambda_j}}} \le b_{\max}.
\end{aligned}
\tag{30}
$$

Let $PFHSEWA(\mathfrak{F}_{\breve{d}_{11}}, \mathfrak{F}_{\breve{d}_{12}}, \ldots, \mathfrak{F}_{\breve{d}_{nm}}) = \mathfrak{F}_{\breve{d}_k}$. Then, inequalities (E) and (F) can be written as $a_{\min} \le a \le a_{\max}$ and $b_{\min} \le b \le b_{\max}$. Thus, $S(\mathfrak{F}_{\breve{d}_k}) = a^2 - b^2 \le a_{\max}^2 - b_{\min}^2 = S(\mathfrak{F}_{\breve{d}_k^{\max}})$ and $S(S(\mathfrak{F}_{\breve{d}_k}) = a^2 - b^2 \ge a_{\min}^2 - b_{\max}^2 = S(\mathfrak{F}_{\breve{d}_k^{\min}})$.

If $S(\mathfrak{F}_{\breve{d}_k}) < S(\mathfrak{F}_{\breve{d}_k^{\max}})$ and $S(\mathfrak{F}_{\breve{d}_k}) > S(\mathfrak{F}_{\breve{d}_k^{\min}})$, then we have

$$
\mathfrak{F}_{\breve{d}_k^{\min}} < PFHSEWA\left(\mathfrak{F}_{\breve{d}_{11}}, \mathfrak{F}_{\breve{d}_{12}}, ..., \mathfrak{F}_{\breve{d}_{nm}}\right) < \mathfrak{F}_{\breve{d}_k^{\min}}, \tag{31}
$$

If $S(\mathfrak{F}_{\breve{d}_k}) = S(\mathfrak{F}_{\breve{d}_k^{\max}})$, then we have $a^2 = a_{\max}^2$ and $b^2 = b_{\max}^2$. Thus, $S(\mathfrak{F}_{\breve{d}_k}) = a^2 - b^2 == a_{\max}^2 - b_{\max}^2 = S(\mathfrak{F}_{\breve{d}_k^{\max}})$. Therefore,

$$
PFHSEWA\left(\mathfrak{F}_{\breve{d}_{11}}, \mathfrak{F}_{\breve{d}_{12}}, \ldots, \mathfrak{F}_{\breve{d}_{nm}}\right) = \mathfrak{F}_{\breve{d}_k^{\max}}. \tag{32}
$$

If $S(\mathfrak{F}_{\breve{d}_k}) = S(\mathfrak{F}_{\breve{d}_k \min})$, then we have $a^2 - b^2 = a_{\min}^2 - b_{\min}^2 \Rightarrow a^2 = a_{\min}^2$ and $b^2 = b_{\min}^2$.

Thus, $A(\mathfrak{F}_{\breve{d}_k}) = a^2 + b^2 = a_{\min}^2 + b_{\min}^2 = A(\mathfrak{F}_{\breve{d}_k^{\min}})$. So,

$$
PFHSEWA\left(\mathfrak{F}_{\breve{d}_{11}}, \mathfrak{F}_{\breve{d}_{12}}, \ldots, \mathfrak{F}_{\breve{d}_{nm}}\right) = \mathfrak{F}_{\breve{d}_k^{\min}}. \tag{33}
$$

$$
\mathfrak{F}_{\breve{d}_k^{\min}} \le PFHSEWA(\mathfrak{F}_{\breve{d}_{11}}, \mathfrak{F}_{\breve{d}_{12}}, \ldots, \mathfrak{F}_{\breve{d}_{nm}}) \le \mathfrak{F}_{\breve{d}_k^{\max}}. \quad \square
$$

3.4.3. Homogeneity. Prove that $PFHSEWA(\mathfrak{F}_{\breve{d}_{11}}, \mathfrak{F}_{\breve{d}_{12}}, \ldots, \mathfrak{F}_{\breve{d}_{nm}}) = \partial P\ FHSEWA(\mathfrak{F}_{\breve{d}_{11}}, \mathfrak{F}_{\breve{d}_{12}}, \ldots, \mathfrak{F}_{\breve{d}_{nm}})$ for $\partial > 0$.

Proof. Let $\mathfrak{F}_{\breve{d}_{ij}}$ be a PFHSN and ∂ is a positive number, then by $\partial\mathfrak{F}_{\breve{d}_{ij}} = (\sqrt{(1+a_{\breve{d}_{ij}}^2)^{\partial} - (1-a_{\breve{d}_{ij}}^2)^{\partial}} / \sqrt{(1+a_{\breve{d}_{ij}}^2)^{\partial} + (1-a_{\breve{d}_{ij}}^2)^{\partial}}), \sqrt{2(b_{\breve{d}_{ij}}^2)^{\partial}} / \sqrt{(2-b_{\breve{d}_{ij}}^2)^{\partial} + (b_{\breve{d}_{ij}}^2)^{\partial}}$. So,

$$
\begin{aligned}
&PFHSEWA\left(\partial\mathfrak{F}_{\breve{d}_{11}}, \partial\mathfrak{F}_{\breve{d}_{12}} \partial\mathfrak{F}_{\breve{d}_{nm}}\right)\\
&= \left\langle \frac{\sqrt{\prod_{j=1}^{m}\left(\prod_{i=1}^{n}\left(1+\alpha_{\breve{d}_{ij}}^2\right)^{\theta_i}\right)^{\lambda_j} - \prod_{j=1}^{m}\left(\prod_{i=1}^{n}\left(1-\alpha_{\breve{d}_{ij}}^2\right)^{\theta_i}\right)^{\lambda_j}}}{\sqrt{\prod_{j=1}^{m}\left(\prod_{i=1}^{n}\left(1+\alpha_{\breve{d}_{ij}}^2\right)^{\theta_i}\right)^{\lambda_j} + \prod_{j=1}^{m}\left(\prod_{i=1}^{n}\left(1-\alpha_{\breve{d}_{ij}}^2\right)^{\theta_i}\right)^{\lambda_j}}}, \frac{\sqrt{2\prod_{j=1}^{m}\left(\prod_{i=1}^{n}\left(b_{\breve{d}_{ij}}^2\right)^{\theta_i}\right)^{\lambda_j}}}{\sqrt{\prod_{j=1}^{m}\left(\prod_{i=1}^{n}\left(2-b_{\breve{d}_{ij}}^2\right)^{\theta_i}\right)^{\lambda_j} + \prod_{j=1}^{m}\left(\prod_{i=1}^{n}\left(b_{\breve{d}_{ij}}^2\right)^{\theta_i}\right)^{\lambda_j}}} \right\rangle\\
&= \left\langle \frac{\sqrt{\left(\prod_{j=1}^{m}\left(\prod_{i=1}^{n}\left(1+\alpha_{\breve{d}_{ij}}^2\right)^{\theta_i}\right)^{\lambda_j}\right)^{\partial} - \left(\prod_{j=1}^{m}\left(\prod_{i=1}^{n}\left(1-\alpha_{\breve{d}_{ij}}^2\right)^{\theta_i}\right)^{\lambda_j}\right)^{\partial}}}{\sqrt{\left(\prod_{j=1}^{m}\left(\prod_{i=1}^{n}\left(1+\alpha_{\breve{d}_{ij}}^2\right)^{\theta_i}\right)^{\lambda_j}\right)^{\partial} + \left(\prod_{j=1}^{m}\left(\prod_{i=1}^{n}\left(1-\alpha_{\breve{d}_{ij}}^2\right)^{\theta_i}\right)^{\lambda_j}\right)^{\partial}}}, \frac{\sqrt{\left(2\prod_{j=1}^{m}\left(\prod_{i=1}^{n}\left(b_{\breve{d}_{ij}}^2\right)^{\theta_i}\right)^{\lambda_j}\right)^{\partial}}}{\sqrt{\left(\prod_{j=1}^{m}\left(\prod_{i=1}^{n}\left(2-b_{\breve{d}_{ij}}^2\right)^{\theta_i}\right)^{\lambda_j}\right)^{\partial} + \left(\prod_{j=1}^{m}\left(\prod_{i=1}^{n}\left(b_{\breve{d}_{ij}}^2\right)^{\theta_i}\right)^{\lambda_j}\right)^{\partial}}} \right\rangle\\
&= PFHSEWA\left(\mathfrak{F}_{\breve{d}_{11}}, \mathfrak{F}_{\breve{d}_{12}} \mathfrak{F}_{\breve{d}_{nm}}\right).
\end{aligned}
\tag{34}
$$

□

4. Novel Multicriteria Decision-Making Approach

This section has developed a DM approach for solving MCDM problems based on the proposed PFHSEWA operator and numerical examples.

4.1. Proposed Approach. Consider $\mathfrak{H} = \{\mathfrak{H}^1, \mathfrak{H}^2, \mathfrak{H}^3, \ldots, \mathfrak{H}^s\}$ be a set of alternatives and $O = \{O_1, O_2, O_3, \ldots, O_r\}$ be a set of experts. The weights of experts are given as $\theta = (\theta_1, \theta_2, \theta_3, \ldots, \theta_n)^T$ such that $\theta_i > 0$, $\sum_{i=1}^{n}\theta_i = 1$. Let L= $\{d_1, d_2, \ldots, d_m\}$ express the set of attributes with their corresponding multi-sub-attributes such as $\mathfrak{L}' = \{(d_{1\rho} \times d_{2\rho} \times \ldots \times d_{m\rho}) \text{ for all } \rho \in \{1, 2, \ldots, t\}\}$ with weights $\theta = (\theta_1, \theta_2, \theta_3, \ldots, \theta_n)^T$ such that $\theta_i > 0$, $\sum_{i=1}^{n}\theta_i = 1$, and can be stated as $\mathfrak{L}' = \{\breve{d}_{\partial} : \partial \in \{1, 2, \ldots, m\}\}$. The group of experts $\{\kappa^i, i = 1, 2, \ldots, n\}$ assess the alternatives $\{\mathfrak{H}^{(z)}, z = 1, 2, \ldots S\}$ under the chosen subattributes $\{\breve{d}_{\partial}, \partial = 1, 2, \ldots, k\}$ in the form of PFHSNs such as $(\mathfrak{H}_{\breve{d}_{ik}}^{(z)})_{n\times m} = (\alpha_{\breve{d}_{ij}}, b_{\breve{d}_{ij}})_{n*m}$, where $0 \le \alpha_{\breve{d}_{ij}}, b_{\breve{d}_{ij}} \le 1$ and $0 \le (\alpha_{\breve{d}_{ij}})^2 + (b_{\breve{d}_{ij}})^2 \le 1$ for all i, k. The experts provide their opinion in the form of PFHSNs $\mathscr{L}_k$ for each alternative and present the step-wise algorithm to obtain the most suitable alternative.

Step 1. Obtain decision matrices $F = (\mathfrak{F}_{\breve{d}_{ij}})_{n*m}$ in the form of PFHSNs for alternatives relative to attributes.

$$
\left(\mathfrak{H}_{\breve{d}_{ik}}^{(z)}, \mathfrak{L}'\right)_{n\times\partial} = \begin{matrix} O_1 \\ O_2 \\ \vdots \\ O_n \end{matrix} \begin{pmatrix} \left(\alpha_{d_{11}}^{(z)}, b_{d_{11}}^{(z)}\right) & \left(\alpha_{d_{12}}^{(z)}, b_{d_{12}}^{(z)}\right) & \cdots & \left(\alpha_{d_{1\,\partial}}^{(z)}, b_{d_{1\,\partial}}^{(z)}\right) \\ \left(\alpha_{d_{21}}^{(z)}, b_{d_{21}}^{(z)}\right) & \left(\alpha_{d_{22}}^{(z)}, b_{d_{22}}^{(z)}\right) & \cdots & \left(\alpha_{d_{2\,\partial}}^{(z)}, b_{d_{2\,\partial}}^{(z)}\right) \\ \vdots & \vdots & \vdots & \vdots \\ \left(\alpha_{d_{n1}}^{(z)}, b_{d_{n1}}^{(z)}\right) & \left(\alpha_{d_{n2}}^{(z)}, b_{d_{n2}}^{(z)}\right) & \cdots & \left(\alpha_{d_{n\,\partial}}^{(z)}, b_{d_{n\,\partial}}^{(z)}\right) \end{pmatrix}. \tag{35}
$$

Step 2. Use the normalization formula to normalize the decision matrix and convert the rating value of the cost type parameter to the benefit type parameter.

$$
M_{\breve{d}_{ij}} = \begin{cases} \mathfrak{F}_{\breve{d}_{ij}}^{c} = \left(b_{\breve{d}_{ij}}, \alpha_{\breve{d}_{ij}}\right) \text{costtypeparameter}, \\ \mathfrak{F}_{\breve{d}_{ij}} = \left(\alpha_{\breve{d}_{ij}}, b_{\breve{d}_{ij}}\right) \text{benefittypeparameter}. \end{cases} \tag{36}
$$

Step 3. Use the settled PFHSEWA operator to collect the PFHSNs $\mathfrak{F}_{\breve{d}_{ij}}$ for each alternative $\mathfrak{H} = \{\mathfrak{H}^1, \mathfrak{H}^2, \mathfrak{H}^3, \ldots, \mathfrak{H}^s\}$ into the decision matrix $\mathscr{L}_k$.

Step 4. Use equation (1) to calculate the scores for all alternatives.

Step 5. Choose the alternative with the highest score.

Step 6. Rank the alternatives.

The graphical demonstration of the planned model is given in Figure 1.

4.2. Numerical Example. In this section, a practical MCDM problem comprises decisive adequate agricultural models in numerous kinds of farming to confirm that the conventional approach is pertinent and reasonable.

4.2.1. Case Study. Green agriculture claims sustainable growth ideas to farming, such as confirming food production and fiber while preserving financial and societal constrictions to ensure the long-term viability of production. For example, sustainable agriculture diminishes the practice of pesticides that are harmful to the health of agriculturalists and customers. Accuracy farming and intellectual farming

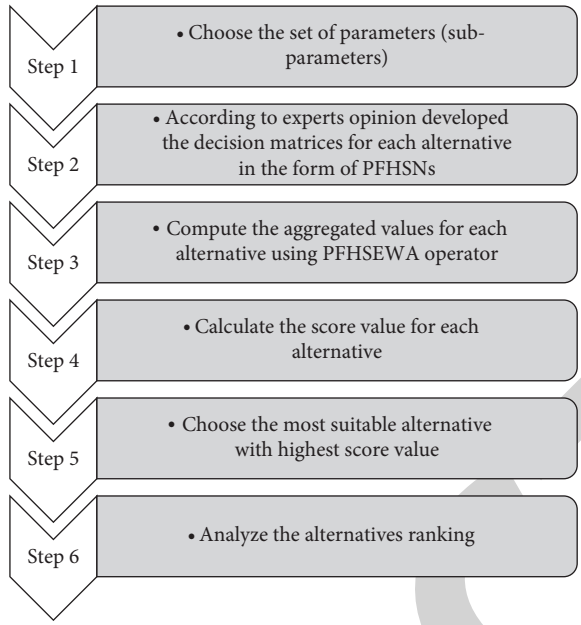

Figure 1: Flowchart of the proposed model.

are the core mechanisms of sustainable farming. Increasing crops and raising livestock are agricultural professions or businesses. Farming comprises raising animals and growing crops, which deliver nutrition and raw ingredients. Agriculture was initiated approximately 5,000 years earlier, but the particular time and source are indefinite. Agriculture is a technique of lifecycle, not just a profession. We are all farmers, and we like farming no matter whether we are at home or in the fields. This love of gardening must be a lifelong practice, regardless of age. Due to this land devastation, food prices will skyrocket, and we will have to pay more for daily food needs. Farmers must focus on increasing production through agricultural robots to get out of this situation. The use of robots in farming is an illustration of inspiration beyond origination. Agriculture, as an industry, will grow into a high-tech sector in the new era. Agribots or agri-robots are other terms for agricultural robots [64]. Five key alternatives are interrelated to sustainable agriculture such as good crop production ($\mathfrak{H}^1$), environmental protection ($\mathfrak{H}^2$), natural resources availability ($\mathfrak{H}^3$), food security and productivity ($\mathfrak{H}^4$), and availability of machines ($\mathfrak{H}^5$). In addition, the abovementioned five alternatives are evaluated using four parameters. The attribute of robotic agriculture is given as follows: $\mathfrak{L}\{d_1 =$ Qualityproduction, $d_2 =$ Completionofatime– consumingproject, $d_3 =$ Consistentroleincompletingaproject, $d_4 =$ Limitingtheneedformanuallabor$\}$. The corresponding subattributes of the considered parameters are Qualityproduction $= d_1 =$ $\{d_{11} =$ High – qualityproduction, $d_{12} =$ Low – qualityproduction$\}\{d_{11} =$ High– qualityproduction, $d_{12} =$ Low – qualityproduction$\}$, Completionofatime – consumingproject $= d_2 = \{d_{21} =$ Shortterm, $d_{22} =$ Longterm$\}=$ $\{d_{21} =$ Shortterm, $d_{22} =$ Long term$\}$, Consistentroleincompletingaproject $= d_3 = \{d_{31} =$ Projectbudgetingandforecasting, $d_{32} =$ Developingariskmanagementplan$\}=$ $\{d_{31} =$ Projectbudgetingandforecasting, $d_{32} =$ Developingariskmanagementplan$\}$, Limiting the need for manual labor $= d_4 = \{d_{41} =$ Limiting the need for manual labor$\}$ $=$ $\{d_{41} =$ Limiting the need for manual labor$\}$. Let $\mathfrak{L}^{'} = d_1 \times d_2 \times d_3 \times d_4$ be a set of subattributes.

$\mathfrak{L}^{'} = d_1 \times d_2 \times d_3 \times d_4 = \{d_{11}, d_{12}\} \times \{d_{21}, d_{22}\} \times \{d_{31}, d_{32}\} \times \{d_{41}\} = \{(d_{11}, d_{21}, d_{31}, d_{41}), (d_{11}, d_{21}, d_{32}, d_{41}), (d_{11}, d_{22}, d_{31}, d_{41}), (d_{11}, d_{22}, d_{32}, d_{41}), (d_{12}, d_{21}, d_{31}, d_{41}), (d_{12}, d_{21}, d_{32}, d_{41}), (d_{12}, d_{22}, d_{31}, d_{41}), (d_{12}, d_{22}, d_{32}, d_{41})\}$, $\mathfrak{L} = \{\check{d}_1, \check{d}_2, \check{d}_3, \check{d}_4, \check{d}_5, \check{d}_6, \check{d}_7, \check{d}_8\}$ be a set of all sub-attributes with weights $(0.12, 0.18, 0.1, 0.15, 0.05, 0.22, 0.08, 0.1)^T$. Let $\{O_1, O_2, O_3\}$ be a set of three experts with weights $(0.143, 0.514, 0.343)^T$. To judge the optimum alternative, specialists provide their preferences in the form of PFHSNs.

4.2.2. PFHSEWA Operator

Step 1. According to the expert's opinion, Pythagorean fuzzy hypersoft decision matrices for all alternatives are given in Tables 1–5.

Step 2. There is no need to normalize because all parameters are the same type.

Step 3. Apply the proposed PFHSEWA operator to the obtained data (Tables 1–5), and then we get the opinions of decision-makers on alternatives in the form of PFHSN, for example,

Table 1: PFHS decision matrix for $\mathfrak{H}^1$.

	$\breve{d}_1$	$\breve{d}_2$	$\breve{d}_3$	$\breve{d}_4$	$\breve{d}_5$	$\breve{d}_6$	$\breve{d}_7$	$\breve{d}_8$
O_1	(0.3,0.8)	(0.7 0.3)	(0.6,0.7)	(0.5,0.4)	(0.2,0.4)	(0.4,0.6)	(0.5,0.8)	(0.9,0.3)
O_2	(0.7,0.6)	(0.3,0.4)	(0.6,0.5)	(0.3,0.9)	(0.5,0.4)	(0.4,0.6)	(0.7,0.5)	(0.4,0.8)
O_3	(0.5,0.7)	(0.8,0.5)	(0.7,0.4)	(0.4,0.3)	(0.4,0.9)	(0.2,0.4)	(0.8,0.4)	(0.7,0.5)

Table 2: PFHS decision matrix for $\mathfrak{H}^2$.

	$\breve{d}_1$	$\breve{d}_2$	$\breve{d}_3$	$\breve{d}_4$	$\breve{d}_5$	$\breve{d}_6$	$\breve{d}_7$	$\breve{d}_8$
O_1	(0.6,0.7)	(0.4,0.6)	(0.3,0.4)	(0.9,0.2)	(0.3,0.8)	(0.2,0.4)	(0.7,0.5)	(0.4,0.5)
O_2	(0.8,0.5)	(0.7,0.4)	(0.9,0.2)	(0.7,0.4)	(0.4,0.5)	(0.9,0.3)	(0.2,0.7)	(0.3,0.8)
O_3	(0.8,0.5)	(0.7,0.4)	(0.8,0.5)	(0.5,0.2)	(0.5,0.7)	(0.7,0.5)	(0.7,0.6)	(0.6,0.4)

Table 3: PFHS decision matrix for $\mathfrak{H}^3$.

	$\breve{d}_1$	$\breve{d}_2$	$\breve{d}_3$	$\breve{d}_4$	$\breve{d}_5$	$\breve{d}_6$	$\breve{d}_7$	$\breve{d}_8$
O_1	(0.7,0.3)	(0.2,0.5)	(0.1,0.6)	(0.3,0.4)	(0.4 0.6)	(0.8,0.4)	(0.6,0.7)	(0.2,0.5)
O_2	(0.3,0.7)	(0.4,0.5)	(0.4,0.8)	(0.3,0.4)	(0.6,0.7)	(0.3,0.4)	(0.9,0.2)	(0.7,0.2)
O_3	(0.6,0.8)	(0.4,0.5)	(0.6,0.5)	(0.6,0.4)	(0.7,0.5)	(0.8,0.4)	(0.5,0.8)	(0.4 0.5)

Table 4: PFHS decision matrix for $\mathfrak{H}^4$.

	$\breve{d}_1$	$\breve{d}_2$	$\breve{d}_3$	$\breve{d}_4$	$\breve{d}_5$	$\breve{d}_6$	$\breve{d}_7$	$\breve{d}_8$
O_1	(0.8,0.4)	(0.2,0.9)	(0.2,0.4)	(0.4,0.6)	(0.6,0.5)	(0.5,0.6)	(0.4,0.5)	(0.8,0.3)
O_2	(0.5,0.4)	(0.7,0.6)	(0.9,0.3)	(0.8,0.5)	(0.9,0.2)	(0.2,0.4)	(0.4,0.6)	(0.6,0.5)
O_3	(0.5,0.7)	(0.9,0.3)	(0.3,0.5)	(0.5,0.7)	(0.3,0.5)	(0.8,0.5)	(0.7,0.5)	(0.2,0.5)

Table 5: PFHS decision matrix for $\mathfrak{H}^5$.

	$\breve{d}_1$	$\breve{d}_2$	$\breve{d}_3$	$\breve{d}_4$	$\breve{d}_5$	$\breve{d}_6$	$\breve{d}_7$	$\breve{d}_8$
O_1	(0.5,0.7)	(0.8,0.5)	(0.7,0.4)	(0.4,0.3)	(0.4,0.9)	(0.2,0.4)	(0.8,0.4)	(0.7,0.5)
O_2	(0.8,0.5)	(0.7,0.4)	(0.8,0.5)	(0.5,0.2)	(0.5,0.7)	(0.7,0.5)	(0.7,0.6)	(0.6,0.4)
O_3	(0.5,0.4)	(0.4,0.8)	(0.5,0.6)	(0.3,0.4)	(0.7,0.6)	(0.7,0.5)	(0.4,0.9)	(0.5,0.2)

$$PFHSEWA\left(\mathfrak{F}_{\breve{d}_{11}}, \mathfrak{F}_{\breve{d}_{12}} \mathfrak{F}_{\breve{d}_{mn}}\right) = \left\langle \frac{\sqrt{\prod_{j=1}^{m}\left(\prod_{i=1}^{n}\left(1+\alpha_{\breve{d}_{ij}}^{2}\right)^{\theta_i}\right)^{\lambda_j} - \prod_{j=1}^{m}\left(\prod_{i=1}^{n}\left(1-\alpha_{\breve{d}_{ij}}^{2}\right)^{\theta_i}\right)^{\lambda_j}}}{\sqrt{\prod_{j=1}^{m}\left(\prod_{i=1}^{n}\left(1+\alpha_{\breve{d}_{ij}}^{2}\right)^{\theta_i}\right)^{\lambda_j} + \prod_{j=1}^{m}\left(\prod_{i=1}^{n}\left(1-\alpha_{\breve{d}_{ij}}^{2}\right)^{\theta_i}\right)^{\lambda_j}}}, \frac{\sqrt{2\prod_{j=1}^{m}\left(\prod_{i=1}^{n}\left(b_{\breve{d}_{ij}}^{2}\right)^{\theta_i}\right)^{\lambda_j}}}{\sqrt{\prod_{j=1}^{m}\left(\prod_{i=1}^{n}\left(2-b_{\breve{d}_{ij}}^{2}\right)^{\theta_i}\right)^{\lambda_j} + \prod_{j=1}^{m}\left(\prod_{i=1}^{n}\left(b_{\breve{d}_{ij}}^{2}\right)^{\theta_i}\right)^{\lambda_j}}} \right\rangle \tag{37}$$

$$\mathscr{L}_2 = \left\langle \frac{\sqrt{\begin{Bmatrix}(1.36)^{0.12}(1.16)^{0.18}(1.09)^{0.1}(1.81)^{0.15}(1.09)^{0.05}(1.04)^{0.22}(1.49)^{0.08}(1.16)0.1\end{Bmatrix}^{0.143}\begin{Bmatrix}(1.64)^{0.12}(1.49)^{0.18}(1.81)^{0.1}(1.49)^{0.15}(1.16)^{0.05}(1.81)^{0.22}(1.04)^{0.08}(1.09)0.1\end{Bmatrix}^{0.514}\begin{Bmatrix}(1.64)^{0.12}(1.49)^{0.18}(1.64)^{0.1}(1.25)^{0.15}(1.25)^{0.05}(1.49)^{0.22}(1.49)^{0.08}(1.36)0.1\end{Bmatrix}^{0.343} - \begin{Bmatrix}(0.64)^{0.12}(0.84)^{0.18}(0.91)^{0.1}(0.19)^{0.15}(0.91)^{0.05}(0.96)^{0.22}(0.51)^{0.08}(0.84)^{0.1}\end{Bmatrix}^{0.143}\begin{Bmatrix}(0.36)^{0.12}(0.51)^{0.18}(0.19)^{0.1}(0.51)^{0.15}(0.84)^{0.05}(0.19)^{0.22}(0.96)^{0.08}(0.91)^{0.1}\end{Bmatrix}^{0.514}\begin{Bmatrix}(0.36)^{0.12}(0.51)^{0.18}(0.36)^{0.1}(0.75)^{0.15}(0.75)^{0.05}(0.51)^{0.22}(0.51)^{0.08}(0.64)^{0.1}\end{Bmatrix}^{0.343}}}{\sqrt{\begin{Bmatrix}(1.36)^{0.12}(1.16)^{0.18}(1.09)^{0.1}(1.81)^{0.15}(1.09)^{0.05}(1.04)^{0.22}(1.49)^{0.08}(1.16)^{0.1}\end{Bmatrix}^{0.143}\begin{Bmatrix}(1.64)^{0.12}(1.49)^{0.18}(1.81)^{0.1}(1.49)^{0.15}(1.16)^{0.05}(1.81)^{0.22}(1.04)^{0.08}(1.09)^{0.1}\end{Bmatrix}^{0.514}\begin{Bmatrix}(1.64)^{0.12}(1.49)^{0.18}(1.64)^{0.1}(1.25)^{0.15}(1.25)^{0.05}(1.49)^{0.22}(1.49)^{0.08}(1.36)0.1\end{Bmatrix}^{0.343} + \begin{Bmatrix}(0.64)^{0.12}(0.84)^{0.18}(0.91)^{0.1}(0.19)^{0.15}(0.91)^{0.05}(0.96)^{0.22}(0.51)^{0.08}(0.84)^{0.1}\end{Bmatrix}^{0.143}\begin{Bmatrix}(0.36)^{0.12}(0.51)^{0.18}(0.91)^{0.1}(0.51)^{0.15}(0.84)^{0.05}(0.91)^{0.22}(0.96)^{0.08}(0.91)^{0.1}\end{Bmatrix}^{0.514}\begin{Bmatrix}(0.36)^{0.12}(0.51)^{0.18}(0.36)^{0.1}(0.75)^{0.15}(0.75)^{0.05}(0.51)^{0.22}(0.51)^{0.08}(0.64)^{0.1}\end{Bmatrix}^{0.343}}}, \frac{\sqrt{2\begin{bmatrix}\begin{Bmatrix}(0.49)^{0.12}(0.36)^{0.18}(0.16)^{0.1}(0.04)^{0.15}(0.64)^{0.05}(0.16)^{0.22}(0.25)^{0.08}(0.25)^{0.1}\end{Bmatrix}^{0.143}\\ \begin{Bmatrix}(0.25)^{0.12}(0.16)^{0.18}(0.04)^{0.1}(0.16)^{0.15}(0.25)^{0.05}(0.09)^{0.22}(0.49)^{0.08}(0.64)^{0.1}\end{Bmatrix}^{0.514}\\ \begin{Bmatrix}(0.25)^{0.12}(0.16)^{0.18}(0.25)^{0.1}(0.04)^{0.15}(0.49)^{0.05}(0.25)^{0.22}(0.36)^{0.08}(0.16)^{0.1}\end{Bmatrix}^{0.343}\end{bmatrix}}}{\sqrt{\begin{Bmatrix}(1.51)^{0.12}(1.64)^{0.18}(1.84)^{0.1}(1.96)^{0.15}(1.36)^{0.05}(1.84)^{0.22}(1.75)^{0.08}(1.75)^{0.1}\end{Bmatrix}^{0.143}\begin{Bmatrix}(1.75)^{0.12}(1.84)^{0.18}(1.96)^{0.1}(1.84)^{0.15}(1.75)^{0.05}(1.91)^{0.22}(1.51)^{0.08}(1.36)^{0.1}\end{Bmatrix}^{0.514}\begin{Bmatrix}(1.75)^{0.12}(1.84)^{0.18}(1.75)^{0.1}(1.96)^{0.15}(1.51)^{0.05}(1.75)^{0.22}(1.64)^{0.08}(1.84)^{0.1}\end{Bmatrix}^{0.343} + \begin{Bmatrix}(0.49)^{0.12}(0.36)^{0.18}(0.16)^{0.1}(0.04)^{0.15}(0.64)^{0.05}(0.16)^{0.22}(0.25)^{0.08}(0.25)^{0.1}\end{Bmatrix}^{0.143}\begin{Bmatrix}(0.25)^{0.12}(0.16)^{0.18}(0.04)^{0.1}(0.16)^{0.15}(0.25)^{0.05}(0.09)^{0.22}(0.49)^{0.08}(0.64)^{0.1}\end{Bmatrix}^{0.514}\begin{Bmatrix}(0.25)^{0.12}(0.16)^{0.18}(0.25)^{0.1}(0.04)^{0.15}(0.49)^{0.05}(0.25)^{0.22}(0.36)^{0.08}(0.16)^{0.1}\end{Bmatrix}^{0.343}}} \right\rangle \tag{38}$$

$$\langle 0.7105, 0.4250 \rangle$$

$$\mathscr{L}_3 = \left\langle \frac{\sqrt{\begin{array}{l}\left\{(1.49)^{0.12}(1.04)^{0.18}(1.01)^{0.1}(1.09)^{0.15}(1.16)0.05(1.64)0.22(1.36)0.08(1.04)0.1\right\}0.143\\ \left\{(1.09)^{0.12}(1.16)^{0.18}(1.16)^{0.1}(1.09)^{0.15}(1.36)0.05(1.09)0.22(1.81)0.08(1.49)0.1\right\}0.514\\ \left\{(1.36)^{0.12}(1.16)^{0.18}(1.36)^{0.1}(1.36)^{0.15}(1.49)0.05(1.64)0.22(1.25)0.08(1.16)0.1\right\}0.343\end{array}} - \sqrt{\begin{array}{l}\left\{(0.51)^{0.12}(0.96)^{0.18}(0.01)^{0.1}(0.91)^{0.15}(0.84)^{0.05}(0.36)^{0.22}(0.64)^{0.08}(0.96)^{0.1}\right\}^{0.143}\\ \left\{(0.91)^{0.12}(0.84)^{0.18}(0.84)^{0.1}(0.91)^{0.15}(0.64)^{0.05}(0.91)^{0.22}(0.19)^{0.08}(0.51)^{0.1}\right\}^{0.514}\\ \left\{(0.64)^{0.12}(0.84)^{0.18}(0.64)^{0.1}(0.64)^{0.15}(0.51)^{0.05}(0.36)^{0.22}(0.75)^{0.08}(0.84)^{0.1}\right\}^{0.343}\end{array}}}{\sqrt{\begin{array}{l}\left\{(1.49)^{0.12}(1.04)^{0.18}(1.01)^{0.1}(1.09)^{0.15}(1.16)^{0.05}(1.64)^{0.22}(1.36)^{0.08}(1.04)^{0.1}\right\}^{0.143}\\ \left\{(1.09)^{0.12}(1.16)^{0.18}(1.16)^{0.1}(1.09)^{0.15}(1.36)^{0.05}(1.09)^{0.22}(1.81)^{0.08}(1.49)^{0.1}\right\}^{0.514}\\ \left\{(1.36)^{0.12}(1.16)^{0.18}(1.36)^{0.1}(1.36)^{0.15}(1.49)^{0.05}(1.64)^{0.22}(1.25)^{0.08}(1.16)^{0.1}\right\}^{0.343}\end{array}} + \sqrt{\begin{array}{l}\left\{(0.51)^{0.12}(0.96)^{0.18}(0.01)^{0.1}(0.91)^{0.15}(0.84)^{0.05}(0.36)^{0.22}(0.64)^{0.08}(0.96)^{0.1}\right\}^{0.143}\\ \left\{(0.91)^{0.12}(0.84)^{0.18}(0.84)^{0.1}(0.91)^{0.15}(0.64)^{0.05}(0.91)^{0.22}(0.19)^{0.08}(0.51)^{0.1}\right\}^{0.514}\\ \left\{(0.64)^{0.12}(0.84)^{0.18}(0.64)^{0.1}(0.64)^{0.15}(0.51)^{0.05}(0.36)^{0.22}(0.75)^{0.08}(0.84)^{0.1}\right\}^{0.343}\end{array}}}, \frac{\sqrt{2\left[\begin{array}{l}\left\{(0.09)^{0.12}(0.25)^{0.18}(0.36)^{0.1}(0.16)0.15(0.36)^{0.05}(0.16)^{0.22}(0.49)^{0.08}(0.25)^{0.1}\right\}^{0.143}\\ \left\{\left\{(0.49)^{0.12}(0.25)^{0.18}(0.64)^{0.1}(0.16)0.15(0.49)^{0.05}(0.16)^{0.22}(0.04)^{0.08}(0.04)^{0.1}\right\}^{0.514}\right\}\\ \left\{(0.64)^{0.12}(0.25)^{0.18}(0.25)^{0.1}(0.16)0.15(0.25)^{0.05}(0.16)^{0.22}(0.64)^{0.08}(0.25)^{0.1}\right\}^{0.343}\end{array}\right]}}{\sqrt{\begin{array}{l}\left\{(1.91)^{0.12}(1.75)^{0.18}(1.64)^{0.1}(1.84)0.15(1.64)^{0.05}(1.84)^{0.22}(1.51)^{0.08}(1.75)^{0.1}\right\}^{0.143}\\ \left\{(1.51)^{0.12}(1.75)^{0.18}(1.36)^{0.1}(1.84)0.15(1.51)^{0.05}(1.84)^{0.22}(1.96)^{0.08}(1.96)^{0.1}\right\}^{0.514}\\ \left\{(1.36)^{0.12}(1.75)^{0.18}(1.75)^{0.1}(1.84)0.15(1.75)^{0.05}(1.84)^{0.22}(1.36)^{0.08}(1.75)^{0.1}\right\}^{0.343}\end{array}} + \sqrt{\begin{array}{l}\left\{(0.09)^{0.12}(0.25)^{0.18}(0.36)^{0.1}(0.16)^{0.15}(0.36)^{0.05}(0.16)^{0.22}(0.49)^{0.08}(0.25)^{0.1}\right\}^{0.143}\\ \left\{(0.49)^{0.12}(0.25)^{0.18}(0.64)^{0.1}(0.16)^{0.15}(0.49)^{0.05}(0.16)^{0.22}(0.04)^{0.08}(0.04)^{0.1}\right\}^{0.514}\\ \left\{(0.64)^{0.12}(0.25)^{0.18}(0.25)^{0.1}(0.16)^{0.15}(0.25)^{0.05}(0.16)^{0.22}(0.64)^{0.08}(0.25)^{0.1}\right\}0.343\end{array}}}\right\rangle \tag{39}$$

$$\langle 0.5834, 0.4680 \rangle$$

$$\mathscr{L}_4 = \left\langle \frac{\sqrt{\begin{array}{l}\left\{(1.64)^{0.12}(1.04)^{0.18}(1.04)^{0.1}(1.16)^{0.15}(1.36)^{0.05}(1.25)^{0.22}(1.16)^{0.08}(1.64)^{0.1}\right\}^{0.143}\\ \left\{(1.25)^{0.12}(1.49)^{0.18}(1.81)^{0.1}(1.64)^{0.15}(1.81)^{0.05}(1.04)^{0.22}(1.16)^{0.08}(1.36)^{0.1}\right\}^{0.514}\\ \left\{(1.25)^{0.12}(1.81)^{0.18}(1.09)^{0.1}(1.25)^{0.15}(1.09)^{0.05}(1.64)^{0.22}(1.49)^{0.08}(1.04)^{0.1}\right\}^{0.343}\\ -\\ \left\{(0.36)^{0.12}(0.96)^{0.18}(0.96)^{0.1}(0.84)^{0.15}(0.64)0.05(0.75)^{0.22}(0.84)^{0.08}(0.36)^{0.1}\right\}^{0.143}\\ \left\{(0.75)^{0.12}(0.51)^{0.18}(0.19)^{0.1}(0.36)^{0.15}(0.19)0.05(0.96)^{0.22}(0.84)^{0.08}(0.64)^{0.1}\right\}^{0.514}\\ \left\{(0.75)^{0.12}(0.19)^{0.18}(0.91)^{0.1}(0.75)^{0.15}(0.91)0.05(0.36)^{0.22}(0.51)^{0.08}(0.96)^{0.1}\right\}^{0.343}\end{array}}}{\sqrt{\begin{array}{l}\left\{(1.64)^{0.12}(1.04)^{0.18}(1.04)^{0.1}(1.16)^{0.15}(1.36)^{0.05}(1.25)^{0.22}(1.16)^{0.08}(1.64)^{0.1}\right\}^{0.143}\\ \left\{(1.25)^{0.12}(1.49)^{0.18}(1.81)^{0.1}(1.64)^{0.15}(1.81)^{0.05}(1.04)^{0.22}(1.16)^{0.08}(1.36)^{0.1}\right\}^{0.514}\\ \left\{(1.25)^{0.12}(1.81)^{0.18}(1.09)^{0.1}(1.25)^{0.15}(1.09)^{0.05}(1.64)^{0.22}(1.49)^{0.08}(1.04)^{0.1}\right\}^{0.343}\\ +\\ \left\{(0.36)^{0.12}(0.96)^{0.18}(0.96)^{0.1}(0.84)^{0.15}(0.64)^{0.05}(0.75)^{0.22}(0.84)^{0.08}(0.36)^{0.1}\right\}^{0.143}\\ \left\{(0.75)^{0.12}(0.51)^{0.18}(0.19)^{0.1}(0.36)^{0.15}(0.19)^{0.05}(0.96)^{0.22}(0.84)^{0.08}(0.64)^{0.1}\right\}^{0.514}\\ \left\{(0.75)^{0.12}(0.19)^{0.18}(0.91)^{0.1}(0.75)^{0.15}(0.91)^{0.05}(0.36)^{0.22}(0.51)^{0.08}(0.96)^{0.1}\right\}^{0.343}\end{array}}}, \frac{\sqrt{2\left[\begin{array}{l}\left\{(0.16)^{0.12}(0.81)^{0.18}(0.16)^{0.1}(0.36)^{0.15}(0.25)^{0.05}(0.36)^{0.22}(0.25)^{0.08}(0.09)^{0.1}\right\}^{0.143}\\ \left\{(0.16)^{0.12}(0.36)^{0.18}(0.09)^{0.1}(0.25)^{0.15}(0.04)^{0.05}(0.16)^{0.22}(0.36)^{0.08}(0.25)^{0.1}\right\}^{0.514}\\ \left\{(0.49)^{0.12}(0.09)^{0.18}(0.25)^{0.1}(0.49)^{0.15}(0.25)^{0.05}(0.25)^{0.22}(0.25)^{0.08}(0.25)^{0.1}\right\}^{0.343}\end{array}\right]}}{\sqrt{\begin{array}{l}(1.84)^{0.12}(1.19)^{0.18}(1.84)^{0.1}(1.64)^{0.15}(1.75)^{0.05}(1.64)^{0.22}(1.75)^{0.08}(1.91)^{0.1}0.143\}\\ \left\{(1.84)^{0.12}(1.64)^{0.18}(1.91)^{0.1}(1.75)^{0.15}(1.96)^{0.05}(1.84)^{0.22}(1.64)^{0.08}(1.75)^{0.1}\right\}^{0.514}\\ \left\{(1.51)^{0.12}(1.91)^{0.18}(1.75)^{0.1}(1.51)^{0.15}(1.75)^{0.05}(1.75)^{0.22}(1.75)^{0.08}(1.75)^{0.1}\right\}^{0.343}\\ +\\ \left\{(0.16)^{0.12}(0.81)^{0.18}(0.16)^{0.1}(0.36)^{0.15}(0.25)^{0.05}(0.36)^{0.22}(0.25)^{0.08}(0.09)^{0.1}\right\}^{0.143}\\ \left\{(0.16)^{0.12}(0.36)^{0.18}(0.09)^{0.1}(0.25)^{0.15}(0.04)^{0.05}(0.16)^{0.22}(0.36)^{0.08}(0.25)^{0.1}\right\}^{0.514}\\ \left\{(0.49)^{0.12}(0.09)^{0.18}(0.25)^{0.1}(0.49)^{0.15}(0.25)^{0.05}(0.25)^{0.22}(0.25)^{0.08}(0.25)^{0.1}\right\}^{0.343}\end{array}}}\right\rangle \quad (40)$$

$$\langle 0.6521, 0.4253 \rangle$$

$$\mathscr{L}_5 = \left\langle \frac{\sqrt{\begin{array}{l}\left\{(1.25)^{0.12}(1.64)0.18(1.49)^{0.1}(1.16)^{0.15}(1.16)^{0.05}(1.04)^{0.22}(1.64)^{0.08}(1.49)^{0.1}\right\}^{0.143}\\ \left\{(1.64)^{0.12}(1.49)0.18(1.64)^{0.1}(1.25)^{0.15}(1.25)^{0.05}(1.49)^{0.22}(1.49)^{0.08}(1.36)^{0.1}\right\}^{0.514}\\ \left\{(1.25)^{0.12}(1.16)0.18(1.25)^{0.1}(1.09)^{0.15}(1.49)^{0.05}(1.49)^{0.22}(1.16)^{0.08}(1.25)^{0.1}\right\}^{0.343}\\ -\\ \left\{(1.25)^{0.12}(1.16)^{0.18}(1.25)^{0.1}(1.09)^{0.15}(1.49)^{0.05}(1.49)^{0.22}(1.16)^{0.08}(1.25)^{0.1}\right\}^{0.343}\\ \left\{(0.36)^{0.12}(0.51)^{0.18}(0.36)^{0.1}(0.75)^{0.15}(0.75)^{0.05}(0.51)^{0.22}(0.51)^{0.08}(0.64)^{0.1}\right\}^{0.514}\\ \left\{(0.75)^{0.12}(0.84)^{0.18}(0.75)0.1(0.91)^{0.15}(0.51)^{0.05}(0.51)^{0.22}(0.84)^{0.08}(0.75)^{0.1}\right\}^{0.343}\end{array}}}{\sqrt{\begin{array}{l}\left\{(1.25)^{0.12}(1.64)^{0.18}(1.49)^{0.1}(1.16)^{0.15}(1.16)^{0.05}(1.04)^{0.22}(1.64)^{0.08}(1.49)^{0.1}\right\}^{0.143}\\ \left\{(1.64)^{0.12}(1.49)^{0.18}(1.64)^{0.1}(1.25)^{0.15}(1.25)^{0.05}(1.49)^{0.22}(1.49)^{0.08}(1.36)^{0.1}\right\}^{0.514}\\ \left\{(1.25)^{0.12}(1.16)^{0.18}(1.25)^{0.1}(1.09)^{0.15}(1.49)^{0.05}(1.49)^{0.22}(1.16)^{0.08}(1.25)^{0.1}\right\}^{0.343}\\ +\\ \left\{(0.75)^{0.12}(0.36)^{0.18}(0.51)^{0.1}(0.84)^{0.15}(0.84)^{0.05}(0.96)^{0.22}(0.36)^{0.08}(0.51)^{0.1}\right\}^{0.143}\\ \left\{(0.36)^{0.12}(0.51)^{0.18}(0.36)^{0.1}(0.75)^{0.15}(0.75)^{0.05}(0.51)^{0.22}(0.51)^{0.08}(0.64)^{0.1}\right\}^{0.514}\\ \left\{(0.75)^{0.12}(0.84)^{0.18}(0.75)^{0.1}(0.91)^{0.15}(0.51)^{0.05}(0.51)^{0.22}(0.84)^{0.08}(0.75)^{0.1}\right\}^{0.343}\end{array}}}, \right.$$

$$\left. \frac{\sqrt{2\left[\begin{array}{l}\left\{(0.49)^{0.12}(0.25)^{0.18}(0.16)^{0.1}(0.09)^{0.15}(0.81)^{0.05}(0.16)^{0.22}(0.16)^{0.08}(0.25)^{0.1}\right\}^{0.143}\\ \left\{(0.25)^{0.12}(0.16)^{0.18}(0.25)^{0.1}(0.04)^{0.15}(0.49)^{0.05}(0.25)^{0.22}(0.36)^{0.08}(0.16)^{0.1}\right\}^{0.514}\\ \left\{(0.16)^{0.12}(0.64)^{0.18}(0.36)^{0.1}(0.16)^{0.15}(0.36)^{0.05}(0.25)^{0.22}(0.81)^{0.08}(0.04)^{0.1}\right\}^{0.343}\end{array}\right]}}{\sqrt{\begin{array}{l}\left\{(1.51)^{0.12}(1.75)^{0.18}(1.84)^{0.1}(1.91)^{0.15}(1.19)^{0.05}(1.84)^{0.22}(1.84)^{0.08}(1.75)^{0.1}\right\}^{0.143}\\ \left\{(1.75)^{0.12}(1.84)^{0.18}(1.75)^{0.1}(1.96)^{0.15}(1.51)^{0.05}(1.75)^{0.22}(1.64)^{0.08}(1.84)^{0.1}\right\}^{0.514}\\ \left\{(1.84)^{0.12}(1.36)^{0.18}(1.64)^{0.1}(1.84)^{0.15}(1.64)^{0.05}(1.75)^{0.22}(1.19)^{0.08}(1.96)^{0.1}\right\}^{0.343}\\ +\\ \left\{(0.49)^{0.12}(0.25)^{0.18}(0.16)^{0.1}(0.09)^{0.15}(0.81)^{0.05}(0.16)^{0.22}(0.16)^{0.08}(0.25)^{0.1}\right\}^{0.143}\\ \left\{(0.25)^{0.12}(0.16)^{0.18}(0.25)^{0.1}(0.04)^{0.15}(0.49)^{0.05}(0.25)^{0.22}(0.36)^{0.08}(0.16)^{0.1}\right\}^{0.514}\\ \left\{(0.16)^{0.12}(0.64)^{0.18}(0.36)^{0.1}(0.16)^{0.15}(0.36)^{0.05}(0.25)^{0.22}(0.81)^{0.08}(0.04)^{0.1}\right\}^{0.343}\end{array}}} \right\rangle$$

$$\langle 0.6260, 0.4583 \rangle$$

$$\mathscr{L}_1 = \left\langle \begin{array}{l} \sqrt{\begin{array}{l} \left\{(1.09)^{0.12}(1.49)^{0.18}(1.36)^{0.1}(1.25)^{0.15}(1.04)^{0.05}(1.16)^{0.22}(1.25)^{0.08}(1.81)^{0.1}\right\}^{0.143} \\ \left\{(1.49)^{0.12}(1.09)^{0.18}(1.36)^{0.1}(1.09)^{0.15)}(1.25)^{0.05}(1.16)^{0.22}(1.49)^{0.08}(1.09)^{0.1}\right\}^{0.514} \\ \left\{(1.25)^{0.12}(1.64)^{0.18}(1.49)^{0.1}(1.16)^{0.15}(1.16)^{0.05}(1.04)^{0.22}(1.64)^{0.08}(1.49)^{0.1}\right\}^{0.343} \end{array}} \\ - \\ \sqrt{\begin{array}{l} \left\{(0.91)^{0.12}(0.51)^{0.18}(0.64)^{0.1}(0.75)^{0.15}(0.96)^{0.05}(0.84)^{0.22}(0.75)^{0.08}(0.19)^{0.1}\right\}^{0.143} \\ \left\{(0.51)^{0.12}(0.91)^{0.18}(0.64)^{0.1}(0.91)^{0.15}(0.75)^{0.05}(0.84)^{0.22}(0.51)^{0.08}(0.91)^{0.1}\right\}^{0.514} \\ \left\{(0.75)^{0.12}(0.36)^{0.18}(0.51)^{0.1}(0.84)^{0.15}(0.84)^{0.05}(0.96)^{0.22}(0.36)^{0.08}(0.51)^{0.1}\right\}^{0.343} \end{array}} \end{array} \right\rangle \tag{41}$$

$$\left\langle \begin{array}{l} \sqrt{\begin{array}{l} \left\{(1.09)^{0.12}(1.49)^{0.18}(1.36)^{0.1}(1.25)^{0.15}(1.04)^{0.05}(1.16)^{0.22}(1.25)^{0.08}(1.81)^{0.1}\right\}^{0.143} \\ \left\{(1.49)^{0.12}(1.09)^{0.18}(1.36)^{0.1}(1.09)^{0.15}(1.25)^{0.05}(1.16)^{0.22}(1.49)^{0.08}(1.09)^{0.1}\right\}^{0.514} \\ \left\{(1.25)^{0.12}(1.64)^{0.18}(1.49)^{0.1}(1.16)^{0.15}(1.16)^{0.05}(1.04)^{0.22}(1.64)^{0.08}(1.49)^{0.1}\right\}^{0.343} \end{array}} \\ + \\ \sqrt{\begin{array}{l} \left\{(0.91)^{0.12}(0.51)^{0.18}(0.64)^{0.1}(0.75)^{0.15}(0.96)^{0.05}(0.84)^{0.22}(0.75)^{0.08}(0.19)^{0.1}\right\}^{0.143} \\ \left\{(0.51)^{0.12}(0.91)^{0.18}(0.64)^{0.1}(0.91)^{0.15}(0.75)^{0.05}(0.84)^{0.22}(0.51)^{0.08}(0.91)^{0.1}\right\}^{0.514} \\ \left\{(0.75)^{0.12}(0.36)^{0.18}(0.51)^{0.1}(0.84)^{0.15}(0.84)^{0.05}(0.96)^{0.22}(0.36)^{0.08}(0.51)^{0.1}\right\}^{0.343} \end{array}} \end{array} \right\rangle$$

$$\sqrt{2\left[\begin{array}{l} \left\{(0.64)^{0.12}(0.09)^{0.18}(0.49)^{0.1}(0.16)^{0.15}(0.16)^{0.05}(0.36)^{0.22}(0.64)^{0.08}(0.09)^{0.1}\right\}^{0.143} \\ \left\{(0.36)^{0.12}(0.16)^{0.18}(0.25)^{0.1}(0.81)^{0.15}(0.16)^{0.05}(0.36)^{0.22}(0.25)^{0.08}(0.64)^{0.1}\right\}^{0.514} \\ \left\{(0.49)^{0.12}(0.25)^{0.18}(0.16)^{0.1}(0.09)^{0.15}(0.81)^{0.05}(0.16)^{0.22}(0.16)^{0.08}(0.25)^{0.1}\right\}^{0.343} \end{array}\right]}$$

$$\left\langle \begin{array}{l} \sqrt{\begin{array}{l} \left\{(1.36)^{0.12}(1.91)^{0.18}(1.51)^{0.1}(1.84)^{0.15}(1.84)^{0.05}(1.64)^{0.22}(1.36)^{0.08}(1.91)^{0.1}\right\}^{0.143} \\ \left\{(1.64)^{0.12}(1.84)^{0.18}(1.75)^{0.1}(1.19)^{0.15}(1.84)^{0.05}(1.64)^{0.22}(1.75)^{0.08}(1.36)^{0.1}\right\}^{0.514} \\ \left\{(1.51)^{0.12}(1.75)^{0.18}(1.84)^{0.1}(1.91)^{0.15}(1.19)^{0.05}(1.84)^{0.22}(1.84)^{0.08}(1.75)^{0.1}\right\}^{0.343} \end{array}} \\ + \\ \sqrt{\begin{array}{l} \left\{(0.64)^{0.12}(0.09)^{0.18}(0.49)^{0.1}(0.16)^{0.15}(0.16)^{0.05}(0.36)^{0.22}(0.64)^{0.08}(0.09)^{0.1}\right\}^{0.143} \\ \left\{(0.36)^{0.12}(0.16)^{0.18}(0.25)^{0.1}(0.81)^{0.15}(0.16)^{0.05}(0.36)^{0.22}(0.25)^{0.08}(0.64)^{0.1}\right\}^{0.514} \\ \left\{(0.49)^{0.12}(0.25)^{0.18}(0.16)^{0.1}(0.09)^{0.15}(0.81)^{0.05}(0.16)^{0.22}(0.16)^{0.08}(0.25)^{0.1}\right\}^{0.343} \end{array}} \end{array} \right\rangle$$

$$\langle 0.5387, 0.5299 \rangle$$

Step 4. Use equation (1) $\mathbb{S} = a^2_{\mathscr{F}(\check{d}_{ij})} - b^2_{\mathscr{F}(\check{d}_{ij})}$ to compute the score values for all alternatives.

$\mathbb{S}(\mathscr{H}_1) = 0.0088$, $\mathbb{S}(\mathscr{H}_2) = 0.2855$, $\mathbb{S}(\mathscr{H}_3) = 0.1154$, $\mathbb{S}(\mathscr{H}_4) = 0.2268$, and $\mathbb{S}(\mathscr{H}_5) = 0.1677$.

Step 5. After calculation, we get the ranking of alternatives $\mathbb{S}(\mathscr{H}_2) > \mathbb{S}(\mathscr{H}_4) > \mathbb{S}(\mathscr{H}_5) > \mathbb{S}(\mathscr{H}_3) > \mathbb{S}(\mathscr{H}_1)$. So, $\mathfrak{H}^2 > \mathfrak{H}^4 > \mathfrak{H}^5 > \mathfrak{H}^3 > \mathfrak{H}^1$.

Hence, the best alternative is $\mathfrak{H}^2$.

Table 6: Feature analysis of different models with a proposed model.

	Fuzzy information	Aggregated parameters information	Einstein aggregated parameters information	Multi-sub-attributes information of each attribute
IFWA [66]	✓	×	×	×
IFEWA [62]	✓	✓	✓	×
IFSWA [35]	✓	✓	×	×
IFHSWA [58]	✓	✓	×	✓
PFSWA [44]	✓	✓	×	×
PFEWA [27]	✓	✓	✓	×
PFSEOWA [46]	✓	✓	✓	×
PFHSWA [65]	✓	✓	×	✓
Proposed operator	✓	✓	✓	✓

Table 7: Comparison of proposed operators with some existing operators.

Approach	H^1	H^2	H^3	H^4	H^5	Alternatives ranking
PFWA operator	0.0039	0.0644	0.0433	−0.0179	−0.0376	$\mathfrak{H}^2 > \mathfrak{H}^3 > \mathfrak{H}^1 > \mathfrak{H}^4 > \mathfrak{H}^5$
PFEWA operator	−0.3306	0.5957	0 .1383	−0.1661	0.1092	$\mathfrak{H}^2 > \mathfrak{H}^3 > \mathfrak{H}^5 > \mathfrak{H}^4 > \mathfrak{H}^1$
PFSWA operator	0.0293	0.0938	0.0783	0.0694	0.0369	$\mathfrak{H}^2 > \mathfrak{H}^3 > \mathfrak{H}^4 > \mathfrak{H}^5 > \mathfrak{H}^1$
PFHSWA operator	0.1975	0.3513	0.2632	0.2297	0.1204	$\mathfrak{H}^2 > \mathfrak{H}^3 > \mathfrak{H}^4 > \mathfrak{H}^1 > \mathfrak{H}^5$
PFHSEWA operator	0.0088	0.2855	0.1154	0.2268	0.1677	$\mathfrak{H}^2 > \mathfrak{H}^4 > \mathfrak{H}^5 > \mathfrak{H}^3 > \mathfrak{H}^1$

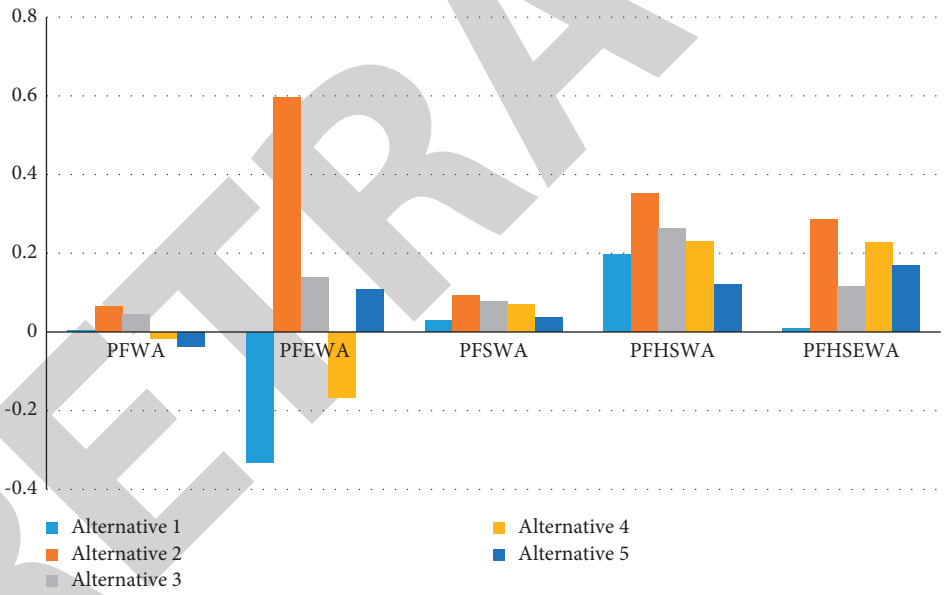

Figure 2: Graphical results of comparative studies.

5. Comparative Studies and Supremacy of the Proposed Model

To demonstrate the efficiency of the anticipated approach, some existing techniques under the PFS, PFSS, and proposed PFHSS model were compared.

5.1. Supremacy of the Proposed Method. The deliberate approach is proficient and convincing; we have constructed a pioneering MCDM model under the PFHSS setting over the PFHSEWA operator. Our advanced model is extra brilliant than prevailing techniques and can convey the utmost subtle connotations in MCDM obstacles. The collective model is flexible and conversant, adjusting to potential instability, commitment, and production. Different models have exhaustive ranking processes, so there is an instantaneous variance among the positions of the offered method to be realistic conferring to their conventions. This systematic exploration and estimation determine that outcomes gained from present techniques are volatile equated to hybrid structures. It is informal to syndicate inadequate and indeterminate facts in DM methods. Hence, our deliberated methodology will be more capable, authoritative, superior, and better than various hybrid-structured FS. Table 6 presents the

supremacy analysis of the anticipated technique and some standing models.

5.2. Comparative Studies. To validate the usefulness of the projected technique, we compare the obtained results with some existing techniques under the environment of PFS and PFSS. A summary of all numerical and graphical outcomes is given in Table 7 and Figure 2. Firstly, we present a comparison with methods proposed by Siddique et al. [65] and Zulqarnain et al. [44]. Their proposed AOs are based on algebraic norms, while the proposed operators in this work are based on Einstein norms. Secondly, we compare the PFEWA operator proposed by Garg [15]. He developed the DM technique for PFNs by utilizing Einstein norms that cannot accommodate the parametrized values of the alternatives. On the other hand, our established approach competently deals with parametrized values of the alternatives and delivers better information than existing techniques. This work recommends innovative Einstein AO, such as PFHSEWA, to integrate the evaluation materials and then use the score function to calculate the substitute score. Therefore, it is inevitable that, based on the above facts, the plan operator in this work is more influential, consistent, and effective. The graphical ranking order of the alternatives of our proposed model with existing models is given in Figure 2.

6. Conclusion

Mathematical validation in agri-farming developments feats all resources while integrating objectives under economic, superior, and protection boundaries. Studies must be delimited for the most acceptable decision, accessing judgment requirements. In genuine DM, the assessment of alternative details carried by the expert is regularly incorrect, rough, and impetuous, so PFHSNs can be used to comport this indeterminate information. The core goal of this research is to use Einstein's norms to develop some operational laws for PFHSS. Then, a new operator, such as PFHSEWA, was developed according to the designed operational laws. In addition, some basic properties are proposed, such as the idempotence, homogeneity, and boundedness of the developed PFHSEWA operator. Furthermore, a DM approach has been designed to address MCDM problems based on endorsed operators. To certify the robustness of the settled approach, we provide an inclusive mathematical illustration for selecting the best agricultural robots in agri-farming. A comparative analysis with some current methods is presented. Finally, based on the outcomes attained, it is determined that the technique projected in this research is the most practical and effective way to solve the problem of MCDM. Future research focuses on developing more decision-making methods in the PFHSS environment using other operators, such as Einstein's hybrid geometric and Einstein's hybrid average operator.

Data Availability

No data were used to support this study.

Conflicts of Interest

The authors declare that they have no conflicts of interest.

Acknowledgments

The authors would like to thank Deanship of Scientific Research at Majmaah University for supporting this work under Project Number No R-2022-47.

References

[1] L. A. Zadeh, "Fuzzy sets," *Inforation and Control*, vol. 8, pp. 338–353, 1965.
[2] K. T. Atanassov, "Intuitionistic fuzzy sets," *Fuzzy Sets and Systems*, vol. 20, no. 1, pp. 87–96, 1986.
[3] W. Wang and X. Liu, "Intuitionistic fuzzy geometric aggregation operators based on Einstein operations," *International Journal of Intelligent Systems*, vol. 26, no. 11, pp. 1049–1075, 2011.
[4] K. T. Atanassov, "Interval valued intuitionistic fuzzy sets," in *Intuitionistic Fuzzy Sets*, pp. 139–177, Physica, Heidelberg, Germany, 1999.
[5] H. Garg and G. Kaur, "Cubic intuitionistic fuzzy sets and their fundamental properties," *Journal of Multiple-Valued Logic and Soft Computing*, vol. 33, no. 6, 2019.
[6] R. R. Yager, "Pythagorean membership grades in multi-criteria decision making," *IEEE Transactions on Fuzzy Systems*, vol. 22, no. 4, pp. 958–965, 2013.
[7] P. A. Ejegwa, "Pythagorean fuzzy set and its application in career placements based on academic performance using max-min-max composition," *Complex & Intelligent Systems*, vol. 5, no. 2, pp. 165–175, 2019.
[8] K. Rahman, S. Abdullah, R. Ahmed, and M. Ullah, "Pythagorean fuzzy Einstein weighted geometric aggregation operator and their application to multiple attribute group decision making," *Journal of Intelligent and Fuzzy Systems*, vol. 33, no. 1, pp. 635–647, 2017.
[9] X. Zhang and Z. Xu, "Extension of TOPSIS to multiple criteria decision making with Pythagorean fuzzy sets," *International Journal of Intelligent Systems*, vol. 29, no. 12, pp. 1061–1078, 2014.
[10] G. Wei and M. Lu, "Pythagorean fuzzy power aggregation operators in multiple attribute decision making," *International Journal of Intelligent Systems*, vol. 33, no. 1, pp. 169–186, 2018.
[11] L. Wang and N. Li, "Pythagorean fuzzy interaction power Bonferroni mean aggregation operators in multiple attribute decision making," *International Journal of Intelligent Systems*, vol. 35, no. 1, pp. 150–183, 2020.
[12] E. Ilbahar, A. Karaşan, S. Cebi, and C. Kahraman, "A novel approach to risk assessment for occupational health and safety using Pythagorean fuzzy AHP & fuzzy inference system," *Safety Science*, vol. 103, pp. 124–136, 2018.
[13] X. Zhang, "A novel approach based on similarity measure for Pythagorean fuzzy multiple criteria group decision making," *International Journal of Intelligent Systems*, vol. 31, no. 6, pp. 593–611, 2016.
[14] X. Peng and Y. Yang, "Some results for Pythagorean fuzzy sets," *International Journal of Intelligent Systems*, vol. 30, no. 11, pp. 1133–1160, 2015.
[15] H. Garg, "A new generalized Pythagorean fuzzy information aggregation using Einstein operations and its application to

decision making," *International Journal of Intelligent Systems*, vol. 31, no. 9, pp. 886–920, 2016.
[16] H. Garg, "Generalized pythagorean fuzzy geometric aggregation operators using einsteint-norm andt-conorm for multicriteria decision-making process," *International Journal of Intelligent Systems*, vol. 32, no. 6, pp. 597–630, 2017.
[17] H. Garg, "New logarithmic operational laws and their aggregation operators for Pythagorean fuzzy set and their applications," *International Journal of Intelligent Systems*, vol. 34, no. 1, pp. 82–106, 2019.
[18] H. Gao, M. Lu, G. Wei, and Y. Wei, "Some novel Pythagorean fuzzy interaction aggregation operators in multiple attribute decision making," *Fundamenta Informaticae*, vol. 159, no. 4, pp. 385–428, 2018.
[19] L. Wang, H. Garg, and N. Li, "Pythagorean fuzzy interactive Hamacher power aggregation operators for assessment of express service quality with entropy weight," *Soft Computing*, vol. 25, no. 2, pp. 973–993, 2021.
[20] M. Zulqarnain and F. Dayan, "Choose best criteria for decision making via fuzzy topsis method," *Mathematics and Computer Science*, vol. 2, no. 6, pp. 113–119, 2017.
[21] X. Peng and H. Yuan, "Fundamental properties of Pythagorean fuzzy aggregation operators," *Fundamenta Informaticae*, vol. 147, no. 4, pp. 415–446, 2016.
[22] L. Wang and H. Garg, "Algorithm for multiple attribute decision-making with interactive archimedean norm operations under pythagorean fuzzy uncertainty," *International Journal of Computational Intelligence Systems*, vol. 14, no. 1, pp. 503–527, 2021.
[23] K. Rahman, S. Abdullah, M. Shakeel, M. S. Ali Khan, and M. Ullah, "Interval-valued Pythagorean fuzzy geometric aggregation operators and their application to group decision making problem," *Cogent Mathematics*, vol. 4, no. 1, Article ID 1338638, 2017.
[24] L. Wang and N. Li, "Continuous interval-valued Pythagorean fuzzy aggregation operators for multiple attribute group decision making," *Journal of Intelligent and Fuzzy Systems*, vol. 36, no. 6, pp. 6245–6263, 2019.
[25] R. Arora and H. Garg, "Group decision-making method based on prioritized linguistic intuitionistic fuzzy aggregation operators and their fundamental properties," *Computational and Applied Mathematics*, vol. 38, no. 2, pp. 1–32, 2019.
[26] H. Garg, "New ranking method for normal intuitionistic sets under crisp, interval environments and its applications to multiple attribute decision making process," *Complex & Intelligent Systems*, vol. 6, no. 3, pp. 559–571, 2020.
[27] Z. Ma and Z. Xu, "Symmetric pythagorean fuzzy weighted geometric/averaging operators and their application in multicriteria decision-making problems," *International Journal of Intelligent Systems*, vol. 31, no. 12, pp. 1198–1219, 2016.
[28] D. Molodtsov, "Soft set theory—first results," *Computers & Mathematics with Applications*, vol. 37, no. 4-5, pp. 19–31, 1999.
[29] P. K. Maji, R. Biswas, and A. R. Roy, "Soft set theory," *Computers & Mathematics with Applications*, vol. 45, no. 4-5, pp. 555–562, 2003.
[30] P. K. Maji, A. R. Roy, and R. Biswas, "An application of soft sets in a decision making problem," *Computers & Mathematics with Applications*, vol. 44, no. 8-9, pp. 1077–1083, 2002.
[31] P. K. Maji, R. Biswas, and A. R. Roy, "Fuzzy soft sets," *Journal of Fuzzy Mathematics*, vol. 9, pp. 589–602, 2001.
[32] P. K. Maji, R. Biswas, and A. R. Roy, "Intuitionistic fuzzy soft sets," *Journal of Fuzzy Mathematics*, vol. 9, pp. 677–692, 2001.
[33] I. Deli and N. Çağman, "Intuitionistic fuzzy parameterized soft set theory and its decision making," *Applied Soft Computing*, vol. 28, pp. 109–113, 2015.
[34] H. Garg and R. Arora, "Maclaurin symmetric mean aggregation operators based on t-norm operations for the dual hesitant fuzzy soft set," *Journal of Ambient Intelligence and Humanized Computing*, vol. 11, no. 1, pp. 375–410, 2020.
[35] R. Arora and H. Garg, "A robust aggregation operators for multi-criteria decision-making with intuitionistic fuzzy soft set environment," *Scientia Iranica*, vol. 25, no. 2, pp. 931–942, 2018.
[36] H. Garg and R. Arora, "Generalized Maclaurin symmetric mean aggregation operators based on Archimedean t-norm of the intuitionistic fuzzy soft set information," *Artificial Intelligence Review*, vol. 54, no. 4, pp. 3173–3213, 2021.
[37] H. Garg, R. Arora, and R. Arora, "TOPSIS method based on correlation coefficient for solving decision-making problems with intuitionistic fuzzy soft set information," *AIMS Mathematics*, vol. 5, no. 4, pp. 2944–2966, 2020.
[38] P. Wang and P. Liu, "Some Maclaurin symmetric mean aggregation operators based on Schweizer-Sklar operations for intuitionistic fuzzy numbers and their application to decision making," *Journal of Intelligent and Fuzzy Systems*, vol. 36, no. 4, pp. 3801–3824, 2019.
[39] P. Liu and P. Wang, "Multiple-attribute decision-making based on Archimedean Bonferroni operators of q-rung orthopair fuzzy numbers," *IEEE Transactions on Fuzzy Systems*, vol. 27, no. 5, pp. 834–848, 2018.
[40] X. D. Peng, Y. Yang, J. Song, and Y. Jiang, "Pythagorean fuzzy soft set and its application," *Computer Engineering*, vol. 41, no. 7, pp. 224–229, 2015.
[41] T. M. Athira, S. J. John, S. Jacob John, and H. Garg, "A novel entropy measure of Pythagorean fuzzy soft sets," *AIMS Mathematics*, vol. 5, no. 2, pp. 1050–1061, 2020.
[42] T. M. Athira, S. J. John, and H. Garg, "Entropy and distance measures of Pythagorean fuzzy soft sets and their applications," *Journal of Intelligent and Fuzzy Systems*, vol. 37, no. 3, pp. 4071–4084, 2019.
[43] K. Naeem, M. Riaz, X. Peng, and D. Afzal, "Pythagorean fuzzy soft MCGDM methods based on TOPSIS, VIKOR and aggregation operators," *Journal of Intelligent and Fuzzy Systems*, vol. 37, no. 5, pp. 6937–6957, 2019.
[44] R. M. Zulqarnain, X. L. Xin, H. Garg, and W. A. Khan, "Aggregation operators of Pythagorean fuzzy soft sets with their application for green supplier chain management," *Journal of Intelligent and Fuzzy Systems*, vol. 40, no. 3, pp. 5545–5563, 2021.
[45] R. M. Zulqarnain, X. L. Xin, H. Garg, and R. Ali, "Interaction aggregation operators to solve multi criteria decision making problem under pythagorean fuzzy soft environment," *Journal of Intelligent and Fuzzy Systems*, vol. 41, no. 1, pp. 1151–1171, 2021.
[46] R. M. Zulqarnain, I. Siddique, S. Ahmad et al., "Pythagorean fuzzy soft Einstein ordered weighted average operator in sustainable supplier selection problem," *Mathematical Problems in Engineering*, vol. 2021, 2021.
[47] R. M. Zulqarnain, I. Siddique, and S. EI-Morsy, "Einstein-ordered weighted geometric operator for pythagorean fuzzy soft set with its application to solve magdm problem," *Mathematical Problems in Engineering*, vol. 2022, Article ID 5199427, 14 pages, 2022.
[48] I. Siddique, R. M. Zulqarnain, R. Ali, A. Alburaikan, A. Iampan, and A. E. W. Khalifa, "A decision-making approach based on score matrix for pythagorean fuzzy soft set,"

Hindawi
Journal of Mathematics
Volume 2022, Article ID 2388199, 7 pages
https://doi.org/10.1155/2022/2388199

Research Article

Generalizations of Fuzzy q-Ideals of *BCI*-Algebras

G. Muhiuddin,[1] **D. Al-Kadi**,[2] **A. Mahboob**,[3] **A. Assiry**,[4] **and Abdullah Alsubhi**[1]

[1]*Department of Mathematics, Faculty of Science, University of Tabuk, P.O. Box 741, Tabuk 71491, Saudi Arabia*
[2]*Department of Mathematics and Statistic, College of Science, Taif University, P.O. Box 11099, Taif 21944, Saudi Arabia*
[3]*Department of Mathematics, Madanapalle Institute of Technology & Science, Madanapalle 517325, India*
[4]*Department of Mathematical Sciences, College of Applied Science, Umm Al-Qura University, Makkah 21955, Saudi Arabia*

Correspondence should be addressed to G. Muhiuddin; chishtygm@gmail.com

Received 8 February 2022; Revised 20 March 2022; Accepted 31 March 2022; Published 6 May 2022

Academic Editor: Naeem Jan

In this paper, we introduce the notion of $(\in, \in\vee(\kappa^*, q_\kappa))$-fuzzy q-ideals of *BCI*-algebras to propose a more general form of fuzzy q-ideals of *BCI*-algebras. We prove that $(\in, \in\vee q)$-fuzzy q-ideals and $(\in\vee(\kappa^*, q_\kappa), \in\vee(\kappa^*, q_\kappa))$-fuzzy q-ideals are $(\in, \in\vee(\kappa^*, q_\kappa))$-fuzzy q-ideals, but the converse assertion is not valid and examples are given to support this. It is proved that every $(\in, \in\vee(\kappa^*, q_\kappa))$-fuzzy q-ideal is an $(\in, \in\vee(\kappa^*, q_\kappa))$-fuzzy ideal, but the converse need not be true in general and an example is provided. In addition, correspondence between $(\in, \in\vee(\kappa^*, q_\kappa))$-fuzzy q-ideals and q-ideals of *BCI*-algebras is considered.

1. Introduction

A fuzzy set, as defined by Zadeh [1], is a powerful methodology for dealing with possibilistic complexity related to expectations, state imprecision, and preferences. Fuzzy set theory has become an essential study subject in research disciplines such as operation research, statistics, graph theory, social science, management, medical science, computer science, machine learning, multicriteria decision-making, information processing, and optimization. Imai and Iseki proposed the notions of *BCK*- and *BCI*-algebras in 1966 [2, 3]. Since then, a large number of studies have been published concerning the theory of *BCK/BCI*-algebras. Many authors, especially Liu et al. [4], Khalid and Ahmad [5], Jun et al. [6–8], Muhiuddin et al. [9, 10], and Al-Masarwah and Ahmad [11], studied different aspects of *BCK/BCI*-algebras based on ideal theory.

The idea of quasi-coincidence of a fuzzy point with a fuzzy set, as stated in [12], was fundamental in the development of various types of fuzzy subgroups, known as (α, β)-fuzzy subgroups, as defined by Bhakat and Das in [13]. The concepts of (α, β)-fuzzy subalgebras and (α, β)-fuzzy ideals in *BCK/BCI*-algebras are also important and useful generalizations of fuzzy subalgebras and fuzzy ideals, which were introduced and studied by Jun [14, 15]. Zhang et al. [16] introduced the concepts of $(\in, \in\vee q)$-fuzzy p-ideals, $(\in, \in\vee q)$-fuzzy q-ideals, and $(\in, \in\vee q)$-fuzzy a-ideals in *BCI*-algebras by using the idea of a quasi-coincidence of a fuzzy point with a fuzzy set in the ideal theory of *BCI*-algebras. Ma et al. [17] proposed and investigated the concepts of (positive implicative, implicative, and commutative) $(\in, \in\vee q)$-interval-valued fuzzy ideals of *BCI*-algebras. Ma et al. [18] also proposed the concepts of $(\in, \in\vee q)$-interval-valued fuzzy (p and q) a-ideals of *BCI*-algebras. Al-Masarwah et al. [19] proposed a new system of m-polar (α, β)-fuzzy ideals and m-polar (α, β)-fuzzy commutative ideals in *BCK/BCI*-algebras by extending the concept of fuzzy point to m-polar fuzzy sets. Muhiuddin et al. [20] established the concept of m-polar $(\in, \in)$-fuzzy q-ideals in *BCI*-algebras and explored the characteristics of m-polar (α, β)-fuzzy q-ideals and m-polar (α, β)-fuzzy ideals/subalgebras. Many researchers have also extended the fuzzy set theory and related concepts to different algebras and other structures (see, for e.g., [10, 21–27]).

It is obvious to provide a generalized version of the existing fuzzy ideals of *BCI*-algebras. To do this, we first review some fundamental concepts from the sequel in Section 2. The notions of $(\in, \in\vee(\kappa^*, q_\kappa))$-fuzzy q-ideals and

$(\in\vee(\kappa^*, q_\kappa), \in\vee(\kappa^*, q_\kappa))$-fuzzy q-ideals are then introduced and associated properties are investigated in Section 3. Moreover, correspondence between $(\in, \in\vee(\kappa^*, q_\kappa))$-fuzzy q-ideals and q-ideals of *BCI*-algebras is presented.

2. Preliminaries

An algebra $\widetilde{\mathscr{A}} = (\widetilde{\mathscr{A}}; *, 0)$ of type $(2, 0)$ is a *BCI*-algebra if

(1) $((\varpi * \Theta) * (\varpi * \varrho)) * (\varrho * \Theta) = 0$

(2) $(\varpi * (\varpi * \Theta)) * \Theta = 0$

(3) $\varpi * \varpi = 0$

(4) $\varpi * \Theta = 0$ and $\Theta * \varpi = 0 \Rightarrow \varpi = \Theta$

$\forall \varpi, \Theta, \varrho \in \widetilde{\mathscr{A}}$

Any *BCI*-algebra $\widetilde{\mathscr{A}}$ satisfies the following:

(1) $\varpi * 0 = \varpi$

(2) $(\varpi * \Theta) * \varrho = (\varpi * \varrho) * \Theta$

Define an order $\leq$ on $\widetilde{\mathscr{A}}$ as $\varpi \leq \Theta \Leftrightarrow \varpi * \Theta = 0$.

Let $\widetilde{\mathscr{A}}$ be a *BCI*-algebra. A mapping $\mathscr{T}: \widetilde{\mathscr{A}} \longrightarrow [0, 1]$ is called a fuzzy subset (briefly, FS) of $\widetilde{\mathscr{A}}$.

Definition 1. Let $a \in \widetilde{\mathscr{A}}$ and $\delta \in (0, 1]$. An *ordered fuzzy point* (briefly, OFP) a_δ of $\widetilde{\mathscr{A}}$ is defined as

$$a_\delta(\varpi) = \begin{cases} \delta, & \text{if } \varpi \in (a], \\ 0, & \text{if } \varpi \notin (a], \end{cases} \quad \forall \varpi \in \widetilde{\mathscr{A}}. \tag{1}$$

Consequently, a_δ is a FS of $\widetilde{\mathscr{A}}$. For a FS $\mathscr{T}$ of $\widetilde{\mathscr{A}}$, we write $a_\delta \subseteq \mathscr{T}$ as $a_\delta \in \mathscr{T}$ in the sequel. So, $a_\delta \in \mathscr{T} \Leftrightarrow \mathscr{T}(a) \geq \delta$.

Definition 2. A *FS* $\mathscr{T}$ of $\widetilde{\mathscr{A}}$ is called an $(\in, \in\vee(\kappa^*, q_\kappa))$-fuzzy ideal (briefly, $(\in, \in\vee(\kappa^*, q_\kappa))$-FI) of $\widetilde{\mathscr{A}}$ if $\varrho_\delta \in \mathscr{T}$ and $\varpi_\epsilon \in \mathscr{T}$ imply $(\varrho * \varpi)_{\delta\wedge\epsilon} \in \vee(\kappa^*, q_\kappa)\mathscr{T}$ for all $\delta, \varepsilon \in (0, 1]$ and $\varrho, \varpi \in \widetilde{\mathscr{A}}$.

Lemma 1. *Let $\mathscr{T}$ be a FS of $\widetilde{\mathscr{A}}$. Then, $\varrho_\delta \in \mathscr{T}$ implies $0_\delta \in \vee(\kappa^*, q_\kappa)$ $\mathscr{T} \Leftrightarrow \forall \varrho \in \widetilde{\mathscr{A}}, \mathscr{T}(0) \geq \mathscr{T}(\varrho) \wedge (\kappa^* - \kappa/2)$.*

Lemma 2. *Let $\mathscr{T}$ be an $(\in, \in\vee(\kappa^*, q_\kappa))$-fuzzy ideal of $\widetilde{\mathscr{A}}$ such that $\varrho \leq \varpi$. Then, $\mathscr{T}(\varrho) \geq \mathscr{T}(\varpi) \wedge (\kappa^* - \kappa/2)$.*

Lemma 3. *Let $\mathscr{T}$ be an $(\in, \in\vee(\kappa^*, q_\kappa))$-fuzzy ideal of $\widetilde{\mathscr{A}}$. Then, for any $\varrho, \varpi, \Theta \in \widetilde{\mathscr{A}}$, $\varrho * \varpi \leq \Theta \Rightarrow \mathscr{T}(\varrho) \geq \mathscr{T}(\varpi) \wedge \mathscr{T}(\Theta) \wedge (\kappa^* - \kappa/2)$.*

3. $(\in, \in\vee(\kappa^*, q_\kappa))$-Fuzzy q-Ideals

Definition 3. Let a_δ be an OFP of $\widetilde{\mathscr{A}}$ and $\kappa^* \in (0, 1]$. Then, a_δ is said to be (κ^*, q)-*quasi-coincident* with a FS $\mathscr{T}$ of $\widetilde{\mathscr{A}}$, written as $a_\delta(\kappa^*, q)\mathscr{T}$, if

$$\mathscr{T}(a) + \delta > \kappa^*. \tag{2}$$

Let $0 \leq \kappa < \kappa^* \leq 1$. For an OFP ϱ_δ, we write

(1) $\varrho_\delta(\kappa^*, q_\kappa)\mathscr{T}$ if $\mathscr{T}(\varrho) + \delta + \kappa > \kappa^*$

(2) $\varrho_\delta \in \vee(\kappa^*, q_\kappa)\mathscr{T}$ if $\varrho_\delta \in \mathscr{T}$ or $\varrho_\delta(\kappa^*, q_\kappa)\mathscr{T}$

(3) $\varrho_\delta \overline{\alpha} \mathscr{T}$ if $\varrho_\delta \alpha \mathscr{T}$ does not hold for $\alpha \in \{(\kappa^*, q_\kappa), \in\vee(\kappa^*, q_\kappa)\}$

Definition 4. A *FS* $\mathscr{T}$ of $\widetilde{\mathscr{A}}$ is called an $(\in, \in\vee(\kappa^*, q_\kappa))$-fuzzy q-ideal (briefly, $(\in, \in\vee(\kappa^*, q_\kappa))$-FQI) of $\widetilde{\mathscr{A}}$ if

(1) $\varrho_\delta \in \mathscr{T}$ implies $0_\delta \in \vee(\kappa^*, q_\kappa)\mathscr{T}$

(2) $(\varpi * (\Theta * \varrho))_\delta \in \mathscr{T}$ and $\Theta_\epsilon \in \mathscr{T}$ imply $(\varpi * \varrho)_{\delta\wedge\varepsilon} \in \vee(\kappa^*, q_\kappa)\mathscr{T} \forall \varpi, \Theta, \varrho \in \widetilde{\mathscr{A}}$ and $\delta, \varepsilon \in (0, 1]$.

Example 1. Consider $\widetilde{\mathscr{A}} = \{0, 1, j, \varrho, \Theta\}$ as a *BCI*-algebra under the operation $(*)$ which is defined in Table 1.

Define a *FS* $\mathscr{T}$ on $\widetilde{\mathscr{A}}$ as

$$\mathscr{T}(\varpi) = \begin{cases} 0.6 & \text{if } \varpi = 0, \\ 0.1 & \text{if } \varpi \in \{1, \Theta\}, \\ 0.3 & \text{if } \varpi = j, \\ 0.2 & \text{if } \varpi = \varrho. \end{cases} \tag{3}$$

Choose $\kappa^* = 0.8$ and $\kappa = 0.4$. It is straightforward to show that $\mathscr{T}$ is an $(\in, \in\vee(\kappa^*, q_\kappa))$-FQI of $\widetilde{\mathscr{A}}$.

Definition 5. A *FS* $\mathscr{T}$ of $\widetilde{\mathscr{A}}$ is called an $(\in, \in\vee q)$-fuzzy q-ideal (briefly, $(\in, \in\vee q)$-FQI) of $\widetilde{\mathscr{A}}$ if

(1) $\varrho_\delta \in \mathscr{T}$ implies $0_\delta \in \vee q\mathscr{T}$

(2) $(\varpi * (\Theta * \varrho))_\delta \in \mathscr{T}$ and $\Theta_\epsilon \in \mathscr{T}$ imply $(\varpi * \varrho)_{\delta\wedge\varepsilon} \in \vee q\mathscr{T}, \forall \varpi, \Theta, \varrho \in \widetilde{\mathscr{A}}$ and $\delta, \varepsilon \in (0, 1]$.

Example 2. Take a *BCI*-algebra $\widetilde{\mathscr{A}} = \{0, 1, j, \varpi\}$ with operation $(*)$ which is described in Table 2.

Define a FS $\mathscr{T}$ on $\widetilde{\mathscr{A}}$ as

$$\mathscr{T}(\vartheta) = \begin{cases} 0.6 & \text{if } \vartheta = 0, \\ 0.1 & \text{if } \vartheta \in \{1, j\}. \end{cases} \tag{4}$$

It is straightforward to check that $\mathscr{T}$ is an $(\in, \in\vee q)$-FQI of $\widetilde{\mathscr{A}}$.

Lemma 4. *In $\widetilde{\mathscr{A}}$, every $(\in, \in\vee q)$-FQI is $(\in, \in\vee(\kappa^*, q_\kappa))$-FQI.*

Proof. Let $\mathscr{T}$ be an $(\in, \in\vee q)$-FQI of $\widetilde{\mathscr{A}}$. Take any $\varrho_\delta \in \mathscr{T}$ for $\varrho \in \widetilde{\mathscr{A}}$ and $\delta \in (0, 1]$. Then, by hypothesis, $0_\delta \in \vee q\mathscr{T}$. It implies that $\mathscr{T}(0) \geq \delta$ or $\mathscr{T}(0) + \delta \geq 1$, and thus, $\mathscr{T}(0) \geq \delta$ or $\mathscr{T}(0) + \kappa + \delta > \kappa^*$. Therefore, $0_\delta \in \vee(\kappa^*, q_\kappa)\mathscr{T}$. Next, take any $(\varpi * (\Theta * \varrho))_\delta \in \mathscr{T}$ and $\Theta_\epsilon \in \mathscr{T}$. So, $(\varpi * \varrho)_{\delta\wedge\epsilon} \in \vee q\mathscr{T}$ implies $\mathscr{T}(\varpi * \varrho) \geq \delta \wedge \varepsilon$ or $\mathscr{T}(\varpi * \varrho) + \delta \wedge \varepsilon > 1$. Therefore, $\mathscr{T}(\varpi * \varrho) \geq \delta \wedge \varepsilon$ or $\mathscr{T}(\varpi * \varrho) + \kappa + \delta \wedge \varepsilon > \kappa^*$. Thus, $(\varpi * \varrho)_{\delta\wedge\epsilon} \in \vee(\kappa^*, q_\kappa)\mathscr{T}$. Hence, $\mathscr{T}$ is an $(\in, \in\vee(\kappa^*, q_\kappa))$-FQI of $\widetilde{\mathscr{A}}$. □

In general, the converse of Lemma 4 is not valid, as illustrated by the following example.

Table 1: Cayley table of the binary operation $*$.

$*$	0	1	j	ϱ	Θ
0	0	0	0	ϱ	ϱ
1	1	0	1	Θ	ϱ
j	j	j	0	ϱ	ϱ
ϱ	ϱ	ϱ	ϱ	0	0
Θ	Θ	ϱ	Θ	1	0

Table 2: Cayley table of the binary operation $*$.

$*$	0	1	j
0	0	0	j
1	1	0	j
j	j	j	0

Example 3. Take a *BCI*-algebra $\widetilde{\mathscr{A}} = \{0, 1, j, \varrho\}$ with the operation $(*)$ described in Table 3.

Define a *FS* $\mathscr{T}$ on $\widetilde{\mathscr{A}}$ as

$$\mathscr{T}(\varpi) = \begin{cases} 0.7 & \text{if } \varpi = 0, \\ 0.6 & \text{if } \varpi = 1, \\ 0.4 & \text{if } \varpi \in \{j, \varrho\}. \end{cases} \tag{5}$$

Choose $\kappa^* = 0.82$ and $\kappa = 0.02$. It is straightforward to show that $\mathscr{T}$ is an $(\in, \in\vee(\kappa^*, q_\kappa))$-FQI of $\widetilde{\mathscr{A}}$ but not an $(\in, \in\vee q)$-FQI because $(\varrho * (0 * 1))_{\delta=0.5} \in \mathscr{T}$ and $0_{\varepsilon=0.5} \in \mathscr{T}$ but $(\varrho * 1)_{\delta\wedge\varepsilon=0.5} \overline{\in\vee q}\mathscr{T}$.

Definition 6. A *FS* $\mathscr{T}$ of $\widetilde{\mathscr{A}}$ is called an $(\in\vee(\kappa^*, q_\kappa), \in\vee(\kappa^*, q_\kappa))$-fuzzy q-ideal (briefly, $(\in\vee(\kappa^*, q_\kappa), \in\vee(\kappa^*, q_\kappa))$-*FQI*) of $\widetilde{\mathscr{A}}$ if

(1) $\varrho_\delta \in\vee(\kappa^*, q_\kappa)\mathscr{T}$ implies $0_\delta \in\vee(\kappa^*, q_\kappa)\mathscr{T}$

(2) $(\varpi * (\Theta * \varrho))_\delta \in\vee(\kappa^*, q_\kappa)\mathscr{T}$ and $\Theta_\epsilon \in\vee(\kappa^*, q_\kappa)\mathscr{T}$ imply $(\varpi * \varrho)_{\delta\wedge\varepsilon} \in\vee(\kappa^*, q_\kappa)\mathscr{T}$ $\forall \varpi, \Theta, \varrho \in \widetilde{\mathscr{A}}$ and $\delta, \varepsilon \in (0, 1]$

Example 4. Take a *BCI*-algebra $\widetilde{\mathscr{A}} = \{0, 1, j, \varrho\}$ with operation $(*)$ which is described in Table 4.

Define $\mathscr{T}: \widetilde{\mathscr{A}} \longrightarrow [0, 1]$ by

$$\mathscr{T}(\varpi) = \begin{cases} 0.9, & \text{if } \varpi = 0, \\ 0.3, & \text{if } \varpi \in \{1, j, \varrho\}. \end{cases} \tag{6}$$

Consider $\kappa^* = 0.2$ and $\kappa = 0.1$. It is easy to check that $\mathscr{T}$ is an $(\in, \in\vee(\kappa^*, q_\kappa))$-FI of $\widetilde{\mathscr{A}}$.

Lemma 5. *In $\widetilde{\mathscr{A}}$, every $(\in\vee(\kappa^*, q_\kappa), \in\vee(\kappa^*, q_\kappa))$-FQI is $(\in, \in\vee(\kappa^*, q_\kappa))$-FQI.*

Proof. Let $\mathscr{T}$ be any $(\in\vee(\kappa^*, q_\kappa), \in\vee(\kappa^*, q_\kappa))$-FQI of $\widetilde{\mathscr{A}}$. Take any $\varrho_\delta \in \mathscr{T}$ for $\varrho \in \widetilde{\mathscr{A}}$ and $\delta \in (0, 1]$. Then, $\varrho_\delta \in\vee(\kappa^*, q_\kappa)\mathscr{T}$. So, by hypothesis, $0_\delta \in\vee(\kappa^*, q_\kappa)\mathscr{T}$. Suppose that $(\varpi * (\Theta * \varrho))_\delta \in \mathscr{T}$ and $\Theta_\epsilon \in \mathscr{T}$. Then, $(\varpi * (\Theta * \varrho))_\delta \in\vee(\kappa^*, q_\kappa)\mathscr{T}$ and $\Theta_\epsilon \in\vee(\kappa^*, q_\kappa)\mathscr{T}$. Therefore, by hypothesis, $(\varpi * \varrho)_{\delta\wedge\varepsilon} \in\vee(\kappa^*, q_\kappa)\mathscr{T}$. Hence, $\mathscr{T}$ is an $(\in, \in\vee(\kappa^*, q_\kappa))$-FQI of $\mathscr{A}$. □

Table 3: Cayley table of the binary operation $*$.

$*$	0	1	j	ϱ
0	0	ϱ	j	1
1	1	0	ϱ	j
j	j	1	0	ϱ
ϱ	ϱ	j	1	0

Table 4: Cayley table of the binary operation $*$.

$*$	0	1	j	ϱ
0	0	0	0	ϱ
1	1	0	0	ϱ
j	j	j	0	ϱ
ϱ	ϱ	ϱ	ϱ	0

In general, the converse of Lemma 5 is not valid, as illustrated in the following example.

Example 5. Take a *BCI*-algebra $\widetilde{\mathscr{A}} = \{0, 1, j, \varrho, \Theta\}$ with the operation $(*)$ described in Table 5.

Define $\mathscr{T}: \widetilde{\mathscr{A}} \longrightarrow [0, 1]$ by

$$\mathscr{T}(\varpi) = \begin{cases} 0.4, & \text{if } \varpi = 0, \\ 0.6, & \text{if } \varpi \in \{1, \varrho\}, \\ 0.1, & \text{if } \varpi = \{j, \Theta\}. \end{cases} \tag{7}$$

Consider $\kappa = 0$ and $\kappa^* = 0.7$. Then, $\mathscr{T}$ is an $(\in, \in\vee(\kappa^*, q_\kappa))$-FQI of $\widetilde{\mathscr{A}}$, but it is not an $(\in\vee(\kappa^*, q_\kappa), \in\vee(\kappa^*, q_\kappa))$-FQI of $\widetilde{\mathscr{A}}$ as $j_{\delta=0.95} = (j * (0 * 1))_{\delta=0.95} \in\vee(\kappa^*, q_\kappa)\mathscr{T}$ and $0_{\varepsilon=0.5} \in\vee(\kappa^*, q_\kappa)\mathscr{T}$, but $j = (j * 1)_{\delta\wedge\varepsilon=0.5} \overline{\in\vee(\kappa^*, q_\kappa)}\mathscr{T}$.

Lemma 6. *Let $\mathscr{T}$ be a FS of $\widetilde{\mathscr{A}}$. Then, $(\varpi * (\Theta * \varrho))_\delta \in \mathscr{T}$ and $\Theta_\epsilon \in \mathscr{T}$ imply $(\varpi * \varrho)_{\delta\wedge\varepsilon} \in\vee(\kappa^*, q_\kappa)\mathscr{T} \Leftrightarrow \mathscr{T}(\varpi * \varrho) \geq \mathscr{T}(\varpi * (\Theta * \varrho))\wedge\mathscr{T}(\Theta)\wedge(\kappa^* - \kappa/2)$.*

Proof. $(\Rightarrow)$ On the contrary, suppose that $\mathscr{T}(\varrho) < \mathscr{T}(\varpi * (\Theta * \varrho))\wedge\mathscr{T}(\Theta)\wedge(\kappa^* - \kappa/2)$ for some $\varpi, \Theta, \varrho \in \widetilde{\mathscr{A}}$. Choose $\delta \in (0, (\kappa^* - \kappa/2)]$ such that $\mathscr{T}(\varrho) < \delta \leq \mathscr{T}(\varpi * (\Theta * \varrho))\wedge\mathscr{T}(\Theta)\wedge(\kappa^* - \kappa/2)$. Then, $(\varpi * (\Theta * \varrho))_\delta \in \mathscr{T}$ and $\Theta_\delta \in \mathscr{T}$, but $\varrho_\delta \overline{\in\vee(\kappa^*, q_\kappa)}\mathscr{T}$, which is not possible. Thus, $\mathscr{T}(\varpi * \varrho) \geq \mathscr{T}(\varpi * (\Theta * \varrho))\wedge\mathscr{T}(\Theta)\wedge(\kappa^* - \kappa/2)$.

$(\Leftarrow)$ Let $(\varpi * (\Theta * \varrho))_\delta \in \mathscr{T}$ and $\Theta_\varepsilon \in \mathscr{T}$, $\forall \delta, \varepsilon \in (0, 1]$. Then, $\mathscr{T}(\varpi * (\Theta * \varrho)) \geq \delta$ and $\mathscr{T}(\Theta) \geq \varepsilon$. Thus,

$$\begin{aligned} \mathscr{T}(\varpi * \varrho) &\geq \mathscr{T}(\varpi * (\Theta * \varrho))\wedge\mathscr{T}(\Theta)\wedge\frac{\kappa^* - \kappa}{2} \\ &\geq \delta\wedge\varepsilon\wedge\frac{\kappa^* - \kappa}{2}. \end{aligned} \tag{8}$$

Now, if $\delta\wedge\varepsilon \leq (\kappa^* - \kappa/2)$, then $\mathscr{T}(\varpi * \varrho) \geq \delta\wedge\varepsilon$; hence, $(\varpi * \varrho)_{\delta\wedge\varepsilon} \in \mathscr{T}$; otherwise, i.e., when $\delta\wedge\varepsilon > (\kappa^* - \kappa/2)$, $\mathscr{T}(\varpi * \varrho) \geq (\kappa^* - \kappa/2)$. So, we have

Table 5: Cayley table of the binary operation $*$.

$*$	0	1	j	ϱ	Θ
0	0	0	0	0	0
1	1	0	1	0	1
j	j	j	0	j	0
ϱ	ϱ	1	ϱ	0	ϱ
Θ	Θ	Θ	j	Θ	0

$$\begin{aligned}\mathscr{T}(\varpi * \varrho) + \delta \wedge \varepsilon &> \frac{\kappa^* - \kappa}{2} + \frac{\kappa^* - \kappa}{2} \\ &= \kappa^* - \kappa.\end{aligned} \tag{9}$$

This implies that $(\varpi * \varrho)_{\delta\wedge\varepsilon}(\kappa^*, q_\kappa)\mathscr{T}$. Hence, $(\varpi * \varrho)_{\delta\wedge\varepsilon} \in \vee(\kappa^*, q_\kappa)\mathscr{T}$, as required. □

By combining Lemma 1 and Lemma 6, we get the following theorem.

Theorem 1. *A FS $\mathscr{T}$ of $\widetilde{\mathscr{A}}$ is an $(\in, \in\vee(\kappa^*, q_\kappa))$-FQI of $\widetilde{\mathscr{A}}$ ⇔*

(1) $\mathscr{T}(0) \geq \mathscr{T}(\varrho) \wedge (\kappa^* - \kappa/2)$

(2) $\mathscr{T}(\varpi * \varrho) \geq \mathscr{T}(\varpi * (\Theta * \varrho)) \wedge \mathscr{T}(\Theta) \wedge (\kappa^* - \kappa/2)$, $\forall \varpi, \Theta, \varrho \in \widetilde{\mathscr{A}}$

Theorem 2. *Every $(\in, \in\vee(\kappa^*, q_\kappa))$-FQI of $\widetilde{\mathscr{A}}$ is an $(\in, \in\vee(\kappa^*, q_\kappa))$-FI.*

Proof. Let $\mathscr{T}$ be an $(\in, \in\vee(\kappa^*, q_\kappa))$-FQI of $\widetilde{\mathscr{A}}$. Then, $\forall\, \varpi, \Theta, \varrho \in \widetilde{\mathscr{A}}$, we have

$$\mathscr{T}(\varpi * \varrho) \geq \mathscr{T}(\varpi * (\Theta * \varrho)) \wedge \mathscr{T}(\Theta) \wedge \frac{\kappa^* - \kappa}{2}. \tag{10}$$

Substitute ϱ by 0, to obtain

$$\mathscr{T}(\varpi * 0) \geq \mathscr{T}(\varpi * (\Theta * 0)) \wedge \mathscr{T}(\Theta) \wedge \frac{\kappa^* - \kappa}{2}. \tag{11}$$

Thus, $\mathscr{T}(\varpi) \geq \mathscr{T}(\varpi * \Theta) \wedge \mathscr{T}(\Theta) \wedge (\kappa^* - \kappa/2)$, as required. □

In general, the converse of Theorem 2 is not valid, as illustrated in the following example.

Example 6. Take a *BCI*-algebra $\widetilde{\mathscr{A}} = \{0, 1, j, \varrho, \Theta\}$ with the operation $(*)$ described in Table 6.

Define a *FS* $\mathscr{T}$ on $\widetilde{\mathscr{A}}$ as

$$\mathscr{T}(\varpi) = \begin{cases} 0.4 & \text{if } \varpi = 0, \\ 0.2 & \text{if } \varpi = 1, \\ 0 & \text{if } \varpi \in \{j, \varrho, \Theta\}. \end{cases} \tag{12}$$

Choose $\kappa = 0.1$ and $\kappa^* = 0.9$. It is straightforward to check that $\mathscr{T}$ is an $(\in, \in\vee(\kappa^*, q_\kappa))$-FI of $\widetilde{\mathscr{A}}$, but it is not an $(\in, \in\vee(\kappa^*, q_\kappa))$-FQI because $0 = \mathscr{T}(\Theta * j) \not\geq \mathscr{T}(\Theta * (0 * j)) \wedge \mathscr{T}(0) \wedge 0.4 = \mathscr{T}(0) = 0.4$.

Theorem 3. *If $\mathscr{T}$ is an $(\in, \in\vee(\kappa^*, q_\kappa))$-FI of $\widetilde{\mathscr{A}}$, then the following statements are equivalent:*

Table 6: Cayley table of the binary operation $*$.

$*$	0	1	j	ϱ	Θ
0	0	0	Θ	ϱ	j
1	1	0	Θ	ϱ	j
j	j	j	0	Θ	ϱ
ϱ	ϱ	ϱ	j	0	Θ
Θ	Θ	Θ	ϱ	j	0

(1) $\mathscr{T}$ *is an* $(\in, \in\vee(\kappa^*, q_\kappa))$-*FQI of* $\widetilde{\mathscr{A}}$

(2) $\mathscr{T}(\varpi * \Theta) \geq \mathscr{T}(\varpi * (0 * \Theta)) \wedge (\kappa^* - \kappa/2)$, $\forall \varpi, \Theta \in \widetilde{\mathscr{A}}$

(3) $\mathscr{T}((\varpi * \Theta) * \varrho) \geq \mathscr{T}(\varpi * (\Theta * \varrho)) \wedge (\kappa^* - \kappa/2)$, $\forall \varpi, \Theta, \varrho \in \widetilde{\mathscr{A}}$

Proof. (1)⇒(2). Let $\mathscr{T}$ be an $(\in, \in\vee(\kappa^*, q_\kappa))$-FQI of $\widetilde{\mathscr{A}}$. Then, $\forall\, \varpi, \Theta, \varrho \in \widetilde{\mathscr{A}}$, we have

$$\mathscr{T}(\varpi * \varrho) \geq \mathscr{T}(\varpi * (\Theta * \varrho)) \wedge \mathscr{T}(\Theta) \wedge (\kappa^* - \kappa/2). \tag{13}$$

Replacing ϱ by Θ and Θ by ϱ, we get

$$\mathscr{T}(\varpi * \Theta) \geq \mathscr{T}(\varpi * (\varrho * \Theta)) \wedge \mathscr{T}(\varrho) \wedge \frac{\kappa^* - \kappa}{2}. \tag{14}$$

Substitute ϱ by 0, to obtain

$$\begin{aligned}\mathscr{T}(\varpi * \Theta) &\geq \mathscr{T}(\varpi * (0 * \Theta)) \wedge \mathscr{T}(0) \\ &= \mathscr{T}(\varpi * (0 * \Theta)) \wedge \frac{\kappa^* - \kappa}{2}.\end{aligned} \tag{15}$$

(2)⇒(3). Let $\varpi, \Theta, \varrho \in \widetilde{\mathscr{A}}$. Then,

$$\mathscr{T}((\varpi * \Theta) * \varrho) \geq \mathscr{T}((\varpi * \Theta) * (0 * \varrho)) \wedge \frac{\kappa^* - \kappa}{2}. \tag{16}$$

Now, we have

$$\begin{aligned}&((\varpi * \Theta) * (0 * \varrho)) * (\varpi * (\Theta * \varrho)) \\ &= ((\varpi * \Theta) * (\varpi * (\Theta * \varrho))) * (0 * \varrho) \\ &\leq ((\Theta * \varrho) * \Theta) * (0 * \varrho) \\ &= ((\Theta * \Theta) * \varrho) * (0 * \varrho) \\ &= (0 * \varrho) * (0 * \varrho) \\ &= 0.\end{aligned} \tag{17}$$

By Lemma 3, we have

$$\mathscr{T}((\varpi * \Theta) * (0 * \varrho)) \geq \mathscr{T}(\varpi * (\Theta * \varrho)) \wedge \frac{\kappa^* - \kappa}{2}. \tag{18}$$

From (16) and (18), we obtain $\mathscr{T}((\varpi * \Theta) * \varrho) \geq \mathscr{T}(\varpi * (\Theta * \varrho)) \wedge (\kappa^* - \kappa/2)$.

(3)⇒(1). As $\mathscr{T}$ is an $(\in, \in\vee(\kappa^*, q_\kappa))$-FI of $\widetilde{\mathscr{A}}$, $\forall\, \varpi, \Theta, \varrho \in \widetilde{\mathscr{A}}$, we have

$$\begin{aligned}\mathscr{T}(\varpi * \varrho) &\geq \mathscr{T}((\varpi * \varrho) * \Theta) \wedge \mathscr{T}(\Theta) \wedge \frac{\kappa^* - \kappa}{2} \\ &\geq \mathscr{T}(\varpi * (\Theta * \varrho)) \wedge \mathscr{T}(\Theta) \wedge \frac{\kappa^* - \kappa}{2}.\end{aligned} \tag{19}$$

□

Lemma 7. *Let $\mathcal{T}$ be an $(\in, \in\vee(\kappa^*, q_\kappa))$-FQI of $\widetilde{\mathcal{A}}$. Then, $\mathcal{T}(0 * \varrho) \geq \mathcal{T}(\varrho) \wedge (\kappa^* - \kappa/2) \forall \varrho \in \widetilde{\mathcal{A}}$.*

Proof. Assume that $\mathcal{T}$ is an $(\in, \in\vee(\kappa^*, q_\kappa))$-FQI of $\widetilde{\mathcal{A}}$. Then, $\forall \varpi, \Theta, \varrho \in \widetilde{\mathcal{A}}$, we have

$$\mathcal{T}(\varpi * \varrho) \geq \mathcal{T}(\varpi * (\Theta * \varrho)) \wedge \mathcal{T}(\Theta) \wedge \frac{\kappa^* - \kappa}{2}. \tag{20}$$

Substitute ϖ by 0 and Θ by ϱ, and we have

$$\mathcal{T}(0 * \varrho) \geq \mathcal{T}(0 * (\varrho * \varrho)) \wedge \mathcal{T}(\varrho) = \mathcal{T}(\varrho) \wedge \frac{\kappa^* - \kappa}{2}. \tag{21}$$

□

Definition 7. Let $\mathcal{T}$ be a FS of $\widetilde{\mathcal{A}}$. The set

$$\mathcal{T}_\delta = \left\{\varrho \in \widetilde{\mathcal{A}} | \mathcal{T}(\varrho) \geq \delta\right\}, \text{ where } \delta \in (0, 1], \tag{22}$$

is called the *level subset* of $\mathcal{T}$.

Theorem 4. *Let $\mathcal{T}$ be a FS of $\widetilde{\mathcal{A}}$. Then, $\mathcal{T}$ is an $(\in, \in\vee(\kappa^*, q_\kappa))$-FQI of $\widetilde{\mathcal{A}} \Leftrightarrow$ the set $\mathcal{T}_\delta (\neq \varnothing)$ is a q-ideal of $\widetilde{\mathcal{A}}$, $\forall \delta \in (0, (\kappa^* - \kappa/2)]$.*

Proof. ($\Rightarrow$) Let $\delta \in (0, (\kappa^* - \kappa/2)]$ with $\mathcal{T}_\delta \neq \varnothing$. From Theorem 1, we have

$$\mathcal{T}(0) \geq \mathcal{T}(\varrho) \wedge \frac{\kappa^* - \kappa}{2}, \tag{23}$$

with $\varrho \in \mathcal{T}_\delta$. It implies that $\mathcal{T}(0) \geq \delta \wedge (\kappa^* - \kappa/2) = \delta$. Therefore, $0 \in \mathcal{T}_\delta$.

Next, assume that $(\varpi * (\Theta * \varrho)) \in \mathcal{T}_\delta$ and $\Theta \in \mathcal{T}_\delta$. Then, $\mathcal{T}(\varpi * (\Theta * \varrho)) \geq \delta$ and $\mathcal{T}(\Theta) \geq \delta$. Again, by Theorem 1, we have

$$\begin{aligned} \mathcal{T}(\varpi * \varrho) &\geq \mathcal{T}(\varpi * (\Theta * \varrho)) \wedge \mathcal{T}(\Theta) \wedge \frac{\kappa^* - \kappa}{2} \\ &\geq \delta \wedge \frac{\kappa^* - \kappa}{2} = \delta. \end{aligned} \tag{24}$$

Therefore, $\varpi * \varrho \in \mathcal{T}_\delta$. Hence, $\mathcal{T}_\delta$ is a q-ideal of $\widetilde{\mathcal{A}}$.

($\Leftarrow$) Assume that $\mathcal{T}_\delta$ is q-ideal of $\widetilde{\mathcal{A}}$, $\forall \delta \in (0, (\kappa^* - k/2)]$. If $\mathcal{T}(0) < \mathcal{T}(\varrho) \wedge (\kappa^* - \kappa/2)$ for some $\varrho \in \widetilde{\mathcal{A}}$, then $\exists \delta \in (0, (\kappa^* - k/2)]$ such that $\mathcal{T}(0) < \delta \leq \mathcal{T}(\varrho) \wedge (\kappa^* - \kappa/2)$. It follows that $\varrho \in \mathcal{T}_\delta$ but $0 \notin \mathcal{T}_\delta$, a contradiction. Therefore, $\mathcal{T}(0) \geq \mathcal{T}(\varrho) \wedge (\kappa^* - \kappa/2)$. Also, if $\mathcal{T}(\varpi * \varrho) < \mathcal{T}(\varpi * (\Theta * \varrho)) \wedge \mathcal{T}(\Theta) \wedge (\kappa^* - \kappa/2)$ for some $\varpi, \Theta, \varrho \in \widetilde{\mathcal{A}}$, then $\exists \delta \in (0, (\kappa^* - k/2)]$ such that

$$\mathcal{T}(\varpi * \varrho) < \delta \leq \mathcal{T}(\varpi * (\Theta * \varrho)) \wedge \mathcal{T}(\Theta) \wedge \frac{\kappa^* - \kappa}{2}. \tag{25}$$

It follows that $(\varpi * (\Theta * \varrho)) \in \mathcal{T}_\delta$ and $\Theta \in \mathcal{T}_\delta$ but $\varpi * \varrho \notin \mathcal{T}_\delta$, which is again a contradiction. Therefore, $\mathcal{T}(\varpi * \varrho) \geq \mathcal{T}(\varpi * (\Theta * \varrho)) \wedge \mathcal{T}(\Theta) \wedge (\kappa^* - \kappa/2)$. Hence, $\mathcal{T}$ is an $(\in, \in\vee(\kappa^*, q_\kappa))$-FQI of $\widetilde{\mathcal{A}}$. □

Definition 8. Let $\mathcal{T}$ be a FS of $\widetilde{\mathcal{A}}$. The set

$$\widetilde{[\mathcal{T}]}_\delta = \left\{\varrho \in \widetilde{\mathcal{A}} | \varrho_\delta \in\vee(\kappa^*, q_\kappa)\mathcal{T}\right\}, \text{ where } \delta \in (0, 1], \tag{26}$$

is called an $(\in\vee(\kappa^*, q_\kappa))$-*level subset* of $\mathcal{T}$.

Theorem 5. *Let $\mathcal{T}$ be a FS of $\widetilde{\mathcal{A}}$. Then, $\mathcal{T}$ is an $(\in, \in\vee(\kappa^*, q_\kappa))$-FQI of $\widetilde{\mathcal{A}} \Leftrightarrow$ the $(\in\vee(\kappa^*, q_\kappa))$-level subset $\widetilde{[\mathcal{T}]}_\delta$ of $\mathcal{T}$ is a q-ideal of $\widetilde{\mathcal{A}}$, $\forall \delta \in (0, 1]$.*

Proof. ($\Rightarrow$) Suppose $\mathcal{T}$ is an $(\in, \in\vee(\kappa^*, q_\kappa))$-FQI of $\widetilde{\mathcal{A}}$. Take any $\varrho \in \widetilde{[\mathcal{T}]}_\delta$. Then, $\varrho_\delta \in\vee(\kappa^*, q_\kappa)\mathcal{T}$. So, $\mathcal{T}(\varrho) \geq \delta$ or $\mathcal{T}(\varrho) + \delta > \kappa^* - \kappa$. Now, by Theorem 1, we have $\mathcal{T}(0) \geq \mathcal{T}(\varrho) \wedge (\kappa^* - \kappa/2)$. Thus, $\mathcal{T}(0) \geq \delta \wedge (\kappa^* - \kappa/2)$ when $\mathcal{T}(\varrho) \geq \delta$. If $\delta > (\kappa^* - \kappa/2)$, then $\mathcal{T}(0) \geq (\kappa^* - \kappa/2)$ implies $0 \in \widetilde{[\mathcal{T}]}_\delta$. Also, if $\delta \leq (\kappa^* - \kappa/2)$, then $\mathcal{T}(0) \geq \delta$ implies $0 \in \widetilde{[\mathcal{T}]}_\delta$. Similarly, $0 \in \widetilde{[\mathcal{T}]}_\delta$ when $\mathcal{T}(\varrho) + \delta > \kappa^* - \kappa$.

Next, take any $(\varpi * (\Theta * \varrho)) \in \widetilde{[\mathcal{T}]}_\delta$ and $\Theta \in \widetilde{[\mathcal{T}]}_\delta$. Then, $(\varpi * (\Theta * \varrho)) \in\vee(\kappa^*, q_\kappa)\mathcal{T}$ and $\Theta \in\vee(\kappa^*, q_\kappa)\mathcal{T}$, i.e., either $\mathcal{T}(\varpi * (\Theta * \varrho)) \geq \delta$ or $\mathcal{T}(\varpi * (\Theta * \varrho)) + \delta > \kappa^* - \kappa$ and either $\mathcal{T}(\Theta) \geq \delta$ or $\mathcal{T}(\Theta) + \delta > \kappa^* - \kappa$. By assumption, $\mathcal{T}(\varrho) \geq \mathcal{T}(\varpi * (\Theta * \varrho)) \wedge \mathcal{T}(\Theta) \wedge (\kappa^* - \kappa/2)$. Thus, the following cases arise. □

Case 1. Let $\mathcal{T}(\varpi * (\Theta * \varrho)) \geq \delta$ and $\mathcal{T}(\Theta) \geq \delta$. If $\delta > (\kappa^* - \kappa/2)$, then

$$\begin{aligned} \mathcal{T}(\varpi * \varrho) &\geq \mathcal{T}(\varpi * (\Theta * \varrho)) \wedge \mathcal{T}(\Theta) \wedge \frac{\kappa^* - \kappa}{2} \\ &\geq \delta \wedge \frac{\kappa^* - \kappa}{2} \\ &= \frac{\kappa^* - \kappa}{2}, \end{aligned} \tag{27}$$

and so, $(\varpi * \varrho)_\delta \in (\kappa^*, q_\kappa)\mathcal{T}$. If $\delta \leq (\kappa^* - \kappa/2)$, then

$$\begin{aligned} \mathcal{T}(\varpi * \varrho) &\geq \mathcal{T}(\varpi * (\Theta * \varrho)) \wedge \mathcal{T}(\Theta) \wedge \frac{\kappa^* - \kappa}{2} \\ &\geq \delta \wedge \frac{\kappa^* - \kappa}{2} \\ &= \delta. \end{aligned} \tag{28}$$

So, $(\varpi * \varrho)_\delta \in \mathcal{T}$. Hence, $\varrho_\delta \in\vee(\kappa^*, q_\kappa)\mathcal{T}$.

Case 2. Let $\mathcal{T}(\varpi * (\Theta * \varrho)) \geq \delta$ and $\mathcal{T}(\Theta) + \delta \geq \kappa^* - \kappa$. If $\delta > (\kappa^* - \kappa/2)$, then

$$\begin{aligned} \mathcal{T}(\varpi * \varrho) &\geq \mathcal{T}(\varpi * (\Theta * \varrho)) \wedge \mathcal{T}(\Theta), \frac{\kappa^* - \kappa}{2} \\ &\geq \delta \wedge \kappa^* - \kappa - \delta \wedge \frac{\kappa^* - \kappa}{2} \\ &= \kappa^* - \kappa - \delta, \end{aligned} \tag{29}$$

i.e., $\mathcal{T}(\varpi * \varrho) + \delta > \kappa^* - \kappa$, and thus, $(\varpi * \varrho)_\delta \in (\kappa^*, q_\kappa)\mathcal{T}$. If $\delta \leq (\kappa^* - \kappa/2)$, then

$$\mathcal{T}(\varpi * \varrho) \geq \mathcal{T}(\varpi * (\Theta * \varrho)) \wedge \mathcal{T}(\Theta) \wedge \frac{\kappa^* - \kappa}{2} \geq \delta \wedge \kappa^* - \kappa - \delta \wedge \frac{\kappa^* - \kappa}{2} = \delta, \tag{30}$$

and so, $(\varpi * \varrho)_\delta \in \mathcal{T}$. Hence, $(\varpi * \varrho)_\delta \in \vee(\kappa^*, q_\kappa)\mathcal{T}$.

Similarly, for other cases, i.e., when $\mathcal{T}(\varpi * (\Theta * \varrho)) + \delta > \kappa^* - \kappa$, $\mathcal{T}(\Theta) \geq \delta$, $\mathcal{T}(\varpi * (\Theta * \varrho)) + \delta > \kappa^* - \kappa$, and $\mathcal{T}(\Theta) + \delta > \kappa^* - \kappa$, we have $(\varpi * \varrho)_\delta \in \vee(\kappa^*, q_\kappa)\mathcal{T}$. Hence, for each case, $(\varpi * \varrho)_\delta \in \vee(\kappa^*, q_\kappa)\mathcal{T}$, and thus, $\varpi * \varrho \in \widetilde{[\mathcal{T}]_\delta}$.

($\Leftarrow$) Let $\widetilde{[\mathcal{T}]_\delta}$ be a q-ideal of $\widetilde{\mathcal{A}}$, $\forall \delta \in (0, 1]$. On the contrary, let

$$\mathcal{T}(0) < \mathcal{T}(\varrho) \wedge \frac{\kappa^* - \kappa}{2}, \tag{31}$$

for some $\varrho \in \widetilde{\mathcal{A}}$. Then, $\exists \delta \in (0, 1]$ such that $\mathcal{T}(0) < \delta \leq \mathcal{T}(\varrho) \wedge (\kappa^* - \kappa/2)$. It follows that $\varrho \in \widetilde{[\mathcal{T}]_\delta}$, but $0 \notin \widetilde{[\mathcal{T}]_\delta}$, which is not possible. Therefore,

$$\mathcal{T}(0) \geq \mathcal{T}(\varrho) \wedge \frac{\kappa^* - \kappa}{2}. \tag{32}$$

Also, if $\mathcal{T}(\varpi * \varrho) < \mathcal{T}(\varpi * (\Theta * \varrho)) \wedge \mathcal{T}(\Theta) \wedge (\kappa^* - \kappa/2)$ for some $\varrho, \varpi \in \widetilde{\mathcal{A}}$, then $\exists \delta \in (0, 1]$ such that

$$\mathcal{T}(\varpi * \varrho) < \delta \leq \mathcal{T}(\varpi * (\Theta * \varrho)) \wedge \mathcal{T}(\Theta) \wedge \frac{\kappa^* - \kappa}{2}. \tag{33}$$

Thus, $(\varpi * (\Theta * \varrho)) \in \widetilde{[\mathcal{T}]_\delta}$ and $\Theta \in \widetilde{[\mathcal{T}]_\delta}$, but $\varpi * \varrho \notin \widetilde{[\mathcal{T}]_\delta}$, which is again a contradiction. Therefore, $\mathcal{T}(\varpi * \varrho) \geq \mathcal{T}(\varpi * (\Theta * \varrho)) \wedge \mathcal{T}(\Theta) \wedge (\kappa^* - \kappa/2)$. Hence, $\mathcal{T}$ is an $(\in, \in \vee(\kappa^*, q_\kappa))$-FQI of $\widetilde{\mathcal{A}}$.

4. Conclusion

The main aim of the present paper is to introduce the concept of $(\in, \in \vee(\kappa^*, q_\kappa))$-FQI in *BCI*-algebras. We provided some equivalent conditions and different characterizations of the $(\in, \in \vee(\kappa^*, q_\kappa))$-FQI in terms of level subsets and $(\in \vee(\kappa^*, q_\kappa))$-level subsets of *BCI*-algebras. It has been shown that in any *BCI*-algebras, the $(\in, \in \vee(\kappa^*, q_\kappa))$-FQI is $(\in, \in \vee(\kappa^*, q_\kappa))$-FI but the converse does not hold and an example is provided to support this. Furthermore, relation between $(\in, \in \vee(\kappa^*, q_\kappa))$-FQI and q-ideal of *BCI*-algebras has been considered. In this investigation, we get to the following conclusions:

(1) If we choose $\kappa^* = 1$ and $k = 0$, then $(\in, \in \vee(\kappa^*, q_\kappa))$-FQI reduces to the notion $(\in, \in \vee q)$-FQI of X as established in [16]

(2) If we choose $\kappa^* = 1$ and $k = k$, then $(\in, \in \vee(\kappa^*, q_\kappa))$-fuzzy subalgebras and $(\in, \in \vee(\kappa^*, q_\kappa))$-FQI reduce to the concepts $(\in, \in \vee q_\kappa)$-fuzzy subalgebras and $(\in, \in \vee q_\kappa)$-FQI of X as introduced in [28]

Consequently, the notions introduced in this paper are more general than the existing notions. In future study, these ideas may be extended to other algebraic structures such as rings, hemirings, *LA*-semigroups, semi-hypergroups, semi-hyper-rings, *BL*-algebras, *MTL*-algebras, *R0*-algebras, *EQ*-algebras, *MV*-algebras, and lattice implication algebras.

Data Availability

No data were used to support this study.

Conflicts of Interest

The authors declare that they have no conflicts of interest.

Acknowledgments

This work was supported by the Taif University Researchers Supporting Project (TURSP-2020/246), Taif University, Taif, Saudi Arabia.

References

[1] L. A. Zadeh, "Fuzzy sets," *Information and Control*, vol. 8, pp. 338–353, 1965.

[2] Y. Imai and K. Iseki, "On axiom systems of propositional calculi," *XIV. Proc. Japan Acad.*vol. 42, pp. 19–22, 1966.

[3] K. Is, ki, An algebra related with a propositional calculus," *Proceedings of the Japan Academy*, vol. 42, pp. 26–29, 1966.

[4] Y. L. Liu, J. Meng, and X. H. Zhang, "q-Ideals and a-Ideals in BCI-Algebras," *SEA bull. math.*vol. 24, pp. 243–253, 2000.

[5] H. M. Khalid and B. Ahmad, "Fuzzy h-ideals in BCI-algebras," *Fuzzy Sets and Systems*, vol. 101, no. 1, pp. 153–158, 1999.

[6] Y. B. Jun, K. J. Lee, and J. Zhan, "Soft p-ideals of soft BCI-algebras," *Computers & Mathematics with Applications*, vol. 58, pp. 2060–2068, 2009.

[7] Y. B. Jun and C. H. Park, "Applications of soft sets in ideal theory of BCK/BCI-algebras," *Information Science*, vol. 178, pp. 2466–2475, 2008.

[8] Y. B. Jun and E. H. Roh, "MBJ-neutrosophic ideals of BCK/BCI-algebras," *Open Mathematics*, vol. 17, no. 1, pp. 588–601, 2019.

[9] G. Muhiuddin, D. Al-Kadi, A. Mahboob, and A. Aljohani, "Generalized fuzzy ideals of BCI-algebras based on interval valued m-polar fuzzy structures," *International Journal of Computational Intelligence Systems*, vol. 14, p. 169, 2021.

[10] G. Muhiuddin, D. Al-Kadi, and A. Mahboob, "Hybrid structures applied to ideals in BCI-algebras," *Journal of Mathematics*, vol. 2020, Article ID 2365078, 7 pages, 2020.

[11] A. Al-Masarwah, "Ahmad m-polar fuzzy ideals of BCK/BCI-algebras," *Journal of King Saud University Science*, vol. 31, pp. 1220–1226, 2019.

[12] P. M. Pu and Y. M. Liu, "Fuzzy topology I, Neighborhood structure of a fuzzy point and Moore-Smith convergence," *Journal of Mathematical Analysis and Applications*, vol. 76, pp. 571–599, 1980.

[13] S. K. Bhakat and P. Das, "-fuzzy subgroup," *Fuzzy Sets and Systems*, vol. 80, pp. 359–368, 1996.

[14] Y. B. Jun, "On (α, β)-fuzzy subalgebras of *BCK*/*BCI*-algebras," *Bull. Korean Math. Soc.*vol. 42, no. 4, pp. 703–711, 2005.

[15] Y. B. Jun, "On (α, β)-fuzzy ideals of *BCK*/*BCI*-algebras," *Scientiae Mathematicae Japonicae*, vol. 60, no. 3, pp. 613–617, 2004.

[16] J. Zhan, Y. B. Jun, and B. Davvaz, "On $(\in, \in \vee q)$-fuzzy ideals of BCI-algebras," *Iranian Journal of Fuzzy Syst.*vol. 6, no. 1, pp. 81–94, 2009.

[17] X. Ma, J. Zhan, B. Davvaz, and Y. B. Jun, "Some kinds of ($\in$, $\in \vee q$)-interval-valued fuzzy ideals of BCI-algebras," *Information Science*, vol. 178, pp. 3738–3754, 2008.

[18] X. Ma, J. Zhan, and Y. B. Jun, "Some types of ($\in$, $\in \vee q$)-interval-valued fuzzy ideals of BCI-algebras," *Iranian Journal of Fuzzy Systems*, vol. 6, pp. 53–63, 2009.

[19] A. Al-Masarwah and A. G. Ahmad, "m-Polar (α, β) -Fuzzy Ideals in BCK/BCI-Algebras," *Symmetry*, vol. 11, no. 1, p. 44, 2019.

[20] G. Muhiuddin, M. M. Takallo, R. A. Borzooei, and Y. B. Jun, "m-polar fuzzy q-ideals in BCI-algebras," *Journal of King Saud University Science*, vol. 32, no. 6, pp. 2803–2809, 2020.

[21] M. Akram, "Spherical fuzzy K-algebras," *Journal of Algebraic Hyperstructures and Logical Algebras*, vol. 2, no. 3, pp. 85–98, 2021.

[22] M. Akram and B. Davvaz, "Generalized fuzzy ideals of K-algebras," *Journal of Multiple-Valued Logic & Soft Computing*, vol. 19, no. 5-6, pp. 475–491, 2012.

[23] M. Akram, K. H. Dar, and K. P. Shum, "Interval-valued -fuzzy K-algebras," *Applied Soft Computing*, vol. 11, no. 1, pp. 1213–1222, 2011.

[24] G. Muhiuddin, "p-ideals of BCI-algebras based on neutrosophic N-structures," *Journal of Intelligent & Fuzzy Systems*, vol. 40, no. 1, pp. 1097–1105, 2021.

[25] G. Muhiuddin and Y. B. Jun, "p-semisimple neutrosophic quadruple BCI-algebras and neutrosophic quadruple p-ideals," *Annals of Communication in Mathematics*, vol. 1, no. 1, pp. 26–37, 2018.

[26] T. Senapati, C. Jana, M. Pal, and Y. B. Jun, "Cubic intuitionistic q-ideals of BCI-algebras," *Symmetry*, vol. 10, no. 12, p. 752, 2018.

[27] X. Yuan, C. Zhang, and Y. Rena, "Generalized fuzzy groups and many-valued implications," *Fuzzy Sets and Systems*, vol. 138, pp. 205–211, 2003.

[28] Y. B. Jun, K. J. Lee, and C. H. Park, "New types of fuzzy ideals in BCK/BCI-algebras," *Computers & Mathematics with Applications*, vol. 60, pp. 771–785, 2010.

Hindawi
Journal of Mathematics
Volume 2023, Article ID 9784719, 1 page
https://doi.org/10.1155/2023/9784719

Retraction

Retracted: Statistical Inference and Mathematical Properties of Burr X Logistic-Exponential Distribution with Applications to Engineering Data

Journal of Mathematics

Received 10 October 2023; Accepted 10 October 2023; Published 11 October 2023

This article has been retracted by Hindawi following an investigation undertaken by the publisher [1]. This investigation has uncovered evidence of one or more of the following indicators of systematic manipulation of the publication process:

(1) Discrepancies in scope

(2) Discrepancies in the description of the research reported

(3) Discrepancies between the availability of data and the research described

(4) Inappropriate citations

(5) Incoherent, meaningless and/or irrelevant content included in the article

(6) Peer-review manipulation

The presence of these indicators undermines our confidence in the integrity of the article's content and we cannot, therefore, vouch for its reliability. Please note that this notice is intended solely to alert readers that the content of this article is unreliable. We have not investigated whether authors were aware of or involved in the systematic manipulation of the publication process.

Wiley and Hindawi regrets that the usual quality checks did not identify these issues before publication and have since put additional measures in place to safeguard research integrity.

We wish to credit our own Research Integrity and Research Publishing teams and anonymous and named external researchers and research integrity experts for contributing to this investigation.

The corresponding author, as the representative of all authors, has been given the opportunity to register their agreement or disagreement to this retraction. We have kept a record of any response received.

References

[1] M. M. Al Sobhi, "Statistical Inference and Mathematical Properties of Burr X Logistic-Exponential Distribution with Applications to Engineering Data," *Journal of Mathematics*, vol. 2022, Article ID 4688871, 21 pages, 2022.

Hindawi
Journal of Mathematics
Volume 2022, Article ID 4688871, 21 pages
https://doi.org/10.1155/2022/4688871

Research Article

Statistical Inference and Mathematical Properties of Burr X Logistic-Exponential Distribution with Applications to Engineering Data

Mashail M. AL Sobhi

Department of Mathematics, Umm-Al-Qura University, Makkah 24227, Saudi Arabia

Correspondence should be addressed to Mashail M. AL Sobhi; mmsobhi@uqu.edu.sa

Received 10 January 2022; Revised 3 March 2022; Accepted 11 March 2022; Published 28 April 2022

Academic Editor: Naeem Jan

The Burr X logistic-exponential distribution is introduced in this study as a novel logistic-exponential distribution extension that may be utilized to efficiently describe engineering data. There are J-shape, symmetrical, left-skewed, reversed-J shape, and right-skewed densities available, as well as decreasing, rising, bathtub, unimodal, J-shape, and reversed-J shape hazard rates. The fundamental mathematical features of the proposed model were obtained. The new model's parameters were estimated using seven different approaches, including maximum likelihood, Anderson–Darling, maximum product of spacing, least-squares, Cramér–von Mises, percentiles, and weighted least squares. To evaluate the performance of the recommended estimation methods, a full simulation study was carried out. Finally, the adaptability of the provided distribution was tested using two real datasets from engineering science, revealing that the new model can yield a close match when compared to competing models.

1. Introduction

Survival and reliability analysis is an important field of statistics with several applications in engineering, actuarial science, biomedical investigations, demography, and dependability. In these applicable disciplines, several writers have constructed generalized distributions to model various data. The exponential distribution is a popular data modeling model because it is analytically tractable and has a low memory need. However, due to its declining probability density function (PDF) and constant hazard rate function, its use was limited (HRF). As a result, various academics have developed generalized variants of the exponential distribution in order to improve its capacity to represent data in applicable domains and increase its flexibility in terms of PDF and HRF. Some important generlizations of the exponential (E) distribution are proposed as follows: the exponentiated-E [1], beta-exponential [2], logoistic-E [15], beta generalized-E [3], Nadarajah–Haghighi [4], transmuted generalized-E [5], Harris extended-E [6], Marshall–Olkin Nadarajah–Haghighi [7], transmuted Topp–Leone E [8], alpha power-E [9], Marshall–Olkin logistic E [10], extended-E [11], odd inverse power generalized Weibull-E [12, 13] studied the heavy-tailed E and Type I half logistic Burr E [14] distributions.

The logistic-E (LE) distribution [15] is a significant generalization of the E distribution. We suggested a more flexible variant of the LE model termed the Burr X logistic-E (BXLE) distribution in this study. The BXLE allows for greater flexibility and application when modeling engineering data. The BXLE distribution was constructed using the Burr X family (Yousof et al. [16]).

The Burr X family's cumulative distribution function (CDF) looks like this:

$$F(x;\kappa,\varphi)=\left\{1-e^{-[G(x;\varphi)/1-(G(x;\varphi))]^2}\right\}^{\kappa},\quad \kappa>0,\ x\in\Re,\quad (1)$$

where $G(x;\varphi)$ is the baseline model CDF and φ is the baseline parameter vector. The Burr X family's PDF shrinks to

$$f(x;\kappa,\varphi)=\frac{2\kappa g(x;\varphi)G(x;\varphi)}{[1-G(x;\varphi)]^3}e^{-\left[G(x;\varphi)/1-(G(x;\varphi))^2\right]}\left\{1-e^{-\left[G(x;\varphi)/1-(G(x;\varphi))^2\right]}\right\}^{\kappa-1},\quad \kappa>0,\ x\in\Re. \tag{2}$$

Some qualities can inspire the suggested BXLE distribution, for example, the BXLE model includes the Burr X E distribution as a special submodel; the BXLE distribution provides J-shape, symmetrical, left-skewed, reversed-J shape, and right-skewed densities, as well as decreasing, increasing, bathtub, then unimodal, J-shape, and reversed-J shape hazard rates; its PDF and CDF have simple closed forms and can thus be used effectively in analyzing censored data, and it has also been employed to model engineering datasets, where it outperforms other competing distributions in terms of fit.

The key goal of this article is to investigate and deduce some of the basic distributional features of a new extension of the LE model based on the Burr X family. We are also interested in investigating the estimation of BXLE parameters using seven classical estimation methods, including maximum likelihood estimators (MLEs), Anderson–Darling estimators (ADEs), maximum product of spacing estimators (MPSEs), least-squares estimators (LSEs), Cramér–von Mises estimators (CVMEs), percentile estimators (PCEs), and weighted least-squares estimators (WLSEs). Extensive simulations were used to examine and analyze the performance of the suggested estimate approaches.

The CDF of the BXLE model is obtained by substituting the CDF of the LE model in (1), as follows:

$$F(x)=\left[1-e^{-(e^{\rho x}-1)^{2\delta}}\right]^{\kappa},\quad \rho,\delta,\kappa>0,\ x>0. \tag{3}$$

The corresponding PDF of the BXLE distribution follows, by inserting the PDF and CDF of the LE model in (2), as

$$f(x)=2\delta\kappa\rho e^{\rho x-(e^{\rho x}-1)^{2\delta}}\left(e^{\rho x}-1\right)^{2\delta-1}\left[1-e^{-(e^{\rho x}-1)^{2\delta}}\right]^{\kappa-1},\quad \rho,\delta,\kappa>0,\ x>0. \tag{4}$$

The BXLE distribution's survival function (SF) and HRF take the required forms:

$$S(x)=1-\left[1-e^{-(e^{\rho x}-1)^{2\delta}}\right]^{\kappa},$$

$$h(x)=\frac{2\delta\kappa\rho e^{\rho x}\left(e^{\rho x}-1\right)^{2\delta-1}\left[1-e^{-(e^{\rho x}-1)^{2\delta}}\right]^{\kappa}}{\left[-e^{(e^{\rho x}-1)^{2\delta}}+1\right]\left\{\left[1-e^{-(e^{\rho x}-1)^{2\delta}}\right]^{\kappa}-1\right\}}. \tag{5}$$

Figures 1 and 2 provide plots of the PDF and HRF of the BXLE distribution, respectively. The BXLE model produces J-shape, symmetrical, left-skewed, reversed-J shape, and right-skewed densities, as well as decreasing, increasing, bathtub, then unimodal, J-shape, and reversed-J shape hazard rates.

The remainder of this work is structured as follows. Section 2 determined some basic distributional features of the BXLE distribution. In Section 3, the BXLE parameters were calculated using seven different approaches. Section 4 investigated the performance of these estimators using numerical simulations. In Section 5, two engineering actual datasets were evaluated to demonstrate the relevance and adaptability of the BLLE distribution. Finally, Section 6 gave the conclusions.

2. Mathematical Properties

In this section, we will introduce some important statistical properties such as linear representation, quantile function, moments, and order statistics.

2.1. Linear Representation. An expansion for (3) can be derived using the power series

$$(1-z)^b=\sum_{j=0}^{\infty}(-1)^j\binom{b}{j}z^j, \tag{6}$$

where $|Z|<1$ and $b>0$.

Then, the BXLE CDF could be written as

$$F(x)=\sum_{j=0}^{\infty}(-1)^j\binom{\kappa}{j}e^{-j(e^{\rho x}-1)^{2\delta}}. \tag{7}$$

Applying the E series,

$$F(x)=\sum_{j,k=0}^{\infty}\frac{(-1)^{j+k}j^k}{k!}\binom{\kappa}{j}e^{2\delta k\rho x}\left(1-e^{-\rho x}\right)^{2\delta k}, \tag{8}$$

and then

$$F(x)=\sum_{j,k,m=0}^{\infty}\frac{(-1)^{j+k+m}j^k}{k!}\binom{\kappa}{j}\binom{2\delta k}{m}e^{-\rho(m-2\delta k)x}. \tag{9}$$

By differentiating the previous equation, we have

$$f(x)=\sum_{k,m=0}^{\infty}\phi_{k,m}g_{\rho(m-2\delta k)}(x), \tag{10}$$

where g_A is the PDF of E model with scale parameter $\rho(m-2\delta k)$ and $\phi_{k,m}=\sum_{j=0}^{\infty}\left((-1)^{j+k+m+1}j^k/k!\right)\binom{\kappa}{j}\binom{2\delta k}{m}$.

2.2. Quantile Function. Obtaining the inverse CDF yields the quantile function (QF) of the BXLE distribution (3) as

$$Q(p)=\frac{\log\left\{\left[-\log\left(1-p^{(1/\kappa)}\right)\right]^{(1/2\delta)}+1\right\}}{\rho},\quad 0<p<1. \tag{11}$$

The QF may be used to generate random data from the BXLE distribution:

$$x_i=\frac{\log\left\{\left[-\log\left(1-p_i^{(1/\kappa)}\right)\right]^{1/2\delta}+1\right\}}{\rho},\quad i=1,2,\ldots,n, \tag{12}$$

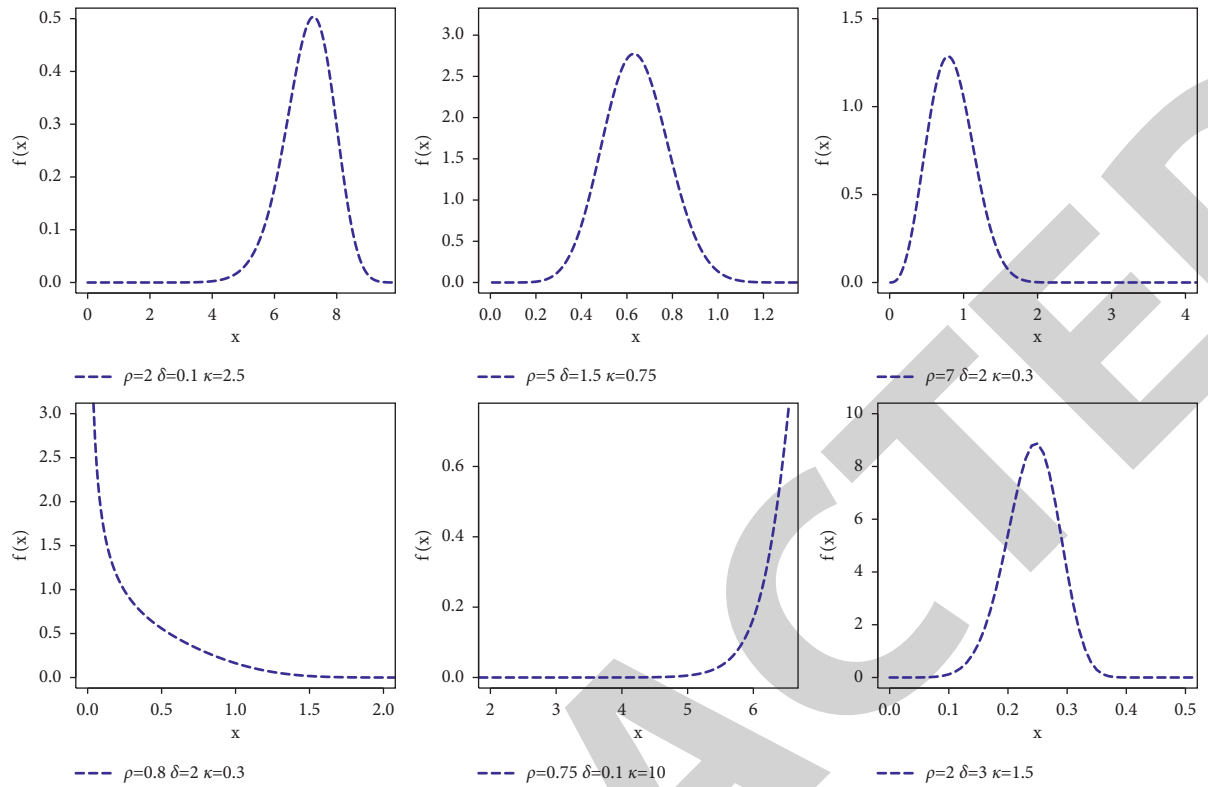

Figure 1: PDF plots of BXLE distribution.

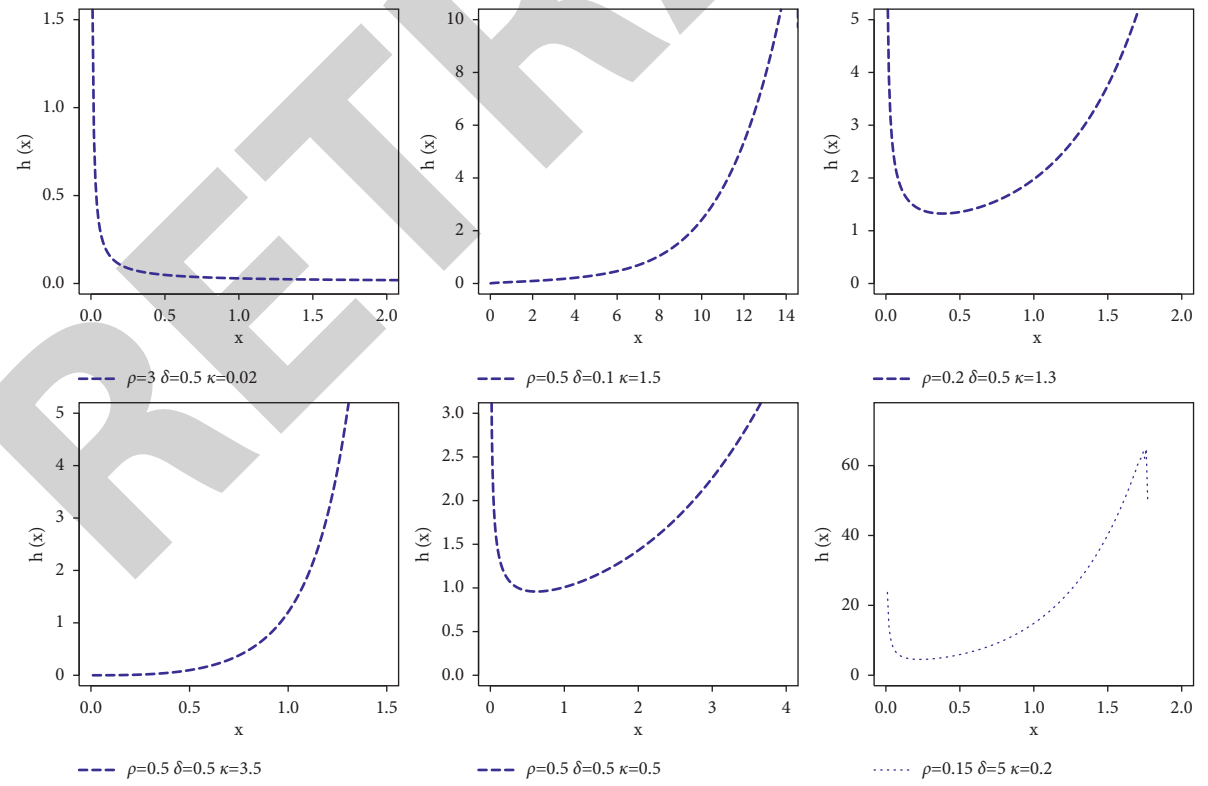

Figure 2: HRF plots of BXLE distribution.

where $p \in (0,1)$ follows the uniform distribution.

2.3. Moments. The rth moment of the BXLE distribution has the form

$$\begin{aligned}\mu_r' &= E(X^r) = \int_0^\infty x^r f(x)\mathrm{d}x \\ &= \sum_{k,m=0}^{\infty} \phi_{k,m}[\rho(m-2\delta k)]^{-r}\Gamma(r+1).\end{aligned} \tag{13}$$

One can obtain the first four original moments of the BXLE distribution by setting $r = 1, 2, 3$, and 4 in the last formula.

The BXLE distribution's moment generating function has the following form:

$$M(t) = \sum_{k,m=0}^{\infty} \phi_{k,m}\frac{\rho(m-2\delta k)}{\rho(m-2\delta k)-t}. \tag{14}$$

Characteristic function of the BXLE distribution follows from the last formula by replacing t with it.

2.4. Order Statistics. The PDF and CDF of the BXLE distribution's ith order statistic (OS) are provided by

$$\begin{aligned} f_{i:n}(x) &= \frac{n!}{(i-1)!(n-i)!}[F(x)]^{i-1}[1-F(x)]^{n-i}f(x) = \frac{2\delta\kappa\rho n! e^{\rho x}\left(e^{\rho x}-1\right)^{2\delta-1}\left[1-e^{-(e^{\rho x}-1)^{2\delta}}\right]^{i\kappa}\left\{1-\left[1-e^{-(e^{\rho x}-1)^{2\delta}}\right]^{\kappa}\right\}^{n-i}}{\Gamma(i)\Gamma(-i+n+1)\left[e^{(e^{\rho x}-1)^{2\delta}}-1\right]}, \\ F_{i:n}(x) &= \sum_{r=i}^{n}\binom{n}{r}(F(x))^r(1-F(x))^{n-r} = \frac{\Gamma(n+1)\left[1-e^{-(e^{\rho x}-1)^{2\delta}}\right]^{i\kappa}\left\{1-\left[1-e^{-(e^{\rho x}-1)^{2\delta}}\right]^{\kappa}\right\}^{n-i}\Omega}{\Gamma(i+1)\Gamma(-i+n+1)}, \end{aligned} \tag{15}$$

where $\Omega = {}_2F_1[1, i-n; i+1; 1+((1/(1-e^{-(-(1+e^{x\rho}))^{2\delta}})^{\kappa}-1))]$ is a hyper-geometric function.

$$\begin{aligned} f_{i:n}(x) &= \frac{f(x)}{B(i,n-i+1)}\sum_{h=0}^{\infty}(-1)^h\binom{n-i}{h}F^{h+i-1}(x) \\ &= \frac{\sum_{k,m=0}^{\infty}\phi_{k,m}g_{\rho(m-2\delta k)}(x)}{B(i,n-i+1)} \\ &\quad \sum_{h=0}^{\infty}(-1)^h\binom{n-i}{h}\left[1-e^{-(e^{\rho x}-1)^{2\delta}}\right]^{\kappa(h+i-1)}, \end{aligned} \tag{16}$$

where $B(\cdot,\cdot)$ is beta function.

3. Different Estimation Methods

In this part, we will look at how to estimate the BXLE parameters using seven different approaches, including the MLE, ADE, MPSE, CVME, LSE, WLSE, and PCE.

3.1. Maximum Likelihood Method of Estimation. Let $x_1, x_2, \ldots, x_n$ be a random sample of size n from the PDF (4); then, the log-likelihood function holds to

$$\begin{aligned} L &= (\kappa-1)\sum_{i=1}^{n}\log\left[1-e^{-(e^{\rho x_i}-1)^{2\delta}}\right] + \sum_{i=1}^{n}\left[\rho x_i - \left(e^{\rho x_i}-1\right)^{2\delta}\right] \\ &\quad + 2(\delta-1)\sum_{i=1}^{n}\log\left(e^{\rho x_i}-1\right) + n\log(2\delta\kappa\rho). \end{aligned} \tag{17}$$

By differentiating (17) with respect to ρ, δ, and κ, respectively, and equating to 0, then

$$\begin{aligned} \frac{\partial L}{\partial\rho} &= (\kappa-1)\sum_{i=1}^{n}\frac{2\delta x_i e^{\rho x_i - (e^{\rho x_i}-1)^{2\delta}}\left(e^{\rho x_i}-1\right)^{2\delta-1}}{1-e^{-(e^{\rho x_i}-1)^{2\delta}}} \\ &\quad + (2\delta-1)\sum_{i=1}^{n}\frac{x_i e^{\rho x_i}}{e^{\rho x_i}-1} + \sum_{i=1}^{n}\left[x_i - 2\delta x_i e^{\rho x_i}\left(e^{\rho x_i}-1\right)^{2\delta-1}\right] + \frac{n}{\rho}, \\ \frac{\partial L}{\partial\delta} &= (\kappa-1)\sum_{i=1}^{n}\frac{2e^{-(e^{\rho x_i}-1)^{2\delta}}\left(e^{\rho x_i}-1\right)^{2\delta}\log\left(e^{\rho x_i}-1\right)}{1-e^{-(e^{\rho x_i}-1)^{2\delta}}} \\ &\quad + \sum_{i=1}^{n}-2\left(e^{\rho x_i}-1\right)^{2\delta}\log\left(e^{\rho x_i}-1\right) + 2\sum_{i=1}^{n}\log\left(e^{\rho x_i}-1\right) + \frac{n}{\delta}, \\ \frac{\partial L}{\partial\kappa} &= \sum_{i=1}^{n}\log\left(1-e^{-(e^{\rho x_i}-1)^{2\delta}}\right) + \frac{n}{\kappa}. \end{aligned} \tag{18}$$

By solving the above equations, we derive MLEs of the BXLE parameters.

3.2. Ordinary and Weighted Least-Squares Methods of Estimations. Let $x_{1:n}, x_{2:n}, \ldots, x_{2:n}$ be the OS of a random sample of size n from the BXLE model. Hence, we have the OLSE of the BXLE parameters by minimizing the next equation:

$$O = \sum_{i=1}^{n}\left[F(x_{i:n}) - \frac{i}{n+1}\right]^2 = \sum_{i=1}^{n}\left\{\left[1 - e^{-(e^{\rho x_{i:\,n}} - 1)^{2\delta}}\right]^{\kappa} - \frac{i}{n+1}\right\}^2. \tag{19}$$

The OLSE of the BXLE parameters may also be calculated by solving the nonlinear equations:

$$\sum_{i=1}^{n}\left\{\left[1 - e^{-(e^{\rho x_{i:\,n}} - 1)^{2\delta}}\right]^{\kappa} - \frac{i}{n+1}\right\}\Delta_s(x_{i:\,n}) = 0, \quad s = 1, 2, 3, \tag{20}$$

where

$$\Delta_1(x_{i:n}) = \frac{\partial}{\partial\rho}F(x_{i:\,n}) = 2\delta\kappa x_{i:\,n}e^{\rho x_{i:\,n} - (e^{\rho x_{i:\,n}} - 1)^{2\delta}}\left(e^{\rho x_{i:\,n}} - 1\right)^{2\delta - 1}\left[1 - e^{-(e^{\rho x_{i:\,n}} - 1)^{2\delta}}\right]^{\kappa - 1}, \tag{21}$$

$$\Delta_2(x_{i:n}) = \frac{\partial}{\partial\delta}F(x_{i:\,n}) = \frac{2\kappa\left(e^{\rho x_{i:\,n}} - 1\right)^{2\delta}\log\left(e^{\rho x_{i:\,n}} - 1\right)\left[1 - e^{-(e^{\rho x_{i:\,n}} - 1)^{2\delta}}\right]^{\kappa}}{e^{(e^{\rho x_{i:\,n}} - 1)^{2\delta}} - 1}, \tag{22}$$

$$\Delta_3(x_{i:n}) = \frac{\partial}{\partial\kappa}F(x_{i:\,n}) = \left[1 - e^{-(e^{\rho x_{i:\,n}} - 1)^{2\delta}}\right]^{\kappa}\log\left[1 - e^{-(e^{\rho x_{i:\,n}} - 1)^{2\delta}}\right]. \tag{23}$$

The WLSE of the BXLE parameters can be calculated by minimizing the following equation:

$$W = \sum_{i=1}^{n}\frac{(n+1)^2(n+2)}{i(n-i+1)}\left[F(x_{i:n}) - \frac{i}{n+1}\right]^2 = \sum_{i=1}^{n}\frac{(n+1)^2(n+2)}{i(n-i+1)}\left\{\left[1 - e^{-(e^{\rho x_{i:\,n}} - 1)^{2\delta}}\right]^{\kappa} - \frac{i}{n+1}\right\}^2. \tag{24}$$

Furthermore, the WLSE of the BXLE parameters can be obtained by solving the following nonlinear equations:

$$\sum_{i=1}^{n}\frac{(n+1)^2(n+2)}{i(n-i+1)}\left[F(x_{i:n}) - \frac{i}{n+1}\right]\Delta_s(x_{i:n}) = 0, \tag{25}$$

where $\Delta_s(x_{i:\,n})$, $s = 1, 2, 3$, were defined in (21), (22), and (23), respectively.

3.3. Anderson–Darling Estimation. The ADEs of the BXLE parameters are obtained by minimizing the following equation:

$$A = -n - \frac{1}{n}\sum_{i=1}^{n}(2i-1)\left[\log F(x_{i:n}) + \log S(x_{i:n})\right]. \tag{26}$$

The ADE can also be calculated by solving the following nonlinear equations:

$$\sum_{i=1}^{n}(2i-1)\left[\frac{\Delta_s(x_{i:n})}{F(x_{i:n})} - \frac{\Delta_s(x_{n+1-i:n})}{S(x_{n+1-i:n})}\right] = 0, \tag{27}$$

where $\Delta_s(x_{i:n})$, $s = 1, 2, 3$, were defined in (21), (22), and (23), respectively.

3.4. Cramér–von Mises Estimators. The CVMEs of BXLE parameters are obtained by minimizing the following equation:

$$\begin{aligned}\mathrm{CV}\,&\frac{1}{12n}\sum_{i=1}^{n}\left[F(x_{i:\,n}) - \frac{2i-1}{2n}\right]^2 \\ &= \frac{2}{12n} + \sum_{i=1}^{n}\left\{\left[1 - e^{-(e^{\rho x_{i:\,n}} - 1)^{2\delta}}\right]^{\kappa} - \frac{2i-1}{2n}\right\}^2,\end{aligned} \tag{28}$$

or by solving the following nonlinear equations:

$$\sum_{i=1}^{n}\left\{\left[1 - e^{-(e^{\rho x_{i:\,n}} - 1)^{2\delta}}\right]^{\kappa} - \frac{2i-1}{2n}\right\}\Delta_s(x_{i:n}) = 0, \tag{29}$$

where $\Delta_s(x_{i:n})$, $s = 1, 2, 3$, were defined in (21), (22), and (23), respectively.

3.5. Maximum Product of Spacing Method of Estimation. As an alternative to the ML approach, the maximum product of spacing (MPS) method is used to estimate the parameters of continuous univariate models. The uniform spacings of a random sample of size n drawn from the BXLE distribution may be defined as follows:

$$D_i = F(x_i) - F(x_{i-1}), \tag{30}$$

where D_i denotes the uniform spacings, $F(x_0) = 0$, $F(x_{n+1} = 1)$, and $\sum_{i=1}^{n+1} D_i = 1$. MPS estimators (MPSEs) of the BXLE parameters can be obtained by maximizing

$$G = \frac{1}{n+1}\sum_{i=1}^{n+1}\log(D_i), \tag{31}$$

with respect to ρ, δ, and κ. Further, the MPSE of the BXLE parameters can also be obtained by solving

$$\frac{1}{n+1}\sum_{i=1}^{n+1}\frac{1}{D_i}\left[\Delta_s(x_{i:n}) - \Delta_s(x_{i-1:n})\right] = 0, \tag{32}$$

where $\Delta_s(x_{i:n})$, $s = 1, 2, 3$, were defined in (21), (22), and (23), respectively.

3.6. Percentile Method of Estimation. If we consider $pi = (i/(n+1))$ to be an estimate of $F(xi{:}\ n)$, then the PCE of the BXLE parameters is derived by minimizing the following expression:

$$\begin{aligned}\mathrm{PCE} &= \sum_{i=1}^{n}\left[x_{i:n} - Q(p_i)\right]^2 \\ &= \sum_{i=1}^{n}\left(x_{i:n} - \frac{\log\left\{\left[-\log\left(1-p_i^{1/\kappa}\right)\right]^{1/2\delta}+1\right\}}{\rho}\right)^2.\end{aligned} \tag{33}$$

Alternatively, solve the associated nonlinear equations:

$$\sum_{i=1}^{n}\left(x_{i:n} - \frac{\log\left\{\left[-\log\left(1-p_i^{1/\kappa}\right)\right]^{1/2\delta}+1\right\}}{\rho}\right)\Phi_s(x_{i:n}) = 0, \quad s = 1, 2, 3, \tag{34}$$

where

$$\begin{aligned}\Phi_1(x_{i:n}) &= \frac{\partial}{\partial\rho}Q(p_i) = -\frac{\log\left\{\left[-\log\left(1-p_i^{1/\kappa}\right)\right]^{1/2\delta}+1\right\}}{\rho^2}, \\ \Phi_2(x_{i:n}) &= \frac{\partial}{\partial\rho}Q(p_i) = -\frac{\log\left[-\log\left(1-p_i^{1/\kappa}\right)\right]}{2\delta^2\rho\left\{\left[-\log\left(1-p_i^{1/\kappa}\right)\right]^{-(1/2\delta)}+1\right\}}, \\ \Phi_3(x_{i:n}) &= \frac{\partial}{\partial\rho}Q(p_i) = -\frac{p_i^{1/\kappa}\log(p_i)\left[-\log\left(1-p_i^{1/\kappa}\right)\right]^{(1/2\delta)-1}}{2\delta\kappa^2\rho\left(p_i^{1/\kappa}-1\right)\left\{\left[-\log\left(1-p_i^{1/\kappa}\right)\right]^{(1/2\delta)}+1\right\}}.\end{aligned} \tag{35}$$

4. Numerical Outcomes

Based on comprehensive simulation findings, this section investigates the performance of the seven estimate approaches in estimating the BXLE parameters. We explore several sample sizes, $n = 20, 30, 50, 100, 200, 400$, as well as some parametric values for ρ, δ, and κ, $\rho = \{0.50, 0.75, 1.5, 2.0, 2.5, 3.0\}$, $\delta = \{0.50, 0.75, 1.5, 2.0, 3.0\}$, and $\kappa = \{0.25, 0.5, 0.75, 1.5, 2.0, 2.5, 3.0\}$. We generate $n = 2000$ random samples from the BXLE distribution using its QF and calculate the average values of the estimates (AVEs) with their associated average mean square errors (MSEs), average absolute biases (AVBs), and average mean relative estimates (MREs) for all sample sizes and parameter combinations using the R software.

The MSE, AVB, and MRE were calculated by the following equations:

$$\begin{aligned}\mathrm{MSE} &= \frac{1}{N}\sum_{i=1}^{N}(\widehat{\eta}-\eta)^2, \\ \mathrm{AVB} &= \frac{1}{N}\sum_{i=1}^{N}|\widehat{\eta}-\eta|, \\ \mathrm{MRE} &= \frac{1}{N}\sum_{i=1}^{\eta}\frac{|\widehat{\eta}-\eta|}{\eta},\end{aligned} \tag{36}$$

where $\eta = (\rho, \delta, \kappa)'$.

Table 1: Simulation results of the AVE, AVB, MSE, and MRE of BXLE distribution for $(\rho = 0.5, \delta = 0.25, \kappa = 0.75)$.

n	Est.	Est. Par.	MLE	ADE	CVME	MPSE	LSE	PCE	WLSE
20	AVE	$\widehat{\rho}$	0.75626	0.74294	0.77114	0.63616	0.66827	0.66066	0.68538
		$\widehat{\delta}$	0.32870	0.32225	0.33404	0.28857	0.30368	0.29438	0.31013
		$\widehat{\kappa}$	1.28915	1.10508	1.29370	1.17167	1.29074	1.29088	1.18169
	AVB	$\widehat{\rho}$	0.57509	0.50104	0.56988	0.44217	0.48610	0.44857	0.48385
		$\widehat{\delta}$	0.13429	0.12232	0.13450	0.10197	0.11572	0.10502	0.11975
		$\widehat{\kappa}$	0.84827	0.68373	0.88523	0.73831	0.86113	0.88817	0.76063
	MSE	$\widehat{\rho}$	0.61131	0.43585	0.55599	0.32051	0.37521	0.30429	0.38361
		$\widehat{\delta}$	0.03684	0.02765	0.03335	0.01838	0.02384	0.01723	0.02682
		$\widehat{\kappa}$	1.34536	0.97456	1.51227	1.16675	1.42122	1.76670	1.13282
	MRE	$\widehat{\rho}$	1.15018	1.00208	1.13975	0.88434	0.97220	0.89714	0.96769
		$\widehat{\delta}$	0.53715	0.48927	0.53801	0.40789	0.46288	0.42008	0.47901
		$\widehat{\kappa}$	1.13103	0.91164	1.18031	0.98441	1.14818	1.18423	1.01418
30	AVE	$\widehat{\rho}$	0.74980	0.73553	0.70742	0.64032	0.68392	0.67673	0.70238
		$\widehat{\delta}$	0.32590	0.31460	0.31839	0.28646	0.30457	0.29386	0.30745
		$\widehat{\kappa}$	1.11324	1.01445	1.23892	1.03511	1.17335	1.14738	1.05079
	AVB	$\widehat{\rho}$	0.53103	0.47971	0.50014	0.40962	0.46876	0.44152	0.46056
		$\widehat{\delta}$	0.12802	0.11374	0.11864	0.09400	0.10969	0.10188	0.10946
		$\widehat{\kappa}$	0.66919	0.59122	0.81142	0.57234	0.74324	0.73838	0.62155
	MSE	$\widehat{\rho}$	0.52477	0.38597	0.40381	0.30499	0.35316	0.28967	0.35777
		$\widehat{\delta}$	0.03443	0.02367	0.02524	0.01729	0.02085	0.01574	0.02189
		$\widehat{\kappa}$	0.79795	0.65169	1.28599	0.65605	1.08587	1.23344	0.75033
	MRE	$\widehat{\rho}$	1.06207	0.95941	1.00028	0.81924	0.93752	0.88303	0.92112
		$\widehat{\delta}$	0.51207	0.45496	0.47458	0.37600	0.43875	0.40753	0.43785
		$\widehat{\kappa}$	0.89226	0.78830	1.08189	0.76313	0.99099	0.98451	0.82873
50	AVE	$\widehat{\rho}$	0.69689	0.71560	0.75253	0.67167	0.67426	0.67517	0.67767
		$\widehat{\delta}$	0.30795	0.31005	0.32236	0.29655	0.30238	0.29341	0.30187
		$\widehat{\kappa}$	0.97495	0.87418	0.99148	0.87106	1.06047	0.97671	0.94581
	AVB	$\widehat{\rho}$	0.43983	0.40735	0.47510	0.37968	0.43243	0.40228	0.39965
		$\widehat{\delta}$	0.10706	0.10000	0.11235	0.09237	0.10150	0.09259	0.09683
		$\widehat{\kappa}$	0.48884	0.42880	0.58480	0.42059	0.61858	0.54587	0.48790
	MSE	$\widehat{\rho}$	0.39635	0.29597	0.36214	0.28129	0.29993	0.24958	0.27337
		$\widehat{\delta}$	0.02674	0.01899	0.02254	0.01768	0.01836	0.01351	0.01783
		$\widehat{\kappa}$	0.41368	0.33758	0.66812	0.33158	0.72395	0.67687	0.46245
	MRE	$\widehat{\rho}$	0.87965	0.81470	0.95020	0.75936	0.86486	0.80455	0.79929
		$\widehat{\delta}$	0.42826	0.40002	0.44939	0.36947	0.40598	0.37038	0.38731
		$\widehat{\kappa}$	0.65178	0.57173	0.77974	0.56079	0.82477	0.72782	0.65053
100	AVE	$\widehat{\rho}$	0.64897	0.66463	0.66279	0.61251	0.63576	0.67257	0.66188
		$\widehat{\delta}$	0.29199	0.29387	0.29946	0.27945	0.28980	0.29256	0.29370
		$\widehat{\kappa}$	0.83676	0.81012	0.93017	0.79547	0.93685	0.80283	0.85312
	AVB	$\widehat{\rho}$	0.32170	0.32725	0.37202	0.27099	0.35471	0.33264	0.34039
		$\widehat{\delta}$	0.08002	0.07787	0.08794	0.06545	0.08167	0.07821	0.07992
		$\widehat{\kappa}$	0.31060	0.31096	0.45045	0.27546	0.44797	0.34072	0.36769
	MSE	$\widehat{\rho}$	0.25320	0.22288	0.24784	0.16443	0.22054	0.19068	0.22617
		$\widehat{\delta}$	0.01776	0.01372	0.01601	0.01102	0.01306	0.01094	0.01367
		$\widehat{\kappa}$	0.16281	0.16200	0.40000	0.13830	0.37298	0.24699	0.25588
	MRE	$\widehat{\rho}$	0.64341	0.65451	0.74405	0.54199	0.70942	0.66528	0.68077
		$\widehat{\delta}$	0.32006	0.31150	0.35174	0.26179	0.32666	0.31284	0.31969
		$\widehat{\kappa}$	0.41413	0.41461	0.60061	0.36728	0.59729	0.45429	0.49026
200	AVE	$\widehat{\rho}$	0.62806	0.61441	0.63894	0.59507	0.62384	0.62830	0.58400
		$\widehat{\delta}$	0.28473	0.28028	0.28828	0.27427	0.28341	0.28064	0.27245
		$\widehat{\kappa}$	0.77515	0.77074	0.81983	0.76058	0.83602	0.76306	0.81231
	AVB	$\widehat{\rho}$	0.25696	0.24422	0.29983	0.21929	0.29219	0.26479	0.23074
		$\widehat{\delta}$	0.06349	0.05754	0.06868	0.05258	0.06628	0.06067	0.05306
		$\widehat{\kappa}$	0.22577	0.22809	0.31003	0.20476	0.31524	0.24611	0.24667
	MSE	$\widehat{\rho}$	0.18981	0.13768	0.17886	0.12369	0.16951	0.13519	0.12078
		$\widehat{\delta}$	0.01303	0.00851	0.01076	0.00816	0.01001	0.00742	0.00712
		$\widehat{\kappa}$	0.08315	0.08413	0.17360	0.07187	0.18961	0.10257	0.11142
	MRE	$\widehat{\rho}$	0.51391	0.48845	0.59966	0.43859	0.58438	0.52959	0.46149
		$\widehat{\delta}$	0.25396	0.23017	0.27474	0.21033	0.26512	0.24267	0.21222
		$\widehat{\kappa}$	0.30102	0.30412	0.41338	0.27302	0.42032	0.32815	0.32889

Table 1: Continued.

n	Est.	Est. Par.	MLE	ADE	CVME	MPSE	LSE	PCE	WLSE
400	AVE	$\widehat{\rho}$	0.54278	0.56400	0.59055	0.54946	0.59618	0.60443	0.55423
		$\widehat{\delta}$	0.26135	0.26722	0.27407	0.26175	0.27455	0.27381	0.26417
		$\widehat{\kappa}$	0.76724	0.76195	0.78147	0.74278	0.76910	0.71854	0.76840
	AVB	$\widehat{\rho}$	0.13906	0.16768	0.21650	0.13422	0.21968	0.18995	0.16118
		$\widehat{\delta}$	0.03348	0.03898	0.04861	0.03165	0.04877	0.04269	0.03623
		$\widehat{\kappa}$	0.14364	0.16593	0.22004	0.13548	0.21739	0.16307	0.17109
	MSE	$\widehat{\rho}$	0.05849	0.07369	0.10487	0.04410	0.10851	0.07949	0.05898
		$\widehat{\delta}$	0.00398	0.00466	0.00608	0.00267	0.00600	0.00419	0.00344
		$\widehat{\kappa}$	0.03479	0.04481	0.08409	0.03130	0.07771	0.04229	0.04917
	MRE	$\widehat{\rho}$	0.27812	0.33536	0.43299	0.26843	0.43937	0.37990	0.32236
		$\widehat{\delta}$	0.13393	0.15593	0.19442	0.12662	0.19509	0.17077	0.14491
		$\widehat{\kappa}$	0.19152	0.22124	0.29339	0.18064	0.28986	0.21742	0.22812

Table 2: Simulation results of the AVE, AVB, MSE, and MRE of BXLE distribution for $(\rho = 0.5, \delta = 0.25, \kappa = 2.5)$.

n	Est.	Est. Par.	MLE	ADE	CVME	MPSE	LSE	PCE	WLSE
20	AVE	$\widehat{\rho}$	1.79838	1.78970	3.72711	1.26641	2.56295	1.37714	2.13722
		$\widehat{\delta}$	0.29334	0.30627	0.34361	0.28445	0.33228	0.28874	0.31289
		$\widehat{\kappa}$	4.18376	3.56065	4.14725	3.59192	3.73590	3.67903	3.50675
	AVB	$\widehat{\rho}$	1.61879	1.55097	3.51563	1.04734	2.34417	1.18384	1.90137
		$\widehat{\delta}$	0.06430	0.07386	0.10995	0.05517	0.10056	0.06101	0.08100
		$\widehat{\kappa}$	2.61040	2.17815	3.01901	2.13379	2.61237	2.20280	2.27485
	MSE	$\widehat{\rho}$	27.24052	18.29810	203.49892	7.90529	41.28473	9.92185	28.59804
		$\widehat{\delta}$	0.02077	0.02546	0.04469	0.01434	0.03817	0.01850	0.02930
		$\widehat{\kappa}$	13.02115	9.19147	17.70745	10.29252	13.32810	8.42028	10.35202
	MRE	$\widehat{\rho}$	3.23757	3.10194	7.03127	2.09468	4.68835	2.36768	3.80274
		$\widehat{\delta}$	0.25720	0.29544	0.43979	0.22068	0.40226	0.24405	0.32402
		$\widehat{\kappa}$	1.04416	0.87126	1.20761	0.85352	1.04495	0.88112	0.90994
30	AVE	$\widehat{\rho}$	0.99099	1.32921	2.07930	0.95420	1.53393	0.98388	1.35775
		$\widehat{\delta}$	0.27125	0.28688	0.31226	0.27055	0.29855	0.27138	0.28670
		$\widehat{\kappa}$	3.61831	3.12526	3.73172	3.20562	3.65227	3.29690	3.28674
	AVB	$\widehat{\rho}$	0.75889	1.04541	1.84504	0.69777	1.31490	0.74802	1.10170
		$\widehat{\delta}$	0.03911	0.05178	0.07787	0.03944	0.06690	0.04132	0.05350
		$\widehat{\kappa}$	1.88820	1.59461	2.40894	1.64291	2.25227	1.71862	1.84758
	MSE	$\widehat{\rho}$	4.30156	8.59982	24.55273	3.60766	11.38860	4.80813	10.04901
		$\widehat{\delta}$	0.00776	0.01501	0.02769	0.00763	0.02158	0.00886	0.01474
		$\widehat{\kappa}$	7.31598	5.21073	11.46680	5.87619	10.04647	5.36600	6.74280
	MRE	$\widehat{\rho}$	1.51779	2.09083	3.69008	1.39553	2.62980	1.49604	2.20341
		$\widehat{\delta}$	0.15645	0.20714	0.31150	0.15778	0.26759	0.16526	0.21402
		$\widehat{\kappa}$	0.75528	0.63784	0.96358	0.65716	0.90091	0.68745	0.73903
50	AVE	$\widehat{\rho}$	0.72897	0.87809	1.30793	0.67147	1.14520	0.68726	0.94686
		$\widehat{\delta}$	0.26094	0.26977	0.28827	0.25766	0.28002	0.25869	0.27062
		$\widehat{\kappa}$	3.19562	2.77012	3.22326	2.88887	3.25550	2.99237	2.97697
	AVB	$\widehat{\rho}$	0.45319	0.54537	1.02266	0.36814	0.87346	0.40681	0.64862
		$\widehat{\delta}$	0.02671	0.03093	0.05103	0.02294	0.04451	0.02554	0.03453
		$\widehat{\kappa}$	1.33854	1.16317	1.78693	1.12205	1.75687	1.25366	1.37743
	MSE	$\widehat{\rho}$	1.88471	2.09399	7.42802	0.81609	5.56387	0.90985	3.96788
		$\widehat{\delta}$	0.00372	0.00481	0.01309	0.00201	0.01061	0.00258	0.00648
		$\widehat{\kappa}$	3.69003	2.59408	6.49205	2.69052	6.21149	2.75350	3.75536
	MRE	$\widehat{\rho}$	0.90638	1.09073	2.04533	0.73627	1.74691	0.81362	1.29724
		$\widehat{\delta}$	0.10683	0.12372	0.20413	0.09177	0.17806	0.10218	0.13811
		$\widehat{\kappa}$	0.53542	0.46527	0.71477	0.44882	0.70275	0.50146	0.55097

Table 2: Continued.

n	Est.	Est. Par.	MLE	ADE	CVME	MPSE	LSE	PCE	WLSE
100	AVE	$\widehat{\rho}$	0.55522	0.59565	0.73694	0.54867	0.65998	0.54406	0.62726
		$\widehat{\delta}$	0.25137	0.25550	0.26245	0.25206	0.25804	0.25193	0.25698
		$\widehat{\kappa}$	2.73597	2.70173	2.92681	2.62728	2.89390	2.79649	2.70926
	AVB	$\widehat{\rho}$	0.20372	0.24386	0.41585	0.19054	0.33922	0.21185	0.27539
		$\widehat{\delta}$	0.01554	0.01542	0.02334	0.01334	0.01982	0.01405	0.01699
		$\widehat{\kappa}$	0.73542	0.78757	1.21745	0.69786	1.11703	0.83807	0.89749
	MSE	$\widehat{\rho}$	0.09625	0.25577	1.05703	0.06916	0.48862	0.10010	0.23843
		$\widehat{\delta}$	0.00092	0.00075	0.00217	0.00031	0.00121	0.00039	0.00079
		$\widehat{\kappa}$	1.02468	1.12126	3.10865	0.93664	2.68427	1.30829	1.54429
	MRE	$\widehat{\rho}$	0.40743	0.48773	0.83169	0.38108	0.67843	0.42371	0.55078
		$\widehat{\delta}$	0.06218	0.06168	0.09337	0.05334	0.07928	0.05621	0.06797
		$\widehat{\kappa}$	0.29417	0.31503	0.48698	0.27914	0.44681	0.33523	0.35900
200	AVE	$\widehat{\rho}$	0.51672	0.54133	0.54552	0.53728	0.56798	0.51174	0.54949
		$\widehat{\delta}$	0.24980	0.25229	0.25268	0.25183	0.25355	0.25036	0.25282
		$\widehat{\kappa}$	2.63383	2.61698	2.79988	2.49776	2.69918	2.67996	2.59225
	AVB	$\widehat{\rho}$	0.13323	0.15520	0.19892	0.13056	0.21263	0.14086	0.16293
		$\widehat{\delta}$	0.01036	0.01015	0.01216	0.00900	0.01281	0.00958	0.01067
		$\widehat{\kappa}$	0.50072	0.55770	0.77807	0.43559	0.76143	0.56505	0.57875
	MSE	$\widehat{\rho}$	0.03135	0.05073	0.09565	0.03116	0.11396	0.03749	0.04950
		$\widehat{\delta}$	0.00051	0.00019	0.00033	0.00014	0.00036	0.00016	0.00020
		$\widehat{\kappa}$	0.44381	0.55024	1.18116	0.34815	1.03225	0.57667	0.60758
	MRE	$\widehat{\rho}$	0.26645	0.31040	0.39784	0.26112	0.42525	0.28173	0.32585
		$\widehat{\delta}$	0.04143	0.04062	0.04864	0.03600	0.05125	0.03831	0.04270
		$\widehat{\kappa}$	0.20029	0.22308	0.31123	0.17423	0.30457	0.22602	0.23150
400	AVE	$\widehat{\rho}$	0.50100	0.52236	0.52823	0.51783	0.52287	0.51285	0.51279
		$\widehat{\delta}$	0.24898	0.25119	0.25180	0.25086	0.25118	0.25060	0.25073
		$\widehat{\kappa}$	2.57622	2.54449	2.61466	2.49300	2.61337	2.55073	2.57562
	AVB	$\widehat{\rho}$	0.08862	0.10704	0.14043	0.08619	0.12979	0.09737	0.10665
		$\widehat{\delta}$	0.00729	0.00722	0.00869	0.00606	0.00825	0.00672	0.00705
		$\widehat{\kappa}$	0.33083	0.39449	0.53050	0.28869	0.50412	0.37270	0.41309
	MSE	$\widehat{\rho}$	0.01298	0.01903	0.03637	0.01352	0.03009	0.01617	0.01763
		$\widehat{\delta}$	0.00037	0.00008	0.00014	0.00006	0.00012	0.00007	0.00008
		$\widehat{\kappa}$	0.18116	0.25401	0.46145	0.16352	0.44900	0.24111	0.28127
	MRE	$\widehat{\rho}$	0.17725	0.21407	0.28086	0.17238	0.25958	0.19474	0.21331
		$\widehat{\delta}$	0.02915	0.02889	0.03476	0.02424	0.03300	0.02690	0.02820
		$\widehat{\kappa}$	0.13233	0.15779	0.21220	0.11548	0.20165	0.14908	0.16523

Table 3: Simulation results of the AVE, AVB, MSE, and MRE of BXLE distribution for $(\rho = 0.75, \delta = 1.50, \kappa = 0.25)$.

n	Est.	Est. Par.	MLE	ADE	CVME	MPSE	LSE	PCE	WLSE
20	AVE	$\widehat{\rho}$	0.99360	0.95711	0.96270	0.86926	0.98110	0.86442	0.92370
		$\widehat{\delta}$	2.42543	2.42282	2.66289	2.08319	2.56447	3.53535	2.35381
		$\widehat{\kappa}$	0.34295	0.30690	0.34230	0.31174	0.31461	0.36856	0.34015
	AVB	$\widehat{\rho}$	0.50582	0.48037	0.45163	0.45122	0.48677	0.50786	0.47104
		$\widehat{\delta}$	1.29066	1.31734	1.45196	1.18737	1.45493	2.70680	1.30148
		$\widehat{\kappa}$	0.19613	0.15841	0.18684	0.15798	0.17649	0.25179	0.19231
	MSE	$\widehat{\rho}$	0.45214	0.46317	0.45474	0.38317	0.49133	0.41989	0.43086
		$\widehat{\delta}$	4.06209	5.56485	7.76750	4.11920	6.57387	48.76375	4.70223
		$\widehat{\kappa}$	0.12030	0.07043	0.14299	0.07264	0.10355	0.39286	0.12948
	MRE	$\widehat{\rho}$	0.67443	0.64049	0.60217	0.60163	0.64902	0.67715	0.62806
		$\widehat{\delta}$	0.86044	0.87823	0.96797	0.79158	0.96995	1.80453	0.86765
		$\widehat{\kappa}$	0.78450	0.63364	0.74735	0.63194	0.70596	1.00714	0.76924

Table 3: Continued.

n	Est.	Est. Par.	MLE	ADE	CVME	MPSE	LSE	PCE	WLSE
30	AVE	$\widehat{\rho}$	0.95938	0.87601	0.92287	0.84252	0.92927	0.87334	0.89492
		$\widehat{\delta}$	2.22733	2.07721	2.38510	1.93928	2.32628	2.82560	2.18518
		$\widehat{\kappa}$	0.30217	0.29895	0.31209	0.29869	0.28824	0.32625	0.30640
	AVB	$\widehat{\rho}$	0.44834	0.39020	0.40942	0.40810	0.42097	0.46867	0.42713
		$\widehat{\delta}$	1.08404	0.96531	1.17402	1.00478	1.17111	1.91451	1.11519
		$\widehat{\kappa}$	0.15229	0.13439	0.15337	0.13590	0.13904	0.20183	0.15072
	MSE	$\widehat{\rho}$	0.34095	0.28513	0.34354	0.29757	0.35432	0.34798	0.34303
		$\widehat{\delta}$	2.66924	2.49728	4.10740	2.68863	4.11698	15.16534	3.64459
		$\widehat{\kappa}$	0.06268	0.04899	0.08541	0.04280	0.06511	0.25334	0.06424
	MRE	$\widehat{\rho}$	0.59779	0.52026	0.54590	0.54413	0.56130	0.62489	0.56950
		$\widehat{\delta}$	0.72269	0.64354	0.78268	0.66985	0.78074	1.27634	0.74346
		$\widehat{\kappa}$	0.60915	0.53757	0.61347	0.54358	0.55616	0.80732	0.60289
50	AVE	$\widehat{\rho}$	0.91163	0.86778	0.92852	0.76703	0.90027	0.84528	0.87249
		$\widehat{\delta}$	2.03322	1.99131	2.22980	1.65948	2.12220	2.31959	2.00310
		$\widehat{\kappa}$	0.29140	0.27962	0.28109	0.29744	0.27958	0.27304	0.28505
	AVB	$\widehat{\rho}$	0.37058	0.36321	0.38886	0.32528	0.38555	0.41703	0.37056
		$\widehat{\delta}$	0.86939	0.87081	1.01492	0.72622	0.98087	1.36792	0.89554
		$\widehat{\kappa}$	0.13116	0.11350	0.12246	0.11279	0.12262	0.13345	0.11958
	MSE	$\widehat{\rho}$	0.23360	0.23192	0.29373	0.18427	0.27272	0.25789	0.25123
		$\widehat{\delta}$	1.56149	1.81361	2.69281	1.25685	2.50704	5.78669	2.05061
		$\widehat{\kappa}$	0.04840	0.02696	0.04590	0.02649	0.04063	0.07676	0.03561
	MRE	$\widehat{\rho}$	0.49411	0.48428	0.51848	0.43371	0.51407	0.55604	0.49408
		$\widehat{\delta}$	0.57959	0.58054	0.67662	0.48415	0.65392	0.91195	0.59703
		$\widehat{\kappa}$	0.52466	0.45399	0.48984	0.45115	0.49050	0.53381	0.47833
100	AVE	$\widehat{\rho}$	0.88398	0.83183	0.86478	0.75635	0.86641	0.81495	0.88168
		$\widehat{\delta}$	1.90133	1.81269	1.95739	1.57353	1.96806	1.94150	1.91637
		$\widehat{\kappa}$	0.27396	0.27360	0.26871	0.28069	0.26751	0.25885	0.26220
	AVB	$\widehat{\rho}$	0.32223	0.30217	0.31393	0.26218	0.32813	0.35825	0.33039
		$\widehat{\delta}$	0.73675	0.66249	0.74721	0.54375	0.78939	0.96608	0.73887
		$\widehat{\kappa}$	0.10653	0.09510	0.09814	0.08624	0.09925	0.10375	0.09643
	MSE	$\widehat{\rho}$	0.16553	0.15050	0.17177	0.11858	0.19127	0.17936	0.17703
		$\widehat{\delta}$	1.03517	0.88563	1.25841	0.64749	1.48242	1.98362	1.04959
		$\widehat{\kappa}$	0.03014	0.01913	0.02273	0.01442	0.02174	0.02017	0.01795
	MRE	$\widehat{\rho}$	0.42964	0.40289	0.41857	0.34957	0.43751	0.47767	0.44052
		$\widehat{\delta}$	0.49117	0.44166	0.49814	0.36250	0.52626	0.64405	0.49258
		$\widehat{\kappa}$	0.42614	0.38039	0.39256	0.34498	0.39698	0.41501	0.38571
200	AVE	$\widehat{\rho}$	0.80515	0.80691	0.82173	0.73513	0.82507	0.74742	0.82156
		$\widehat{\delta}$	1.67192	1.71497	1.78058	1.50274	1.79591	1.66370	1.74915
		$\widehat{\kappa}$	0.26800	0.26074	0.26166	0.27287	0.26112	0.27281	0.26201
	AVB	$\widehat{\rho}$	0.24761	0.24322	0.25420	0.17948	0.26823	0.29254	0.26068
		$\widehat{\delta}$	0.52815	0.52432	0.55804	0.34659	0.60818	0.69585	0.56620
		$\widehat{\kappa}$	0.07914	0.07238	0.07655	0.05840	0.07850	0.09053	0.07860
	MSE	$\widehat{\rho}$	0.09236	0.09356	0.10633	0.06331	0.11724	0.11168	0.10681
		$\widehat{\delta}$	0.45233	0.51497	0.64130	0.30021	0.76518	0.89761	0.60677
		$\widehat{\kappa}$	0.01156	0.00903	0.01146	0.00740	0.01110	0.00987	0.01097
	MRE	$\widehat{\rho}$	0.33015	0.32430	0.33894	0.23930	0.35763	0.39005	0.34758
		$\widehat{\delta}$	0.35210	0.34954	0.37203	0.23106	0.40545	0.46390	0.37747
		$\widehat{\kappa}$	0.31656	0.28951	0.30622	0.23360	0.31400	0.36213	0.31439
400	AVE	$\widehat{\rho}$	0.78216	0.79246	0.80316	0.72550	0.80397	0.72395	0.79052
		$\widehat{\delta}$	1.61856	1.64791	1.70873	1.46216	1.69433	1.53857	1.64473
		$\widehat{\kappa}$	0.26564	0.25990	0.26092	0.26924	0.25947	0.27606	0.26031
	AVB	$\widehat{\rho}$	0.20920	0.21347	0.22881	0.12526	0.22547	0.24047	0.20776
		$\widehat{\delta}$	0.44192	0.44367	0.49432	0.22955	0.48918	0.52659	0.43133
		$\widehat{\kappa}$	0.06805	0.06447	0.06871	0.04216	0.06758	0.07965	0.06396
	MSE	$\widehat{\rho}$	0.06600	0.06737	0.07930	0.03591	0.07975	0.07370	0.06616
		$\widehat{\delta}$	0.31604	0.32293	0.44119	0.15385	0.43808	0.41215	0.31885
		$\widehat{\kappa}$	0.00854	0.00694	0.00854	0.00456	0.00798	0.00813	0.00710
	MRE	$\widehat{\rho}$	0.27893	0.28462	0.30508	0.16702	0.30062	0.32062	0.27702
		$\widehat{\delta}$	0.29461	0.29578	0.32955	0.15304	0.32612	0.35106	0.28755
		$\widehat{\kappa}$	0.27218	0.25786	0.27486	0.16864	0.27031	0.31859	0.25582

Table 4: Simulation results of the AVE, AVB, MSE, and MRE of BXLE distribution for $(\rho = 2, \delta = 0.75, \kappa = 0.5)$.

n	Est.	Est. Par.	MLE	ADE	CVME	MPSE	LSE	PCE	WLSE
20	AVE	$\widehat{\rho}$	2.19972	2.10860	2.18055	1.83387	2.02412	1.89513	2.04918
		$\widehat{\delta}$	0.80464	0.82806	0.81834	0.76080	0.84119	0.76588	0.83656
		$\widehat{\kappa}$	1.28376	0.95015	1.24156	0.96376	1.19295	0.97828	1.11270
	AVB	$\widehat{\rho}$	1.48464	1.27651	1.42915	0.84619	1.22818	1.09457	1.33954
		$\widehat{\delta}$	0.32012	0.32444	0.31584	0.22769	0.33701	0.26718	0.34797
		$\widehat{\kappa}$	0.92999	0.60028	0.89061	0.60676	0.85783	0.63555	0.76614
	MSE	$\widehat{\rho}$	3.08643	2.61610	3.47436	1.56670	2.76591	1.78122	3.07681
		$\widehat{\delta}$	0.20631	0.36524	0.20891	0.26242	0.58276	0.13725	0.36637
		$\widehat{\kappa}$	3.21804	1.35341	2.97730	1.80724	2.82349	1.49541	2.12508
	MRE	$\widehat{\rho}$	0.74232	0.63826	0.71457	0.42310	0.61409	0.54729	0.66977
		$\widehat{\delta}$	0.42683	0.43259	0.42111	0.30359	0.44934	0.35624	0.46396
		$\widehat{\kappa}$	1.85999	1.20057	1.78123	1.21352	1.71567	1.27109	1.53228
30	AVE	$\widehat{\rho}$	2.07208	2.09879	1.93054	1.81643	1.87920	1.80982	1.97688
		$\widehat{\delta}$	0.77345	0.79470	0.75483	0.73911	0.76213	0.73608	0.79586
		$\widehat{\kappa}$	1.02110	0.82572	1.17015	0.81542	1.10133	0.84551	0.93708
	AVB	$\widehat{\rho}$	1.35315	1.18342	1.27698	0.78084	1.20001	1.03024	1.23836
		$\widehat{\delta}$	0.29055	0.27508	0.27860	0.20257	0.28535	0.24667	0.30605
		$\widehat{\kappa}$	0.65961	0.46780	0.79891	0.44044	0.73575	0.47929	0.57549
	MSE	$\widehat{\rho}$	2.35464	2.20850	2.39316	1.25677	2.26625	1.50754	2.29529
		$\widehat{\delta}$	0.10427	0.14760	0.10481	0.22213	0.21766	0.10972	0.31649
		$\widehat{\kappa}$	1.51082	0.78721	2.20739	0.85698	1.93455	0.76941	1.10169
	MRE	$\widehat{\rho}$	0.67657	0.59171	0.63849	0.39042	0.60000	0.51512	0.61918
		$\widehat{\delta}$	0.38739	0.36677	0.37147	0.27009	0.38047	0.32889	0.40807
		$\widehat{\kappa}$	1.31923	0.93561	1.59783	0.88089	1.47150	0.95859	1.15098
50	AVE	$\widehat{\rho}$	2.21638	2.01940	1.98735	1.84738	1.91368	1.98021	1.99521
		$\widehat{\delta}$	0.80572	0.76881	0.77159	0.73132	0.75873	0.76822	0.77033
		$\widehat{\kappa}$	0.70792	0.69409	0.86623	0.67736	0.83730	0.67283	0.78059
	AVB	$\widehat{\rho}$	1.20455	1.04262	1.16157	0.69744	1.07214	0.97911	1.14091
		$\widehat{\delta}$	0.26408	0.23746	0.26207	0.17030	0.24731	0.23206	0.26052
		$\widehat{\kappa}$	0.35563	0.32068	0.49499	0.28592	0.46832	0.31635	0.41074
	MSE	$\widehat{\rho}$	1.82687	1.42665	1.96539	0.91267	1.64635	1.30571	1.78899
		$\widehat{\delta}$	0.08468	0.08372	0.10039	0.04297	0.08239	0.06919	0.14433
		$\widehat{\kappa}$	0.37512	0.29818	0.78968	0.28940	0.73692	0.26978	0.50205
	MRE	$\widehat{\rho}$	0.60228	0.52131	0.58079	0.34872	0.53607	0.48956	0.57045
		$\widehat{\delta}$	0.35210	0.31662	0.34943	0.22707	0.32975	0.30941	0.34736
		$\widehat{\kappa}$	0.71126	0.64136	0.98999	0.57184	0.93664	0.63270	0.82148
100	AVE	$\widehat{\rho}$	2.16724	2.14223	1.97914	1.95534	1.97042	2.11936	2.02067
		$\widehat{\delta}$	0.79778	0.79347	0.76016	0.75013	0.76123	0.79596	0.76815
		$\widehat{\kappa}$	0.59543	0.58523	0.68696	0.56600	0.67915	0.57161	0.63676
	AVB	$\widehat{\rho}$	1.02791	0.93518	1.01950	0.51636	1.00702	0.91638	0.97203
		$\widehat{\delta}$	0.23146	0.21315	0.22653	0.13179	0.23056	0.21854	0.21899
		$\widehat{\kappa}$	0.23138	0.21866	0.30926	0.15552	0.30441	0.21339	0.25835
	MSE	$\widehat{\rho}$	1.32814	1.11433	1.26780	0.60659	1.28261	1.12964	1.17428
		$\widehat{\delta}$	0.06693	0.05548	0.05985	0.03010	0.06435	0.06556	0.05745
		$\widehat{\kappa}$	0.10069	0.09467	0.24364	0.06331	0.23705	0.08434	0.14838
	MRE	$\widehat{\rho}$	0.51395	0.46759	0.50975	0.25818	0.50351	0.45819	0.48601
		$\widehat{\delta}$	0.30861	0.28420	0.30204	0.17572	0.30742	0.29139	0.29199
		$\widehat{\kappa}$	0.46277	0.43732	0.61852	0.31105	0.60881	0.42678	0.51670
200	AVE	$\widehat{\rho}$	2.20581	2.15610	2.13158	1.92166	2.01104	2.22879	2.12827
		$\widehat{\delta}$	0.80440	0.79620	0.79485	0.73774	0.76525	0.81614	0.78879
		$\widehat{\kappa}$	0.54241	0.54382	0.58959	0.54591	0.61300	0.51987	0.55222
	AVB	$\widehat{\rho}$	0.89638	0.83000	0.95399	0.34023	0.91264	0.84794	0.84106
		$\widehat{\delta}$	0.20432	0.19064	0.21694	0.08864	0.20523	0.19965	0.19182
		$\widehat{\kappa}$	0.17065	0.17054	0.22367	0.10093	0.23182	0.16210	0.17306
	MSE	$\widehat{\rho}$	1.06258	0.86982	1.12036	0.36602	1.01362	0.93002	0.89204
		$\widehat{\delta}$	0.05631	0.04548	0.05775	0.01784	0.04974	0.05204	0.04582
		$\widehat{\kappa}$	0.04495	0.04693	0.09351	0.03008	0.10902	0.04136	0.04966
	MRE	$\widehat{\rho}$	0.44819	0.41500	0.47700	0.17012	0.45632	0.42397	0.42053
		$\widehat{\delta}$	0.27242	0.25418	0.28926	0.11819	0.27364	0.26620	0.25576
		$\widehat{\kappa}$	0.34131	0.34107	0.44733	0.20186	0.46365	0.32421	0.34612

Table 4: Continued.

n	Est.	Est. Par.	MLE	ADE	CVME	MPSE	LSE	PCE	WLSE
400	AVE	$\widehat{\rho}$	2.19928	2.23351	2.12434	1.98656	2.10487	2.22701	2.12101
		$\widehat{\delta}$	0.80281	0.81210	0.78777	0.74960	0.78419	0.81309	0.78822
		$\widehat{\kappa}$	0.52140	0.50938	0.54236	0.51222	0.54996	0.50616	0.52888
	AVB	$\widehat{\rho}$	0.78212	0.76831	0.80115	0.16129	0.81774	0.77148	0.74657
		$\widehat{\delta}$	0.17915	0.17629	0.18084	0.04812	0.18478	0.18059	0.17113
		$\widehat{\kappa}$	0.13703	0.13600	0.15975	0.04871	0.16807	0.13728	0.14135
	MSE	$\widehat{\rho}$	0.87125	0.74539	0.78899	0.16253	0.81562	0.76414	0.69966
		$\widehat{\delta}$	0.04720	0.03958	0.04038	0.00823	0.04167	0.04256	0.03742
		$\widehat{\kappa}$	0.02671	0.02624	0.03959	0.00944	0.04442	0.02600	0.02909
	MRE	$\widehat{\rho}$	0.39106	0.38416	0.40057	0.08064	0.40887	0.38574	0.37329
		$\widehat{\delta}$	0.23887	0.23505	0.24112	0.06415	0.24637	0.24079	0.22817
		$\widehat{\kappa}$	0.27406	0.27201	0.31950	0.09742	0.33613	0.27455	0.28269

Table 5: Simulation results of the AVE, AVB, MSE, and MRE of BXLE distribution for $(\rho = 1.5, \delta = 2, \kappa = 3)$.

n	Est.	Est. Par.	MLE	ADE	CVME	MPSE	LSE	PCE	WLSE
20	AVE	$\widehat{\rho}$	1.48426	1.50143	1.53919	1.39727	1.49729	1.40027	1.51141
		$\widehat{\delta}$	1.99585	1.99840	2.00021	1.98168	1.99476	1.97884	1.99683
		$\widehat{\kappa}$	3.35961	3.25344	3.30962	3.15830	3.21190	3.23687	3.19768
	AVB	$\widehat{\rho}$	0.45024	0.46569	0.47307	0.49942	0.49706	0.52360	0.49561
		$\widehat{\delta}$	0.07124	0.07666	0.08052	0.08212	0.08343	0.08790	0.08176
		$\widehat{\kappa}$	0.70369	0.68421	0.70003	0.72208	0.73740	0.70854	0.70656
	MSE	$\widehat{\rho}$	0.23741	0.25537	0.25762	0.29410	0.28450	0.31937	0.28166
		$\widehat{\delta}$	0.00716	0.00859	0.00915	0.00938	0.01012	0.01065	0.00953
		$\widehat{\kappa}$	0.61438	0.58270	0.61510	0.64382	0.66424	0.62750	0.61700
	MRE	$\widehat{\rho}$	0.30016	0.31046	0.31538	0.33295	0.33137	0.34907	0.33041
		$\widehat{\delta}$	0.03562	0.03833	0.04026	0.04106	0.04172	0.04395	0.04088
		$\widehat{\kappa}$	0.23456	0.22807	0.23334	0.24069	0.24580	0.23618	0.23552
30	AVE	$\widehat{\rho}$	1.49349	1.52758	1.50013	1.40873	1.48982	1.40388	1.48786
		$\widehat{\delta}$	1.99440	2.00095	1.99698	1.98237	1.99378	1.97927	1.99263
		$\widehat{\kappa}$	3.32788	3.18310	3.29192	3.16789	3.19937	3.23034	3.21322
	AVB	$\widehat{\rho}$	0.44356	0.45161	0.45218	0.47739	0.49011	0.49857	0.45999
		$\widehat{\delta}$	0.06403	0.06994	0.07372	0.07541	0.07839	0.08068	0.07318
		$\widehat{\kappa}$	0.61983	0.61354	0.68297	0.65874	0.69034	0.66390	0.65282
	MSE	$\widehat{\rho}$	0.23018	0.23337	0.23855	0.26956	0.27263	0.28904	0.24734
		$\widehat{\delta}$	0.00581	0.00670	0.00751	0.00792	0.00839	0.00884	0.00743
		$\widehat{\kappa}$	0.51057	0.49647	0.58501	0.55431	0.59566	0.55794	0.54755
	MRE	$\widehat{\rho}$	0.29571	0.30107	0.30146	0.31826	0.32674	0.33238	0.30666
		$\widehat{\delta}$	0.03202	0.03497	0.03686	0.03771	0.03919	0.04034	0.03659
		$\widehat{\kappa}$	0.20661	0.20451	0.22766	0.21958	0.23011	0.22130	0.21761
50	AVE	$\widehat{\rho}$	1.52272	1.48816	1.50716	1.44609	1.50200	1.42613	1.48624
		$\widehat{\delta}$	1.99826	1.99351	1.99775	1.98939	1.99568	1.98419	1.99475
		$\widehat{\kappa}$	3.23116	3.20837	3.24415	3.11142	3.17626	3.18904	3.17970
	AVB	$\widehat{\rho}$	0.43070	0.43099	0.44992	0.44334	0.45581	0.46098	0.43779
		$\widehat{\delta}$	0.06190	0.06572	0.06765	0.06812	0.06835	0.07124	0.06679
		$\widehat{\kappa}$	0.57289	0.58429	0.62487	0.58566	0.62722	0.60344	0.59943
	MSE	$\widehat{\rho}$	0.21395	0.21883	0.22988	0.23618	0.23900	0.25058	0.22438
		$\widehat{\delta}$	0.00509	0.00574	0.00603	0.00613	0.00623	0.00684	0.00597
		$\widehat{\kappa}$	0.44440	0.45749	0.50946	0.46032	0.51462	0.48127	0.47750
	MRE	$\widehat{\rho}$	0.28713	0.28733	0.29994	0.29556	0.30387	0.30732	0.29186
		$\widehat{\delta}$	0.03095	0.03286	0.03382	0.03406	0.03418	0.03562	0.03340
		$\widehat{\kappa}$	0.19096	0.19476	0.20829	0.19522	0.20907	0.20115	0.19981

Table 5: Continued.

n	Est.	Est. Par.	MLE	ADE	CVME	MPSE	LSE	PCE	WLSE
100	AVE	$\widehat{\rho}$	1.49861	1.49854	1.48977	1.49453	1.48220	1.45097	1.52141
		$\widehat{\delta}$	1.99659	1.99520	1.99600	1.99676	1.99332	1.98899	1.99940
		$\widehat{\kappa}$	3.18175	3.17224	3.20354	3.07278	3.19864	3.16300	3.13747
	AVB	$\widehat{\rho}$	0.37760	0.39828	0.42841	0.37844	0.43741	0.40096	0.40783
		$\widehat{\delta}$	0.05390	0.05817	0.06213	0.05587	0.06380	0.05892	0.05851
		$\widehat{\kappa}$	0.49406	0.51521	0.57305	0.47351	0.57208	0.51239	0.52015
	MSE	$\widehat{\rho}$	0.17340	0.19014	0.21242	0.18343	0.22034	0.19669	0.19731
		$\widehat{\delta}$	0.00384	0.00442	0.00486	0.00423	0.00519	0.00459	0.00445
		$\widehat{\kappa}$	0.34608	0.37380	0.44334	0.32961	0.43920	0.36842	0.37435
	MRE	$\widehat{\rho}$	0.25173	0.26552	0.28560	0.25230	0.29161	0.26730	0.27189
		$\widehat{\delta}$	0.16469	0.17174	0.19102	0.15784	0.19069	0.17080	0.17338
		$\widehat{\kappa}$	0.02695	0.02908	0.03107	0.02793	0.03190	0.02946	0.02926
200	AVE	$\widehat{\rho}$	1.52112	1.51905	1.50244	1.50740	1.51074	1.47311	1.51276
		$\widehat{\delta}$	1.99975	1.99985	1.99705	1.99890	1.99808	1.99255	1.99789
		$\widehat{\kappa}$	3.11370	3.09869	3.15336	3.03961	3.13256	3.12542	3.11391
	AVB	$\widehat{\rho}$	0.33664	0.36135	0.39323	0.30583	0.39643	0.35301	0.36308
		$\widehat{\delta}$	0.04711	0.05190	0.05530	0.04539	0.05535	0.05108	0.05125
		$\widehat{\kappa}$	0.41955	0.44732	0.50282	0.37172	0.49959	0.44572	0.44781
	MSE	$\widehat{\rho}$	0.14564	0.16292	0.18432	0.13545	0.18676	0.15976	0.16363
		$\widehat{\delta}$	0.00296	0.00350	0.00386	0.00304	0.00384	0.00348	0.00340
		$\widehat{\kappa}$	0.26202	0.28263	0.35606	0.23001	0.34779	0.28964	0.28877
	MRE	$\widehat{\rho}$	0.22443	0.24090	0.26215	0.20389	0.26429	0.23534	0.24205
		$\widehat{\delta}$	0.02355	0.02595	0.02765	0.02270	0.02768	0.02554	0.02563
		$\widehat{\kappa}$	0.13985	0.14911	0.16761	0.12391	0.16653	0.14857	0.14927
400	AVE	$\widehat{\rho}$	1.50952	1.51872	1.48852	1.50735	1.51329	1.46800	1.50446
		$\widehat{\delta}$	1.99977	2.00038	1.99609	1.99982	1.99935	1.99288	1.99783
		$\widehat{\kappa}$	3.07239	3.07818	3.14157	3.02834	3.10499	3.11262	3.08511
	AVB	$\widehat{\rho}$	0.27199	0.30058	0.34299	0.23273	0.34738	0.29709	0.29563
		$\widehat{\delta}$	0.03884	0.04181	0.04737	0.03348	0.04864	0.04239	0.04145
		$\widehat{\kappa}$	0.33349	0.35723	0.43772	0.27538	0.43071	0.37178	0.35158
	MSE	$\widehat{\rho}$	0.10212	0.12074	0.14913	0.09413	0.15349	0.11852	0.11873
		$\widehat{\delta}$	0.00211	0.00238	0.00294	0.00192	0.00311	0.00247	0.00239
		$\widehat{\kappa}$	0.16775	0.19116	0.27750	0.14899	0.27192	0.20760	0.19001
	MRE	$\widehat{\rho}$	0.18132	0.20039	0.22866	0.15515	0.23159	0.19806	0.19709
		$\widehat{\delta}$	0.01942	0.02091	0.02369	0.01674	0.02432	0.02119	0.02072
		$\widehat{\kappa}$	0.11116	0.11908	0.14591	0.09179	0.14357	0.12393	0.11719

Table 6: Simulation results of the AVE, AVB, MSE, and MRE of BXLE distribution for $(\rho = 0.5, \delta = 3, \kappa = 1.5)$.

n	Est.	Est. Par.	MLE	ADE	CVME	MPSE	LSE	PCE	WLSE
20	AVE	$\widehat{\rho}$	1.09013	1.09301	1.59993	1.05621	1.26885	1.03708	1.36696
		$\widehat{\delta}$	3.75659	3.72276	4.23521	3.65787	3.88774	3.70788	4.01329
		$\widehat{\kappa}$	2.49700	2.17462	2.41294	2.16578	2.48830	2.16685	2.19013
	AVB	$\widehat{\rho}$	0.89701	0.85443	1.37656	0.83944	1.08015	0.82323	1.13763
		$\widehat{\delta}$	1.10098	1.06444	1.53775	1.06360	1.30483	1.12174	1.36835
		$\widehat{\kappa}$	1.59407	1.32878	1.74556	1.36212	1.72736	1.34914	1.46963
	MSE	$\widehat{\rho}$	2.88732	2.87882	7.28783	2.42481	4.15889	2.50272	8.32081
		$\widehat{\delta}$	3.85325	3.46515	6.77092	3.19793	4.71999	5.88239	6.48326
		$\widehat{\kappa}$	4.90730	3.52543	6.19279	3.88614	5.63150	3.31593	4.40429
	MRE	$\widehat{\rho}$	1.79403	1.70886	2.75312	1.67889	2.16030	1.64646	2.27525
		$\widehat{\delta}$	0.36699	0.35481	0.51258	0.35453	0.43494	0.37391	0.45612
		$\widehat{\kappa}$	1.06271	0.88585	1.16371	0.90808	1.15158	0.89943	0.97975

Table 6: Continued.

n	Est.	Est. Par.	MLE	ADE	CVME	MPSE	LSE	PCE	WLSE
30	AVE	$\widehat{\rho}$	0.94954	1.00033	1.30323	0.86314	1.10217	0.88577	1.11377
		$\widehat{\delta}$	3.59034	3.65031	3.96094	3.42215	3.74420	3.56056	3.76013
		$\widehat{\kappa}$	2.26098	1.89910	2.17864	1.93524	2.17345	1.99736	2.02340
	AVB	$\widehat{\rho}$	0.74141	0.72104	1.05990	0.60505	0.86941	0.64025	0.86180
		$\widehat{\delta}$	0.93953	0.94579	1.25724	0.77415	1.09003	0.92673	1.09069
		$\widehat{\kappa}$	1.28238	1.01758	1.44164	1.03514	1.37325	1.09947	1.21207
	MSE	$\widehat{\rho}$	2.25949	2.20718	3.66942	1.39781	2.63789	1.53392	2.77654
		$\widehat{\delta}$	3.14915	4.08395	4.36029	1.95861	3.59800	5.64114	4.08607
		$\widehat{\kappa}$	3.05310	2.03374	4.07271	2.34656	3.61853	2.29771	2.85553
	MRE	$\widehat{\rho}$	1.48282	1.44208	2.11981	1.21010	1.73882	1.28050	1.72360
		$\widehat{\delta}$	0.31318	0.31526	0.41908	0.25805	0.36334	0.30891	0.36356
		$\widehat{\kappa}$	0.85492	0.67839	0.96110	0.69009	0.91550	0.73298	0.80805
50	AVE	$\widehat{\rho}$	0.69172	0.79182	1.00863	0.70484	0.91721	0.74754	0.82745
		$\widehat{\delta}$	3.26123	3.39251	3.64936	3.25112	3.55590	3.30188	3.40601
		$\widehat{\kappa}$	1.98831	1.68950	2.00656	1.74926	1.97113	1.76822	1.82594
	AVB	$\widehat{\rho}$	0.43423	0.47355	0.74483	0.40840	0.65350	0.45431	0.53521
		$\widehat{\delta}$	0.56234	0.63452	0.92003	0.54596	0.85673	0.60527	0.68306
		$\widehat{\kappa}$	0.89780	0.72426	1.14282	0.75930	1.07921	0.78071	0.87385
	MSE	$\widehat{\rho}$	0.74115	0.79329	1.97914	0.55856	1.50196	0.82328	1.15166
		$\widehat{\delta}$	1.18160	1.39180	2.76212	0.99183	2.54417	1.45508	1.75732
		$\widehat{\kappa}$	1.54985	0.98647	2.50926	1.14006	2.36698	1.14811	1.55161
	MRE	$\widehat{\rho}$	0.86846	0.94710	1.48966	0.81681	1.30700	0.90863	1.07042
		$\widehat{\delta}$	0.18745	0.21151	0.30668	0.18199	0.28558	0.20176	0.22769
		$\widehat{\kappa}$	0.59853	0.48284	0.76188	0.50620	0.71947	0.52047	0.58257
100	AVE	$\widehat{\rho}$	0.56807	0.64665	0.71324	0.57865	0.74440	0.59553	0.65737
		$\widehat{\delta}$	3.09793	3.18688	3.27587	3.08497	3.30720	3.11328	3.20582
		$\widehat{\kappa}$	1.69720	1.62676	1.81135	1.58225	1.73585	1.60584	1.61359
	AVB	$\widehat{\rho}$	0.23193	0.30342	0.40499	0.22032	0.42918	0.23957	0.30949
		$\widehat{\delta}$	0.31118	0.39824	0.49846	0.29956	0.54175	0.32289	0.40949
		$\widehat{\kappa}$	0.50544	0.56005	0.78929	0.44830	0.74598	0.48990	0.54703
	MSE	$\widehat{\rho}$	0.18046	0.26910	0.55243	0.14965	0.66605	0.16895	0.34042
		$\widehat{\delta}$	0.31402	0.43605	0.84022	0.25285	1.02444	0.29370	0.58959
		$\widehat{\kappa}$	0.49210	0.56994	1.26854	0.39231	1.10382	0.46066	0.56457
	MRE	$\widehat{\rho}$	0.46387	0.60684	0.80998	0.44065	0.85836	0.47914	0.61898
		$\widehat{\delta}$	0.10373	0.13275	0.16615	0.09985	0.18058	0.10763	0.13650
		$\widehat{\kappa}$	0.33696	0.37336	0.52619	0.29887	0.49732	0.32660	0.36468
200	AVE	$\widehat{\rho}$	0.52163	0.55192	0.58775	0.53757	0.57761	0.53850	0.56014
		$\widehat{\delta}$	3.03469	3.06770	3.11509	3.04118	3.09781	3.04023	3.07489
		$\widehat{\kappa}$	1.57260	1.56649	1.65780	1.52635	1.65208	1.54260	1.54055
	AVB	$\widehat{\rho}$	0.13096	0.17348	0.23565	0.14386	0.23109	0.14610	0.17219
		$\widehat{\delta}$	0.17941	0.23151	0.29393	0.20012	0.28508	0.19715	0.22459
		$\widehat{\kappa}$	0.29963	0.36415	0.51977	0.30460	0.50699	0.32327	0.35146
	MSE	$\widehat{\rho}$	0.03047	0.07002	0.15686	0.04158	0.13620	0.03915	0.06129
		$\widehat{\delta}$	0.05648	0.12205	0.25027	0.07665	0.22107	0.06870	0.10343
		$\widehat{\kappa}$	0.15729	0.22493	0.56042	0.17224	0.50982	0.18505	0.21295
	MRE	$\widehat{\rho}$	0.26191	0.34695	0.47130	0.28772	0.46218	0.29219	0.34437
		$\widehat{\delta}$	0.05980	0.07717	0.09798	0.06671	0.09503	0.06572	0.07486
		$\widehat{\kappa}$	0.19975	0.24277	0.34651	0.20307	0.33799	0.21551	0.23431
400	AVE	$\widehat{\rho}$	0.51200	0.52689	0.53675	0.52540	0.53707	0.52883	0.51915
		$\widehat{\delta}$	3.01624	3.03684	3.04806	3.02951	3.04637	3.03206	3.02435
		$\widehat{\kappa}$	1.53588	1.52257	1.55591	1.48598	1.55730	1.50231	1.54437
	AVB	$\widehat{\rho}$	0.09003	0.11149	0.14263	0.09413	0.14921	0.10498	0.11394
		$\widehat{\delta}$	0.12499	0.15018	0.18267	0.13220	0.18794	0.14136	0.15208
		$\widehat{\kappa}$	0.20697	0.24149	0.32007	0.19607	0.33507	0.22659	0.26217
	MSE	$\widehat{\rho}$	0.01375	0.02398	0.04397	0.01641	0.04258	0.01933	0.02252
		$\widehat{\delta}$	0.02570	0.04117	0.07023	0.03113	0.06597	0.03384	0.03974
		$\widehat{\kappa}$	0.07078	0.09843	0.18096	0.06585	0.19442	0.08545	0.11580
	MRE	$\widehat{\rho}$	0.18006	0.22298	0.28526	0.18825	0.29843	0.20997	0.22788
		$\widehat{\delta}$	0.04166	0.05006	0.06089	0.04407	0.06265	0.04712	0.05069
		$\widehat{\kappa}$	0.13798	0.16099	0.21338	0.13071	0.22338	0.15106	0.17478

Table 7: Simulation results of the AVE, AVB, MSE, and MRE of BXLE distribution for $(\rho = 2.5, \delta = 0.75, \kappa = 2)$.

n	Est.	Est. Par.	MLE	ADE	CVME	MPSE	LSE	PCE	WLSE
20	AVE	$\widehat{\rho}$	1.93468	2.02949	1.92525	1.88766	1.93247	1.87049	1.91932
		$\widehat{\delta}$	0.71610	0.72405	0.71885	0.71756	0.72157	0.71711	0.71864
		$\widehat{\kappa}$	4.58878	3.56315	5.02440	3.97201	4.37834	3.55651	4.10333
	AVB	$\widehat{\rho}$	1.03764	0.96413	1.06606	1.00392	1.05027	1.05225	1.04019
		$\widehat{\delta}$	0.05603	0.05330	0.05959	0.06013	0.06046	0.06039	0.05869
		$\widehat{\kappa}$	2.73667	1.77733	3.23614	2.28332	2.67764	1.83243	2.34900
	MSE	$\widehat{\rho}$	1.60674	1.36611	1.71018	1.59658	1.66744	1.60003	1.59770
		$\widehat{\delta}$	0.00514	0.00448	0.00546	0.00569	0.00558	0.00550	0.00527
		$\widehat{\kappa}$	35.74006	16.09120	47.41465	26.43301	33.13628	14.69811	27.01181
	MRE	$\widehat{\rho}$	0.41506	0.38565	0.42642	0.40157	0.42011	0.42090	0.41608
		$\widehat{\delta}$	0.07471	0.07106	0.07946	0.08017	0.08061	0.08052	0.07825
		$\widehat{\kappa}$	1.36834	0.88867	1.61807	1.14166	1.33882	0.91621	1.17450
30	AVE	$\widehat{\rho}$	2.07335	2.11612	2.00259	2.06720	1.92691	2.01205	2.00773
		$\widehat{\delta}$	0.72414	0.72853	0.72285	0.72763	0.71952	0.72425	0.72425
		$\widehat{\kappa}$	3.31432	2.88686	3.82660	2.76187	3.84179	2.85758	3.23246
	AVB	$\widehat{\rho}$	0.89648	0.87194	0.97766	0.82608	1.03461	0.93578	0.95710
		$\widehat{\delta}$	0.04775	0.04680	0.05296	0.04633	0.05807	0.05184	0.05307
		$\widehat{\kappa}$	1.48215	1.09070	2.02785	1.02366	2.08143	1.12326	1.47502
	MSE	$\widehat{\rho}$	1.20422	1.10883	1.45171	1.09246	1.57836	1.27435	1.34196
		$\widehat{\delta}$	0.00379	0.00352	0.00448	0.00352	0.00512	0.00420	0.00429
		$\widehat{\kappa}$	11.76096	5.59121	19.43984	5.97968	19.49340	4.77205	10.10694
	MRE	$\widehat{\rho}$	0.35859	0.34878	0.39106	0.33043	0.41384	0.37431	0.38284
		$\widehat{\delta}$	0.06367	0.06240	0.07061	0.06177	0.07742	0.06912	0.07077
		$\widehat{\kappa}$	0.74107	0.54535	1.01392	0.51183	1.04072	0.56163	0.73751
50	AVE	$\widehat{\rho}$	2.17426	2.20516	2.05871	2.15930	2.00776	2.03987	2.19373
		$\widehat{\delta}$	0.73060	0.73417	0.72631	0.73224	0.72417	0.72536	0.73278
		$\widehat{\kappa}$	2.64343	2.51874	3.09799	2.40827	3.06424	2.56593	2.61239
	AVB	$\widehat{\rho}$	0.78267	0.76088	0.89548	0.72196	0.94080	0.86487	0.80352
		$\widehat{\delta}$	0.79162	0.71054	1.26072	0.66060	1.27875	0.76711	0.82421
		$\widehat{\kappa}$	0.03975	0.03932	0.04529	0.03996	0.04997	0.04549	0.04171
	MSE	$\widehat{\rho}$	0.89336	0.84562	1.17762	0.86059	1.29162	1.06094	0.95492
		$\widehat{\delta}$	0.00260	0.00249	0.00330	0.00267	0.00388	0.00317	0.00285
		$\widehat{\kappa}$	2.73791	1.90731	8.16773	1.58877	6.84234	1.77905	3.10024
	MRE	$\widehat{\rho}$	0.31307	0.30435	0.35819	0.28878	0.37632	0.34595	0.32141
		$\widehat{\delta}$	0.05300	0.05242	0.06039	0.05328	0.06663	0.06065	0.05561
		$\widehat{\kappa}$	0.39581	0.35527	0.63036	0.33030	0.63937	0.38355	0.41210
100	AVE	$\widehat{\rho}$	2.25841	2.26598	2.18105	2.29193	2.16943	2.20190	2.28508
		$\widehat{\delta}$	0.73682	0.73771	0.73260	0.74043	0.73263	0.73487	0.73828
		$\widehat{\kappa}$	2.28788	2.30145	2.48144	2.17275	2.45347	2.29386	2.29980
	AVB	$\widehat{\rho}$	0.66104	0.66707	0.77255	0.55686	0.78640	0.70841	0.66816
		$\widehat{\delta}$	0.03198	0.03297	0.03822	0.02917	0.03944	0.03547	0.03311
		$\widehat{\kappa}$	0.44198	0.46307	0.64902	0.38714	0.63041	0.47545	0.46638
	MSE	$\widehat{\rho}$	0.60785	0.62747	0.84610	0.52706	0.86283	0.70227	0.63059
		$\widehat{\delta}$	0.00158	0.00170	0.00228	0.00142	0.00238	0.00192	0.00172
		$\widehat{\kappa}$	0.45389	0.55123	1.32059	0.37179	1.10366	0.52812	0.63115
	MRE	$\widehat{\rho}$	0.26442	0.26683	0.30902	0.22274	0.31456	0.28336	0.26727
		$\widehat{\delta}$	0.04264	0.04397	0.05095	0.03890	0.05258	0.04729	0.04414
		$\widehat{\kappa}$	0.22099	0.23154	0.32451	0.19357	0.31521	0.23772	0.23319

Table 7: Continued.

n	Est.	Est. Par.	MLE	ADE	CVME	MPSE	LSE	PCE	WLSE
200	AVE	$\widehat{\rho}$	2.38319	2.36681	2.32689	2.38031	2.26972	2.26997	2.35139
		$\widehat{\delta}$	0.74284	0.74250	0.74039	0.74490	0.73778	0.73805	0.74156
		$\widehat{\kappa}$	2.14738	2.16018	2.23583	2.07987	2.26382	2.18058	2.17066
	AVB	$\widehat{\rho}$	0.54258	0.56624	0.64209	0.39355	0.66561	0.58906	0.57429
		$\widehat{\delta}$	0.02548	0.02693	0.03106	0.02074	0.03193	0.02832	0.02726
		$\widehat{\kappa}$	0.28846	0.31529	0.40522	0.24417	0.42483	0.32890	0.32415
	MSE	$\widehat{\rho}$	0.39884	0.43566	0.57162	0.31207	0.61496	0.47433	0.45050
		$\widehat{\delta}$	0.00097	0.00108	0.00146	0.00080	0.00152	0.00119	0.00111
		$\widehat{\kappa}$	0.16655	0.21034	0.38818	0.13295	0.42311	0.21135	0.22558
	MRE	$\widehat{\rho}$	0.21703	0.22650	0.25683	0.15742	0.26624	0.23562	0.22972
		$\widehat{\delta}$	0.03397	0.03591	0.04141	0.02765	0.04257	0.03776	0.03635
		$\widehat{\kappa}$	0.14423	0.15765	0.20261	0.12208	0.21242	0.16445	0.16208
400	AVE	$\widehat{\rho}$	2.46565	2.44224	2.38062	2.43642	2.37639	2.38323	2.40852
		$\widehat{\delta}$	0.74731	0.74643	0.74325	0.74681	0.74287	0.74408	0.74470
		$\widehat{\kappa}$	2.06535	2.07995	2.14420	2.04099	2.14149	2.09305	2.10390
	AVB	$\widehat{\rho}$	0.42714	0.46076	0.56325	0.24706	0.54240	0.47087	0.48153
		$\widehat{\delta}$	0.01936	0.02167	0.02617	0.01321	0.02534	0.02215	0.02216
		$\widehat{\kappa}$	0.20133	0.22996	0.30180	0.15109	0.29189	0.23358	0.24279
	MSE	$\widehat{\rho}$	0.24466	0.28492	0.41630	0.17369	0.40917	0.30357	0.31548
		$\widehat{\delta}$	0.00054	0.00067	0.00097	0.00041	0.00096	0.00071	0.00072
		$\widehat{\kappa}$	0.07472	0.09483	0.18202	0.05741	0.17759	0.09695	0.11244
	MRE	$\widehat{\rho}$	0.17086	0.18430	0.22530	0.09883	0.21696	0.18835	0.19261
		$\widehat{\delta}$	0.02582	0.02889	0.03490	0.01762	0.03379	0.02953	0.02955
		$\widehat{\kappa}$	0.10066	0.11498	0.15090	0.07554	0.14595	0.11679	0.12139

Table 8: Simulation results of the AVE, AVB, MSE, and MRE of BXLE distribution for $(\rho = 3, \delta = 1.5, \kappa = 0.5)$.

n	Est.	Est. Par.	MLE	ADE	CVME	MPSE	LSE	PCE	WLSE
20	AVE	$\widehat{\rho}$	2.25922	2.27161	2.30386	2.56517	2.31245	2.22016	2.11469
		$\widehat{\delta}$	1.28865	1.33928	1.33780	1.46675	1.37558	1.33183	1.31017
		$\widehat{\kappa}$	1.44443	1.06799	1.47947	0.89627	1.25029	1.04311	1.34574
	AVB	$\widehat{\rho}$	1.24102	1.15163	1.10023	0.65276	1.04342	1.14332	1.28963
		$\widehat{\delta}$	0.38019	0.37841	0.36227	0.28477	0.36259	0.38376	0.42134
		$\widehat{\kappa}$	0.99257	0.64230	1.04387	0.51867	0.84803	0.63293	0.92532
	MSE	$\widehat{\rho}$	2.49321	2.18957	2.28668	1.29495	2.14546	2.24551	2.64590
		$\widehat{\delta}$	4.24912	1.78742	5.28595	1.98167	3.57678	1.73329	3.57683
		$\widehat{\kappa}$	0.22030	0.20938	0.20249	0.15387	0.20329	0.21702	0.24799
	MRE	$\widehat{\rho}$	0.41367	0.38388	0.36674	0.21759	0.34781	0.38111	0.42988
		$\widehat{\delta}$	0.25346	0.25227	0.24151	0.18985	0.24172	0.25584	0.28089
		$\widehat{\kappa}$	1.98514	1.28459	2.08774	1.03734	1.69606	1.26587	1.85063
30	AVE	$\widehat{\rho}$	2.37795	2.35231	2.30591	2.58777	2.26834	2.31186	2.22954
		$\widehat{\delta}$	1.32796	1.34465	1.33708	1.43656	1.34068	1.34833	1.31035
		$\widehat{\kappa}$	0.99171	0.91347	1.14839	0.75291	1.15454	0.86102	0.99014
	AVB	$\widehat{\rho}$	1.12486	1.10341	1.12391	0.59610	1.11783	1.10276	1.21249
		$\widehat{\delta}$	0.34291	0.34590	0.35695	0.24323	0.36800	0.36261	0.37609
		$\widehat{\kappa}$	0.54142	0.47675	0.70968	0.34657	0.73060	0.44939	0.55049
	MSE	$\widehat{\rho}$	1.99694	1.96454	2.20519	1.16656	2.24897	2.02286	2.26525
		$\widehat{\delta}$	0.17757	0.17668	0.19166	0.11519	0.20274	0.19130	0.20194
		$\widehat{\kappa}$	1.43681	1.00028	2.28948	0.78501	2.48222	0.76471	1.18992
	MRE	$\widehat{\rho}$	0.37495	0.36780	0.37464	0.19870	0.37261	0.36759	0.40416
		$\widehat{\delta}$	0.22861	0.23060	0.23796	0.16216	0.24533	0.24174	0.25073
		$\widehat{\kappa}$	1.08283	0.95351	1.41936	0.69315	1.46121	0.89878	1.10098

Table 8: Continued.

n	Est.	Est. Par.	MLE	ADE	CVME	MPSE	LSE	PCE	WLSE
50	AVE	$\hat{\rho}$	2.41563	2.44759	2.33970	2.65901	2.34853	2.46812	2.33817
		$\hat{\delta}$	1.33871	1.36030	1.33053	1.43464	1.34434	1.37902	1.33240
		$\hat{\kappa}$	0.81702	0.72635	0.92425	0.63296	0.88870	0.72036	0.80824
	AVB	$\hat{\rho}$	1.07805	1.02476	1.08837	0.50426	1.08137	1.01465	1.13162
		$\hat{\delta}$	0.31870	0.31530	0.32707	0.19814	0.33465	0.32299	0.34249
		$\hat{\kappa}$	0.36429	0.28073	0.47801	0.20502	0.45484	0.29865	0.36362
	MSE	$\hat{\rho}$	1.77579	1.59334	1.99108	0.92871	1.96795	1.64311	1.92550
		$\hat{\delta}$	0.15294	0.14211	0.16498	0.08597	0.16787	0.15183	0.16718
		$\hat{\kappa}$	0.54310	0.23512	0.97545	0.22440	0.91236	0.30409	0.44341
	MRE	$\hat{\rho}$	0.35935	0.34159	0.36279	0.16809	0.36046	0.33822	0.37721
		$\hat{\delta}$	0.21247	0.21020	0.21804	0.13209	0.22310	0.21533	0.22833
		$\hat{\kappa}$	0.72859	0.56147	0.95601	0.41005	0.90969	0.59730	0.72724
100	AVE	$\hat{\rho}$	2.50497	2.54496	2.50903	2.82909	2.35625	2.59121	2.51501
		$\hat{\delta}$	1.36222	1.38965	1.37429	1.47182	1.33673	1.40815	1.37591
		$\hat{\kappa}$	0.66422	0.64091	0.71243	0.54529	0.74151	0.62469	0.66829
	AVB	$\hat{\rho}$	0.95829	0.93129	0.98960	0.28308	1.06864	0.91262	0.97376
		$\hat{\delta}$	0.27993	0.28231	0.29390	0.12694	0.31529	0.28449	0.28950
		$\hat{\kappa}$	0.20841	0.19472	0.26368	0.09863	0.29472	0.19449	0.21911
	MSE	$\hat{\rho}$	1.33183	1.26898	1.53254	0.45669	1.76001	1.23869	1.40130
		$\hat{\delta}$	0.11403	0.11208	0.12961	0.04257	0.14476	0.11340	0.12035
		$\hat{\kappa}$	0.10638	0.08990	0.20465	0.04885	0.23498	0.09389	0.12633
	MRE	$\hat{\rho}$	0.31943	0.31043	0.32987	0.09436	0.35621	0.30421	0.32459
		$\hat{\delta}$	0.41682	0.38945	0.52735	0.19725	0.58944	0.38899	0.43823
		$\hat{\kappa}$	0.18662	0.18821	0.19593	0.08463	0.21019	0.18966	0.19300
200	AVE	$\hat{\rho}$	2.68622	2.63929	2.54449	2.91341	2.52655	2.77992	2.57827
		$\hat{\delta}$	1.41291	1.40348	1.38300	1.48787	1.38236	1.45466	1.39272
		$\hat{\kappa}$	0.58701	0.59670	0.64583	0.51505	0.64304	0.56015	0.61597
	AVB	$\hat{\rho}$	0.79267	0.82070	0.93297	0.13418	0.93781	0.76320	0.86433
		$\hat{\delta}$	0.22912	0.24048	0.27404	0.07519	0.27461	0.23440	0.25492
		$\hat{\kappa}$	0.13258	0.14285	0.19532	0.04978	0.19404	0.12768	0.16375
	MSE	$\hat{\rho}$	0.87772	0.95246	1.28415	0.19687	1.27774	0.83111	1.07875
		$\hat{\delta}$	0.07403	0.08190	0.10702	0.01894	0.10602	0.07514	0.09153
		$\hat{\kappa}$	0.03721	0.04421	0.09242	0.01387	0.09175	0.03414	0.05970
	MRE	$\hat{\rho}$	0.26422	0.27357	0.31099	0.04473	0.31260	0.25440	0.28811
		$\hat{\delta}$	0.15275	0.16032	0.18270	0.05013	0.18307	0.15627	0.16995
		$\hat{\kappa}$	0.26516	0.28570	0.39063	0.09955	0.38808	0.25536	0.32749
400	AVE	$\hat{\rho}$	2.81400	2.78651	2.67628	2.97841	2.68454	2.84482	2.72588
		$\hat{\delta}$	1.45146	1.44724	1.41857	1.49984	1.42069	1.46642	1.42676
		$\hat{\kappa}$	0.54913	0.55669	0.59135	0.49916	0.58688	0.53957	0.56863
	AVB	$\hat{\rho}$	0.65747	0.70065	0.80308	0.03702	0.79883	0.66605	0.73811
		$\hat{\delta}$	0.19107	0.20580	0.23258	0.03920	0.23358	0.19898	0.21271
		$\hat{\kappa}$	0.09696	0.10719	0.13937	0.02315	0.13700	0.09832	0.11442
	MSE	$\hat{\rho}$	0.59368	0.68521	0.92646	0.04280	0.91585	0.60649	0.75292
		$\hat{\delta}$	0.05023	0.05802	0.07557	0.00509	0.07574	0.05308	0.06228
		$\hat{\kappa}$	0.01849	0.02262	0.04460	0.00308	0.04000	0.01828	0.02615
	MRE	$\hat{\rho}$	0.21916	0.23355	0.26769	0.01234	0.26628	0.22202	0.24604
		$\hat{\delta}$	0.12738	0.13720	0.15505	0.02613	0.15572	0.13265	0.14180
		$\hat{\kappa}$	0.19392	0.21439	0.27874	0.04630	0.27400	0.19663	0.22884

Table 9: Estimated parameters with their standard errors of the BXLE model and other fitted models for first dataset.

Model	Estimated parameters (standard errors)			
BXLE	$\widehat{\rho} = 16.6547\ (6215.44)$	$\widehat{\delta} = 0.01708\ (6.37703)$	$\widehat{\kappa} = 39.5297\ (7.64793)$	
FWME	$\widehat{\alpha} = 2.77136\ (1.2456043)$	$\widehat{\lambda} = 2.88091\ (0.0012536)$	$\widehat{k} = 3.11453\,(1.256135)$	$\widehat{a} = 3.84424\ (0.012989)$
BE	$\widehat{\lambda} = 0.07354\,(0.00071)$	$\widehat{a} = 24.2815\,(8.98448)$	$\widehat{b} = 121.998\,(7.64793)$	
APExE	$\widehat{\alpha} = 46.3239\,(65.8173)$	$\widehat{a} = 2.52118\,(0.217317)$	$\widehat{c} = 91.0457\,(52.8461)$	
GExE	$\widehat{\lambda} = 0.25249\,(0.382442)$	$\widehat{\alpha} = 35.2218\,(14.7076)$	$\widehat{\delta} = 27.6803\,(49.284)$	
TGE	$\widehat{\alpha} = 90.1525\,(38.8898)$	$\widehat{\lambda} = -0.697529\,(0.20628)$	$\widehat{\theta} = 2.21536\,(0.187642)$	
ExE	$\widehat{b} = 89.4374\,(33.3448)$	$\widehat{a} = 2.01918\,(0.002538)$		
TE	$\widehat{\beta} = 0.585265\,(0.0672482)$	$\widehat{\lambda} = -1.00000\,(0.459119)$		
LE	$\widehat{\beta} = 1.74693 \times 10^{-22}\,(0.375895)$	$\widehat{\theta} = 0.313899\,(0.162698)$		
E	$\widehat{a} = 0.40367\,(0.0469257)$			
NH	$\widehat{\alpha} = 38.5268\,(26.7975)$	$\widehat{\lambda} = 0.0082434\,(0.0057971)$		

Table 10: Estimated parameters with their standard errors of the BXLE model and other fitted models for second dataset.

Model	Estimated parameters (standard errors)			
BXLE	$\widehat{\rho} = 0.626149\ (0.970701)$	$\widehat{\delta} = 0.293385\,(0.432376)$	$\widehat{\kappa} = 6.24390\,(9.78511)$	
FWME	$\widehat{\alpha} = 1.90568\,(0.024546)$	$\widehat{\lambda} = 2.84917\,(0.567416)$	$\widehat{k} = 2.16087\,(0.005413)$	$\widehat{a} = 1.71784\,(0.025468)$
BE	$\widehat{\lambda} = 0.056844\,(0.000868)$	$\widehat{a} = 5.95815\,(2.13741)$	$\widehat{b} = 37.5763\,(0.821257)$	
APExE	$\widehat{\alpha} = 32.2179\,(58.4502)$	$\widehat{a} = 1.23847\,(0.103739)$	$\widehat{c} = 4.60025\,(2.54393)$	
GExE	$\widehat{\lambda} = 0.269724\,(0.257315)$	$\widehat{\alpha} = 8.07549\,(2.2026)$	$\widehat{\delta} = 6.15979\,(6.82518)$	
TGE	$\widehat{\alpha} = 6.18732\,(1.92831)$	$\widehat{\lambda} = -0.683705\,(0.279297)$	$\widehat{\theta} = 1.10199\,(0.094658)$	
ExE	$\widehat{b} = 7.78824\,(33.3448)$	$\widehat{a} = 1.01317\,(0.002538)$		
TE	$\widehat{\beta} = 32.2179\,(0.557692)$	$\widehat{\lambda} = -1.00000\ (0.398622)$		
LE	$\widehat{\beta} = 4.07405 \times 10^{-10}\,(0.0859971)$	$\widehat{\theta} = 0.253513\,(0.0475148)$		
E	$\widehat{a} = 0.381476\,(0.0381476)$			
NH	$\widehat{\alpha} = 38.3038\,(24.8412)$	$\widehat{\lambda} = 0.007253\ (0.004764)$		

Table 11: Discrimination measures of the BXLE model and other competing models for first dataset.

Model	AKI	CAKI	BAI	HAQUI	ANDA	CRVMI	KOSM	p value
BXLE	110.123	110.466	117.036	112.881	0.380356	0.059098	0.056529	0.972044
FWME	116.084	116.664	125.301	119.761	0.56027	0.0775639	0.0693095	0.927044
BE	112.344	112.687	119.257	115.102	0.565112	0.086484	0.068130	0.882162
APExE	115.308	115.651	122.22	118.066	0.715941	0.0965186	0.0697025	0.864808
GExE	112.777	113.12	119.689	115.534	0.600183	0.0920141	0.0700697	0.860604
TGE	119.542	119.885	126.454	122.3	1.08865	0.15413	0.084345	0.668357
ExE	121.607	121.776	126.215	123.445	1.50244	0.223549	0.0953139	0.512098
TE	237.473	237.642	242.081	239.311	15.8457	3.1266	0.359161	00000
LE	192.302	192.471	196.91	194.14	13.3126	2.65435	0.339298	00000
E	284.259	284.315	286.563	285.178	22.1407	4.67218	0.44947	00000
NH	239.564	239.733	244.172	241.402	23.9619	5.22339	0.468589	00000

Table 12: Discrimination measures of the BXLE model and other competing models for second dataset.

Model	AKI	CAKI	BAI	HAQUI	ANDA	CRVMI	KOSM	p value
BXLE	288.775	289.025	296.591	291.938	0.41295	0.067419	0.060811	0.853353
FWME	300.559	300.98	310.98	304.776	1.10367	0.167555	0.0902804	0.388871
BE	292.486	292.736	300.301	295.649	0.760458	0.15047	0.09349	0.346368
APExE	291.673	291.923	299.489	294.837	0.664769	0.125778	0.0870556	0.43464
GExE	293.482	293.732	301.297	296.645	0.834621	0.164551	0.0963921	0.310696
TGE	294.83	295.08	302.646	297.993	0.927332	0.174829	0.0966358	0.307819
ExE	296.365	296.488	301.575	298.473	1.22463	0.229158	0.107725	0.196182
TE	342.209	342.333	347.419	344.318	8.42304	1.4915	0.21033	0.000287
LE	303.002	303.126	308.212	305.111	3.5464	0.634098	0.138342	0.0435195
E	394.742	394.783	397.347	395.796	17.3021	3.43402	0.320593	00000
NH	347.224	347.348	352.434	349.333	13.8496	2.83065	0.288983	00000

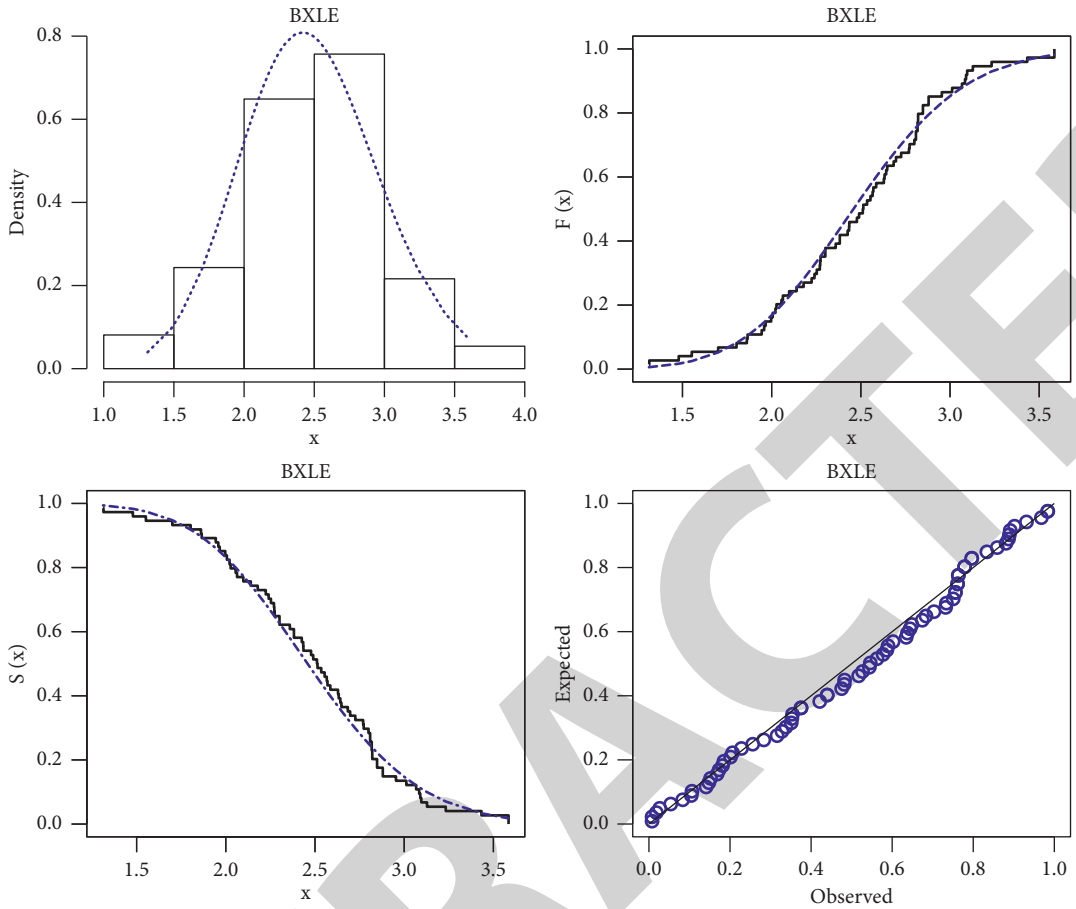

Figure 3: The fitted BXLE PDF, CDF, SF, and P-P plots for first dataset.

Tables 1–8 provide the simulation results for the BXLE parameters utilizing the seven estimate methodologies, including AVE, AVB, MSE, and MRE. The estimates of the BXLE parameters derived from all seven estimation techniques are fully good, that is, they are extremely trustworthy and very near to the real values, with negligible biases, MSE, and MRE in all parameter combinations. For all parameter combinations, all estimators exhibit the consistency property, in which the MSE, AVB, and MRE drop as sample size grows. We find that the MLE, ADE, CVME, LSE, MPSE, PCE, and WLSE approaches do an excellent job at estimating BXLE parameters.

5. Application

In this part, we will look at two real-world datasets. The first dataset has 74 observations and represents gauge lengths of 20 mm [17]. The second set is made up of 100 observations and reflects the breaking stress of carbon fiber [18].

We compare the BXLE model with some other well-known competitive distributions such as the beta E (BE) [19], transmuted generalized-E (TGE) [5], exponentiated E (ExE), alpha power exponentiated E (APExE) transmuted E (TE) [23], exponetial (E), Nadarajah-Haghighi (NH) [4], Fréchet Weibull mixture E (FWME) [21], gamma exponentiated E (GExE) [22], and linear E (LE) [23] distributions.

Some discriminatory practice measures, such as Akaike information (AKI), Hannan–Quinn information (HAQUI), Bayesian information (BAI), and consistent Akaike information (CAKI), can be used to compare competing models. Other discrimination measures include the Anderson–Darling (ANDA), Cramér–von Mises (CRVMI), and the p value of the Kolmogorov–Smirnov (KOSM).

The estimated parameters using the maximum likelihood method and their standard errors for the BXLE model and other compared models are reported in Tables 9 and 10 for the two datasets, respectively. The values of discrimination measures are listed in Tables 11 and 12. The values in Tables 11 and 12 indicate that the proposed BXLE distribution provides better fit for the two analyzed datasets than other competing models.

The fitted functions are displayed graphically, including the PDF, CDF, SF, and PP plots, in Figures 3 and 4. These plots supports the numerical values in Tables 11 and 12 that the proposed BXLE model provides the best fit for the two datasets.

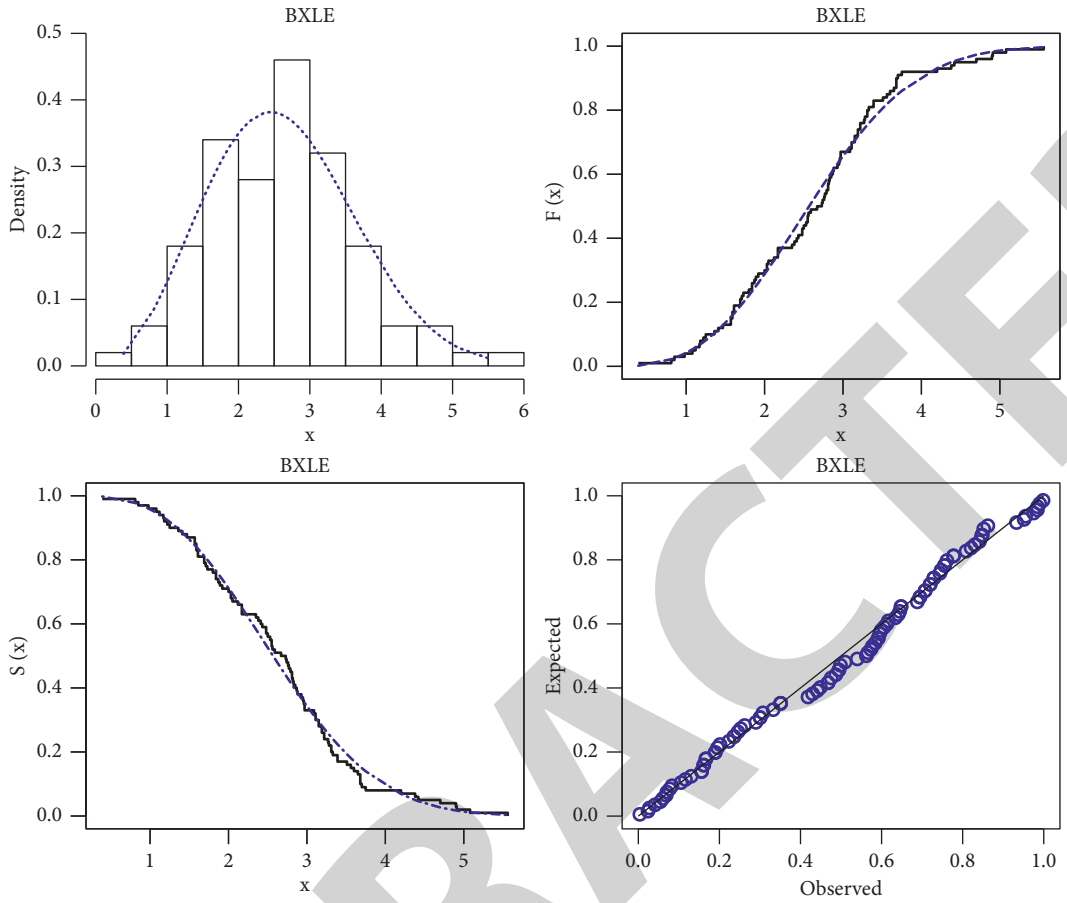

Figure 4: The fitted BXLE PDF, CDF, SF, and P-P plots for second dataset.

6. Concluding Remarks

This study proposed a unique three-parameter Burr *X* logistic-exponential (BXLE) distribution for modeling engineering data and other applications. The BXLE model generalizes and extends the logistic-exponential distribution. The hazard rate of the BXLE distribution might be declining, increasing, bathtub, unimodal, J-shape, or reversed-J shape. In certain circumstances, its mathematical properties were derived. Its density was determined as a mixture of exponential densities. The maximum likelihood estimators, Cramér–von Mises estimators, Anderson–Darling estimators, maximum product of spacing estimators, least-squares estimators, percentile estimators, and weighted least-squares estimators were used to estimate the unknown parameters of the BXLE model. All estimators perform brilliantly in predicting the BXLE parameters, as proved by simulation data. According to our findings, the maximum likelihood approach delivers the best accurate estimations of the parameters of the BXLE distribution. The BXLE distribution's practical importance was proved using two authentic engineering datasets, proving its acceptable fits and benefits over other competing contemporary models.

Data Availability

The datasets used to support the findings of this study are included within the article.

Conflicts of Interest

The author declares that there are no conflicts of interest.

References

[1] R. D. Gupta and D. Kundu, "Generalized exponential distribution: different method of estimations," *Journal of Statistical Computation and Simulation*, vol. 69, pp. 315–337, 2001.

[2] M. C. Jones, "Families of distributions arising from distributions of order statistics," *Test*, vol. 13, pp. 1–43, 2004.

[3] W. Barreto-Souza, A. H. Santos, and G. M. Cordeiro, "The beta generalized exponential distribution," *Journal of Statistical Computation and Simulation*, vol. 80, pp. 159–172, 2010.

[4] S. Nadarajah and F. Haghigh, "An extension of the exponential distribution," *Statistics*, vol. 45, pp. 543–558, 2011.

[5] M. S. Khan, R. King, and I. L. Hudson, "Transmuted generalized exponential distribution: a generalization of the exponential distribution with applications to survival data,"

Hindawi
Journal of Mathematics
Volume 2024, Article ID 9857507, 1 page
https://doi.org/10.1155/2024/9857507

Retraction

Retracted: Dynamic Wavelength Scheduling by Multiobjectives in OBS Networks

Journal of Mathematics

Received 23 January 2024; Accepted 23 January 2024; Published 24 January 2024

This article has been retracted by Hindawi following an investigation undertaken by the publisher [1]. This investigation has uncovered evidence of one or more of the following indicators of systematic manipulation of the publication process:

(1) Discrepancies in scope

(2) Discrepancies in the description of the research reported

(3) Discrepancies between the availability of data and the research described

(4) Inappropriate citations

(5) Incoherent, meaningless and/or irrelevant content included in the article

(6) Manipulated or compromised peer review

The presence of these indicators undermines our confidence in the integrity of the article's content and we cannot, therefore, vouch for its reliability. Please note that this notice is intended solely to alert readers that the content of this article is unreliable. We have not investigated whether authors were aware of or involved in the systematic manipulation of the publication process.

Wiley and Hindawi regrets that the usual quality checks did not identify these issues before publication and have since put additional measures in place to safeguard research integrity.

We wish to credit our own Research Integrity and Research Publishing teams and anonymous and named external researchers and research integrity experts for contributing to this investigation.

The corresponding author, as the representative of all authors, has been given the opportunity to register their agreement or disagreement to this retraction. We have kept a record of any response received.

References

[1] V. K. A. Kumar, M. R. Kumar, N. Shribala et al., "Dynamic Wavelength Scheduling by Multiobjectives in OBS Networks," *Journal of Mathematics*, vol. 2022, Article ID 3806018, 10 pages, 2022.

Hindawi
Journal of Mathematics
Volume 2022, Article ID 3806018, 10 pages
https://doi.org/10.1155/2022/3806018

Research Article

Dynamic Wavelength Scheduling by Multiobjectives in OBS Networks

V. Kishen Ajay Kumar,[1] M. Rudra Kumar,[2] N. Shribala,[3] Ninni Singh,[4] Vinit Kumar Gunjan,[4] Kazy Noor-e-alam Siddiquee,[5] and Muhammad Arif[6]

[1]*Department of ECE, Institute of Aeronautical Engineering, Hyderabad, Telangana 501401, India*
[2]*Department of CSE, GPCET, Kurnool, Andhra Pradesh, India*
[3]*Department of ECE, Matrusri Engineering College, Hyderabad, Telangana 501401, India*
[4]*Department of Computer Science and Engineering, CMR Institute of Technology, Hyderabad, Telangana 501401, India*
[5]*Department of Computer Science and Engineering, University of Science and Technology, Chittagong, Bangladesh*
[6]*Department of Computer Science and Information Technology, University of Lahore, Lahore, Pakistan*

Correspondence should be addressed to Kazy Noor-e-alam Siddiquee; knalam@ustc.ac.bd

Received 12 February 2022; Revised 7 March 2022; Accepted 24 March 2022; Published 28 April 2022

Academic Editor: Naeem Jan

The burst dropping ratio is witnessed in the contemporary literature as a considerable constraint of optical burst switching (OBS) networks that attained many researchers' efforts in the recent past. Among the multiple practices endeavoring to reduce the burst drop ratio, the optimal burst scheduling is one dimension in this regard. The transmission channel scheduling and appropriate wavelength allocation are critical objectives to achieve optimal burst scheduling in regard to minimal burst drop ratio. Many of the scheduling models depicted in the contemporary literature aimed to achieve the optimum scheduling by electing the channels, which depend on optimum utilization of idle time. Some of the studies tried to select channels by any metrics of quality, and significantly minimal amount of studies focused on wavelength allocation for lowering BDR. Moreover, in regard to this, this study tried to achieve optimum wavelength allocation beneath manifold objective QoS metrics, which is identified as "multi-objective dynamic wavelength scheduling (DyWaS)." The experimental study carried through the simulations evinced that the proposed model DyWaS escalated the optimality of burst scheduling through wavelength allocation compared with other existing methods represented in the contemporary literature.

1. Introduction

Growing Internet access and penetration rate across the world is resulting in high traffic congestion among system networks. Further, the increase in multi-media applications is causing further load over existing bandwidth. Accordingly, the need for additional traffic rates, which have already crossed the maximum capacity limits of networks, is on the rise. As these traffic rates focus more on backbone networks, the impact is largely felt on core networks. To overcome these limitations, highly effective and optimal resource distribution to clients must be designed [1]. Most of the network programmers rely on the optical-switching model to address the congestion issues in networks [2].

In commercial networks, circuit switching is the most common optical-switching model. Light can travel a longer distance through the circuit-switching model. It is known as the "WR network" because of the light paths it allows to pass through the fibres. The projected wavelengths of these rays also influence their trajectories. It is true that the traditional WR model is not as effective in high-traffic situations, and its performance can change over time. WR light paths are bandwidth-assured tunnels, resulting in insufficient or unused bandwidth due to information transmission inefficiency, which is the case here.

The OBS model [3–11] has emerged as a reliable option for next-generation optical networking to efficiently handle heavy congestion scenario along with dynamically varying traffic conditions. The model [12] integrates the optimal optical circuit with packet switching in order to explore large bandwidth. Hence, this approach is regarded as a preferred option for managing high-speed backbone networks. It incorporates burst assembly, where data packets are integrated into bursts at the ingress-edge nodes and then disintegrates these bursts at the egress. The model considers a burst as the primary switching granularity consisting of a cluster of data packets transmitted between nodes. Together with the burst, a control message is also transmitted through the pre-determined path to construct the fabrics of every in-between node before the delivery of burst to the particular node. These guarantees cut-through at every in-between node for the burst, which is open to the control layer. The duration of the transmission of the control message and the delivery of related burst is termed as offset duration.

Though the approach has multiple pros, it also involves certain challenges, hindering QoS of the network like buffering lags, occasional burst conflicts arousing from single-way signaling norms, and regular retro-blocking of bursts. Packet dropping is the major challenge observed in higher layers, mandating redelivery of the dropped packets and thereby adding to overall transmission lags.

There are a number of possible explanations for this burst reduction in the OBS environment, including data contention, path congestion, and ineffective resource reservation coding or retro-blocking. Numerous studies in the current literature focus on burst-based models and the switching framework associated with them. Another intriguing area of study in the context of OBS is data contention [13]. Environmental factors can complicate multiplexing and switching.

As a result, these issues can result in a decrease in network efficiency, particularly when a transmission request consumes nearly all of the available bandwidth capacity. In these networks, a more nuanced version of unfairness is observed, with a higher probability of bursts dropping.

1.1. Motivation. The OBS default transmission model does not support burst buffering during transmission. As a result, burst drop is frequently observed as the default loss class constraint for networks. This is because buffering based on burst transmission reduces the QoS in OBS when compared to IP networks. Typically, for OBS network provisioning of QoS, wavelength contention occurs when two or more data bursts attempt to achieve identical output at the same time using the same wavelength. In this case, for OBS networks, the possibility of burst loss is minimized by lowering the level of wavelength contentions during data bursts.

1.2. Problem Statement. Scheduling an OBS network can be defined as the process of allocating or reserving resources in anticipation of a burst entering the network. The primary goal of scheduling is to minimize any idle spaces created by the burst and schedules. Unlike the traditional Internet, there is little support for optical buffers for temporary storage and forwarding in the event of a contention in OBS networks. Thus, bursts are typically forwarded to the next node in the destination direction within a short turnaround time, or the burst is dropped.

The scheduling algorithm must effectively handle bursts while also ensuring that any existing voids are filled in an efficient manner. A void can be defined as the space between two consecutive bursts scheduled for a channel that is left unused or idle.

2. Related Research

In JET models, the probability of burst loss varies with each hop in the OBS environment. This is because the duration of the offset decreases with each hop. As a burst approaches its final node, the likelihood of it dropping increases. This concept results in a decrease in both throughput and resource consumption. Additionally, it may result in a great deal of injustice [14].

A bi-state Markov chain approach was proposed in [15] for managing burst drops in the JET context. It used the FF-VF filling context for path sequencing. In [16], a tool for estimating the probability of an FDL buffering granularity-specific loss was developed. Researchers in [17, 18] developed an estimation tool by utilizing retransmission and deflection models. The authors proposed a more advanced form of JET signaling, dubbed VFO, in their study [19]. The VFO's time sequencer takes the burst's arrival time into account. S-JET, a new JET signaling variant, was proposed in [20] as a means of increasing JET processing speed by registering at the end of the list. The authors in [21] developed an asymptotic scenario for the possibility of a null burst drop at various projected wavelengths. This assists in identifying areas with a remote possibility of a burst drop.

The researchers in [22] paid greater attention to the effect of offset duration. They devised a method for supplying the patterns of offset time distribution seen in control frame headers. The researchers demonstrated that the variance of the pattern can affect the total burst loss. Because the burst loss is less dependent on reservation coding in the header span, a lower threshold value is required. Barakat and Darcie [6] conducted a study to determine the effect of control frame dispensation on the throughput of a channel. A new technique was been developed in order to better understand the effect of the control-header sequencing procedure on primary nodes. According to the researchers' findings, high-speed control message transmission is not required to achieve superior performance in OBS networks. According to another study, the mean control delay on existing long-haul routes can be significantly longer than the delay in the header sequences.

The researchers in [23] developed a probabilistic method for determining the likelihood of burst loss when channel usage convertor sharing is used. To manage traffic distributions, the method employs the Markovian arrival procedure, which views the burst onset as the burst's onset. The burst volume appears to disperse rapidly. According to [24], this study developed an optimal burst sequencing code. The

code makes use of invariant time burst rescheduling. The primary purpose of this method is to eliminate any offset duration errors. As a result, duration-based priority mechanisms are prohibited. The possibility of data contention and loss is examined in the context of multiple routing codes [25]. The model in [26] is a lower load fixed-point method for determining the likelihood of data loss. For both JIT and JET concepts, the method utilizes data segmentation and path-based priorities. According to the theory, data segmentation reduces the risk of data loss the least, while path-based priority theory also reduced losses more significantly, but the difference was not statistically significant.

Pre-emption is the most frequently used technique for ensuring fairness in OBS networks [27]. The LHP mechanism as a means of redressing environmental injustices is another contemporary model [28]. The researchers discovered that if the total number of hops exceeds a predetermined threshold, it is possible to prevent a second burst at the final hop. However, in OBS, the method fails because pre-emption occurs only once, at the very end of the network path. The authors in [29] proposed an alternative to this solution. This concept is founded on two pre-determined threshold levels. Additionally, Gao et al. [30] proposed a fair FPP model. This calculation is based on the first offset duration, the mean burst volume, the successful hops, and the leftover hops. In the context of data contention, the FPP method of pre-emption is used to balance network fairness and throughput. In an experimental study, the FPP model outperformed the approaches proposed in [27, 28].

As suggested by the authors in [31], the FCSA sequencing program can be used to strike a balance between fairness and blocking efficiency. The algorithm incorporates a dynamic priority into each burst. The critical characteristics of a burst are determined by the priority assigned by the appropriate authority. In the context of data contention, this approach uses these priorities to select a desirable burst and ignore another. The researchers in [32] considered the role of a subcarrier in path capacity.

The study in [33] employed sequencing mechanisms in order to accommodate a large number of participants. As part of this effort to ensure short-term fairness, bandwidth is weighted. The model in [34] proposes the use of the DPCC system, which is designed to ensure equitable distribution of traffic and resources. Additionally, the method modifies the message transmission's speed and reliability. It adjusts these parameters based on data from traffic congestion, pricing, and user feedback. The model is based on feedback data, which can be scarce. As a result, when input flows are limited, certain bursts experience a high rate of loss. This can result in an asymmetrical network utilization. A route based on an ant scenario, a wavelength, and a time-slot distribution program was proposed [35] for lowering the burst drop ratio and achieving a high overall efficiency.

The preceding studies concentrated on reducing the likelihood of burst loss and increasing network throughput as a result. However, these contributions were limited to determining the channel's optimal idle time. The purpose of this paper is to propose a new model for increasing efficiency that can be used with both JIT and JET. It considers multiple quality metrics at the channel level, such as data offset duration and burst transmission realization time, in addition to traffic inference resolution methods. In this model, burst segmentation can also be used to optimize scheduling.

3. Dynamic Wavelength Scheduling (DyWaS)

Dynamic wavelength scheduling (DyWaS) is an extension of our previous work, proximate optimal channel selection via void filling (POCS-VF) [36]. When it comes to wireless networks, the POCS-VF is an adaptive channel scheduling system that maximizes the utilization of data bursts by utilizing idle time between channel schedules (pools of packets). POCS-VF is a scheduling strategy for data bursts that prioritizes them based on available bandwidth and the possibility of utilizing idle time. However, other aspects of quality of service (QoS) are ignored when channel scheduling is determined. As a result, it frequently performs below average at public access points. In comparison to POCS-VF, the proposed DyWaS evaluates the effect of multiple transmission quality objectives on the transmission quality of proposed wavelengths. The wavelength optimality ratio (*wor*) has been proposed as a new scale for examining the application of various channel quality metrics in this context. The greater the wavelength optimality ratio is, the more critical that particular communication channel is. The DyWaS strategy is as follows.

Each access point's controller buffers packets to ensure consistent transmission latency. When a transmission session is created, the collection of packets is divided into bursts and information about each burst is passed to a scheduler. This information sharing can be determined using a burst transmission control packet. Arrival time is the time required for a burst to arrive at an access point and the time required to share information about that burst, which is commonly referred to as offset time.

For simplicity, we will use $p(cf_i)$ as the processing time, $\tau(cf_i)$ as the time it takes for control frame cf_i to attain the scheduling system after it leaves the assembler, and$\tau(b_i)$ as an estimate of how long it will take to send burst bi from the assembler to the scheduler. The total estimated transmission time $ett(b_i)$ is calculated as follows:

$$ett(b_i) = p(cf_i) + \tau(cf_i) + \tau(b_i). \quad (1)$$

Here in equation (1), the representation could be the entire expected time consumed by burst for reaching towards scheduler. Table 1 describes the annotation used to describe the equations.

3.1. DyWaS Strategy. The scheduler starts the scheduling procedure if the control frame has arrived. In this regard, the scheduler introduces the essential properties of transmission called optimum wavelength, which requires the existence of wavelength time. Moreover, wavelength allocation procedure under DyWaS is discussed in the following.

Primarily, the abovesaid method evaluates the shown wavelength transmission values of entire available presented

Table 1: Notations for DyWaS.

Wavelength optimality ratio	(wor)
Processing time	$p(cf_i)$
Control frame	cf_i
Estimated transmission time	$ett(b_i)$
Wavelength arbitration rate	$arr(w_i)$
Elapsed schedules of the wavelength	$es(w_i)$
Total number of schedules	$ts(w_i)$
Nanometers and the representation	$nw(i)$
Deserted schedules	$\mathrm{ds}(w_i)$
Inference threshold	irt
Wavelength existence span	wes
Existence span threshold	est
Residual life span	$rls(w_i)$
Transmission realization rate	(trr)
Inference rate	(ir)
Wavelengths possessing primary score	W_{ps}

wavelengths and sequences these wavelengths as per the one of shown quality metrics, which is deliberated as main transmission quality requirement. The planned method for evaluating the opportunity of every transmission metric quality, projected in respect to available estimated wavelengths, is discussed in the following segment.

The scheduler transmission controller receives the DPs from manifold consumers and buffers as per their arrival time latency, and later bursts are the buffered DP pool. Moreover, these bursts are scheduled by the access points towards optimal shown wavelengths, which transfer data towards target. This paper's objective is to attain maximum quality of transmission.

The projected wavelengths are scheduled and controlled by the scheduler (set of wavelengths). Therefore, the wavelength allocation under the scheduler is from the sets, which indicates the available wavelengths.

The wavelength scheduling towards burst is required for transmitting the particular quality. The wavelength, which is scheduler, is not often optimal under entire considered quality metrics. The priority sequence in respect to chosen metrics quality could be the contextual position. Here, wavelength that is highly rated under 1 metric of quality is not optimal often under other metrics of quality. Therefore, it is evident for choosing the wavelength, which is reasonably rated under many of the most preferable quality metrics for scheduling.

The selection of wavelength by the optimality rate of wavelength scheduled towards respective burst is suggested. The metric quality is adapted for evaluating optimality ratio of wavelength in the following way:

(i) Wavelength arbitration rate: this metric signifies ratio of wavelength elapsed schedules in averse to count of times where the wavelength is scheduled. This could be measured in the following equation:

$$arr(w_i) = \frac{es(w_i)}{ts(w_i)}. \tag{2}$$

(a) The notation $arr(w_i)$ in equation (2) is the wavelength arbitration rate, which is the ratio of elapsed schedules $es(w_i)$ of the wavelength w_i against total schedules $ts(w_i)$.

(ii) Desertion rate: this metric indicates the failure transmissions noticed in averse to entire amount of times the respective wavelength is scheduled. Equation (3) represents the metric assessment:

$$dr(w_i) = \frac{\mathrm{ds}(w_i)}{ts(w_i)}. \tag{3}$$

(a) The notation $dr(w_i)$ in equation (3) depicts the ratio of abandoned transmissions $\mathrm{ds}(w_i)$ against the total number of schedules $ts(w_i)$ of respective wavelengthw_i.

(iii) Transmission realization rate: this metric denotes transmission realization ratio in averse to count of times, in which wavelength is the scheduler that could be measured in the following way:

$$trr(w_i) = \frac{ts(w_i) - \mathrm{ds}(w_i)}{ts(w_i)}. \tag{4}$$

(a) The notation $trr(w_i)$ in equation (4) claims the transmission realization rate of wavelength w_i, and the difference between total schedules $ts(w_i)$ and the deserted schedules $\mathrm{ds}(w_i)$ depicts the total number of successful schedules.

(iv) Inference rate: adequate amount of wavelength is required for performing transmission with less assurance. The wavelength that is available needs to be compatible towards respective transmission of burst, so that at bottom side, the attenuation needs to be overcome, and at top side, it should not enable noise inference. When wavelength is lower than essential level or higher than level that allows noise inference, then it depicts that respective wavelength could not be optimal, and when it is in between pre-requisite levels, then respective wavelength needs to be considered. The wavelength in the specified level is divergent at the specified threshold from other shown wavelengths, which is scheduled as per the wavelength compatibility measuring using the following equation:

$$ir(w_i) = \sqrt{(w(i) - nw(i))^2}. \tag{5}$$

(a) The notation $ir(w_i)$ in equation (5) finalizes the distance of resulting wavelength distance from its neighbor wavelength, the representation $w(i)$ signifies respective wavelength in the nanometers, and the representation $nw(i)$ denotes the neighbor wavelength in the nanometers.

(b) This $ir(w_i)$ must be greater than the given inference thresholdirt, since $ir(w_i) < irt$ indicates that wavelengthw_i causes inference with wavelengthw_j for current scheduling requirement.

(v) Wavelength data rate: this parameter is the main QoS aspect since data rate acts as crucial role for

attaining less assured delivery of burst at destination. When rate of data is lower than needed or more than cumulative of pre-requisite data rate and residual data rate of threshold, then it represents that corresponding wavelength could not be optimal for scheduling; if they are in between requisite rate of data and residual threshold data rate, then respective wavelength could be optimal. Here, data rate measuring compatibility is given in the following:

$$wdr(w_i) = dra(w_i) - drr(w_i). \quad (6)$$

(a) Here notation $w\ dr(w_i)$ in equation (6) finalizes the data rate of wavelength w_i, $dr\ a(w_i)$ is indicating the data rate available at wavelengthw_i, and "$dr\ r(w_i)$" is the data rate required at w_i for corresponding burst to be scheduled.

(b) This $dr\ c(w_i)$ needs to be lower than the specified "residual data rate threshold" $r\ dr\ t$, as $dr\ c(w_i) > r\ dr\ t$ denotes that w_i wavelength is large for present scheduling requirement data rate that could be reserved for further scheduling with maximum requirement of data rate.

(vi) Wavelength existence span (*wes*): if the "wavelength existence span" is more than residual life time of respective burst, then corresponding wavelength is not suitable for scheduling as span existence is more than residual life time of burst and absolute variance of *est* (existence span threshold). When the absolute variance among "wavelength existence span" and residual life time of burst is more than $r\ dr\ t$, then it could be infeasible for scheduling because the respective wavelength could be reserved aimed at future load, which required more wavelength existence span. This could be measured in the following way:

$$wes(w_i) = aes(w_i) - rls(b). \quad (7)$$

(a) The notation $wes(w_i)$ in equation (7) evinces the wavelength existence span of wavelength w_i, the notation $aes(w_i)$ signifies the available existence span of w_i wavelength, and representation $rls(w_i)$ signifies the residual life span of b burst for transmitting the required burst.

(b) If $0 < wes(w_i) \leq est$, then the wavelengthw_i is optimal; otherwise, it is infeasible for scheduling.

3.2. Evaluation Strategy of Optimality Ratio of Projected Wavelengths. Let wavelength arbitration rate (*arr*), desertion rate (*dr*), transmission realization rate (*trr*), inference rate (*ir*), wavelength data rate ($w\ dr$), and wavelength existence span (*wes*) be a set of QoS metrics $M = \{[arr(w_i), dr(w_i), trr(w_i), ir\ (w_i), w\ dr(w_i), wes(w_i)] \forall i = 1 \ldots x\}$ of available projected wavelengths $W = \{w_1, w_2, \ldots w_x\}$ under scheduler s_j.

The QoS factors $w\ dr(w_i)$, $wes(w_i)$ are primary metrics, which are main metrics that are utilized for detecting every wavelength compatibility scope. This prime score is utilized for sequencing the presented wavelengths that are evaluated in the following way.

Then, identify primary score in the following way.

Initial procedure normalizes the compatibility of bandwidth and span existence.

Step 1. $\forall_{i=1}^{x}\{w_i \exists w_i \in W\}$, begin.

Step 2. diff$\leftarrow r\ dr\ t - w\ dr(w_i)$: the set diff comprises the variance among the residual data rate $w\ dr(w_i)$ of each wavelengthw_i in averse to $r\ dr\ t$ residual bandwidth threshold.

Step 3. diff$_{abs}\leftarrow abs(\text{diff}\{w_i\})$ //the set diff$_{abs}$ comprises the absolute entries values in diff.

Step 4. End.

Step 5. $\forall_{i=1}^{x}\{w_i \exists w_i \in W\}$, begin.

Step 6. $w\ dr(w_i) = 1 - (1/(\text{diff}\{w_i\} + \max(\text{diff}_{abs}) + 1))$: normalize the data rate of wavelength so that optimal wavelength in respect to data rate might possess greater value that is between 0 and 1.

Step 7. End.

Step 8. $\forall_{i=1}^{x}\{w_i \exists w_i \in W\}$, begin.

Step 9. diff$\leftarrow est - wes(w_i)$//the set diff comprises the variance among the residual existence span$wes(w_i)$ of the probable wavelengths in averse to residual *est*.

Step 10. diff$_{abs}\leftarrow abs(\text{diff}\{w_i\})$ //the set diff$_{abs}$ comprises the absolute entry values in diff.

Step 11. End.

Step 12. $\forall_{i=1}^{x}\{w_i \exists w_i \in W\}$, begin.

Step 13. $wes(w_i) = 1 - (1/(\text{diff}\{w_i\} + \max(\text{diff}_{abs}) + 1))$ //normalizing "wavelength existence span" so that the optimal wavelength existence span might possess greater value that is in between 0 and 1.

Step 14. End.

Step 15. $\forall_{i=1}^{x}\{w_i \exists w_i \in W\}$, begin.

Step 16. $ps(w_i) = 1 - (w\ dr(w_i) \times wes(w_i))$//product of 2 decimal fractions gives the minor decimal fraction. Therefore, product of represented data rate $w\ dr(w_i)$ and $wes(w_i)$ is deducted from 1 to achieve higher product value.

Step 17. End.

Moreover, these probable wavelengths could be indexed as per the metric values of QoS, so that every probable wavelength could have diverse indices for divergent QoS metrics, and greater than 1 wavelength might possess similar index regarding 1 of QoS. The wavelength index in respect to QoS might be achieved by arranging the presented wavelengths in increasing sequence of corresponding metrics of QoS that is optimal through higher values. When metric QoS is optimal by lesser values, then probable wavelengths could

be arranged in decreasing sequence of corresponding metric values of QoS. In respect to any of QoS, the index greater than 1 wavelength in sequenced list could be same, when corresponding QoS metric values for respective wavelengths were identical. As per the description,

(i) These projected wavelengths are deliberated as W_{ps} set, which are arranged in increasing sequence of their main score.

(ii) These projected wavelengths are deliberated as W_{arr} set, which are arranged in decreasing sequence of arbitration rate of wavelength.

(iii) These projected wavelengths are deliberated as W_{dr} set, which are arranged in decreasing sequence of ratio of desertion.

(iv) These projected wavelengths are deliberated as W_{trr} set, which are arranged in increasing sequence of ratio of transmission realization.

(v) These projected wavelengths are considered as W_{ir} set, which are arranged in decreasing sequence of inference ratio.

Moreover, the method represents the "wavelength optimality rate" for every projected wavelength in the following way.

$\forall_{i=1}^{x}\{w_i \exists w_i \in W\}$, Begin for each projected wavelength.

$$\mu(w_i) = \frac{\{W_{ps}\{w_i\} + W_{arr}\{w_i\} + W_{dr}\{w_i\} + W_{trr}\{w_i\} + W_{ir}\{w_i\}\}}{|Q|}. \tag{8}$$

Equation (8) evaluates the projected indices' mean for manifold wavelength metrics w_i. The representations $W_{ps}\{w_i\}$, $W_{arr}\{w_i\}$, $W_{dr}\{w_i\}$, $W_{trr}\{w_i\}$, $W_{ir}\{w_i\}$ denote the wavelength index w_i in corresponding sets.

$$d(w_i) = \sqrt{\frac{1}{|Q|}\left\{\begin{array}{c}(\mu(w_i) - W_{ps}\{w_i\})^2 + (\mu(w_i) - W_{arr}\{w_i\})^2 + \\ (\mu(w_i) - W_{dr}\{w_i\})^2 + (\mu\{w_i\} - W_{trr}\{w_i\})^2 + \\ (\mu(w_i) - W_{ir}\{w_i\})^2\end{array}\right\}}. \tag{9}$$

Equation (9) expressed from statistical metric is known as "root mean square deviation" of indices assigned towards respective wavelength over diverse metrics of QoS. The representation $\mu(w_i)$, which is utilized in the equation, finalizes the index average of respective w_i wavelength attained for diverse metrics of QoS.

$$wor(w_i) = \frac{1}{d(w_i)}. \tag{10}$$

Then, equation (10) selects optimal entry sets W_{ps} that are probable wavelengths possessing primary score more than specified threshold. Moreover, arrange these chosen wavelengths in decreasing sequence of *wor*, and similar sequence is recommended for selecting the probable wavelength in respect to schedule respective burst.

The negative parameters like (a) no availability of wavelength with required values of QoS metrics and (b) threshold lapses of burst incoming time could be managed under DyWaS in the following way.

If projection of required wavelength is not occurred, when delay identified in arrival of burst that exhibits in wavelength utilization arbitration or if manifold burst competent towards respective wavelength then restructuring of burst into manifold bursts could be done & scheduling of DyWaS would be recursively done till the scheduling procedure is succeeded.

Here, in the DyWaS procedure, it endeavors initially for tracking the optimal wavelength under the influence of diverse metrics of QoS; when scheduling procedure is unsuccessful in connecting burst with respective wavelength, then corresponding burst is restructured into two bursts so that one will definitely be suitable for contemporary wavelength. Nevertheless, repeat the represented method on other burst part till it is scheduled towards optimum wavelength.

4. Simulation Result

The results of the staged experiment are discussed in this section. Through JAVOBS integration, connecting 38 senders via a one-way communication path enables two-way order [37]. Each burst volume is limited to 1,024 data packets of 64 bytes each. The experimentation process utilizes sixteen communication paths, each with a unique time and bandwidth constraint. Each experiment lasted an average of ten minutes. Along with standard approaches, the simulation was conducted using the DyWaS method. POCS-VF [36] and MSBFVF [38–40] are two well-established techniques that share a common concept but differ in their implementation.

The burst drop rate against variable loads and non-variable time periods; the drop rate against variable time periods and non-variable load; the transmission path usage ratio against variable loads and non-variable time periods; the transmission path usage ratio against variable period and non-variable load; and the mean scheduling duration are all parameters used to assess the efficiency of the tested models. The burst drop rate is the total number of bursts that were scheduled for transmission divided by the total number of scheduled bursts. The utilization rate of transmission paths is calculated by dividing the number of active paths by the total number of paths. On average, scheduling each of the sequenced bursts takes the same amount of time as the total number of bursts considered. The simulation's burst load volume ranged from ten to ninety, and the study's time durations ranged from ten to fifty milliseconds.

4.1. Performance Assessment. The experimental results established that the proposed sequencing model DyWaS outperformed the industry-standard MSBFVF. In comparison to POCS-VF, it solved the scheduling optimization problem at a higher level. The preceding paragraph detailed the metrics used to evaluate the performances. As illustrated in Figure 1, the burst dropping rate is 2% smaller than that of

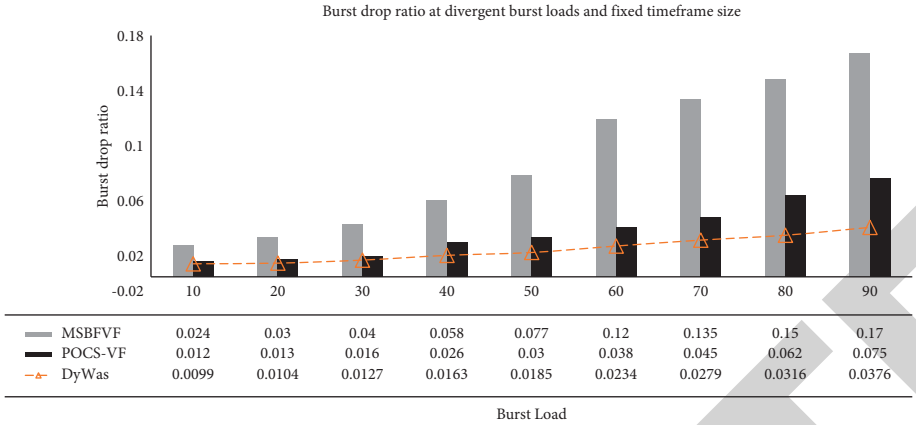

Figure 1: Ratio of burst drop to divergent burst load for a fixed timeframe of 35 μs.

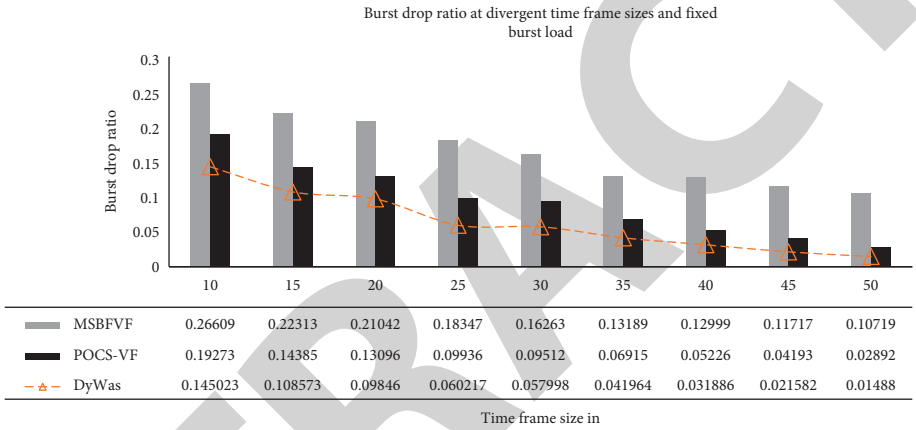

Figure 2: Burst drop ratio changing with the change of size of the timeframes and the burst size staying the same.

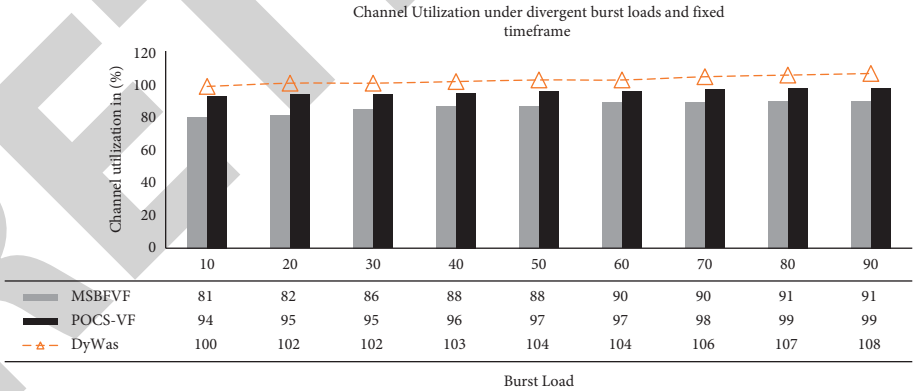

Figure 3: The ratio of channel utilization when a constant timeframe of 35 μs and a varied burst load are used.

POCS-VF and 8% narrower than that of MSBFVF strategy under various loads and a constant timeframe of 35 μs.

Figure 2 illustrates the burst drop ratio for non-variable load burst models with varying timeframes. The ratios are shown for burst drops of 35 and 840 and various other models. The proposed model's burst dropping was found to be 2.5% and 7.5% less than that of POCS-VF and MBSFVF, respectively.

As shown in Figure 3, the transmission path usage ratio for the DyWaS model is 3% higher than that of the PCS-VF approach and 7% higher than that of the MSBFVF approach for burst sizes that are both variable in size but not in duration.

As shown in Figure 4, the proposed DyWaS model had a transmission path utilization ratio that was 2% higher than that of POCS-VF and 8% higher than that of MSBFVF under burst load as constant and variable time duration conditions.

To further evaluate DyWaS's scheduling performance, the study compared it to two other benchmark approaches

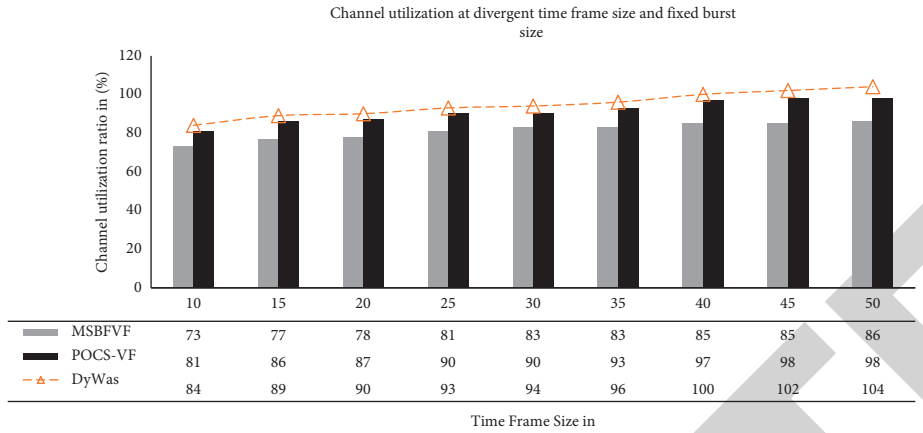

Figure 4: A depiction of how many bytes each channel uses under a wide range of timeframes and a burst load of 35680 bytes.

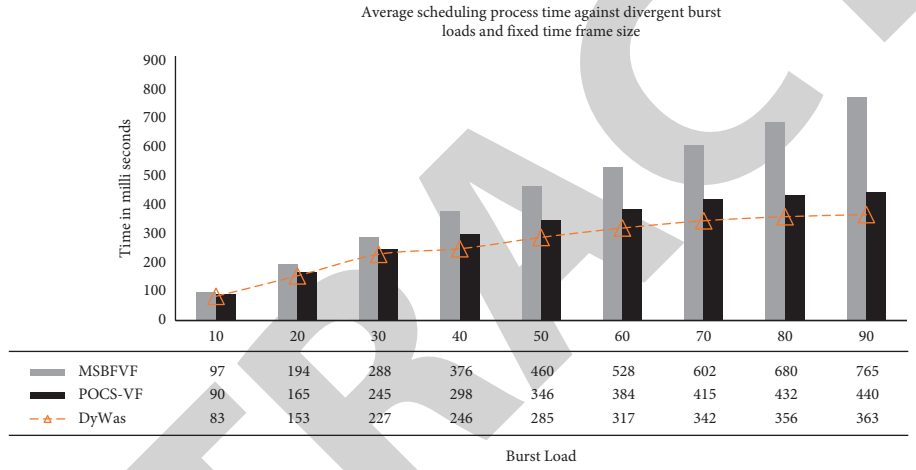

Figure 5: Depiction of average time to schedule burst: divergent burst loads with the fixed time frame of size 25.

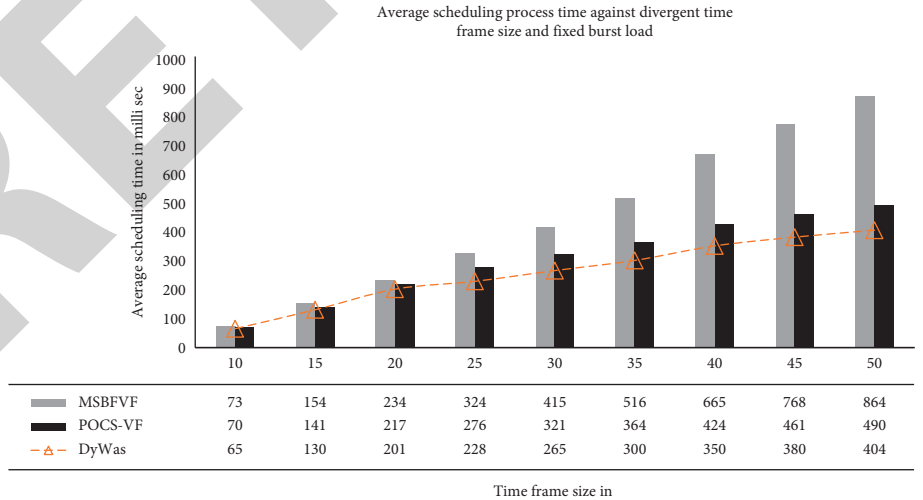

Figure 6: Average time depiction for scheduling of bursts: diversified sizes of timeframes and constant 35680 bytes of burst load.

in terms of scheduling time. Figure 5 depicts a system with a constant duration of 35 μs and a wide range of burst sizes. Figure 6 shows a non-varying burst size of 35,680 bytes with a variable time duration. DyWaS scheduling times were comparable to POCS-VF scheduling times and significantly less than MSBFVF scheduling times in both conditions.

Figure 5 illustrates the average time required to schedule bursts for disparate burst loads with a specific timeframe of 35 μs.

5. Conclusion

The novel proposal and objective of this paper can be regarded as a new approach for scheduling bursts in OBS networks using wavelength allocation. In contrast to other contemporary models, the proposed model is a multi-objective dynamic wavelength scheduling strategy (DyWaS) that evaluates the wavelength's competence in relation to the burst to be scheduled using multiple quality metrics. The proposal's core competency is to achieve the lowest burst drop ratio possible under volatile burst sizes and timeframes, as demonstrated by an experimental study conducted in a simulation environment. Performance analysis was conducted using a variety of different performance statistics, and the proposed model was compared with other contemporary models. The performance metrics burst drop ratio, transmission channel utilization ratio, and time required for scheduling were used to evaluate performance. The proposed model DyWaS outperformed the contemporary models MSB-FVF and POCS-VF by 2.5% and 8%, respectively, in terms of burst drop ratio. When compared to MSB-VF, the model DyWaS required the least amount of processing time; however, when compared to POCS-VF, the model DyWaS required approximately the same amount of processing time. The proposal's results motivate us to extend further by utilizing the depicted metrics as fitness functions in evolutionary strategies to construct an end-to-end route with optimal wavelength allocation between source and destination via multiple nodes.

Data Availability

The processed data are available upon request from the corresponding author.

Conflicts of Interest

The authors declare that they have no conflicts of interest.

References

[1] Y. V. Kumar, A. B. Reddy, B. R. Reddy, and D. Abhishekh, "Bandwidth management in wireless mesh networks," *International Journal of Scientific & Engineering Research*, vol. 4, pp. 1–5, 2013.

[2] J. P. Jue and V. M. Vokkarane, *Optical Burst Switched Networks*, Springer Science & Business Media, Berlin, Germany, 2006.

[3] F. Farahmand, M. De Leenheer, P. Thysebaert et al., "A multi-layered approach to optical burst-switched based grids," in *Proceedings of the 2nd International Conference on Broadband Networks*, pp. 1050–1057, IEEE, Boston, MA, USA, October 2005.

[4] M. Myungsik Yoo, C. Chunming Qiao, and S. Sudhir Dixit, "QoS performance of optical burst switching in IP-over-WDM networks," *IEEE Journal on Selected Areas in Communications*, vol. 18, no. 10, pp. 2062–2071, 2000.

[5] A. Detti, V. Eramo, and M. Listanti, "Performance evaluation of a new technique for IP support in a WDM optical network: optical composite burst switching (OCBS)," *Journal of Lightwave Technology*, vol. 20, no. 2, pp. 154–165, 2002.

[6] N. Barakat and T. E. Darcie, "Control-plane congestion in optical-burst-switched networks," *Journal of Optical Communications and Networking*, vol. 1, no. 3, pp. B98–B110, 2009.

[7] W. Hosny, M. Mahmoud, M. H. Aly, and E. A. EI-Badawy, "New optical parameters dependent metric for OSPF protocol for OBS networks," in *Proceedings of the 2009 IFIP International Conference on Wireless and Optical Communications Networks*, April 2009.

[8] A. Elrasad, S. Rabia, M. Mahmoud, M. H. Aly, and B. Shihada, "Dropping probability reduction in OBS networks: a simple approach," *Optik*, vol. 127, no. 20, pp. 9947–9960, 2016.

[9] A. Das, S. Chakraborty, S. Saha, and A. K. Das, "Traffic statistics and optical burst overlap reduction in core router of OBS networks," in *Proceedings of the 2009 First Asian Himalayas International Conference on Internet*, pp. 1–5, IEEE, Kathmundu, Nepal, November 2009.

[10] P. Zhang, B. Guo, J. Li, Y. He, Z. Chen, and H. Wu, "Collision-free bandwidth-variable optical burst switching ring network," *Journal of Optical Communications and Networking*, vol. 5, no. 9, pp. 1043–1056, 2013.

[11] S.-W. Kau, W.-T. Lu, W.-P. Chen, T.-F. Lee, and C.-N. Tsai, "Performance study of asymmetric traffic load for OBS ring networks," in *Proceedings of the 2009 Fifth International Conference on Intelligent Information Hiding and Multimedia Signal Processing*, pp. 226–229, IEEE, Kyoto, Japan, September 2009.

[12] H. Li, M. W. L. Tan, and I. L.-J. Thng, "Fairness issue and monitor-based algorithm in optical burst switching networks," *Computer Networks*, vol. 50, no. 9, pp. 1384–1405, 2006.

[13] R. Jankuniene and P. Tervydis, "The contention resolution in OBS network," *Elektronika ir Elektrotechnika*, vol. 20, no. 6, pp. 144–149, 2014.

[14] S. Tariq and M. Bassiouni, "Performance evaluation of MPTCP over optical burst switching in data centers," in *Proceedings of the 2014 International Telecommunications Symposium (ITS)*, August 2014.

[15] A. M. Kaheel, H. Alnuweiri, and F. Gebali, "A new analytical model for computing blocking probability in optical burst switching networks," *IEEE Journal on Selected Areas in Communications*, vol. 24, no. 12, 2006.

[16] X. Zhu and J. M. Kahn, "Queueing models of optical delay lines in synchronous and asynchronous optical packet-switching networks," *Optical Engineering*, vol. 42, no. 6, pp. 1741–1748, 2003.

[17] Q. Zhang, N. Charbonneau, V. M. Vokkarane, and J. P. Jue, "TCP over optical burst-switched networks with controlled burst retransmission," *Photonic Network Communications*, vol. 22, no. 3, pp. 299–312, 2011.

[18] C.-F. Hsu, Te-L. Liu, and N.-Fu Huang, "Performance analysis of deflection routing in optical burst-switched networks," in *Proceedings of the Twenty-First Annual Joint Conference of the IEEE Computer and Communications Societies*, vol. 1, IEEE, New York, NY, USA, June 2002.

[19] J. Li, C. Qiao, J. Xu, and D. Xu, "Maximizing throughput for optical burst switching networks," *IEEE/ACM Transactions on Networking*, vol. 15, no. 5, pp. 1163–1176, 2007.

[20] B. Sansò, F. Vázquez-Abad, and E. Gutiérrez-Cabrera, "S-JET: efficient reservation scheduling algorithm for optical burst

Hindawi
Journal of Mathematics
Volume 2023, Article ID 9768364, 1 page
https://doi.org/10.1155/2023/9768364

Retraction

Retracted: Leveraging Digital Library to Enhance Research and Learning Experience of College Students: An In-Depth Study

Journal of Mathematics

Received 10 October 2023; Accepted 10 October 2023; Published 11 October 2023

This article has been retracted by Hindawi following an investigation undertaken by the publisher [1]. This investigation has uncovered evidence of one or more of the following indicators of systematic manipulation of the publication process:

(1) Discrepancies in scope

(2) Discrepancies in the description of the research reported

(3) Discrepancies between the availability of data and the research described

(4) Inappropriate citations

(5) Incoherent, meaningless and/or irrelevant content included in the article

(6) Peer-review manipulation

The presence of these indicators undermines our confidence in the integrity of the article's content and we cannot, therefore, vouch for its reliability. Please note that this notice is intended solely to alert readers that the content of this article is unreliable. We have not investigated whether authors were aware of or involved in the systematic manipulation of the publication process.

Wiley and Hindawi regrets that the usual quality checks did not identify these issues before publication and have since put additional measures in place to safeguard research integrity.

We wish to credit our own Research Integrity and Research Publishing teams and anonymous and named external researchers and research integrity experts for contributing to this investigation.

The corresponding author, as the representative of all authors, has been given the opportunity to register their agreement or disagreement to this retraction. We have kept a record of any response received.

References

[1] C. Yang, "Leveraging Digital Library to Enhance Research and Learning Experience of College Students: An In-Depth Study," *Journal of Mathematics*, vol. 2022, Article ID 8046962, 8 pages, 2022.

Hindawi
Journal of Mathematics
Volume 2022, Article ID 8046962, 8 pages
https://doi.org/10.1155/2022/8046962

Research Article

Leveraging Digital Library to Enhance Research and Learning Experience of College Students: An In-Depth Study

Chunying Yang

School of Special Education, Zhengzhou Normal University, Zhengzhou, Henan 450044, China

Correspondence should be addressed to Chunying Yang; chunying_yang66@163.com

Received 18 January 2022; Revised 21 February 2022; Accepted 1 March 2022; Published 21 April 2022

Academic Editor: Naeem Jan

A digital library is a platform that contains collections of books, services, and personnel to support the sharing of knowledge with creation, dissemination, and preservation. In this context, any university library should comprehensively embrace the developmental trend occurring in the library setting, which should be strictly followed by university libraries as a special mission. Digital libraries should also actively promote the updating of the embedded service model and further upgrade the various resources of the university library. Thus, the digital library provides a platform to assist students to develop an inclination towards learning and emotional shaping. Its functional system thus serves both comprehensive and harmonious development of students. Especially, the knowledge service module of the digital library incorporates users' scientific research context. Most of the existing research studies focus on the individual researcher and neglects the context of the entire research team. Knowledge recommendation for the context of team-based scientific research activities can better serve more scientific research activities and team cooperation. In this work, we propose a knowledge recommendation algorithm for digital libraries based on team research-knowledge application in context matching. We leverage the context-aware learning model to construct the corresponding application context of the digital library knowledge and the context model of team scientific research. Subsequently, we select alternative knowledge and neighbor users as active users and further complete knowledge sorting and recommendation. According to the knowledge recommendation system in a digital library, it is confirmed that the proposed method can effectively deliver the knowledge of researchers in the context of the digital library.

1. Introduction

According to the definition proposed by the United Nations Educational, Scientific, and Cultural Organization (UNESCO), new media refer to the medium of information dissemination based on digital technology and its network [1]. Common new media platforms include mobile TV, digital TV, and mobile media as well as new online media such as WeChat, Weibo, Wiki, and podcasts based on Web2.0 technology. The new media technology has changed information interaction from conventional one-way communication to two-way interactive communication [2]. Besides, new media technology is extremely efficient in sharing information and supports multiformat digital resources. Moreover, some of the new media platforms support resource linking, which enables users to log in, access, download, and read digital resources when needed. Most of these new media platforms have a rich variety of functions and provide more convenience to users. Their popularity among users can effectively realize the transmission and exchange of information.

New media platforms emerge as a supplemental tool to break down the barriers of information exchange between libraries and readers and can facilitate to reach more book collections. Nevertheless, university digital libraries lack effective reading/browsing promotion and do not enable users to exchange information. Using the available new media platforms to assist the construction of resources on the platform of the digital library can provide more conveniences since conventional libraries cannot compete with them due to the limited funds and not up-to-date technological conditions. Reading promotions and improving both

satisfaction of teachers and students significantly could be achieved by developing digital libraries at universities. Libraries cannot ignore their most fundamental role as an instructor since they play an indispensable role as components of universities. Thus, the ministry of education has proclaimed that "conducting information and literacy programs, cultivating information awareness in university students, and the ability to obtain and utilize documents" are some of the university libraries' key roles [2, 3]. Most university libraries have currently provided information literacy education by offering literature retrieval courses and special lectures for undergraduates. However, instructors have to fully consider the requirements of different learning groups in an international environment. Besides, instructors should constantly enrich teaching content, introduce internationally advanced innovative teaching methods, adopt modern information technology, and strive to be diverse. They should make it interesting and provide the instructions with the necessary knowledge that could be applied globally. According to the objective of developing an international university, the language barriers that are encountered should be first eliminated.

With the increasing volumes of exchange activities internationally at the university level, libraries should increase the bilingual literacy education programs applicable to international students. Hence, they may increase international students' information retrieval as well as help international students who are interested in studying abroad to develop themselves by attending mini courses and lectures. Therefore, information retrieval ability means increasing their chances of participating in international exchanges. The digital library should be designed to meet the requirements of special groups. The instructors should not only deal with the university students but should also take into account the requirements of retired staff. Besides, instructors can also cooperate with other school departments to conduct a series of lectures to assist retired staff. Digital libraries can integrate conventional instructing modes with microclasses, flipped classrooms, and MOOCs to substantially improve the retrospectives and reproducibility of courses for knowledge dissemination. The integration with other professional courses and international activities could be utilized to improve knowledge utilization. Typical schemes should start with including information retrieval courses in courses taught in English. Besides, some creative methods should be applied such as incorporating games into international cultural exchange activities.

The knowledge that digital libraries contained has increased rapidly. Moreover, the phenomenon of knowledge overload has become an overwhelming issue. Providing an ideal knowledge dissemination service becomes difficult since the process of matching the searching words of users with resource keywords turns out to be optimized [4]. The knowledge recommendation system of the digital library can analyze and predict the requirements of users and suggest the corresponding knowledge to them. Thus, it has become an effective scientific tool for conducting academic research [5]. However, the increasingly complex scientific research tasks and highly specialized scientific research situations make researchers deal with diverse knowledge requirements. For example, most of the knowledge sources of researchers in science and medicine are the latest papers published in academic journals and conferences, while many social science researchers focus on the value of classic works. More specifically, large-scale scientific research tasks can no longer be completed by a single researcher independently or in cooperation with a small number of researchers since many research projects require a multidisciplinary framework. Thus, many scientific research talents with diverse knowledge backgrounds and complementary roles are required [6]. The context information of the research team is the key to influencing scientific research.

We propose a context-aware learning method that can acquire users' contextual information in real time. The recommendation system that integrates contextual factors can be considered as an important direction in the knowledge services of digital libraries [7]. Hence, the focused key issue is that when scientific research is carried out by teamwork, scientific research will acquire contextual information about the team and its members. Besides, we investigate how to match these knowledge requirements with the knowledge application of the digital library to realize knowledge recommendations. Considering the research context of the scientific team and the knowledge application context utilizing digital libraries, a knowledge recommendation algorithm called TKCM (Team-Knowledge Context Matching) for digital libraries is proposed. Application of the context matching for the team research-knowledge is the motivation of this algorithm. An overview of the proposed TKCM framework is presented in Figure 1.

The proposed method called the TKCM can provide information for the related research of digital library knowledge service according to the research situation and new ideas. The main contributions of this work include the following components: (1) realizing the active recommendation of knowledge according to the application situation of digital library knowledge (this can improve the quality of knowledge service in the digital library; we also emphasize that the knowledge service of the digital library should be oriented to the situation of team scientific research); (2) integrating team situation and individual situation of scientific researchers to meet the knowledge requirements of team research and individual research.

The rest of the paper is organized as follows. Section 2 presents the related work that covers the issues of digital library and information retrieval using models. The proposed method is presented in Section 3. Experimental results and their analysis are presented and discussed in Section 4. Section 5 concludes the research.

2. Related Work

In this section, we present the studies available in the literature whose scope is related to various knowledge recommendation methods and their properties in the formwork of the digital library. Most of the existing research studies focus on the individual researcher and neglects the context of the entire research team. Thus, knowledge

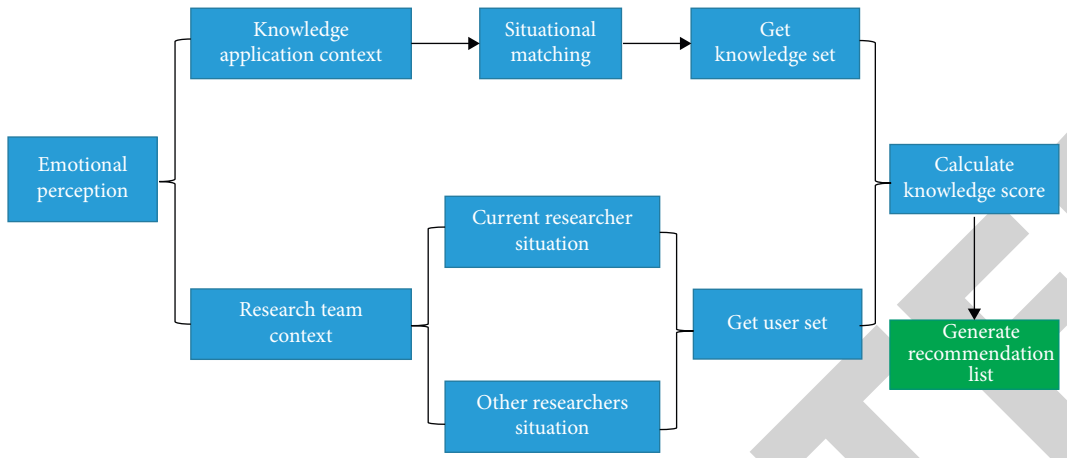

Figure 1: An overview of the proposed TKCM framework.

recommendations for the context of team-based scientific research activities are needed more and can trigger more scientific research activities and team cooperation. Therefore, several studies have been conducted concerning it.

In the era of "big science" characterized by team research and teamwork, the knowledge requirements of scientific researchers are highly individualized, specialized, complex, and volatile. They have strong situational sensitivity. Context refers to any information that can be leveraged to describe the characteristics of an entity's situation. An entity can be a person, a location, or either a physical or virtual object related to user and application interaction [8]. Context can be divided into seven categories: user, user social environment, task, location, infrastructure, physical condition, and time [9]. The context as computing context, user context, physical context, and time was defined in [10]. Digital library service includes the scientific research context. The specific contextual information generally includes such elements as a subject area, scientific research background, scientific research environment, and personnel. Hence, context information can be acquired, processed, and analyzed using smart terminal devices such as sensors, the Internet, and radio frequency identification. All these operations are context-aware [11]. Real-time acquisition of context information through context awareness enables fast-tracking of changes in user requirements and preferences [12]. It can not only effectively enhance the overall performance of the information system but also realize the precise mining of users' personalized requirements as well as improve the user experience of system services. In the domain of digital libraries, context awareness algorithms have been used to acquire user context information, including location Information context, social network context, and so on. They have substantially improved the immediacy and practicability of the user information in the demand model [13]. Knowledge recommendations at the digital library can optimally encode scientific research context. Some researchers introduced the scientific research context into the digital library knowledge recommendation system. They researched the identification of scientific research situations and the construction of situational models. The context elements of digital library knowledge services generally include dimensions such as resource context, user context, and knowledge context [14]. The context-aware system of personalized services for digital libraries can be divided into multiple layers such as sensor access layer, data processing layer, personalized recommendation layer, and application layer [15]. The corresponding service process includes context information acquisition, integration, and personalized semantic matching [16].

Researchers have proposed a variety of knowledge recommendation algorithms for digital libraries to conduct scientific research. Generally, these algorithms can be divided into three categories according to the application of context information. (1) The context information is employed to perform secondary screening on the retrieved list of the recommender system, which uses the item scores predicted by the collaborative filtering algorithm. The context condition entropy is used calculate the weight of each context attribute as well as the user's weighted score of the item in different contexts to generate a recommendation list [17]. The well-known Naive Bayes method with context awareness was combined. Hence, a collaborative recommendation based on the attribute weighted Bayes method is performed in the first place, and subsequently, the influence of context attributes on recommended resources is calculated, and finally, the score list of collaborative recommendations is adjusted [18]. (2) To leverage the context information as a system recommends items to implement contextual recommendations: for the problem of knowledge recommendation in digital libraries, Liu et al. [19] formulated the context similarity calculation to obtain a two-dimensional scoring model of "user-resources" of context sets that are similar to the user's current context. They further generated a recommendation list according to the use of collaborative filtering [20]. The contextual information in integrated into a content recommendation, the similarity between the user's current context and historical context is calculated, and the rankings of users' interest in resources with similar contexts are finally obtained [21]. The contextual information is integrated into the recommendation model to generate new recommendation algorithms.

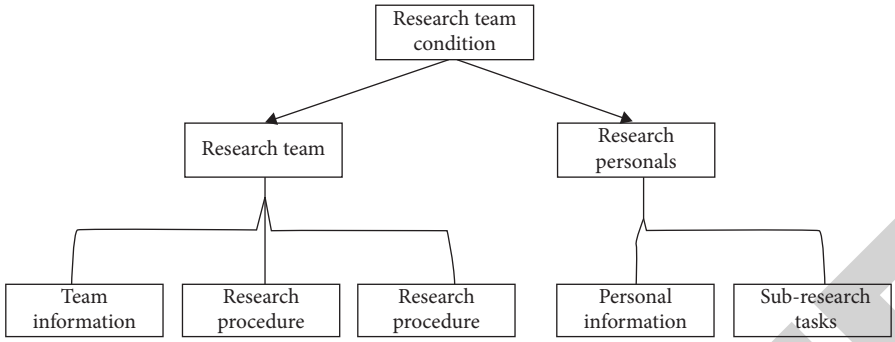

Figure 2: The illustration of the metadata produced by TKCM.

Information recommendation is achieved by matching custom rules with contextual semantic information. The contextual information is used to discover common interests among user groups, and then an information recommendation model is built by leveraging the association and collaboration of common interests [22]. Besides, some of the current novel research and systematic review can be found in [23–25].

3. The Proposed Method

In this section, a novel approach called Team-Knowledge Context Matching (TKCM) is proposed. We propose a context-aware learning method that can acquire users' contextual information in real time. The recommendation system combining contextual factors will be the main direction to match two different types of resources, which are called the knowledge services of digital libraries and research teams.

The research of the team is matched with the knowledge application of the digital library. The knowledge recommendation method called TKCM for the digital library is designed and proposed based on the construction of the situation modeling. Hence, the recommended knowledge can find the actual situation of the scientific research team. The TKCM framework can be expressed by four steps: (1) acquiring contextual information, (2) acquiring knowledge of candidate sets, (3) acquiring neighbor user sets, and (4) generating recommendation lists. The first step collaboratively incorporates the context-aware technique to learn the knowledge application context and team research context utilizing digital libraries. In the second step, the knowledge application of the digital library is matched with the current research of the researchers where the knowledge with high situation similarity is selected as the candidate set. The third step is to match the team research context of other researchers with the context of the current researcher and thus further select researchers with higher contextual similarity as the neighbor user set. The higher the similarity between neighbor users and the current researcher, the greater the influence of their preferences. The fourth step is to calculate the comprehensive preference score of each piece of knowledge in the candidate set according to the preferences of the researchers in the neighbor user set. It is, then, further used to generate a recommendation list. An example of metadata generated by the TKCM recommendation method is elaborated in Figure 2.

The research information includes the knowledge application situation and team research situation of the digital library calculated by the proposed situational awareness technique. It involves two steps, which are called situational information collection and situational information processing. Besides, there are two main ways to collect contextual information. (1) Digital library service records: personal information and knowledge request information are obtained by the registration items of researchers in the digital library as well as user records of search engines. (2) Situation monitoring towards scientific researchers: the location information, working environment, and voice information of researchers in daily life through sensors, radio frequency identification, global positioning system, voice recognition, and other channels are accurately obtained. Thus, we further deliver this information to the digital library in the database. Subsequently, the redundant information in the context is eliminated based on integrating the remaining context information into the knowledge application context of the digital library. Moreover, they are also integrated into the team scientific research context model.

We define the quintuple $C = (T, P, A, R, S)$ to represent the data structure of the situation modeling where $T(\cdot), P(\cdot)\ A(\cdot), R(\cdot)$, and $S(\cdot)$ represent the team's scientific research information, the scientific research process, the scientific research task, the information of researchers, and the sub-research task, respectively. Subsequently, the data structure of the knowledge application situation modeling for the digital library is defined by

$$C_l = (T_l, P_l, A_l, R_l, S_l), \tag{1}$$

where the data structure of the team scientific research situation modeling is represented by

$$C_m = (T_m, P_m, A_m, R_m, S_m). \tag{2}$$

The five situations of library knowledge application and team research are normalized into the so-called situation vectors in a multidimensional space. Thus, their similarities were further compared. More specifically, the knowledge application context and team research context vectors of the digital library are obtained through a backpropagated (BP) neural network that is divided into two components. The

first component is to construct a research context database according to the context information obtained by the context perception technique. BP neural network training is performed by integrating the original data in the research context database running several iterations. In the second step, given the historical application of digital library knowledge i and the context elements of researcher j, the maximum value of the closeness between the context category k of the two users and the context categories in the library can be obtained after the training is completed. Afterward, the historical application situation vector l_i and the team scientific research situation vector j are expressed by

$$\mathrm{Sim}(ji, li) \cdot m, \ldots. \tag{3}$$

We define $M_a = \{jl_{\mathrm{Sim}}(m_a, l_i) > \alpha\}$ as the knowledge candidate set of researcher a, where α represents l_i. The similarity threshold of m_a, $0 < \alpha < 1$, when $\mathrm{Sim}(\mathrm{mai}, l.)$ is greater than α, and the digital library knowledge i is incorporated into the knowledge selection set. Thereafter, the amount of knowledge in the knowledge selection set is denoted by t. It is noticeable that the basic idea of recommender systems is to calculate items with similar user preferences to those active users. In this research, we assume that researchers who are similar to team research contexts such as their teams, research directions, and research tasks have similar knowledge requirements. Thus, the similarity computation of their knowledge can be determined by the contextual similarity between researchers. More specifically, the higher the situational similarity between researchers, the higher the similarity of their knowledge requirements. The similarity between jıs team situation and the current researcher's team situation m_a can be expressed by the cosine of the respective situation information vector defined by

$$\mathrm{Sim}\left(m_a, m_y\right) = \frac{m_a \times X_m}{\sqrt{\sum m_a^2 \times m_j^2}}, \tag{4}$$

where the team research situation and digital library knowledge application situation of multiple researchers can be integrated into matrix L and M, respectively.

Afterward, we calculate the similarity between the current researcher's team context m_a and the digital library knowledge's application context l_i. Then, the similarity can be expressed as the cosine of its vector angle. It is defined by

$$M_a = \{j_l \, \mathrm{Sim}(m_a, l_i) > \alpha\}. \tag{5}$$

It is the knowledge candidate set of researchers, where α represents the similarity threshold between l_i and m_a, $0 < \alpha < 1$. Noticeably, when $\mathrm{Sim}(m_a, l_i)$ is greater than α, we put the digital library knowledge i into the knowledge candidate set. We let the number of knowledge in the knowledge candidate set be t.

Then, we obtain the neighbor user set. The basic idea of the recommendation system is to offer items to university students with similar preferences of active users. We assume that researchers who are similar in team research contexts such as team members, directions, and tasks have similar knowledge requirements in the proposed method. The similarity of their knowledge requirements can be determined by the contextual similarity between researchers. More specifically, the higher the situational similarity between researchers, the higher the similarity of their knowledge requirements. The situation similarity between the team of researcher j with a research situation i_e and the team of researcher a with a research situation m_a can be calculated by the cosine of their respective situational information vectors defined by $N_a = \{\mathrm{Sim}(m_a, m_j) > \beta\}$ The neighbor set of the researcher a is denoted by $(0 < 0 < 1)$ where beta denotes the similarity threshold between m_j and m_a. Thus, $\mathrm{Sim}(m_a, m_j)$ between 0 and 1. We then put researcher j into the neighbor user settings and set the neighbor user. The number of centralized researchers is set to n. Afterward, we generate a recommendation list. Researchers' preferences for knowledge, including behavioral data such as access, citation, and collection, can be obtained correspondingly. Let P_{ih} represent the preference degree of the researcher j in the neighbor user set to the knowledge i in the alternative set. The recommendation score of knowledge i can be obtained by weighted average. The calculation is defined by

$$\mathrm{Score}_i = \mathrm{Shift}\left[\mathrm{Sim}\left(m_a, m_j\right)\right] P_{ij}. \tag{6}$$

We sort the recommendation score of each knowledge in descending order to obtain the recommended list. The obtained recommendation list can guide the research and learning activities of university students. An overview of the proposed framework is presented in the Algorithm 1.

(i) Input: a digital library and its corresponding parameters, N; university students; learning rate and recommendation parameters; output: recommendation list to learners;

(1) Calculate the data situation context model and construct a quintuple to represent the research and learning attributes;

(2) Calculate the similarity matrix based on the context model to capture the complicated relationships among learners in a digital library;

(3) Calculate the recommendation list and score based on equations presented in (5) and (6), respectively. Use them to guide the learning process of university students.

4. Experimental Results and Analysis

In this section, we discuss the experimental results and provide a comprehensive analysis to better present the practicality of the knowledge recommendation system proposed in this paper.

To verify the knowledge recommendation performance of the proposed TCKM framework, knowledge application information and user information are collected from the official websites of ten universities' digital libraries, and 100 scientific research teams are randomly selected from the user information, and 620 of these teams were found to be

Table 1: Researchers' R01 and its situational context.

Research context	Context type	Context elements	Description
Research participants	Basic information	Team background	The knowledge service team at a digital library
		Research scope	Digital library for knowledge recommendation
		Research history	Context perception; resource recommendation; data mining
		Team members	{R01, R13, R76, R43, R51}
	Research procedure	Sub-procedure set	{Sub-procedure-1, sub-procedure-2, sub-procedure-3,. . ...}
		Start of procedure	{Data, resource,. . ..}
		Termination of procedure	{Data, resources, papers,. . ..}
	Research task	Task types	Research of knowledge discovery
		Task objective	Conduct knowledge discovery at the digital library
		Task target	Knowledge from the digital library; users
		Sub-task	{Sub-task1; sub-task2; sub-task3,. . ..}
Research subjects	Basic information	Education background	University students
		Research experience	Knowledge recommendation; data analysis
		Knowledge structure	Data mining; knowledge recommendation; context modeling
	Team		Research team T01
	Sub-research tasks	Sub-task objective	Research of recommendation algorithms
		Sub-task object	Recommendation algorithms
		Sub-task target	Recommendation algorithms in digital libraries
		Tasks' relation	Implementable recommendation algorithms

Table 2: Knowledge alternative set from researchers R01.

Knowledge ID	T	P	A	R	S
K19	T37	Knowledge accumulation	Context perception technique and applications	R73	Data collection
K46	T63	Form items	Personal knowledge recommendation	R04	Personal recommendation algorithm
K92	T10	Conduct experiments	Digital library knowledge recommendation	R67	Recommendation algorithm
K58	T56	Data analysis	Knowledge recommendation by context perception	T12	Algorithm application instance
K67	T28	Form items	Context perception	R73	Context perception

Table 3: University students' R01 neighboring users.

Researchers	$\mathrm{sim}(m_a, m_i)$
R10	0.5865
R90	0.6334
R35	0.7435
R67	0.9032
R04	0.8543

scientific researchers. Domain experts, as a sample for analyzing the application cases of the TCKM recommendation algorithm, randomly select a researcher in each team to conduct recommendation algorithms analysis such as knowledge push for researcher R01 in research team T01. After obtaining the application context knowledge through context-aware technology, we report the current research context of scientific research staff R01 displayed in Table 1.

In the research, we focus on not only the research subject but also the personnel or teams that research subjects. Thus, we combine those two to infer more detailed outcomes in the framework of knowledge discovery. Table 1 illustrates the subdimensions of two pillars related to knowledge discovery.

According to equations (1) to (3), the similarity between the knowledge application situation and the team research situation of each university student can be calculated. Afterward, the knowledge with higher similarity is leveraged as the candidate set shown inTables 2 and 3. We thus generate a neighbor user set. According to equations (1)–(4), we abandon the list of researchers with high similarity by calculating the similarity between the research context of researcher R01 and the scientific research context of other researchers whose some representative results are presented in Table 3. We generate a recommendation list and further utilize the context-aware technique to obtain the interest level of each neighboring user shown in Table 3 and each knowledge shown in Table 2 in our experiment. We further calculate the final score of the six kinds of knowledge according to (5). The ranking of R01 knowledge recommendation is K92, K46, K58, K67, and K19. Thus, the recommended knowledge takes into account the team research situation of T01 in the domain of knowledge recommendation in digital libraries. Besides, the individual research situation of R01 in the knowledge recommendation algorithms is calculated in digital libraries. Hence, the TKCM recommendation algorithm can accurately discover the knowledge requirements of university students in the context of team research. These details are shown in Table 2.

The presentation strategy is three-dimensional and diverse, which is called the combination of virtuality and reality, strong game interactivity, and strong platform

Table 4: The list of knowledge recommendation.

Knowledge	Item title	Score
K92	Research context-based digital library knowledge recommendation	24.15
K44	Data recommendation algorithm by digital libraries	22.43
K54	Mobile digital library context-sensitive knowledge recommendation	19.43
K67	Perception-based mobile digital library for user data collection	17.55
K19	Service context research by digital library	18.56

scalability. The combination of reality and virtual techniques can satisfy the creative construction of libraries with different characteristics. The combination of auditory, visual, and tactile senses presents a highly realistic and three-dimensional digital library, which is the best medium for reader training and library publicity. Combining the original system of the library with a rationally developed one in a three-dimensional space, the library service will be more personalized and humanized. The creative display of library digital resources can improve the utilization rate of library resources. As the navigation document claims, the navigation function of the system can click on the retrieved books to navigate the databases university students are interested in. The system will automatically calculate the best path and present it to the user in the form of screenshots and 3D navigation. Thus, they will lead different users to reach different locations where the book could be retrieved. For the interaction between personal centers, users can create their nicknames and personal profile in the personal center. Students then use their virtual identities to participate in virtual community activities, such as interacting and chatting with other readers, broadcasting, and occupying a reading room, fire drills, and escapes.

Noticeably, we also observed interactions of university students that chat with friends, make friends, and find and meet new friends. Also, they conduct interactive online communication to increase the fun. They conduct interactive and virtual consultations, which means that creating a consultation desk on a virtual floor and setting up virtual characters are realized. Hence, readers can click on the consultant desk to ask questions about the digital library. Moreover, the virtual consultant can also propose common consulting questions that are responded to by the digital library instructor online. The functional structure design is shown in Table 2. For the virtual exhibition, the movie screening hall is a virtual screening room for the library. University students thus can choose their films to watch, and the library can also upload videos of student activities to display. The digital library can also build a virtual online lecture hall to display video lectures by experts worldwide. Virtual exhibition hall especially contains a rich collection of ancient books. These ancient books collected by the library can be displayed in a three-dimensional virtual manner and are open to university students for reference, as shown in Table 4.

5. Conclusions

In this work, we utilize the context-aware learning model to construct the knowledge application situation and team research situation for the digital library. We further propose the knowledge recommendation method TKCM for the digital library by leveraging the situation of team scientific research-knowledge application. The proposed method called the TKCM can provide information for the related research of knowledge service in the application of the digital library according to the research situation and new ideas.

The main contributions of this work include the following components: (1) realizing the active recommendation of knowledge according to the application situation of digital library knowledge (this can improve the quality of knowledge service in the digital library; we also emphasize that the knowledge service of the digital library should be oriented to the situation of team scientific research); (2) integrating team situation and individual situation of scientific researchers to meet the knowledge requirements of team research and individual research.

Despite the articulated advantages, the disadvantage of the proposed method is that it mainly studies the application context of digital library knowledge and lacks a careful analysis of the content of knowledge and the context information. Thus, how to comprehensively utilize all the context information of digital library knowledge remains an unresolved challenge. To complete a more accurate digital library recommendation system, further studies related to a detailed analysis of the content of knowledge and the context information are needed to obtain more refined outcomes in future research.

Data Availability

The data used to support the findings of this study are available from the corresponding author upon request.

Conflicts of Interest

The author declares that there are no conflicts of interest.

References

[1] X. Zhang, X. Zhao, and X. Liu, "Research on knowledge resource recommendation of university mobile library based on context-awareness," *Information Science*, vol. 38, no. 1, pp. 48–52, 2020.

[2] Y. Sun, R. Qiu, and C. Huang, "Analysis of the theme evolution of personalized service research in domestic digital libraries," *Information Theory and Practice*, vol. 37, no. 8, pp. 41–47, 2014.

[3] G. Li, C. Li, and Li Xiang, "Research on the discovery of scientific research teams based on social network analysis," *Library and Information Work*, no. 7, pp. 63–70, 2014.

Hindawi
Journal of Mathematics
Volume 2023, Article ID 9785391, 1 page
https://doi.org/10.1155/2023/9785391

Retraction

Retracted: Linguistic Analysis of Hindi-English Mixed Tweets for Depression Detection

Journal of Mathematics

Received 10 October 2023; Accepted 10 October 2023; Published 11 October 2023

This article has been retracted by Hindawi following an investigation undertaken by the publisher [1]. This investigation has uncovered evidence of one or more of the following indicators of systematic manipulation of the publication process:

(1) Discrepancies in scope

(2) Discrepancies in the description of the research reported

(3) Discrepancies between the availability of data and the research described

(4) Inappropriate citations

(5) Incoherent, meaningless and/or irrelevant content included in the article

(6) Peer-review manipulation

The presence of these indicators undermines our confidence in the integrity of the article's content and we cannot, therefore, vouch for its reliability. Please note that this notice is intended solely to alert readers that the content of this article is unreliable. We have not investigated whether authors were aware of or involved in the systematic manipulation of the publication process.

Wiley and Hindawi regrets that the usual quality checks did not identify these issues before publication and have since put additional measures in place to safeguard research integrity.

We wish to credit our own Research Integrity and Research Publishing teams and anonymous and named external researchers and research integrity experts for contributing to this investigation.

The corresponding author, as the representative of all authors, has been given the opportunity to register their agreement or disagreement to this retraction. We have kept a record of any response received.

References

[1] C. M. B. M. J, R. S, M. Arif, D. K. V, A. K. K, and A. G, "Linguistic Analysis of Hindi-English Mixed Tweets for Depression Detection," *Journal of Mathematics*, vol. 2022, Article ID 3225920, 7 pages, 2022.

Hindawi
Journal of Mathematics
Volume 2022, Article ID 3225920, 7 pages
https://doi.org/10.1155/2022/3225920

Research Article

Linguistic Analysis of Hindi-English Mixed Tweets for Depression Detection

Carmel Mary Belinda M J,[1] **Ravikumar S**,[1] **Muhammad Arif**,[2] **Dhilip Kumar V**,[1] **Antony Kumar K**,[1] **and Arulkumaran G**[3]

[1]*Department of Computer Science & Engineering, Vel Tech Rangarajan Dr Sagunthala R and D Institute of Science and Technology, Chennai, India*
[2]*Department of Computer Science and Information Technology, University of Lahore, Lahore, Pakistan*
[3]*Department of Electrical and Computer Engineering, Bule Hora University, Bule Hora, Ethiopia*

Correspondence should be addressed to Arulkumaran G; erarulkumaran@gmail.com

Received 31 January 2022; Revised 15 February 2022; Accepted 21 February 2022; Published 12 April 2022

Academic Editor: Naeem Jan

According to recent studies, young adults in India faced mental health issues due to closures of universities and loss of income, low self-esteem, distress, and reported symptoms of anxiety and/or depressive disorder (43%). This makes it a high time to come up with a solution. A new classifier proposed to find those individuals who might be having depression based on their tweets from the social media platform Twitter. The proposed model is based on linguistic analysis and text classification by calculating probability using the TF ∗ IDF (term frequency-inverse document frequency). Indians tend to tweet predominantly using English, Hindi, or a mix of these two languages (colloquially known as Hinglish). In this proposed approach, data has been collected from Twitter and screened via passing them through a classifier built using the multinomial Naive Bayes algorithm and grid search, the latter being used for hyperparameter optimization. Each tweet is classified as depressed or not depressed. The entire architecture works over English and Hindi languages, which shall help in implementation globally and across multiple platforms and help in putting a stop to the ever-increasing depression rates in a methodical and automated manner. In the proposed model pipeline, composed techniques are used to get the better results, as 96.15% accuracy and 0.914 as the F1 score have been attained.

1. Introduction

Recent studies by the World Health Organization (WHO) [1] have revealed that 56 million Indians suffer from depression and another 38 million Indians suffer from anxiety disorders, and only a fraction of them receive adequate treatment. Even though this disorder is highly treatable, only a fraction of those suffering receive treatment, due to the societal stigma associated with mental health. Diagnosis and subsequent treatment for depression are often delayed, imprecise, and/or missed entirely. The social media activity of individuals presents a revolutionary approach to transforming early depression intervention services, especially for young adults [2, 3]. Many depressed individuals seldom choose not to discuss their mental health with their family and friends because the taboo surrounding depression is still high, especially in India. Such individuals, when they tweet, consciously and subconsciously use words that indicate their mental health. The advent of social media platforms has made it relatively easier to find these individuals [4, 5]. Since it is nearly impossible to check the hints from the posts of each user across all platforms for a human being or even a team of them, automating the entire process becomes the need of the hour. One such approach accepted globally is sentiment analysis [6, 7]. It is a cross platform ML approach that can be implemented to filter out a particular user based on the pattern of their social media posts.

2. Related Works

The ability of algorithms to evaluate text has substantially improved as a result of recent advances in the field of deep learning [8, 9]. Sentiment analysis and opinion mining algorithms for social multimedia [10, 11] summarizes existing research on multimodal sentiment analysis, which incorporates numerous media outlets. Data mining to detect depressed people on social networking platforms in the field of psychology [12, 13]. To begin, a sentiment analysis method is proposed that uses vocabulary and man-made rules to calculate the depression inclination of each post or microblog. A hybrid model for identifying depressed individuals via CNN and LSTM models is based on normal conversation-based text data obtained from Twitter [14]. However, the vast majority of these studies were conducted with an audience that spoke only English. There has not been much work done on the subject of sentiment analysis for an audience that predominantly uses Indian languages in microblogging websites. Instead of learning character or word-level representation, a model was proposed that includes learning subword-level representation in the LSTM architecture [7]. In excessively noisy text with misspellings, the model performs well. Twitter-based annotated corpus of mixed social media material in Hindi, English, and Hinglish for coding [6,15]. To create a more diverse canvas, the study used words with ambiguous meanings and irregular spellings in both languages [16,17].

3. Proposed System

The proposed system uses a classifier model to classify tweets as "depressed" or "not depressed". The model utilizes a pipeline composed of the TF ∗ IDF and multinomial Naive Bayes (MNB) algorithms, with MNB serving as the classifier. The implementation of the Bayes algorithm takes minimal effort, thus keeping the development phase short and elongating the testing phase to perfect it [18]. The proposed model is based on linguistic analysis and text classification by calculating probability using the TF ∗ IDF weight instead of word count, as the TF ∗ IDF weight reflects how important the word is to the document; this is an improvement over probability calculated using word count. Grid search is included to perform hyperparameter optimization to determine the optimal values for the model. The performance of a model significantly depends on the hyperparameters used by the estimators; selecting optimal parameters manually can take a considerable amount of time and resources [19]. Thus, grid search has been used to automate this entire process.

As for the working of the model, a tweet from the Twitter API serves as the input for the model. This tweet can be written in English, Hindi, or a mix of these two languages (Hinglish). The model classifies the tweet into one of the two target class labels, depressed (denoted by 0 in the dataset) and not depressed (denoted by 1 in the dataset) based on the words present in the tweet (for instance, depressed tweets most commonly include the keywords "depressed," "anxiety," "sad," etc.), and the class of the tweet is displayed on the screen. Figure 1 represents the architecture of the proposed model.

4. Technique Used

4.1. Data Collection. The tweets in the dataset were obtained using the Python module Tweepy via the Twitter API. Hashtags (#) like #depressed, #anxiety, and #sad were used to filter out depressed tweets, whereas #happy and #life were used to filter out tweets that were not depressed. These tweets were then turned into a 670-data-point raw dataset with three columns: TID (unique Twitter ID), TWEET, and LABEL. Figure 2 represents the output derived. The tweets were then compiled into a CSV file, shown in Table 1.

4.2. Data Preprocessing. The raw dataset was preprocessed to bring all the textual data into a form that is predictable and analyzable for the model. Figure 1 depicts the flow of processes in data preprocessing. The Python modules stopwords, RegexpTokenizer, WordNetLemmatizer, and PorterStemmer from NLTK were used along with String. We also included Hindi stopwords [20] separately as NLTK does not have this provision.

4.3. Undersampling. Initially, the dataset contained 670 data points, out of which 409 were associated with label 1, and 260 were associated with label 0. This created a bias, which if not rectified, would skew the results of the model. So, we proceeded with undersampling the data associated with label 1, after which there was an equal distribution of data for both target class labels, consisting of 520 data points in the dataset.

*4.4. TF*IDF.* The TF*IDF algorithm was applied to generate a score that implied how relevant a word was to the proposed model. The Python libraries CountVectorizer and Tfidftransformer are used for this purpose. The mathematical formula for the TF ∗ IDF algorithm is given as follows:

$$w_{i,j} = tf_{i,j} X \ \log\left(\frac{N}{df_i}\right), \tag{1}$$

where $tf_{i,j}$ = number of occurrences of i in j, df_i = number of documents containing i, and N = number of documents.

4.5. Multinomial Naive Bayes. The MNB algorithm is used as the primary classifier because it is more accurate than the Naive Bayes (NB) algorithm [5]. While NB considers the independent probability of each feature, MNB considers a feature vector where each term represents the TF ∗ IDF weight of each word, i e., not only considering the frequency of the word but also how important that word is in the entire document. This allows us to make classifications using only the most important words in each line of text. MNB can be represented mathematically by

$$C_{NB} = \text{argmax}_{k\varepsilon K}\left(\log\ P(C_k) + \sum_{i=1}^{n} x_i \cdot \ \log\ Pk_i\right), \tag{2}$$

where p_{ki} = probability of $i-th$ event occurring in class k, x_i = frequency of $i-th$ event.

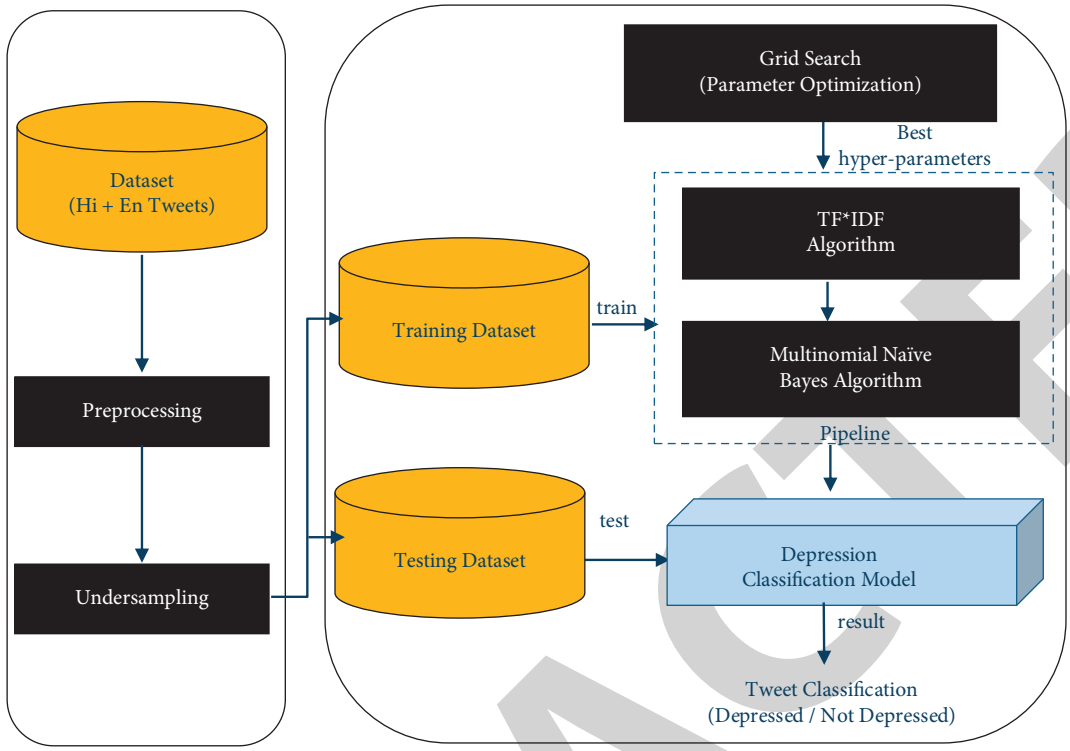

Figure 1: The model architecture of the depression classification system as a hybrid of MNB and grid search.

4.6. Grid Search. Selecting the best hyperparameters for tuning the model can be exhaustive and time-consuming if performed manually. To automate this process, grid search has been used [21]. These are the best hyperparameters that were determined for the proposed model.

An important feature to note is that the value of $\alpha = 1$ for the MNB algorithm, indicating that Laplace smoothing has been used for smoothing categorical data. A small-sample correction, or pseudocount, is incorporated into every probability estimate. Consequently, no probability will be zero. This is a fairly efficient method to regularize the MNB algorithm.

5. Implementation

The model is an application of supervised machine learning, and the requirement of a user is to deploy and collect the result. Deploying this application needs basic interaction where it asks for the keys and tokens to access the database (as for Twitter, it needs access_token, secret access token, consumer key, and consumer secret key, respectively). The application later requires minimal to no intervention from the user until the output is provided by the application. The application collects a collection of tweets from the database (Twitter), which is fed into the core of the application. The core contains a trained model to classify the tweets into one of two classifications: depressed or not depressed. The model is trained in one of the best methods, using grid search. Grid search as already mentioned in the previous section, chooses the best combination of parameters and derives an output. The parameters have chosen for the model are a pipeline of TFIDF, countvectorizer, and multinomial Naive Bayes. The model is capable of prioritizing accuracy in different types of data provided to it. The model can successfully read Hindi tweets as well and classify them using its knowledge of the different Hinglish terms that are commonly used over social media. After classification, the application can provide an accurate result of up to 96.15% (data based on training dataset) and can provide a visual representation of the different key lexicons it has encountered throughout the dataframe.

One of the best features of the implementation is its modularized approach, where each of the jobs is assigned to different modules and each of the major module clusters is capable of working individually without interference from other module clusters. This improves the implementation, upgradability, and readability of code. A vivid test report for different types of tweets is provided by Table 2.

6. Experimental Setup

The 670 data point raw dataset taken from Twitter has a collection of real tweets that include the Hindi and English language. The dataset has been split into 2 groups: the train set, which is to be input as training samples, and the development set, which is to verify the accuracy of the checkpoint of the grid search; for each of the datasets, the train set represents around 90% of the whole data amount, and the development set is around 10%. For the testing, we train the grid search model several times and choose the one with the highest average development accuracy, as shown in Table 3.

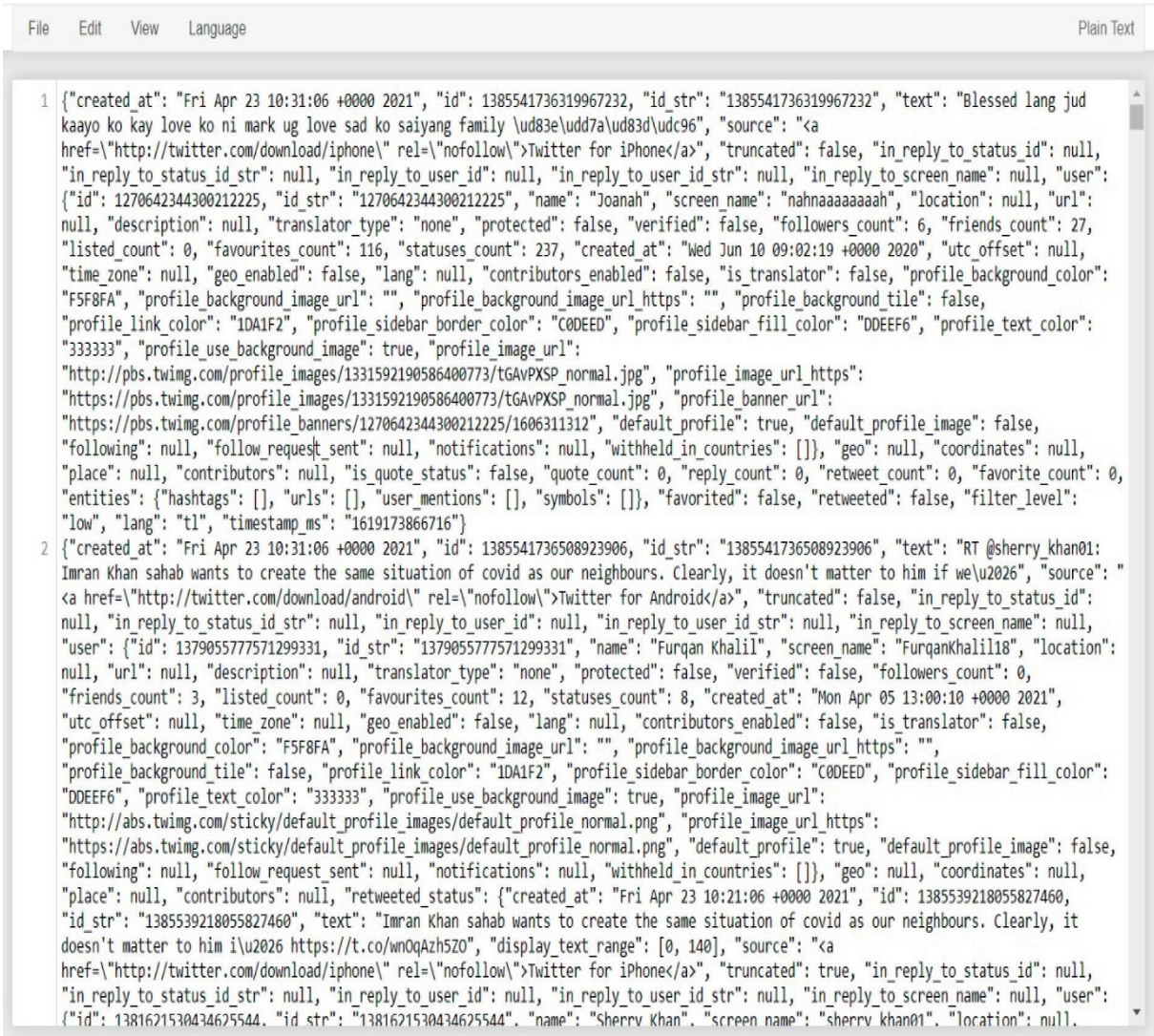
File Edit View Language Plain Text
1 {"created_at": "Fri Apr 23 10:31:06 +0000 2021", "id": 1385541736319967232, "id_str": "1385541736319967232", "text": "Blessed lang jud kaayo ko kay love ko ni mark ug love sad ko saiyang family \ud83e\udd7a\ud83d\udc96", "source": "Twitter for iPhone", "truncated": false, "in_reply_to_status_id": null, "in_reply_to_status_id_str": null, "in_reply_to_user_id": null, "in_reply_to_user_id_str": null, "in_reply_to_screen_name": null, "user": {"id": 1270642344300212225, "id_str": "1270642344300212225", "name": "Joanah", "screen_name": "nahnaaaaaaaah", "location": null, "url": null, "description": null, "translator_type": "none", "protected": false, "verified": false, "followers_count": 6, "friends_count": 27, "listed_count": 0, "favourites_count": 116, "statuses_count": 237, "created_at": "Wed Jun 10 09:02:19 +0000 2020", "utc_offset": null, "time_zone": null, "geo_enabled": false, "lang": null, "contributors_enabled": false, "is_translator": false, "profile_background_color": "F5F8FA", "profile_background_image_url": "", "profile_background_image_url_https": "", "profile_background_tile": false, "profile_link_color": "1DA1F2", "profile_sidebar_border_color": "C0DEED", "profile_sidebar_fill_color": "DDEEF6", "profile_text_color": "333333", "profile_use_background_image": true, "profile_image_url": "http://pbs.twimg.com/profile_images/1331592190586400773/tGAvPXSP_normal.jpg", "profile_image_url_https": "https://pbs.twimg.com/profile_images/1331592190586400773/tGAvPXSP_normal.jpg", "profile_banner_url": "https://pbs.twimg.com/profile_banners/1270642344300212225/1606311312", "default_profile": true, "default_profile_image": false, "following": null, "follow_request_sent": null, "notifications": null, "withheld_in_countries": []}, "geo": null, "coordinates": null, "place": null, "contributors": null, "is_quote_status": false, "quote_count": 0, "reply_count": 0, "retweet_count": 0, "favorite_count": 0, "entities": {"hashtags": [], "urls": [], "user_mentions": [], "symbols": []}, "favorited": false, "retweeted": false, "filter_level": "low", "lang": "tl", "timestamp_ms": "1619173866716"}
2 {"created_at": "Fri Apr 23 10:31:06 +0000 2021", "id": 1385541736508923906, "id_str": "1385541736508923906", "text": "RT @sherry_khan01: Imran Khan sahab wants to create the same situation of covid as our neighbours. Clearly, it doesn't matter to him if we\u2026", "source": "Twitter for Android", "truncated": false, "in_reply_to_status_id": null, "in_reply_to_status_id_str": null, "in_reply_to_user_id": null, "in_reply_to_user_id_str": null, "in_reply_to_screen_name": null, "user": {"id": 1379055777571299331, "id_str": "1379055777571299331", "name": "Furqan Khalil", "screen_name": "FurqanKhalil18", "location": null, "url": null, "description": null, "translator_type": "none", "protected": false, "verified": false, "followers_count": 0, "friends_count": 3, "listed_count": 0, "favourites_count": 12, "statuses_count": 8, "created_at": "Mon Apr 05 13:00:10 +0000 2021", "utc_offset": null, "time_zone": null, "geo_enabled": false, "lang": null, "contributors_enabled": false, "is_translator": false, "profile_background_color": "F5F8FA", "profile_background_image_url": "", "profile_background_image_url_https": "", "profile_background_tile": false, "profile_link_color": "1DA1F2", "profile_sidebar_border_color": "C0DEED", "profile_sidebar_fill_color": "DDEEF6", "profile_text_color": "333333", "profile_use_background_image": true, "profile_image_url": "http://abs.twimg.com/sticky/default_profile_images/default_profile_normal.png", "profile_image_url_https": "https://abs.twimg.com/sticky/default_profile_images/default_profile_normal.png", "default_profile": true, "default_profile_image": false, "following": null, "follow_request_sent": null, "notifications": null, "withheld_in_countries": []}, "geo": null, "coordinates": null, "place": null, "contributors": null, "retweeted_status": {"created_at": "Fri Apr 23 10:21:06 +0000 2021", "id": 1385539218055827460, "id_str": "1385539218055827460", "text": "Imran Khan sahab wants to create the same situation of covid as our neighbours. Clearly, it doesn't matter to him i\u2026 https://t.co/wnOqAzh5ZO", "display_text_range": [0, 140], "source": "Twitter for iPhone", "truncated": true, "in_reply_to_status_id": null, "in_reply_to_status_id_str": null, "in_reply_to_user_id": null, "in_reply_to_user_id_str": null, "in_reply_to_screen_name": null, "user": {"id": 1381621530434625544, "id_str": "1381621530434625544", "name": "Sherry Khan", "screen_name": "sherry_khan01", "location": null,

Figure 2: Snapshot of the output of the Tweepy code.

Table 1: Generated classification report of the model.

	Precision	Recall	F1-score	Support
0	0.9815	0.9464	0.9636	56
1	0.9400	0.9792	0.9592	48
Accuracy			0.9615	104
Macro avg	0.9607	0.9628	0.9614	104
Weighted avg	0.9623	0.9615	0.9616	104

7. Results and Discussions

The model, which is a hybrid of MNB, TF ∗ IDF, and grid search, is able to classify tweets as depressed or not depressed with an accuracy of 96.15%. The full classification report of the proposed model is shown in Table 1. The model is trained on the full development set and the scores are computed on the full evaluation set.

When applying MNB, TF ∗ IDF, and grid search to the dataset, TF ∗ IDF got the best results. We trained, tested, and validated the dataset with a batch size of 500, the number of epochs = 20, the drop out size of any network = 0.4, vocabulary size that we applied our models to it was 5000, with 32 hidden layers for every DL model, and finally the embedding size was equaled to 60. The evaluation splitting parameter was tested on 90%, 80%, and 70% for training with dividing equally the remaining for testing and validation.

After training, the model applies the evaluation measures to check how the model is performing. Accordingly, the following evaluation parameters are used to check the performance of the models, respectively:

(i) Accuracy score

Table 2: Test cases for testing the model.

Test case ID	Test condition	Tweets	Expected result	Actual result	Status
01	Test MNB (TF * IDF) with grid search (for English not depressed tweet)	Hello hk im soooo happi luv soooo much	Not depressed	Not depressed	Pass
02	Test MNB (TF * IDF) with grid search (for Hindi depressed tweet)	@Rishabverma740 Tere dukh tere he rahenge Phir tu isko suna Ya usko suna Kya farak padta hai #Depressed	Depressed	Depressed	Pass
03	Test MNB (TF * IDF) with grid search (for Hindi not depressed tweet)	Udaas rehne ki wajah to bohot hai life me..!! Par fookat me khush rehne ka maza hi kuch aur hai.!! #happy #sad #life	Not depressed	Depressed	Fail
04	Test MNB (TF*IDF) with grid search(for English not depressed tweet	Depress start counsel next monthal want happi	Not depressed	Depressed	Pass
05	Test MNB (TF * IDF) with grid search (for English depressed tweet)	I Feel lost inside myself! #illness #lifelessons #useless #depressed #Ignored #worthless #pathetic.	Depressed	Depressed	Pass
06	Test MNB, (TF * IDF) with grid search (for Hinglish not depressed tweet)	@sidnaaz_ka Happy birthday preeti di Lots of love and prayers! □□☺☺☺ Hamesha khush rehna app! ☺	Not depressed	Not depressed	Pass

Table 3: Model metrics.

Metric	Value derived for proposed model
MAE (mean absolute error)	0.038461538461538464
R2 score	0.85
Log loss	1.3284375420378214
IoU (Jaccard score)	0.9215686274509803
MSE (mean squared error)	0.038461538461538464
RMSE (root mean squared error)	0.19611613513818404
MSLE (mean squared log error)	0.018478962073776976
NAE (normalized absolute error	0.20450490315512837

Table 4: Comparison between existing models and proposed model.

Method	Reported in	Accuracy (%)	F1-score
Char-LSTM	Joshi, A. et al. (2016)	59.8	0.511
Subword-LSTM	Joshi, A. et al. (2016)	69.7	0.658
CNN-BiLSTM	Garg, N., and Sharma, K. (2020)	83.21	0.556
MNB (TF*IDF)-grid search	Proposed	96.15	0.914

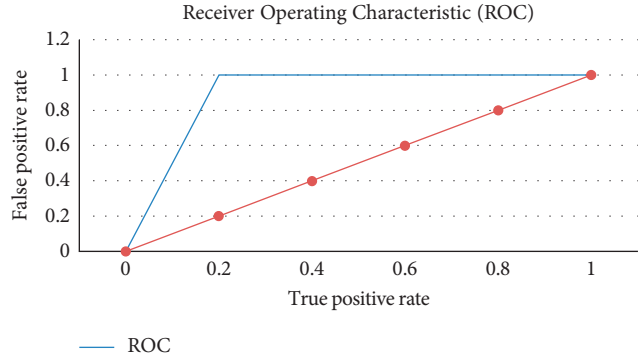

Figure 3: ROC curve.

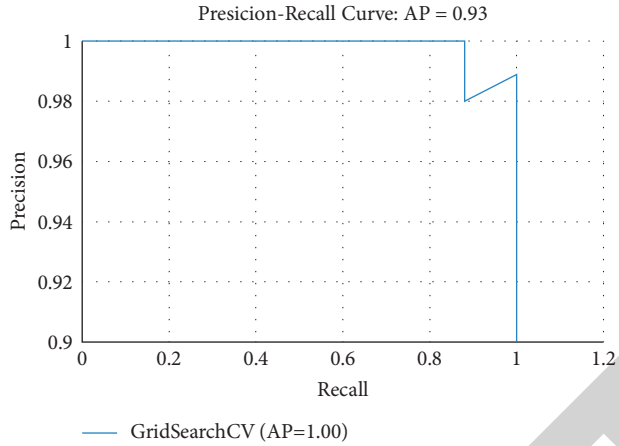

Figure 4: Precision-recall curve.

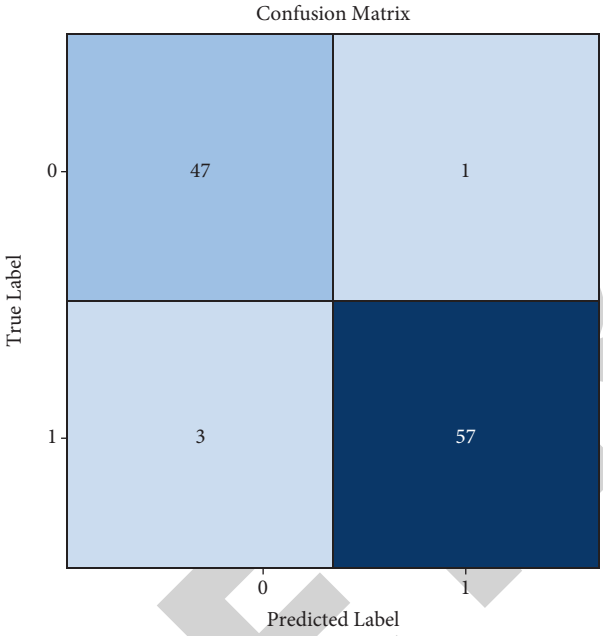

Figure 5: Confusion matrix.

(ii) Confusion matrix with plot

(iii) ROC-AUC Curve

Accuracy: as far as the accuracy of the model is concerned, MNB (TF ∗ IDF)-Grid search performs better than Char-LSTM, Subword-LSTM, and CNN-BiLSTM.

F1-score: MNB(TF ∗ IDF)-Grid search (F1-score = 0.914) < , Subword-LSTM (F1-score = 0.658) < CNN-BiLSTM. (F1-score = 0.556) < Char-LSTM (F1-score = 0.92).

The model has been evaluated against several metrics to compare the model's predictions with the (known) values of the dependent variable in a dataset. Table 1 describes the model metrics derived for the classification model.

A study has been conducted to compare the proposed model metrics, specifically the accuracy and F1-score, with preexisting works, and the results of this study is shown in Table 4.

Figure 3 and Figure 4 represent the ROC curve and precision-recall curve obtained for the proposed model, respectively, and Figure 5 represents the confusion matrix of the model.

8. Conclusion and Future Enhancement

The proposed model helps to identify those depressed individuals from the large data pool and easily identify them using a quick-fix solution that is done with minimal changes and hardly any human intervention. Another distinguishing factor of the proposed model is that it is able to classify tweets written in English, Hindi, and Hinglish languages. The entire architecture works over English and Hindi languages, which shall help in implementation globally, especially in India and across multiple platforms. This will help put a stop to the ever-increasing depression rates in an automated manner.

This work can be readily upgraded into an interactive bot. The bot adapts himself to the depressed person and makes him/her able to express themselves. This would help people to spend time working on their mental health and have a regular conversation with the bot. This can be extended to include several other Indian languages.

Data Availability

The data used to support the findings of this study are available from the corresponding author upon request.

Conflicts of Interest

The authors declare that they have no conflicts of interest.

References

[1] World Health Organization, "WHO Director-General's opening remarks at the media briefing on COVID," Geneva, Switzerland, March 2020, https://www.who.int/dg/speeches/detail/who-director-general-s-opening-remarks-at-the-media-briefing-on-covid-19-11-march-2020.

Hindawi
Journal of Mathematics
Volume 2022, Article ID 1813717, 6 pages
https://doi.org/10.1155/2022/1813717

Research Article

Complex-Valued Migrativity of Complex Fuzzy Operations

Yingying Xu, Haifeng Song, Lei Du, and Songsong Dai

School of Electronics and Information Engineering, Taizhou University, Taizhou 318000, Zhejiang, China

Correspondence should be addressed to Songsong Dai; ssdai@stu.xmu.edu.cn

Received 17 February 2022; Revised 8 March 2022; Accepted 10 March 2022; Published 6 April 2022

Academic Editor: Lazim Abdullah

Complex fuzzy sets (CFSs), as an important extension of fuzzy sets, have been investigated in the literature. Operators of CFSs are of high importance. In addition, α–migrativity for various fuzzy operations on [0, 1] has been well discussed, where α is a real number and $\alpha \in [0, 1]$. Thus, this paper studies α–migrativity for binary functions on the unit circle of the complex plane $\mathbf{O}$, where α is a complex number and $\alpha \in \mathbf{O}$. In particular, we show that a binary function is α–migrativity for all $\alpha \in \mathbf{O}$ if and only if it is α–migrativity for all $\alpha \in [0, 1] \cup \overline{\mathbf{O}}$, where $\overline{\mathbf{O}}$ is the boundary point subset of $\mathbf{O}$. Finally, we discuss the relationship between migrativity and rotational invariance of binary operators on $\mathbf{O}$.

1. Introduction

Complex fuzzy sets (CFSs) were introduced by Ramot et al. [1, 2], whose membership degree is a complex number on the unit disc of the complex plane $\mathbf{O}$, where $\mathbf{O} = \{\alpha \in \mathbb{C} \mid |\alpha| \leq 1\}$. Operations are of high importance in the theory of CFSs. Various concepts and properties have been developed for complex fuzzy operations. Dick [3] introduced the rotational invariance of operators of CFSs. Dai [4, 5] generalized Dick's works on rotational invariance and order induced by algebraic product operation. Zhang et al. [6] studied operation properties and δ-equalities of CFSs. Dick, Yager, and Yazdanbahksh [7] gave some complex fuzzy operations based on Pythagorean fuzzy operations, which was developed by Liu et al. [8]. Then Dick [9] considered complex fuzzy S-implications. Hu et al. [10–13] discussed orthogonality preserving operators and parallelity preserving operators of CFSs.

The α-migrativity [14] as an important property of binary fuzzy operators has been discussed in the cases of overlap/grouping functions [15, 16], uninorms [17–22], triangular subnorm [23], t-norms [24], nullnorm [25], copulas [26, 27], and aggregation functions [28–30]. In the aforementioned migrative functions, their research domain is limited to real numbers on [0, 1]. For example, a binary function $f: \mathbf{I}^2 \longrightarrow \mathbf{I}$ is migrative if $f(\alpha x, y) = f(\mu, \alpha v)$ holds for all $\mu, v \in \mathbf{I}$ and $\alpha \in \mathbf{I}$, where $\mathbf{I} = [0, 1]$.

This paper focuses on the α-migrativity of complex fuzzy binary operations, i.e., functions $f: \mathbf{O}^2 \longrightarrow \mathbf{O}$, where $\alpha \in \mathbf{O}$ is a complex number. Moreover, since a CFS is composed of a magnitude term and a phase term, we consider magnitude-migrativity and phase-migrativity, which respectively limits $\alpha \in \mathbf{I}$ and $\alpha \in \overline{\mathbf{O}}$, where $\overline{\mathbf{O}}$ is the boundary point subset of $\mathbf{O}$, i.e., $\overline{\mathbf{O}} = \{\alpha \in \mathbb{C} \mid |\alpha| = 1\}$.

As far as we know, migrativity including magnitude-migrativity and phase-migrativity of complex fuzzy operations have not been studied yet. Moreover, we note that phase-migrativity and rotational invariance [3, 4] of complex fuzzy operations are similar with respect to angle rotation operations. It is essential to straighten out the relationship between phase-migrativity and rotational invariance for complex fuzzy operations.

This article is structured as follows: in Section 2, we introduce the concepts of migrativity, magnitude-migrativity, and phase-migrativity for complex fuzzy binary operations. In Section 3, we give characterizations of these migrativity properties of complex fuzzy binary operations. In Section 4, the relationship between rotational invariance and migrativity is studied. In Section 5, concluding remarks are given.

2. Migrativity

Definition 1. Consider a fixed point $\alpha \in \mathbf{O}$, a binary operation $f\colon \mathbf{O}^2 \longrightarrow \mathbf{O}$ is said to be α–migrative if

$$f(\alpha\mu, \nu) = f(\mu, \alpha\nu), \quad \text{for all } \mu, \nu \in \mathbf{O}. \tag{1}$$

Note that α– migrativity refers to a fixed complex number α. This can be generalized as follows:

Definition 2. A binary operation $f\colon \mathbf{O}^2 \longrightarrow \mathbf{O}$ is said to be migrative if and only if (briefly, iff)

$$f(\alpha\mu, \nu) = f(\mu, \alpha\nu), \quad \text{for all } \mu, \nu \in \mathbf{O} \text{ and } \alpha \in \mathbf{O}. \tag{2}$$

A complex vector includes the amplitude term and the phase part. So, we introduce the following concepts:

Definition 3. A binary operation $f\colon \mathbf{O}^2 \longrightarrow \mathbf{O}$ is said to be amplitude-migrative iff

$$f(r\mu, \nu) = f(\mu, r\nu), \quad \text{for all } \mu, \nu \in \mathbf{O} \text{ and } r \in \mathbf{I}. \tag{3}$$

Definition 4. A binary operation $f\colon \mathbf{O}^2 \longrightarrow \mathbf{O}$ is said to be phase-migrative if and only if

$$f\left(e^{j\theta}\mu, \nu\right) = f\left(\mu, e^{j\theta}\nu\right), \quad \text{for all } \mu, \nu \in \mathbf{O} \text{ and } \theta \in \mathbb{R}, \tag{4}$$

where $j = \sqrt{-1}$.

Note that phase-migrativity means α-migrativity for all $\alpha \in \overline{\mathbf{O}}$.

Theorem 1. *A binary operation $f\colon \mathbf{O}^2 \longrightarrow \mathbf{O}$ is migrative iff, for all $r \in \mathbf{I}$ and $\theta \in \mathbb{R}$, it holds that*

$$\left.\begin{aligned} f\left(e^{j\theta}\mu, \nu\right) &= f\left(\mu, e^{j\theta}\nu\right) \\ f(r\mu, \nu) &= f(\mu, r\nu) \end{aligned}\right\}. \tag{5}$$

Proof. ($\Rightarrow$) Trivial.

($\Leftarrow$) For any $\alpha \in \mathbf{O}$, denote $\alpha = r_\alpha \cdot e^{j\theta_\alpha}$ where $r_\alpha \in \mathbf{I}$. Then $f(\alpha\mu, \nu) = f(r_\alpha \cdot e^{j\theta_\alpha}\mu, \nu) = f\ (e^{j\theta_\alpha}\mu, r_\alpha \cdot \nu) = f\ (\mu, e^{j\theta_\alpha} \cdot r_\alpha\nu) = f(\mu, \alpha\nu)$. □

For a complex fuzzy binary function f, as shown in Figure 1(a) and 1(b), if it is phase-migrative, then we have $\beta_1 = \beta_2$ for any θ and inputs $\mu, \nu \in \mathbf{O}$.

A binary operation is migrative if and only if it is amplitude-migrative and phase-migrative. From this result, we have the following result: □

Corollary 1. *Let $f\colon \mathbf{O}^2 \longrightarrow \mathbf{O}$ be a binary operation. Then the following statements are equivalent.*

(1) $f(\alpha\mu, \nu) = f(\mu, \alpha\nu)$, for all $\mu, \nu \in \mathbf{O}$ and $\alpha \in \mathbf{O}$;

(2) $f(\alpha\mu, \nu) = f(\mu, \alpha\nu)$, for all $\mu, \nu \in \mathbf{O}$ and $\alpha \in \mathbf{I} \cup \overline{\mathbf{O}}$.

Note that f is α–migrative for all $\alpha \in \mathbf{O}$ if and only if it is α–migrative for all $\alpha \in \mathbf{I} \cup \overline{\mathbf{O}}$. This is very interesting because $\mathbf{I} \cup \overline{\mathbf{O}}$ is a proper subset of $\mathbf{O}$, i.e., $(\mathbf{I} \cup \overline{\mathbf{O}}) \subsetneq \mathbf{O}$, and the size of $\mathbf{I} \cup \overline{\mathbf{O}}$ is much smaller than that of $\mathbf{O}$. Obviously, in the above corollary, $\mathbf{I} \cup \overline{\mathbf{O}}$ could be replaced by other subsets, such as $[-1, 0] \cup \overline{\mathbf{O}}$.

Example 1. The operations $f_1, f_2, f_3\colon \mathbf{O}^2 \longrightarrow \mathbf{O}$ are respectively defined by

$$\begin{aligned} f_1(\mu, \nu) &= \mu \cdot \nu, \\ f_2(\mu, \nu) &= |\mu| \cdot \nu, \\ f_3(\mu, \nu) &= |\mu| \cdot \mu \cdot \nu. \end{aligned} \tag{6}$$

Obviously, f_1 is migrative. Interestingly, for all $r \in \mathbf{I}$, we have $f_2(r\mu, \nu) = f_2(\mu, r\nu)$. Thus f_2 is amplitude-migrative. Similarly, for all $\theta \in \mathbb{R}$, we have $f_3(e^{j\theta}\mu, \nu) = f_3(\mu, e^{j\theta}\nu)$. Thus, f_3 is phase-migrative. But f_2 is not phase-migrative, f_3 is not amplitude-migrative, thus, they are not migrative.

3. Characterization of Migrativity

One of the important results of migrative real-valued functions is the following theorem:

Theorem 2 (see [28]). *A binary operation $f\colon \mathbf{I}^2 \longrightarrow \mathbf{I}$ is migrative iff there exists a function $g\colon \mathbf{I} \longrightarrow \mathbf{I}$ such that $f(\mu, \nu) = g(xy)$ for all $\mu, \nu \in \mathbf{I}$.*

This result is not true for amplitude-migrative (or phase-migrative) functions (see Example 1), but it is true for migrative complex-valued functions.

Theorem 3. *A binary operation $f\colon \mathbf{O}^2 \longrightarrow \mathbf{O}$ is migrative iff there exists a function $f\colon \mathbf{O} \longrightarrow \mathbf{O}$ such that $f(\mu, \nu) = g(xy)$ for all $\mu, \nu \in \mathbf{O}$.*

Proof. ($\Leftarrow$) If g exists, then $f(\alpha\mu, \nu) = g(\alpha\mu\nu) = f(\mu, \alpha\nu)$.

($\Rightarrow$) If f is migrative, then $f(\mu, \nu) = f(\mu \cdot 1, \nu) = f(1, \mu\nu)$, thus, $g(\mu\nu) = f(1, \mu\nu)$ is the function.

In this way, the function g is the migrative generator of the migrative binary operation f.

The following result is immediate: □

Theorem 4. *Let $f\colon \mathbf{O}^2 \longrightarrow \mathbf{O}$ be a migrative binary operation. Then*

(1) $f(1, 1) = 1$ if and only of $g(1) = 1$;

(2) $f(0, 0) = 0$ if and only of $g(0) = 0$;

Example 2. We give some migrative functions and their migrative generators.

(1) *The migrative generator of $f(\mu, \nu) = \mu\nu$ is $g(\mu) = \mu$;*

(2) *The migrative generator of $f(\mu, \nu) = |\mu\nu|$ is $g(\mu) = |\mu|$;*

(3) *The migrative generator of $f(\mu, \nu) = 1 - |\mu\nu|$ is $g(\mu) = 1 - |\mu|$.*

Moreover, we have the following results.

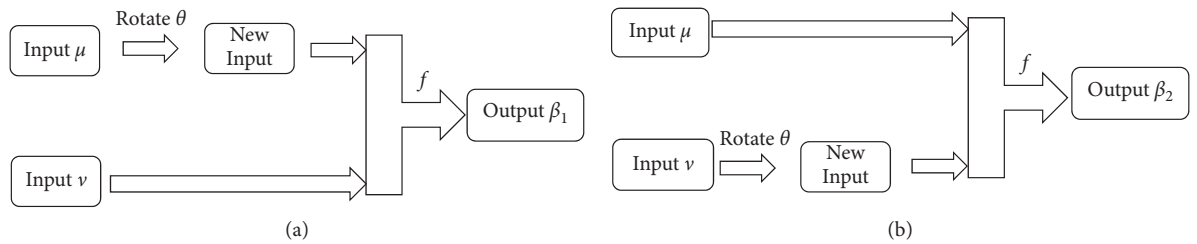

Figure 1: Phase-migrative function (a) $f(\mu \cdot e^{j\theta}, \nu)$ and (b) $f(\mu, \nu \cdot e^{j\theta})$.

Theorem 5. *Let $f\colon \mathbf{O}^2 \longrightarrow \mathbf{O}$ be a migrative function. Then f is commutative, i.e., $f(\mu, \nu) = f(\nu, \mu)$.*

Proof. If f is migrative, then $f(\mu, \nu) = f(\mu \cdot 1, \nu) = f(1, \mu\nu) = f(\nu \cdot 1, \mu) = f(\nu, \mu)$ for all $\mu, \nu \in \mathbf{O}$.

This result is not true for amplitude-migrative (or phase-migrative) functions (see Example 1). The following result is true even for amplitude-migrative (or phase-migrative) functions. □

Theorem 6. *If a binary operation $f\colon \mathbf{O}^2 \longrightarrow \mathbf{O}$ is amplitude-migrative (or phase-migrative), then for all $\mu, \nu \in \mathbf{O}$,*

(1) $f(-\mu, -\nu) = f(\mu, \nu)$;

(2) $f(-\mu, \nu) = f(\mu, -\nu)$.

Proof. Here we only give the proof of (1). If f is amplitude-migrative, then

$$f(-\mu, -\nu) = f(\mu, (-1)(-1)\nu) = f(\mu, \nu), \tag{7}$$

for all $\mu, \nu \in \mathbf{O}$.

If f is phase-migrative, then

$$f(-\mu, -\nu) = f\left(e^{j\pi}\mu, e^{j\pi}\nu\right) = f\left(\mu, e^{j\pi}e^{j\pi}\nu\right) = f(\mu, \nu), \tag{8}$$

for all $\mu, \nu \in \mathbf{O}$. □

Corollary 2. *If a binary operation $f\colon \mathbf{O}^2 \longrightarrow \mathbf{O}$ is migrative, then $f(-\mu, -\nu) = f(\mu, \nu)$ for all $\mu, \nu \in \mathbf{O}$.*

Theorem 7. *A binary operation $f\colon \mathbf{O}^2 \longrightarrow \mathbf{O}$ is phase-migrative iff it is the convex sum of a finite family of phase-migrative functions.*

Proof. ($\Rightarrow$) f is the convex sum of itself.

($\Leftarrow$) Let $f(\mu, \nu) = \sum_{i=1}^{n} w_i f_i(\mu, \nu)$ with $\sum_{i=1}^{n} w_i$ and $w_i \in \mathbf{I}$. If f_i $(i = 12, \ldots, n)$ is amplitude-migrative, then for any $\theta \in \mathbb{R}$, $f(e^{j\theta}\mu, \nu) = \sum_{i=1}^{n} w_i f_i(e^{j\theta}\mu, \nu) = \sum_{i=1}^{n} w_i f_i(\mu, e^{j\theta}\nu) = f(\mu, e^{j\theta}\nu)$ for all $\mu, \nu \in \mathbf{O}$.

Similarly, we have the following results. □

Theorem 8. *A binary operation $f\colon \mathbf{O}^2 \longrightarrow \mathbf{O}$ is amplitude-migrative iff it is the convex sum of a finite family of amplitude-migrative functions.*

Corollary 3. *A binary operation $f\colon \mathbf{O}^2 \longrightarrow \mathbf{O}$ is migrative iff it is the convex sum of a finite family of migrative functions.*

4. Migrativity and Rotational Invariance

Now we consider the relation between migrativity and rotational invariance [3, 4].

Definition 5. (see [3]). Let $f\colon \mathbf{O}^2 \longrightarrow \mathbf{O}$ be a binary function, then f is rotationally invariant if

$$f\left(\mu \cdot e^{j\theta}, \nu \cdot e^{j\theta}\right) = f(\mu, \nu) \cdot e^{j\theta}, \tag{9}$$

for any $\theta \in \mathbb{R}$ and $\mu, \nu \in \mathbf{O}$.

Dick's concept of rotational invariance was generalized as follows:

Definition 6. (see [4]). Let $f\colon \mathbf{O}^2 \longrightarrow \mathbf{O}$ be a binary function, then f is h-rotationally invariant if, for a function $h\colon \mathbb{R}^2 \longrightarrow \mathbb{R}$,

$$f\left(\mu \cdot e^{j\theta_1}, \nu \cdot e^{j\theta_2}\right) = f(\mu, \nu) \cdot e^{jh(\theta_1, \theta_2)}, \tag{10}$$

for any $\theta_1, \theta_2 \in \mathbb{R}$ and $\mu, \nu \in \mathbf{O}$.

Theorem 9. *A binary operation $f\colon \mathbf{O}^2 \longrightarrow \mathbf{O}$ is h-rotationally invariant iff it is the convex sum of a finite family of h-rotationally invariant functions.*

Proof. ($\Rightarrow$) f is the convex sum of itself.

($\Leftarrow$) Let $f(\mu, \nu) = \sum_{i=1}^{n} w_i f_i(\mu, \nu)$ with $\sum_{i=1}^{n} w_i$ and $w_i \in \mathbf{I}$. If f_i $(i = 12, \ldots, n)$ is h-rotationally invariant, then for any $\theta_1, \theta_2 \in \mathbb{R}$, $f(e^{j\theta_1}\mu, e^{j\theta_2}\nu) = \sum_{i=1}^{n} w_i f_i(e^{j\theta_1}\mu, e^{j\theta_2}\nu) = \sum_{i=1}^{n} w_i f_i(\mu, \nu)e^{jh(\theta_1, \theta_2)} = f(\mu, \nu)e^{jh(\theta_1, \theta_2)}$ for all $\mu, \nu \in \mathbf{O}$. □ □

Corollary 4. *A binary operation $f\colon \mathbf{O}^2 \longrightarrow \mathbf{O}$ is rotationally invariant iff it is the convex sum of a finite family of rotationally invariant functions.*

First, for binary operations, there is no direct relation between migrativity and Dick's rotational invariance [3]. For example, $f(\mu, \nu) = \mu\nu$ is migrative but not rotational invariance. $f(\mu, \nu) = (\mu + \nu)/2$ is rotational invariance but not migrative.

Theorem 10. *Let $f\colon \mathbf{O}^2 \longrightarrow \mathbf{O}$ be a migrative binary operation and $g\colon \mathbf{O} \longrightarrow \mathbf{O}$ be its migrative generator, then g is rotationally invariant iff*

$$f\left(\mu \cdot e^{j\theta_1}, \nu \cdot e^{j\theta_2}\right) = f(\mu, \nu) \cdot e^{j(\theta_1 + \theta_2)}, \tag{11}$$

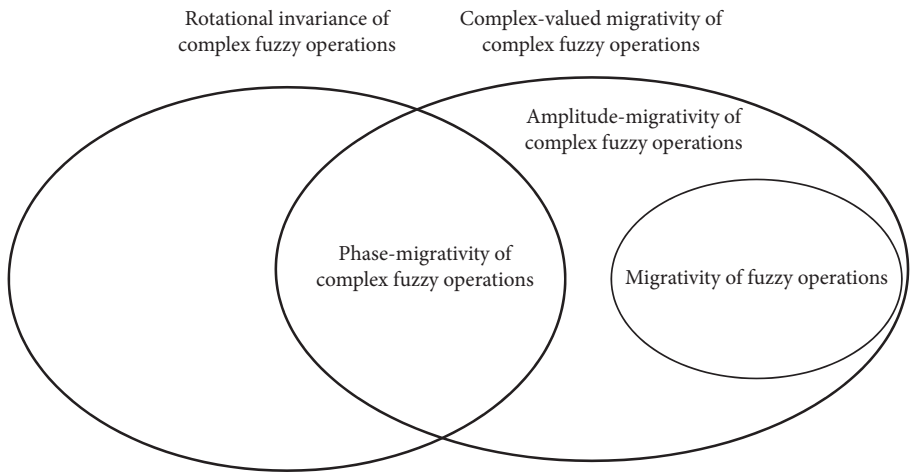

Figure 2: Relations between complex-valued migrativity of complex fuzzy operations, amplitude migrativity of complex fuzzy operations, phase valued migrativity of complex fuzzy operations, rotational invariance of complex fuzzy operations, and the migrativity of fuzzy operations.

for any $\theta_1, \theta_2 \in \mathbb{R}$ *and* $\mu, \nu \in \mathbf{O}$.

Proof. ($\Rightarrow$) g is rotationally invariant, i.e., $g(\mu \cdot e^{j\theta}) = g(\mu) \cdot e^{j\theta}$ for any $\theta \in \mathbb{R}$ and $\mu, \nu \in \mathbf{O}$. Then $f(\mu \cdot e^{j\theta_1}, \nu \cdot e^{j\theta_2}) = g(\mu \cdot e^{j\theta_1} \cdot \nu \cdot e^{j\theta_2}) = e^{j(\theta_1+\theta_2)} \cdot g(\mu\nu) = e^{j(\theta_1+\theta_2)} \cdot f(\mu, \nu)$.

($\Leftarrow$) If f satisfies equation (11), then for any $\theta \in \mathbb{R}$ and $\mu \in \mathbf{O}$, we have $g(\mu \cdot e^{j\theta}) = f(1, \mu \cdot e^{j\theta}) = f(1, \mu) \cdot e^{j\theta} = g(\mu) \cdot e^{j\theta}$.

Moreover, we consider the relation between phase-migrativity and conditional rotational invariance [4]. □

Theorem 11. *A binary operation* $f: \mathbf{O}^2 \longrightarrow \mathbf{O}$ *satisfies*

$$f\left(\mu \cdot e^{j\theta_1}, \nu \cdot e^{j\theta_2}\right) = f(\mu, \nu) \cdot e^{j(\theta_1+\theta_2)}, \tag{12}$$

for any $\theta_1, \theta_2 \in \mathbb{R}$ *and* $\mu, \nu \in \mathbf{O}$. *Then it is phase-migrative. But the converse is not true.*

Proof. For any $\theta \in \mathbb{R}$ and $\mu, \nu \in \mathbf{O}$, $f(e^{j\theta}\mu, \nu) = f(\mu, \nu) \cdot e^{j\theta} = f(\mu, e^{j\theta}\nu)$. Moreover, $f(\mu, \nu) = (\mu\nu)^2$ is phase-migrative but does not satisfy equation (12). □

Corollary 5. *A binary operation* $f: \mathbf{O}^2 \longrightarrow \mathbf{O}$ *satisfies*

$$\left.\begin{aligned} f\left(\mu \cdot e^{j\theta_1}, \nu\right) &= f(\mu, \nu) \cdot e^{j\theta_1} \\ f\left(\mu, \nu \cdot e^{j\theta_2}\right) &= f(\mu, \nu) \cdot e^{j\theta_2} \end{aligned}\right\}, \tag{13}$$

for any $\theta_1, \theta_2 \in \mathbb{R}$ *and* $\mu, \nu \in \mathbf{O}$. *Then it is phase-migrative. But the converse is not true.*

Proof. Because equation (12) is equivalent to equation (13), □

Theorem 12. *Let* $f: \mathbf{O}^2 \longrightarrow \mathbf{O}$ *be a commutative binary operation, if it satisfies* $f(e^{j\theta}\mu, \nu) = f(\mu, \nu) \cdot e^{j\theta}$ *for all* $\theta \in \mathbb{R}$ *and* $\mu, \nu \in \mathbf{O}$. *Then*

(1) it is phase-migrative;

(2) it is h*–rotationally invariant, where* $h(\theta_1, \theta_2) = \theta_1 + \theta_2$.

Proof

(1) For any $\theta \in \mathbb{R}$ and $\mu, \nu \in \mathbf{O}$, we have $f(\mu, e^{j\theta}\nu) = f(e^{j\theta}\nu, \mu) = f(\nu, \mu) \cdot e^{j\theta} = f(\mu, \nu) \cdot e^{j\theta} = f(\mu \cdot e^{j\theta}, \nu)$.

(2) For any $\theta_1, \theta_2 \in \mathbb{R}$ and $\mu, \nu \in \mathbf{O}$, we have $f(\mu \cdot e^{j\theta_1}, \nu \cdot e^{j\theta_2}) = f(\mu, \nu \cdot e^{j\theta_2}) \cdot e^{j\theta_1} = f(\nu \cdot e^{j\theta_2}, \mu) \cdot e^{j\theta_1} = f(\nu, \mu) \cdot e^{j\theta_1} \cdot e^{j\theta_2} = f(\mu, \nu) \cdot e^{j(\theta_1+\theta_2)}$.

We give a binary operation f without commutativity, $f(\mu, \nu) = \mu|\nu|$ satisfies $f(e^{j\theta}\mu, \nu) = f(\mu, \nu) \cdot e^{j\theta}$ for all $\theta \in \mathbb{R}$ and $\mu, \nu \in \mathbf{O}$. But it is neither commutative nor phase-migrative. Moreover, it is h'–rotationally invariant, where $h'(\theta_1, \theta_2) = \theta_2$.

The relations between complex-valued migrativity of complex fuzzy operations, amplitude migrativity of complex fuzzy operations, phase valued migrativity of complex fuzzy operations, rotational invariance of complex fuzzy operations, and the migrativity of fuzzy operations are shown in Figure 2. □

Theorem 13. *Let* $f: \mathbf{O}^2 \longrightarrow \mathbf{O}$ *be a commutative binary operation, if it satisfies* $f(r\mu, \nu) = rf(\mu, \nu)$ *for all* $r \in \mathbf{I}$ *and* $\mu, \nu \in \mathbf{O}$. *Then*

(1) it is amplitude-migrative;

(2) it satisfies $f(r_1\mu, r_2\nu) = r_1 r_2 f(\mu, \nu)$. *for all* $r_1, r_2 \in \mathbf{I}$ *and* $\mu, \nu \in \mathbf{O}$.

Proof. For any $r \in \mathbf{I}$ and $\mu, \nu \in \mathbf{O}$, we have

(1) $f(\mu, r\nu) = f(r\nu, \mu) = r \cdot f(\nu, \mu) = r \cdot f(\mu, \nu) = f(r\mu, \nu)$.

(2) $f(r_1\mu, r_2\nu) = r_1 \cdot f(\mu, r_2\nu) = r_1 \cdot f(r_2\nu, \mu) = r_2 \cdot r_1 \cdot f(\nu, \mu) = r_1 r_2 \cdot f(\mu, \nu)$.

We observe that it is homogeneous of order 2, i.e., $f(r\mu, r\nu) = r^2 f(\mu, \nu)$ when $r_1 = r_2$.

We give a binary operation f without commutativity, $f(\mu, \nu) = \mu \cdot \nu \cdot |\nu|$ satisfies $f(r\mu, \nu) = r \cdot f(\mu, \nu)$ for all $r \in \mathbf{I}$ and $\mu, \nu \in \mathbf{O}$. But it is neither commutative nor amplitude-migrative. Moreover, it is homogeneous of order 3, i.e., $f(r\mu, r\nu) = r^3 f(\mu, \nu)$. □

Corollary 6. *Let $f: \mathbf{O}^2 \longrightarrow \mathbf{O}$ be a commutative binary operation, if it satisfies $f(\alpha\mu, \nu) = \alpha \cdot f(\mu, \nu)$ for all $\alpha \in \mathbf{O}$ and $\mu, \nu \in \mathbf{O}$. Then it is migrative*

Theorem 14. *If a binary operation $f: \mathbf{O}^2 \longrightarrow \mathbf{O}$ is h−rotationally invariant where $h_1(\theta_1, \theta_2) = k(\theta_1, \theta_2)$ for some $k > 0$. Then f is phase-migrative,*

Proof. For any $\theta \in \mathbb{R}$ and $\mu, \nu \in \mathbf{O}$, we have $f(\mu \cdot e^{j\theta}, \nu) = f(\mu, \nu) \cdot e^{jk\theta} = f(\mu, \nu \cdot e^{j\theta})$ for some $k > 0$. □

Theorem 15. *If a binary operation $f: \mathbf{O}^2 \longrightarrow \mathbf{O}$ satisfies $f(r_1\mu, r_2\nu) = (r_1 \cdot r_2)^k f(\mu, \nu)$ for all $r_1, r_2 \in \mathbf{I}$, all $\mu, \nu \in \mathbf{O}$, and some $k > 0$. Then f is amplitude-migrative.*

Proof. For any $r \in \mathbf{I}$ and $\mu, \nu \in \mathbf{O}$, we have $f(r\mu, \nu) = r^k f(\mu, \nu) = f(\mu, r\nu)$ for some $k > 0$. □

Corollary 7. *If a binary operation $f: \mathbf{O}^2 \longrightarrow \mathbf{O}$ satisfies $f(\alpha_1\mu, \alpha_2\nu) = (\alpha_1 \cdot \alpha_2)^k f(\mu, \nu)$ for all $\alpha_1, \alpha_2 \in \mathbf{O}$, all $\mu, \nu \in \mathbf{O}$, and some $k > 0$. Then f is migrative.*

5. Conclusions

In this paper, we study the migrative binary complex fuzzy operators

$$f(\alpha\mu, \nu) = f(\mu, \alpha\nu), \quad \forall \mu, \nu \in \mathbf{O}, \tag{14}$$

for three cases $\alpha \in \mathbf{I}$, $\alpha \in \overline{\mathbf{O}}$, and $\alpha \in \mathbf{O}$. Interestingly, this equation holds for all $\alpha \in \mathbf{O}$ if and only if it holds for all $\alpha \in \mathbf{I} \cup \overline{\mathbf{O}}$ (see Theorem 1). Note that the size of $\mathbf{I} \cup \overline{\mathbf{O}}$ is much smaller than that of $\mathbf{O}$. Then we give the relationship among phase-migrativity, amplitude-migrativity, migrativity, and rotational invariance for complex fuzzy operations (see Figure 1). We show that phase-migrativity is a special case of conditional rotational invariance (see Theorem 12).

Note that this paper focused on binary complex fuzzy operators. Future research should consider the migrativity of n-dimensional complex fuzzy aggregation operators. Naturally, other properties of complex fuzzy operators are possible topics for future consideration.

In [31], Yager and Abbasov used complex numbers of the form $r \cdot e^{j\theta}$ as Pythagorean membership grades, where $r \in [0, 1]$ and $\theta \in [0, \pi/2]$. These complex numbers are called $\pi - i$ numbers, which belong to the upper-right quadrant of the unit disk in the complex plane. Viewed in this way, studying the migrativity of Pythagorean fuzzy operators is a special case of migrativity of complex fuzzy operators by limiting the domain to $\pi - i$ numbers. Obviously, a more detailed discussion of the migrativity of Pythagorean fuzzy aggregation operators [32], Pythagorean t-norm [33], will be both necessary and interesting.

Data Availability

No data were used to support this study.

Conflicts of Interest

The authors declare that they have no conflicts of interest.

Acknowledgments

This research was funded by the National Science Foundation of China (Grant nos. 62006168 and 62101375) and the Zhejiang Provincial Natural Science Foundation of China (Grant nos. LQ21A010001 and LQ21F020001).

References

[1] D. Ramot, R. Milo, M. Friedman, and A. Kandel, "Complex fuzzy sets," *IEEE Transactions on Fuzzy Systems*, vol. 10, no. 2, pp. 171–186, 2002.

[2] D. Ramot, M. Friedman, G. Langholz, and A. Kandel, "Complex fuzzy logic," *IEEE Transactions on Fuzzy Systems*, vol. 11, no. 4, pp. 450–461, 2003.

[3] S. Dick, "Toward complex fuzzy logic," *IEEE Transactions on Fuzzy Systems*, vol. 13, no. 3, pp. 405–414, 2005.

[4] S. Dai, "A generalization of rotational invariance for complex fuzzy operations," *IEEE Transactions on Fuzzy Systems*, vol. 29, no. 5, pp. 1152–1159, 2021.

[5] S. Dai, "On partial orders in complex fuzzy logic," *IEEE Transactions on Fuzzy Systems*, vol. 29, no. 3, pp. 698–701, 2021.

[6] G. Zhang, T. S. Dillon, K. y. Cai, J. Ma, and J. Lu, "Operation properties and δ-equalities of complex fuzzy sets δ-equalities of complex fuzzy sets," *International Journal of Approximate Reasoning*, vol. 50, no. 8, pp. 1227–1249, 2009.

[7] S. Dick, R. R. Yager, and O. Yazdanbakhsh, "On pythagorean and complex fuzzy set operations," *IEEE Transactions on Fuzzy Systems*, vol. 24, no. 5, pp. 1009–1021, 2016.

[8] L. Liu and X. Zhang, "Comment on pythagorean and complex fuzzy set operations," *IEEE Transactions on Fuzzy Systems*, vol. 26, no. 6, pp. 3902–3904, 2018.

[9] S. Dick, "On complex fuzzy S-implications," *IEEE Transactions on Emerging Topics in Computational Intelligence*, pp. 1–7, 2020.

[10] L. Bi, B. Hu, S. Li, and S. Dai, "The parallelity of complex fuzzy sets and parallelity preserving operators," *Journal of Intelligent & Fuzzy Systems*, vol. 34, no. 6, pp. 4173–4180, 2018.

[11] B. Hu, L. Bi, and S. Dai, "The orthogonality between complex fuzzy sets and its application to signal detection," *Symmetry*, vol. 9, no. 9, p. 175, 2017.

[12] B. Hu, L. Bi, S. Dai, and S. Li, "The approximate parallelity of complex fuzzy sets," *Journal of Intelligent & Fuzzy Systems*, vol. 35, no. 6, pp. 6343–6351, 2018.

[13] B. Hu, L. Bi, and S. Dai, "Approximate orthogonality of complex fuzzy sets and approximately orthogonality preserving operators," *Journal of Intelligent & Fuzzy Systems*, vol. 37, no. 4, pp. 5025–5030, 2019.

[14] F. Durante and P. Sarkoci, "A note on the convex combinations of triangular norms," *Fuzzy Sets and Systems*, vol. 159, no. 1, pp. 77–80, 2008.

[15] J. Qiao and B. Q. Hu, "On generalized migrativity property for overlap functions," *Fuzzy Sets and Systems*, vol. 357, pp. 91–116, 2019.
[16] H. Zhou and X. Yan, "Migrativity properties of overlap functions over uninorms," *Fuzzy Sets System*, vol. 403, 2021.
[17] J. Qiao and B. Q. Hu, "On the migrativity of uninorms and nullnorms over overlap and grouping functions," *Fuzzy Sets and Systems*, vol. 346, pp. 1–54, 2018.
[18] Y. Su, H. W. Liu, J. V. Riera, D. Ruiz-Aguilera, and J. Torrens, "The migrativity equation for uninorms revisited," *Fuzzy Sets and Systems*, vol. 323, pp. 56–78, 2017.
[19] Y. Su, W. Zong, and H. W. Liu, "Migrativity property for uninorms," *Fuzzy Sets and Systems*, vol. 287, pp. 213–226, 2016.
[20] Y. Su, W. Zong, H. W. Liu, and P. Xue, "Migrativity property for uninorms and semi t-operators," *Information Sciences*, vol. 325, pp. 455–465, 2015.
[21] Y. Su, W. Zong, H. W. Liu, and F. Zhang, "On migrativity property for uninorms," *Information Sciences*, vol. 300, pp. 114–123, 2015.
[22] M. Mas, M. Monserrat, D. Ruiz-Aguilera, and J. Torrens, "An extension of the migrative property for uninorms," *Information Sciences*, vol. 246, pp. 191–198, 2013.
[23] L. Wu and Y. Ouyang, "On the migrativity of triangular subnorms," *Fuzzy Sets and Systems*, vol. 226, pp. 89–98, 2013.
[24] Y. Ouyang, "Generalizing the migrativity of continuous t-norms," *Fuzzy Sets and Systems*, vol. 211, pp. 73–83, 2013.
[25] W. Zong and H. W. Liu, "Migrative property for nullnorms," *International Journal of Uncertain Fuzziness Knowledge Based System*, vol. 22, no. 5, pp. 749–759, 2014.
[26] F. Durante, J. Fernández-Sánchez, and J. J. Quesada-Molina, "On the α-migrativity of multivariate semi-copulas α-migrativity of multivariate semi-copulas," *Information Sciences*, vol. 187, pp. 216–223, 2012.
[27] R. Mesiar, H. Bustince, and J. Fernandez, "On the α-migrativity of semicopulas, quasi-copulas, and copulas," *Informative Science*, vol. 180, 2010.
[28] H. Bustince, J. Montero, and R. Mesiar, "Migrativity of aggregation functions," *Fuzzy Sets and Systems*, vol. 160, no. 6, pp. 766–77710, 2009.
[29] H. Bustince, B. De Baets, J. Fernandez, R. Mesiar, and J. Montero, "A generalization of the migrativity property of aggregation functions," *Information Sciences*, vol. 191, pp. 76–85, 2012.
[30] C. Lopez-Molina, B. De Baets, H. Bustince, E. Induráin, A. Stupňanová, and R. Mesiar, "Bimigrativity of binary aggregation functions," *Information Sciences*, vol. 274, pp. 225–235, 2014.
[31] R. R. Yager and A. M. Abbasov, "Pythagorean membership grades, complex numbers, and decision making," *International Journal of Intelligent Systems*, vol. 28, no. 5, pp. 436–452, 2013.
[32] L. Wang and H. Garg, "Algorithm for multiple attribute decision-making with interactive archimedean norm operations under pythagorean fuzzy uncertainty," *International Journal of Computational Intelligence Systems*, vol. 14, no. 1, pp. 503–527, 2020.
[33] T. Nan, H. Zhang, and Y. He, "Pythagorean fuzzy full implication multiple I method and corresponding applications," *Journal of Intelligent & Fuzzy Systems*, vol. 41, no. 1, pp. 1741–1755, 2021.